NAVAL POSTGRADUATE SCHOOL
Monterey, California

THESIS

AN ANALYSIS OF SYMMETRIC REINFORCEMENT OF GRAPHITE/EPOXY HONEYCOMB SANDWICH PANELS WITH A CIRCULAR CUTOUT UNDER UNIAXIAL COMPRESSIVE LOADING

by

Patrick D. Sullivan

December 1985

Thesis Advisor: M. H. Bank

SECURITY CLASSIFICATION OF THIS PAGE

REPORT DOCUMENTATION PAGE

1a. REPORT SECURITY CLASSIFICATION	1b. RESTRICTIVE MARKINGS
2a. SECURITY CLASSIFICATION AUTHORITY 2b. DECLASSIFICATION / DOWNGRADING SCHEDULE	3. DISTRIBUTION / AVAILABILITY OF REPORT Approved for public release; distribution unlimited.
4. PERFORMING ORGANIZATION REPORT NUMBER(S)	5. MONITORING ORGANIZATION REPORT NUMBER(S)
6a. NAME OF PERFORMING ORGANIZATION Naval Postgraduate School 6b. OFFICE SYMBOL (If applicable) Code 67	7a. NAME OF MONITORING ORGANIZATION Naval Postgraduate School
6c. ADDRESS (City, State, and ZIP Code) Monterey, California 93943-5100	7b. ADDRESS (City, State, and ZIP Code) Monterey, California 93943-5100
8a. NAME OF FUNDING / SPONSORING ORGANIZATION 8b. OFFICE SYMBOL (If applicable)	9. PROCUREMENT INSTRUMENT IDENTIFICATION NUMBER
8c. ADDRESS (City, State, and ZIP Code)	10. SOURCE OF FUNDING NUMBERS PROGRAM ELEMENT NO. | PROJECT NO. | TASK NO. | WORK UNIT ACCESSION NO.

11. TITLE (Include Security Classification)
AN ANALYSIS OF SYMMETRIC REINFORCEMENT OF GRAPHITE/EPOXY HONEYCOMB SANDWICH PANELS WITH A CIRCULAR CUTOUT UNDER UNIAXIAL COMPRESSIVE LOADING

12. PERSONAL AUTHOR(S)
Sullivan, Patrick D.

13a. TYPE OF REPORT	13b. TIME COVERED	14. DATE OF REPORT (Year, Month, Day)	15. PAGE COUNT
Engineer's thesis	FROM ____ TO ____	1985 December	343

16. SUPPLEMENTARY NOTATION

17. COSATI CODES			18. SUBJECT TERMS (Continue on reverse if necessary and identify by block number)
FIELD	GROUP	SUB-GROUP	Composite; reinforced composite; circular hole; graphite epoxy panel; compression

19. ABSTRACT (Continue on reverse if necessary and identify by block number)

An experimental and computational analysis was made of stress/strain concentrations around a reinforced ciruclar 1.00 inch diameter circular cutout in HMF330C/34 (cloth) graphite/epoxy (G/Ep) and fiberglass/phenolic honeycomb sandwich panels under uniaxial compressive loading. The test specimens were 10.00" x 8.50", eight ply quasi-isotropic ($[0,\pm 45,90,\text{core}]_s$) panels. The reinforcement consisted of either one or two additional G/Ep plies co-cured to the outside of each facesheet. Three general reinforcement configurations were considered: round, square and strips parallel to the applied load. The analytical results demonstrated that small amounts of reinforcement could greatly increase the strength-to-weight ratio. The indication was that concentrating the reinforcement close to the cutout yielded the greatest decrease in stress concentration. A program of experimental validation of the analytical results experienced some problems

20. DISTRIBUTION / AVAILABILITY OF ABSTRACT ☒ UNCLASSIFIED/UNLIMITED ☐ SAME AS RPT ☐ DTIC USERS	21. ABSTRACT SECURITY CLASSIFICATION Unclassified
22a. NAME OF RESPONSIBLE INDIVIDUAL L. H. Bank	22b. TELEPHONE (Include Area Code) (408) 646-2582 22c. OFFICE SYMBOL Code 034Bt

DD FORM 1473, 84 MAR — 83 APR edition may be used until exhausted. All other editions are obsolete. — SECURITY CLASSIFICATION OF THIS PAGE

Block 3. (cont'd)

with prematrue panel failure caused by the facesheets separating from the core. It generally confirmed the analytical results, however. Further experimental tests on promising reinforcement configurations are justified based on these results. Properly designed reinforcement around cutouts in composite panels can significantly reduce the stress concentration and holds the promise of far lighter and stronger aerospace structures.

An Analysis of Symmetric Reinforcement of Graphite/Epoxy Honeycomb Sandwich Panels with a Circular Cutout Under Uniaxial Compressive Loading

by

Patrick D. Sullivan
Commander, United States Navy
B.S., United States Naval Academy 1969

Submitted in partial fulfillment of the
requirements for the degree of

AERONAUTICAL ENGINEER

from the

NAVAL POSTGRADUATE SCHOOL
December 1985

ABSTRACT

An experimental and computational analysis was made of stress/strain concentrations around a reinforced circular 1.00 inch diameter circular cutout in HMF330C/34 (cloth) graphite/epoxy (G/Ep) and fiberglass/phenolic honeycomb sandwich panels under uniaxial compressive loading. The test specimens were 10.00" x 8.50", eight ply quasi-isotropic ($[0,\pm45,90,\overline{core}]_s$) panels. The reinforcement consisted of either one or two additional G/Ep plies co-cured to the outside of eacn facesheet. Three general reinforcement configurations were considered: round, square and strips parallel to the applied load. The analytical results demonstrated that small amounts of reinforcement could greatly increase the strength-to-weight ratio. The indication was that concentrating the reinforcement close to the cutout yielded the greatest decrease in stress concentration. A program of experimental validation of the analytical results experienced some problems with premature panel failure caused by the facesheets separating from the core. It generally confirmed the analytical results, however. Further experimental tests on promising reinforcement configurations are justified based on these results. Properly designed reinforcement around cutouts in composite panels can significantly reduce the stress concentration and holds the promise of far lighter and stronger aerospace structures.

TABLE OF CONTENTS

LIST OF TABLES

LIST OF FIGURES

LIST OF SYMBOLS

A	Area (in^2)
[A]	Iaminate inplane stiffness matrix (Eqn. 3.11)
a_o	Characteristic length for the average stress failure criterion (Eqn. 2.5)
a	Radius of cutout (0.500 inch)
[B]	Force resultnat-moment coupling matrix (Eqn. 3.16)
[C]	Material elastic constant tensor (Eqn. 3.1)
[D]	Laminate moment stiffness matrix (Eqn. 3.15)
d	Diameter of cutout (1.00 inch)
E	Modulus of Elasticity (tension and compression) (psi)
E	Strain gage excitation level (volts) (Eqn. 4.1)
$\{F\}$	Force vector (lbf) (Eqn. 3.29)
h	Thickness of a laminate ply (inch)
G	Shear modulus of elasticity (psi)
K	Stress concentration factor
[K]	Finite element stiffness matrix (Eqn. 3.29)
k	Radius of curvature (Eqn. 3.17)
l	Panel length (in)
$\{M\}$	Moment vector (Eqn. 3.13)
$\{N\}$	Stress resultant vector (Eqn. 3.12)
PD	Power density (watt/in^2) (Eqn. 4.1)
R	Resistnace (ohms) (Eqn. 4.1)
r	Radial distance from the origin (inch)
[Q]	Reduced laminate stiffness matrix (Eqn. 3.5)
[Q']	Reduced transformed laminate stiffness matrix (Eqn. 3.10)
S	Applied stress (psi)

S	Compliance (Eqn. 3.23)
[T]	Rotation transorm matrix (Eqn. 3.9)
w	Panel width (in)
X,Y,Z	Rectangular
$\{\delta\}$	Displacement vector (Eqn. 3.27)
$\overline{\sigma}_n$	Direct stress
ϵ	Direct strain
σ	Applied far-field normal stress
ν	Poisson's ratio
ξ	$d/[2(d/2 + a_\circ)]$
$\mu\epsilon$	microstrain ($*10^6$)
γ	Shear strain

Subscripts

avg	Average
c	Compression
i,j,k	Indices of summation
l	Lateral direction (parallel to load line)
max	Maximum
n	Notched panel
σ	Stress
ϵ	Strain
t	Tension
t	Transverse direction (prependicular to load line)
u	Unnotched panel
ult	Ultimate strength (indicating total failure)
1,2	Directions parallel and perpendicular to principal fiber direction respectively
∞	Infinite panel width

Abbreviations

ASFC	Average Stress Failure Criterion
DOF	Degrees of freedom (at a node)
Eps-X	Strain in the x direction (ϵ_x)
Eps-Y	Strain in the y direction (ϵ_y)
Eps-XY	Shear Strain (ϵ_{xy})
FAPF	First Audible Ply Failure
FEA	Finite Element Analysis
G/Ep	Graphite /Epoxy
ksi	Thousand pound force per square inch
LEFEA	Linear Elastic Finite Element Analysis
LEFM	Linear Elastic Fracture Mechanics
msi	Million pound force per square inch
NDI	Non-Distructive Inspection
SCF	Stress Concentration Factor

ACKNOWLEDGEMENTS

For inspiration and guidance I turn to Lao Tsu. He set these words down during the sixth century B.C. in the province of Honan, China:

Thirty spokes share the wheel's hub;
It is the center hole that makes it useful.
Shape clay into a vessel;
It is the space within that makes it useful.
Cut doors and windows for a room;
It is the holes which make it useful.
Therefore profit comes from what is there;
Usefulness from what is not there.

It was upon that passage that this paper was based.

The author owes an incalculable debt of gratitude to the people who made this research possible, for their unflagging patience, if nothing else. The first among these is Professor Milton Bank who was initially drafted to the task of Thesis Advisor but who then adopted my project as his own. His zest and enthusiasm for knowledge changed my life. Professor E.M. Wu entered the project at the last stage and gave it a fine polish.

Robert Besel, Glenn Middleton and Ted Dunton of the Naval Postgraduate School, Department of Aeronautics devoted untold hours to helping me prepare the test apparatus and contributed no end of advice and assistance. Drs. J.A. Bailie, Norman Cyr of Lockheed Missiles and Space Corp, Sunnyvale, CA never tired of my endless questions. The success of this research is due to their most subtle guidance. My debt to both of them goes beyond what can be told. The funds for this research were wholly provided by the U.S. Navy Strategic System Project Office, Washington, DC.

Last, I thank Professor Robert Zucker of the Department of Aeronautics for his faith and for his example.

I. INTRODUCTION

The ratio of strength to weight is one of the principal means of determining the efficiency of a structure. In aerospace applications this comparison can be the most meaningful measure. The dilemma of designing an airframe for both strength and lightness has been with us since the days of daVinci. The quest for ever higher ratios of strength-to-weight has led to the development and use of high modulus advanced composite materials, principally graphite or carbon fibers bonded together in a polymer matrix, in the place of metal.

Major airframe structural components such as wings or bulkheads require cutouts for bolted or riveted attachment, access to interior space and passage of control and fuel lines. Timoshenko and Goodier [Ref. 1: pp. 78-84], among others, point out that such holes in load-bearing structures act to greatly increase the local stress and to reduce ultimate strength. This characteristic is referred to as the stress (or strain) concentration factor (SCF or K). It seems the SCF may have several definitions, depending on the material and the researcher. In this report it shall be defined as the highest plane strain existing around a cutout divided by the far-field strain; generally called the gross SCF or K_{gross}. Taking into consideration Saint-Venant's principle, the far-field strain is assumed to be equal to the strain which would exist in an ideal, thin, stressed infinite plate if a cutout was not present. Stress and strain concentrations, while inextricably linked in elastic materials, are not the same. However, since in the application discussed here, there is little appreciable numerical difference, the term "SCF" will be used to indicate either the stress or strain concentration factor.

When holes or cutouts are necessary in a structural component, airframe designers generally have the choice of accepting either a significantly lower ultimate load or greatly increasing the component's strength, and thus its weight. In either case the ratio of strength-to-weight is reduced in proportion to the highest SCF existing within the member. Properly designed ductile metal structures mitigate the effects of SCF by plastically deforming under high load conditions. This response delays ultimate failure, but can also lead to unacceptable reductions in both stiffness and fatigue life.

The metals used in aircraft construction, principally aluminum and titanium, can almost always be considered isotropic (many manufacturing processes, however, introduce some minor directional properties). The magnitude of the orthogonal strains (X, Y and shear) existing at a point in a plane isotropic panel result from the orthogonal stress resultant at that point and are in proportion determined by the elastic modulus and Poisson's ratio. An applied in-plane stress on an isotropic plate will not induce curvature other than, of course, the possibility of the plate buckling under compression. Composite plates are termed "quasi-isotropic" when they are composed of anisotropic or orthotropic laminae stacked with the directional properties arranged in a manner to react identically to a true isotropic material to both moments and inplane loads.

Composite laminates typically lack the ductility of metals. The high-modulus graphite/epoxy (G/Ep) fibers in general use in the aerospace industry allow approximately 1% strain (10,000μ)

in tension and compression to complete failure. Depending on the fiber orientation, panels constructed of laminated advanced composites with notches or cutouts can demonstrate from slightly less to much more sensitivity to holes or cutouts than otherwise identical isotropic metal panels. As shown by Rybicki and Hopper [Ref. 2: pp. 15-27], among others, this sensitivity principally depends on the type of weave and the orientation of the plies in the laminate; that is, it depends on the degree of orthotropy.

The inherently brittle nature of advanced composite materials, their characteristically low strain to failure, coupled with manufacturing limitations make their design a far more demanding task than that for metals. Other characteristics, however, including fatigue and corrosion resistance, light weight, and easily tailored directional properties make the design of composite structures very attractive, particularly to the aerospace designer.

A. OBJECTIVES AND SCOPE

This study was designed to investigate the effect of relatively simple co-cured reinforcement of a cutout on the strain field and failure behavior in G/Ep honeycomb sandwich panels subjected to uniaxial compression. Honeycomb construction allows very light yet exceptionally stiff structures. The objective was to determine if a simple and inexpensive reinforcement geometry using small volumes of co-cured G/Ep lamina near the cutout could significantly reduce local stress concentrations and increase the ultimate failure strength in the honeycomb laminate. The idea of local reinforcement around holes is not new; Timoshenko noted [Ref. 1: p. 82] that "reinforcing rings" could decrease the SCF in plates with cutouts. The point was to examine the reaction of an advanced composite, a material whose characteristics differ markedly from those Timoshenko addressed.

The research was undertaken with the manufacturer principally in mind. Complex or exceptionally thick reinforcement geometries are difficult and expensive to manufacture cost-effectively or with a high degree of quality assurance. This research used only very thin (maximum thickness: 0.028") ply reinforcement in three relatively simple geometries. Since facesheets with reinforcing plies on both sides would require machining a precise shallow depression in both the face of the the honeycomb core and the surface of the layup plate, each difficult and expensive tasks, reinforcement was restricted to the outside surface of each facesheet.

This study was limited to one panel size (10.00" x 8.50"), a single loading condition (uniaxial compression) and three relatively simple reinforcement geometries. The 1.00 inch diameter circular cutout was reinforced with concentric co-cured round and square G/Ep plies around the hole and stiffening strips displaced 0.50 inch (1 hole radius) laterally from the cutout edge. The total amount of reinforcement used varied from 1 to 5 times the G/Ep removed from the cutout. Reinforcement was either one or two plies symmetrically applied to the outside of both facesheets of the panel. A honeycomb core was used, as it would be in an actual application, to increase the panel bending stiffness and thus eliminate the buckling of the whole panel as a mode of failure.

The basic panel facesheets were four layer [0,±45,90] HMF330C/34 G/Ep cured to a thickness of 0.056 inch. Cured sheets were bonded to both sides of a 0.50 inch thick fiberglass/phenolic honeycomb core using 3M, Inc.'s AF-126 (250°F) cured adhesive.

The result was a very light, thin quasi-isotropic laminate: $[0,\pm45,90,\overline{core}]_s$ with a great resistance to bending. The HMF330C/34 is a woven, high-temperature epoxy (350°F) G/Ep fabric manufactured by the Fiberite Corporation of Winona, MN. In order to reduce the number of design variables the principal axis of the reinforcement plies was oriented only in the direction of the applied compressive load. This theoretically gives the highest stress concentration and could be considered the worst case.

B. REVIEW OF LITERATURE

1. Background and Historical Research

The subject of notch-induced stress concentrations in plates has been extensively documented. The effects reinforcement have on the SCF in plates have received considerably less attention. Early research concentrated on metals (isotropic materials) and focused on defining the stress and strain fields around circular and elliptic cutouts. Recent research has been primarily in characterizing the response of orthotropic and anisotropic materials.

Kirsch [Ref. 3] is commonly cited as the first to determine exactly the stress concentration factor of a cutout in an isotropic material from the theory of elasticity. Howland [Ref. 4] applied the solution to Airy's equation in polar coordinates to determine the magnitude of the SCF. One of the earliest papers addressing reinforced holes was by Levy, Woolley, and Kroll [Ref. 5]. They investigated the effect of both reinforced and unreinforced holes on the buckling strength of square isotropic plates. They determined that presence of a hole caused only a relatively minor reduction in the buckling (ultimate) load.

A thorough theoretical, closed-form mathematical treatment of anisotropic materials with stress concentrations can be found in the work of two Russian applied mathematicians, S.G. Lekhnitskii and G.N. Savin. Lekhnitskii [Ref. 6] principally addressed the distribution of stress around the edge of variously shaped cutouts in unreinforced anisotropic plates and shells under a variety of loading conditions. He determined that a plate with high anisotropy, as found in strictly unidirectional fiber construction, could produce a stress concentration factor near 9 when the load was parallel (0°) to the principal fiber direction, and slightly more than 2 with the load perpendicular (90°) to it. It must be pointed out that, in composite materials, the SCF may not have a exactly proportional effect on the reduction in the ultimate strength of the plate. Due to the composite's ability to redirect the load path once fibers are broken or lose stiffness through matrix degradation, the ultimate strength is not degraded as much as would be expected by the presence of the stress concentration. This phenomenon is discussed in more detail in section II.D.4.

Savin [Ref. 7] treated the stress and strain fields in a plate resulting from a cutout. He addressed the SCF as a function of a plate's linear material properties, ply orientation and stacking, and its loading. Hole size, reinforcement and geometry were not addressed. A computer program was developed by Garbo and Ogonowski of McDonnell-Douglas [Ref. 8: Vol. 3] which computes the stress and strain field around a cutout based on Lekhnitskii's and Savin's analyses. It was modified by the author for the IBM 370 and is listed in Appendix P.

Substantial research in stress concentrations in composite plates was done by Greszczuk [Ref. 9]. He developed a theoretical solution for failure stress and stress concentrations in both orthotropic and anisotropic material under tension. His method was based on the Hencky-Von Mises distortion energy method, and gave both magnitude and locations of the ultimate stress. Rybicki and Schmueser [Ref. 10] investigated the effects of laminate stacking sequence, lay-up angles, fabrication temperature and thickness on panel stress concentrations using finite element analysis.

There is relatively little research into the effects of reinforcement around holes in composite plates which has been reported in the open literature. Virtually nothing is available on the behavior of notched reinforced plates in compression or on the effect on the type of failure of using honeycomb in such structures.

Kocher and Cross [Ref. 11] demonstrated experimentally that titanium, graphite and steel reinforcement around a circular cutout in a composite plate could reduce the SCF and increase the ultimate failure load in tension. Their results, however, were based on relatively complex, thick reinforcement geometries that have not found acceptance in aeronautical design.

A novel cutout reinforcement method using bonded hoop-wound G/Ep disks was addressed by McKenzie [Ref. 12]. The disks were used to reinforce both aluminum and G/Ep plates under tensile loads. The method proved effective both in reducing the stress around the cutout and increasing the plates' strength.

The team of Daniel, Rowlands and Whiteside [Refs. 13-17] did extensive experimental work in characterizing the effects of cutouts on a variety of composite materials. They did some limited testing of reinforced specimens in tension and found proportionately reduced SCFs and increased strength. They determined that interlaminar deformations occurred in the boundary region of the cutout, an area they defined as extending about one laminate thickness from the free edge. This deformation was very nonlinear and could cause delamination at relatively low loads. Strain levels next to the cutout, prior to failure, were found to be higher than the ultimate failure strain of panels without cutouts. Based on that, they determined that the SCF did not necessarily produce a proportional reduction in strength. They recommended keeping the reinforcement close to the hole, using stepped diameter plies ("wedding cake") to facilitate the load transfer, and using 45° plies in the reinforcement where possible.

Knauss, Starnes, Henneke [Ref. 18] tested unreinforced 0.15 and 0.24 inch thick T300/5208 panels in compression for unbuckled and postbuckled strength. They found that under high, but less than normally ultimate stress levels, the laminate around the hole could buckle locally, delaminate and initiate total panel failure. A micro-mechanical failure mode was postulated where limited fiber buckling at the point of stress concentration caused by local imperfections such as voids, matrix cracking or poor fiber-matrix bonds led to total failure.

2. Summary of Recent Related Research

This report is the fourth in a series of investigations on the character of stress concentrations in composite plates made of HMF330C/34 G/Ep. This particular material was chosen because of its current use in both the Trident submarine launched ballistic missile (SLBM) and the prototype Lear Fan propjet aircraft and the fact that it has a relatively small data base compared to other G/Ep prepreg material currently in aerospace use. This research was funded by the Strategic Systems Project Office of the Naval Sea Systems Command and greatly assisted by Lockheed Missiles and Space Co. (LMSC), Sunnyvale, CA.

The initial project was undertaken by Herman [Ref. 19] who investigated the pre- and postbuckled strength of HMF330C/34 panels loaded strictly in shear. He used a molded-in 45° flange around the cutout to add strength to the shear web. He determined that this reinforcement method was well-suited to adding stiffness to panels that were not buckled but that the panels did not see a significant increase in ultimate strength once buckling had occurred.

O'Neill [Ref. 20] demonstrated that reinforcement of only one face of a notched panel under tensile loading provided limited additional strength. Initially, the reinforcement of only one side of a cutout was considered attractive since only a small additional manufacturing effort was required. Asymmetric reinforcement, however, displaces the midplane of the laminate (under the reinforced area) toward the reinforced side. Uniaxial tension tends to pull this local midplane toward the load line, causing out-of-plane bending at the hole, which results in high shear stress between plies, delamination and premature failure. The delamination counteracts most of the decrease in stress concentration provided by the reinforcement.

Pickett and Sullivan [Ref. 21] and Bank, et al. [Ref. 22] continued O'Neill's research examining tension panels with symmetric reinforcement. They showed that suitably designed reinforcement which was symmetric along the axis extending through the panel's thickness could both reduce strain concentrations and proportionately increase the ultimate strength. No delamination was noted in their test panels.

The work reported here extends the idea of symmetric hole reinforcement to compression specimens with a honeycomb core.

II. APPROACH TO THE PROBLEM

A thorough investigation into the effect of reinforcement around stress concentrations in composite plates must examine various materials, hole sizes, panel and reinforcement layups and geometries as well as the means and directions of load application. This research addressed only a small portion of the total problem. The material, hole and panel size, layup and loading method remained constant--only the amount and the shape of the reinforcement was varied. Reducing the number of design variables to only two allowed an analysis of the sensitivity of the SCF to certain thin reinforcement geometries.

A. METHOD OF INVESTIGATION

To investigate the effects of co-cured reinforcement around cutouts, linear elastic finite element analysis (LEFEA) was employed to determine the strain field in each panel configuration. Plots were drawn of the strains existing on a line from the point of highest stress concentration at the cutout across the middle of the panel (the X axis) and around the cutout and contours of the three inplane strain fields (Y, X, and shear). These are included as figures in the appendices for each geometry. Specimens of each configuration were manufactured, instrumented with strain gages and finally loaded in compression to failure. The analytical and experimental results were compared and the failure mode of each panel evaluated.

Total failure, in this report, is assumed to be facesheet delamination, separation and buckling with massive fiber failure such that the panel could not withstand a full reversal of the load. Partial failure was facesheet delamination and separation without the massive fiber failure and infers that there could be significant tensile strength remaining.

B. COORDINATE SYSTEM

There are several different right-hand coordinate systems that have been used in the analysis of laminated materials. Analysis is, of course, independent of the the system used, but more than one student has lost his way attempting to compare methods or results expressed in different systems by various recognized authorities in the field.

The data presented in this report is based in a cartesian system with the plane of the laminated panel aligned in the X-Y plane. Individual ply orientations are considered to be rotated counter-clockwise from the X axis an angle of theta (θ) degrees. These plies in the layup are assigned a local orthogonal coordinate system designated the 1-2 axes. The 1 axis, also referred to as the principal axis, is considered to be in the fiber direction with the highest elastic modulus (E_1).

Figure 2.1 shows the upper right quadrant of a typical panel in the X-Y (global) coordinate system as well as the ply 1-2 (local) coordinates. This coordinate system was used by R.M. Jones in Mechanics of Composite Materials and Ashton, Halpin, and Petit [Ref. 23]. Tsai and Hahn [Ref. 24] chose instead to fix the X-Y axes to the ply and the 1-2 axes to the panel. The principal researchers in the field do not use the same system.

The panel is oriented so that the area of greatest interest, a horizontal plane bisecting the circular cutout, is aligned with the X axis, where y = 0.0". The origin is assigned to the center

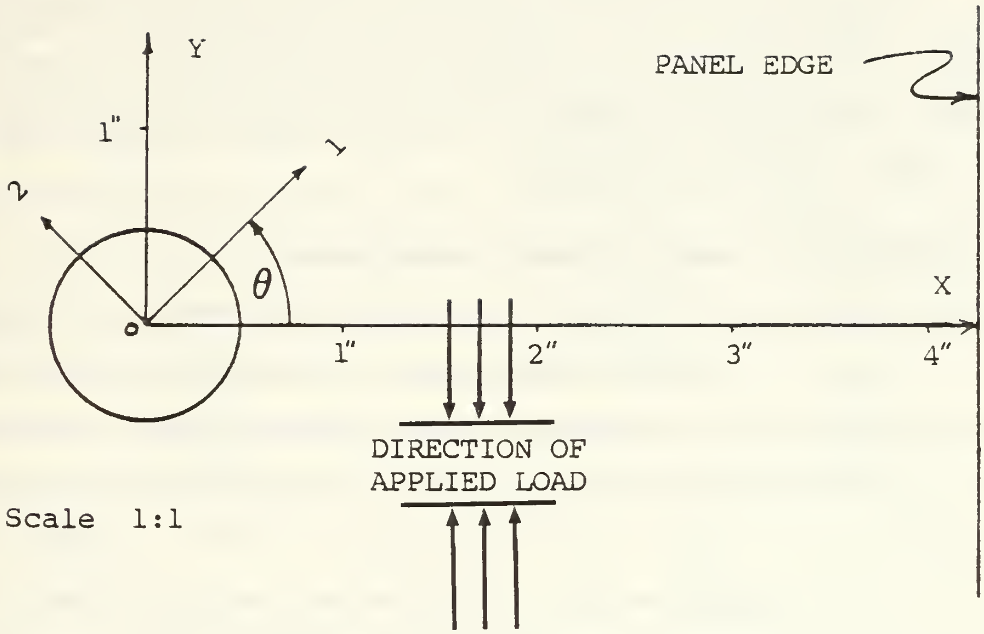

Panel Coordinate System (X-Y)

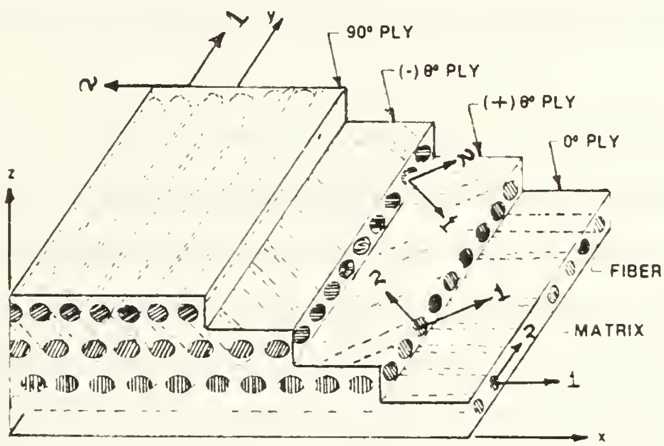

Ply Coordinate System (1-2)

Figure 2.1 Panel and Ply Coordinate Systems.

of the circular cutout. The compressive load is applied to the panel 90° to this plane, parallel to the Y axis, and referred to as $\overline{\sigma}_n$. The Z axis is centered at the midplane of the panel and extends through the thickness toward the viewer, completing a right-hand coordinate system.

C. SELECTION OF TEST SPECIMEN CONFIGURATION

The dimensions of the test specimens were chosen to approximate, at least in order of magnitude, a typical honeycomb panel with a cutout found in many aerospace applications. The overall size was limited by the size of the test machine and compression test frame.

Hong and Crews [Ref. 25], among others, demonstrated that the stress concentration in orthotropic composites under uniaxial loading was dependent on the ratio of hole diameter to panel width (d/w). Whitney and Nuismer [Refs. 26 & 27] pointed out that the absolute hole size had a significant effect on the stress gradient and ultimate strength when the hole diameter (d) was less than 1.0 inch.

The cutout's 1.00 inch diameter was chosen, therefore, to limit, as much as possible, hole-size effects. The panel was then designed as large as practical to reduce the effect of finite panel dimensions and still fit into the test frame and machine. Hole-size and finite-width effects are addressed in more detail in Section II.D.3. The specimen size, 10.00" x 8.50", gave a diameter-to-width ratio (d/w) of 0.118 and a diameter-to-length ratio (d/l) of 0.100. A comparison is made in Section III.C.3 between the solutions for finite and infinite plates of otherwise equal thickness and material constants.

A fabric G/Ep prepreg material was chosen because it has been somewhat less studied than tape and because it is finding increased use in airframe construction. The cured fabric laminate has slightly less in-plane stiffness and strength per unit thickness than uniaxial tape made from identical fibers. This is due to the nature of the weave, where the fibers (or tows) are cured with "crimps" rather than straight. Fabric has, however, demonstrated significant advantages over tape in its damage tolerance [Ref. 28] and ease of manufacture [Ref. 29].

Graphite/epoxy unidirectional tape can be most effectively applied in flat or slightly curved structures such as wings and access panels. Fabric, on the other hand, lends itself to applications requiring high curvature or complex shapes. Tape cannot be used in small inside or outside radius applications without fiber separation, inducing matrix-rich/fiber-poor areas and suffering severe loss of strength.

HMF330C/34 fabric G/Ep manufactured by Fiberite Inc. was chosen because it is a high modulus fabric, using Thornel T300 graphite fibers, found in many aerospace applications. It is an eight harness satin (8HS) weave cloth which minimizes the number of fiber crimps while maintaining many of the desirable characteristics of cloth. Figure 2.2 illustrates some details of its weave.

1. <u>Panel Reinforcement Configuration</u>

Reinforcement of the panel cutout was of three general types: round, square, and strip. The round and square were concentric with the hole, the "stiffening" strips were centered 0.750 inch away from the hole edge, parallel to the applied load. Table I lists the panel designations, reinforcement geometries and amounts; Figure 2.3 shows representative configurations.

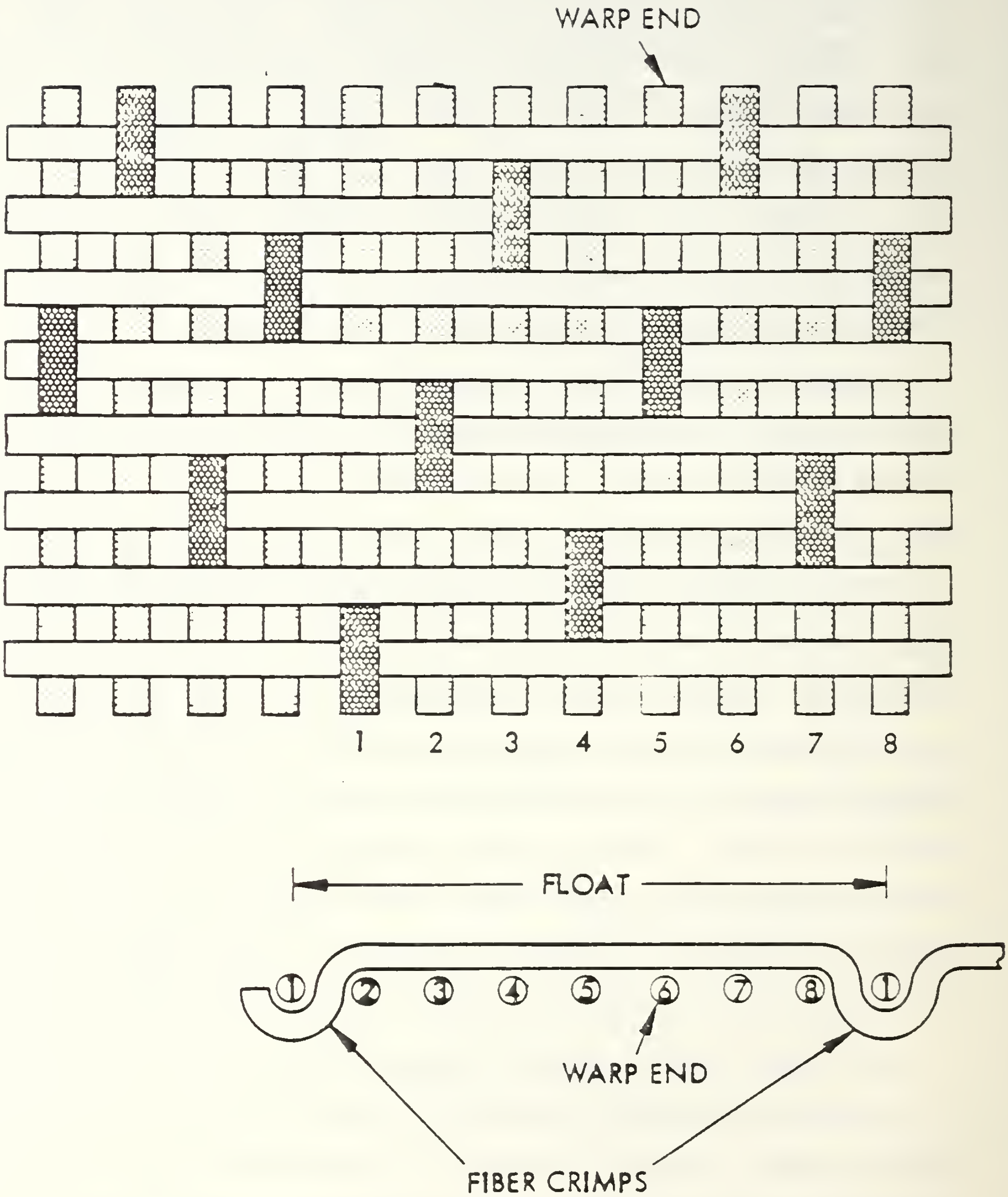

Figure 2.2 8 Harness Satin (8HS) Weave Cloth.

The basic panel was a quasi-isotropic eight ply (nine separate layers including the core) G/Ep panel. For more simple comparison, the amount of reinforcement was normalized by the amount of G/Ep removed from the 1.00 inch diameter cutout in the facesheets of the unreinforced panel. The relative volume of the reinforcement ply(s) was determined from this volume (0.088 in^3) of G/Ep. The round and strip reinforced panels had 5 increments of 100% of the removed reinforcement volume and the square reinforcement had increments of 100, 300 and 500%. The 200% and 400% reinforcements were each two plies thick.

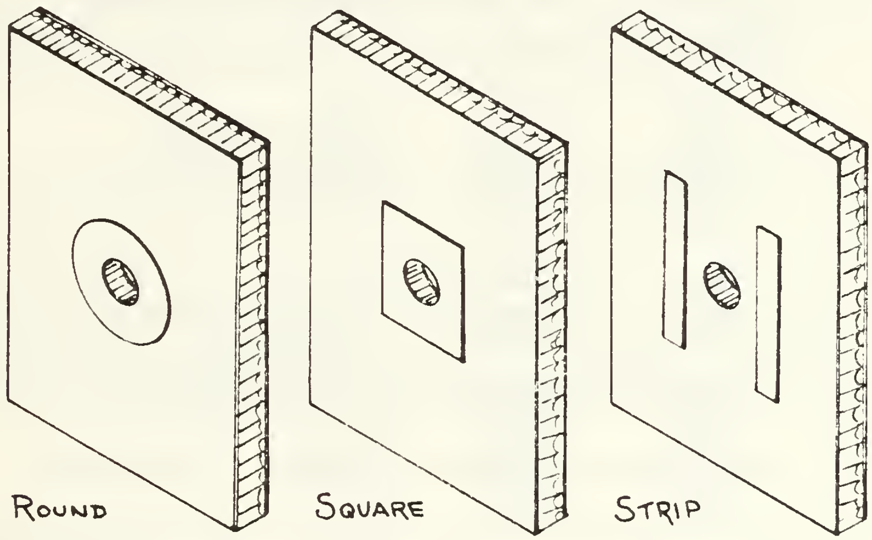

Figure 2.3 Panel Reinforcement Configurations.

The panel designation was devised to be somewhat descriptive of the test specimen. The first letter, P or R, refers to either a plain (unreinforced) or reinforced configuration, respectively. The second letter indicates the type of reinforcement: none (O), round (R), square (S) or strip (H); X indicates no hole was present. The first numeral represents the normalized percent of reinforcement, 1 to 5 for 100% to 500% (Ø indicates no reinforcement). The second numeral is the number of reinforcing plies on each facesheet. For example, RH42 is a reinforced panel with four times the removed hole volume (0.352 in^3) arranged in a strip configuration, 2 plies thick on each facesheet.

TABLE I

TEST SPECIMEN MATRIX

	Reinforcement		
Panel Designation	Type	Normalized Volume (%)	Ply(s) per Facesheet
PXØØ	No cutout or reinforcement		
POØØ	None	0	0
RR11	Round	100	1
RR22	Round	200	2
RR31	Round	300	1
RR42	Round	400	2
RR51	Round	500	1
RS11	Square	100	1
RS31	Square	300	1
RS51	Square	500	1
RH11	Strip	100	1
RH22	Strip	200	2
RH31	Strip	300	1
RH42	Strip	400	2
RH51	Strip	500	1

Figure 2.4 shows a typical laminate cross-section from the midplane. Each panel was symmetric about all three axes. Exceptional care was required and taken during the manufacturing process to ensure that the reinforcement plies were placed directly opposite each other on the opposing facesheets. When

measured, no reinforcement was more than 0.05" off center; the average was less than 0.02".

D. SOME CHARACTERISTICS OF NOTCHED GRAPHITE/EPOXY PLATES

The characteristics of composite materials differ radically from those of the metals they replace. As previously noted, composite fibers, particularly G/Ep, are by nature very brittle. Tensile failures in composite plates with cutouts are, almost without exception, load dependent. [Refs. 20-22]

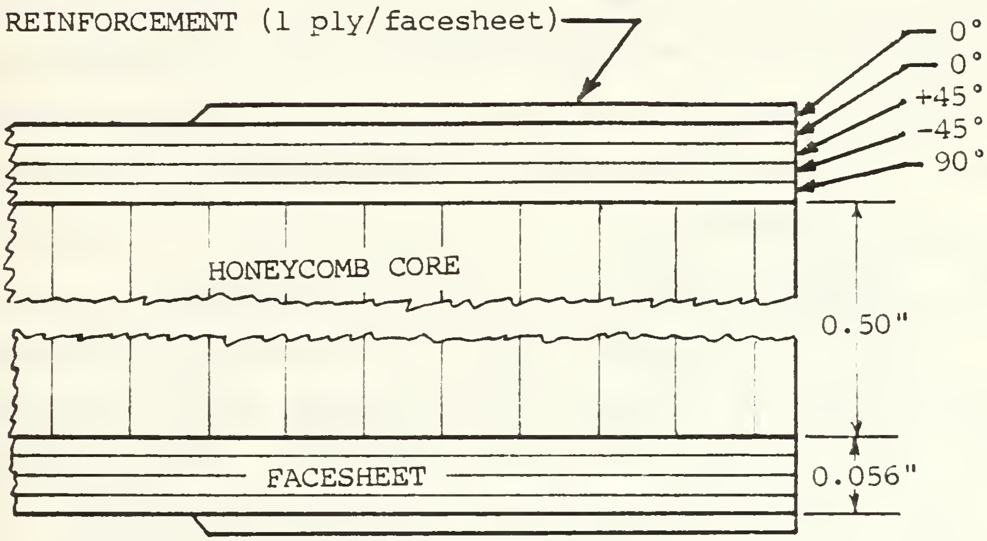

Figure 2.4 Typical Laminate Cross-Section.

Compressive failure, the type dealt with here, is more dependent on the type and thickness of the laminate, the use of honeycomb to overcome the tendency to buckle, the size of cutouts and the presence of imperfections. The compressive failure modes tend to be complex, composed of one or more types of failure: stability, ply delamination, matrix cracking, etc. Stability failure is principally the buckling of either fibers within the matrix (micro-mechanical) or the structure itself (macro-mechanical). These test specimens and the frame were designed to preclude macro-mechanical buckling (in the Euler column mode) since little would be learned about the reinforcement effects and this type of failure has been well documented beginning with Levy, Woolley and Kroll [Ref. 5].

1. Stress Concentration due to Notch Effects

It is well known that notches and cutouts in plates act as stress risers. For circular holes in plane elastic isotropic infinite plates under uniaxial tension or compression, the stress at the hole edge 90° to the applied load will be exactly three times the far-field stress. The distribution of stress around the hole edge and the stress field around it can be predicted using Airy's stress function. Dally and Riley [Ref. 30: pp. 67-83] give a clear and concise derivation of the stress field equations which will not be repeated here.

2. Orthotropic Effects on Stress Distribution

When an orthotropic plate with a stress riser is loaded, the SCF depends on the degree of orthotropy, that is, how much the elastic modulii change with radial direction. This is sometimes referred to, not always correctly, as the ratio of E_l/E_t. The subscripts "l" and "t" refer to the effective lateral and transverse modulii where the lateral direction is parallel to the applied load and transverse is 90° to it. In the coordinate system used in this report, the load is applied parallel to the Y axis and the ratio is expressed as: E_y/E_x. Note that a ratio of 1.0 does not ensure isotropy; it must be accompanied by the appropriate shear modulus (G_{xy}) and Poisson's ratio (ν_{xy}). For a circular hole in an infinite-width plane orthotropic plate, the stress concentration K_∞ on the cutout edge 90° to the applied load was given by Nuismer and Whitney [Ref. 27: Eqn. 3] as:

$$K_{\infty} = 1 + \sqrt{2\left(\sqrt{E_1/E_t} - \nu_{1t}\right) + E_1/G_{1t}} \,. \qquad (2.1)$$

In an idealized infinite laminated plate, this equation must be equally valid in both tension and compression. This stress concentration factor (K_{∞}) may be considered a far better indication of the orthotropy of a material than the ratio E_1/E_t.

The distribution of stress in the Y direction along the X axis ($\sigma_y(x,0)$) due to an applied (far-field) normal stress ($\overline{\sigma}_n$) may be approximated using the following equation:

$$\sigma_y(x,0) = [(\overline{\sigma}_n/2)(2+b^2+3b^4-(K_{\infty}-3)(5b^5-7b^8)], \qquad (2.2a)$$

where:

$$b = a/(x-d/2) \quad \text{and} \quad x > d/2. \qquad (2.2b)$$

The variable "d" is the diameter of the circular cutout and "x" is a location along the X axis (y = 0.0") when the coordinate system is concentric with the hole. This relationship is a quite accurate polynomial approximation developed by Konish and Whitney [Ref. 31].

3. Effects of Finite Plate Width and Hole Size on SCF

Compared to infinite plate width under uniaxial stress, finite plate width acts to increase the SCF. This fact becomes obvious in plates with a high d/w ratio. The applied stress must be carried by a greatly reduced net cross-section. The increase in SCF is due more to the net section effect than the presence of the cutout. Peterson [Ref. 32: pp. 110-111] gives the following equation to approximate the SCF at the edge of an unreinforced circular cutout in a finite-width isotropic plate:

$$K_f = [2 + (1-(d/w)^3)]/[1-(d/w)] \qquad (2.3a)$$

This can be extended to an orthotropic plate where K_∞ does not equal exactly three using:

$$K_f = (K_\infty/3)\ 2+[1-(d/w)^3]\ /[1-(d/w)] \qquad (2.3b)$$

The test specimens used in this report had a d/w ratio of 0.118; K_f was then calculated to be 3.045 for the unreinforced, quasi-isotropic panel PO∅∅. At $\overline{\sigma}_n$ = -10.0 ksi this would theoretically make the maximum stress -30,450 psi at the θ = 0° position on the cutout (90° to the applied load) compared with 30,000 psi predicted for an infinitely wide plate. This is an increase of 1.5%. Thus panel width has little more than a negligible effect on the SCF of the test specimens in this report.

Further data that relate a plate's dimensions to its SCF are given by Hong and Crews [Ref. 25: pp. 8-10]. They calculated stress concentration factors in finite-width orthotropic plates under uniaxial loads using finite element analysis. They used a different definition of SCF, one based on the net cross-sectional area stress concentration (K_{net}). This report uses the SCF based on far-field stress or the gross SCF (K_{gross}). The two are related by the equation:

$$K_{gross} = K_{net}/[1-(d/w)]. \qquad (2.4)$$

To make valid comparisons with SCF data presented in this report selected results of Hong and Crews' analysis, converted from K_{net} to K_{gross}, are listed in Table II.

Their results show that quasi-isotropic layups ($[0,\pm45,90]_s$) give results very close to the theoretical isotropic values. Greater orthotropy in the load direction results in a correspondingly greater SCF. It is interesting to note that the ratio of length to width (l/w) has an increasing effect on the SCF as the ratio d/w increases.

Nuismer and Whitney [Ref. 27: p. 118] point out the effect of absolute hole size on panel failure: ". . . attention was called to a phenomenon that since became known as the 'hole size effect,' that is, for tension specimens containing various sized circular cutouts, larger holes cause greater strength reductions than do smaller holes." They state that the classical stress concentration approach does not explain such an effect and they go on to propose that while the stress concentration factor is the same, the distribution and gradient near the hole is different. Figure 2.5 reproduced from Ref. 27 illustrates this point.

4. <u>Failure Stress Criteria</u>

As previously noted, the SCF does not explain the "hole size effect" on failure. Nuismer and Whitney rejected linear elastic fracture mechanics (LEFM) to explain the inverse relationship between hole size and strength. They noted that while all circular holes in infinite width plates should have the same theoretical SCF, the distribution in fact changes with hole radius. The smaller the hole the more concentrated the stress near the edge appears [Ref. 27: p. 118]. Nuismer and Whitney proposed that when the notched stress (σ_N) reached an average value of $\sigma_{U,ult}$, the unnotched ultimate stress over some characteristic distance a_o, that the panel's ultimate strength had been reached and failure resulted. This characteristic distance a_o must be arrived at by testing a statistically significant number of panels. This distance a_o is defined:

$$\frac{1}{a_o}\int_0^{a_o} \sigma_y(x,0)\,dx = \sigma_{U,ult} \qquad (2.5)$$

TABLE II

STRESS CONCENTRATION FACTORS-K_{gross} (HONG & CREWS)

				Diameter-to-Width Ratio: d/w				
Layup	E_l/E_t	K	L/w	0.05	0.10	0.33	0.50	0.67
$[0,\pm45,90]_s$	1.00	3.00	1	3.00	2.74	3.33	4.02	5.76
$[0,\pm45,90]_s$	1.00	3.00	2	3.01	3.03	3.49	4.36	6.36
[90]	0.07	2.48	1	2.48	2.51	2.97	3.78	5.61
[90]	0.07	2.48	2	2.48	2.51	2.97	3.78	5.88
$[\pm45]_s$ *	1.00	2.06	1	2.88	2.93	3.38	3.84	5.16
$[\pm45]_s$ *	1.00	2.06	2	2.88	2.92	3.36	3.80	5.28
$[0,90]_s$ *	1.00	3.78	1	4.78	4.69	5.61	5.08	6.93
$[0,90]_s$ *	1.00	3.78	2	4.82	4.84	5.22	6.06	8.16
[0]	13.49	5.43	1	6.36	6.07	5.24	5.82	8.01
[0]	13.49	5.43	2	6.44	6.44	6.54	7.30	9.54

* Indicates an E_l/E_t ratio of 1.00, but not a quasi-isotropic laminate.

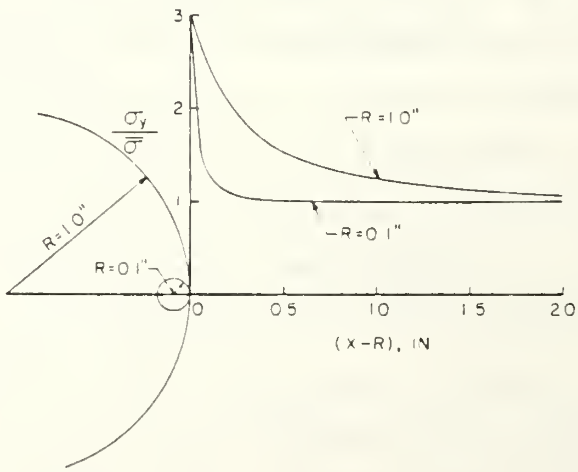

(Reproduced from Reference 27)

Figure 2.5 Hole Size Effect on Normal Stress Distribution

The ratio of notched to unnotched ultimate strength $(\sigma_n/\sigma_u)_{ult}$ for infinite plates is:

$$\sigma_n/\sigma_u = 2(1-\xi)/[2-\xi^2-\xi^4+(K_\infty-3)(\xi^6-\xi^8)] \qquad (2.6a)$$

where:

$$\xi = d/(d/2 + a_o) \quad \text{and} \quad x > a_o. \qquad (2.6b)$$

Nuismer and Labor [Ref. 33: p. 55] determined that for AS/3501-5 G/Ep (tape) in compression this characteristic length was 6.2 mm (0.24"). They also note that the characteristic length for tape in tension was only 2.3 mm (0.091"). Test data provided by LMSC indicates that for HMF330C/34 fabric G/Ep this characteristic length is close to 7.3 mm (0.33") in compression.

5. Effect of Poisson and Interlaminar Stresses on Failure

Isotropic materials may be modeled using classical plate theory neglecting out-of-plane stresses ($\pm z$ in this coordinate system). Orthotropic materials, however, develop complex interlaminar stress fields near the edge of a cutout. The subject has received much theoretical attention [Refs. 34 through 36]. Tang [Ref. 34: p. 1631] states that ". . . radial and shear stresses of each layer along the contour of the hole are in general not zero because there exists a three-dimensional state of stress at the free edge of each layer which the plane stress solution cannot predict." Greszczuk [Ref. 9: p. 372] pointed out that "In orthotropic and anisotropic plates containing openings, the failure will take place not as a result of stress concentration, but rather as a result of interaction of various stress components."

Under uniaxial compressive loading the laminate will have a Poisson expansion induced out-of-plane tensile stress (σ_z) which is highest at the hole's edge at point of the greatest stress concentration. This stress is added to any local stress due to machining and imperfections and combined tend to hasten delamination and the ultimate failure. In the experimental results reported here it was not possible to effectively quantify the effect on failure of this out-of-plane stress.

III. COMPUTATIONAL ANALYSIS

Before an experimental program could be developed, it was necessary to understand and be able to analyze the strain field resulting from a cutout in a representative panel and to be able to predict the reaction of test specimens to an applied compressive load. Three analysis methods were used: classical laminate theory, the linear elastic stress function and linear elastic finite element analysis (LEFEA).

Laminate analysis provides the basic stress-strain relation at a point, once the material properties of each constituent ply are specified. The stress function was used to predict the theoretical stress-strain fields in an infinite unreinforced orthotropic elastic plate with a circular cutout. These two can be solved in closed-form and require relatively little computation time using modern computers. The finite element method allows detailed analysis of reinforced finite-width reinforced panels, but requires a significant allocation of computer resources for an accurate representation of the strain field.

There are several coordinate systems and notations in general use in laminate analysis. The following section presents the method used in this report, explicitly defines the notation and gives justification for some of the assumptions that were made.

A. LAMINATE THEORY AND ANALYSIS

Laminate theory seeks to predict the properties of a multi-directional composite laminate based on the properties and orientation of its constituent lamina. Individual laminae are usually either unidirectional (tape) or woven (cloth) fibers embedded in a polymer matrix (generally a thermoset resin whose molecules are linked in three dimensions and which exhibits elastic properties in normal use) and tend to have strongly directional properties. The theory assumes that the state of stress is plane, displacements are small compared to laminate thickness and that strain is much smaller than unity.

Pipes [Ref. 37: pp. 4-1, 5-1] presented the micro- and macro-mechanical models that are the basis of the theory. An anisotropic material's elastic response at a point to applied stresses may be defined using generalized Hooke's Law. The constitutive relation is Equation 3.1, where σ_{ij} and ϵ_{kl} are the components of the stress and strain tensors and C_{ijkl} is the tensor of elastic constants. Using this most general of equations there are 3^4 or 81 material constants.

$$\sigma_{ij} = \sum_{k=1}^{3} \sum_{l=1}^{3} C_{ijkl} \, \epsilon_{kl} \tag{3.1}$$

This equation may be greatly simplified using the symmetry of stress and strain and the requirement that the strain energy density function be positive definite [Love, Ref. 38: pp. 97-111 and Feynman, Ref. 39: v. 2, ch. 31-7] reducing the independent elastic constants from 81 to 21. Symmetry reduces both σ_{ij} and ϵ_{kl} from nine to six different values. Feynman explains that the elastic response of a crystal with <u>no</u> symmetry in the three axes can be completely defined using 21 independent coefficients. The notation can be contracted using the following convention where the index: i = 1,2,3:

$$\sigma_{ii} = \sigma_i \qquad \sigma_{23} = \sigma_4 \qquad \sigma_{13} = \sigma_5 \qquad \sigma_{12} = \sigma_6$$
$$\epsilon_{ii} = \epsilon_i \qquad \epsilon_{23} = \epsilon_4 \qquad \epsilon_{13} = \epsilon_5 \qquad \epsilon_{12} = \epsilon_6 \qquad (3.2)$$

The constitutive relation can now be expressed as:

$$\sigma_i = \sum_{j=1}^{6} C_{ij} \, \epsilon_j. \qquad (3.3)$$

This is a sixth-order symmetric matrix (where $C_{ij} = C_{ji}$).

Idealized thin laminate theory neglects stress and strain in the $\pm z$ direction; the equations are reduced to plane strain and stress, further contracting the elastic constant tensor to a third-order symmetric matrix. In orthotropic systems (axes at right angles to each other) the "1" direction is the principal fiber direction (or the direction with the highest elastic modulus), "2" is 90° to it and "6" is the shear in the 1-2 plane.

$$\sigma_i = \sum_{j=1,2,6} Q_{ij} \, \epsilon_j. \qquad (3.4)$$

The matrix [Q] is termed the reduced laminate stiffness matrix, is symmetric and is related to [C] by:

$$Q_{ij} = C_{ij} - \frac{C_{i3} \, C_{j3}}{C_{33}} \qquad (i,j = 1,2,6) \qquad (3.5)$$

The matrix [Q] may be expressed explicitly in terms of modulii and Poisson's ratios:

$$Q_{11} = \frac{E_1}{1 - \nu_{12} \nu_{21}} \qquad Q_{12} = \frac{\nu_{12} E_2}{1 - \nu_{12} \nu_{21}} \qquad (3.6)$$

$$Q_{22} = \frac{E_2}{1 - \nu_{12}\nu_{21}} \qquad Q_{21} = Q_{12} = 0 \tag{3.6}$$

$$Q_{66} = G_{12} \qquad Q_{16} = Q_{61} = 0$$

$$Q_{26} = Q_{62} = 0$$

To determine the ply's elastic response defined in the laminate coordinate system (X-Y), both the stress and strain vectors must be rotated an angle θ about the "3" axis (Note: the "3" and Z axes are colocated):

$$\sigma'_i = \sum_{j=1,2,6} T_{\sigma ij}\,\sigma_j \qquad (i = x,y,xy) \tag{3.7}$$

$$\epsilon'_i = \sum_{j=1,2,6} T_{\epsilon ij}\,\epsilon_j \qquad (i = x,y,xy) \tag{3.8}$$

The transform matrix $[T_\sigma]$ (for the case of stress) is derived from the trigonometric relations:

$$T_{\sigma ij} = \begin{bmatrix} m^2 & n^2 & 2mn \\ n^2 & m^2 & -2mn \\ -mn & mn & m^2-n^2 \end{bmatrix} \qquad \begin{aligned} m &= \cos \\ n &= \sin \end{aligned} \tag{3.9}$$

Recall that engineering shear strain (γ_6) differs from tensorial shear strain (ϵ_6) by a factor of 2: $\epsilon_6 = 2\gamma_6$. The strain transform matrix elements $T_{\epsilon 16}$ and $T_{\epsilon 26}$ become **mn** and $T_{\epsilon 61}$ and $T_{\epsilon 62}$ become **2mn**. Using matrix algebra, the now transformed reduced laminate stiffness matrix [Q'] can be expressed in matrix form as:

$$[Q'] = [T_\sigma]\,[Q]\,[T_\epsilon]^{-1} \tag{3.10}$$

A laminate is built from the stacking of a number of these rotated plies. The designer may easily tailor the laminate using various ply thicknesses and orientations.

The integration of each ply's [Q'] matrix through the laminate thickness (h) gives the normalized inplane stiffness matrix:

$$[A] = \int_{-h/2}^{h/2} [Q']\, dz \tag{3.11}$$

Stress and moment resultants are defined by integrating stress through the laminate thickness:

$$\{N\} = \int_{-h/2}^{h/2} \{\sigma\}\, dz \tag{3.12}$$

$$\{M\} = \int_{-h/2}^{h/2} \{\sigma\}\, z\, dz. \tag{3.13}$$

The stress resultant vector $\{N\}$ is related to the strain vector $\{\epsilon\}$ by the laminate inplane stiffness matrix [A] in equation 3.14:

$$\begin{Bmatrix} N_x \\ N_y \\ N_{xy} \end{Bmatrix} = \begin{bmatrix} A_{11} & A_{12} & A_{16} \\ A_{21} & A_{22} & A_{26} \\ A_{61} & A_{62} & A_{66} \end{bmatrix} \begin{Bmatrix} \epsilon_x \\ \epsilon_y \\ \epsilon_{xy} \end{Bmatrix} \tag{3.14}$$

The laminate, while thin, demonstrates resistance to bending governed by the ply stiffness and the square of the distance from the midplane $(\pm z)^2$. Integrating through the laminate's thickness:

$$[D] = \int_{-h/2}^{h/2} [Q'] \, z^2 \, dz. \qquad (3.15)$$

Laminates with unsymmetric layups (where opposing plies at $\pm z$ do not have identical thickness, properties and principal axis orientation) exhibit coupling between strain and curvature (k). This follows since each side of the midplane exhibits different material properties. Any applied inplane stress will induce some curvature. The bending-extension coupling matrix [B] is:

$$[B] = \int_{-h/2}^{h/2} [Q'] \, z \, dz \qquad (3.16)$$

It follows, therefore, that in perfectly symmetric laminates [B] must evaluate to zero.

The combined bending-extension properties of a laminated plate can be expressed as a sixth-order symmetric matrix which relates stress and moment resultants to strain and curvature:

$$\begin{Bmatrix} N \\ M \end{Bmatrix} = \begin{bmatrix} A & B \\ B & D \end{bmatrix} \begin{Bmatrix} \epsilon \\ k \end{Bmatrix} . \qquad (3.17)$$

1. Laminate Properties

LMSC provided the initial data on material properties of cured HMF330C/34 G/Ep fabric. In order to validate it for this program, a solid panel (PXØØ), one without the 1.00 inch cutout, was manufactured and tested. The laminate material properties required slight revision (less than 4%) to match the the actual response of the solid panels to loading. These results are discussed in detail in Section V.B.1. The $[0,\pm45,90,\overline{core}]_s$ solid laminate exhibited different modulii in tension and compression. In addition, it exhibited a slightly nonlinear stress-strain curve in compression (see Table VI and Figure 5.4). The elastic modulus parallel to the applied load (principal modulus, E_y) varied from 7.8 to $6.5*10^6$ psi as the applied load varied from 0 to panel failure at -57 ksi; as the load increased the panel stiffness monotonically decreased. This characteristic is most probably due to the woven plies (Figure 2.2) compressing within the elastic matrix, but it was not further investigated.

The finite elements chosen for this analysis assumed linear elastic material properties. Nonlinear analysis was possible using different elements, but would have yielded little more accuracy at a tremendous increase in computation time. At an applied far-field stress (σ_n) of -10.0 ksi the stress induced in an unreinforced quasi-isotropic panel with a cutout varies from -10 to -30 ksi and thus E_y would vary from 7.46 to about 6.95 msi. Since the compressive stress field and thus the material properties vary continuously over a panel with a cutout, it became necessary to select one principal modulus, indeed, all the material constants (E_1, E_2, G_{12}, ν_{12} and ν_{21}) for use in the FEA. The material properties listed in Table III are valid (at 70°F) throughout the range of tension but in compression they are exact only at -15 ksi; for other values they are approximate but introduce only a small error.

Jones [Ref. 40: pp. 16-21] discussed the bimodulus phenomenon and proposed an improved analysis method he called the

TABLE III

MATERIAL PROPERTIES OF HMF330C/34 CLOTH G/EP

Tension	E_1:	10.9×10^6 psi	E_2:	10.3×10^6 psi
Compression	E_1:	10.2×10^6 psi	E_2:	9.6×10^6 psi
Shear	G_{12}:	1.0×10^6 psi		
Poisson ratio	ν_{12}:	0. 09	ν_{21}:	0. 09
Thickness	t:	0. 014 inch (fully cured ply)		

TABLE IV

LAMINATE STRESS RESULTANT AND MOMENT PROPERTIES (COMPRESSION)

A MATRIX

8.876E+05	2.212E+05	1.362E-01
2.212E+05	8.876E+05	-1.467E-01
1.362E-01	-1.467E-01	3.334E+05

B MATRIX

6.250E-02	0.0	1.221E-04
0.0	6.250E-02	1.221E-04
1.221E-04	1.221E-04	5.078E-02

D MATRIX

6.907E+04	1.711E+04	3.270E+01
1.711E+04	6.868E+04	3.268E+01
3.270E+01	3.268E+01	2.580E+04

weighted compliance matrix. If a more complete analysis is required, this model should be considered.

The bending-extension matrices (Eqn. 3.17) were calculated using conventional thin laminate analysis (based on experimentally derived material properties) for the HMF330C/34 $[0,\pm45,90,\overline{core}]_s$ laminate in compression. The results (the [A], [B] and [D] matrices) are listed in Table IV.

The symmetry of the basic laminate is apparent from the magnitude of the [B] matrix particularly in relation to [A] and [D]. The reinforced laminate also had [B] = 0 since it was symmetric. The very small relative values of the elements of the [B] matrix (as well as elements A_{31}, A_{32}, A_{13} and A_{23}) are more due to round-off error in the computer, using single precision numbers, than an indication of an unsymmetric layup.

Pipes [Ref. 37: pp. 5-4] notes that when analyzing composite laminates it is often more convenient to treat them as homogeneous plates. For symmetric laminates it is possible to express orthotropic material constants in terms of the inplane stiffness matrix [A]. The laminate material properties may be determined in the X-Y plane from [A] using equations 3.18 through 3.22.

$$E_x = (A_{11} * A_{22} - A_{12}^2)/(h * A_{22}) \tag{3.18}$$

$$E_y = (A_{11} * A_{22} - A_{12}^2)/(h * A_{11}) \tag{3.19}$$

$$\nu_{xy} = A_{11}/A_{22} \tag{3.20}$$

$$\nu_{yx} = A_{12}/A_{11} \tag{3.21}$$

$$G_{yx} = A_{66}/h \tag{3.22}$$

Table V lists the (experimentally derived) panel material properties at -15.0 ksi. For the purpose of linear elastic analysis these are assumed to be constant over the stress field for the particular laminate at any load. When these modulii were used in the finite element analysis ($\overline{\sigma}_n$ = -10.0 ksi) the maximum error in strain at any point in the field was less than ±3%.

B. LINEAR ELASTIC STRESS FIELD SOLUTION

Savin [Ref 7: Chapt. II] gives a solution for the stress distribution in various anisotropic plates and beams with cutouts. Garbo and Ogonowski [Refs. 8 and 41] coded the solutions in FORTRAN for the case of a for the case of a thin, infinite-width orthotropic plate with a circular cutout. Their program, revised by the author for the IBM 370, is listed in Appendix P.

TABLE V

MATERIAL PROPERTIES OF THE LAMINATES

Layup	Plies	E_x	E_y	G_{xy}	ν_{xy}	SCF
$[0,\pm45,90,\overline{c}]_s$	8	7.28	7.28	2.78	0.321	3.00
$[0_2,\pm45,90,\overline{c}]_s$	10	7.94	7.79	2.40	0.269	3.19
$[0_3,\pm45,90,\overline{c}]_s$	12	8.36	8.11	2.17	0.236	3.33

(Modulii $*10^6$ psi)

Note: The 0.50" thick honeycomb core ($\overline{c}$) had no effect on the inplane modulii. The panel had an 8 ply layup except under the reinforcement. The 10 and 12 ply layup gives the material properties under the one and two ply reinforcement.

The general biharmonic equation for an orthotropic material is given in Equation 3.24. The S coefficients are members of the third order laminate compliance matrix [S], the inverse of [A]:

$$\{\varepsilon\} = [S]\ \{N\} \tag{3.23}$$

$$S_{22}\frac{\partial^4 F}{\partial X^4} - 2S_{26}\frac{\partial^4 F}{\partial X^3 \partial Y} + (2S_{12} + S_{66})\frac{\partial^4 F}{\partial X^2 \partial Y^2}$$

$$- 2S_{26}\frac{\partial^4 F}{\partial X \partial Y^3} + S_{11}\frac{\partial^4 F}{\partial Y^4} = 0 \tag{3.24}$$

Based on the original research by Savin [Ref. 7], Garbo and Ogonowski point out that the stress function F depends upon the roots of the associated characteristic equation:

$$F = 2\mathrm{Re}[F_1(Z_1) + F_2(Z_2)]. \tag{3.25}$$

$F_1(Z_1)$ and $F_2(Z_2)$ are the analytic functions of the complex variables $Z_1 = X + R_1Y$ and $Z_2 = X + R_2Y$ where R_1 and R_2 are the complex roots of the characteristic equation. The expressions for the three inplane stresses are:

$$\sigma_x = 2\mathrm{Re}[R_1^2 \phi_1'(Z_1) + R_2^2 \phi_2'(Z_2)] \tag{3.26}$$

$$\sigma_y = 2\mathrm{Re}[\phi_1'(Z_1) + \phi_2'(Z_2)] \tag{3.27}$$

$$\sigma_{xy} = -2\mathrm{Re}[R_1 \phi_1'(Z_1) + R_2 \phi_2'(Z_2)] \tag{3.28}$$

The functions $\phi_1(Z_1)$ and $\phi_2(Z_2)$ are defined:

$$\phi_1(Z_1) = \frac{\partial F(Z_1)}{\partial Z_1} \qquad \phi_2(Z_2) = \frac{\partial F(Z_2)}{\partial Z_2} \tag{3.29}$$

These equations have been slightly modified from their original form in order to apply in this report where there is no internal load on the hole. For a full development and explanation of the equations, the reader should refer to Garbo [Ref. 41: p. 586] or Savin [Ref. 7].

C. FINITE ELEMENT ANALYSIS

Finite-width and reinforcement effects cannot be addressed using these two methods because of the discontinuities in thickness and material properties at the edge of the reinforcement. Finite element analysis has demonstrated its ability to accurately analyze the majority of problems in elasticity. The quality of the solution is, however, dependent on the size of both the available computer core memory and the analysis budget, since the quality and cost of the solution are functions of the fineness of the element mesh. The solution time and cost increase at least with the cube of the degrees of nodal freedom (DOF) in the model [Ref. 42: pp. 391-402]. In a full three-dimensional analysis each element node point may be displaced in the X, Y and Z directions and also rotated about each of the three axes. Thus there are six possible DOF per node: three displacements and three rotations. The dimension of the stiffness matrix is the sum of the degrees of freedom at each node point in the model.

The structural finite element analysis method, in its simplest form, is the determination of the relationship between the load on and the displacements in a body. The two are related by the stiffness characteristics of the body. The body is divided into a number of smaller volumes (or areas) termed elements, each element is then assigned a local "stiffness" and these are then combined in matrix form to establish their inter-relation. The result is termed the stiffness matrix [K]. Each element is made up of nodes at its corner points which can be fixed, at which a force can act and which can deflect if not fixed. The vector of forces $\{F\}$

acting on each node equals the product of [K] and the vector of deflections $\{\delta\}$.

$$\{F\} = [K]\{\delta\} \tag{3.30}$$

Since the forces are generally known and it is the displacements which are desired, the stiffness matrix must be inverted:

$$\{\delta\} = [K]^{-1}\{F\} \tag{3.31}$$

The order of the [K] matrix is determined by the sum of nodal degrees of freedom. The matrix inversion to $[K]^{-1}$ is not a trivial computational task in any realistic finite element model.

The art in FEA is in defining a mesh fine enough to give adequate solution accuracy while suppressing as many DOF as possible to keep the cost of solution within reason. Zienkiewicz, in his excellent text on the subject [Ref. 43], covers this method of structural analysis in some depth.

1. DIAL finite Element Program

A finite element analysis program named DIAL as well as a significant allocation of computer time on a Digital Equipment Corporation VAX 11/780 was made available by LMSC for this research. DIAL is a flexible, general purpose finite element code for the analysis of two- and three-dimensional structures. It has a modular architecture in which individual subprograms are executed as the model is being defined, the mesh generated, the equation bandwidth optimized and the solution found. As each subprogram (called a "processor") is executed, it extracts required data from a data base, processes it, updates the solution and adds to the data base. This architecture provides an invaluable restart capability at the last successful process which

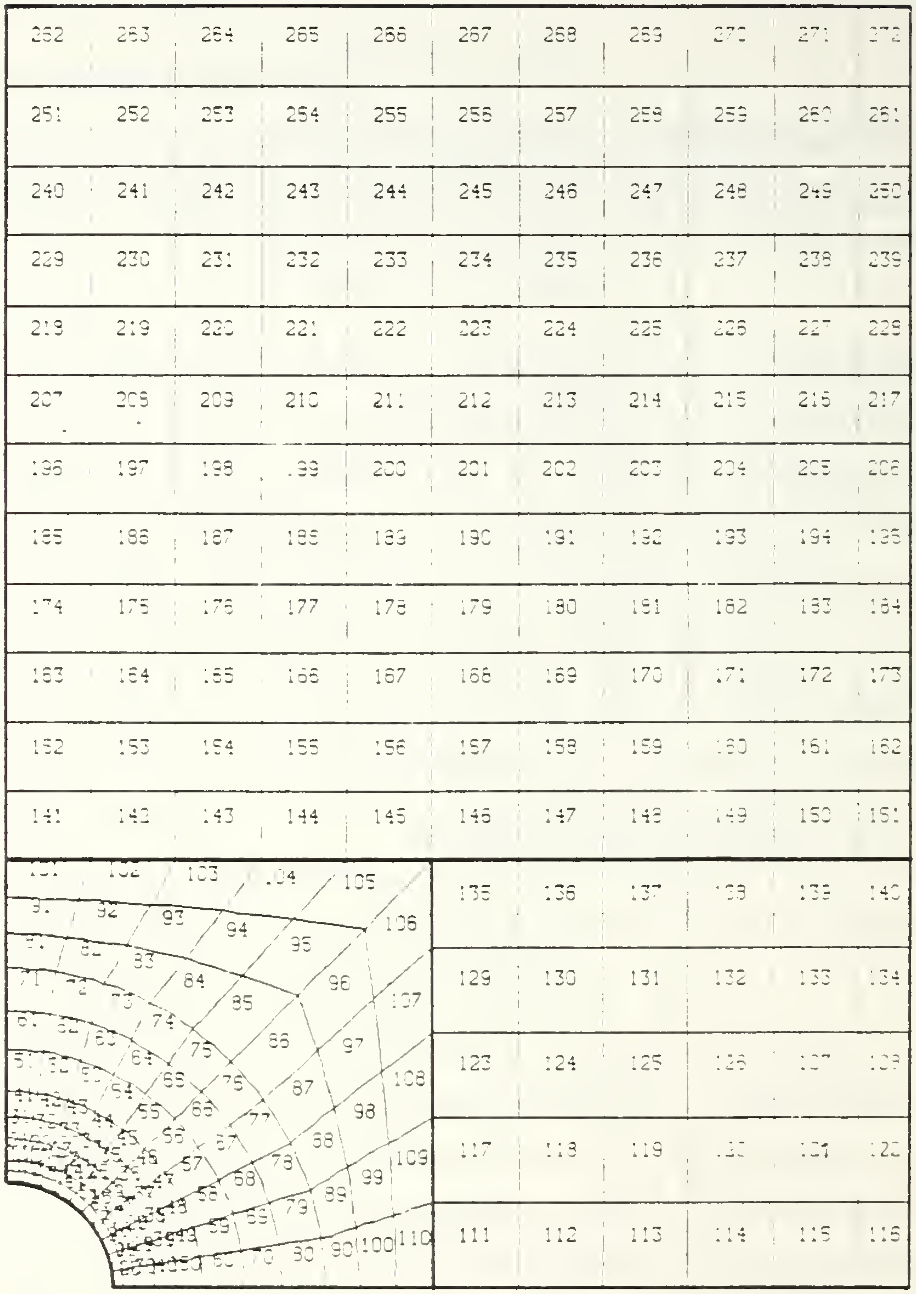

Figure 3.1 Typical Finite Element Mesh

can significantly conserve analysis time [Ref. 44]. The following DIAL processors were used in the linear elastic analysis of the experimental test panels:

* **MESH** The geometric grid of elements to be analyzed, called a mesh, is generated by specifying points coincident with the quadralateral element corner nodes in an orthogonal I-J coordinate system. Certain points key in the I-J system are then givenlocations in the X-Y plane and the MESH processor automatically maps appropriately shaped elements. Figure 3.1 show a typical element mesh. The processor allows partial meshes to be generated individually and then merged to each other creating a larger model. The heavy lines in Figure 3.1 outline these. Building a complete FEA model from a series of smaller partial meshes reduces the manhours required to generate the model and allows more complex geometry. Merging adjacent partial meshes eliminates any redundant nodes and degrees of freedom. The panel models for this analysis used from three to five partial meshes. Boundary conditions are specified and DOF suppressed within the MESH processor to adequately simulate the structure.

* **BAND** It is not necessary to store the entire finite element stiffness matrix; the Betti-Maxwell reciprocal theorem requires that the stiffness matrix must be symmetric. It can be decomposed into a lower and upper triangular matrix, recovering almost half the memory or storage area originally required. Further improvement can be gained by reordering the node numbers to optimize the matrix bandwidth and storing it using the "skyline" method. BAND offers a number of options to do this including Collin's and the Gibbs-Poole-Stockmeyer algorithms.

* **SETUP** The undeformed finite element data sets are generated and a series of error checks are done verifying the element grid.

* **MATL** The material properties of each ply are defined in MATL. The processor uses classical laminate theory to compute the bending-extensional properties. The strength of the processor architecture now becomes apparent. It possible to vary the material properties of the model without regenerating the complete element mesh, optimizing the band width or generating new element data sets.

* **LOAD** The LOAD processor generates consistent load vectors for any combination of pressure, traction, body forces, inertia loads and temperature variations. It allows the variation of loads without regeneration of the stiffness matrix.

* **DIAL** The nodal deflection analysis and stress-strain computation is done within the DIAL processor. It uses the total Lagrangian formulation method to handle geometric nonlinearities. FORTRAN double precision representation (64 bit) and sequential improvement to convergence was used to increase the accuracy of the solution. This insured the best possible solution but increased the equation solution time by a factor of about eight. The effect of using double precision and convergence can be seen in the figures in Appendices A-N where shear strain is resolved to as low as $\pm 0.003\%$ of the value of E_y long the X axis.

* **GEOM** The data generated by even a small model is extensive and difficult to evaluate in tabular form. DIAL provides an extensive array of post-processing choices to present the data in graphical or tabular form. GEOM generated the strain contours for each panel which are presented in the appendices as

well as the extrapolation of strain data from element Gauss points to the nodes.

2. Formulation of the Finite Element Model

Each panel reinforcement configuration required a separate finite element model. A modified thick-shell elastic quadralateral element was used for the analysis. It used the laminate material properties developed in the MATL processor and ply thickness with any offset from the Z axis (specified during the mesh development) to define and individual element stiffness matrix. The greater the Z offset--the greater the resistance to bending. Several of these elements may be stacked through the thickness by merging partial meshes. Stacking meshes results in the direct addition of element stiffness. Element properties are projected to a reference plane ($z = 0.0''$ for this model) which contains the nodes points. Element bending resistance is determined by its stiffness and offset from this reference plane. The advantage of this type of element is that it allows modeling a thin three-dimensional laminate using a two dimensional element, thereby greatly reducing the number of individual element nodes. The modified thick shell element's shortcoming is that it cannot give stresses in any of the stacked partial meshes and the strain is valid only at $z = 0$. Further, thin plate theory is used which gives strain and the stress resultant $\{N\}$ vector. In these models the true thickness varied over the surface of the panels. Plots of stress resultants in this case would be, at best, misleading. Strain was used as the basis for comparison among the panel configurations.

During the experimental phase of the research, premature facesheet separation from the honeycomb core became an unpredicted failure mode of some of the specimens (panels RR22, RR42, RR51, RS51 & RH31). This type of stability failure could not be predicted employing two-dimensional analysis only. It was postulated that the [0,±45,90] facesheet layup or the [0_2,±45,90] (or [0_3,±45,90]) reinforcement could be generating sufficient out-of-plane (±z) forces to tear the facesheet away from the core.

To answer the question, a three-dimensional analysis using thick shell elements representing the facesheet, combined with isoparametric solid elements, representing the honeycomb core, for a 3-D analysis. These results (for panel RR22) are given in Appendix O (results showed no significant out-of-plane stress). While DIAL can handle a 2-D element with an aspect ratio (length/width) up to 20 with little loss in accuracy, an effort was made to keep this ratio below three. At high aspect ratios the interpolation assumptions within each element are no longer valid. The meshes employed were also designed to keep interior element angles as close to 90° as possible, again to increase the accuracy of the solution. Figure 3.2 shows the elements (numbered from 1 to 30) and node points (numbered from 1 to 117) next to the cutout. These elements' dimensions remained unchanged (except for the added reinforcement thickness) for each model, allowing direct comparison among reinforcing configurations in the region near the cutout. Since the plate was symmetric about all three axes only the upper right quadrant of each specimen was modeled.

In the experimental fixture, the compressive load was applied to each 8.50" wide specimen using clamps 8.00 inches wide. The outside edges of each panel had 1/4 of an inch inside a slot in the vertical member which could not be loaded. To simulate a -10 ksi far-field load in the FEA model a constant line load $\{N\}$

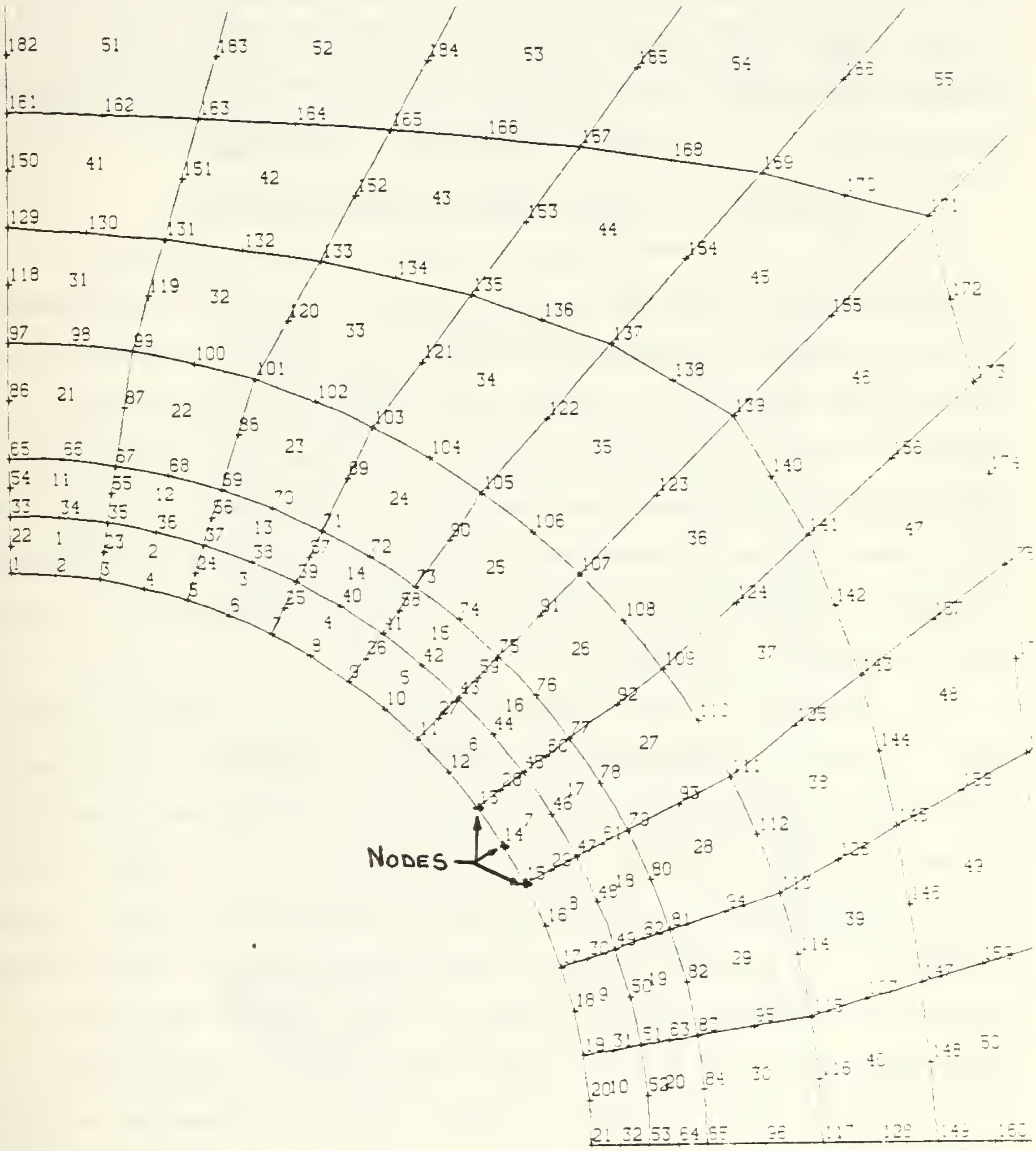

Figure 3.2 Elements and Nodes Next to the Cutout.

of -1,120 lb/in was applied to the 0.112 inch thick plate (neglecting the core). The effect of modeling the test fixture can be seen in the quarter-panel contour plots in the appendices (for example Figure A.4): there is an obvious stress concentration in the upper right-hand corner of the panel. The effects of this stress concentration die out rapidly as the distance into the panel from the line of load application increases.

3. Interpreting Finite Element Analysis Results

DIAL, like most finite element programs, produces voluminous data files giving the stress, strain and displacement at each element's integration points. Meaningful comparison of these files among the various panel configurations would be tedious as well as unenlightening. The items of interest were the distribution of stress along the X axis and around the cutout and the strain fields on each panel resulting from the reinforcement. Graphical comparison was chosen as the best method both to present and to compare the panels.

The results from tests of each of the 14 test specimens with a cutout is presented in individual appendices (A through N). Each configuration has a plot of the element mesh and a comparison of strain both along the X axis and around the hole under a far-field normal stress load of -10 ksi. In addition, strain contours for $\overline{\sigma}_n$ = -10 ksi are shown for each panel's upper right quadrant and for the region near the cutout. Experimental data are correlated with the finite element analysis for each panel.

A plot of a deflected element mesh is presented in Figures 3.3 and 3.4 to illustrate the analytical and experimental boundary conditions imposed on the test panels. Figure 3.3 shows the entire upper right quadrant of the panel. Figure 3.4 shows the elements close to the cutout. The dashed lines represent the outlines of the elements prior to the application of the load. The solid lines show the elements in the panel compressed under a -10 ksi load. The deflections shown are, of course, an exaggeration of those actually present in the panel, but they are accurate representation in relative scale.

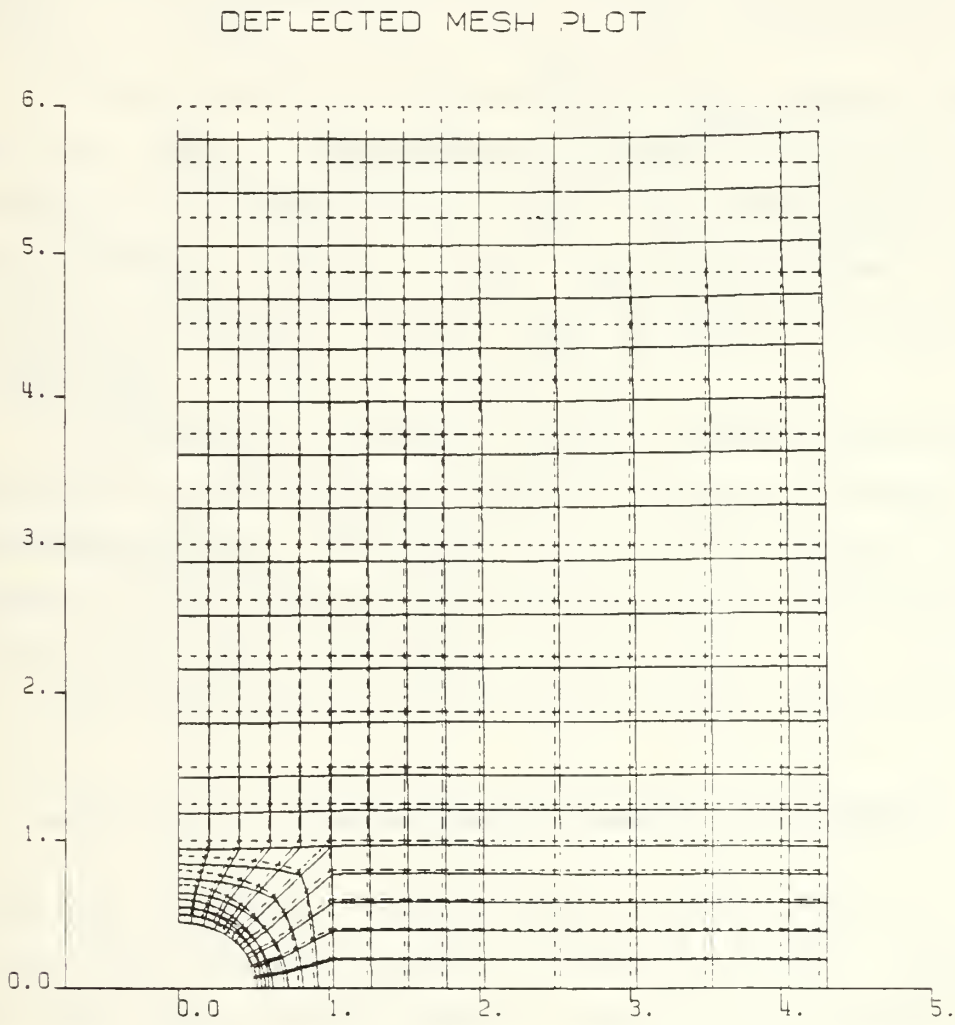

Figure 3.3 Typical Deflected Mesh Plot.

The boundary conditions imposed on the quarter panel are clear: the X axis, representing the longitudinal bisection of the panel allows no movement in the Y direction but allows Poisson expansion the X direction. The panel boundary on the Y axis was constrained in X displacement but was allowed to move vertically.

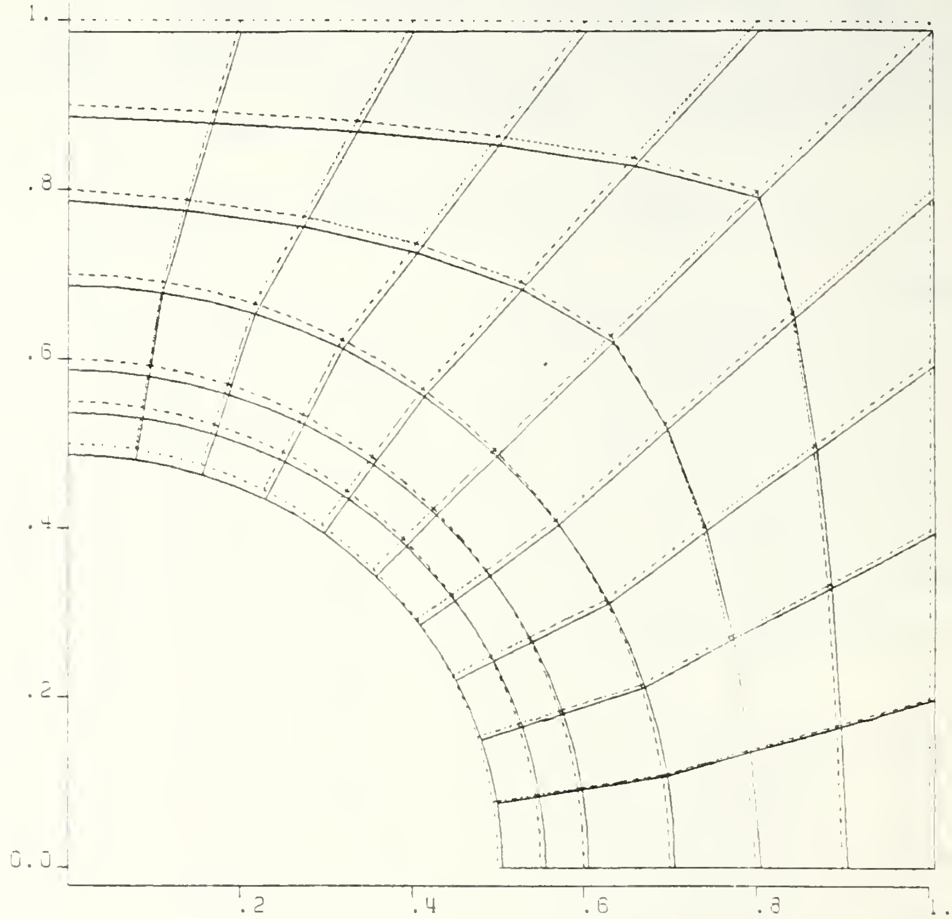

Figure 3.4 Element Deflection Next to the Cutout.

A point to note is the boundary condition at the top of the panel. It was necessary to firmly clamp the upper 8.00" x 1.00" inch area of the panel to assure complete and even load transfer into the G/Ep facesheets. The results of the boundary condition can be seen in the deflected mesh plot; Poisson expansion was not allowed where the panel was clamped. This very closely modeled the experimental setup.

In Figure 3.3 the top edge of the panel has a slight slope upward as X increases from 0.0 to 4.25". This is the result of applying a constant stress boundary condition along the edge rather than constant displacement, which would more closely model the experimental apparatus. This tends to slightly increase the SCF at the hole because the panel finite element model appears somewhat less stiff directly above the cutout than the solid portion.

A test case using constant displacement boundary conditions, which closely approximated the experimental setup, produced less than a 0.5% increase in the SCF. Since each panel has a slightly different stiffness in the Y direction, it would have been exceptionally difficult to impose an identical load on each for comparison.

Hong and Crews [Ref. 25: pp. 4-6] reported significant differences in results between constant stress and constant displacement boundary conditions. In the final analysis, the researcher, understanding the differences and the compromises, must choose the model best suited to his work.

IV. EXPERIMENTAL ANALYSIS

A program of experimental verification was developed in order to determine if the analytical results of the finite element analysis represented the actual strain field. Each reinforcement geometry previously described was manufactured, instrumented and tested.

A. TEST SPECIMEN MANUFACTURE

The test panels were manufactured by Lockheed Missiles and Space Company using methods similar to those for verification of Trident missile structures. The initial uncured prepreg plies of HMF330C/34 cloth G/Ep were laid up on a stainless steel plate in a 4 ply ([0,±45,90]) facesheet. A precut uncured reinforcement (one or two plies) was then placed in position on the top of the uncured layup and retained in place by a small pin. Two identical facesheets were made for each geometry. A standard "bagging" process and cure cycle for the 350°F (450°K) Fiberite 934 epoxy prepreg was used. This included a hold in the autoclave at 360 ±10°F (455 ±5°K) for two hours. Using acid digestion techniques this cycle typically yields a fiber volume of 62 ±2% and a void content less than 1%. One facesheet was joined and cured to a 0.50 inch thick Hexel fiberglass/phenolic honeycomb sheet using 3M Inc.'s AF-126 (250°F curing temperature) film adhesive (known as "Blue Glue"). Once the first facesheet and honeycomb had been bonded an aluminum/epoxy potting compound was poured into the honeycomb cells within 1.25 inches of each end. The aluminum/ epoxy potting compound provided dimensional stability for the panel, assisted the load transfer and prevented crushing the honeycomb in the panel ends when they were clamped into the compression test frame. The second facesheet was then joined and the now complete rough panel put through a third and final cure cycle. The panel configuration, excluding the one or two ply 0° reinforcement, became $[0,\pm 45,90,\overline{core}]_s$. The core's elastic modulii in the X and Y directions were virtually nil and did not contribute to the panel's inplane stiffness.

The center of the reinforcement was marked and a starter hole drilled with a No. 4 carbide-tipped steel drill rotating at approximately 2200 rpm. The hole was enlarged in steps using 0.50 and 0.75 inch diameter carbide-tipped drill bits. The final 1.00 inch finished hole was cut using a carbide-tipped boring head rotating at 1600 rpm moving in depth at 0.0015" per revolution. This method provided a very smooth and almost perfectly circular cutout. Each facesheet was drilled using stiff fiberglass sheets as backing to minimize the breaking of fibers on the bottom ply when the drill bit broke through. Fiberglass tabs (8.0" x 1.0" x 0.25") were applied on both sides at either end to provide for load transfer from the test frame into the panel. The rough panel was then cut to the specified size (8.50" x 10.00") using a diamond-coated circular saw. Great care was taken to both keep tne cutout in the center of the panel and to insure the two edges to be loaded were parallel. The general dimensions of the specimens are shown in Figure 4.1.

B. TEST APPARATUS AND PROCEDURES

In compression, much more so than tension, lack of attention to maintaining proper boundary conditions can quickly invalidate experimental results. Great care was taken in the design and

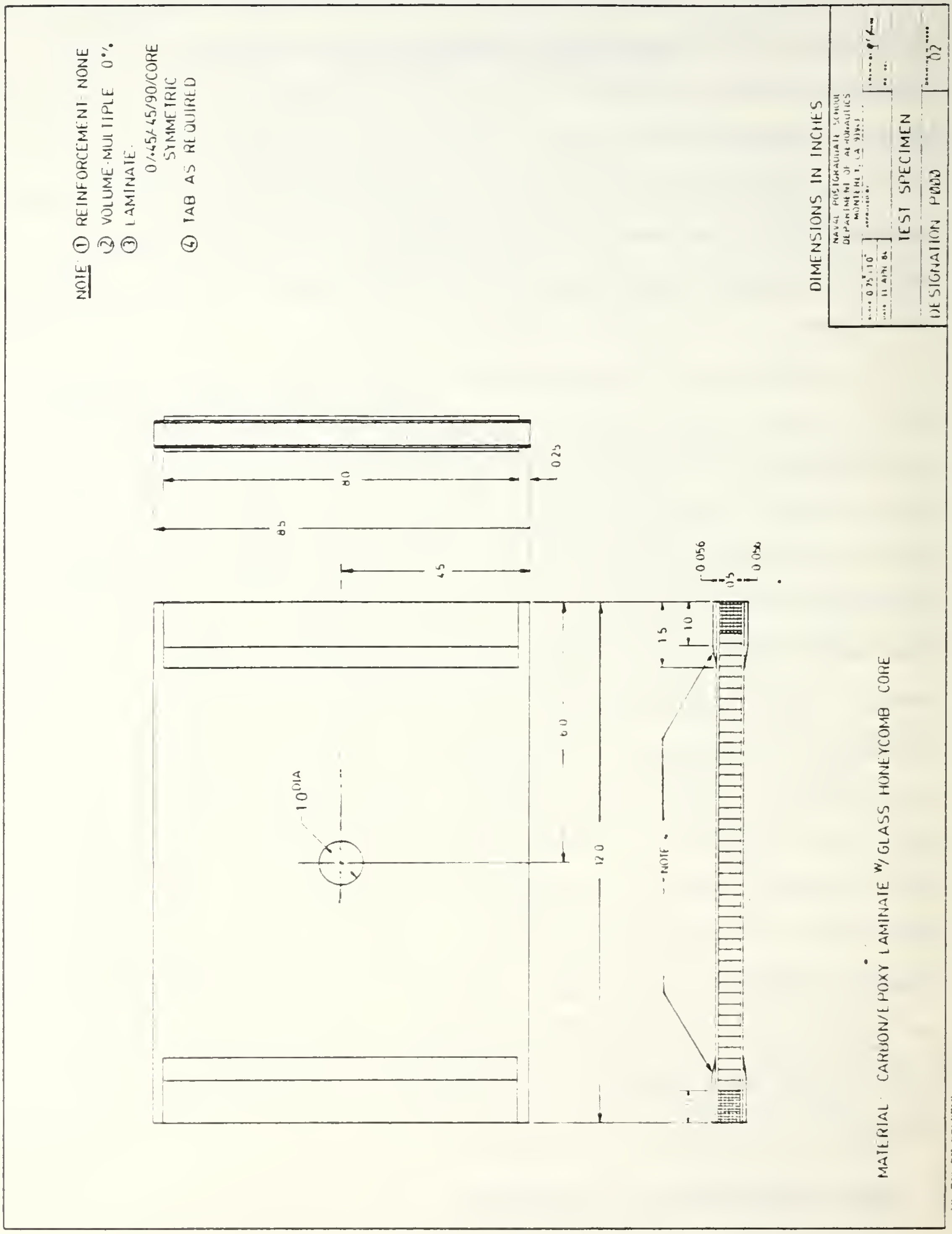

Figure 4.1 Compression Panel Dimensions

construction of the test frame to insure that it was extremely stiff, that the compression surfaces were parallel and that they would remain so during the entire compression sequence.

1. Test Apparatus

a. Load Application

A Material Test System (MTS) Series 810 hydraulic test machine was used produce the compressive loading. The compression test frame was designed to be strong enough to utilize the 100,000 lb. maximum load of the MTS machine. It consisted of a fixed horizontal base and vertical side posts and a sliding horizontal top cross member. Both horizontal members were machined from 7075-T6 aircraft-grade aluminum. The vertical posts were turned to a diameter of 2.000" from diameter mild steel bar stock. The horizontal members were fitted with a means of clamping the test specimens. Each had a 0.250" thick tempered tool steel base plate positioned to transfer the compressive load into the test specimen and to prevent damage to the surface of the aluminum frame. These load plates were carefully adjusted during installation to ensure that they were parallel within a tolerance of ±0.0005 inch.

A 0.614 ±0.001" slot was milled in both steel vertical members to accommodate the panel and to allow some vertical movement while preventing out-of-plane deflection. The lower horizontal member was held fixed relative to the frame while the top one was allowed to slide vertically. Bronze bushings were pressed into the upper and lower frame members and then machined to within a ±0.001" tolerance. The vertical posts' ends were fitted into these bushings. A special effort was made during the design and manufacture of the test frame to keep tolerances as small as possible to maintain proper and repeatable test boundary conditions.

Figure 4.2 shows some details of the compression test frame. The following numbers indicate some of the parts and features of the frame and correspond to the numbers in Figure 4.2:

1. Tempered tool steel compression support plate.

2. Bottom horizontal frame member.

3. Vertical steel post.

4. Slot to hold edge of the test specimen.

5. Bronze bushing.

The test frame was allowed to "float" in the MTS machine. Steel bearing surfaces were fitted to the top and bottom which allowed the test fixture to slide parallel to the floor for centering. These also eliminated the possibility of transfer of any moments from the MTS machine to the frame. Each steel bearing block was made of three pieces: one threaded to mate to the MTS moving piston, a circular 2.000" diameter lubricated cylindrical bearing and one threaded to mate with the test frame. Figure 4.3 show the test frame positioned in the MTS for a test. The bearing blocks can be seen in the figure between the test frame and the machine.

b. Strain Measurement Equipment

A Vishay Measurements Group, Inc System 4ØØØ, shown in Figure 4.4, was used to record the strain gage indications. It consisted of a Hewlett-Packard 9825B microcomputer linked through a Measurements Group, Inc., Instrument Division Model 4200

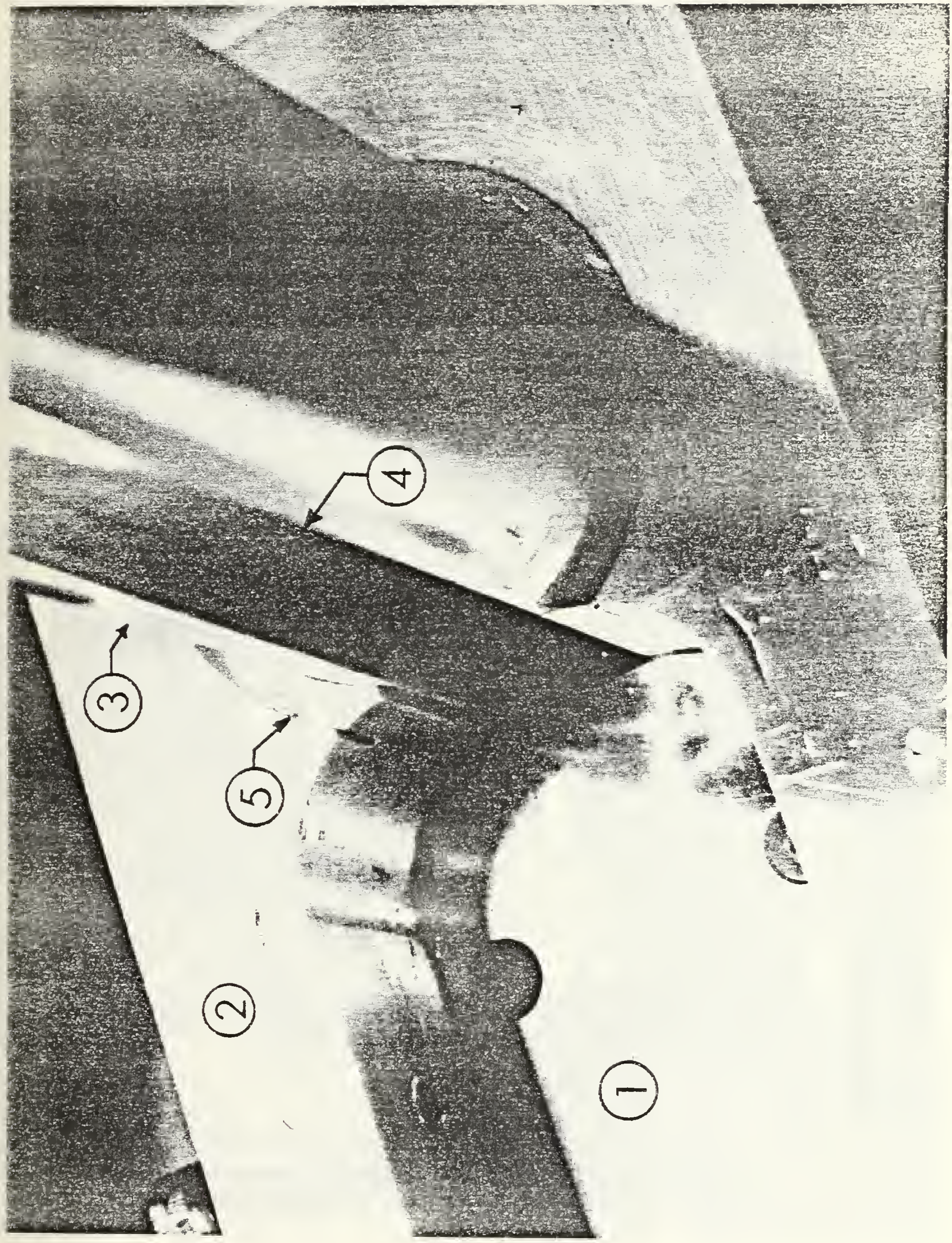

Figure 4.2 Compression Test Frame Details.

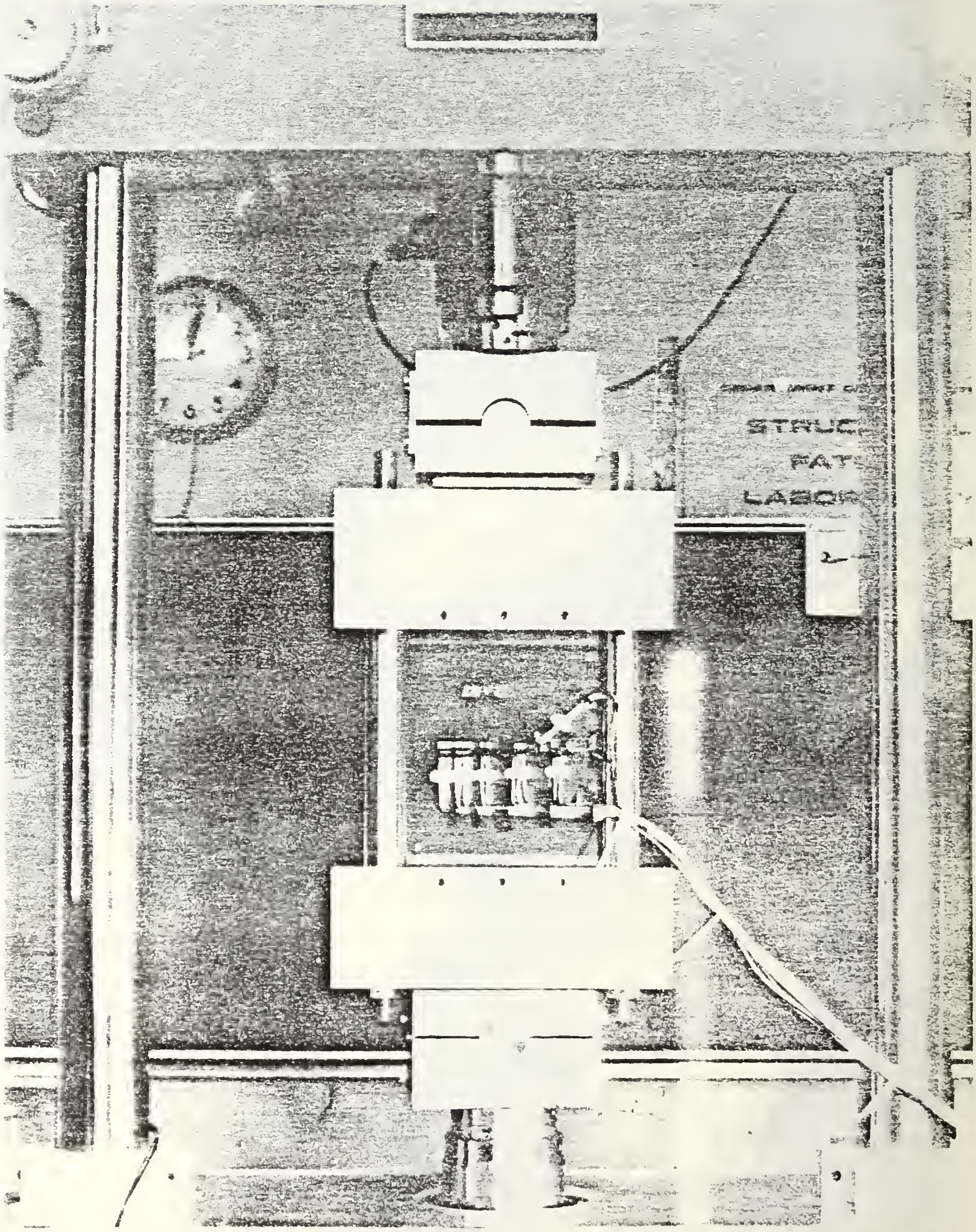

Figure 4.3 Compression Test Frame.

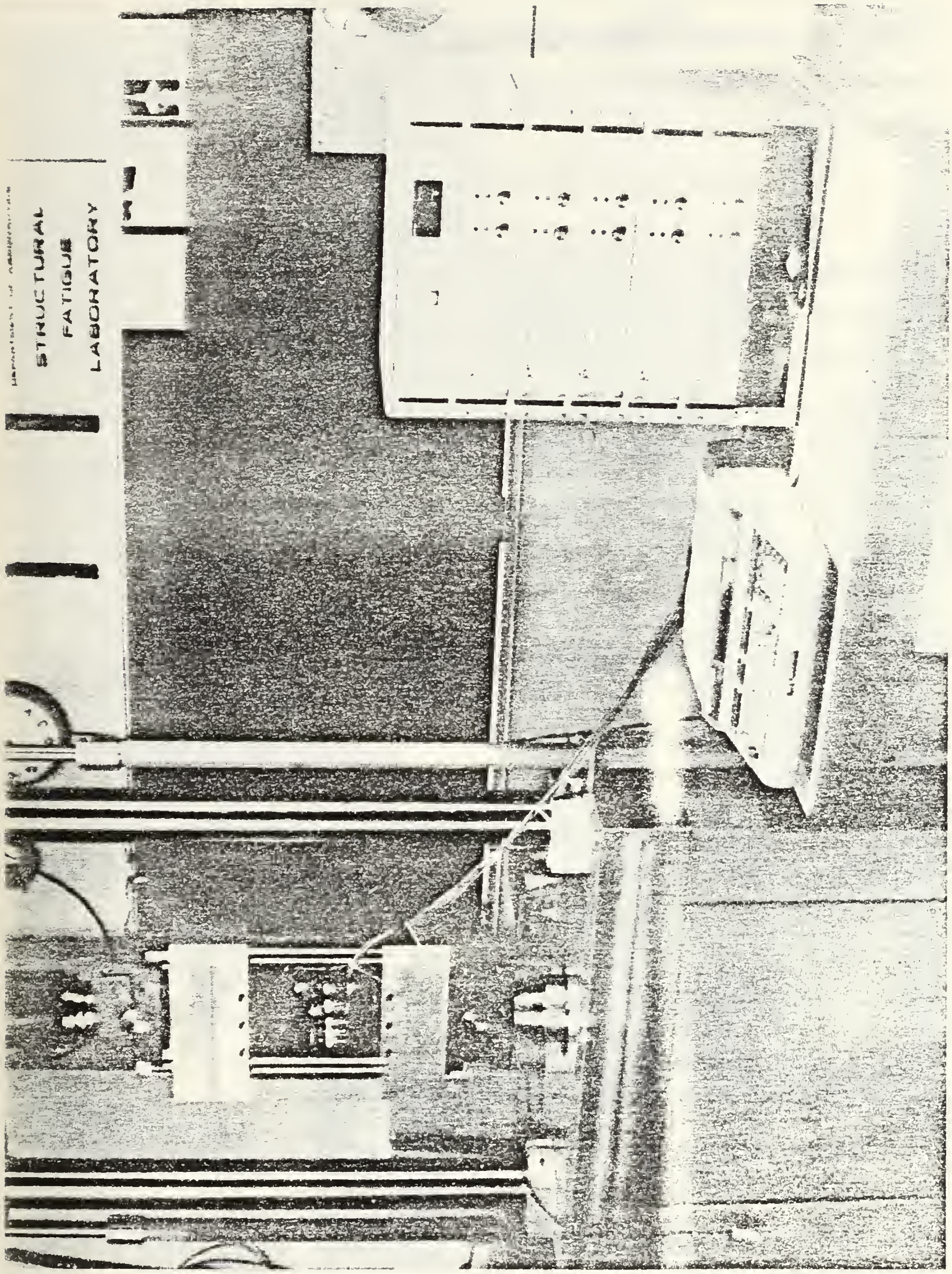

Figure 4.4 System 4ØØØ.

controller to Model 4270 strain gage scanners. Integral software provided for gage identification, calibration and strain reading, conversion and printing. The entire experimental test station is shown in Figure 4.5.

2. Instrumentation Procedures

Each panel was instrumented with a variety of strain gages principally located along the X axis and oriented in the Y direction. The primary purpose of the reinforcement was to reduce the maximum strain, and thus the SCF, at the edge of the hole 90° to the applied load. The 0.50 inch honeycomb core was used to eliminate panel buckling. The panel was designed to maintain, as closely as possible, equal strain on opposite facesheets. The gages were located on either side of the hole, but on only one facesheet. In retrospect, gages on both sides of the cutout on both facesheets would have given additional insight into the failure mechanisms.

The choice of strain gages was based on the strain gradient near the cutout, the panel strain field and the heat transfer properties of the G/Ep panel.

a. Measurement of Strain Near a Cutout

The measurement of strain near a cutout in the presence of very high strain gradients is not a straight-forward exercise. Reference 45 points out that an electrical gage effectively integrates the strain field under its grid. When that field changes very rapidly the accuracy of the measurement can be strongly affected. The typical strain field studied here demonstrated gradients as high as 16,000 microstrain per inch within 0.025" of the cutout at -10.0 ksi far-field load.

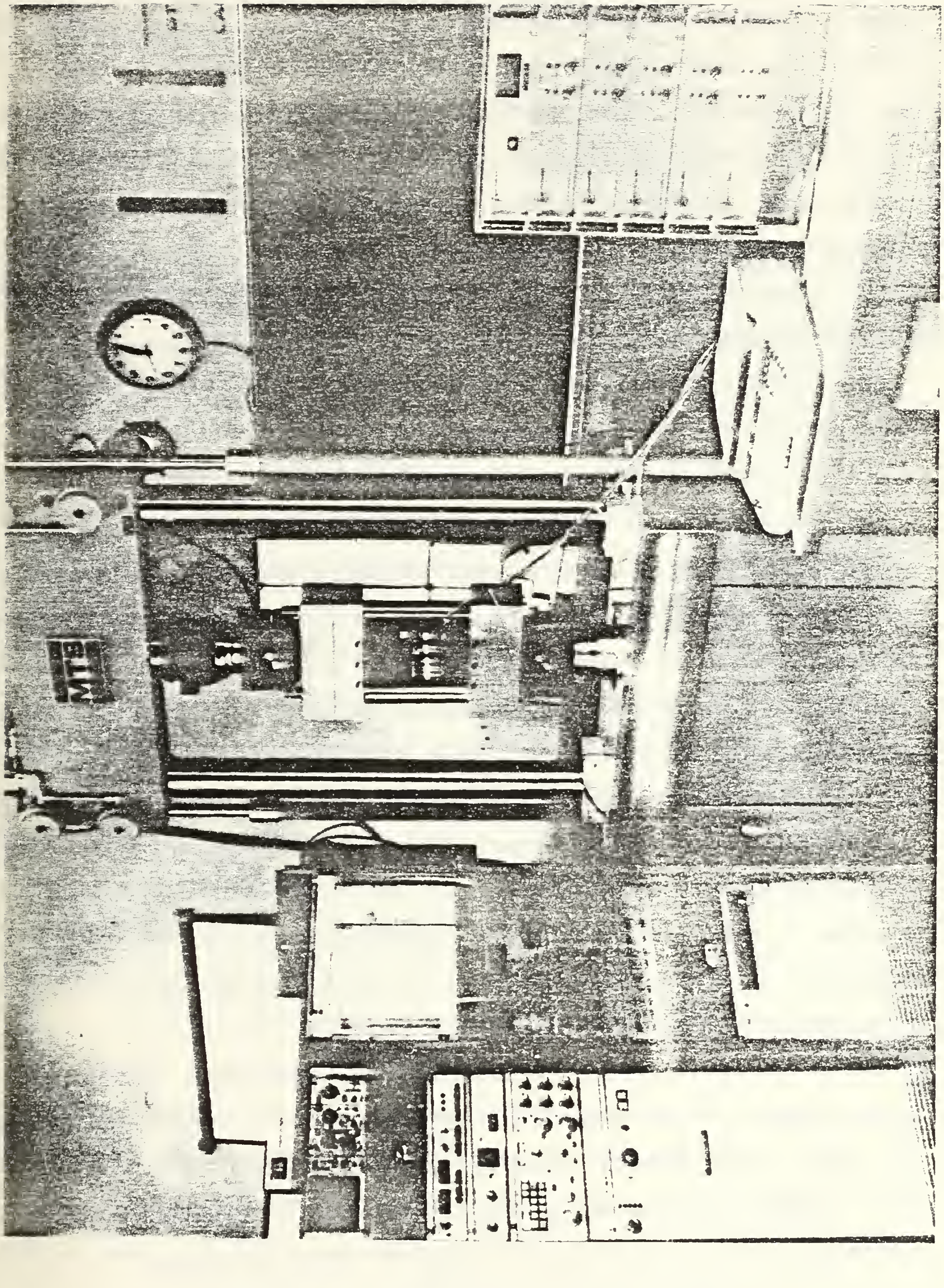

Figure 4.5 Experimental Test Station.

As recommended by Ref. 45, a number of techniques were used to accurately measure the strain field along the X axis. The smallest possible gages were chosen for use for next to the cutout; a series of in-line gages close to the hole gave strain gradient data. Special care was taken to accurately measure the position of each gage. A Rockwell Corp. electronic, digital-readout gurney gave the gage center location to within ± 0.002 inch. This resulted, at the -10.0 ksi test point, in about ± 30 microstrain or $\pm 1\%$ maximum uncertainty in strain due to gage position error.

b. Strain Gage Excitation Level

Strain gages require some electrical excitation to allow measurement of the change in resistance in the gage grid caused by tension or compression. This results in some degree of resistive self-heating within the grid. This self-heating characteristic can cause significant drift in indicated strain from the true value. When measuring strain in most metals, there is little heat buildup due to their superior heat transfer characteristics. What little there is can usually allowed for by self-temperature-compensation (STC) in the gage. STC requires the matching of coefficients of thermal expansion (α) of the gage and the specimen. The heat transfer characteristic of G/Ep is low compared to metals: The temperature under a gage can rise enough to invalidate the indicated strain reading.

Reference 46 recommends a maximum power density of 0.1-0.2 watt/in^2 for materials with low thermal conductivity such as G/Ep. Power density (PD, watts/in^2) is a function of gage active grid area (A, in^2), gage resistance (R, ohms), and gage excitation level (E, volts) according to the relation:

$$PD = E/(4*R*A). \quad (4.1)$$

A typical 120 Ω, 0.040 in^2 gage at 5.0 volts excitation has a PD of 1.3 watt/in^2. As noted above, gages with a small grid area were necessary to accurately measure high-gradient strain. A Measurements Group, Inc. EA-xx-030CM-030 gage (A = 0.0025 in^2) [Ref. 47: p. 7L] which could meet the size requirements has a PD in excess of 21 watts/in^2.

Clearly, high strain gradients and composite materials require extreme care in selecting and using strain gages. A combination of lower than usual excitation levels and higher gage resistance were used too in this research, where required, to keep the power density within acceptable limits.

c. Strain Gage Application

Gages were applied to the panels one facesheet on either side of the cutout along the X axis. They were applied in accordance with the manufacturer's recommended procedures [Refs. 48 through 51] using M-Bond 200 adhesive. Figure 4.6 shows a typical strain gage layout on a test panel. It should be noted that, although similar, each panel had a unique gage layout. Several gages were mounted at points other than along the X axis to verify the analytical strain field.

3. <u>Test Procedures</u>

The test specimens were allowed to age for 180 days at 70°F and 50% relative humidity to reach hygrothermal equilibrium. Immediately after the strain gages were installed the panel was mounted in the compression test frame and loaded to failure.

The test consisted of initially loading the panel to -2000 psi to set it in the test fixture. The load was then removed and the gage readings reset to indicate zero strain and then recaliorated. The compressive load was slowly reapplie[illegible] [illegible]ments to failure. The MTS load control was adjusted [illegible] to give each sequentially increasing load, held for [illegible] seconds for strain gage reading and then increased. Panels [illegible], POØØ, RR11 and RR22 were loaded in 2000 psi steps.

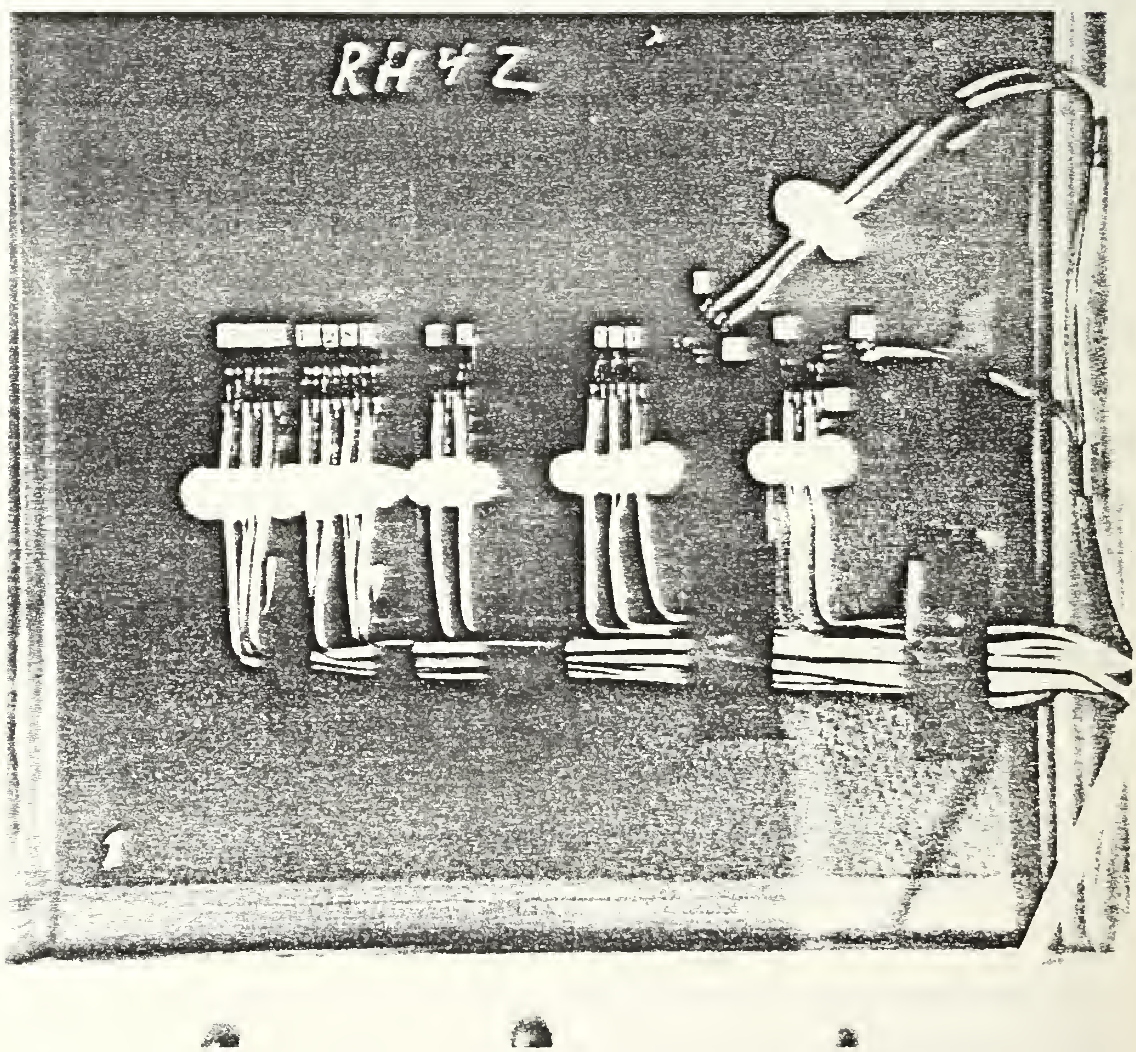

Figure 4.6 Typical Strain Gage Layout

When it became apparent that finer increments were required, 1000 psi steps were used in all subsequent tests. [illegible] typical test required 15-20 minutes to complete. There were some variations in this straight line load procedure which are noted in the appendices for the affected panels.

V. DISCUSSION OF RESULTS

A. COMPARISON OF COMPUTATIONAL RESULTS

All computational analysis were done at a far-field applied stress of -10.0 ksi. These analyses assumed the material had linear elastic properties. This assumption was adequate to reasonably predict the strain field below the material yield point. There are some significant nonlinear yield characteristics of composite materials that require more sophisticated treatment than is given in this report.

1. Open Versus Closed-Form Analysis for an Unreinforced Panel

A comparison of open and closed-form strain distribution around a cutout in an unreinforced panel (PO∅∅)is shown in Figure 5.1. The lines represent the infinite plate width strain computed using the stress function (Equation 3.24) by the FORTRAN program "RBSFM" in Appendix P [Refs. 8 & 40]. The triangular points indicate the LEFEA strains at the node points for the finite-width (8.50") plate The effect of the finite panel width and the constant stress loading boundary condition may perhaps be more easily seen in Figure 5.2 where the FEA strain results are represented by crosses. The maximum FEA computed strain is higher increased at the edge of the cutout (x = 0.50") compared with the closed-form results. At distances more than 2 hole diameters away from the cutout ($x > 2.0"$) the FEA model gives slightly less strain. The differences between the two analysis in Figures 5.1 and 5.2 are small; it is the similarity of the two that is striking.

The increased FEA strain at the hole is due to the constant stress loading boundary condition. A constant displacement

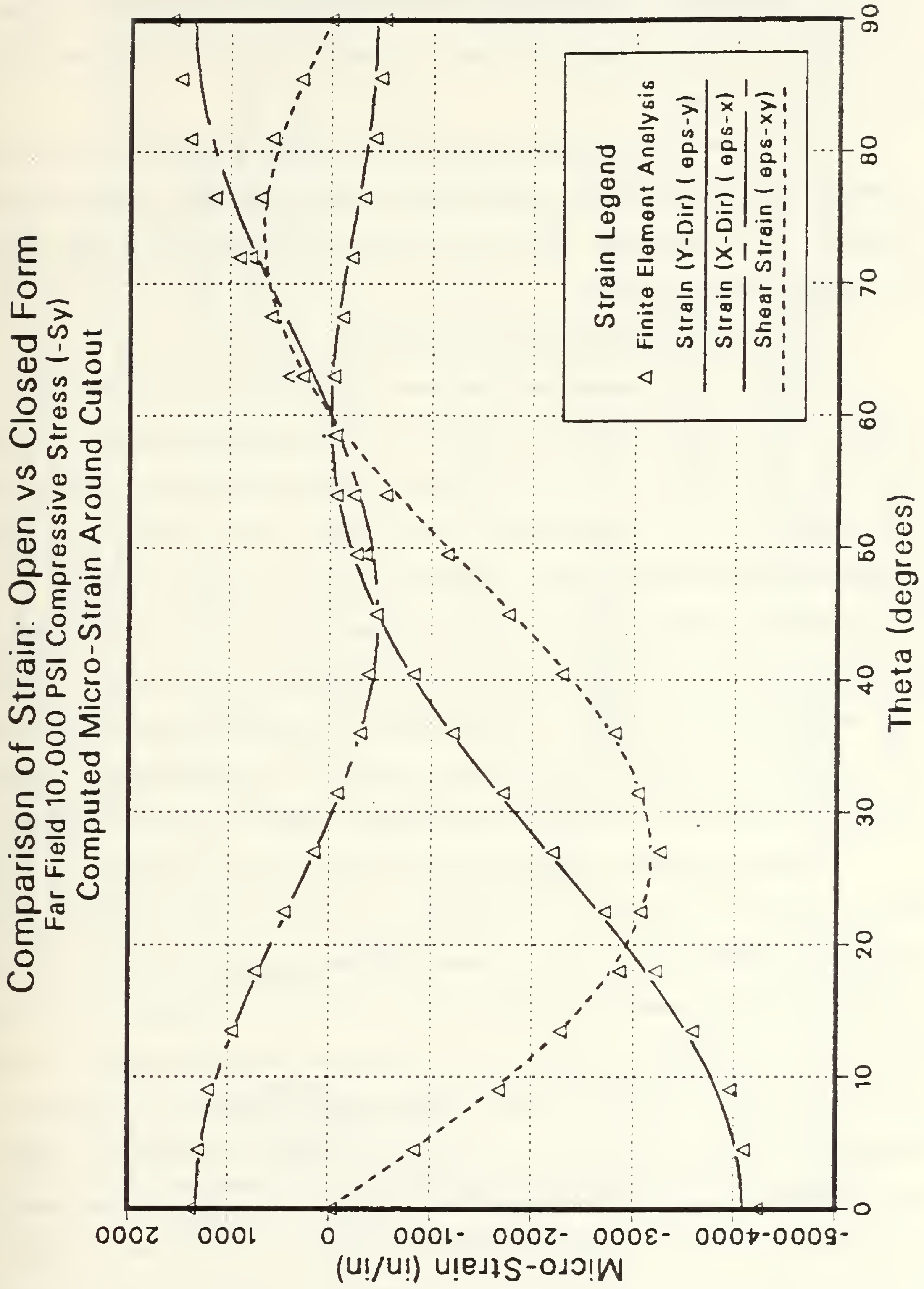

Figure 5.1 Strain Comparison Around the Cutout.

boundary condition would have almost entirely eliminated even this small difference. The reduced strain toward the panel's free edge is due to not applying the load to the outter 0.25 inches of the panel's top edge.

The point of these comparisons is to validate the finite element analysis method, the type element and the configuration chosen. It is assumed that the computational results are as valid for reinforced panels.

2. Finite Element Analysis Results

Table VI summarizes the most important data from the LEFEA. The three maximum strains (Y, X and shear) are given for each configuration as well as the finite-width stress concentration factors. The locations at the edge of the cutout are listed at the bottom of the table. These values are best used as a means of comparison among reinforcement geometries, not for and exact prediction of the micro-strain at the edge of the cutout. Recall the assumption made that the compressive modulus was constant for all strain. Two SCF's are given, one for a theoretical "infinite" plate and one for the 8.50" width panel used in this research.

These stress concentration factors are theoretical only. They are valid solely for a totally elastic strain field. Nuismer and Labor [Ref. 33: p. 50], among others, point out that at high strains (in the case of HMF330C/34 at strain in excess of 9000 $\mu\epsilon$) the fibers immediately next to the hole at the SCF begin to fail and transfer the load through the matrix to adjacent fibers. Compressive failure usually consists of matrix cracking, fiber micro-buckling, ply delamination and the transfer of the load from the failing region next to the hole away to fibers/matrix able to sustain the load. Failure in this manner is difficult to analyze

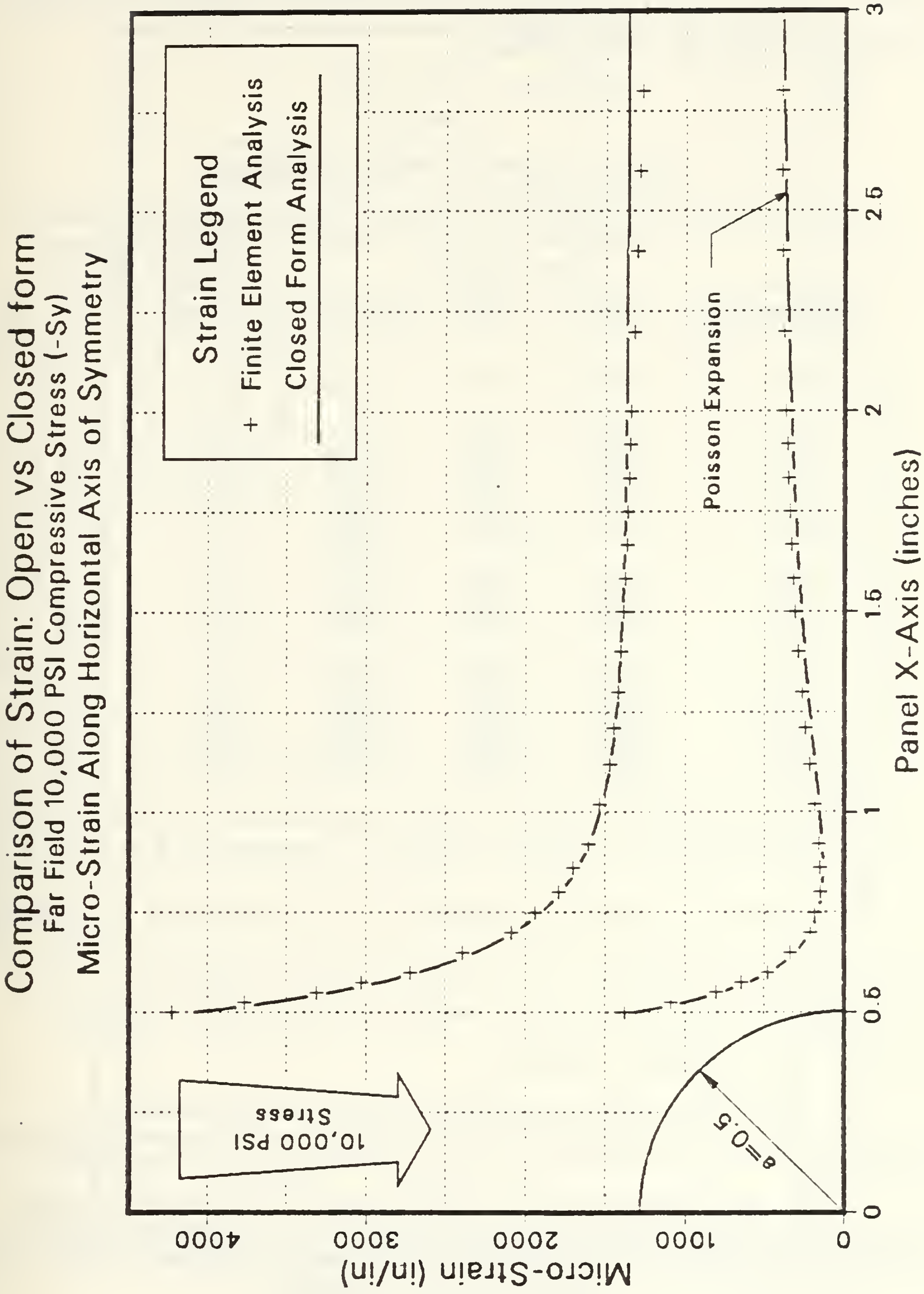

Figure 5.2 Strain Comparison on the X Axis.

using linear methods because of the rapidly changing material properties during the process.

TABLE VI

FINITE ELEMENT ANALYSIS RESULTS

Panel Designation	Maximum Strain Around the Cutout			Strain Concentration Factor	
	eps-y	eps-x	eps-xy	w = ∞	w = 8.5"
POØØ	-4230	1596	-3253	3.00	3.11
RR11	-3739	1420	-3211	2.65	2.75
RR22	-3363	1284	-3113	2.39	2.48
RR31	-3605	1320	-3106	2.56	2.65
RR42	-3231	1186	-2998	2.29	2.37
RR51	-3539	1267	-3056	2.51	2.60
RS11	-3719	1382	-3170	2.64	2.74
RS31	-3545	1254	-3058	2.51	2.60
RS51	-3465	1193	-2999	2.46	2.55
RH11	-4261	1777	-3298	3.02	3.13
RH22	-4097	1821	-3188	2.91	3.02
RH31	-3983	1545	-3097	2.82	2.92
RH42	-3727	1645	-2947	2.64	2.74
RH51	-3997	1475	-3094	2.83	2.93

eps-y @ $\theta = 0°$, eps-x @ $\theta = 90°$, eps-xy @ $\theta = 27.0°$

Figure 5.3 shows a comparison of the maximum Y direction strains (eps-y in Table VI) at the edge of the cutout. These correspond to the theoretical stress concentration factors. Several facts become apparent:

- Panels RR22 and RR42 gave the best theoretical reduction in SCF. They had most of their reinforcement concentrated next to the cutout in 2 plies (thick) per facesheet.

- In no case was the 500% (single ply) reinforcement appreciably superior to the 300% (single ply) configuration in reducing the SCF. Reinforcement relatively far removed from the hole edge added little strength to the panel.

- The square reinforcement configuration provided very slightly more strain reduction compared with equivalent round.

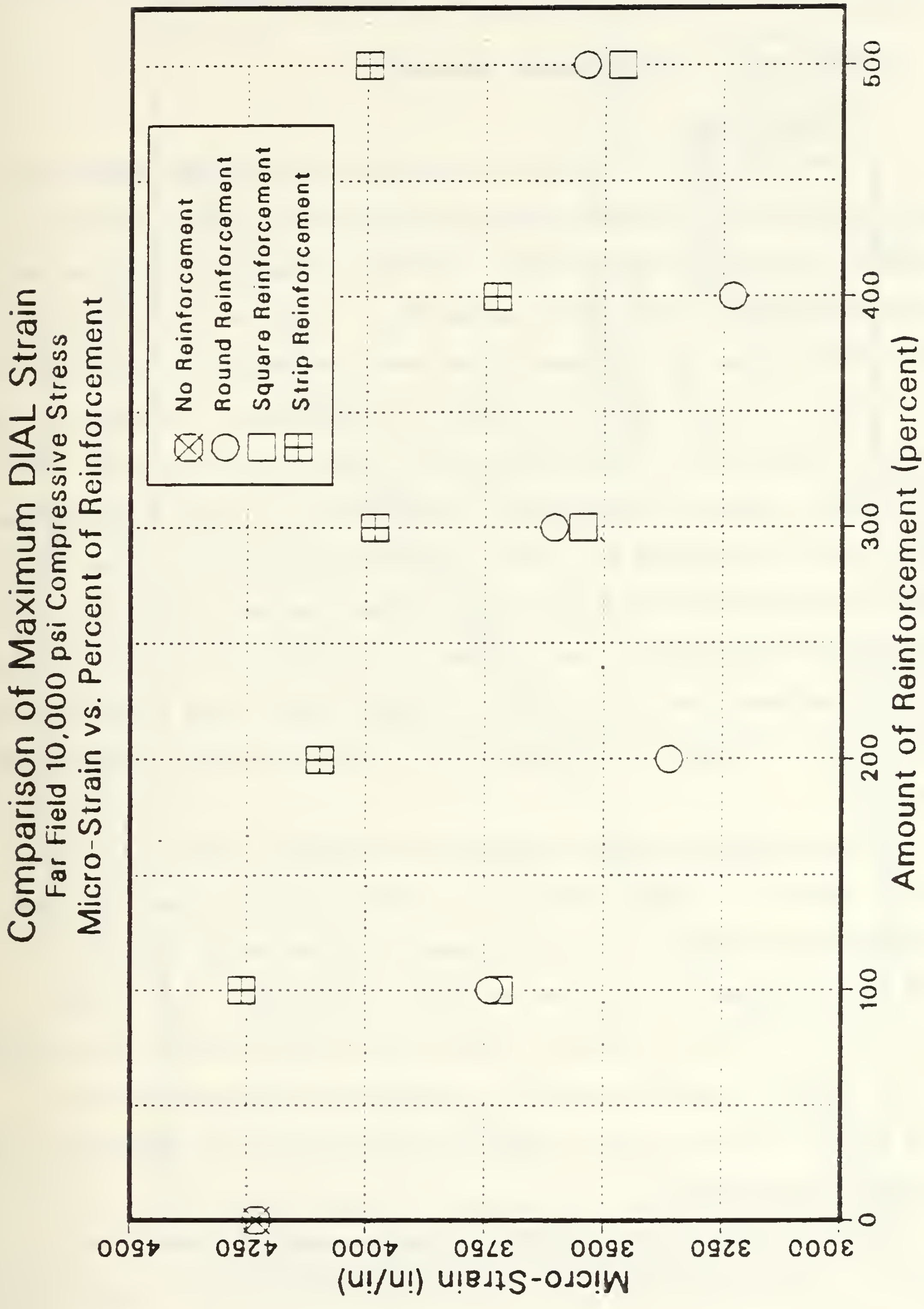

Figure 5.3 Comparison of Maximum FEA Strains.

▪ The strip reinforcement resulted in about 12% higher strain for the same amount (percentage) of reinforcement compared with the other two configurations.

B. COMPARISON OF EXPERIMENTAL RESULTS

1. Solid Panel

Panel PXØØ was tested to provide a basis for comparison and an indication of the ultimate strength of a panel without a cutout or stress concentration. The panel was subjected to two loading sequences: the first up to $\overline{\sigma}_n$ = -45.0 ksi (about two-thirds the estimated ultimate load) and the second to failure at -57.0 ksi. Two load runs were used to determine if there was any residual damage from the first load. After the first run, residual damage would be indicated by reduction in inplane stiffness (the effective modulus E_y) due to matrix degradation. Table VII shows the results of the test. The first run was a maximum load of approximately 80% of the ultimate; no significant difference is apparent between the two runs. It appears that this G/Ep material is elastic, at least up to about 80% of its ultimate compressive strength.

The monotonically decreasing stress-strain curve (noted in Section III.A.1) is significant. It most probably results from the decreasing ability of the crimped harness weave fibers to carry the compressive load as the load increases. The close correlation in strain (Eps-y) and modulus (E_y) between runs 1 and 2 would seem to eliminate matrix cracking or delamination, at least below -45.0 ksi, as a source of the nonlinear behavior; it's nonlinear and elastic.

Figure 5.4 shows the stress-strain curves for both load sequences. Test sequence No. 1 is almost exactly duplicated by No. 2. These curves came from the average of 10 gages mounted

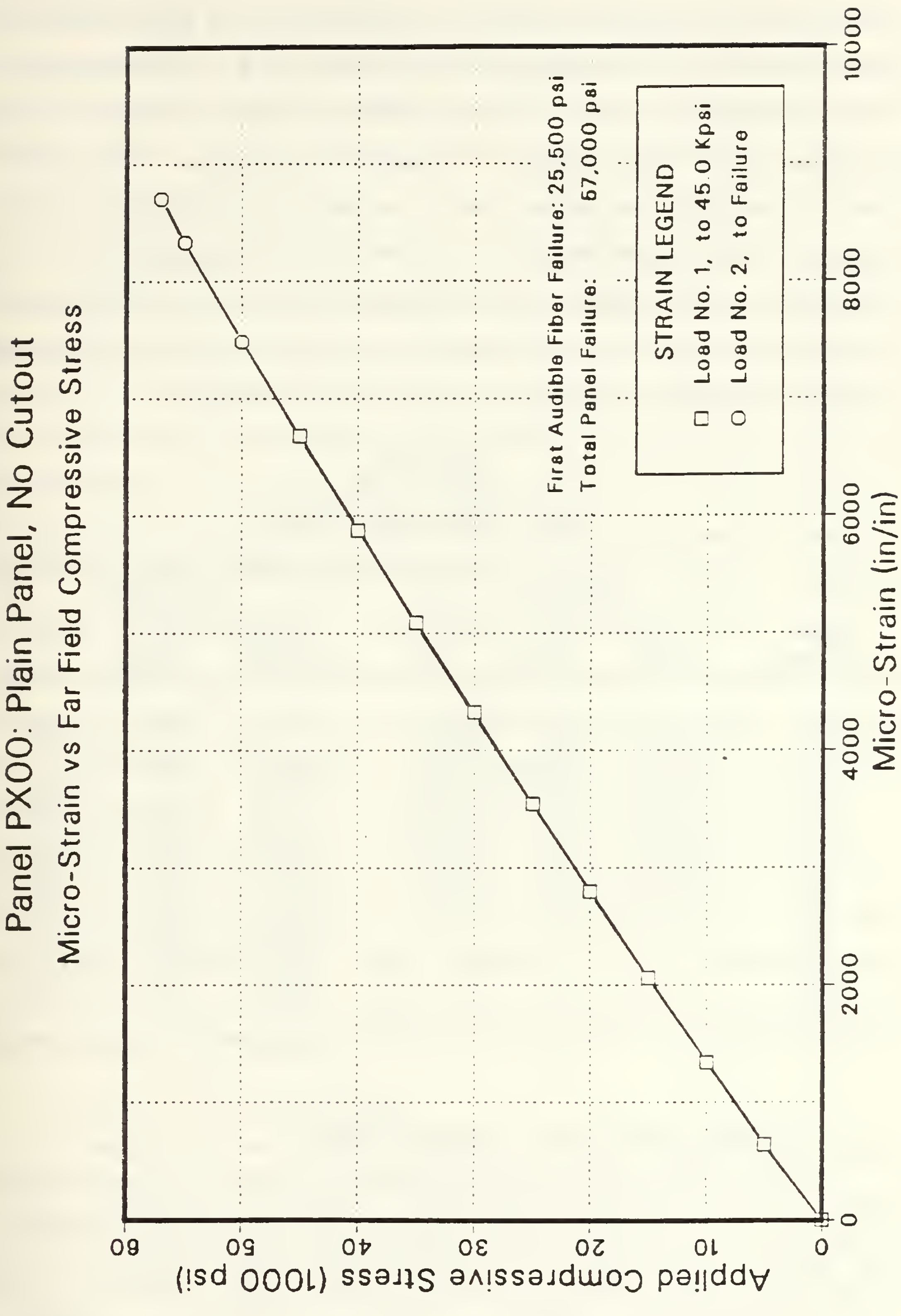

Figure 5.4 Stress-Strain Curve for Solid Panel (PXØØ).

transversely (on the X axis) on the panel. The gages were all the various sizes and resistance values used on the other panels. The standard deviation of all the values was within ±4% of the average for each load. This could be taken as the typical limit of accuracy for any one gage. When including consideration for the position error noted above it would not be unreasonable to consider any experimentally measured strain to be within about ±4% of the true value. It is doubtful that more accurate measurement is possible without taking extraordinary measures.

TABLE VII

PANEL PXØØ TEST RESULTS

	Run #1			Run #2		
Load (- ksi)	eps-y ($\mu\epsilon$)	E_y (msi)	ν_{12}	eps-y ($\mu\epsilon$)	E_y (msi)	ν_{12}
5	644	7.76	0.311	636	7.86	0.336
10	1341	7.46	0.315	1342	7.45	0.322
15	2065	7.26	0.314	2060	7.28	0.320
20	2799	7.15	0.314	2793	7.16	0.319
25	3543	7.06	0.315	3544	7.05	0.318
30	4323	6.94	0.315	4302	6.97	0.318
35	5092	6.87	0.316	5073	6.90	0.319
40	5879	6.80	0.317	5891	6.79	0.319
45	6683	6.73	0.318	6663	6.75	0.320
50	--	--	--	7485	6.68	0.321
55	--	--	--	8328	6.60	0.321
57	--	--	--	8702	6.55	0.322

2. Panels with Stress Concentrations

The results of the experimental program are summarized in Table VIII. Individual panel experimental and computational results are discussed in the appendices. The loads in (ksi) are listed for the first audible ply failure (FAPF) and ultimate. The

FAPF was nothing more than the first "pop" heard during the loading sequence. While this hardly seems to be a rigorous definition, in every case the FAPF appeared to be a predictor of the ultimate load. Stress concentration factors (SCF) were taken from the finite element analysis. In the strength reduction column the calculated value came from equation 2.6 using a_o = 0.33", the value determined by LMSC for HMF330C/34 cloth G/Ep. Nuismer and Whitney [Ref. 26: pp. 122-3] state that there is some evidence that the value of a_o remains "constant for all laminates of all fiber reinforced/resin matrix composites...at least for what has been referred to as 'fiber of filament-dominated' laminates in glass/epoxy, boron/epoxy, and graphite/epoxy systems." There seems to be some difference, however, between tape (a_o = 0.28" for AS/3501-5) and fabric (a_o = 0.33" for HMF330C/34). The actual strength reduction is based on the ratio of the solid panel (PXØØ) ultimate strength to that of each panel with the stress concentration. The percent difference ($\%\Delta$) between calculated and actual strength reduction is [(calculated-actual)*(100/calculated)]. This value serves to compare the relative magnitude of observed strength among test specimens. A positive value of $\%\Delta$ indicates a panel which demonstrated higher strength than predicted by the SCF computed by the LEFEA. Note the close correlation among FAPF, actual strength reduction and failure type.

3. Types of Panel Failure

There were two types of panel failure: (Type-1) delamination at the point of highest stress concentration (θ = 0° on the edge of the cutout) followed immediately by total failure and (Type-2) facesheet separation followed at some higher load by catastrophic failure. Type-2 failures occurred far below the expected stress level. A panel with a Type-2 failure not taken to to a complete failure was designated Type-2'.

TABLE VIII

COMPARISON OF EXPERIMENTAL RESULTS

Panel Desig.	FAPF Ultimate Load	FAPF Ultimate (psi)	SCF	Strength Reduction Calc.	Strength Reduction Actual	Strength Reduction %Δ	Failure Type
PXØØ	25,500	57,460	1.00	0.00	0.00	0.0	1
POØØ	17,000	30,000	3.00	1.89	1.88	+ 0.5	1
RR11	18,500	29,950	2.65	1.87	1.92	- 2.7	1
RR22	16,000	21,050	2.39	1.87	2.73	-46.0	2
RR31	17,500	28,000	2.56	1.87	2.05	-9.6	1
RR42	13,500	21,900	2.29	1.86	2.61	-40.3	2
RR51	5,500	16,000	2.51	1.87	**	**	2
RS11	17,000	31,000	2.64	1.87	1.85	+1.1	1
RS31	17,500	32,550	2.51	1.87	1.77	+5.3	1
RS51	7,000	19,600	2.46	1.87	**	**	2
RH11	19,000	29,960	3.02	1.89	1.92	-1.6	1
RH22	18,000	31,640	2.91	1.88	1.82	+3.2	1
RH31	9,500	21,530	2.82	1.88	2.67	-42.0	2
RH42	21,000	36,990	2.64	1.87	1.55	+17.1	1
RH51	16,500	31,630	2.83	1.88	1.82	+3.2	1

Strength reduction calculation used a_o = 0.33 in. from LMSC test data. Panels marked with ** were not taken to total failure.

Failure Types:
- 1 - Failure originates at Strain Concentration
- 2 - Facesheet Separation & Buckle
- 2' - Facesheet Separation & Buckle (not loaded to ultimate)

It has been noted that in compression there exists a tensile Poisson stress ($+\sigma_z$) which is greatest at the point of highest stress concentration on the edge of of the cutout and tends to pull the plies apart. It was not possible from this experimental procedure to determine if ply delamination, interlaminar shear stress or micro-mechanical fiber buckling was the initiator of the failure. In fact, failure probably resulted from two or all three of these working together, possibly in conjunction with both fiber and matrix flaws. Figure 5.5 shows a typical compressive panel (Type-1) failure. All Type-1 failures were almost identical in appearance; they differed only in the ultimate load sustained.

All Type-2 and Type-2' failures were also similar to eacn other; the facesheet began to pull away from the core at some point away from the edge of the cutout. This began with the formation of a small bulge or "bubble" which increased in total area and distance from the face of the core to inside surface of the facesheet. The initial separation was not visible until well into the load cycle, however, in some cases the FAPF may have well been the sound of the initial adhesive failure. Once the leading edge of the separation reached the cutout the panel failed totally.

Type-2' failure was this facesheet separation not taken to total failure. The partially failed panels were removed from the test apparatus and subjected to non-destructive (NDI) and destructive inspections in an attempt to determine the possible cause of the core-facesheet separation.

Panels RR22, RR42, RR51 RS51 and RH31 failed by facesheet separation. The stress-strain curves for these panels appear in the individual appendices and all clearly show the result of the facesheet separation--the slope of the curve dramatically increased. This was due to the decreasing panel stiffness and the picking-up of the load as the area of separation and facesheet curvature increased.

When this failure mode appeared an additional FEA was considered necessary to examine in detail the core-facesheet

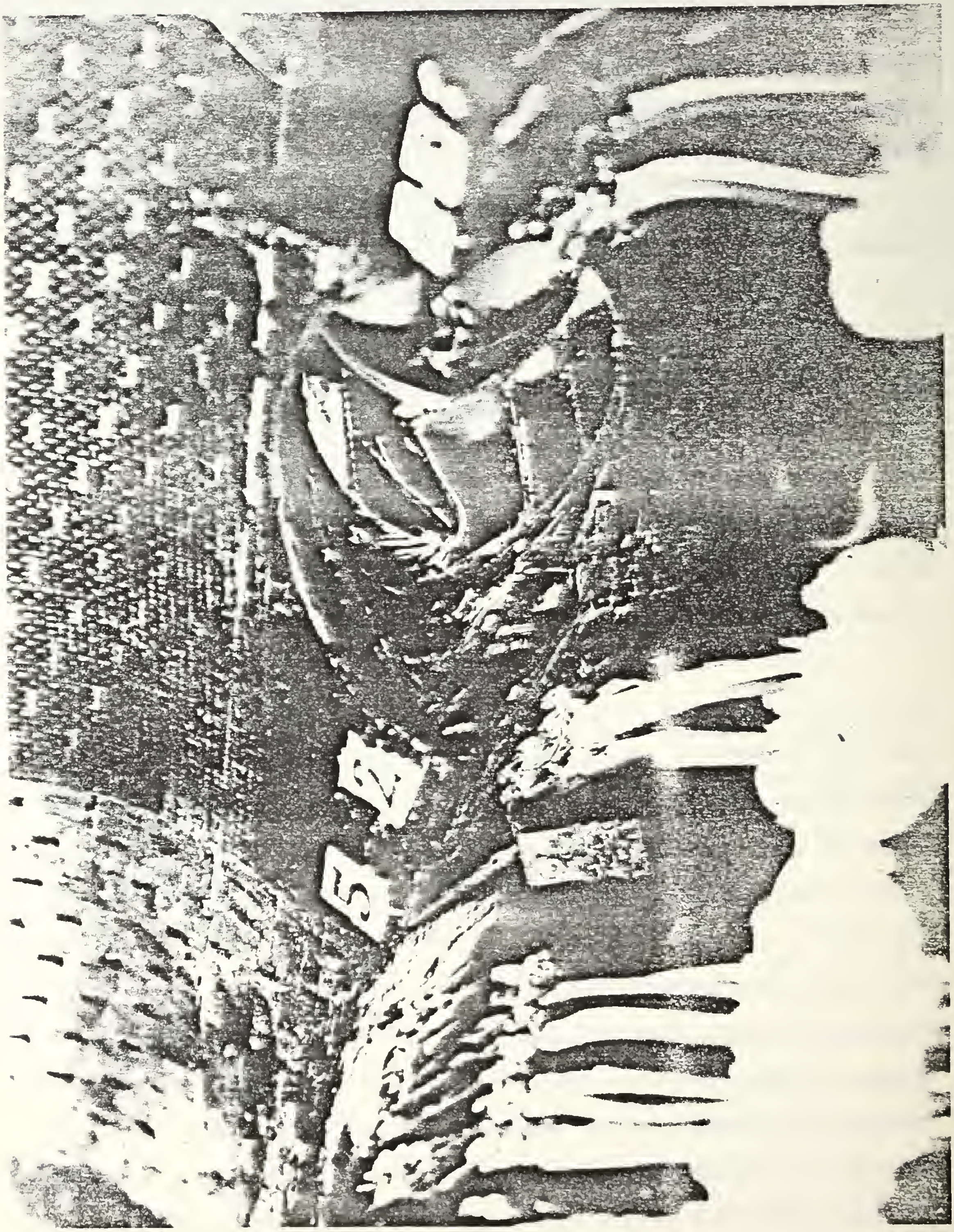

Figure 5.5 Typical Test Panel Failure in Compression.

interface. A three-dimensional analysis was made of panel RR22 to determine if any significant out-of-plane stress was causing the separation. The results are given in Appendix O. The interface (the idealized adhesive surface) showed very low stresses in the ±z, or out-of-plane, direction. From this it may be assumed that facesheet separation was the result of an incomplete or bonding process or other manufacturing error.

The Type-2' failure panels were subjected to non-destructive inspection using C-Scan and X-ray methods to attempt to locate the source of the defect(s). No obvious flaws or manufacturing errors were apparent. Panels virtually identical to those Type-2 and -2' failures were manufactured and tested under the same experimental conditions. In each case the panels sustained Type-1 failure and carried an ultimate load into the -29 to -35 ksi range.

VI. SUMMARY, CONCLUSIONS AND RECOMMENDATIONS

A. SUMMARY

This study examined three geometric configurations of co-cured reinforcement of graphite/epoxy honeycomb plates with circular cutouts subjected to uniaxial compressive loading and compared them to identically loaded unreinforced notched and solid plates. The test specimens were modeled using linear elastic finite element analysis (LEFEA) to analyze the strain field around the cutout. The objective of the study was to determine if a relatively simple, inexpensively manufactured reinforcement of a cutout could significantly reduce the stress concentration it induced, decrease the local strain and thereby increase the ultimate (failure) strength of the panel.

Table IX is a summary of the important analytical and experimental results. The computed SCF is derived from the LEFEA. The predicted failure stress is based on the actual failure of the unreinforced panel (PO∅∅) and the analytical SCF. More than many any other experimental results, compressive failure in composite plates should be classed a stochastic function. It would take a number of identical panels of each configuration to arrive at a statistically significant predicted failure stress. However, from the data of this study, the average of the eight Type-1 failures was 93.5% of the predicted failure stress. The strip reinforcement (four Type-1 failures) failed at 100.5% of the predicted applied stress. A three-dimensional linear finite element analysis of a typical Type-2 failure (Panel RR22) was attempted (see Appendix O). It failed, however, to predict the actual failure loading or to provide a reason for the premature facesheet separation.

The test program reported here confirmed that, properly used, the linear elastic finite element method provided an exceptionally accurate strain field representation even in a material with nonlinear response (see Appendices A-O). The failure stresses were harder to predict using linear methods, but this is hardly surprising considering the material is a composite and the loading is compression.

TABLE IX

SUMMARY OF ANALYTICAL AND EXPERIMENTAL RESULTS

Test Panel	Computed SCF	Failure Stress (psi) Predicted	Failure Stress (psi) Actual	% Predicted Load	Failure Type
POØØ	3.00	———	30,500	100	1
RR11	2.65	34,500	29,950	86.8	1
RR22	2.39	38,250	21,050	55.0	2
RR31	2.56	35,750	28,000	78.3	1
RR42	2.29	39,950	13,500	33.8	2
RR51	2.51	36,500	0	0.0	2'
RS11	2.64	34,650	31,000	89.5	1
RS31	2.51	36,500	32,550	89.2	1
RS51	2.46	37,200	19,000	51.1	2'
RH11	3.02	30,250	29,960	99.0	1
RH22	2.91	31,500	31,640	100.0	1
RH31	2.82	32,500	12,000	36.9	2
RH42	2.64	34,650	36,990	106.8	1
RH51	2.83	32,300	31,630	97.9	1

B. CONCLUSIONS

From data in Table IX it can be seen that reinforcement reduced computed stress concentrations up to 20% in some configurations. The reinforcement added little more than 1 to 4%

additional weight to each panel. While it is difficult to directly compare the improvement reported here with configurations in an actual application in a large, complex structure, it is easy to see that for a small increase in weight a significant reduction in stress concentration is both predicted and realized.

Small amounts of graphite/epoxy reinforcing lamina(e) co-cured with thin composite sheets of the same material can significantly reduce stress concentrations and increase ultimate failure load. This reinforcement method involves some additional manufacturing effort, but it yields excellent strength-to-weight comparisons. The analytical results indicate that using several small reinforcement plies concentrated close to the cutout provides the most attractive strength-to-weight ratios. The strip configuration also gives excellent results and seemingly very predictable failure levels.

This experimental program reaffirmed the well-known fact that even minor manufacturing defects can be a severe problem in compression testing. Improper or incomplete bonding of the face-sheets to the honeycomb core can significantly affect the ultimate failure load in graphite/epoxy specimens. In five cases the facesheet began separating from the core at a point away from the cutout. A "bubble" then formed reducing the facsheet's load resistance and transferring the load to the opposite, still intact facesheet. The panel then began to exhibit greatly decreased stiffness. As the load was increased, panel stiffness decreased in proportion--similar to Euler column buckling.

It was not possible to locate the source of the bonding failure or even prove conclusively that improper bonding was the source of the premature failure. However, since the "bubble" usually initiated at low load levels and at points well away from the stress concentration, bonding failure appears to be the most logical explanation. Prior to testing the panels were subjected to NDI which failed to discover any unbonded areas between the core and facesheet. These failures could have been a case of weak or only partial adhesive bonding.

C. RECOMMENDATIONS

The research reported here investigated only a few of the possible reinforcement geometries. Any number of significant questions remain unanswered in the research reported here. Additional work is suggested in the following areas:

1. <u>Further Testing of Reported Geometries</u>

Time and money limited testing to one specimen of each geometry. Several of the most promising reinforcement configurations (RR22, RR42, RH42, etc.) should be subjected to further testing to obtain statistical confirmation of these results.

The reaction of some of the strain gages remains unexplained, at least in part. For example, panel RS31 (Appendix H, Figure H.4) the gages closest to the cutout show points where an increase in load causes no corresponding strain increase. At a higher applied stress the gage begins to react normally and stress-strain curve resumes an offset but parallel course (also see panel RH22, Figure K.4).

2. <u>Additional Reinforcement Geometries</u>

The three geometries reported here hardly exhaust the possibilities. Some additional promising configurations include oval (when the principal load direction is known or is predictable), several different "wedding cake" methods and moving the strip configuration closer to the cutout.

3. The Effects of Reinforcement Stiffness

Reinforcement plies identical to the reinforced material was used in this study. It would be interesting to observe the effects of stiffer reinforcement such as laying G/Ep tape reinforcement 0° to the applied load.

4. Improvements to Experimental Methods

A dense strain gage network next to the cutout on both sides of each facesheet may better explain the mechanics of failure. Mucn closer load increments are necessary, 1000 psi steps were not sufficient for a full explanation of the high strain notched panel response.

A micro-photographic sequence of the stress concentration at the edge of the cutout at high load (starting at 80% of σ_{ult}) might yield significant information on the way the graphite/epoxy panels fail in compression.

The MTS machine used in this research maintained a constant (or constantly increasing) load using an electronic feed-back loop. When the panel began yeilding, stiffness was reduced and the rate of head travel increased in an attempet to maintain the indicated load. At failure, the head moved about 1/3" - 1/2" and crushed the panel. This precluded detailed examination of the delamination at the stress concentration at failure. A constant displacement compression test machine is recommended in subsequent research.

APPENDIX A

PANEL POØØ: ANALYTICAL AND EXPERIMENTAL DATA

Panel POØØ served as the basis for comparison between reinforced and unreinforced compression specimens. It had a centered 1.00" diameter hole with no reinforcement around the cutout. Two identical specimens were produced, instrumented and tested. They both failed at the hole edge (Type-1) at an average applied normal compressive stress ($\bar{\sigma}_n$) of -30,500 psi.

The panel finite element model (mesh) is illustrated in Figure A.1. Figure 5.1 shows the distribution of strain around the cutout comparing open and closed-form computation methods. Table X gives the (finite element) computed strain data around the cutout. Figure A.2 shows the correlation between computed strain (solid and dashed lines) and the experimentally measured strain (triangles) along the X axis at an applied normal stress of -10,000 psi. Figure 5.2 shows the correlation between open and closed-form analysis along the X axis. Table XI lists the computed values of the strain parallel to the applied load (Eps-Y) and Poisson expansion (Eps-X) along the X axis.

Note that in Figure A.2 between the 1.25 and 2.75 inch stations on the panel's X axis the indicated gage strain seems to alternate slightly up and down. Gages indicating high were on the right side of the hole while those indicating slightly lower were on the left. In order to best illustrate the effect of the stress concentration, left and right side gages are superimposed on the right side of the cutout. It appears that the right side saw about 1 to 2% higher strain than the left. The strain difference is attributed to either a very slight test fixture misalignment or a difference in panel length between each side of the hole amounting to about to somewhat less than 0.0005"

Figure A.3 shows graphically the experimentally measured values of strain at different locations on the X axis. The numerical strain data are given in Table XII. The center of gage #1's resistive grid at x = 0.570" was 0.070" from the edge of the hole. The strain indicated was appropriate to the applied load taking into account the nonlinearities discussed in Chapter 5. Between -7,000 and -9,000 microstrain on gage #1, there appears to be a slight anomaly where the strain does not increase as fast as it had up to that point, but it then appears to "catch up." This may be attributed to minor fiber failure, nonlinear load transfer or local delamination. This is a phenomenon that becomes <u>much</u> more apparent in the tests of reinforced panels.

Figures A.4 through A.7 show the strain field contours at an applied normal stress of -10,000 psi computed and plotted using DIAL. Figure A.4 is the full quarter panel which shows the effect of not loading the full width of the top edge. Figures A.5 through A.7 show the strains contours close to the cutout. The computed strains are very close to that for the ideal infinite-width panel.

Figures A.8 through A.11 plot panel <u>stress</u> contours at the -10,000 psi loading. The type of element used in the LEFEA required the applied load to be input as a stress resultant (N, lb/in) and produced plots in the same units. Since all the reinforced panels had different thicknesses over their surfaces, the plots of stress resultant were not valid and are not given for any other panels. Plots of stress are included to be compared with the classic notched plate solution to validate the analysis.

Figure A.8 shows the full quarter panel with the stress concentration in the upper right corner due to the panel clamping modeling and the imposed boundary conditions. Figures A.8 and A.9 show the maximum resulting stress parallel to the load. The maximum induced stress (at $\theta = 0°$) is 31,100 psi which compares to 30,500 psi (Equation 2.3) for the finite-width panel. This is just 3.6% over that predicted for an infinite plate. This minor difference is accounted for by the loading and boundary conditions.

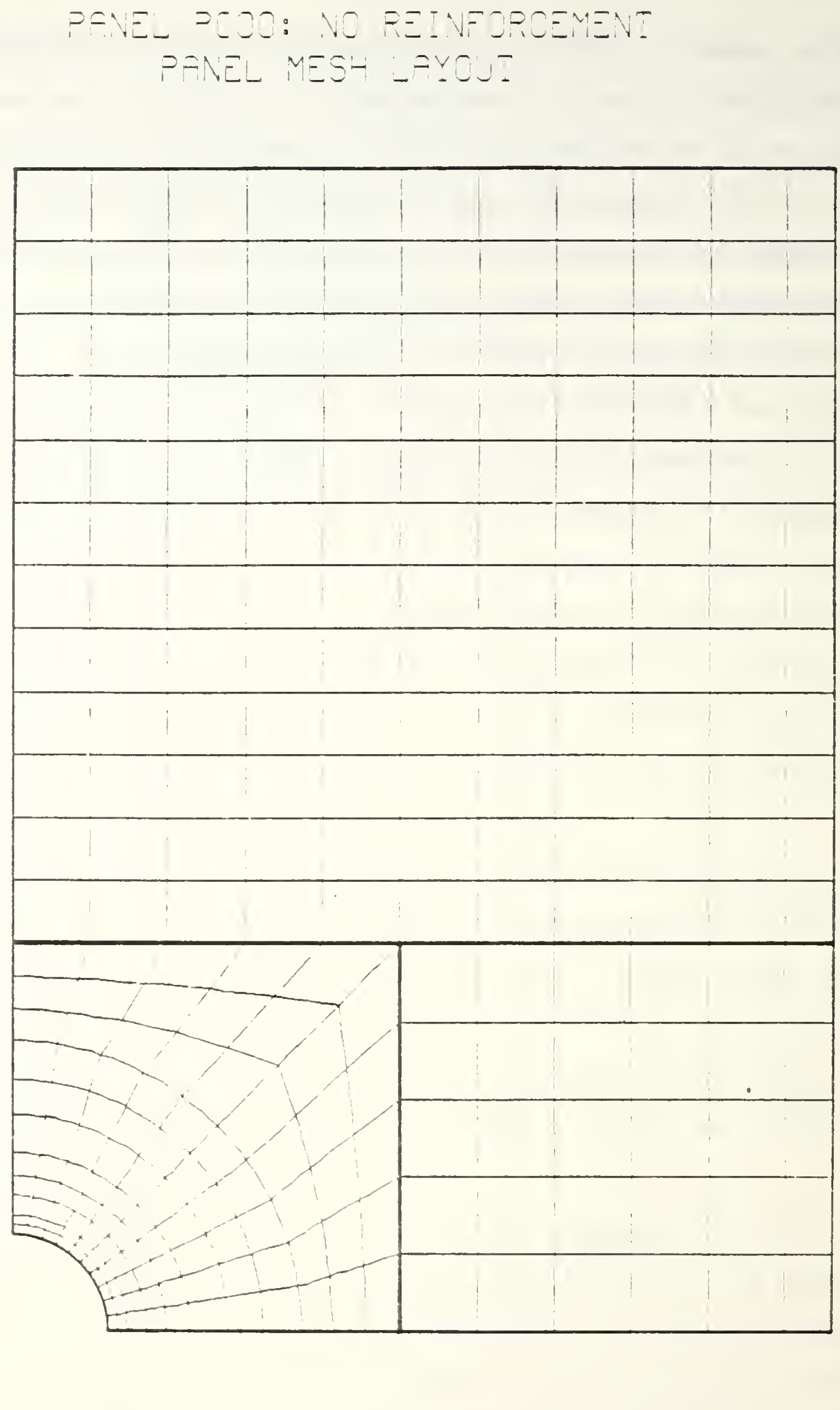

Figure A.1 Panel PO∅∅: DIAL Finite Element Mesh.

TABLE X

PANEL POØØ: LEFEA STRAIN DISTRIBUTION AROUND THE CUTOUT (-10,000 PSI).

NODE	X COORD	Y COORD	EPS-Y	EPS-X	EPS-XY
1	0.0000E+00	0.5000E+00	-0.5152E-03	0.1596E-02	0.1718E-04
2	0.3923E-01	0.4985E+00	-0.4706E-03	0.1504E-02	0.2980E-03
3	0.7822E-01	0.4938E+00	-0.4216E-03	0.1406E-02	0.5928E-03
4	0.1167E+00	0.4862E+00	-0.3133E-03	0.1159E-02	0.7030E-03
5	0.1545E+00	0.4755E+00	-0.2026E-03	0.9073E-03	0.8046E-03
6	0.1913E+00	0.4619E+00	-0.1095E-03	0.5966E-03	0.6153E-03
7	0.2270E+00	0.4455E+00	-0.1711E-04	0.2857E-03	0.4154E-03
8	0.2612E+00	0.4263E+00	-0.3336E-04	0.2764E-04	-0.5635E-04
9	0.2939E+00	0.4045E+00	-0.5333E-04	-0.2274E-03	-0.5365E-03
10	0.3247E+00	0.3802E+00	-0.2464E-03	-0.3383E-03	-0.1145E-02
11	0.3536E+00	0.3536E+00	-0.4449E-03	-0.4440E-03	-0.1757E-02
12	0.3802E+00	0.3247E+00	-0.8223E-03	-0.3704E-03	-0.2283E-02
13	0.4045E+00	0.2939E+00	-0.1205E-02	-0.2914E-03	-0.2804E-02
14	0.4263E+00	0.2612E+00	-0.1704E-02	-0.6603E-04	-0.3033E-02
15	0.4455E+00	0.2270E+00	-0.2205E-02	0.1627E-03	-0.3253E-02
16	0.4619E+00	0.1913E+00	-0.2709E-02	0.4492E-03	-0.3063E-02
17	0.4755E+00	0.1545E+00	-0.3211E-02	0.7360E-03	-0.2862E-02
18	0.4862E+00	0.1167E+00	-0.3585E-02	0.9709E-03	-0.2272E-02
19	0.4938E+00	0.7822E-01	-0.3956E-02	0.1203E-02	-0.1673E-02
20	0.4985E+00	0.3923E-01	-0.4096E-02	0.1295E-02	-0.8381E-03
21	0.5000E+00	0.0000E+00	-0.4230E-02	0.1382E-02	-0.2038E-04

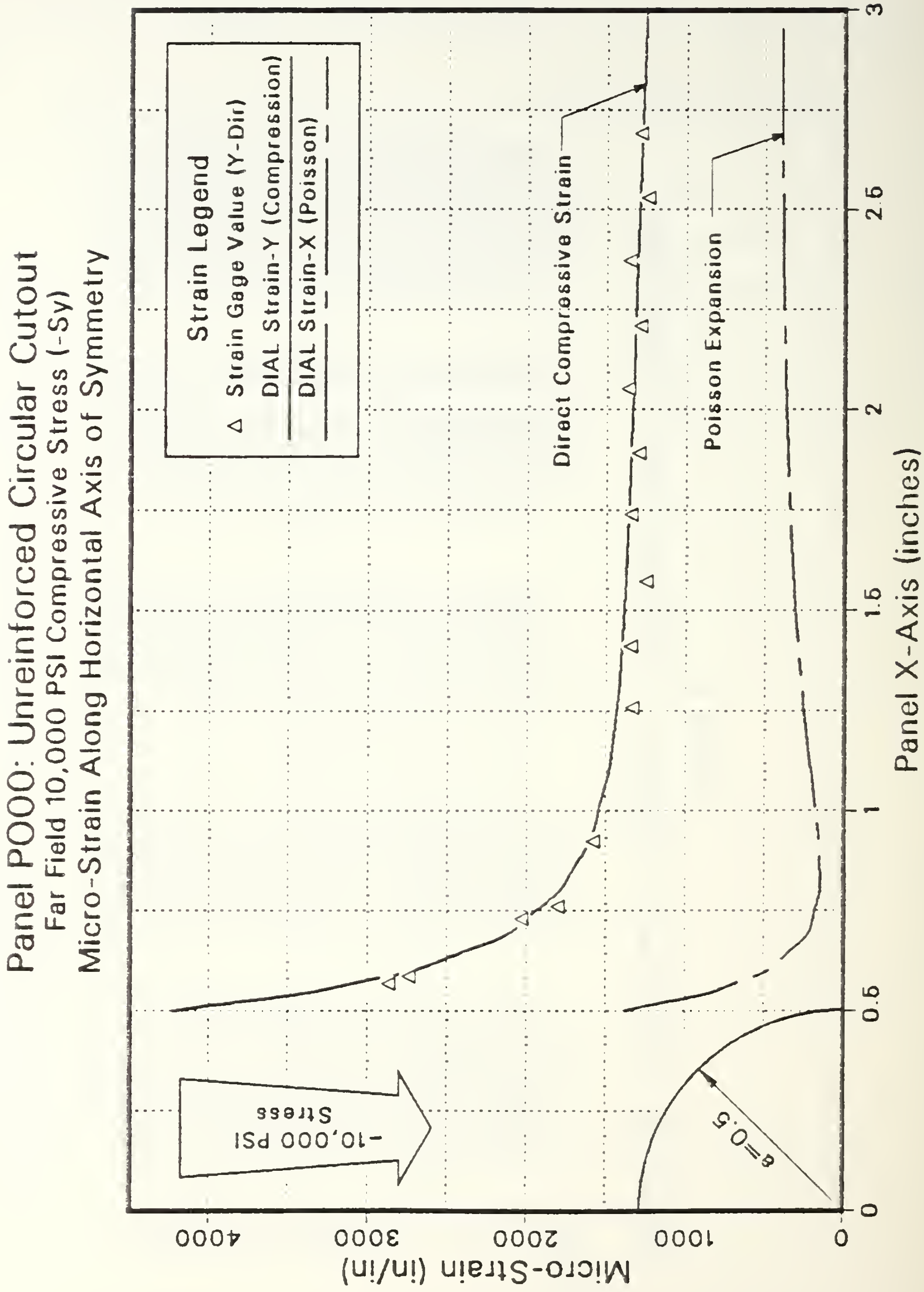

Figure A.2 Panel POØØ: Strain Comparison Along the X Axis.

TABLE XI

PANEL POØØ: LEFEA STRAIN DISTRIBUTION ALONG THE X AXIS (-10,000 PSI).

NODE	X COORD	Y COORD	EPS-Y	EPS-X	EPS-XY
21	0.5000E+00	0.0000E+00	-0.4230E-02	0.1382E-02	-0.2038E-04
32	0.5250E+00	0.0000E+00	-0.3769E-02	0.1092E-02	-0.1446E-04
53	0.5500E+00	0.0000E+00	-0.3315E-02	0.8070E-03	-0.8141E-05
64	0.5750E+00	0.0000E+00	-0.3030E-02	0.6514E-03	-0.7239E-05
85	0.6000E+00	0.0000E+00	-0.2727E-02	0.4830E-03	-0.4355E-05
96	0.6500E+00	0.0000E+00	-0.2397E-02	0.3389E-03	0.8460E-07
117	0.7000E+00	0.0000E+00	-0.2088E-02	0.2096E-03	0.1773E-05
128	0.7500E+00	0.0000E+00	-0.1944E-02	0.1817E-03	0.2602E-05
149	0.8000E+00	0.0000E+00	-0.1793E-02	0.1482E-03	0.3816E-05
160	0.8605E+00	0.0000E+00	-0.1701E-02	0.1521E-03	0.3929E-05
181	0.9210E+00	0.0000E+00	-0.1607E-02	0.1551E-03	0.4066E-05
192	0.1021E+01	0.0000E+00	-0.1539E-02	0.1843E-03	0.3851E-05
213	0.1120E+01	0.0000E+00	-0.1475E-02	0.2135E-03	0.3470E-05
224	0.1210E+01	0.0000E+00	-0.1451E-02	0.2400E-03	0.3597E-05
245	0.1300E+01	0.0000E+00	-0.1424E-02	0.2655E-03	0.3691E-05
256	0.1400E+01	0.0000E+00	-0.1408E-02	0.2875E-03	0.1777E-05
277	0.1500E+01	0.0000E+00	-0.1391E-02	0.3089E-03	0.5370E-06
288	0.1583E+01	0.0000E+00	-0.1381E-02	0.3211E-03	0.1137E-05
309	0.1667E+01	0.0000E+00	-0.1371E-02	0.3338E-03	0.1085E-05
320	0.1750E+01	0.0000E+00	-0.1363E-02	0.3437E-03	0.1865E-05
341	0.1833E+01	0.0000E+00	-0.1355E-02	0.3536E-03	0.2925E-05
352	0.1917E+01	0.0000E+00	-0.1348E-02	0.3610E-03	0.4569E-05
373	0.2000E+01	0.0000E+00	-0.1341E-02	0.3689E-03	0.5184E-05
374	0.2200E+01	0.0000E+00	-0.1324E-02	0.3805E-03	0.3177E-05
375	0.2400E+01	0.0000E+00	-0.1308E-02	0.3910E-03	0.2227E-05
376	0.2600E+01	0.0000E+00	-0.1291E-02	0.3937E-03	0.1675E-05
377	0.2800E+01	0.0000E+00	-0.1273E-02	0.3967E-03	0.1063E-05
378	0.3000E+01	0.0000E+00	-0.1255E-02	0.3955E-03	0.8669E-06
379	0.3200E+01	0.0000E+00	-0.1236E-02	0.3945E-03	0.5930E-06
380	0.3400E+01	0.0000E+00	-0.1217E-02	0.3911E-03	0.4959E-06
381	0.3600E+01	0.0000E+00	-0.1198E-02	0.3879E-03	0.3731E-06
382	0.3800E+01	0.0000E+00	-0.1177E-02	0.3828E-03	0.2843E-06
383	0.4000E+01	0.0000E+00	-0.1156E-02	0.3778E-03	0.1688E-06
384	0.4125E+01	0.0000E+00	-0.1141E-02	0.3733E-03	0.9013E-07
385	0.4250E+C1	0.0000E+00	-0.1127E-02	0.3689E-03	0.3698E-07

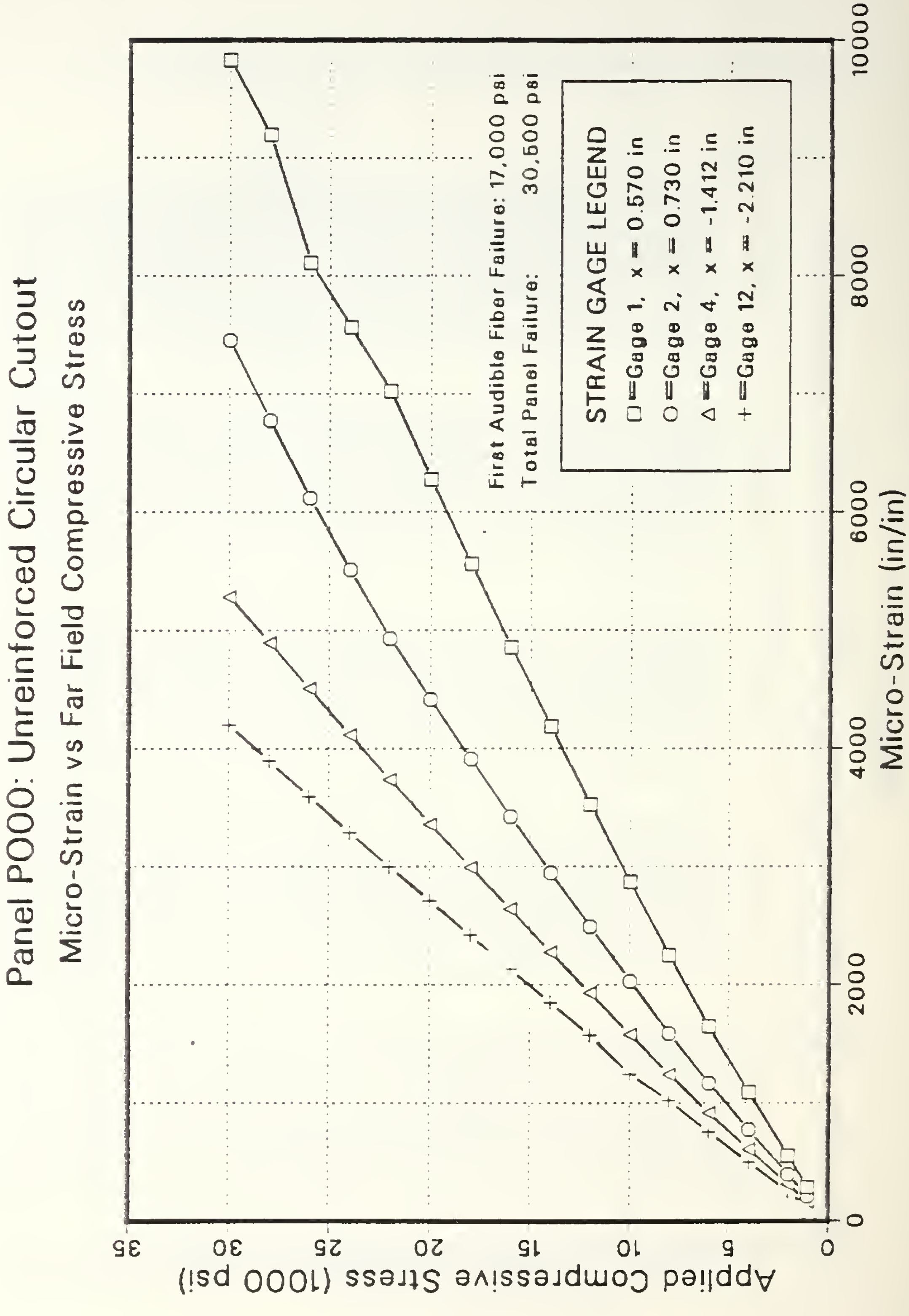

Figure A.3 Panel PO∅∅: Mircostrain vs. Cmpressive Stress.

TABLE XII

PANEL PO∅∅: SELECTED STRAIN GAGE VALUES DURING LOAD.

Load (psi)	Micrc-strain Indicated by gage: #1	#2	#4	#12
2000	-285	-207	-157	-115
4000	-554	-395	-311	-249
6000	-1091	-773	-609	-495
8000	-1648	-1168	-914	-753
10000	-2245	-1586	-1243	-1020
12000	-2869	-2031	-1581	-1244
14000	-3521	-2487	-1923	-1569
16000	-4183	-2948	-2277	-1851
18000	-4857	-3421	-2638	-2130
20000	-5559	-3910	-2996	-2420
22000	-6278	-4416	-3360	-2711
24000	-7022	-4932	-3741	-2997
26000	-7566	-5509	-4117	-3291
28000	-8111	-6115	-4507	-3592
30000	-9192	-6774	-4900	-3895
32000	-9829	-7456	-5283	-4202

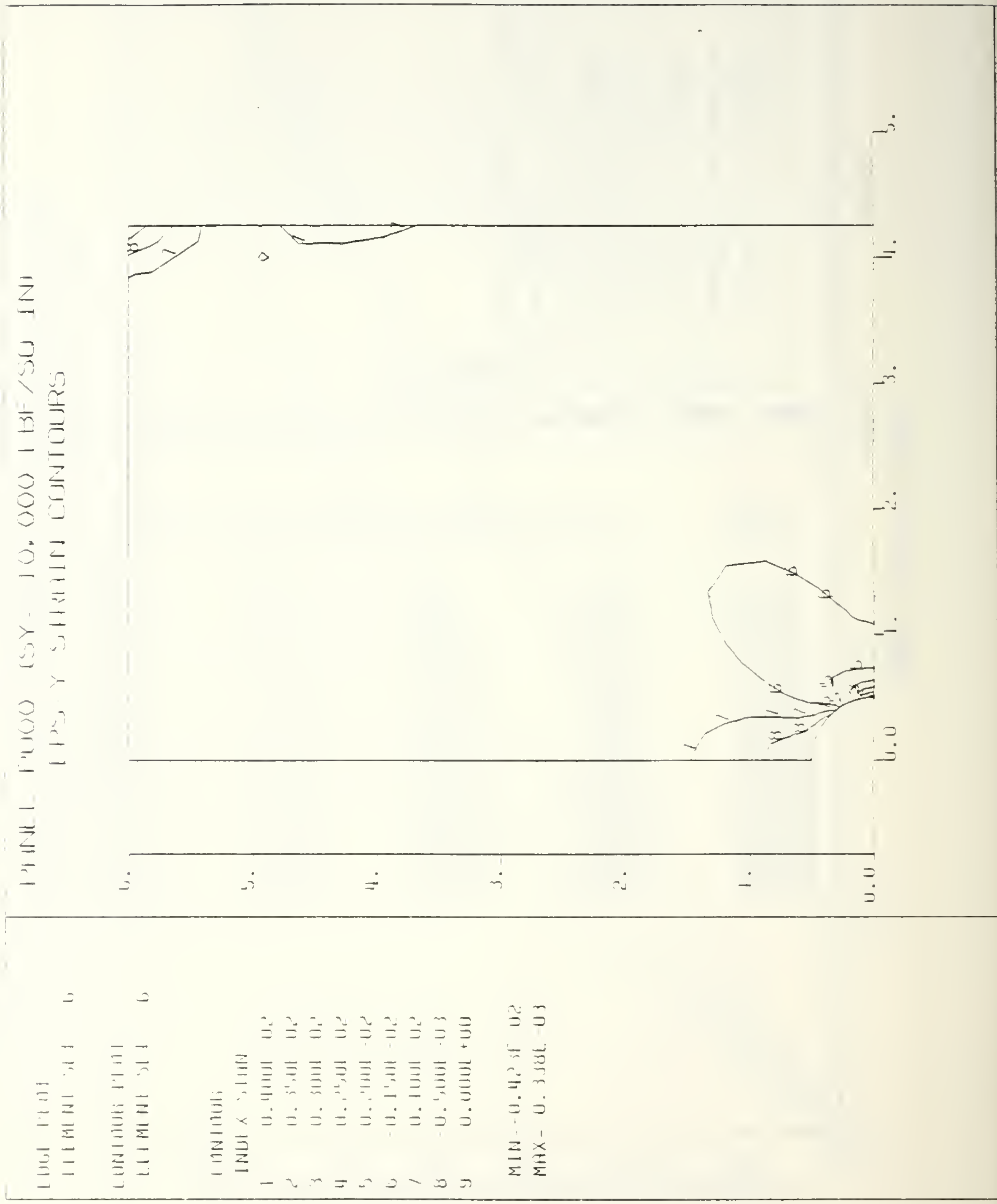

Figure A.4 Panel PO∅∅: Eps-Y FEA Contours.

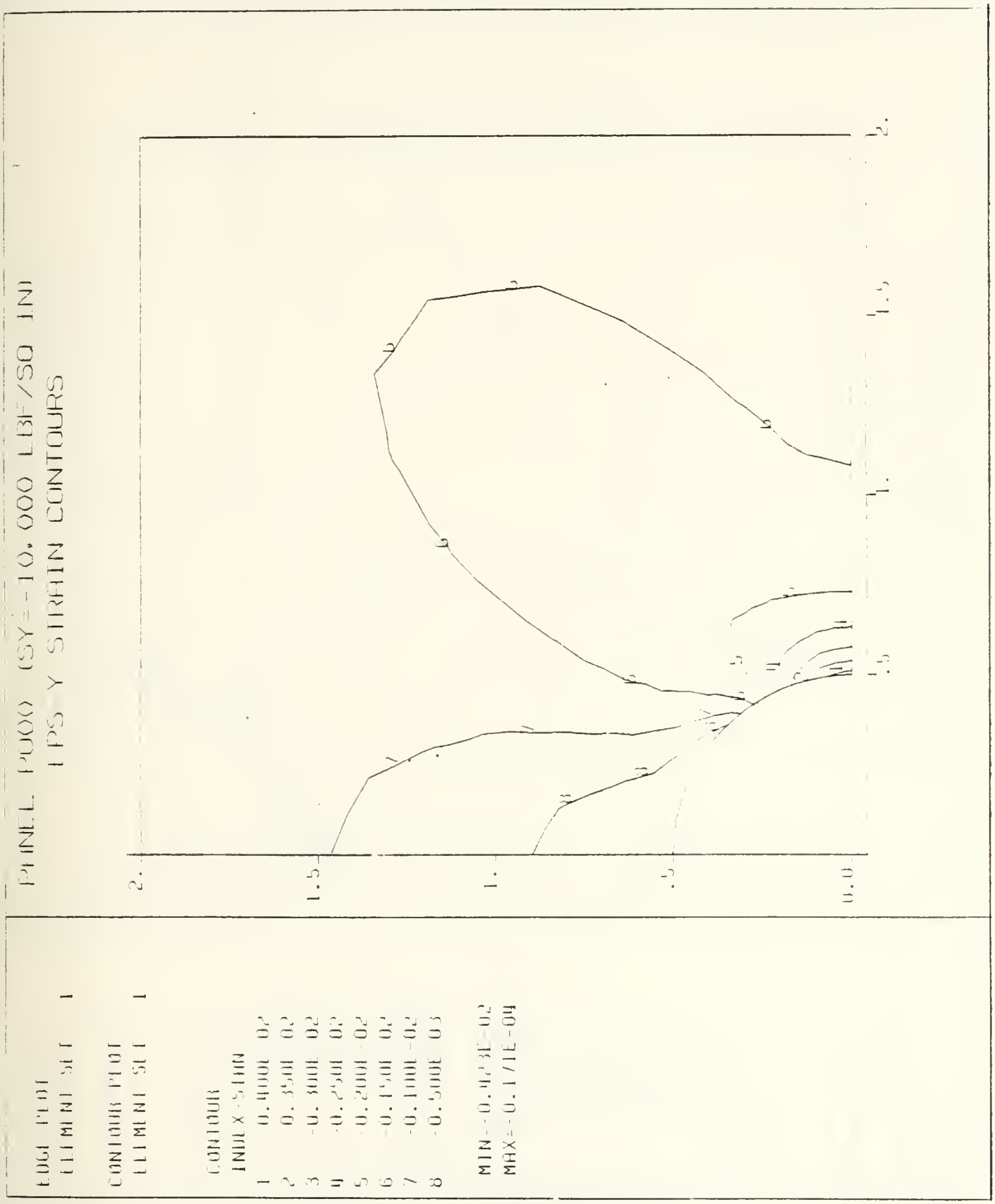

Figure A.5 Panel PO∅∅: Eps-Y FEA Contours Near the Cutout.

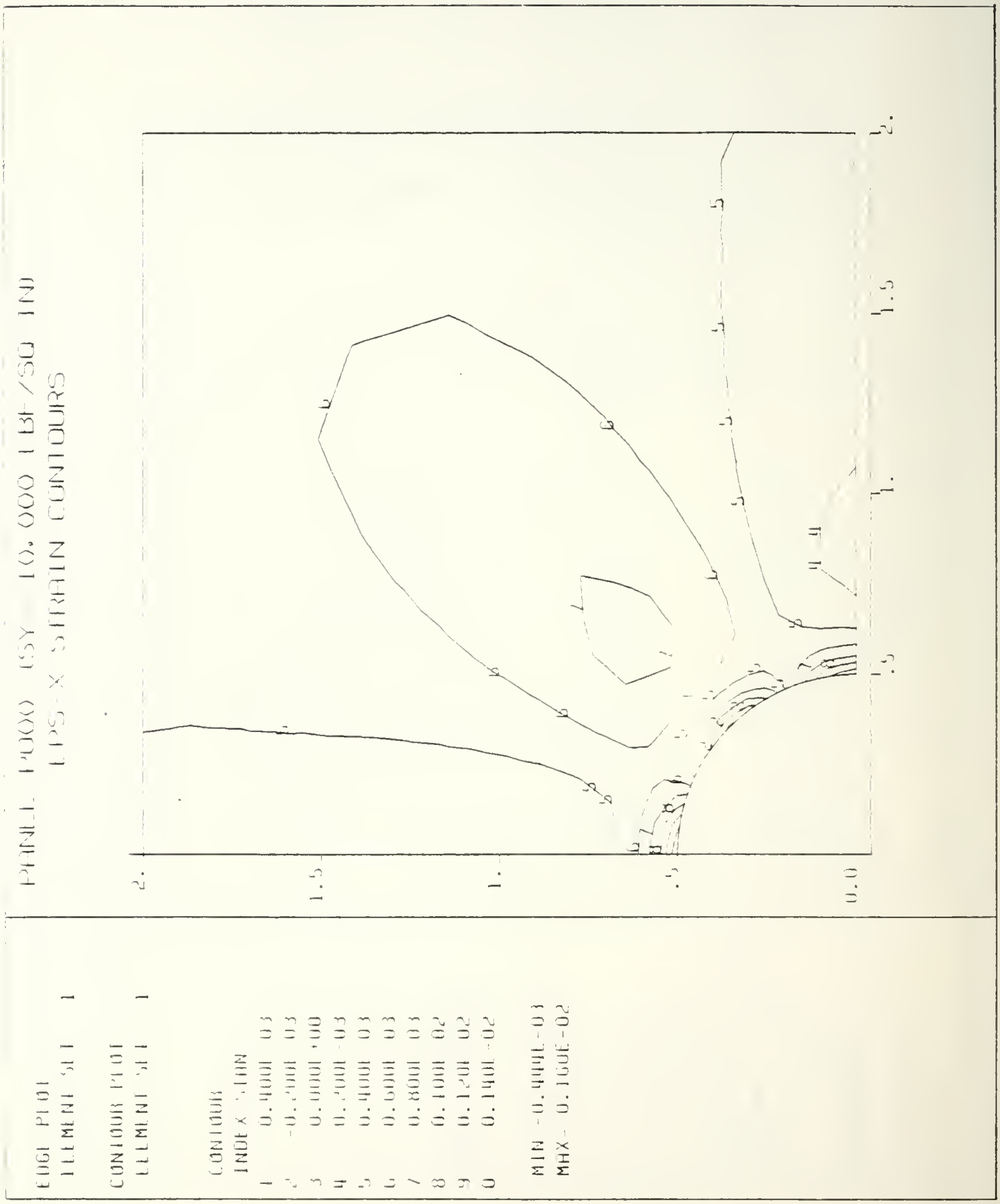

Figure A.6   Panel PO∅∅: Eps-X FEA Contours Near the Cutout.

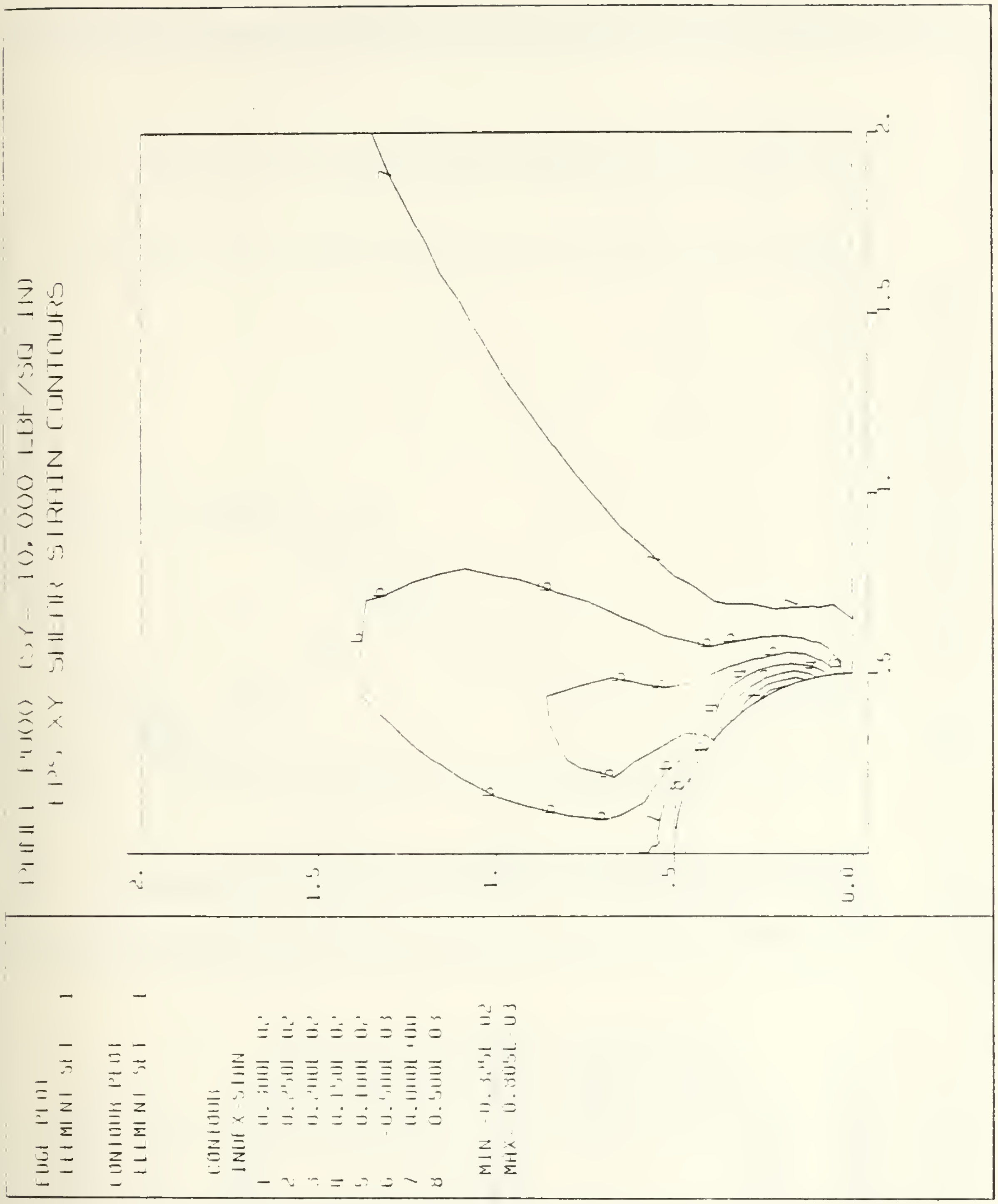

Figure A.7 Panel POØØ: Eps-XY FEA Contours Near the Cutout.

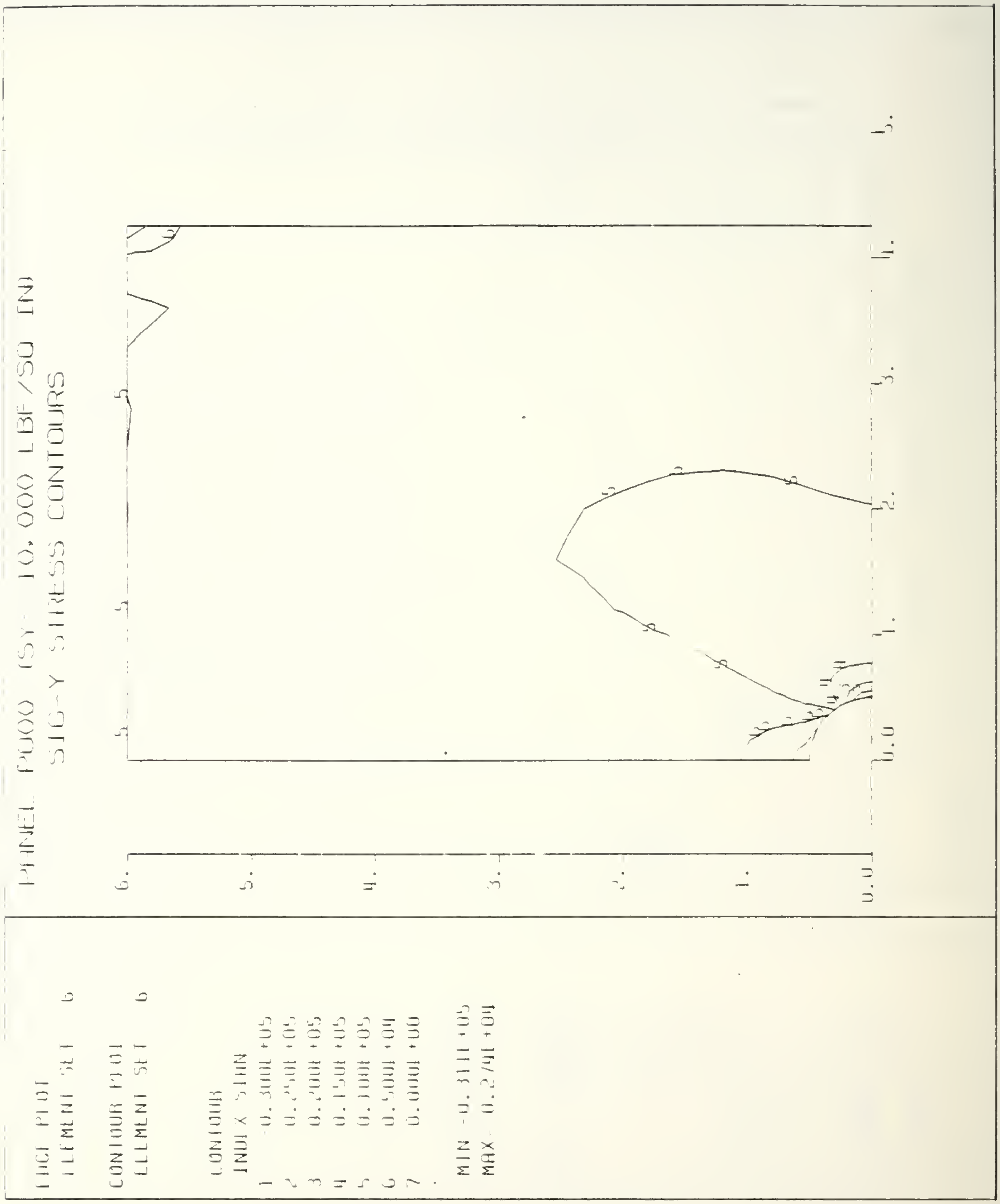

Figure A.8 Panel PO∅∅: Sig-Y FEA Contours.

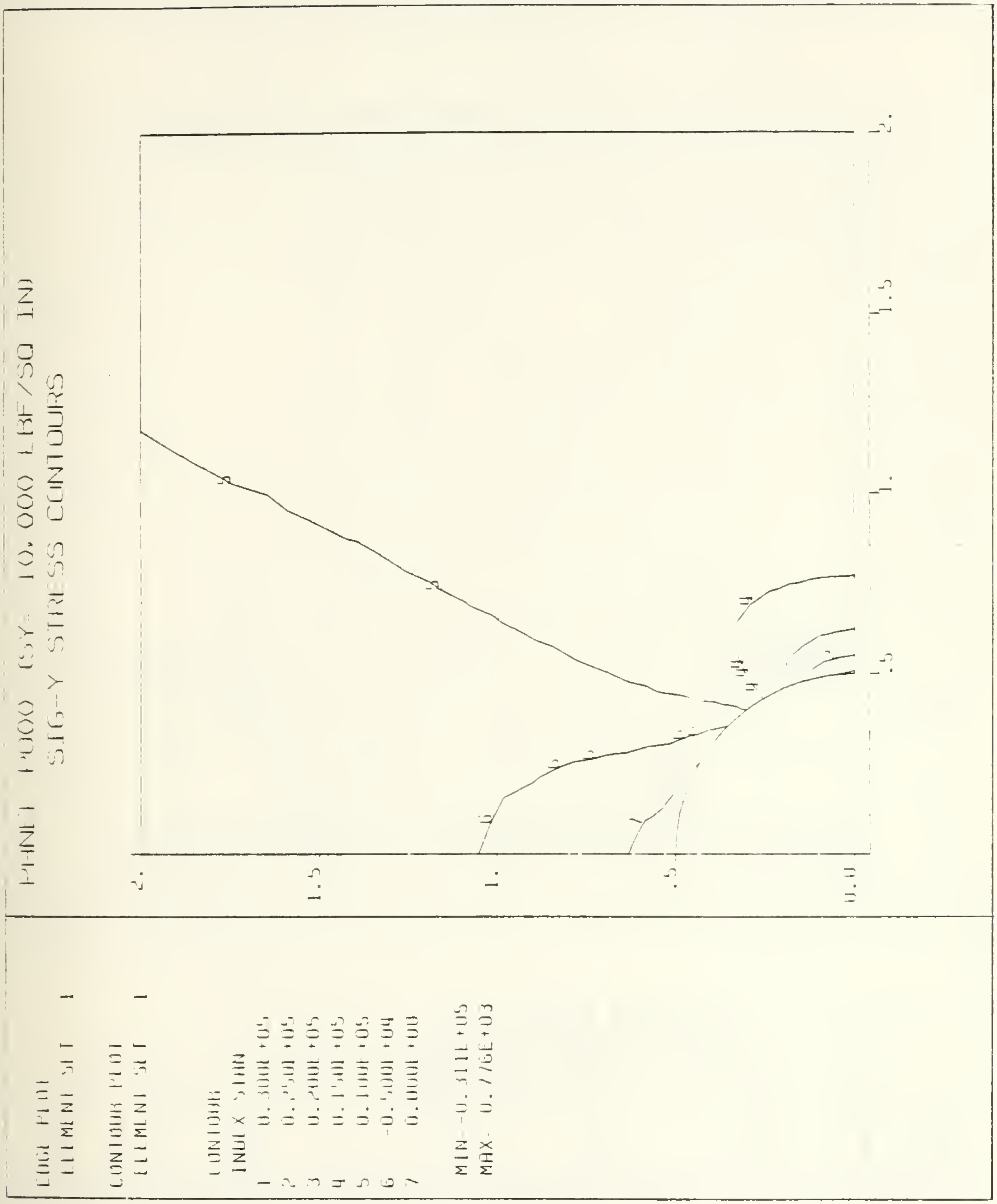

Figure A.9 Panel PØØØ: Sig-Y FEA Contours Near the Cutout.

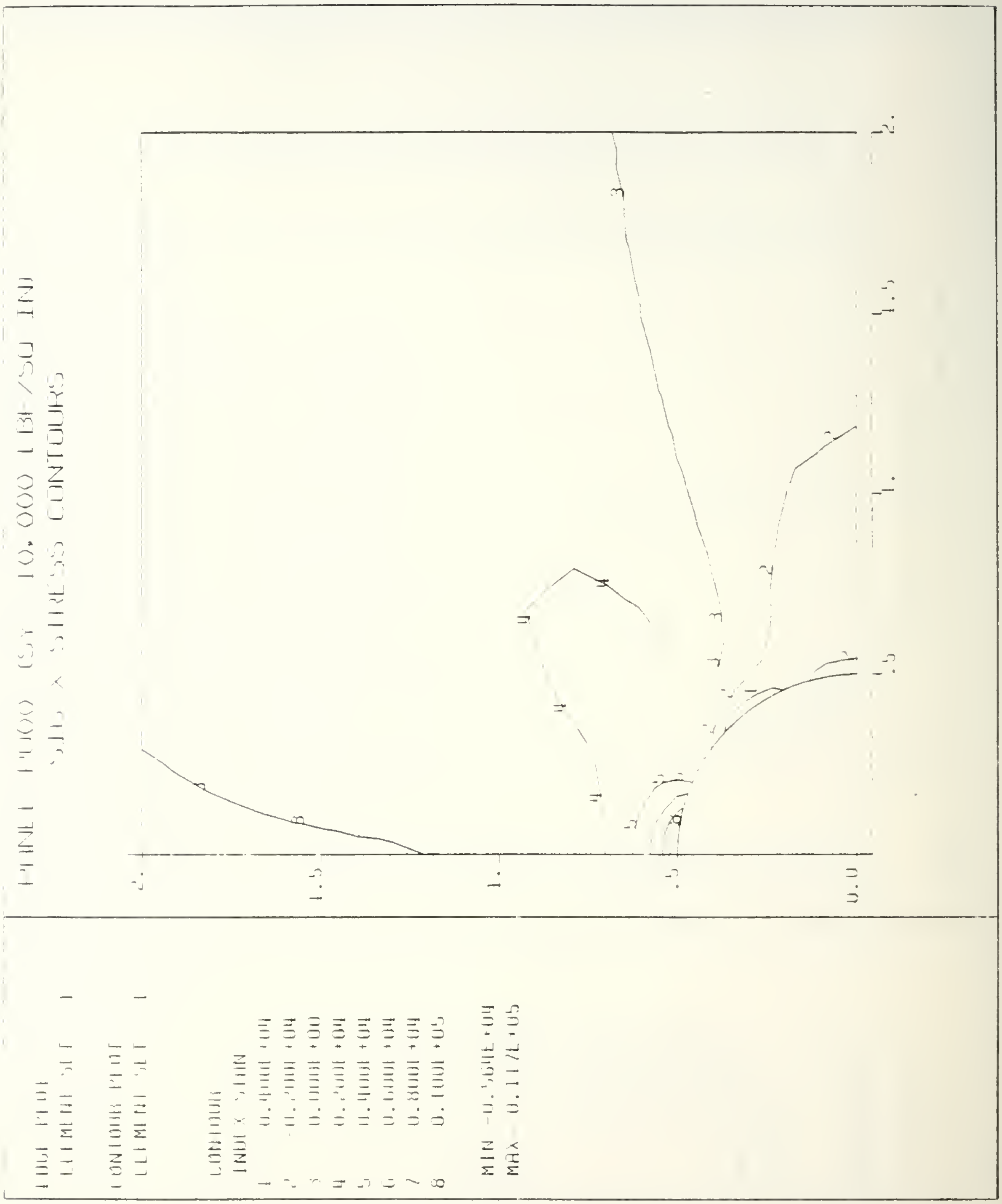

Figure A.10 Panel PO∅∅: Sig-X FEA Contours Near the Cutout.

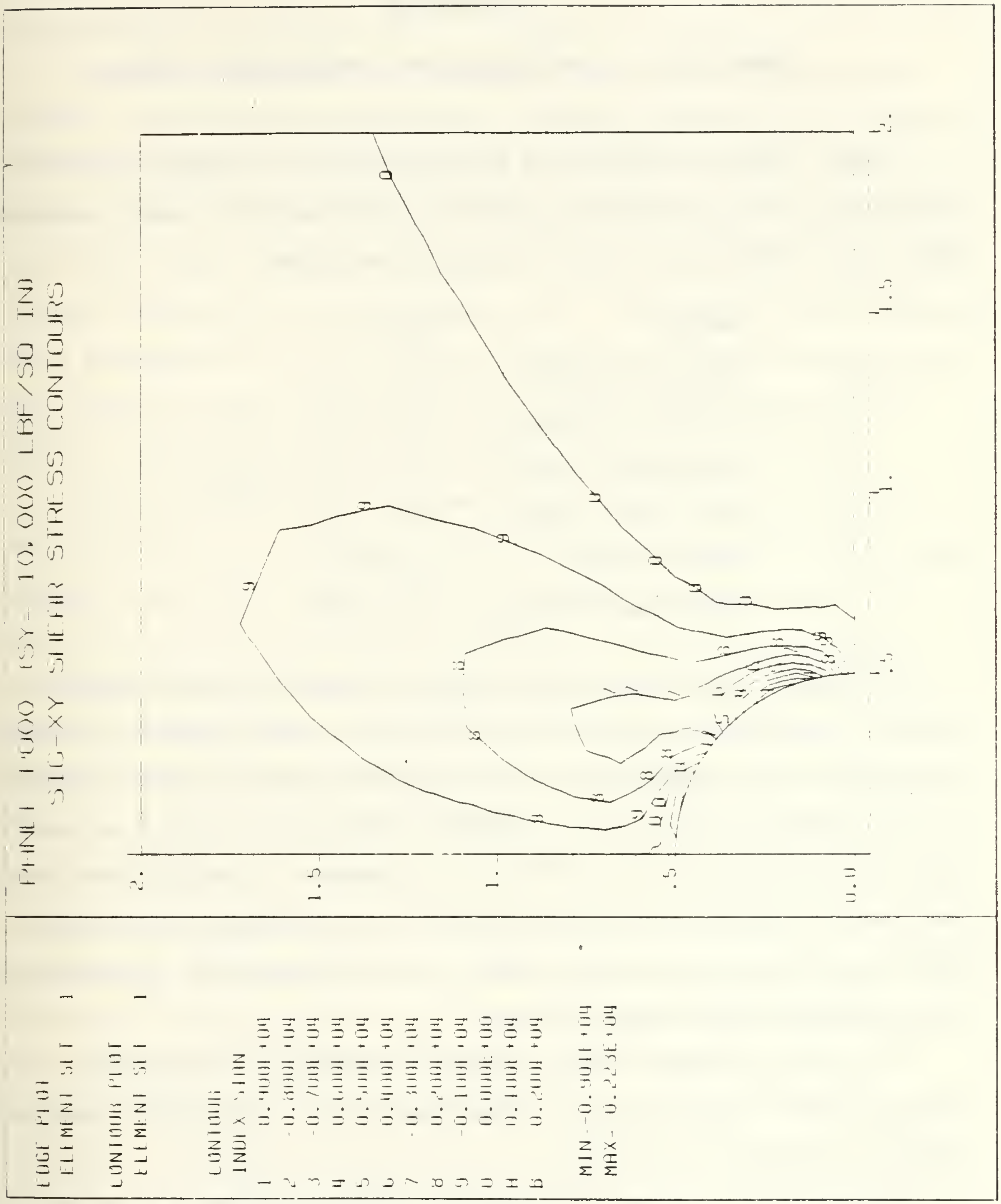

Figure A.11 Panel POØØ: Sig-XY FEA Contours Near the Cutout.

APPENDIX B

PANEL RR11: ANALYTICAL AND EXPERIMENTAL DATA

Panel RR11 was reinforced with one round co-cured ply of G/Ep concentric with the cutout placed on the outside of each facesheet. The reinforcement had the following dimensions:

Shape:	Round
Inside Diameter:	1.00 in
Outside Diameter:	2.24 in
Thickness (each):	0.014 in (1 ply)
Area (each face):	3.16 in^2
Total Volume:	0.088 in^3
Net Cross Section:	0.035 in^2

The panel failed at the hole edge (Type-1) at an applied normal compressive stress of -29,950 psi. Based strictly on the failure of the unreinforced panel and the computed stress concentration factor of 2.65, the predicted failure was $\bar{\sigma}_n$ = -34,500 psi. Failure was at only **87%** of the predicted load. There was no obvious reason for the early failure. No manufacturing errors were apparent on post-test visual or non-destructive inspection of the facesheet-honeycomb bonding.

The finite element model (mesh) is shown in Figure B.1. The area of round reinforcement is denoted by the area inside the bold outline around the cutout.

Figure B.2 compares the computed (finite element) strains around the cutout between the unreinforced panel (PO∅∅) and RR11.

Table XIII gives the computed distribution of strains around the cutout in the Y and X directions as well as shear (Eps-X, Eps-Y and Eps-XY).

Figure B.3 compares the finite element models (solid and dashed lines) and the experimental values (triangles) of strain at -10,000 psi applied normal stress. It shows the very close correlation between the analytically predicted and experimental strain with some minor variation on either side of the panel. The LEFEA strain values are listed in Table XIV. The edge of the reinforcement extended to 1.12" in on the X axis. This is apparent from the figure as the inflection point in the direct compressive strain (solid line) where it abruptly begins to increase.

Figure B.4 shows the stress-strain state during the load sequence from 0 to -30 ksi. Experimentally measured strain gage values are given in Table XV. At -16 ksi the gage next to the hole (x = -0.571") suddenly indicates a severe loss of local stiffness. This is reflected to a smaller, but no less dramatic degree in gage #3 on the other side of the cutout at x = 0.749". Gage #1 demonstrates what appears to be a continuous increase in local stiffness starting at -18 ksi; as the load increases the strain decreases. Between -22 and -24 ksi the strain is rapidly changing from compressive to tensile next to the hole. No visible buckling or delamination, which might help to explain part of this behavior, was noted next to the cutout under visual inspection.

Figures B.5 through B.8 show the LEFEA computed strain contours at an applied normal compressive stress of -10,000 psi computed and plotted using DIAL. Figure B.5 is the full quarter panel with strain parallel to the applied load. This shows some strain contours at the top right of the panel illustrating the effect of not loading the full width of the top edge. Figures B.5 through B.8 (Eps-Y, Eps-X and Eps-XY) show the strains in detail close to the cutout.

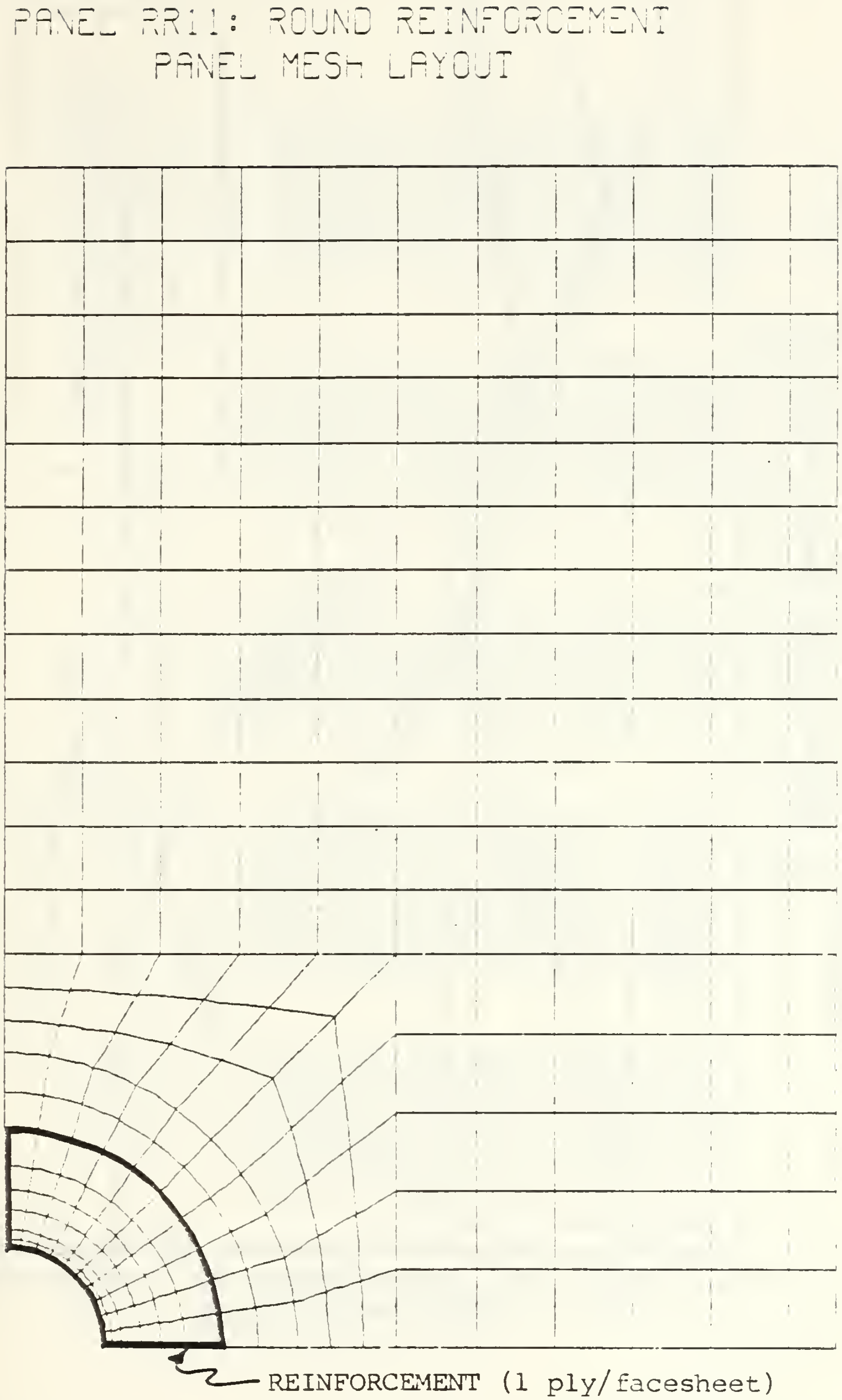

Figure B.1 Panel RR11: DIAL Finite Element Mesh.

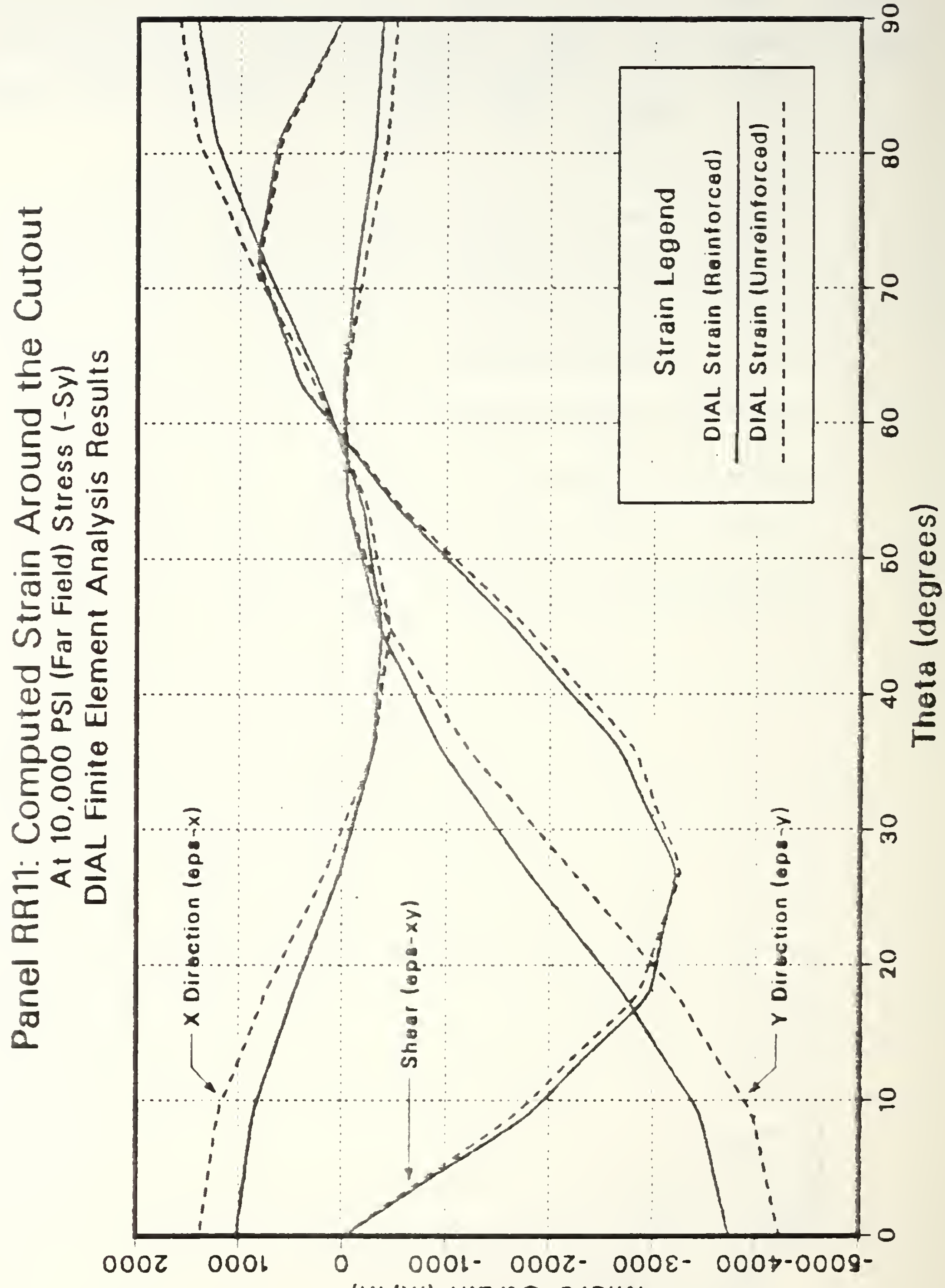

Figure B.2 Panel RR11: Strain Comparison Around the Cutout.

TABLE XIII

PANEL RR11: LEFEA STRAIN DISTRIBUTION AROUND THE CUTOUT (-10,000 PSI).

NODE	X COORD	Y COORD	EPS-Y	EPS-X	EPS-XY
1	0.0000E+00	0.5000E+00	-0.3778E-03	0.1420E-02	0.1837E-04
2	0.3923E-01	0.4985E+00	-0.3408E-03	0.1331E-02	0.3173E-03
3	0.7822E-01	0.4938E+00	-0.3009E-03	0.1236E-02	0.6303E-03
4	0.1167E+00	0.4862E+00	-0.2162E-03	0.1006E-02	0.7349E-03
5	0.1545E+00	0.4755E+00	-0.1300E-03	0.7732E-03	0.8291E-03
6	0.1913E+00	0.4619E+00	-0.6533E-04	0.5037E-03	0.6280E-03
7	0.2270E+00	0.4455E+00	-0.1024E-05	0.2366E-03	0.4173E-03
8	0.2612E+00	0.4263E+00	-0.2328E-04	0.2558E-04	-0.3669E-04
9	0.2939E+00	0.4045E+00	-0.4702E-04	-0.1816E-03	-0.4963E-03
10	0.3247E+00	0.3802E+00	-0.1982E-03	-0.2764E-03	-0.1065E-02
11	0.3536E+00	0.3536E+00	-0.3519E-03	-0.3681E-03	-0.1635E-02
12	0.3802E+00	0.3247E+00	-0.6449E-03	-0.3298E-03	-0.2148E-02
13	0.4045E+00	0.2939E+00	-0.9420E-03	-0.2889E-03	-0.2661E-02
14	0.4263E+00	0.2612E+00	-0.1355E-02	-0.1333E-03	-0.2939E-02
15	0.4455E+00	0.2270E+00	-0.1773E-02	0.2435E-04	-0.3211E-02
16	0.4619E+00	0.1913E+00	-0.2233E-02	0.2454E-03	-0.3094E-02
17	0.4755E+00	0.1545E+00	-0.2696E-02	0.4673E-03	-0.2963E-02
18	0.4862E+00	0.1167E+00	-0.3073E-02	0.6657E-03	-0.2389E-02
19	0.4938E+00	0.7822E-01	-0.3447E-02	0.8626E-03	-0.1800E-02
20	0.4985E+00	0.3923E-01	-0.3598E-02	0.9442E-03	-0.9030E-03
21	0.5000E+00	0.0000E+00	-0.3739E-02	0.1022E-02	-0.2575E-04

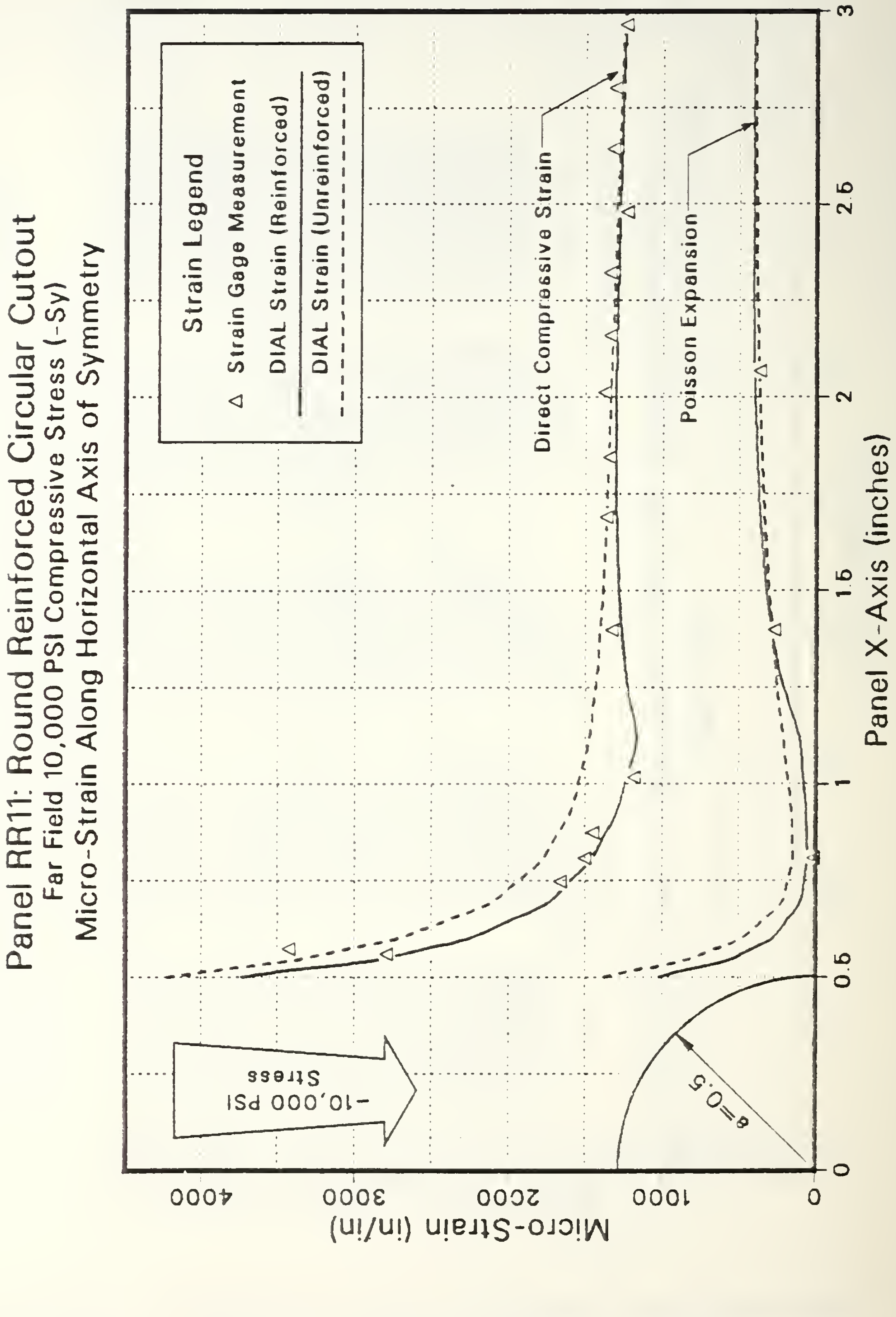

Figure B.3 Panel RR11: Strain Comparison Along the X Axis.

TABLE XIV

PANEL RR11, LEFEA STRAIN DISTRIBUTION ALONG THE X AXIS (-10,000 PSI).

NODE	X COORD	Y COORD	EPS-Y	EPS-X	EPS-XY
21	0.5000E+00	0.0000E+00	-0.3739E-02	0.1022E-02	-0.2575E-04
32	0.5250E+00	0.0000E+00	-0.3261E-02	0.7696E-03	-0.1634E-04
53	0.5500E+00	0.0000E+00	-0.2795E-02	0.5255E-03	-0.5262E-05
64	0.5750E+00	0.0000E+00	-0.2541E-02	0.4111E-03	-0.3572E-05
85	0.6000E+00	0.0000E+00	-0.2267E-02	0.2836E-03	-0.2090E-05
96	0.6500E+00	0.0000E+00	-0.1985E-02	0.1829E-03	0.7482E-06
117	0.7000E+00	0.0000E+00	-0.1723E-02	0.9263E-04	0.1754E-05
128	0.7500E+00	0.0000E+00	-0.1601E-02	0.7537E-04	0.2090E-05
149	0.8000E+00	0.0000E+00	-0.1472E-02	0.5362E-04	0.2743E-05
160	0.8605E+00	0.0000E+00	-0.1389E-02	0.5781E-04	0.2913E-05
181	0.9210E+00	0.0000E+00	-0.1304E-02	0.6139E-04	0.3094E-05
192	0.1021E+01	0.0000E+00	-0.1231E-02	0.8354E-04	0.3340E-05
213	0.1120E+01	0.0000E+00	-0.1163E-02	0.1063E-03	0.4021E-05
224	0.1210E+01	0.0000E+00	-0.1206E-02	0.1768E-03	0.4919E-05
245	0.1300E+01	0.0000E+00	-0.1245E-02	0.2453E-03	0.5330E-05
256	0.1400E+01	0.0000E+00	-0.1268E-02	0.2867E-03	0.2917E-05
277	0.1500E+01	0.0000E+00	-0.1289E-02	0.3273E-03	0.1069E-05
288	0.1583E+01	0.0000E+00	-0.1295E-02	0.3445E-03	0.1617E-05
309	0.1667E+01	0.0000E+00	-0.1303E-02	0.3630E-03	0.1845E-05
320	0.1750E+01	0.0000E+00	-0.1305E-02	0.3744E-03	0.2363E-05
341	0.1833E+01	0.0000E+00	-0.1307E-02	0.3859E-03	0.3022E-05
352	0.1917E+01	0.0000E+00	-0.1306E-02	0.3930E-03	0.4107E-05
373	0.2000E+01	0.0000E+00	-0.1306E-02	0.4005E-03	0.4127E-05
373	0.2000E+01	0.0000E+00	-0.1306E-02	0.4005E-03	0.4127E-05
374	0.2200E+01	0.0000E+00	-0.1297E-02	0.4080E-03	0.2322E-05
375	0.2400E+01	0.0000E+00	-0.1288E-02	0.4142E-03	0.1368E-05
376	0.2600E+01	0.0000E+00	-0.1274E-02	0.4125E-03	0.9859E-06
377	0.2800E+01	0.0000E+00	-0.1260E-02	0.4112E-03	0.6114E-06
378	0.3000E+01	0.0000E+00	-0.1244E-02	0.4067E-03	0.4840E-06
379	0.3200E+01	0.0000E+00	-0.1228E-02	0.4023E-03	0.2911E-06
380	0.3400E+01	0.0000E+00	-0.1211E-02	0.3968E-03	0.2428E-06
381	0.3600E+01	0.0000E+00	-0.1195E-02	0.3914E-03	0.1857E-06
382	0.3800E+01	0.0000E+00	-0.1179E-02	0.3860E-03	0.1393E-06
383	0.4000E+01	0.0000E+00	-0.1163E-02	0.3807E-03	0.8201E-07
384	0.4125E+01	0.0000E+00	-0.1153E-02	0.3775E-03	0.4409E-07
385	0.4250E+01	0.0000E+00	-0.1144E-02	0.3744E-03	0.1498E-07

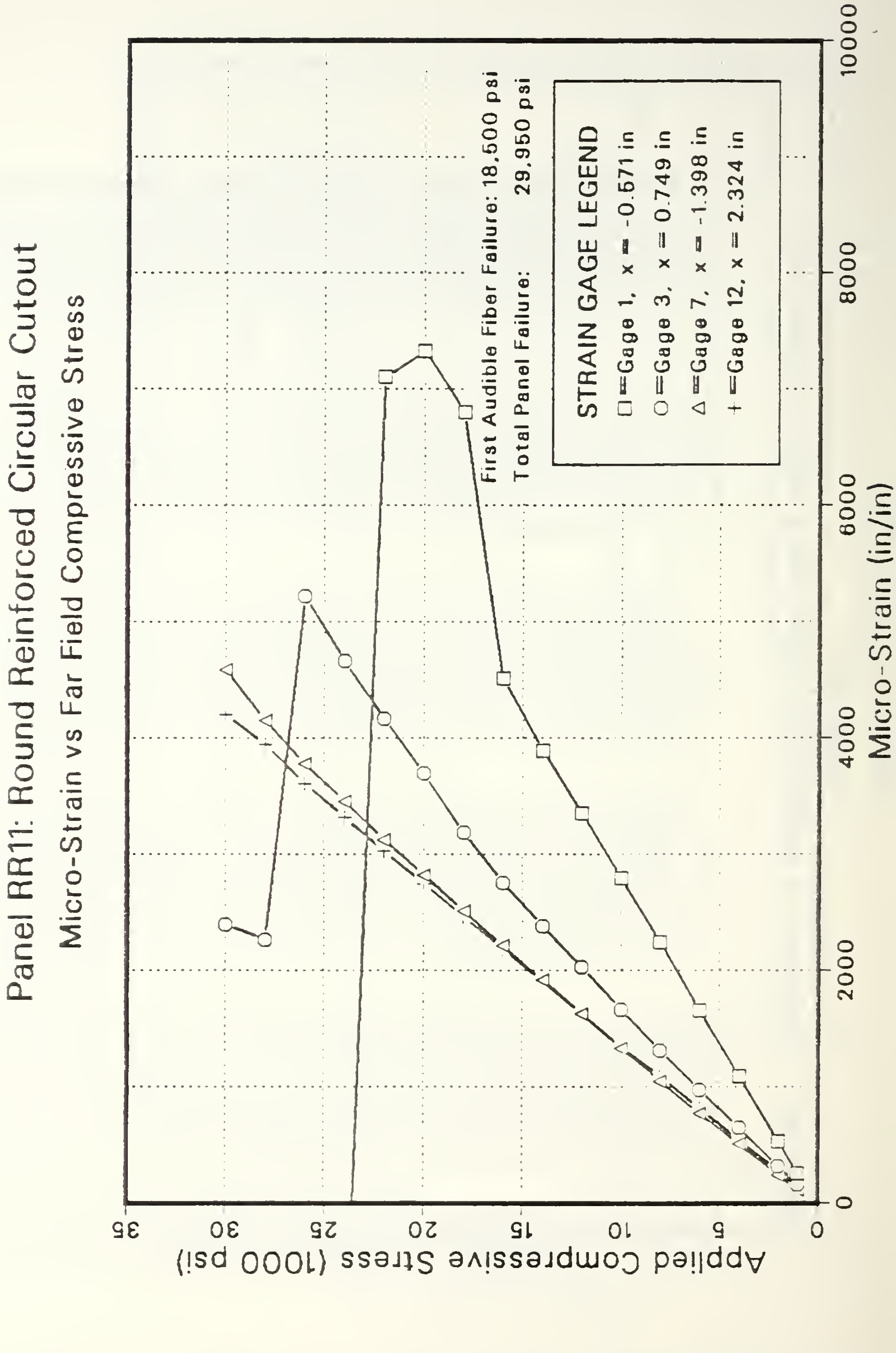

Figure B.4 Panel RR11: Microstrain vs. Compressive Stress.

TABLE XV

PANEL RR11: SELECTED STRAIN GAGE VALUES DURING LOAD.

Load (psi)	Micrc-Strain Indicated by Gage: #1	#3	#7	#12
2000	-254	-156	-110	-146
4000	-530	-320	-240	-278
6000	-1091	-649	-507	-548
8000	-1656	-975	-773	-816
10000	-2241	-1312	-1050	-1089
12000	-2792	-1665	-1334	-1349
14000	-3350	-2026	-1628	-1627
16000	-3893	-2382	-1914	-1905
18000	-4507	-2755	-2211	-2182
20000	-6803	-3183	-2512	-2464
22000	-7326	-3696	-2822	-2747
24000	-7101	-4165	-3125	-3026
26000	+1899	-4661	-3456	-3317
28000	+3785	-5219	-3778	-3609
30000	+3670	-2264	-4149	-3943
32000	+3550	-2396	-4583	-4202

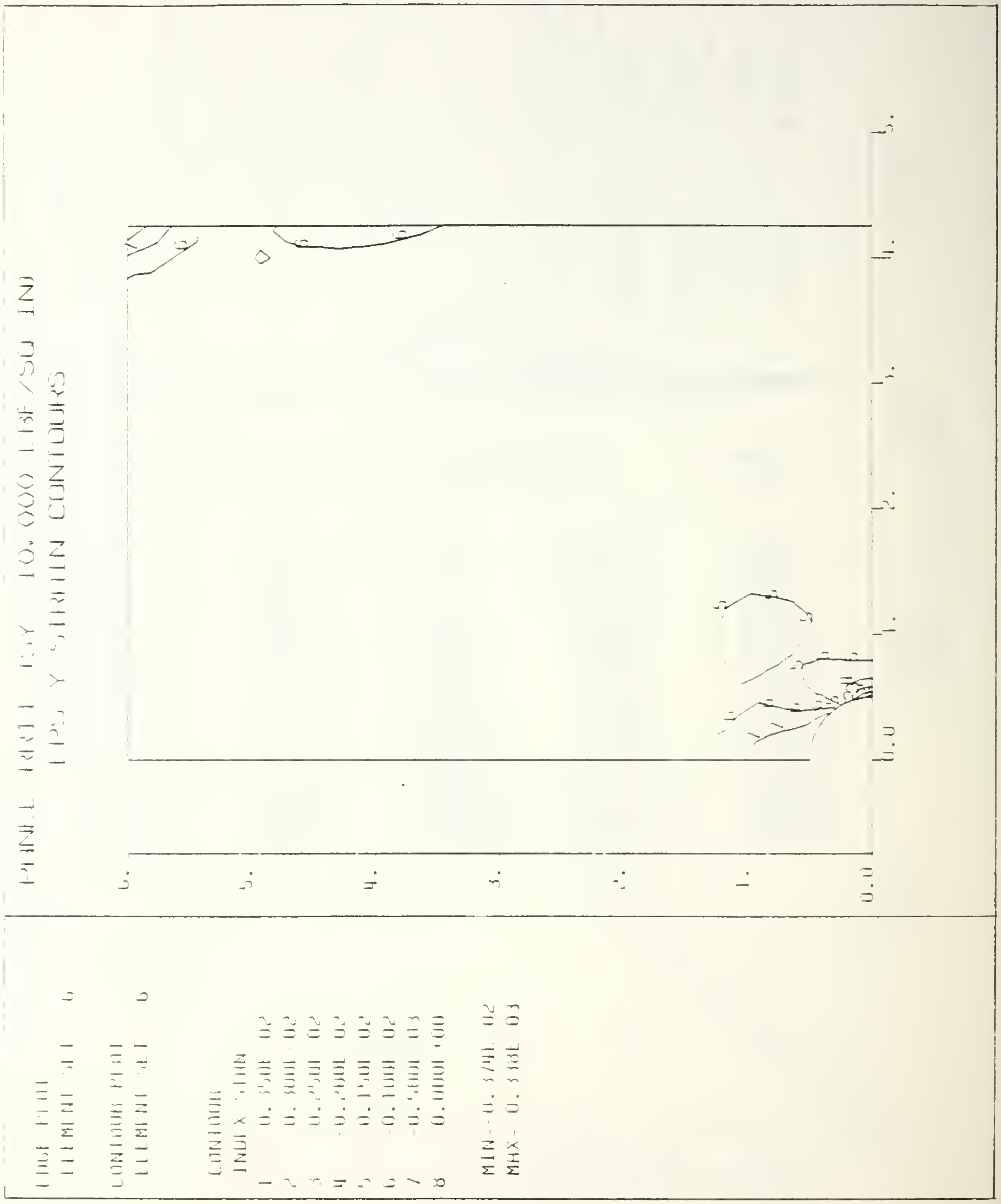

Figure B.5 Panel RR11: Eps-Y FEA Contours.

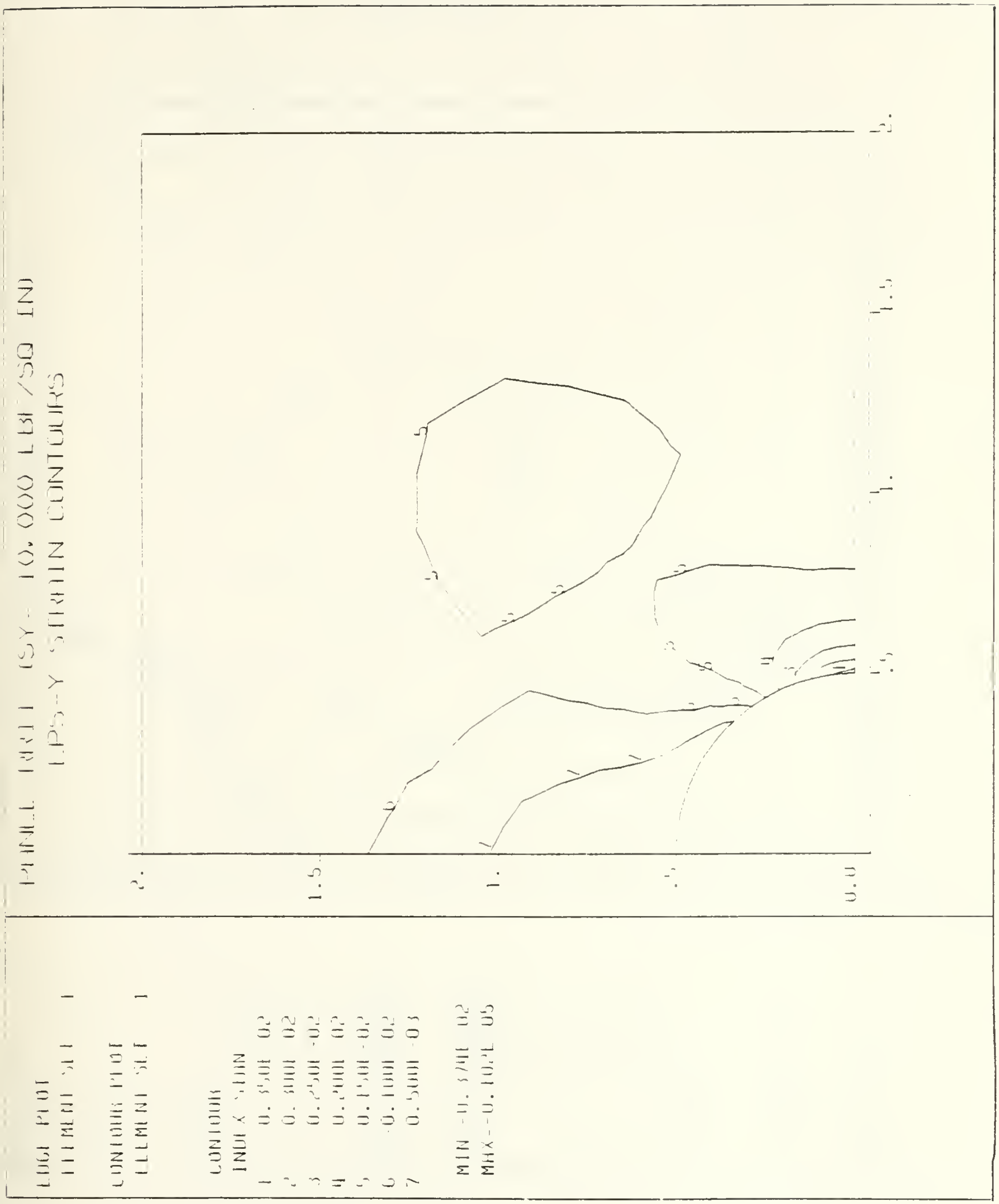

Figure B.6 Panel RR11: Eps-Y FEA Contours Near the Cutout.

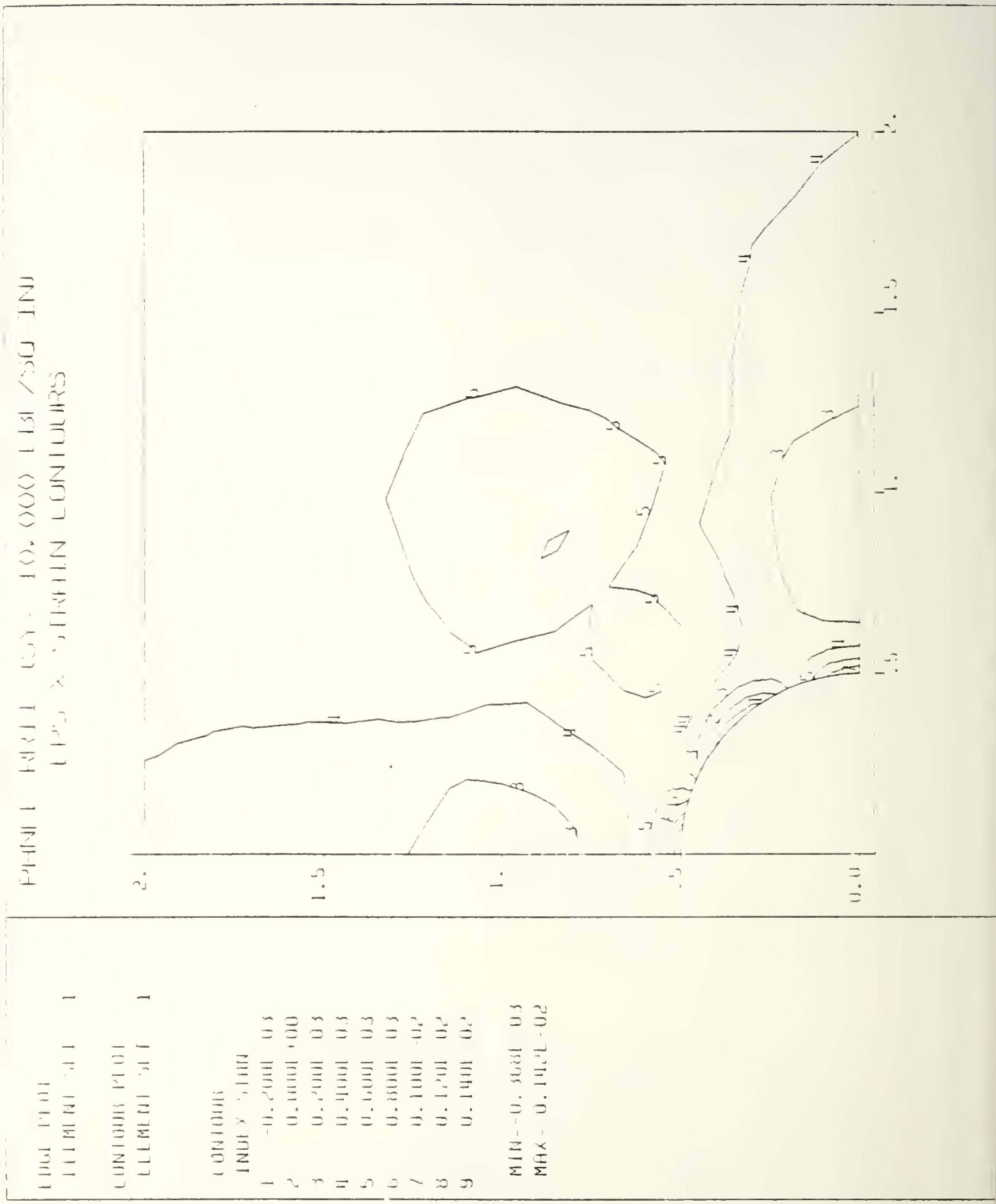

Figure B.7   Panel RR11: Eps-X FEA Contours Near the Cutout.

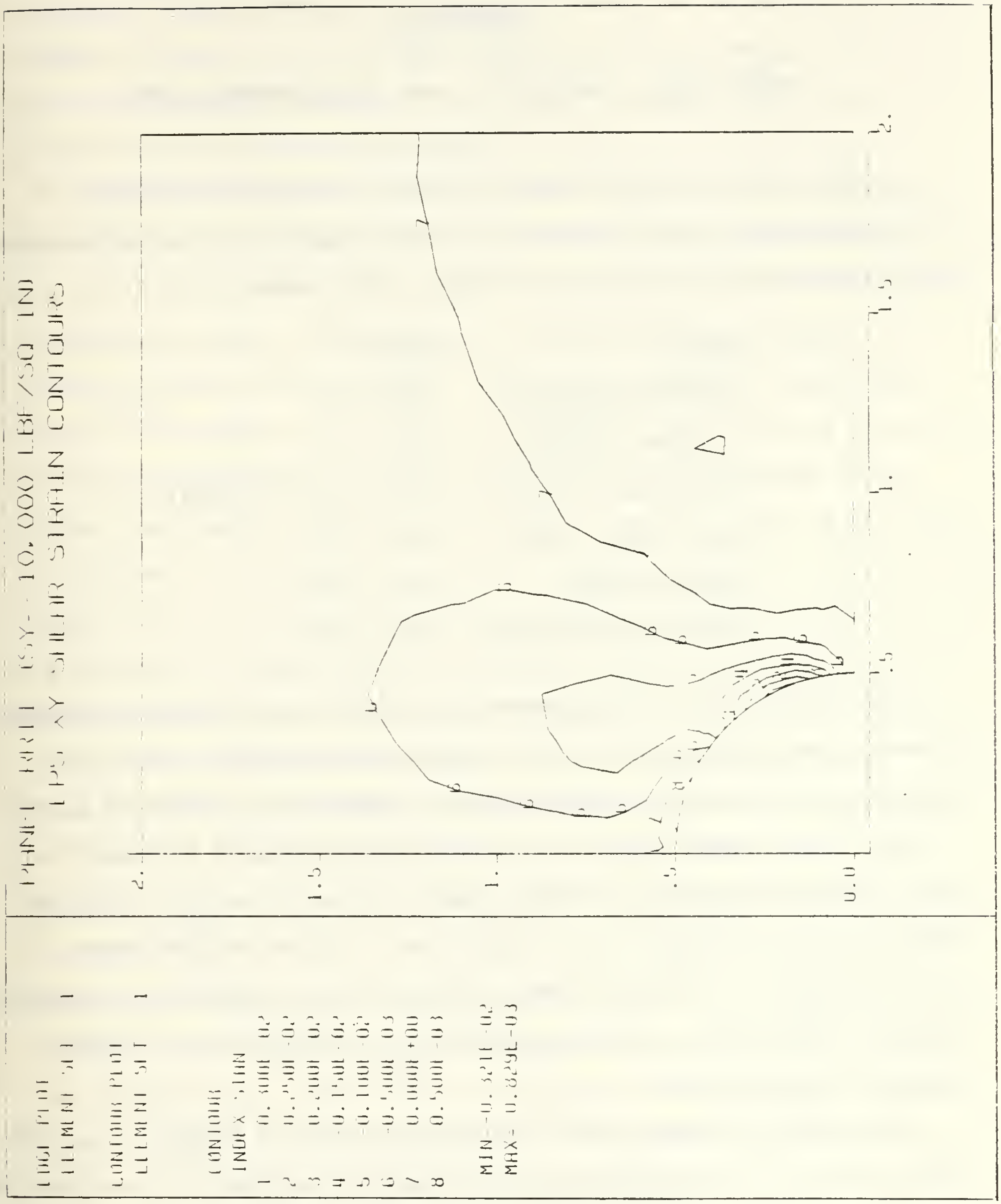

Figure B.8 Panel RR11: Eps-XY FEA Contours Near the Cutout.

APPENDIX C

PANEL RR22: ANALYTICAL AND EXPERIMENTAL DATA

Panel RR22 was reinforced with two round co-cured plies of G/Ep concentric with the cutout on the outside of each facesheet. The reinforcement had the following dimensions:

Shape:	Round	
Inside Diameter:	1.00 in	
Outside Diameter:	2.24 in	
Thickness (each):	0.028 in	(2 plies)
Area (each face):	3.16 in^2	
Total Volume:	0.176 in^3	
Net Cross Section:	0.069 in^2	

The panel failed by facesheet separation and buckling (Type-2) almost immediately upon initial application of the load. It failed totally at an applied normal compressive stress ($\bar{\sigma}_n$) of -21,050 psi. Based strictly on the failure of the unreinforced panel and the computed stress concentration factor of 2.39, the predicted failure was $\bar{\sigma}_n$ = -38,250 psi. This reinforcement configuration should have been among the most efficient: stacking the most additional thickness closest to the point of highest stress concentration.

The finite element model (mesh) is shown in Figure C.1. The round area of reinforcement is outlined by the heavy lines next to the cutout. The reinforcement is two plies thick on the outside of both facesheets.

Figure C.2 shows the comparison between finite element computed strains around the cutout between the unreinforced panel (POØØ) and RR22 at -10,000 psi applied normal stress. Table XVI gives the computed values of the three strains (Eps-Y, Eps-X and Eps-XY) for the reinforced panel.

Figure C.3 compares the analytical (solid and dashed lines) and experimentally measured strain values (triangles) at $\bar{\sigma}_n = -10$ ksi. The alternating strain gage values between x = 1.0" and 2.5" indicate the small experimental difference between gages on opposite sides of the cutout. While the facesheet separation began at the onset of the load, it covered only a small area and the strain gages were on the opposite side of the panel still giving reasonable indications at $\bar{\sigma}_n = -10$ ksi. The edge of the reinforcement extended to x = 1.12". This can be seen clearly in Figure C.3 as the point where the strain along the X axis has an inflection point and begins increasing after a steady decrease moving away from the cutout edge. Table XVII gives the (finite element) computed distribution of strains around the cutout in the Y and X directions as well as shear (Eps-Y, Eps-X and Eps-XY).

Figure C.4 shows the stress-strain state during the load sequence from 0 to -20 ksi. Numerical strain gage data are given in Table XVIII. Gages #1, #3 and #4 all indicate a decreasing compressive strain rate with load application. It appears that a facesheet separated from the honeycomb core at or shortly after load application. When this is compared with the strain levels shown in Figure C.3, it appears that significant separation did not occur until after the -10 ksi load level.

Figures C.5 through C.8 show the analytical strain contours at an applied normal compressive stress of -10,000 psi computed and plotted using DIAL. Figure C.5 is the full quarter panel with strain parallel to the applied load. This shows some strain contours at the top right of the panel illustrating the effect of not loading the full width of the top edge. Figures C.5 through C.8 (Eps-Y, Eps-X and Eps-XY) show the strains in detail close to the cutout.

Panel RR22 should have been the most efficient reinforcement configuration with the best ratio of volume-to-strength. While the volume of reinforcement was small, most of it was concentrated adjacent to the hole in the area of highest stress concentration.

Note: After this research program showed premature panel failure due to facesheet separation, two additional RR22 panels were fabricated by LMSC using identical materials (a different lot, however) and methods. They failed at $\bar{\sigma}_n$ = -41.5 and -38.0 ksi or an average 104% of the predicted applied normal stress of -38.3 ksi.

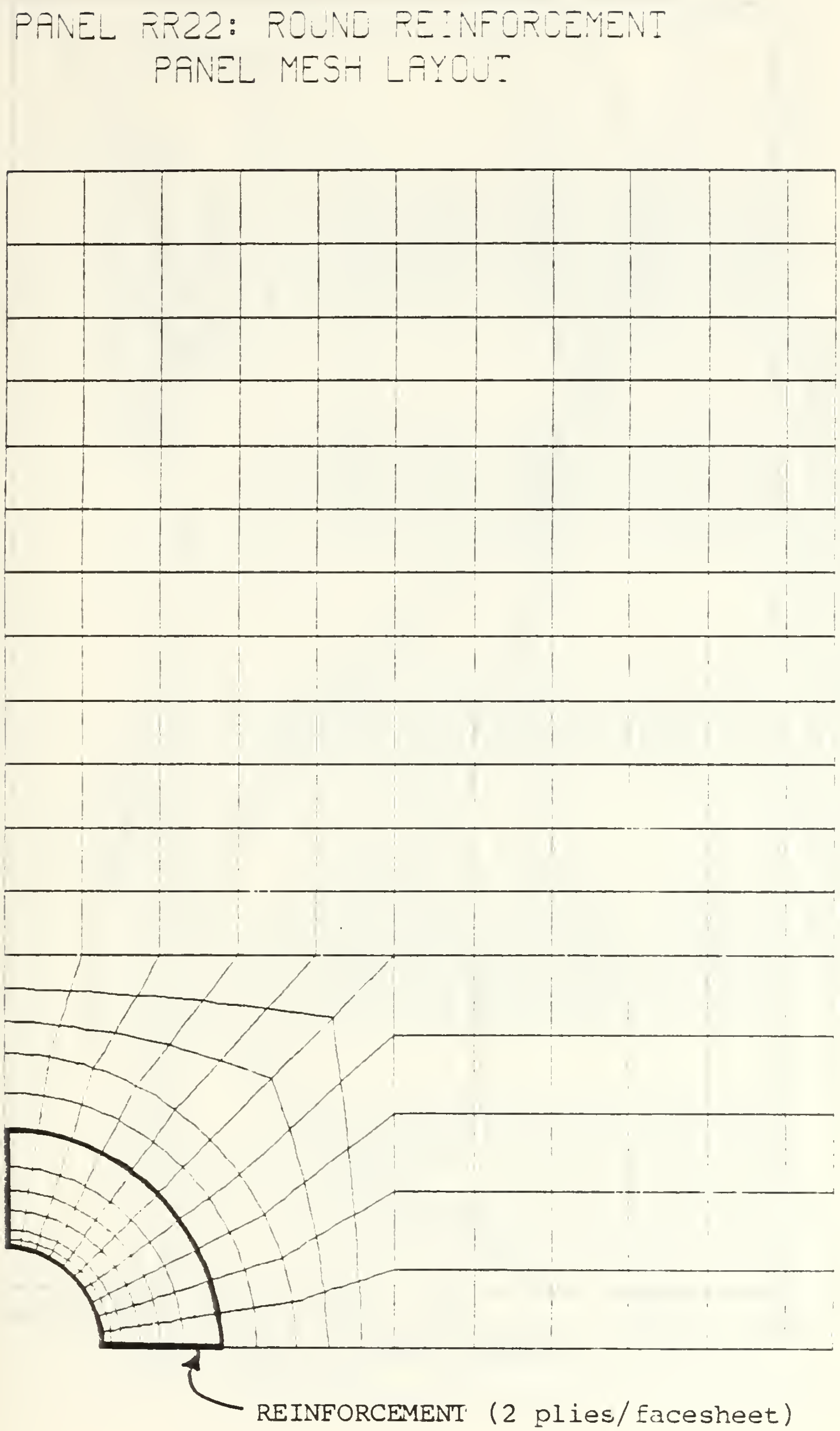

Figure C.1 Panel RR22: DIAL Finite Element Mesh.

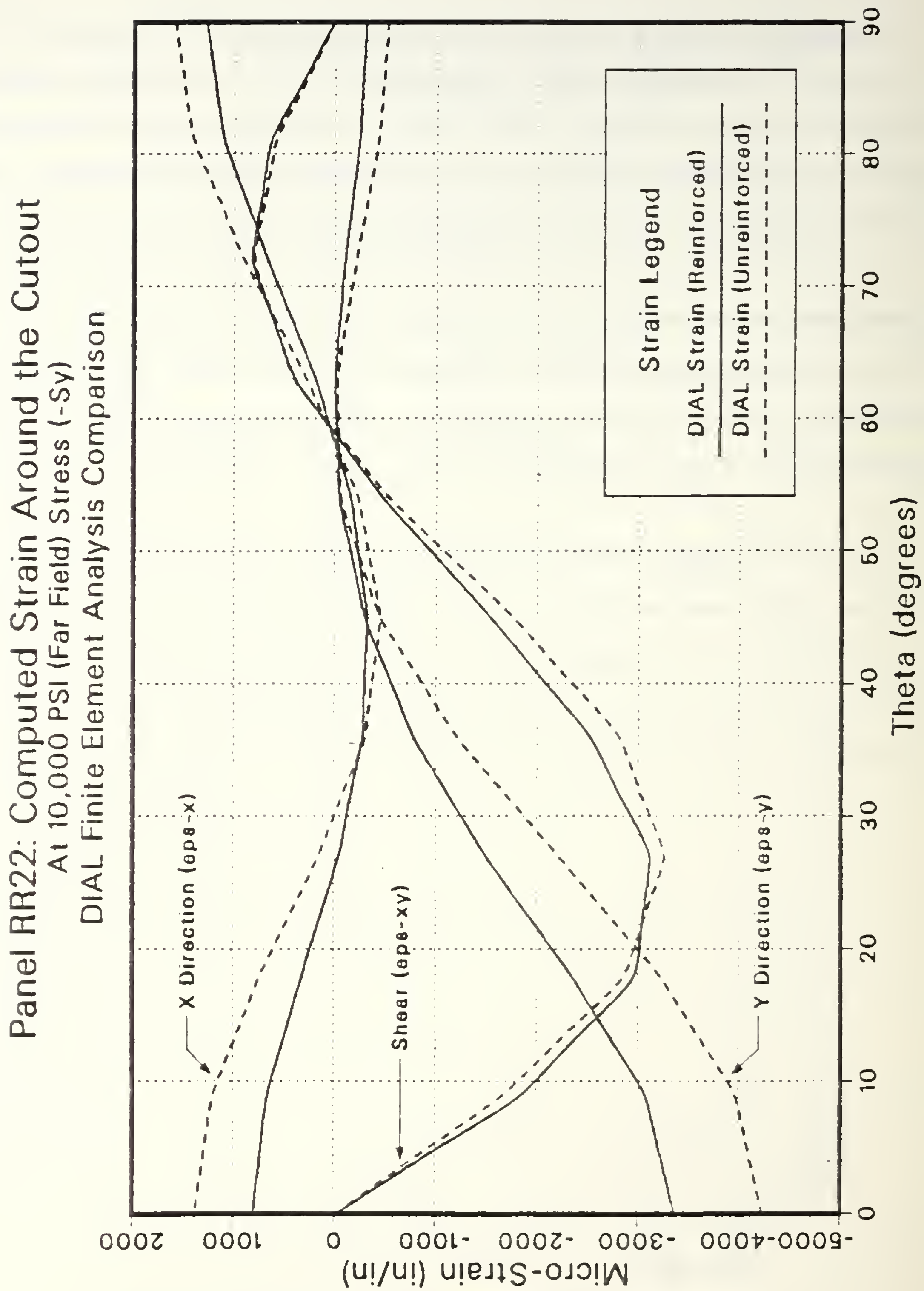

Figure C.2 Panel RR22: Strain Comparison Around the Cutout.

TABLE XVI

PANEL RR22: LEFEA STRAIN DISTRIBUTION AROUND THE CUTOUT (-10,000 PSI).

NODE	X COORD	Y COORD	EPS-Y	EPS-X	EPS-XY
1	0.0000E+00	0.5000E+00	-0.2968E-03	0.1284E-02	0.1872E-04
2	0.3923E-01	0.4985E+00	-0.2651E-03	0.1199E-02	0.3242E-03
3	0.7822E-01	0.4938E+00	-0.2312E-03	0.1106E-02	0.6434E-03
4	0.1167E+00	0.4862E+00	-0.1615E-03	0.8912E-03	0.7402E-03
5	0.1545E+00	0.4755E+00	-0.9080E-04	0.6747E-03	0.8259E-03
6	0.1913E+00	0.4619E+00	-0.4243E-04	0.4349E-03	0.6187E-03
7	0.2270E+00	0.4455E+00	0.5853E-05	0.1990E-03	0.4025E-03
8	0.2612E+00	0.4263E+00	-0.1799E-04	0.2001E-04	-0.3225E-04
9	0.2939E+00	0.4045E+00	-0.4232E-04	-0.1549E-03	-0.4710E-03
10	0.3247E+00	0.3802E+00	-0.1674E-03	-0.2361E-03	-0.1002E-02
11	0.3536E+00	0.3536E+00	-0.2934E-03	-0.3152E-03	-0.1534E-02
12	0.3802E+00	0.3247E+00	-0.5337E-03	-0.2929E-03	-0.2025E-02
13	0.4045E+00	0.2939E+00	-0.7772E-03	-0.2693E-03	-0.2517E-02
14	0.4263E+00	0.2612E+00	-0.1130E-02	-0.1526E-03	-0.2817E-02
15	0.4455E+00	0.2270E+00	-0.1489E-02	-0.3471E-04	-0.3113E-02
16	0.4619E+00	0.1913E+00	-0.1909E-02	0.1441E-03	-0.3045E-02
17	0.4755E+00	0.1545E+00	-0.2335E-02	0.3237E-03	-0.2965E-02
18	0.4862E+00	0.1167E+00	-0.2702E-02	0.4944E-03	-0.2416E-02
19	0.4938E+00	0.7822E-01	-0.3067E-02	0.6641E-03	-0.1849E-02
20	0.4985E+00	0.3923E-01	-0.3221E-02	0.7367E-03	-0.9286E-03
21	0.5000E+00	0.0000E+00	-0.3363E-02	0.8066E-03	-0.2845E-04

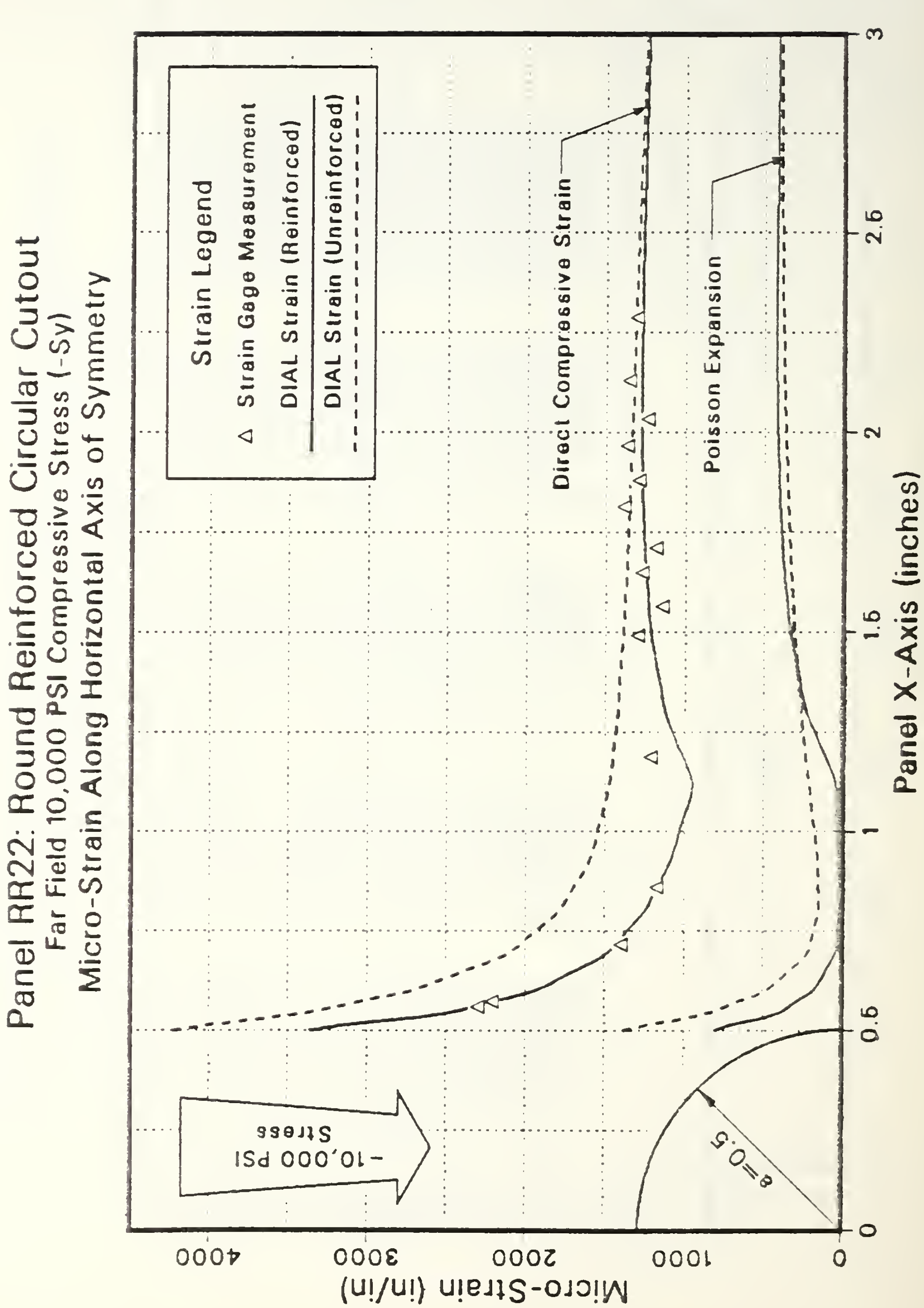

Figure C.3 Panel RR22: Strain Comparison Along the X Axis.

TABLE XVII

PANEL RR22, LEFEA STRAIN DISTRIBUTION ALONG THE X AXIS (-10,000 PSI).

NODE	X COORD	Y COORD	EPS-Y	EPS-X	EPS-XY
21	0.5000E+00	0.0000E+00	-0.3363E-02	0.8066E-03	-0.2845E-04
32	0.5250E+00	0.0000E+00	-0.2886E-02	0.5846E-03	-0.1699E-04
53	0.5500E+00	0.0000E+00	-0.2426E-02	0.3726E-03	-0.3140E-05
64	0.5750E+00	0.0000E+00	-0.2200E-02	0.2838E-03	-0.1134E-05
85	0.6000E+00	0.0000E+00	-0.1950E-02	0.1820E-03	-0.8063E-06
96	0.6500E+00	0.0000E+00	-0.1702E-02	0.1056E-03	0.1003E-05
117	0.7000E+00	0.0000E+00	-0.1472E-02	0.3704E-04	0.1690E-05
128	0.7500E+00	0.0000E+00	-0.1365E-02	0.2503E-04	0.1758E-05
149	0.8000E+00	0.0000E+00	-0.1250E-02	0.9333E-05	0.2133E-05
160	0.8605E+00	0.0000E+00	-0.1174E-02	0.1340E-04	0.2311E-05
181	0.9210E+00	0.0000E+00	-0.1095E-02	0.1702E-04	0.2469E-05
192	0.1021E+01	0.0000E+00	-0.1022E-02	0.3518E-04	0.2965E-05
213	0.1120E+01	0.0000E+00	-0.9526E-03	0.4477E-04	0.4317E-05
224	0.1210E+01	0.0000E+00	-0.1040E-02	0.1344E-03	0.5697E-05
245	0.1300E+01	0.0000E+00	-0.1124E-02	0.2310E-03	0.6269E-05
256	0.1400E+01	0.0000E+00	-0.1172E-02	0.2851E-03	0.3581E-05
277	0.1500E+01	0.0000E+00	-0.1219E-02	0.3383E-03	0.1379E-05
288	0.1583E+01	0.0000E+00	-0.1236E-02	0.3588E-03	0.1891E-05
309	0.1667E+01	0.0000E+00	-0.1254E-02	0.3813E-03	0.2309E-05
320	0.1750E+01	0.0000E+00	-0.1264E-02	0.3939E-03	0.2662E-05
341	0.1833E+01	0.0000E+00	-0.1273E-02	0.4065E-03	0.3067E-05
352	0.1917E+01	0.0000E+00	-0.1277E-02	0.4133E-03	0.3782E-05
373	0.2000E+01	0.0000E+00	-0.1281E-02	0.4206E-03	0.3413E-05
374	0.2200E+01	0.0000E+00	-0.1278E-02	0.4255E-03	0.1748E-05
375	0.2400E+01	0.0000E+00	-0.1274E-02	0.4290E-03	0.7959E-06
376	0.2600E+01	0.0000E+00	-0.1262E-02	0.4244E-03	0.5279E-06
377	0.2800E+01	0.0000E+00	-0.1250E-02	0.4204E-03	0.3103E-06
378	0.3000E+01	0.0000E+00	-0.1235E-02	0.4137E-03	0.2277E-06
379	0.3200E+01	0.0000E+00	-0.1221E-02	0.4071E-03	0.9059E-07
380	0.3400E+01	0.0000E+00	-0.1206E-02	0.4002E-03	0.7603E-07
381	0.3600E+01	0.0000E+00	-0.1192E-02	0.3934E-03	0.6269E-07
382	0.3800E+01	0.0000E+00	-0.1179E-02	0.3877E-03	0.4249E-07
383	0.4000E+01	0.0000E+00	-0.1167E-02	0.3823E-03	0.2358E-07
384	0.4125E+01	0.0000E+00	-0.1160E-02	0.3800E-03	0.1403E-07
385	0.4250E+01	0.0000E+00	-0.1154E-02	0.3777E-03	0.1117E-08

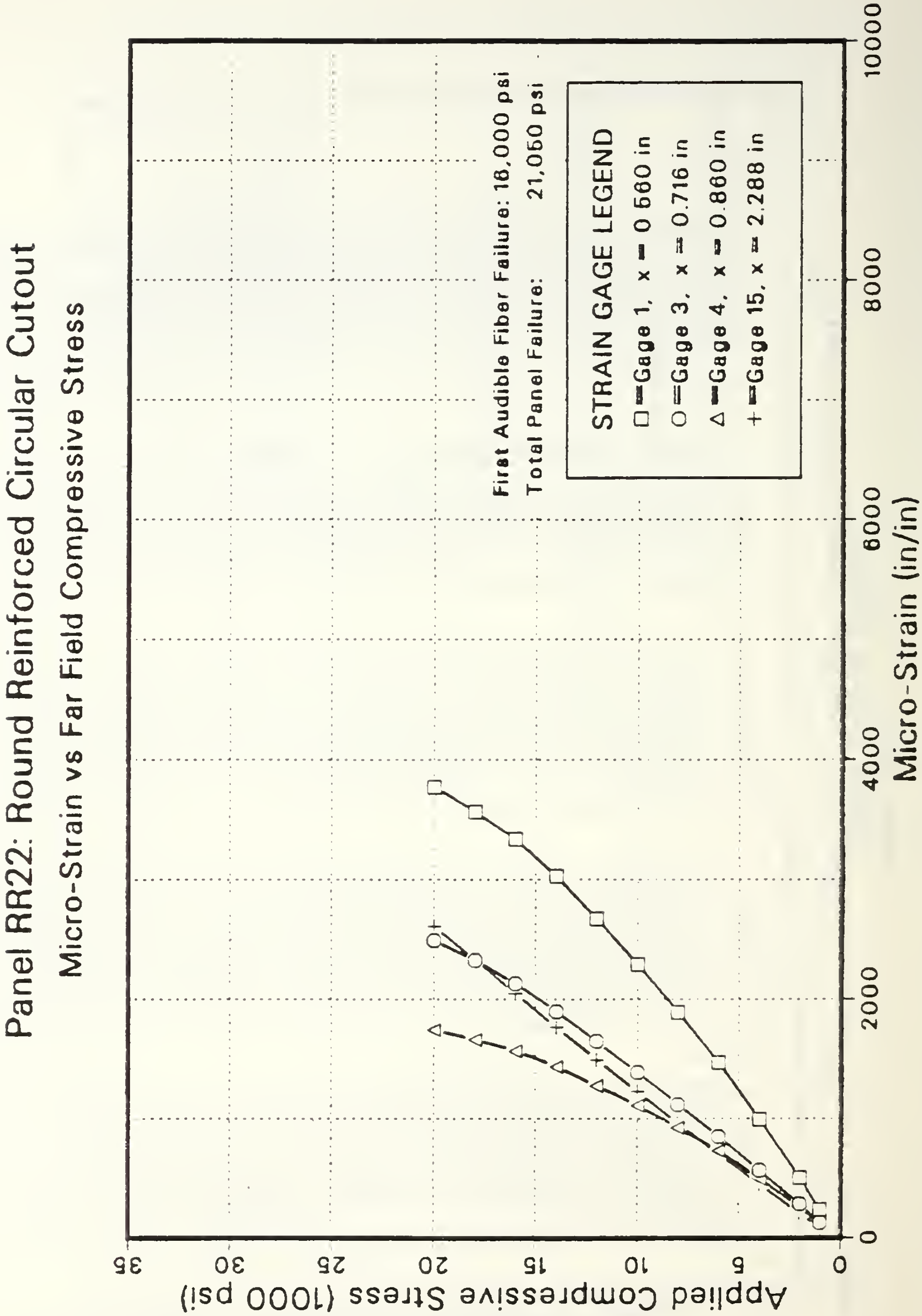

Figure C.4 Panel RR22: Microstrain vs. Compressive Stress.

TABLE XVIII

PANEL RR22: SELECTED STRAIN GAGE VALUES DURING LOAD.

Load (psi)	Micro-Strain Indicated by Gage: #1	#3	#4	#15
1000	-233	-126	-120	-75
2000	-504	-281	-253	-205
4000	-995	-566	-499	-449
6000	-1470	-850	-729	-701
8000	-1891	-1120	-924	-960
10000	-2290	-1387	-1108	-1225
12000	-2666	-1645	-1277	-1493
14000	-3026	-1900	-1437	-1765
16000	-3335	-2134	-1568	-2046
18000	-3566	-2321	-1661	-2328
20000	-3775	-2491	-1742	-2608

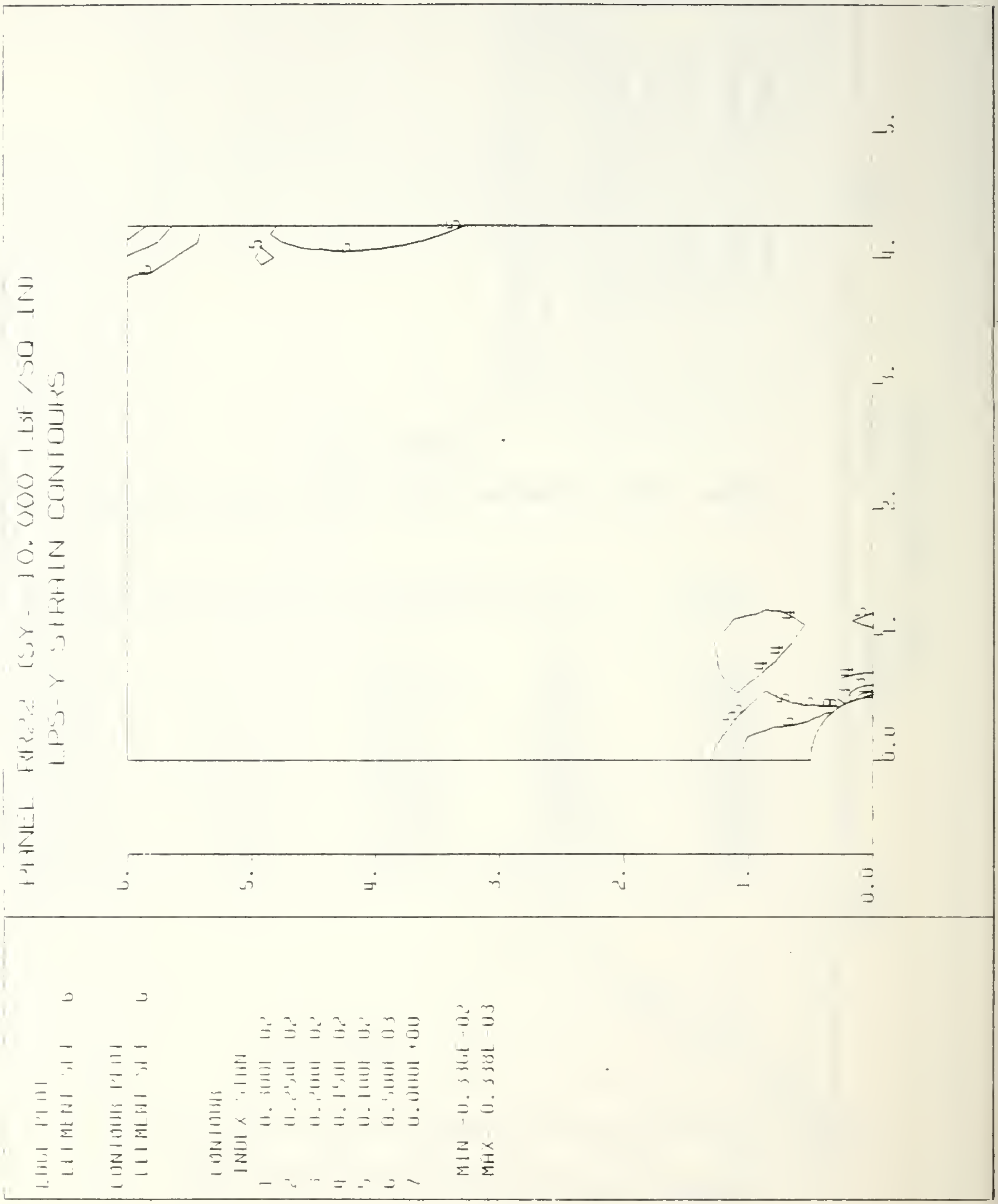

Figure C.5 Panel RR22: Eps-Y FEA Contours.

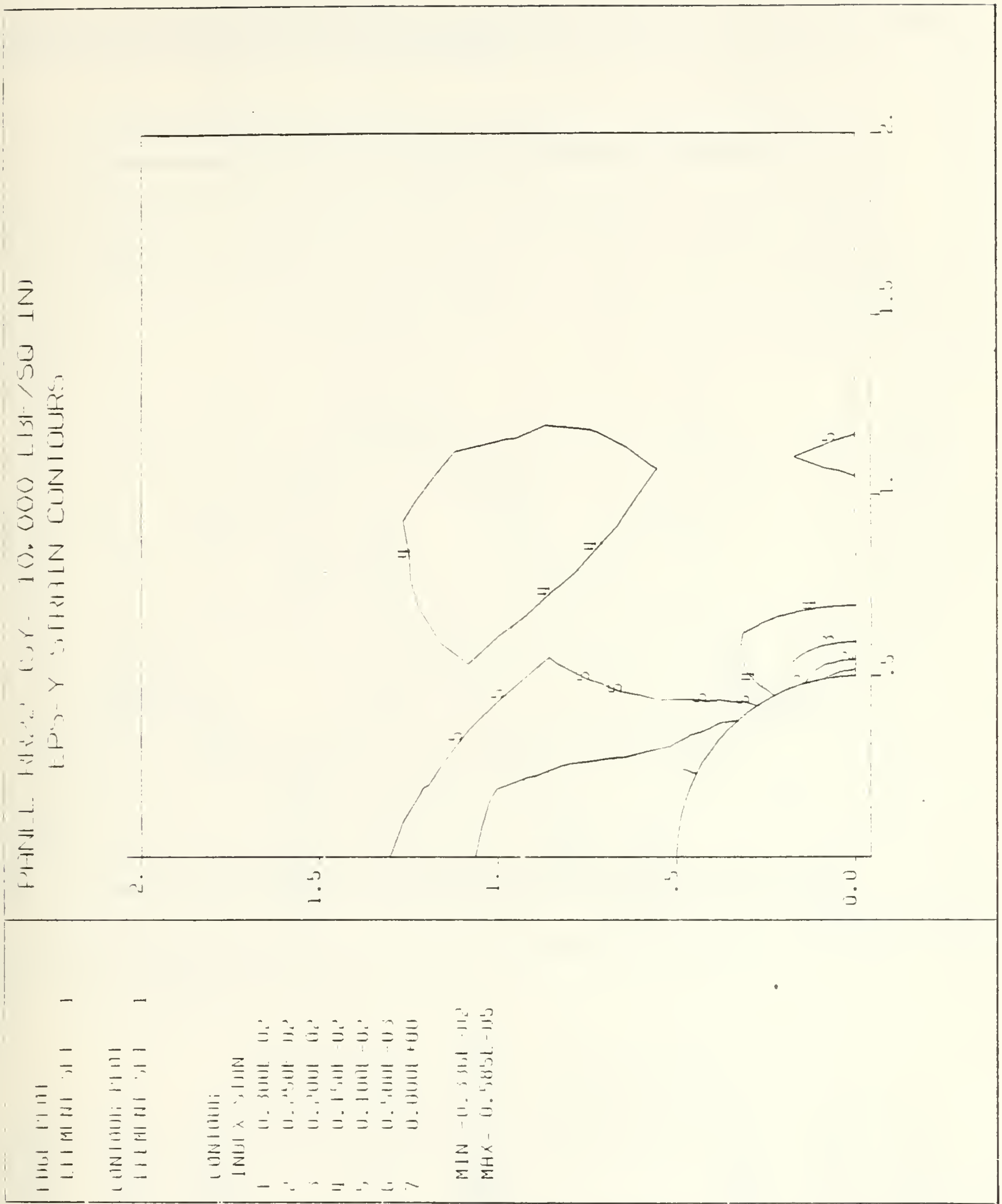

Figure C.6   Panel RR22: Eps-Y FEA Contours Near the Cutout.

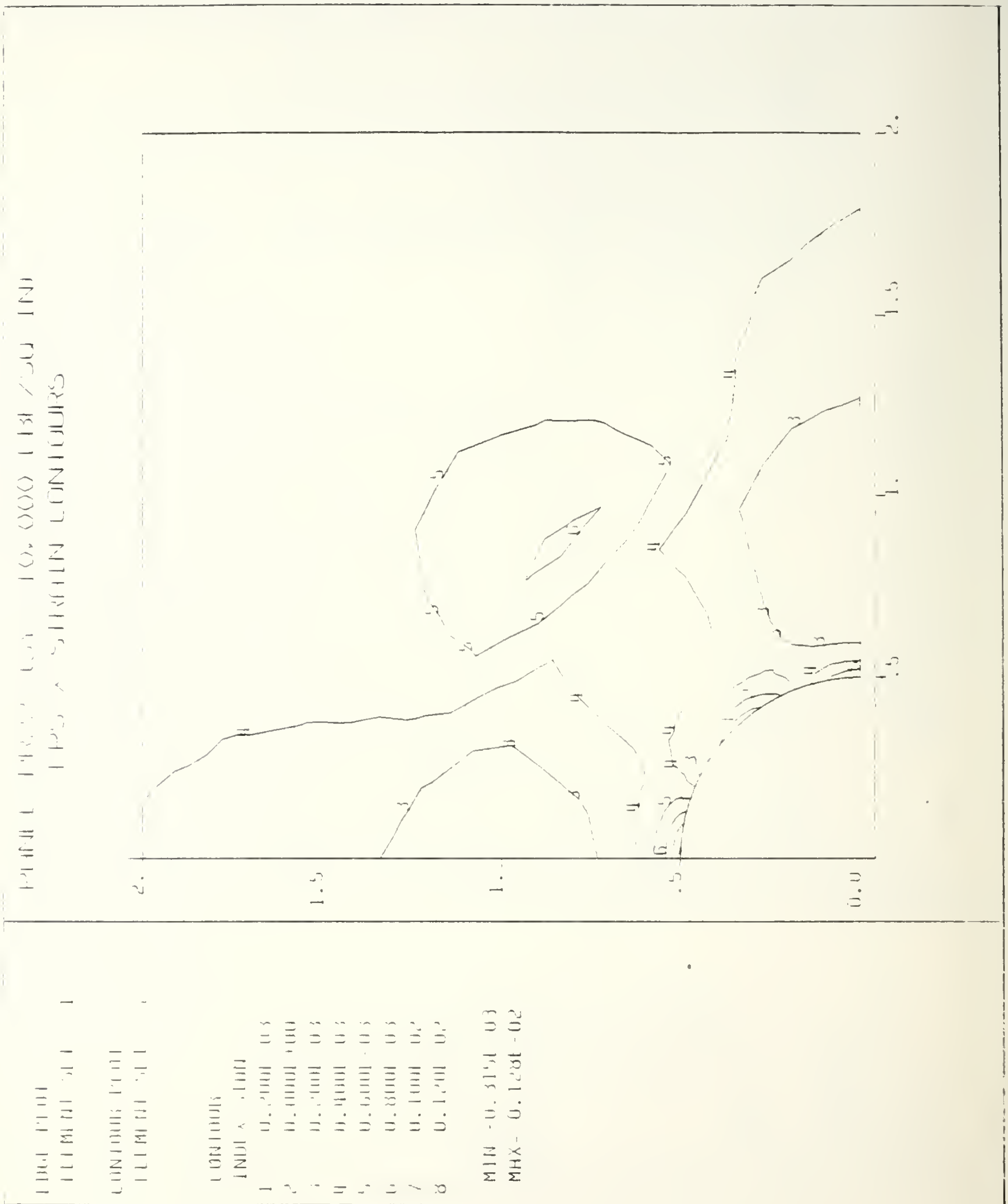

Figure C.7 Panel RR22: Eps-X FEA Contours Near the Cutout.

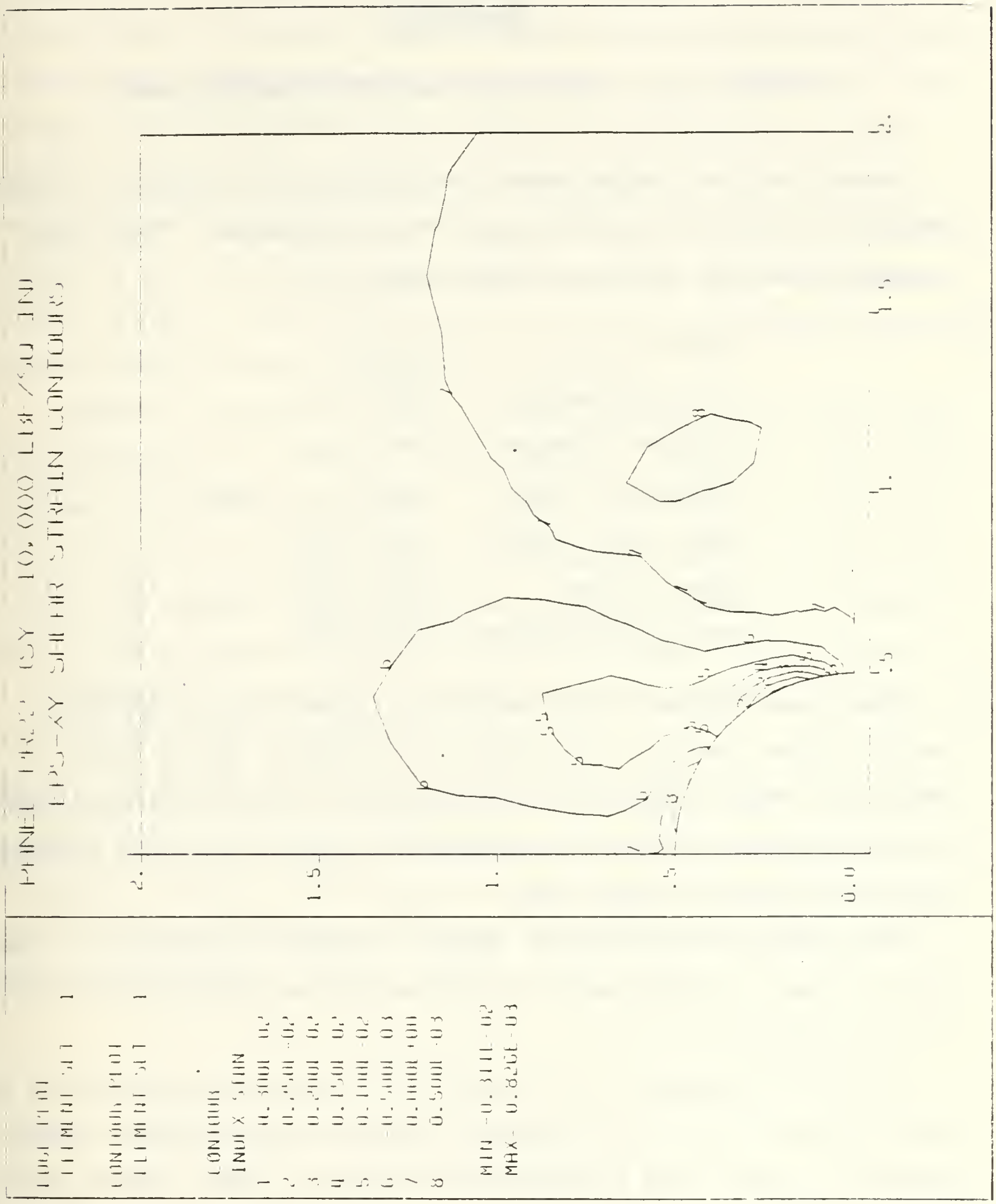

Figure C.8 Panel RR22: Eps-XY FEA Contours Near the Cutout.

APPENDIX D

PANEL RR31: ANALYTICAL AND EXPERIMENTAL DATA

Panel RR31 was reinforced with one round co-cured ply of G/EP around the cutout on the outside of each facesheet. The reinforcement had the following dimensions:

Shape:	Round
Inside Diameter:	1.00 in
Outside Diameter:	3.60 in
Thickness (each):	0.014 in (1 ply)
Area (each face):	9.39 in^2
Total Volume:	0.263 in^3
Net Cross Section:	0.073 in^2

The panel failed at the hole edge (Type-1) at an applied normal stress (σ_n) of -28,000 psi, only about 78% of that expected. Based strictly on the failure of the unreinforced panel and the computed stress concentration factor of 2.56 the predicted failure was $\bar{\sigma}_n$ = -35,700 psi.

The finite element model (mesh) is shown in Figure D.1. The area of round reinforcement is denoted by the area inside the bold outline around the cutout.

Figure D.2 compares the analytical values of strain around the cutout from $\theta = 0°$ to 90° between the unreinforced panel (PO∅∅) and RR31 in the Y and X directions as well as shear (Eps-Y, Eps-X and Eps-XY). Table XIX lists these computed strains around the cutout.

Figure D.2 compares the finite element model (lines) and the experimentally measured strain data (triangles) of strain at $\overline{\sigma}_n$ = -10,000 psi. It shows an almost perfect correlation between the analytically predicted and experimentally measured strain. The edge of the reinforcement extended to 1.80" in on the X axis. This is apparent from the figure as the slight inflection point where the strain begins increasing slightly. The computed strain field in an unreinforced panel (POØØ) is shown as dashed lines (Eps-Y & Eps-X). Table XX gives the values of the computed strain in the Y and X directions as well as shear.

Figure D.4 shows the stress-strain relation during the load sequence from 0 to -28 ksi. Experimentally measured strain gage values are given in Table XXI. Other than a minor "glitch" at $\overline{\sigma}_n$ = -21 ksi, no exceptional anomalies were noted. Gage #3 at x = -0.770" showed little increase in strain between -21 and -22 ksi. This is not reflected in any of the other gage readings.

Figures D.5 through D.8 show the strain contours at an applied normal stress of -10,000 psi computed and plotted using DIAL. Figure D.5 is the full quarter panel with strain parallel to the applied load. As before, the strain contours at the top right of the panel are due to the effect of not loading the full width of the top edge. Figures D.6 through D.8 (Eps-Y, Eps-X and Eps-XY) show the strains in detail close to the cutout.

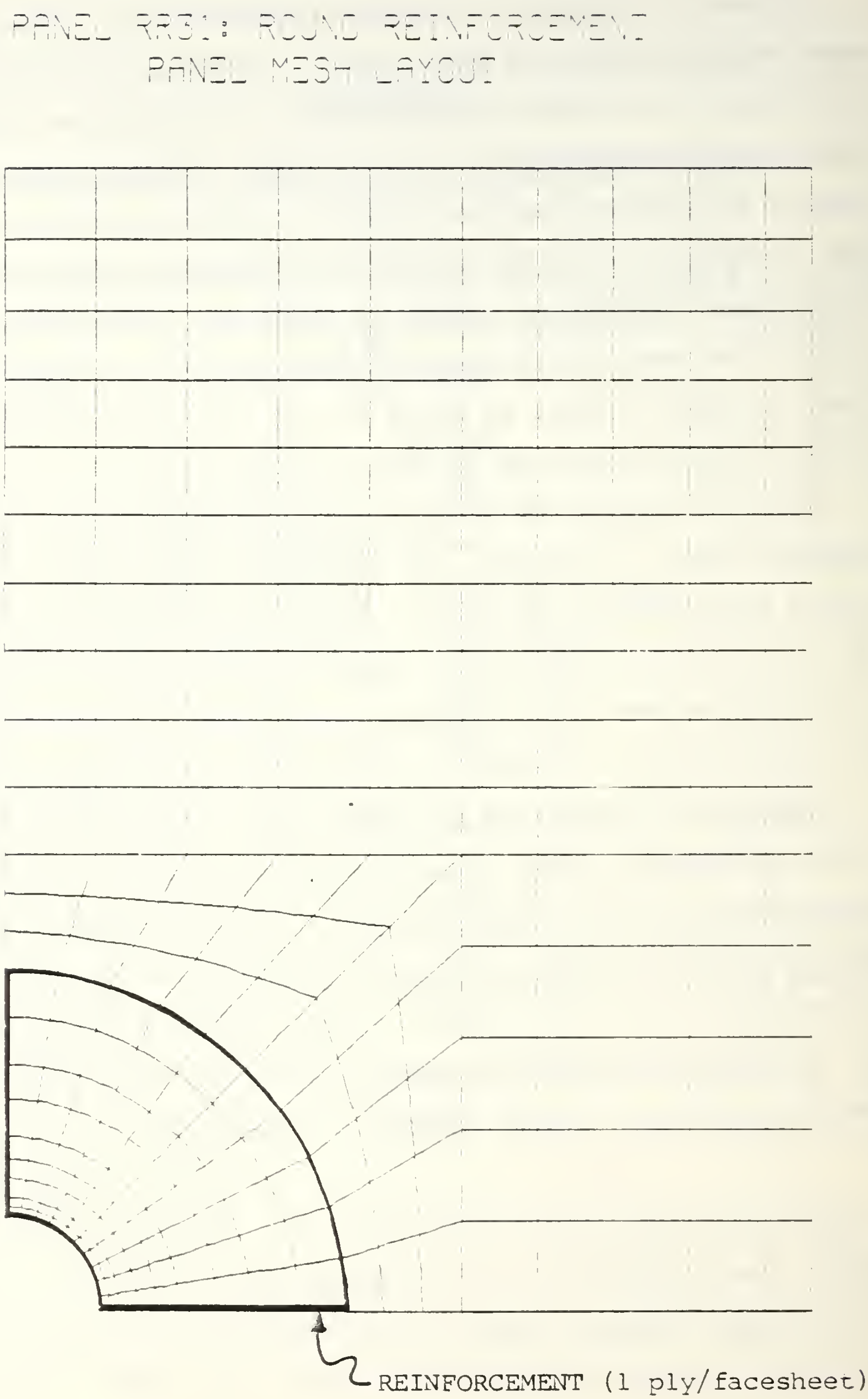

Figure D.1 Panel RR31: DIAL Finite Element Mesh.

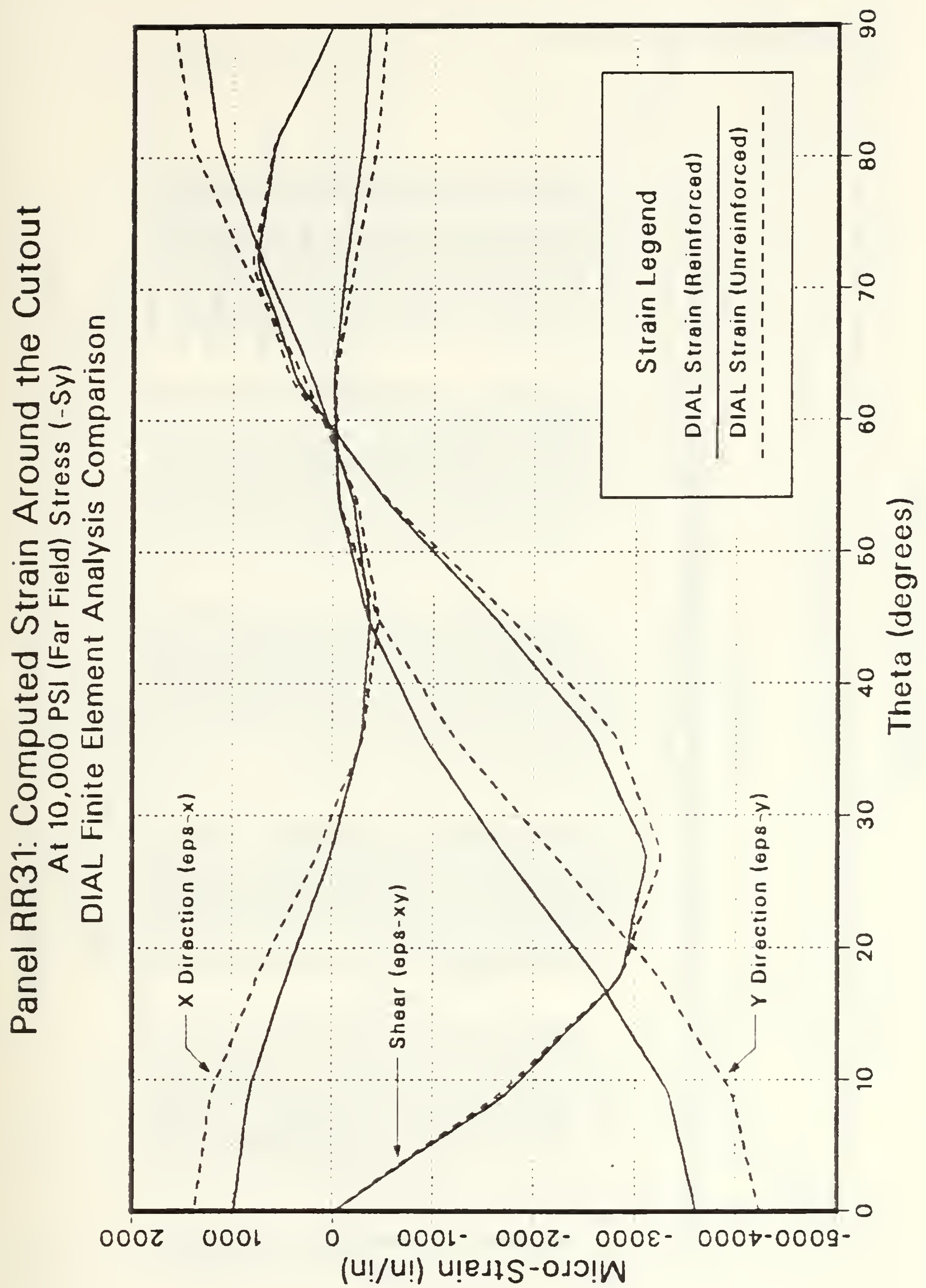

Figure D.2 Panel RR31: Strain Comparison Around the Cutout.

TABLE XIX

PANEL RR31: LEFEA STRAIN DISTRIBUTION AROUND THE CUTOUT (-10,000 PSI).

NODE	X COORD	Y COORD	EPS-Y	EPS-X	EPS-XY
1	0.0000E+00	0.5000E+00	-0.3512E-03	0.1320E-02	0.1761E-04
2	0.3923E-01	0.4985E+00	-0.3165E-03	0.1237E-02	0.2944E-03
3	0.7822E-01	0.4938E+00	-0.2791E-03	0.1146E-02	0.5844E-03
4	0.1167E+00	0.4862E+00	-0.1999E-03	0.9296E-03	0.6776E-03
5	0.1545E+00	0.4755E+00	-0.1193E-03	0.7103E-03	0.7612E-03
6	0.1913E+00	0.4619E+00	-0.5980E-04	0.4564E-03	0.5652E-03
7	0.2270E+00	0.4455E+00	-0.6373E-06	0.2046E-03	0.3600E-03
8	0.2612E+00	0.4263E+00	-0.2428E-04	0.6183E-05	-0.7542E-04
9	0.2939E+00	0.4045E+00	-0.4931E-04	-0.1885E-03	-0.5162E-03
10	0.3247E+00	0.3802E+00	-0.1962E-03	-0.2765E-03	-0.1060E-02
11	0.3536E+00	0.3536E+00	-0.3455E-03	-0.3613E-03	-0.1605E-02
12	0.3802E+00	0.3247E+00	-0.6282E-03	-0.3221E-03	-0.2095E-02
13	0.4045E+00	0.2939E+00	-0.9150E-03	-0.2805E-03	-0.2584E-02
14	0.4263E+00	0.2612E+00	-0.1312E-02	-0.1294E-03	-0.2848E-02
15	0.4455E+00	0.2270E+00	-0.1715E-02	0.2364E-04	-0.3106E-02
16	0.4619E+00	0.1913E+00	-0.2157E-02	0.2370E-03	-0.2989E-02
17	0.4755E+00	0.1545E+00	.2603E-02	0.4511E-03	-0.2860E-02
18	0.4862E+00	0.1167E+00	-0.2965E-02	0.6422E-03	-0.2305E-02
19	0.4938E+00	0.7822E-01	-0.3324E-02	0.8319E-03	-0.1736E-02
20	0.4985E+00	0.3923E-01	-0.3469E-02	0.9106E-03	-0.8710E-03
21	0.5000E+00	0.0000E+00	-0.3605E-02	0.9856E-03	-0.2505E-04

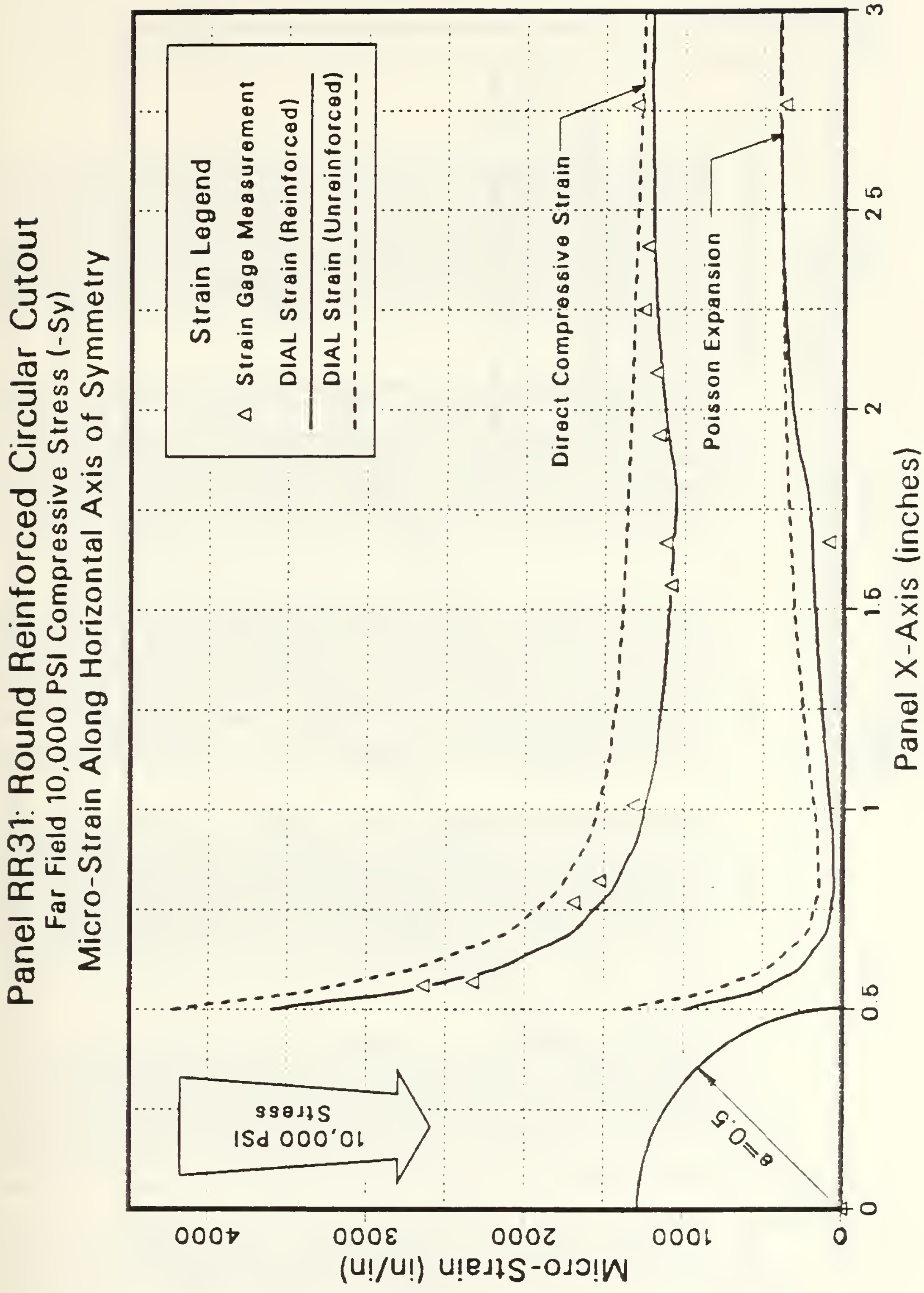

Figure D.3 Panel RR31: Strain Comparison Along the X Axis.

TABLE XX

PANEL RR31: LEFEA STRAIN DISTRIBUTION ALONG THE X AXIS (-10,000 PSI).

NODE	X COORD	Y COORD	EPS-Y	EPS-X	EPS-XY
21	0.5000E+00	0.0000E+00	-0.3605E-02	0.9856E-03	-0.2505E-04
32	0.5250E+00	0.0000E+00	-0.3148E-02	0.7430E-03	-0.1571E-04
53	0.5500E+00	0.0000E+00	-0.2703E-02	0.5085E-03	-0.5085E-05
64	0.5750E+00	0.0000E+00	-0.2462E-02	0.3983E-03	-0.3515E-05
85	0.6000E+00	0.0000E+00	-0.2200E-02	0.2757E-03	-0.1993E-05
96	0.6500E+00	0.0000E+00	-0.1934E-02	0.1785E-03	0.6216E-06
117	0.7000E+00	0.0000E+00	-0.1685E-02	0.9132E-04	0.1590E-05
128	0.7500E+00	0.0000E+00	-0.1572E-02	0.7453E-04	0.1928E-05
149	0.8000E+00	0.0000E+00	-0.1452E-02	0.5342E-04	0.2560E-05
160	0.8605E+00	0.0000E+00	-0.1378E-02	0.5756E-04	0.2613E-05
181	0.9210E+00	0.0000E+00	-0.1301E-02	0.6111E-04	0.2829E-05
192	0.1021E+01	0.0000E+00	-0.1242E-02	0.8349E-04	0.3091E-05
213	0.1120E+01	0.0000E+00	-0.1186E-02	0.1059E-03	0.3085E-05
224	0.1210E+01	0.0000E+00	-0.1162E-02	0.1261E-03	0.2818E-05
245	0.1300E+01	0.0000E+00	-0.1135E-02	0.1460E-03	0.2709E-05
256	0.1425E+01	0.0000E+00	-0.1113E-02	0.1668E-03	0.3000E-05
277	0.1550E+01	0.0000E+00	-0.1091E-02	0.1870E-03	0.3125E-05
288	0.1675E+01	0.0000E+00	-0.1074E-02	0.1999E-03	0.1354E-05
309	0.1800E+01	0.0000E+00	-0.1056E-02	0.2289E-03	0.6156E-06
320	0.1900E+01	0.0000E+00	-0.1093E-02	0.2823E-03	0.2049E-05
341	0.2000E+01	0.0000E+00	-0.1129E-02	0.3198E-03	0.3380E-05
352	0.2100E+01	0.0000E+00	-0.1151E-02	0.3419E-03	0.4232E-05
373	0.2200E+01	0.0000E+00	-0.1173E-02	0.3639E-03	0.5054E-05
384	0.2300E+01	0.0000E+00	-0.1184E-02	0.3762E-03	0.5917E-05
405	0.2400E+01	0.0000E+00	-0.1197E-02	0.3889E-03	0.5306E-05
406	0.2600E+01	0.0000E+00	-0.1203E-02	0.3981E-03	0.3049E-05
407	0.2800E+01	0.0000E+00	-0.1209E-02	0.4056E-03	0.1377E-05
408	0.3000E+01	0.0000E+00	-0.1202E-02	0.4026E-03	0.8350E-06
409	0.3200E+01	0.0000E+00	-0.1196E-02	0.4002E-03	0.5338E-06
410	0.3400E+01	0.0000E+00	-0.1187E-02	0.3949E-03	0.3455E-06
411	0.3600E+01	0.0000E+00	-0.1177E-02	0.3897E-03	0.1136E-06
412	0.3800E+01	0.0000E+00	-0.1169E-02	0.3852E-03	0.7076E-07
413	0.4000E+01	0.0000E+00	-0.1162E-02	0.3808E-03	0.5249E-07
414	0.4125E+01	0.0000E+00	-0.1159E-02	0.3795E-03	0.3093E-07
415	0.4250E+01	0.0000E+00	-0.1156E-02	0.3782E-03	0.2969E-08

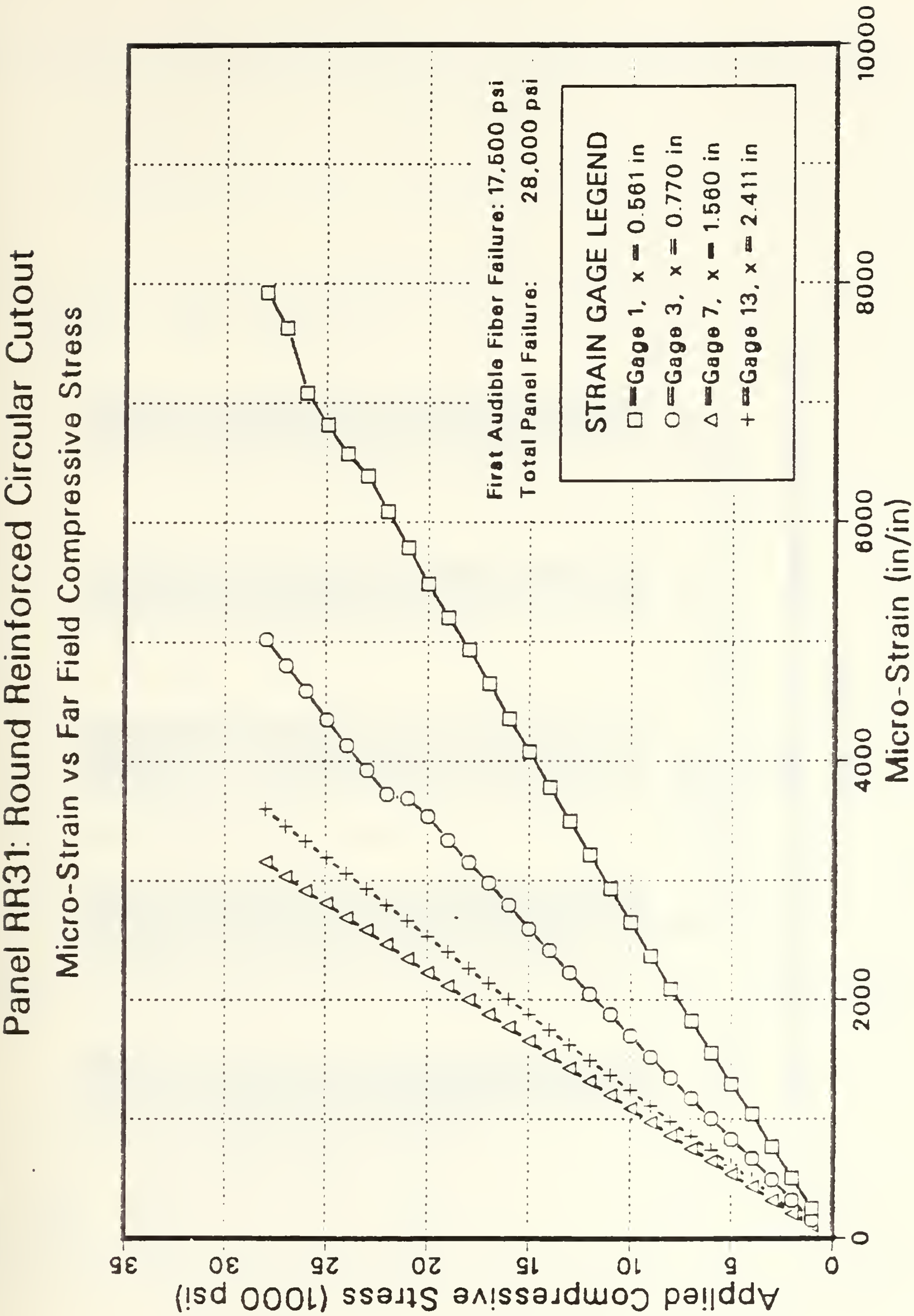

Figure D.4 Panel RR31: Microstrain vs. Compressive Stress.

TABLE XXI

PANEL RR31: SELECTED STRAIN GAGE VALUES DURING LOAD.

Load (PSI)	Micro-Strain Indicated by Gage:			
	#1	#3	#7	#13
1000	-248	-155	-103	-117
2000	-503	-320	-209	-239
3000	-763	-490	-318	-361
4000	-1040	-672	-434	-494
5000	-1287	-830	-536	-611
6000	-1553	-1000	-646	-735
7000	-1820	-1169	-754	-857
8000	-2090	-1343	-863	-981
9000	-2368	-1516	-975	-1109
10000	-2648	-1695	-1089	-1238
11000	-2928	-1873	-1200	-1364
12000	-3212	-2051	-1315	-1491
13000	-3494	-2229	-1426	-1618
14000	-3781	-2411	-1539	-1746
15000	-4073	-2591	-1657	-1876
16000	-4355	-2793	-1769	-2006
17000	-4645	-2978	-1884	-2135
18000	-4934	-3151	-2000	-2265
19000	-5199	-3341	-2115	-2398
20000	-5484	-3537	-2231	-2530
21000	-5784	[illegible]91	-2347	-2664
22000	-6090	-3721	-2464	-2795
23000	-6387	-3923	-2583	-2931
24000	-6570	-4129	-2692	-3062
25000	-6811	-4346	-2805	-3193
26000	-7085	-4585	-2920	-3328
27000	-7625	-4802	-3035	-3456
28000	-7923	-5020	-3161	-3599

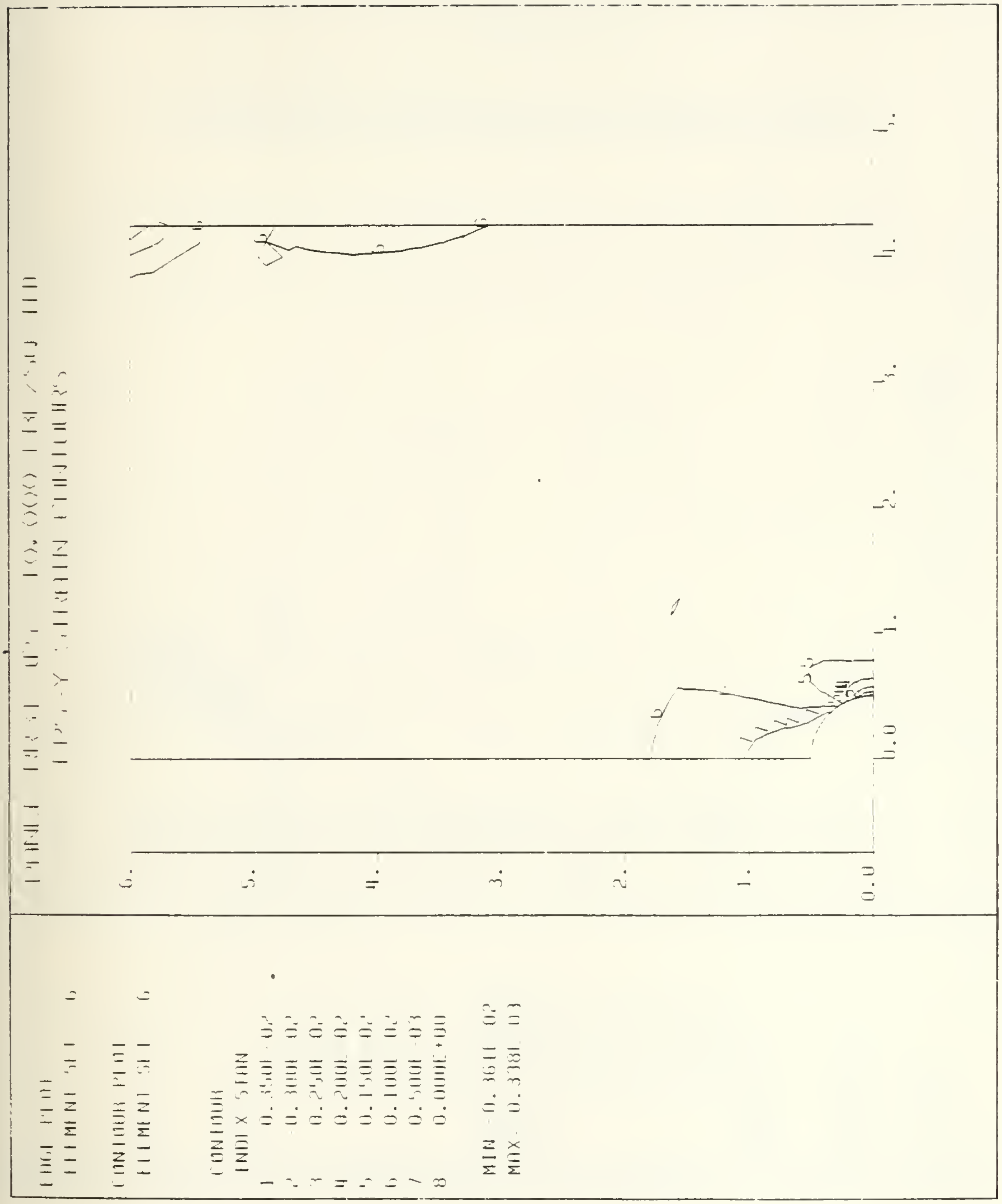

Figure D.5   Panel RR31: Eps-Y FEA Contours.

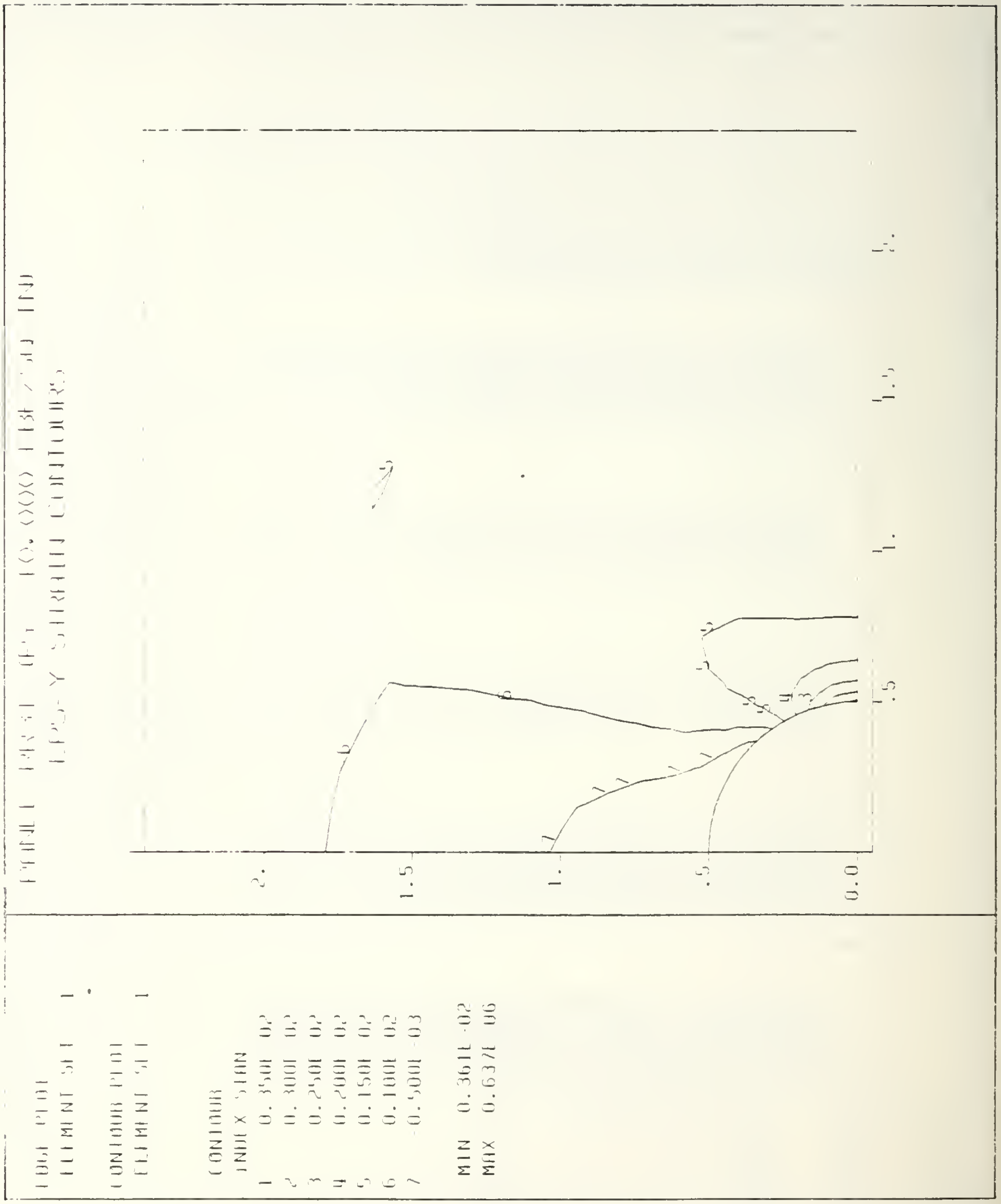

Figure D.6 Panel RR31: Eps-Y FEA Contours Near the Cutout.

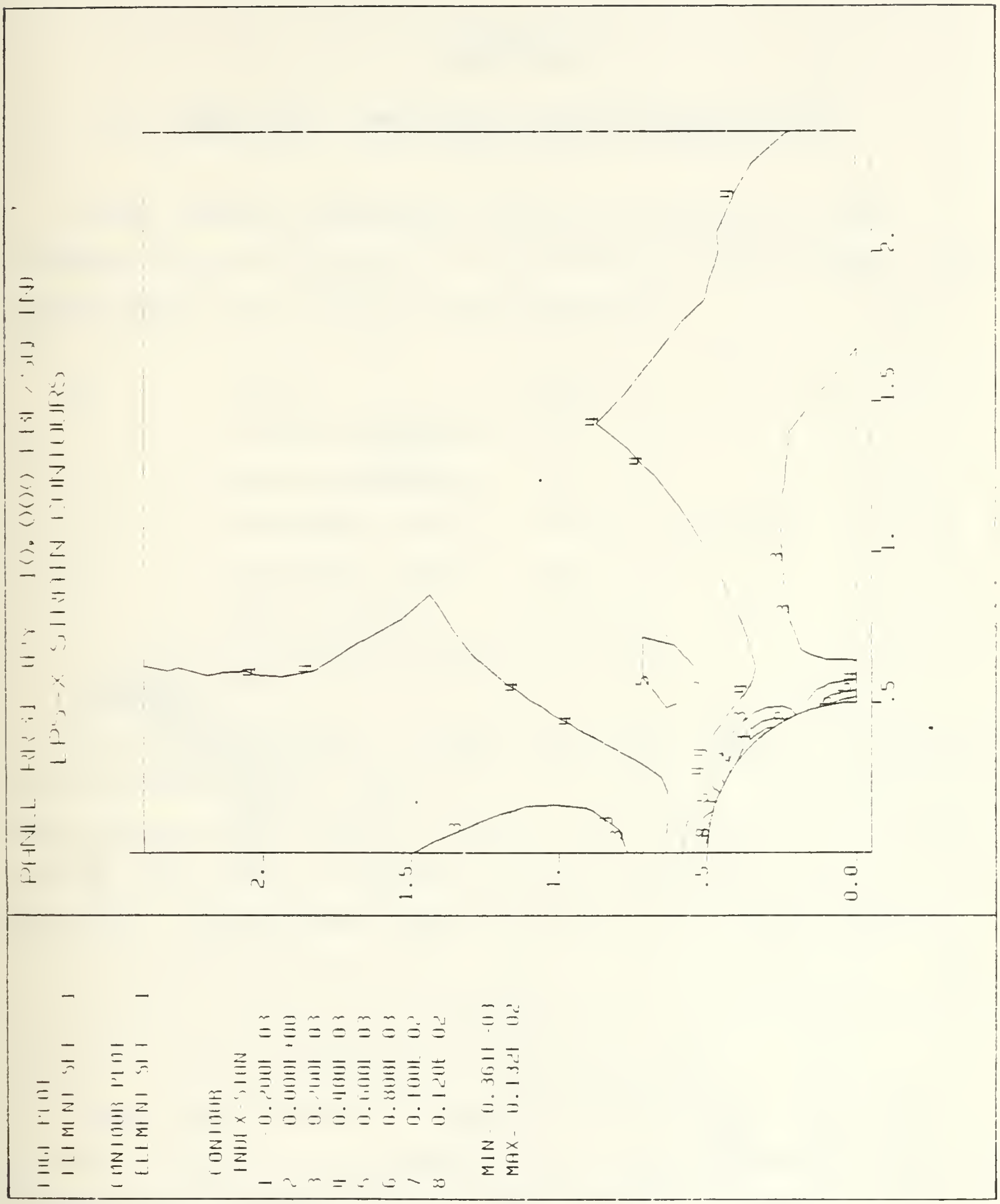

Figure D.7 Panel RR31: Eps-X FEA Contours Near the Cutout.

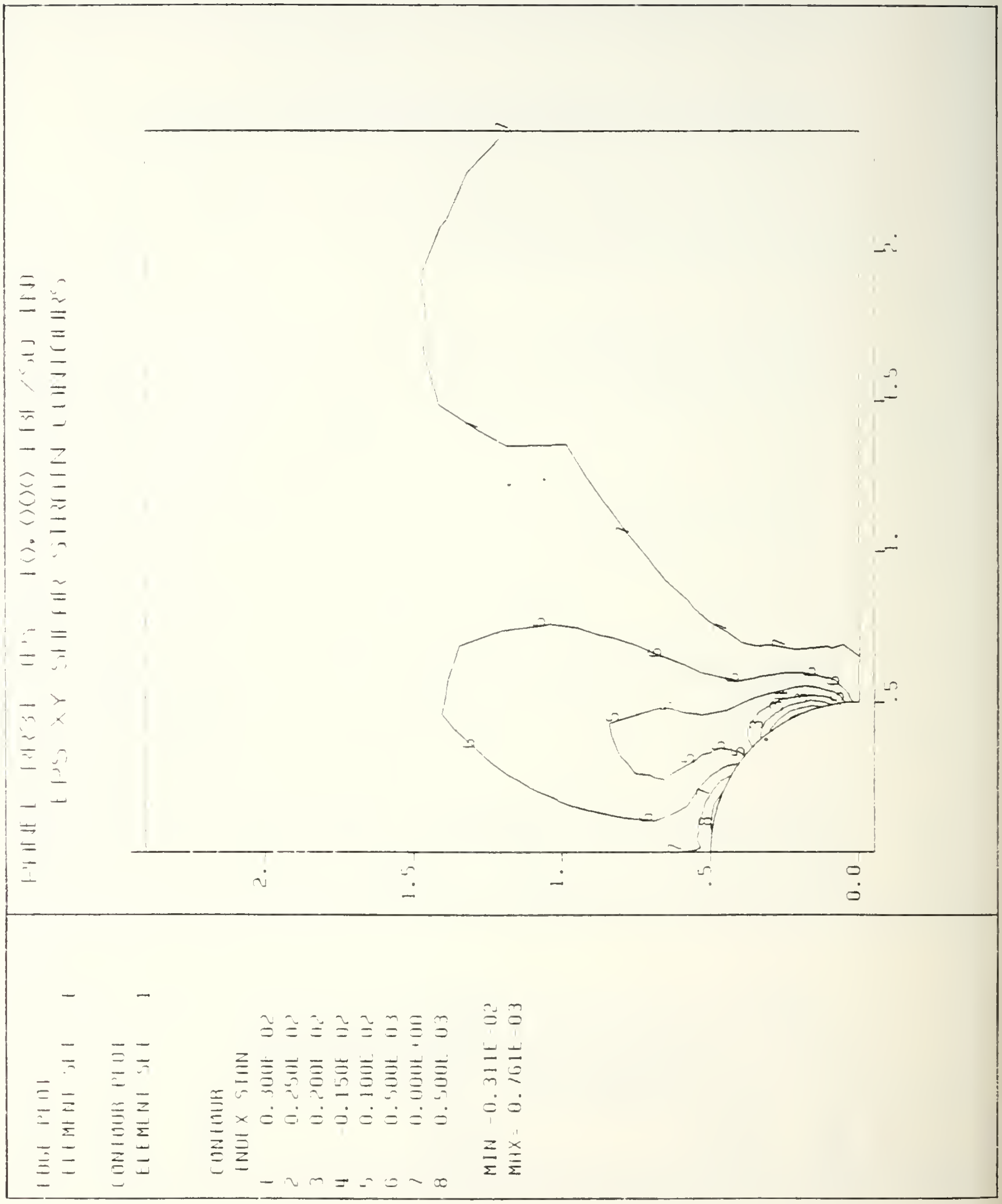

Figure D.8 Panel RR31: Eps-XY FEA Contours Near the Cutout.

APPENDIX E

PANEL RR42: ANALYTICAL AND EXPERIMENTAL DATA

Panel RR42 was reinforced with one co-cured ply of G/EP concentric with the cutout on the outside of each facesheet. The reinforcement had the following dimensions:

Shape:	Round
Inside Diameter:	1.00 in
Outside Diameter:	3.00 in
Thickness (each):	0.028 in (2 ply)
Area (each face):	6.28 in^2
Total Volume:	0.176 in^3
Net Cross Section:	0.112 in^2

The panel failed by facesheet separation and buckling (Type-2) at an applied normal stress ($\bar{\sigma}_n$) of -13,500 psi, less that 34% of the expected value. Based strictly on the failure of the unreinforced panel and the computed stress concentration factor of 2.29 for RR42, the predicted panel failure was $\bar{\sigma}_n$ = -40,000 psi.

The finite element model (mesh) is shown in Figure E.1. The area of round reinforcement is denoted by the area inside the bold outline around the cutout.

Figure E.2 compares the LEFEA values of strain around the cutout between the unreinforced panel (PO∅∅) and RR42 in the Y and X directions as well as shear (Eps-Y, Eps-X and Eps-XY). Table XXII lists these computed strains around the cutout.

Figure E.3 compares the finite element model (lines) and the experimentally measured strain data (triangles) of strain at $\bar{\sigma}_n$ = -10,000 psi. It shows very poor correlation between the analytically predicted and measured strain. At least one facesheet separated from the honeycomb core over a significant area prior to the -10 ksi test point. The strain field at that applied stress was little more than 80% of that predicted. The computed strain field in an unreinforced panel (PO∅∅) is shown as dotted lines (Eps-Y & Eps-X). Table XXIII gives the values of the LEFEA computed strain in the Y and X directions as well as in shear.

Figure E.4 shows the stress-strain relation during the load sequence from σ_n = 0 to -21.9 ksi (failure). Measured strain gage values are given in Table XXIV. The strain, particularly in gages #3, #8 and #14, indicate that the panel stiffness decreased from the initiation of the load. The notable difference in slope between gages #3, #8 and #14 and gage #1 next to the cutout indicate that the separation "bubble" occurred <u>away</u> from the cutout. Failure seemed to occur when the bubble's edge reached the cutout.

This type of failure probably indicates that at least one facesheet was improperly bonded to the honeycomb core. Nondestructive inspection before and after testing did not indicate unbonded areas between the facesheet and the core. I suspect, in this and other panels that failed in a similar manner, that the adhesive was in place but either weak from an improper mixing or aging or was applied too thinly.

Figures E.5 through E.8 show the strain contours at an applied normal stress of -10,000 psi computed and plotted using DIAL. Figure E.5 is the full quarter panel with strain parallel to the applied load. As before, the strain contours at the top right of the panel are due to the effect of not loading the full width of the top edge. Figures E.6 through E.8 (EPS-Y, EPS-X and EPS-XY) show the strains in detail close to the cutout.

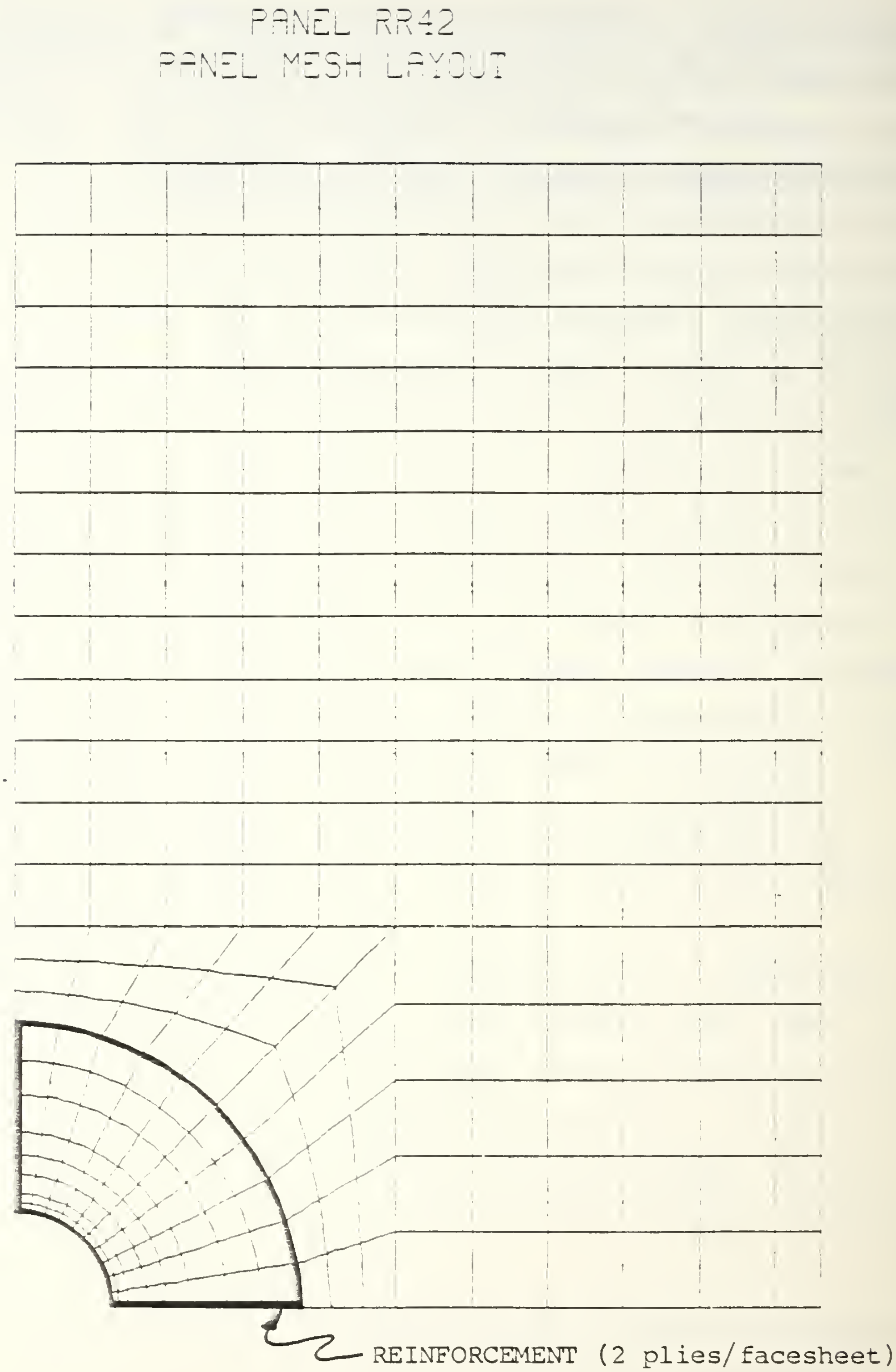

Figure E.1 Panel RR42: DIAL Finite Element Mesh.

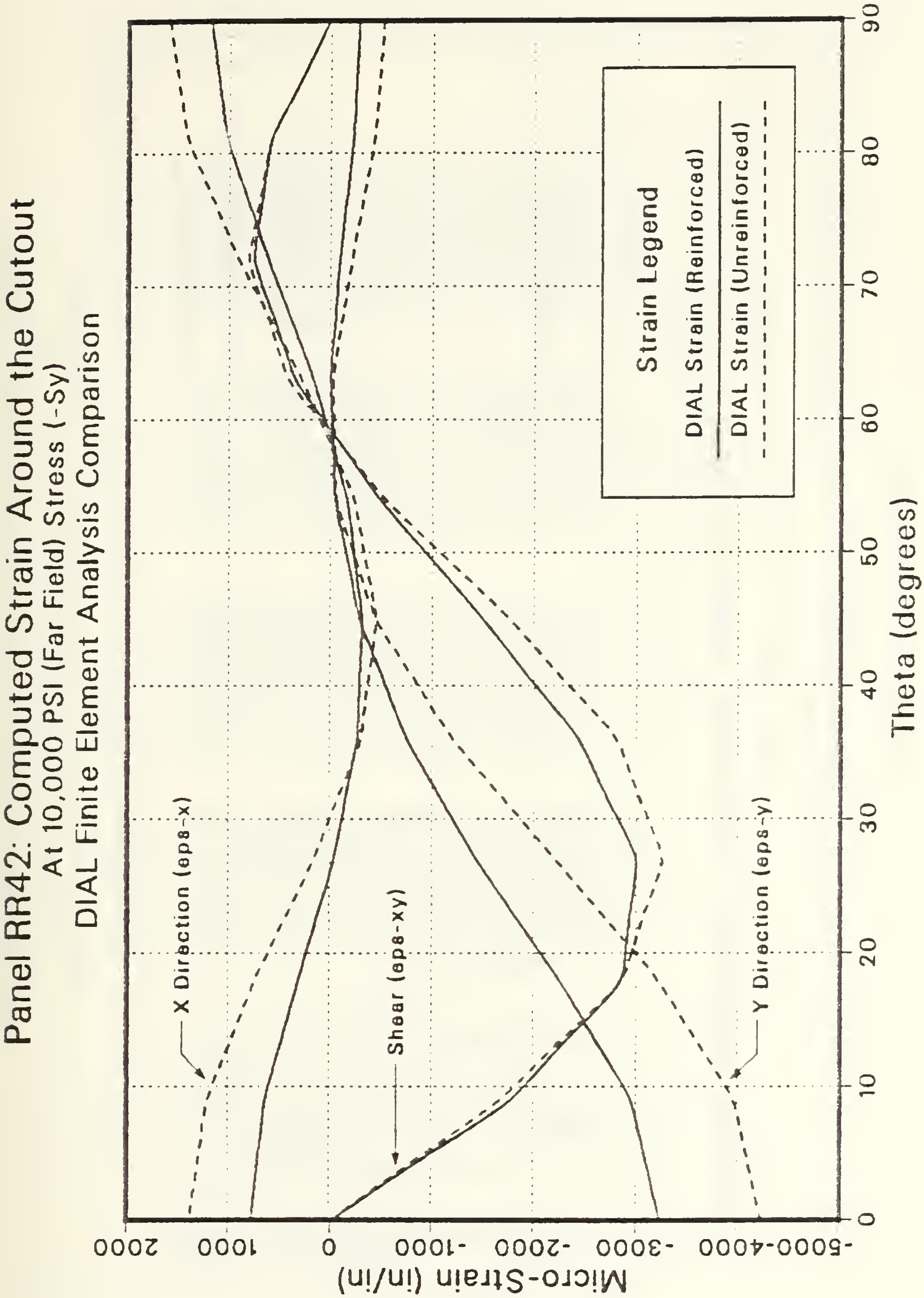

Figure E.2 Panel RR42: Strain Comparison Around the Cutout.

TABLE XXII

PANEL RR42: LEFEA STRAIN DISTRIBUTION AROUND THE CUTOUT (-10,000 PSI).

NODE	X COORD	Y COORD	EPS-Y	EPS-X	EPS-XY
1	0.0000E+00	0.5000E+00	-0.2743E-03	0.1186E-02	0.1755E-04
2	0.3923E-01	0.4985E+00	-0.2447E-03	0.1107E-02	0.2992E-03
3	0.7822E-01	0.4938E+00	-0.2133E-03	0.1021E-02	0.5937E-03
4	0.1167E+00	0.4862E+00	-0.1486E-03	0.8197E-03	0.6798E-03
5	0.1545E+00	0.4755E+00	-0.8294E-04	0.6173E-03	0.7555E-03
6	0.1913E+00	0.4619E+00	-0.3874E-04	0.3930E-03	0.5563E-03
7	0.2270E+00	0.4455E+00	0.5406E-05	0.1723E-03	0.3486E-03
8	0.2612E+00	0.4263E+00	-0.1892E-04	0.4917E-05	-0.6540E-04
9	0.2939E+00	0.4045E+00	-0.4369E-04	-0.1587E-03	-0.4832E-03
10	0.3247E+00	0.3802E+00	-0.1644E-03	-0.2339E-03	-0.9884E-03
11	0.3536E+00	0.3536E+00	-0.2860E-03	-0.3072E-03	-0.1495E-02
12	0.3802E+00	0.3247E+00	-0.5169E-03	-0.2842E-03	-0.1963E-02
13	0.4045E+00	0.2939E+00	-0.7507E-03	-0.2601E-03	-0.2432E-02
14	0.4263E+00	0.2612E+00	-0.1089E-02	-0.1474E-03	-0.2717E-02
15	0.4455E+00	0.2270E+00	-0.1434E-02	-0.3345E-04	-0.2998E-02
16	0.4619E+00	0.1913E+00	-0.1837E-02	0.1386E-03	-0.2931E-02
17	0.4755E+00	0.1545E+00	-0.2245E-02	0.3113E-03	-0.2852E-02
18	0.4862E+00	0.1167E+00	-0.2597E-02	0.4752E-03	-0.2323E-02
19	0.4938E+00	0.7822E-01	-0.2947E-02	0.6382E-03	-0.1777E-02
20	0.4985E+00	0.3923E-01	-0.3095E-02	0.7079E-03	-0.8924E-03
21	0.5000E+00	0.0000E+00	-0.3231E-02	0.7750E-03	-0.2726E-04

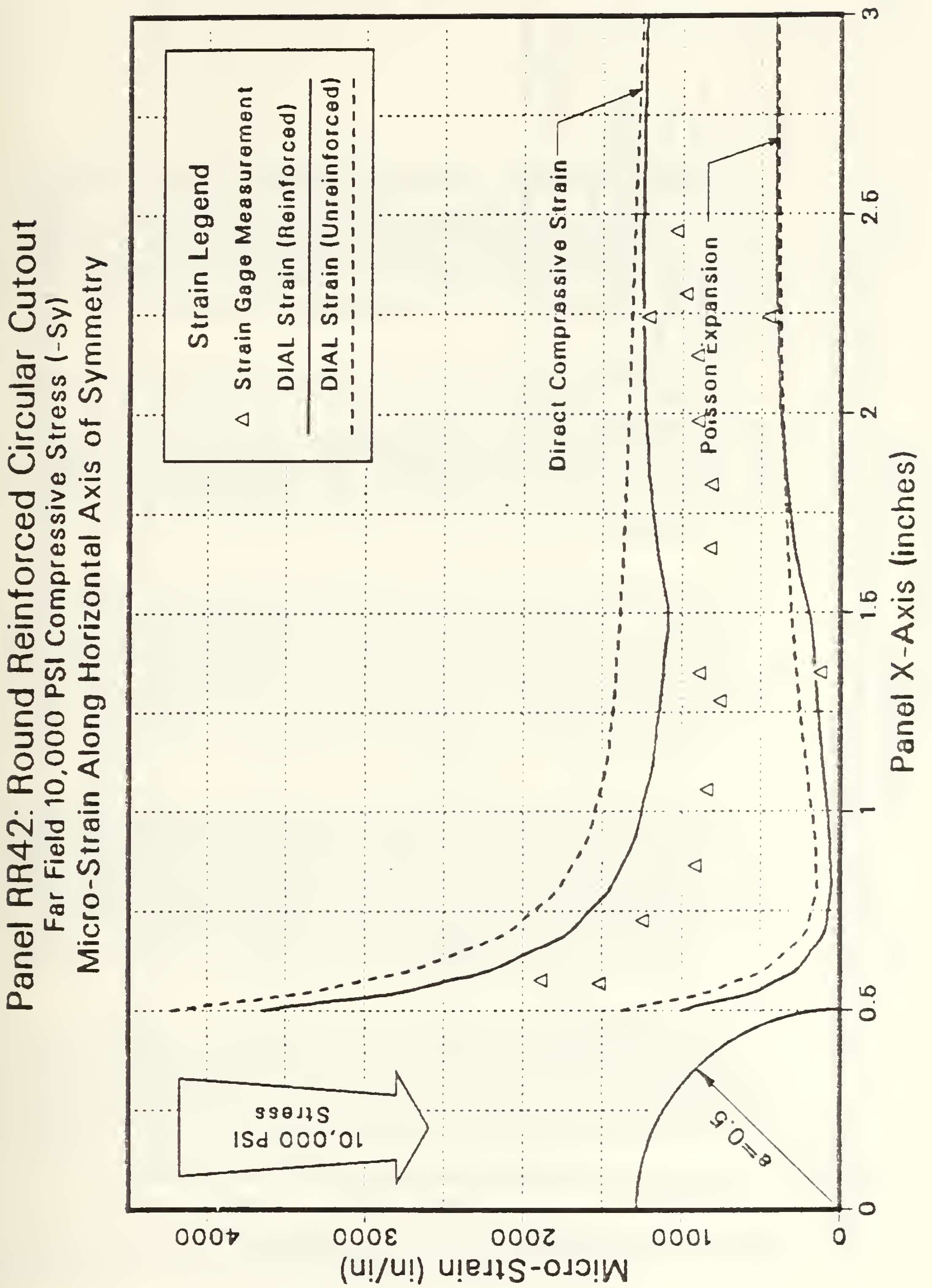

Figure E.3 Panel RR42: Strain Comparison Along the X Axis.

TABLE XXIII

PANEL RR42: LEFEA STRAIN DISTRIBUTION ALONG THE X AXIS (-10,000 PSI).

NODE	X COORD	Y COORD	EPS-Y	EPS-X	EPS-XY
21	0.5000E+00	0.0000E+00	-0.3231E-02	0.7750E-03	-0.2726E-04
32	0.5250E+00	0.0000E+00	-0.2778E-02	0.5627E-03	-0.1631E-04
53	0.5500E+00	0.0000E+00	-0.2340E-02	0.3598E-03	-0.3055E-05
64	0.5750E+00	0.0000E+00	-0.2126E-02	0.2748E-03	-0.1159E-05
85	0.6000E+00	0.0000E+00	-0.1890E-02	0.1773E-03	-0.8493E-06
96	0.6500E+00	0.0000E+00	-0.1658E-02	0.1040E-03	0.8765E-06
117	0.7000E+00	0.0000E+00	-0.1442E-02	0.3831E-04	0.1525E-05
128	0.7500E+00	0.0000E+00	-0.1345E-02	0.2687E-04	0.1566E-05
149	0.8000E+00	0.0000E+00	-0.1241E-02	0.1188E-04	0.1899E-05
160	0.8605E+00	0.0000E+00	-0.1174E-02	0.1610E-04	0.2067E-05
181	0.9210E+00	0.0000E+00	-0.1106E-02	0.1988E-04	0.2332E-05
192	0.1021E+01	0.0000E+00	-0.1049E-02	0.3851E-04	0.2485E-05
213	0.1120E+01	0.0000E+00	-0.9945E-03	0.5719E-04	0.2447E-05
224	0.1210E+01	0.0000E+00	-0.9674E-03	0.7389E-04	0.3185E-05
245	0.1300E+01	0.0000E+00	-0.9387E-03	0.9012E-04	0.3769E-05
256	0.1400E+01	0.0000E+00	-0.9142E-03	0.1038E-03	0.1456E-05
277	0.1500E+01	0.0000E+00	-0.8884E-03	0.1265E-03	0.6855E-06
288	0.1583E+01	0.0000E+00	-0.9537E-03	0.1979E-03	0.3013E-05
309	0.1667E+01	0.0000E+00	-0.1020E-02	0.2605E-03	0.5353E-05
320	0.1750E+01	0.0000E+00	-0.1063E-02	0.2991E-03	0.6768E-05
341	0.1833E+01	0.0000E+00	-0.1107E-02	0.3375E-03	0.8086E-05
352	0.1917E+01	0.0000E+00	-0.1134E-02	0.3604E-03	0.9726E-05
373	0.2000E+01	0.0000E+00	-0.1162E-02	0.3846E-03	0.8418E-05
374	0.2200E+01	0.0000E+00	-0.1190E-02	0.4073E-03	0.4025E-05
375	0.2400E+01	0.0000E+00	-0.1215E-02	0.4262E-03	0.1397E-05
376	0.2600E+01	0.0000E+00	-0.1214E-02	0.4237E-03	0.8002E-06
377	0.2800E+01	0.0000E+00	-0.1214E-02	0.4229E-03	0.3700E-06
378	0.3000E+01	0.0000E+00	-0.1206E-02	0.4157E-03	0.2069E-06
379	0.3200E+01	0.0000E+00	-0.1198E-02	0.4090E-03	-0.8925E-07
380	0.3400E+01	0.0000E+00	-0.1189E-02	0.4013E-03	-0.8554E-07
381	0.3600E+01	0.0000E+00	-0.1180E-02	0.3937E-03	-0.6176E-07
382	0.3800E+01	0.0000E+00	-0.1174E-02	0.3884E-03	-0.5938E-07
383	0.4000E+01	0.0000E+00	-0.1168E-02	0.3834E-03	-0.4430E-07
384	0.4125E+01	0.0000E+00	-0.1168E-02	0.3827E-03	-0.1993E-07
385	0.4250E+01	0.0000E+00	-0.1168E-02	0.3819E-03	-0.1514E-07

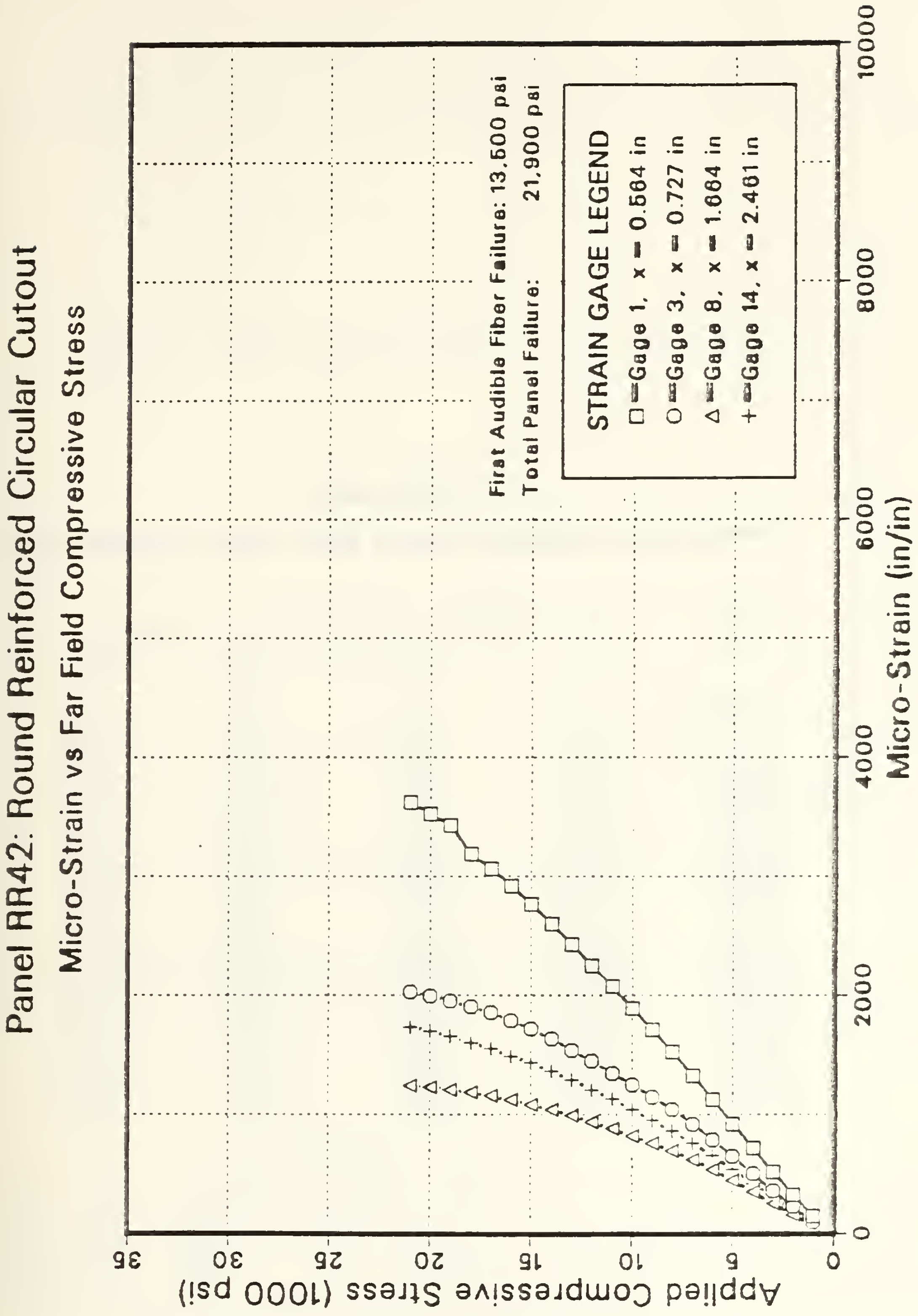

Figure E.4 Panel RR42: Microstrain vs. Compressive Stress.

TABLE XXIV

PANEL RR42: SELECTED STRAIN GAGE VALUES DURING LOAD.

Load (psi)	Micro-Strain Indicated by Gage: #1	#3	#8	#14
1000	-143	-94	-63	-74
2000	-327	-227	-159	-197
3000	-516	-361	-25[illegible]	-306
4000	-717	-502	-3[illegible]	-423
5000	-920	-645	-44[illegible]	-537
6000	-1125	-788	-541	-654
7000	-1327	-919	-624	-761
8000	-1522	-1038	-69[illegible]	-860
9000	-1710	-1146	-76[illegible]	-951
10000	-1890	-1250	-823	-1039
11000	-2073	-1348	-883	-1132
12000	-2250	-1446	-939	-1210
13000	-2425	-1540	-992	-1293
14000	-2603	-1634	-1041	-1363
15000	-2764	-1714	-1085	-1432
16000	-2917	-1788	-1123	-14[illegible]2
17000	-3065	-1855	-1156	-1549
18000	-3183	-1902	-1183	-1603
19000	-3427	-1955	-1210	-1653
20000	-3522	-1993	-1229	-1698
21000	-3620	-2025	-1241	-1732

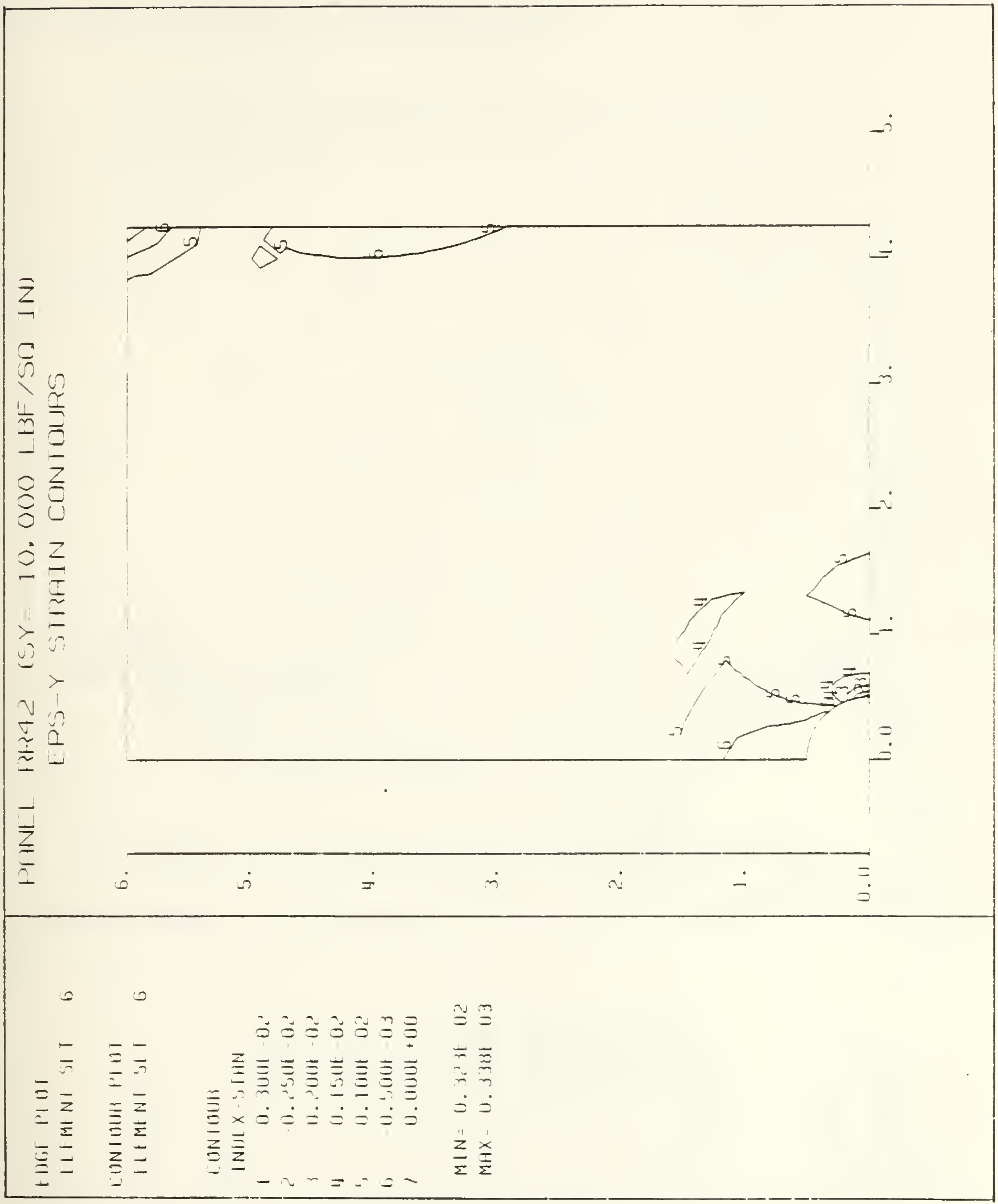

Figure E.5 Panel RR42: Eps-Y FEA Contours.

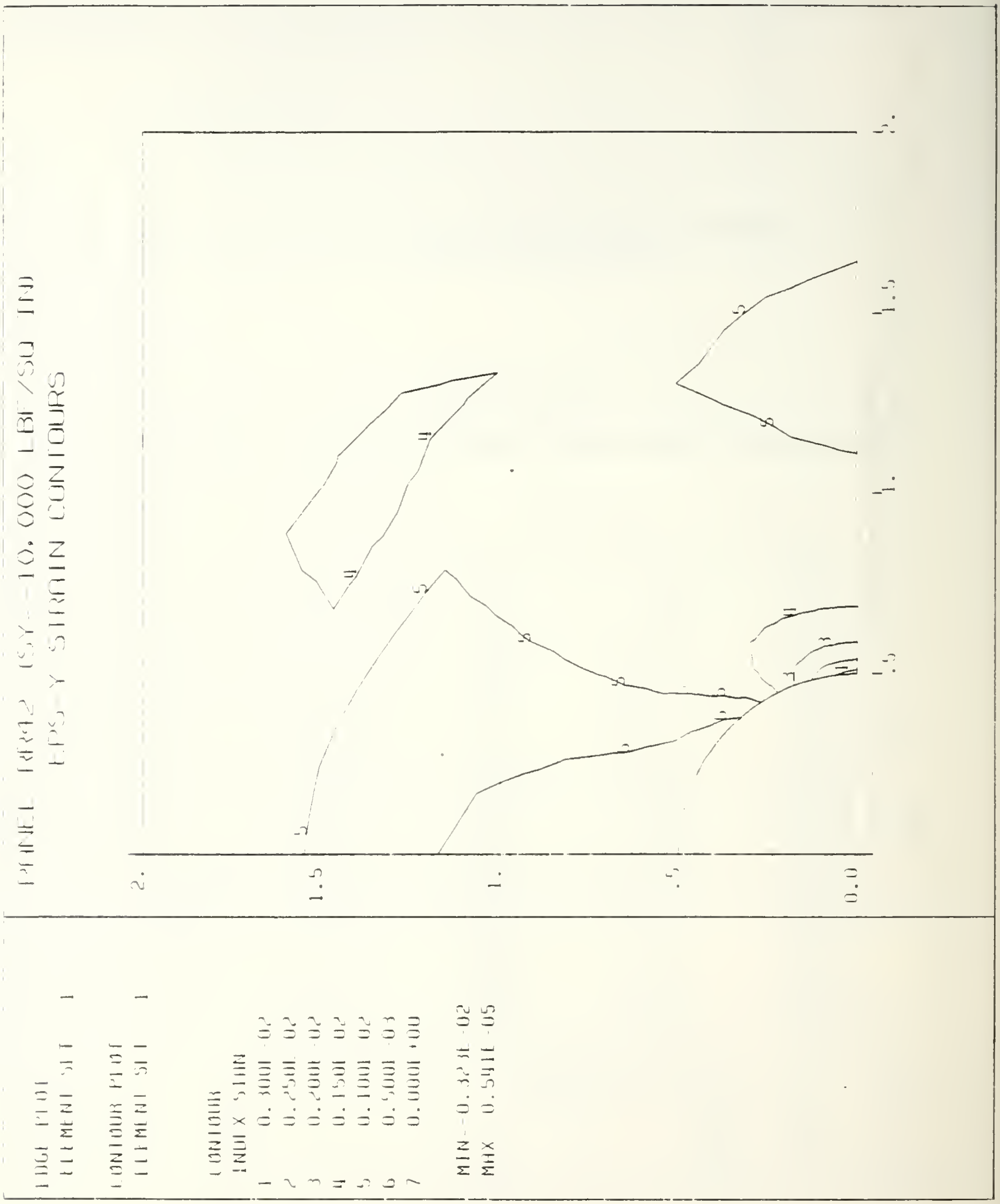

Figure E.6 Panel RR42: Eps-Y FEA Contours Near the Cutout.

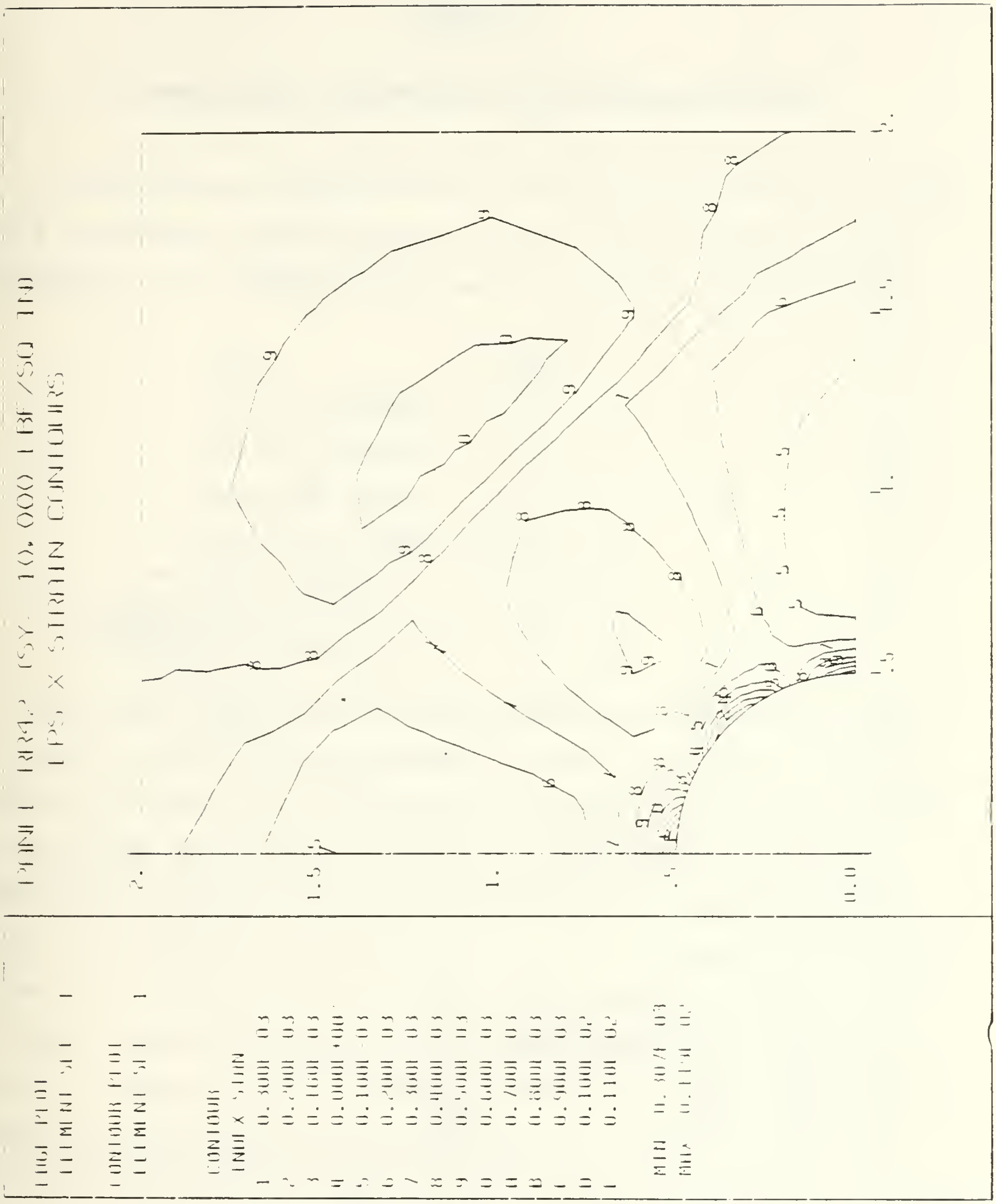

Figure E.7   Panel RR42: Eps-X FEA Contours Near the Cutout.

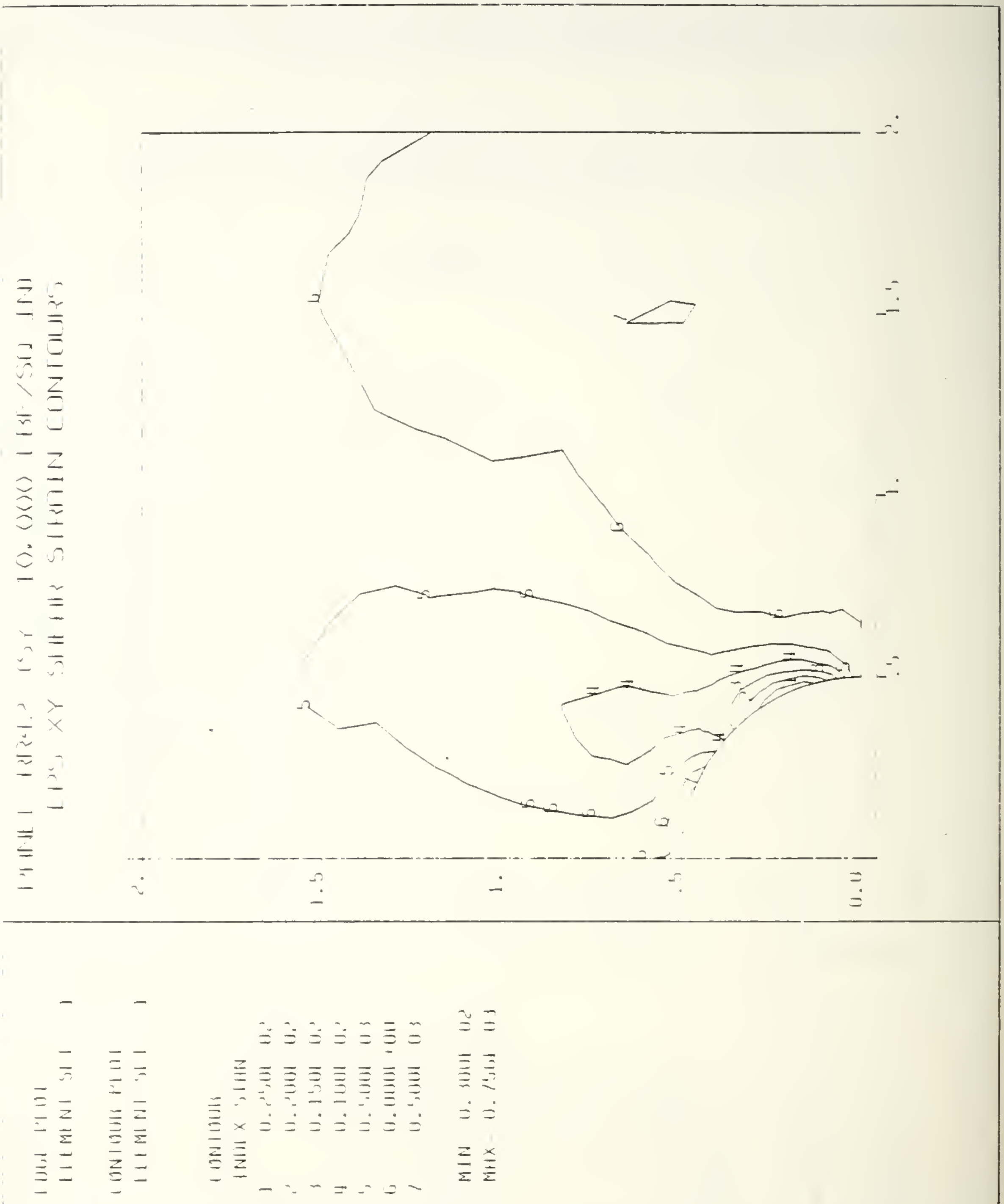

Figure E.8 Panel RR42: Eps-XY FEA Contours Near the Cutout.

APPENDIX F

PANEL RR51: ANALYTICAL AND EXPERIMENTAL DATA

Panel RR51 was reinforced with one round co-cured ply of G/Ep in a concentric with the cutout placed on the outside of each facesheets. The reinforcement had the following dimensions:

Shape:	Round	
Inside Diameter:	1.00	in
Outside Diameter:	4.60	in
Thickness (each):	0.014	in (1 ply)
Area (each face):	15.83	in^2
Total Volume:	0.443	in^3
Net Cross Section:	0.101	in^2

The panel failed by facesheet separation and buckling (Type-2') and was taken only to an applied normal stress of -16,000 psi, not to total failure. The series of premature panel failures due to facesheet separation required an intact panel for testing. Subsequent non-destructive testing showed the separation, but could not determine the reason for it. It is suspected that the adhesive, while properly applied, was not properly mixed or was overage. Based strictly on the failure of the unreinforced panel and the computed stress concentration factor of 2.51, failure was predicted at about $\bar{\sigma}_n$ = -36,400 psi.

The finite element model (mesh) is shown in Figure F.1. The 15.83 square inch area of the one-ply reinforcement is outlined by the bold lines next to the cutout.

Figure F.2 compares the three (finite element) computed strains around the cutout between the unreinforced panel (POØØ) and RR51. These computed strain values are listed in Table XXV. Note the very significant decrease in the strain due to the reinforcement at the point of highest stress concentration (θ = 0°) compared to the unreinforced panel. A significant decrease in all three strains can be seen around the hole from 0 to 90 degrees.

Figure F.3 compares the LEFEA computed (solid and dashed lines) and experimental strains (triangles) in the Y and X (poisson expansion) directions in the panel and shows that there was a great disparity between opposite sides of the hole on the same facesheet. One side showed much higher strain than predicted at σ_n = -10,000 psi. This is due to load transfer from the side with the buckled facesheet. The edge of the reinforcement can be seen in the figure by the very slight inflection point at x = 2.3". The effects of the one-ply reinforcement is apparent in the far-field as a significant decrease in computed Eps-Y compared to the unreinforced panel (POØØ). Table XXVI gives the computed values of the strains along the X axis.

Figure F.4 shows the stress-strain state during the load sequence from 0 to -16 ksi. Experimentally measured strain gage values are given in Table XXVII. Gage #1 and #4, on either side of the hole, show a positive slope of the derivative $\Delta\sigma/\Delta\varepsilon$. This is unusual and indicates some panel-honeycomb separation close to the hole.

Figures F.5 through F.8 show the strain contours at an $\bar{\sigma}_n$ = -10,000 psi computed and plotted using DIAL. Figure F.5 is the full quarter panel with strain (Eps-Y) parallel to the applied load. Figures F.6 through F.8 (Eps-Y, Eps-X and Eps-XY) show the strains in detail close to the cutout.

The result of the wide reinforcement is to effect a thicker overall panel. A separate LEFEA of a $[0_2,+45,90,\overline{core}]_s$ panel without reinforcement had an almost identical strain field near the cutout.

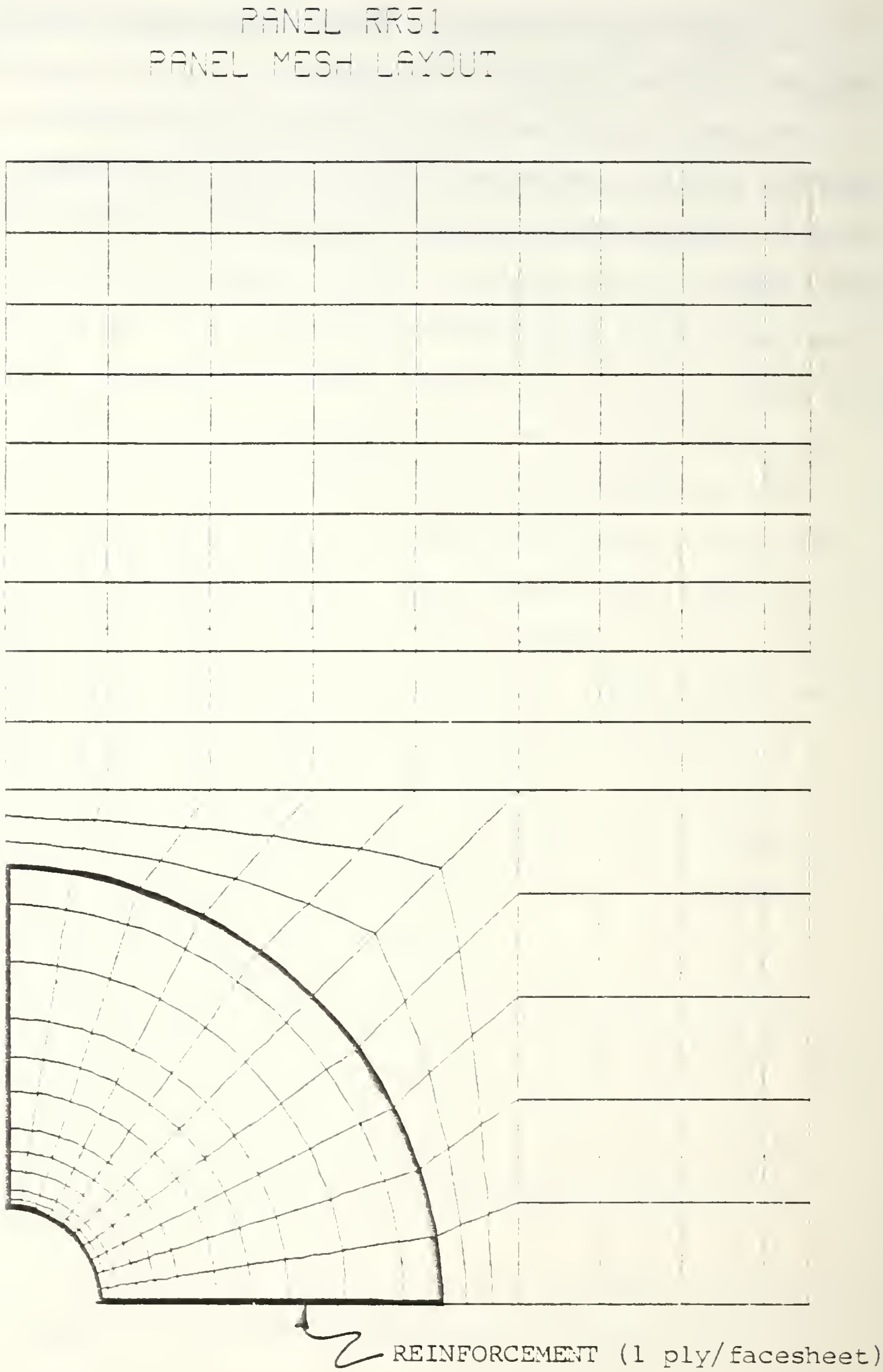

Figure F.1 Panel RR51: DIAL Finite Element Mesh.

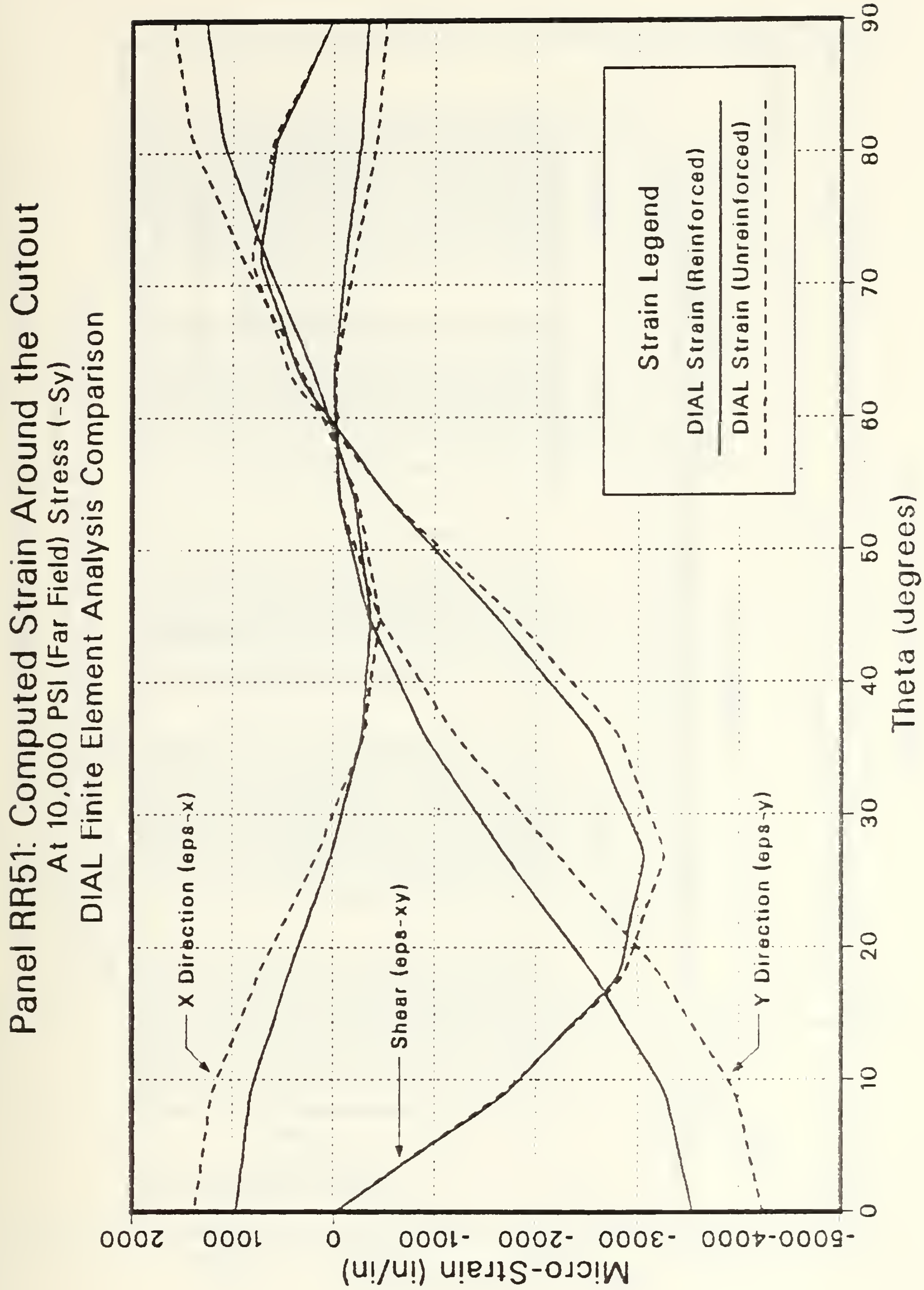

Figure F.2 Panel RR51: Strain Comparison Around the Cutout.

TABLE XXV

PANEL RR51: LEFEA STRAIN DISTRIBUTION AROUND THE CUTOUT (-10,000 PSI).

NODE	X COORD	Y COORD	EPS-Y	EPS-X	EPS-XY
1	0.0000E+00	0.5000E+00	-0.3369E-03	0.1267E-02	0.1695E-04
2	0.3923E-01	0.4985E+00	-0.3035E-03	0.1186E-02	0.2821E-03
3	0.7822E-01	0.4938E+00	-0.2673E-03	0.1099E-02	0.5601E-03
4	0.1167E+00	0.4862E+00	-0.1910E-03	0.8882E-03	0.6468E-03
5	0.1545E+00	0.4755E+00	-0.1133E-03	0.6756E-03	0.7240E-03
6	0.1913E+00	0.4619E+00	-0.5662E-04	0.4295E-03	0.5297E-03
7	0.2270E+00	0.4455E+00	-0.2300E-06	0.1855E-03	0.3266E-03
8	0.2612E+00	0.4263E+00	-0.2491E-04	-0.6197E-05	-0.1001E-03
9	0.2939E+00	0.4045E+00	-0.5096E-04	-0.1943E-03	-0.5320E-03
10	0.3247E+00	0.3802E+00	-0.1961E-03	-0.2782E-03	-0.1063E-02
11	0.3536E+00	0.3536E+00	-0.3436E-03	-0.3592E-03	-0.1596E-02
12	0.3802E+00	0.3247E+00	-0.6213E-03	-0.3192E-03	-0.2074E-02
13	0.4045E+00	0.2939E+00	-0.9029E-03	-0.2769E-03	-0.2550E-02
14	0.4263E+00	0.2612E+00	-0.1293E-02	-0.1278E-03	-0.2806E-02
15	0.4455E+00	0.2270E+00	-0.1688E-02	0.2321E-04	-0.3056E-02
16	0.4619E+00	0.1913E+00	-0.2121E-02	0.2328E-03	-0.2939E-02
17	0.4755E+00	0.1545E+00	-0.2557E-02	0.4432E-03	-0.2811E-02
18	0.4862E+00	0.1167E+00	-0.2912E-02	0.6308E-03	-0.2264E-02
19	0.4938E+00	0.7822E-01	-0.3264E-02	0.8169E-03	-0.1704E-02
20	0.4985E+00	0.3923E-01	-0.3406E-02	0.8940E-03	-0.8552E-03
21	0.5000E+00	0.0000E+00	-0.3539E-02	0.9676E-03	-0.2425E-04

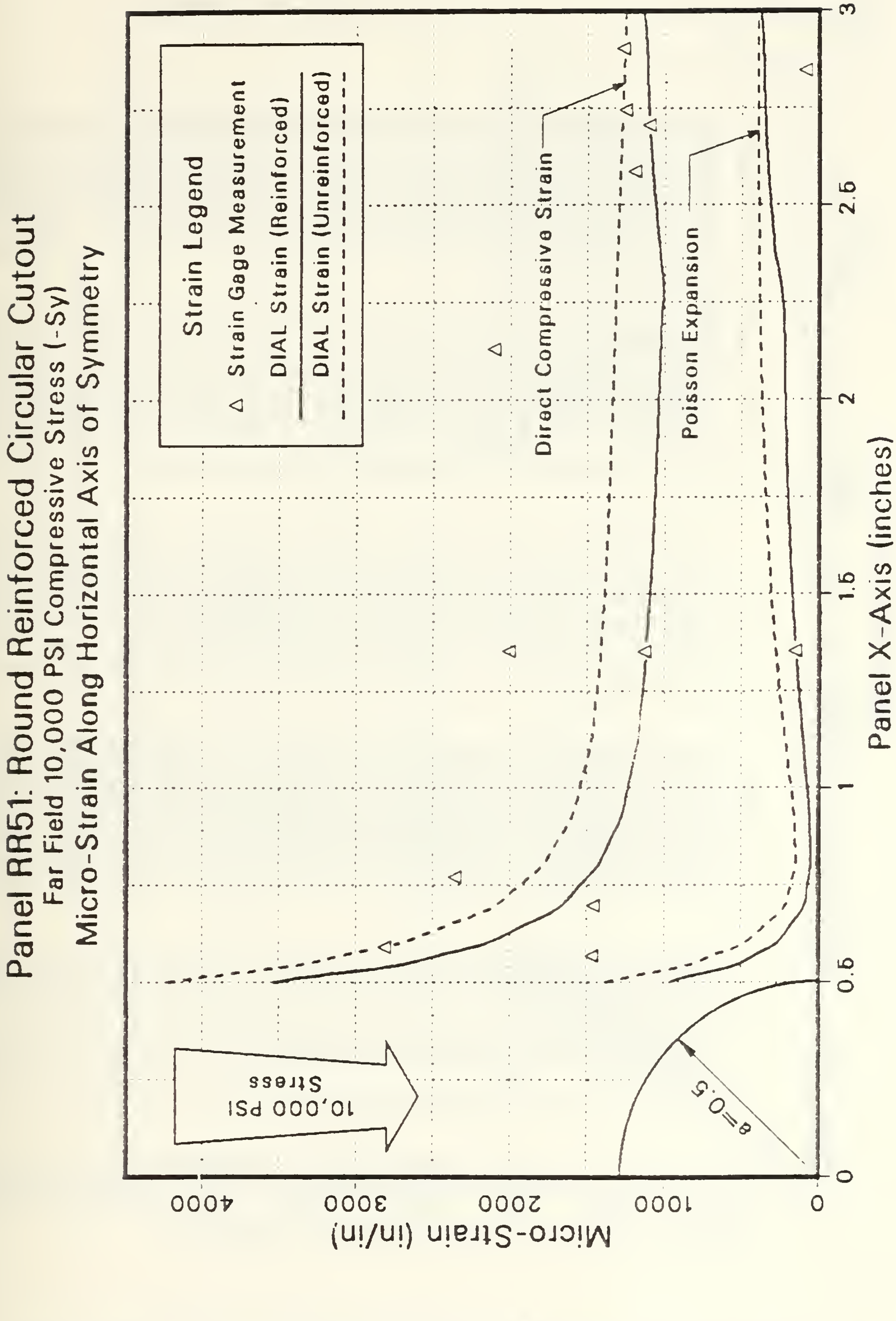

Figure F.3 Panel RR51: Strain Comparison Along the X Axis.

TABLE XXVI

PANEL RR51: LEFEA STRAIN DISTRIBUTION ALONG THE X AXIS (-10,000 PSI).

NODE	X COORD	Y COORD	EPS-Y	EPS-X	EPS-XY
21	0.5000E+00	0.0000E+00	-0.3539E-02	0.9676E-03	-0.2425E-04
32	0.5250E+00	0.0000E+00	-0.3092E-02	0.7296E-03	-0.1537E-04
53	0.5500E+00	0.0000E+00	-0.2656E-02	0.4997E-03	-0.4987E-05
64	0.5750E+00	0.0000E+00	-0.2420E-02	0.3914E-03	-0.3423E-05
85	0.6000E+00	0.0000E+00	-0.2164E-02	0.2709E-03	-0.2016E-05
96	0.6500E+00	0.0000E+00	-0.1903E-02	0.1750E-03	0.6076E-06
117	0.7000E+00	0.0000E+00	-0.1660E-02	0.8895E-04	0.1538E-05
128	0.7500E+00	0.0000E+00	-0.1550E-02	0.7196E-04	0.1861E-05
149	0.8000E+00	0.0000E+00	-0.1432E-02	0.5072E-04	0.2477E-05
160	0.8605E+00	0.0000E+00	-0.1360E-02	0.5429E-04	0.2537E-05
181	0.9210E+00	0.0000E+00	-0.1285E-02	0.5727E-04	0.2728E-05
192	0.1021E+01	0.0000E+00	-0.1228E-02	0.7868E-04	0.2963E-05
213	0.1120E+01	0.0000E+00	-0.1174E-02	0.1001E-03	0.2921E-05
224	0.1210E+01	0.0000E+00	-0.1152E-02	0.1197E-03	0.2783E-05
245	0.1300E+01	0.0000E+00	-0.1128E-02	0.1387E-03	0.2789E-05
256	0.1400E+01	0.0000E+00	-0.1111E-02	0.1554E-03	0.2674E-05
277	0.1500E+01	0.0000E+00	-0.1095E-02	0.1724E-03	0.2530E-05
288	0.1650E+01	0.0000E+00	-0.1077E-02	0.1892E-03	0.2185E-05
309	0.1800E+01	0.0000E+00	-0.1061E-02	0.2054E-03	0.1899E-05
320	0.1950E+01	0.0000E+00	-0.1046E-02	0.2144E-03	0.1995E-05
341	0.2100E+01	0.0000E+00	-0.1032E-02	0.2232E-03	0.1955E-05
352	0.2200E+01	0.0000E+00	-0.1022E-02	0.2260E-03	0.4435E-06
373	0.2300E+01	0.0000E+00	-0.1011E-02	0.2473E-03	-0.1352E-05
384	0.2367E+01	0.0000E+00	-0.1029E-02	0.2830E-03	-0.6789E-06
405	0.2433E+01	0.0000E+00	-0.1048E-02	0.3010E-03	0.1969E-05
416	0.2500E+01	0.0000E+00	-0.1064E-02	0.3144E-03	0.3665E-05
437	0.2567E+01	0.0000E+00	-0.1079E-02	0.3279E-03	0.5033E-05
448	0.2633E+01	0.0000E+00	-0.1090E-02	0.3377E-03	0.7189E-05
469	0.2700E+01	0.0000E+00	-0.1103E-02	0.3485E-03	0.7082E-05
470	0.2917E+01	0.0000E+00	-0.1122E-02	0.3645E-03	0.4129E-05
471	0.3133E+01	0.0000E+00	-0.1139E-02	0.3778E-03	0.1897E-05
472	0.3350E+01	0.0000E+00	-0.1141E-02	0.3775E-03	0.1138E-05
473	0.3567E+01	0.0000E+00	-0.1142E-02	0.3780E-03	0.7185E-06
474	0.3783E+01	0.0000E+00	-0.1141E-02	0.3758E-03	0.4329E-06
475	0.4000E+01	0.0000E+00	-0.1141E-02	0.3741E-03	0.1236E-06
476	0.4125E+01	0.0000E+00	-0.1142E-02	0.3741E-03	0.7999E-07
477	0.4250E+01	0.0000E+00	-0.1143E-02	0.3742E-03	0.5878E-07

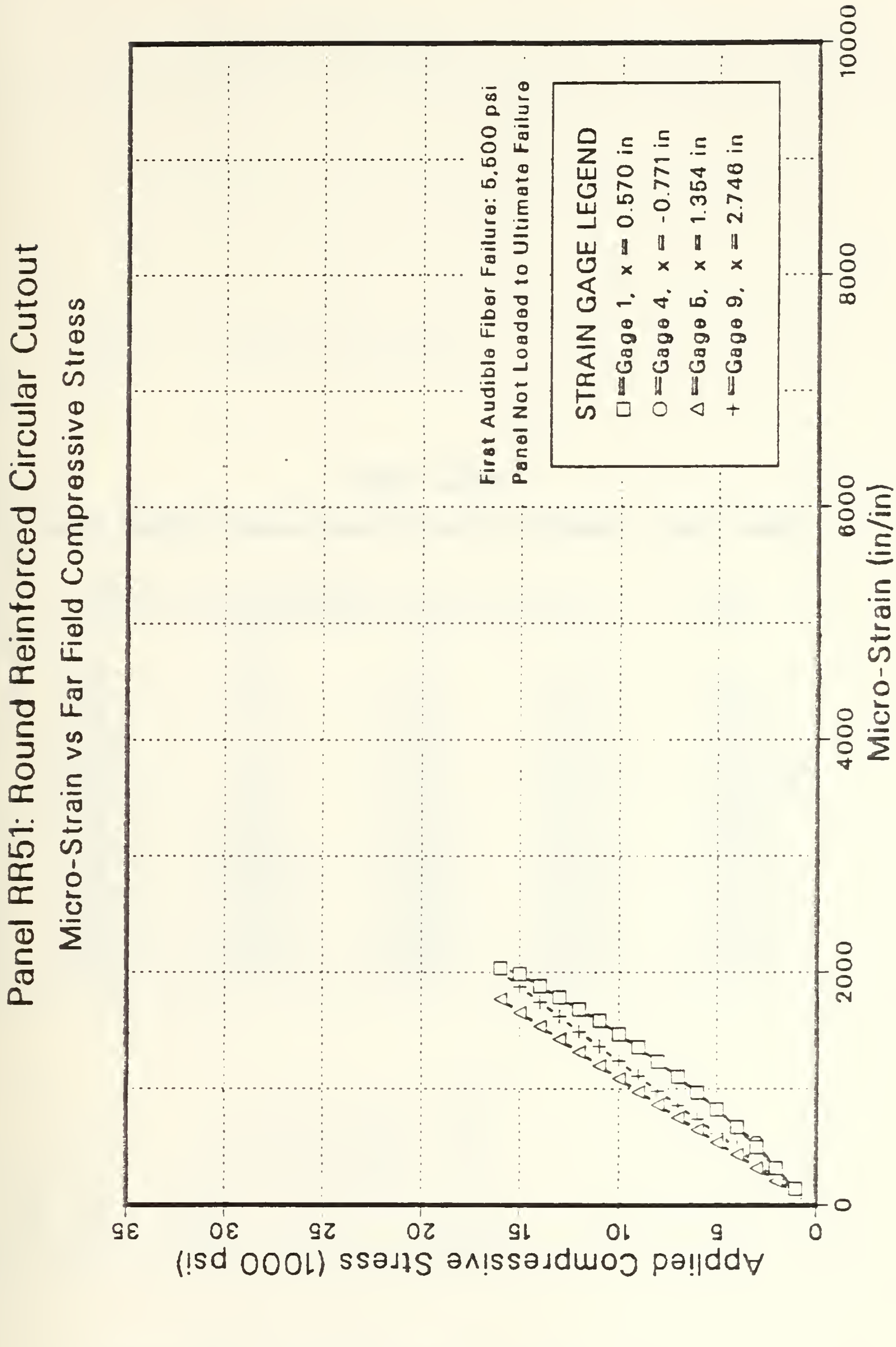

Figure F.4 Panel RR51: Microstrain vs. Compressive Stress.

TABLE XXVII

PANEL RR51: SELECTED STRAIN GAGE VALUES DURING LOAD.

Load (psi)	Micro-Strain Indicated by Gage:			
	#1	#4	#5	#9
1000	-135	-127	-103	-117
2000	-319	-312	[illegible]	-239
3000	-497	-534	[illegible]	-361
4000	-670	-670	[illegible]	-494
5000	-820	-820	[illegible]	-611
6000	-963	-963	[illegible]	-735
7000	-1103	-1103	-754	-857
8000	-1232	-1232	-863	-981
9000	-1357	-1357	-975	-1109
10000	-1467	-1467	-1089	-1238
11000	-1583	-1583	-1200	-1364
12000	-1684	-1684	-1315	-1491
13000	-1783	-1783	-1426	-1618
14000	-1882	-1882	-1539	-1746
15000	-1988	-1988	-1657	-1876
16000	-2032	-2032	-1769	-2006

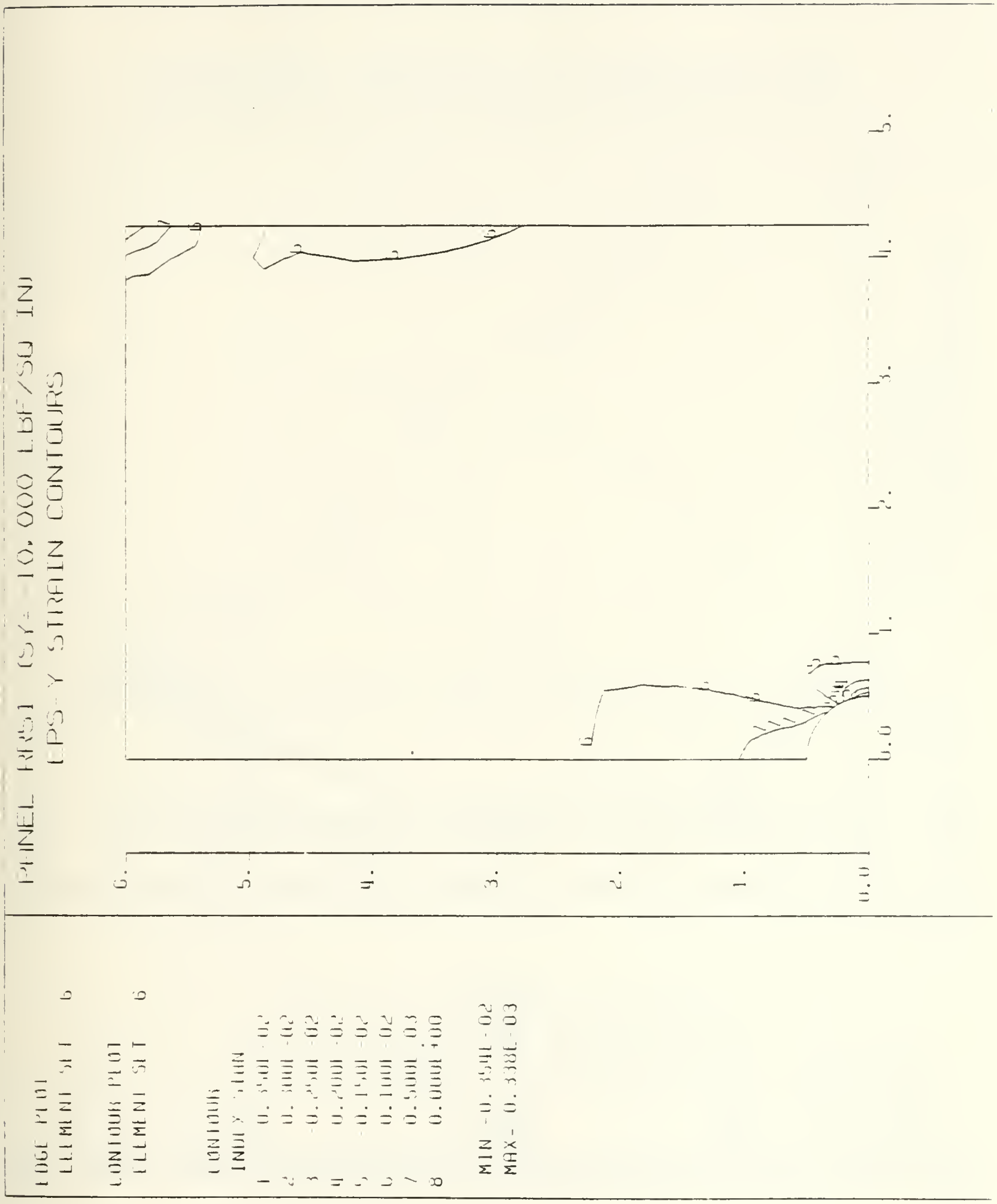

Figure F.5 Panel RR51: Eps-Y FEA Contours.

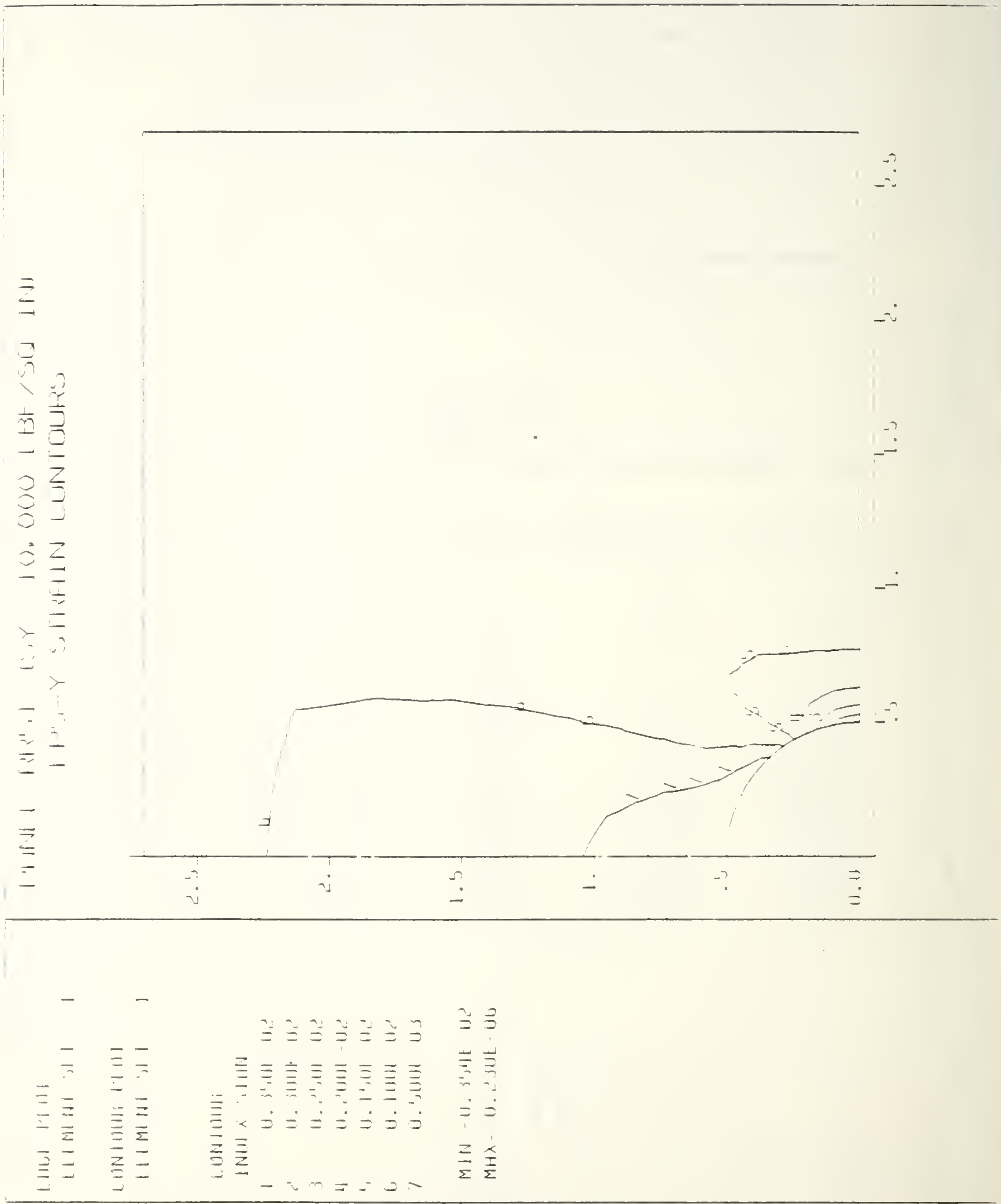

Figure F.6 Panel RR51: Eps-Y FEA Contours Near the Cutout.

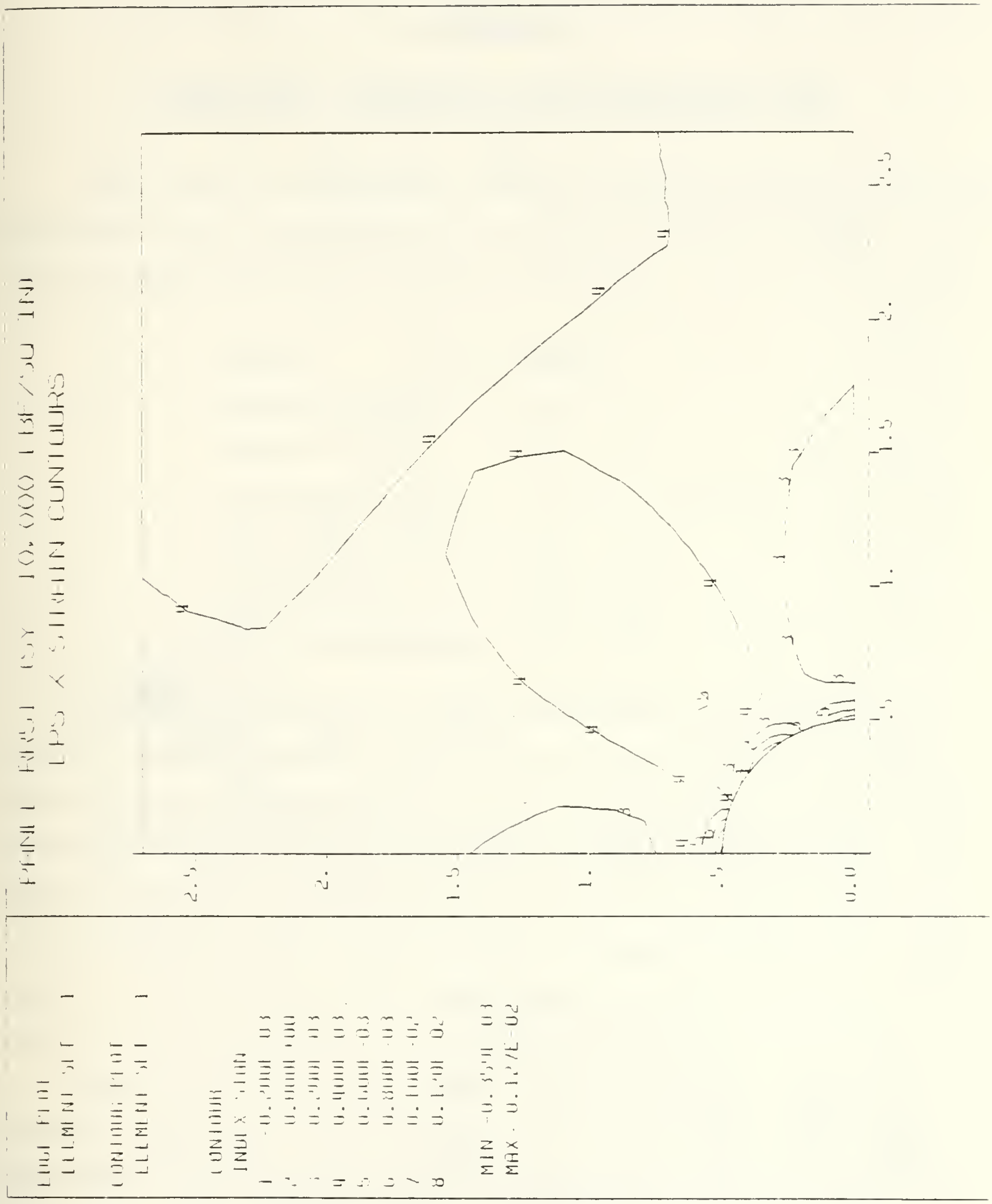

Figure F.7 Panel RR51: Eps-X FEA Contours Near the Cutout.

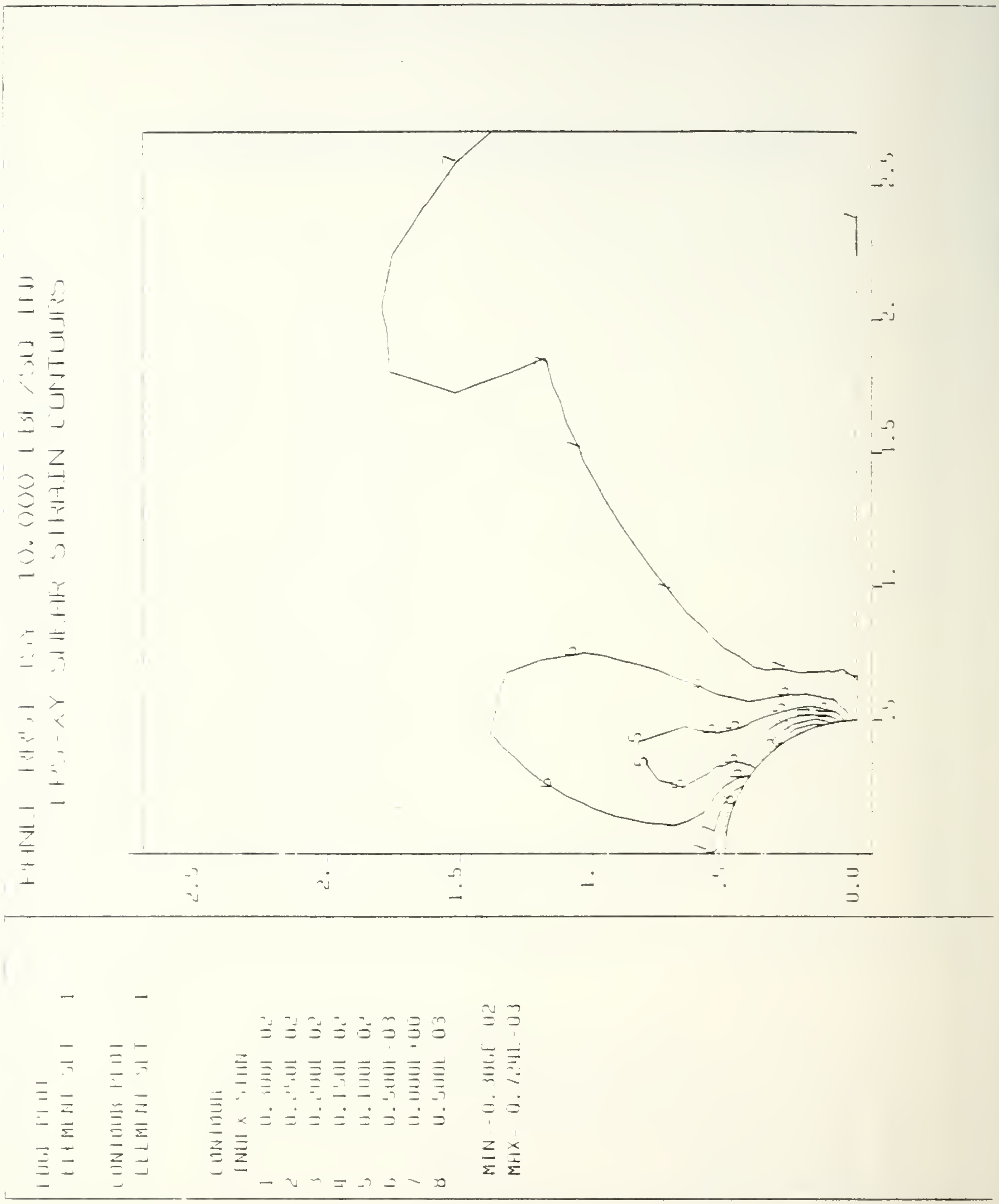

Figure F.8 Panel RR51: Eps-XY FEA Contours Near the Cutout.

APPENDIX G

PANEL RS11: ANALYTICAL AND EXPERIMENTAL DATA

Panel RS11 was reinforced with one square co-cured ply of G/Ep concentric with the cutout on the outside of each facesheet. The reinforcement had the following dimensions:

Shape:	Square
Inside Diameter:	1.00 in
Length & Width:	2.00 in
Thickness (each):	0.014 in (1 ply)
Area (each face):	3.22 in^2
Total Volume:	0.088 in^3
Net Cross Section:	0.028 in^2

The panel failed at the hole edge (Type-1) at an applied normal stress of -31,000 psi, about 90% of the load predicted. Based strictly on the failure of the unreinforced panel and the computed stress concentration factor of 2.64, the predicted failure was $\overline{\sigma}_n$ = -34,600 psi.

The finite element model (mesh) is shown in Figure G.1. The square area of reinforcement is denoted by the heavy outline around the cutout.

Figure G.2 compares the three (finite element) computed strains around the cutout between the unreinforced panel (PO∅∅) and RS11. These computed strain values are listed in Table XXVIII.

Figure G.3 compares the computed (solid and dashed lines) and experimentally measured (triangles) strain along the X axis in the Y and X (poisson expansion) directions in the panel and shows the excellent correlation between analytical and experimental strain at $\bar{\sigma}_n$ = -10,000 psi. There was some minor strain variation between the left and right sides of the hole. Both are represented in the figure as strain gage values on the right side. The difference was small, but visible. The outside edge of the reinforcement can be seen in the figure as an inflection point in the direct compressive strain where it begins increasing at x = 1.1". Table XXVIX gives the computed values of the strain along the X axis.

Figure G.4 is the stress-strain state during the load sequence from $\bar{\sigma}_n$ = 0 to -30 ksi. Experimentally measured strain values are given in Table XXX. Up to about -20 ksi the gage next to the hole (x = +0.561") shows an almost linear stress-strain relation. Gage #4 at x = -0.737" shows the expected degree of loss in local stiffness up to -20 ksi (see Table VI, Figure 5.4 and section III A.1 for a discussion). Gage #1 indicates, starting at about -20 ksi, what at first appears to be a slow but continuous increase in local stiffness indicated by a decreasing strain rate. At corresponding stress values gage #4 indicates an increasing strain rate. These gages were on opposite sides of the panel. What is actually happening is that $\bar{\sigma}_n$ = -28 ksi the right side of the panel is showing significant matrix degradation and the load is being transferred to the left side of the panel next to the cutout. Gage #1 is probably not indicating the true state of strain under its grid. Since the panel was evenly loaded and well constrained the strain at each side of the cutout 90° to the applied load should have been almost identical up to failure.

Figures G.5 through G.8 show the strain contours at $\bar{\sigma}_n$ = -10,000 psi computed and plotted using DIAL. Figure G.5 is the full quarter panel with strain (Eps-Y) parallel to the applied load. Figures G.6 through G.8 (Eps-Y, Eps-X and Eps-XY) show the strains in detail close to the cutout.

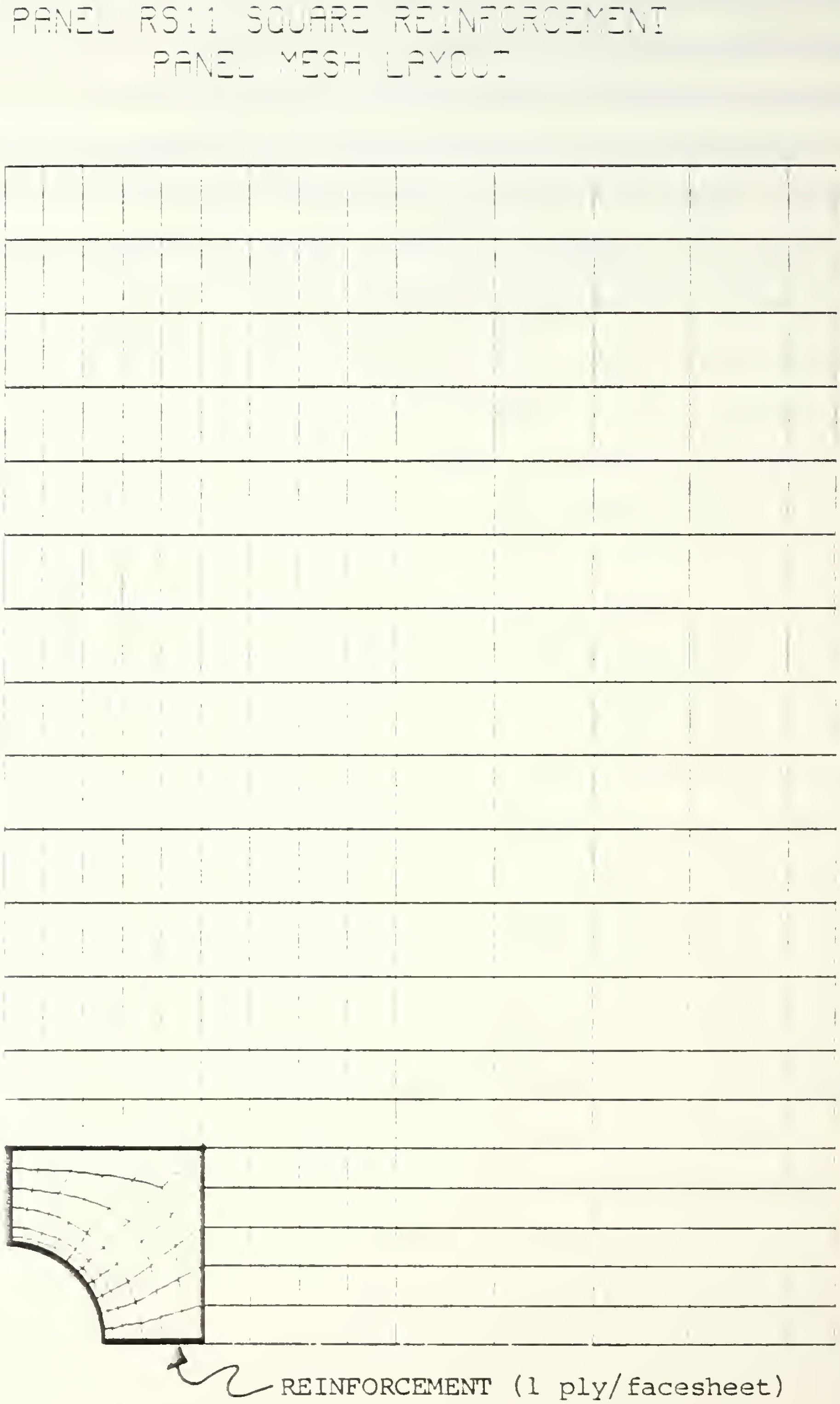

Figure G.1 Panel RS11: DIAL Finite Element Mesh.

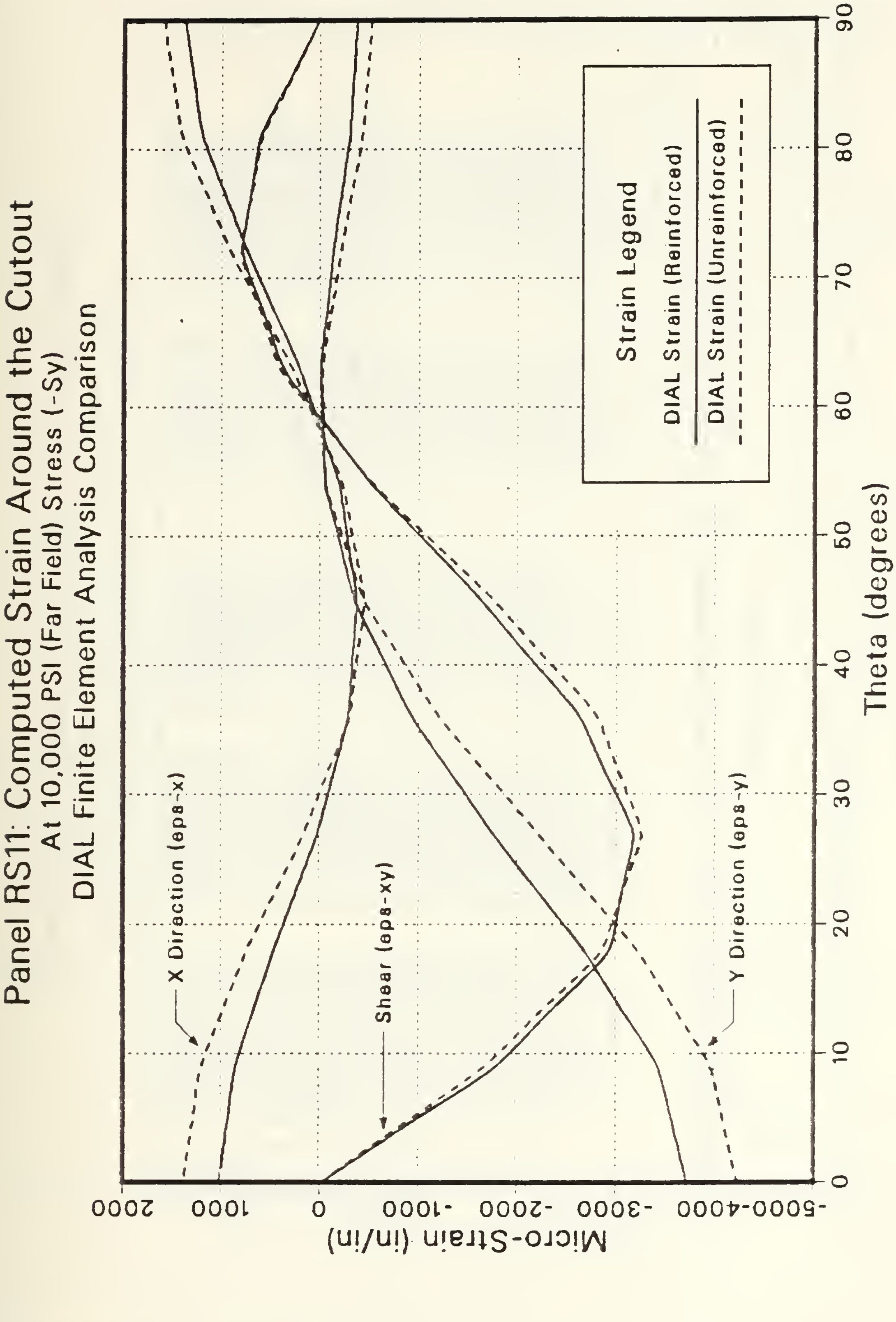

Figure G.2 Panel RS11: Strain Comparison Around the Cutout.

TABLE XXVIII

PANEL RS11: LEFEA STRAIN DISTRIBUTION AROUND THE CUTOUT (-10,000 PSI).

NODE	X COORD	Y COORD	EPS-Y	EPS-X	EPS-XY
1	0.0000E+00	0.5000E+00	-0.3677E-03	0.1382E-02	0.1812E-04
2	0.3923E-01	0.4985E+00	-0.3312E-03	0.1294E-02	0.3077E-03
3	0.7822E-01	0.4938E+00	-0.2918E-03	0.1198E-02	0.6109E-03
4	0.1167E+00	0.4862E+00	-0.2087E-03	0.9701E-03	0.7070E-03
5	0.1545E+00	0.4755E+00	-0.1243E-03	0.7394E-03	0.7925E-03
6	0.1913E+00	0.4619E+00	-0.6227E-04	0.4749E-03	0.5888E-03
7	0.2270E+00	0.4455E+00	-0.7012E-06	0.2129E-03	0.3757E-03
8	0.2612E+00	0.4263E+00	-0.2445E-04	0.8898E-05	-0.7043E-04
9	0.2939E+00	0.4045E+00	-0.4962E-04	-0.1911E-03	-0.5216E-03
10	0.3247E+00	0.3802E+00	-0.1988E-03	-0.2805E-03	-0.1074E-02
11	0.3536E+00	0.3536E+00	-0.3503E-03	-0.3669E-03	-0.1629E-02
12	0.3802E+00	0.3247E+00	-0.6379E-03	-0.3273E-03	-0.2128E-02
13	0.4045E+00	0.2939E+00	-0.9295E-03	-0.2853E-03	-0.2627E-02
14	0.4263E+00	0.2612E+00	-0.1337E-02	-0.1316E-03	-0.2901E-02
15	0.4455E+00	0.2270E+00	-0.1750E-02	0.2416E-04	-0.3170E-02
16	0.4619E+00	0.1913E+00	-0.2208E-02	0.2430E-03	-0.3059E-02
17	0.4755E+00	0.1545E+00	-0.2670E-02	0.4629E-03	-0.2934E-02
18	0.4862E+00	0.1167E+00	-0.3049E-02	0.6606E-03	-0.2369E-02
19	0.4938E+00	0.7822E-01	-0.3424E-02	0.8569E-03	-0.1788E-02
20	0.4985E+00	0.3923E-01	-0.3577E-02	0.9386E-03	-0.8970E-03
21	0.5000E+00	0.0000E+00	-0.3719E-02	0.1017E-02	-0.2601E-04

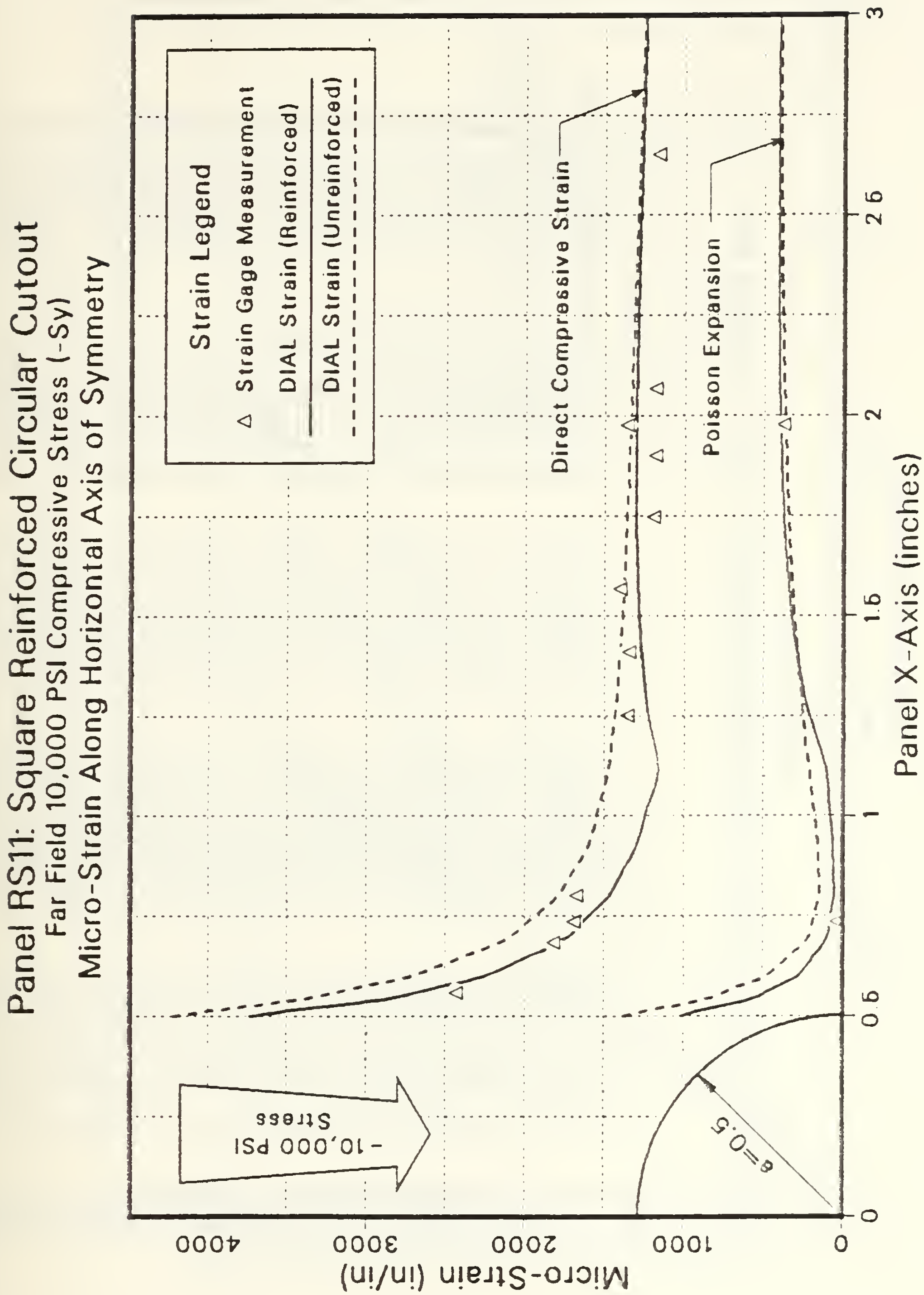

Figure G.3 Panel RS11: Strain Comparison Along the ¯ Axis.

TABLE XXIX

PANEL RS11, LEFEA STRAIN DISTRIBUTION ALONG THE X AXIS (-10,000 PSI).

NODE	X COORD	Y COORD	EPS-Y	EPS-X	EPS-XY
21	0.5000E+00	0.0000E+00	-0.3719E-02	0.1017E-02	-0.2601E-04
32	0.5250E+00	0.0000E+00	-0.3247E-02	0.7667E-03	-0.1635E-04
53	0.5500E+00	0.0000E+00	-0.2787E-02	0.5255E-03	-0.4922E-05
64	0.5750E+00	0.0000E+00	-0.2540E-02	0.4141E-03	-0.2909E-05
85	0.6000E+00	0.0000E+00	-0.2272E-02	0.2895E-03	-0.1167E-05
96	0.6500E+00	0.0000E+00	-0.2003E-02	0.1939E-03	0.1864E-07
117	0.7000E+00	0.0000E+00	-0.1753E-02	0.1085E-03	0.1714E-06
128	0.7500E+00	0.0000E+00	-0.1646E-02	0.9598E-04	0.6064E-06
149	0.8000E+00	0.0000E+00	-0.1531E-02	0.7889E-04	-0.7076E-06
160	0.8500E+00	0.0000E+00	-0.1470E-02	0.8579E-04	0.1112E-05
181	0.9000E+00	0.0000E+00	-0.1409E-02	0.9251E-04	0.2942E-05
192	0.9500E+00	0.0000E+00	-0.1370E-02	0.1055E-03	0.6938E-05
213	0.1000E+01	0.0000E+00	-0.1326E-02	0.1163E-03	0.1029E-04
214	0.1125E+01	0.0000E+00	-0.1297E-02	0.1721E-03	0.6693E-05
215	0.1250E+01	0.0000E+00	-0.1277E-02	0.2302E-03	0.6247E-05
216	0.1375E+01	0.0000E+00	-0.1286E-02	0.2749E-03	0.4728E-05
217	0.1500E+01	0.0000E+00	-0.1291E-02	0.3182E-03	0.2451E-05
218	0.1625E+01	0.0000E+00	-0.1297E-02	0.3441E-03	0.1984E-05
219	0.1750E+01	0.0000E+00	-0.1301E-02	0.3698E-03	0.1297E-05
220	0.1875E+01	0.0000E+00	-0.1301E-02	0.3834E-03	0.1386E-05
221	0.2000E+01	0.0000E+00	-0.1302E-02	0.3981E-03	0.8998E-06
222	0.2250E+01	0.0000E+00	-0.1291E-02	0.4073E-03	0.2243E-06
223	0.2500E+01	0.0000E+00	-0.1280E-02	0.4148E-03	0.2445E-06
224	0.2750E+01	0.0000E+00	-0.1261E-02	0.4110E-03	0.2382E-06
225	0.3000E+01	0.0000E+00	-0.1243E-02	0.4079E-03	-0.3645E-07
226	0.3250E+01	0.0000E+00	-0.1223E-02	0.4011E-03	0.3425E-07
227	0.3500E+01	0.0000E+00	-0.1203E-02	0.3946E-03	0.3496E-07
228	0.3750E+01	0.0000E+00	-0.1183E-02	0.3878E-03	0.2767E-07
229	0.4000E+01	0.0000E+00	-0.1164E-02	0.3812E-03	0.7884E-08
230	0.4125E+01	0.0000E+00	-0.1155E-02	0.3782E-03	0.1325E-07
231	0.4250E+01	0.0000E+00	-0.1146E-02	0.3752E-03	-0.4745E-08

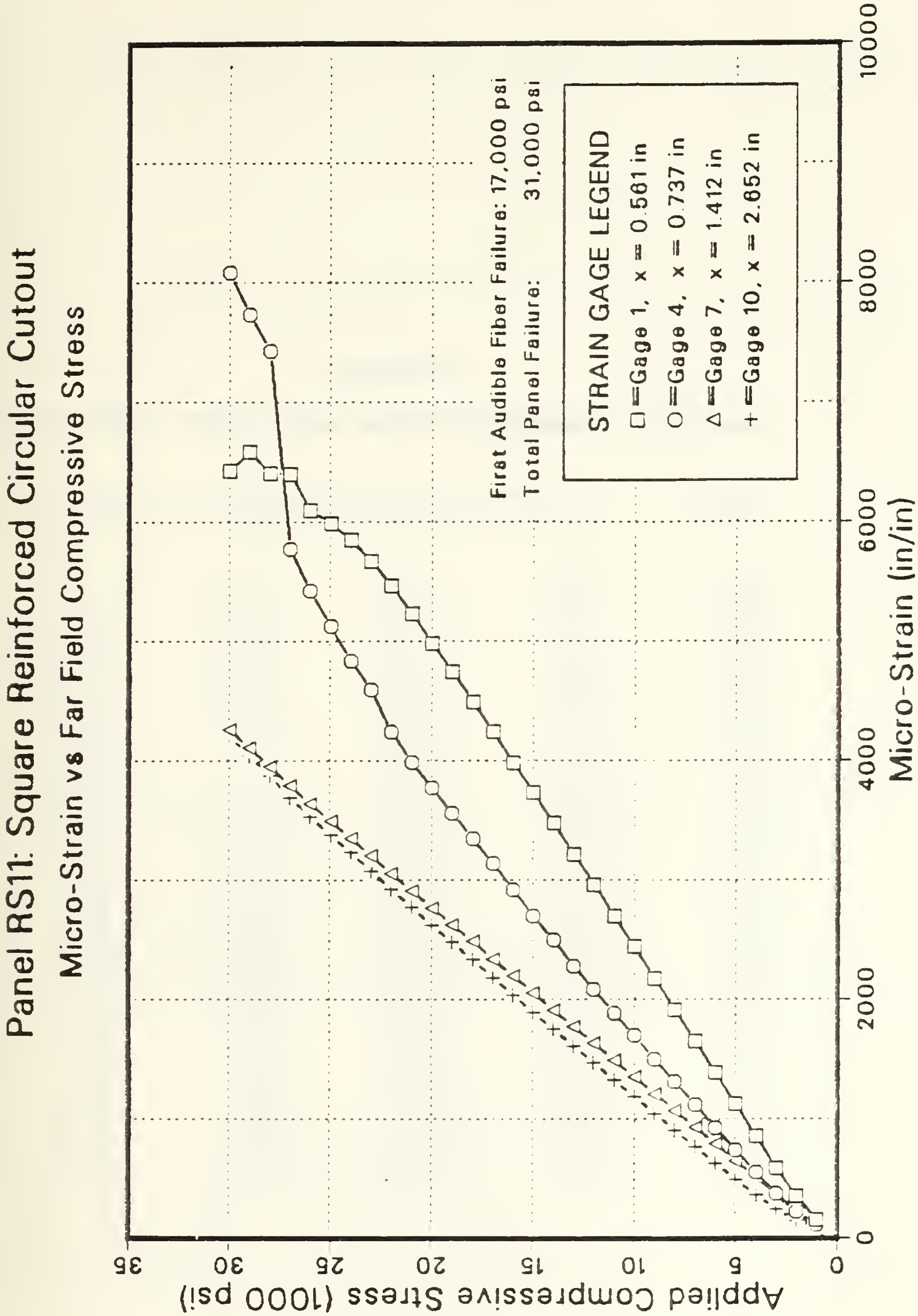

Figure G.4 Panel RS11: Microstrain vs. Compressive Stress.

TABLE XXX

PANEL RS11: SELECTED STRAIN GAGE VALUES DURING LOAD.

Load (psi)	Micro-Strain Indicated by Gage: #1	#4	#7	#10
1000	-151	-108	-72	-86
2000	-349	-221	-217	-144
3000	-587	-371	-357	-240
4000	-857	-554	-508	-361
5000	-1123	-740	-650	-492
6000	-1383	-925	-790	-628
7000	-1650	-1118	-930	-765
8000	-1910	-1308	-1071	-905
9000	-2174	-1500	-1210	-1044
10000	-2439	-1695	[illegible]	-1187
11000	-2697	-1886	[illegible]	-1325
12000	-2962	-2081	[illegible]	-1466
13000	-3217	-2276	-1771	-1607
14000	-3475	-2494	[illegible]	-1750
15000	-3729	-2695	[illegible]	-1892
16000	-3978	-2919	[illegible]	-2037
17000	-4242	-3136	-2337	-2182
18000	-4492	-3344	-2481	-2330
19000	-4744	-3556	-2623	-2473
20000	-4980	-3769	-2766	-2621
21000	-5229	-3988	-2910	-2771
22000	-5460	-4240	-3054	-2922
23000	-5666	-4594	-3205	-3078
24000	-5848	-4835	-3352	-3233
25000	-5988	-5124	-3494	-3379
26000	-6098	-5421	-3641	-3533
27000	-6403	-5773	-3790	-3692
28000	-6407	-7431	-3955	-3379
29000	-6583	-7731	-4107	-4043
30000	-6429	-8081	-4264	-4207

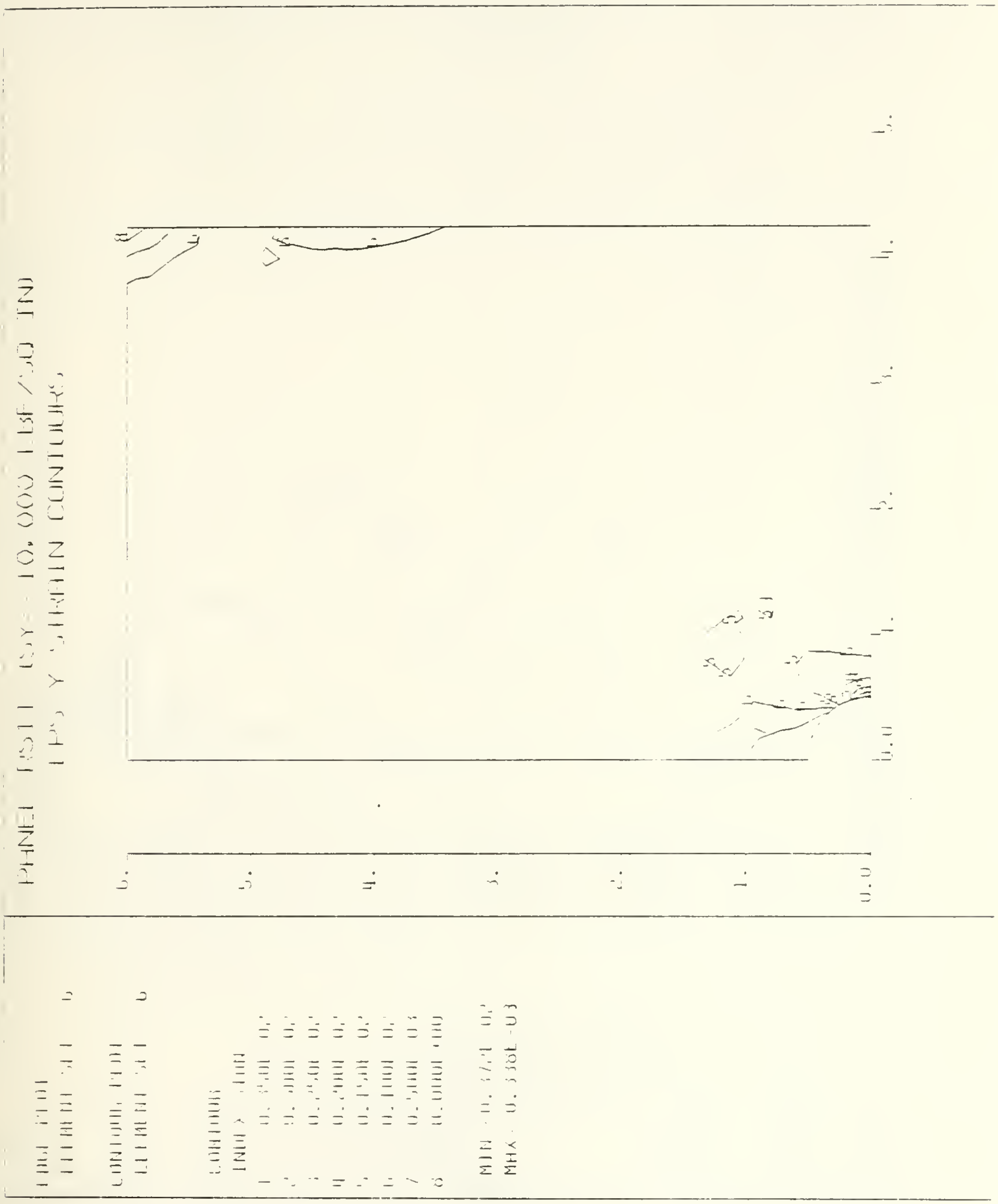

Figure G.5 Panel RS11: Eps-Y FEA Contours.

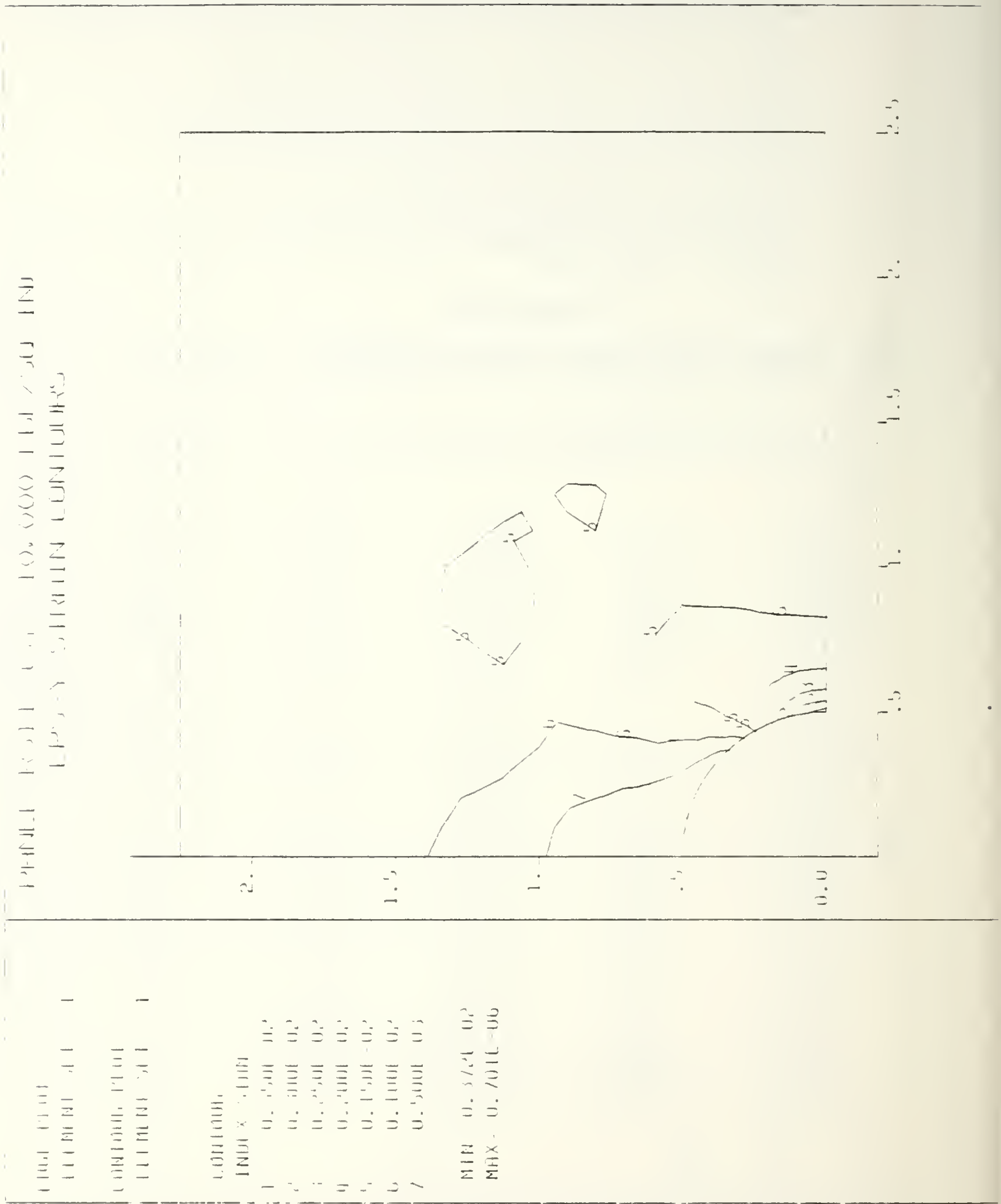

Figure G.6 Panel RS11: Eps-Y FEA Contours Near the Cutout.

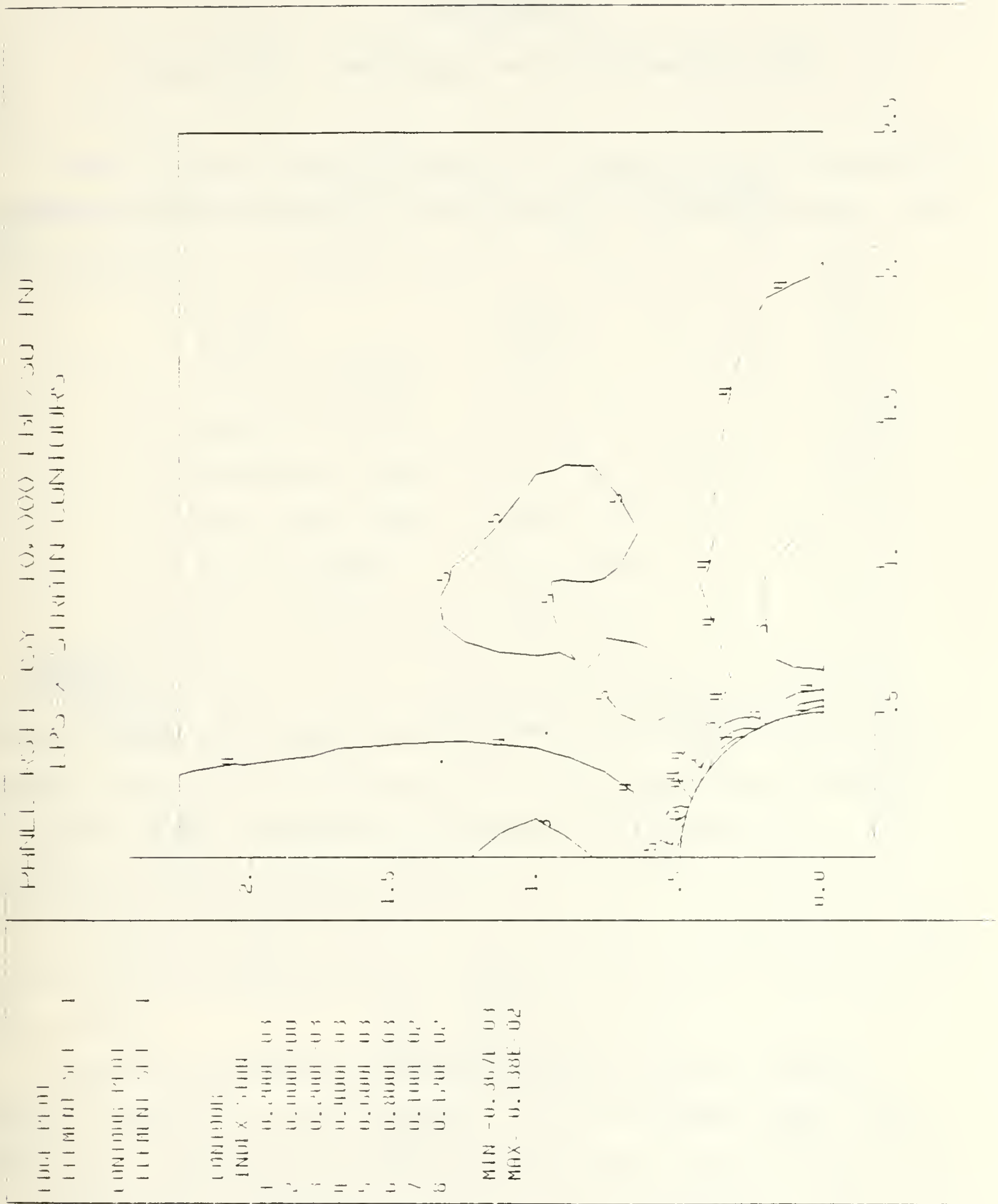

Figure G.7   Panel RS11: Eps-X FEA Contours Near the Cutout.

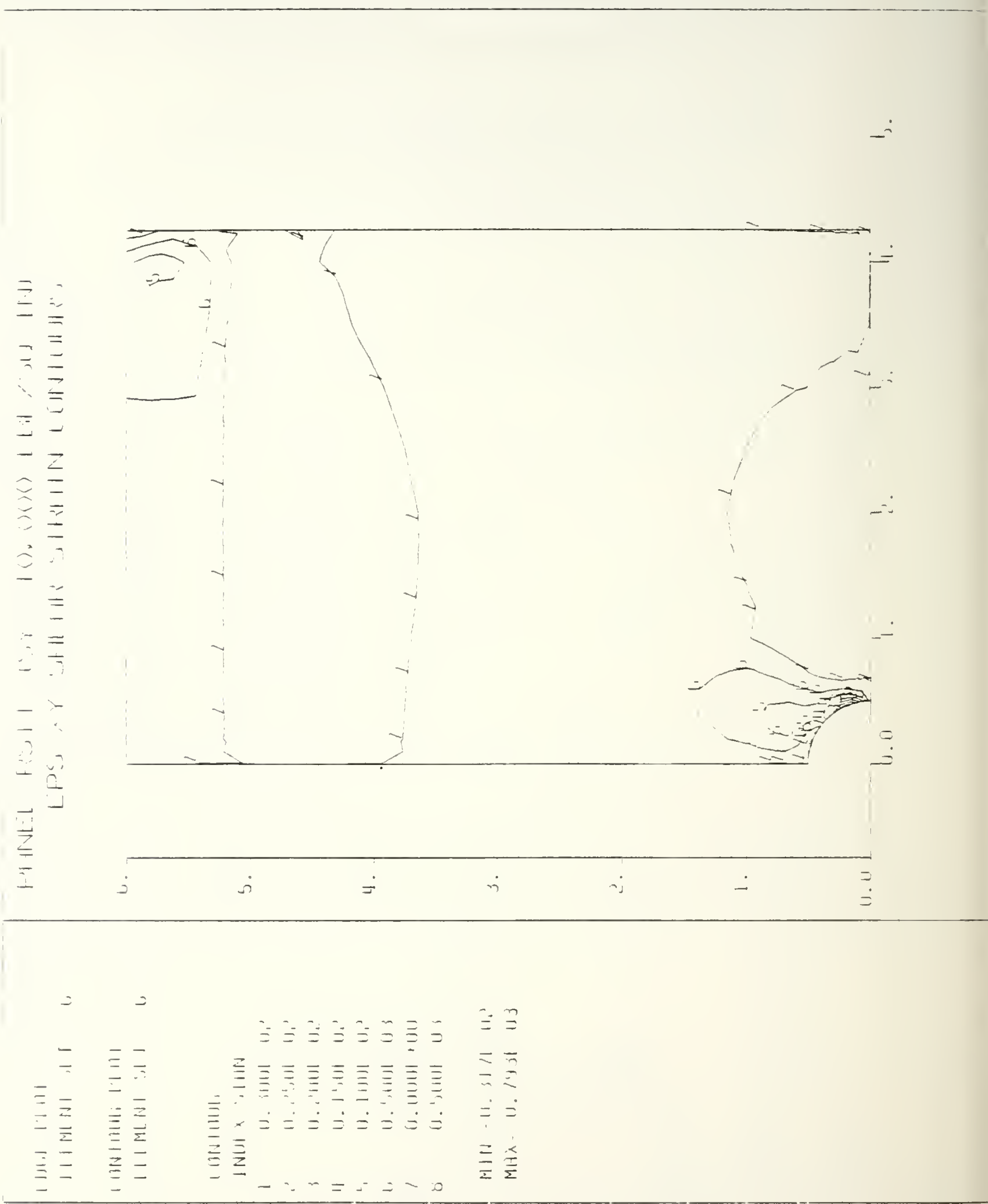

Figure G.8 Panel RS11: Eps-XY FEA Contours Near the Cutout.

APPENDIX H

PANEL RS31: ANALYTICAL AND EXPERIMENTAL DATA

Panel RS31 was reinforced with one square co-cured ply of G/Ep concentric with the cutout on the outside of each facesheet. The reinforcement had the following dimensions:

Shape:	Square
Inside Diameter:	1.00 in
Length & Width:	3.20 in
Thickness (each):	0.014 in (1 ply)
Area (each face):	9.455 in^2
Total Volume:	0.265 in^3
Net Cross Section:	0.062 in^2

The panel failed at the hole edge (Type-1) at an applied normal stress of -32,550 psi, 89% of the ultimate load predicted. Based strictly on the failure of the unreinforced panel and the computed stress concentration factor of 2.51, failure was predicted at $\bar{\sigma}_n = -36{,}400$ psi.

The finite element model (mesh) is shown in Figure H.1. The square area of reinforcement is denoted by the bold lines next to the cutout.

Figure H.2 compares the three (finite element) computed strains around the cutout between the unreinforced panel (PO∅∅) and RS31. These computed strain values are listed in Table XXXI.

Figure H.3 compares the computed and experimental strains in the Y and X (poisson expansion) directions in the panel and shows an almost perfect correlation between analytical and experimental strain at $\bar{\sigma}_n$ = -10,000 psi. There was virtually no strain variation between the left and right sides of the hole. The edge of the reinforcement is somewhat difficult to see in the Figure H.3 as a slight inflection point at about x = 1.6". Table XXXII gives the LEFEA computed strain values along the X axis.

Figure H.4 graphically shows the stress-strain state during the load sequence from $\bar{\sigma}_n$ = 0 to -32 ksi. The experimentally measured strain gage values are given in Table XXXIII. Up to about 20 ksi gage #1 next to the hole (x = +0.553") shows an almost linear stress-strain relation. At or just above -20 ksi, however, there appears what seems to be a sudden decrease in strain rate on the right side of the cutout which just as suddenly ends at -23 ksi where the previous stress-strain ratio resumes. I believe that this is, instead, a transfer of very localized stress (or the load path) away from the area next to the cutout to some other path in the field or possibly the opposite facesheet. It is important to note that gage #2 on the left side of the cutout at x = -0.597" shows no corresponding increase in strain that would be caused by the transfer of load. Gage #3 at x = +0.666" shows some correspondence with gage #1 degree of loss in local stiffness up to -20 ksi. If it were a malfunction of the strain gage or a partial debonding from the surface of the composite the strain rate would change.

Another anomaly occurs at $\bar{\sigma}_n$ above -27 ksi where the "stair-step" phenomenon occurs again. Gage #3 at x = 0.666" reflects what is occurring next to the cutout edge. This is not true of gages #6 and #11 at x = -1.48" and 2.54" respectively; they reflect only the expected stress-strain relation. At -30 ksi gage

#1 indicated a rapidly increasing rate of strain and subsequently failed.

Figures H.5 through H.8 show the strain contours at $\bar{\sigma}_n$ = -10,000 psi computed and plotted using DIAL. Figure H.5 is the full quarter panel with strain (Eps-Y) parallel to the applied load. Figures H.6 through H.8 (Eps-Y, Eps-X and Eps-XY) show the strains in detail close to the cutout.

PANEL RS31: SQUARE REINFORCEMENT
PANEL MESH LAYOUT

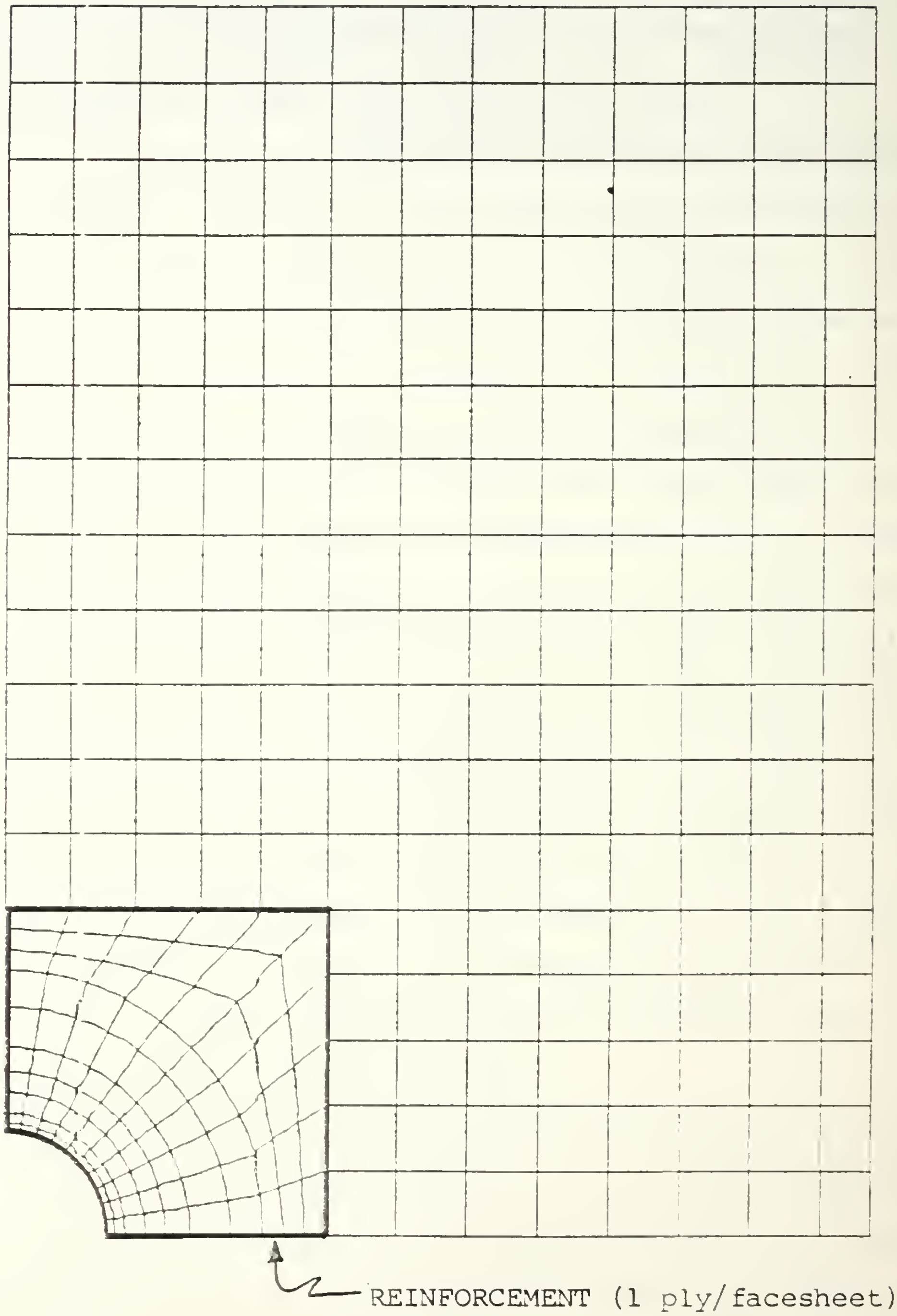

Figure H.1 Panel RS31: DIAL Finite Element Mesh.

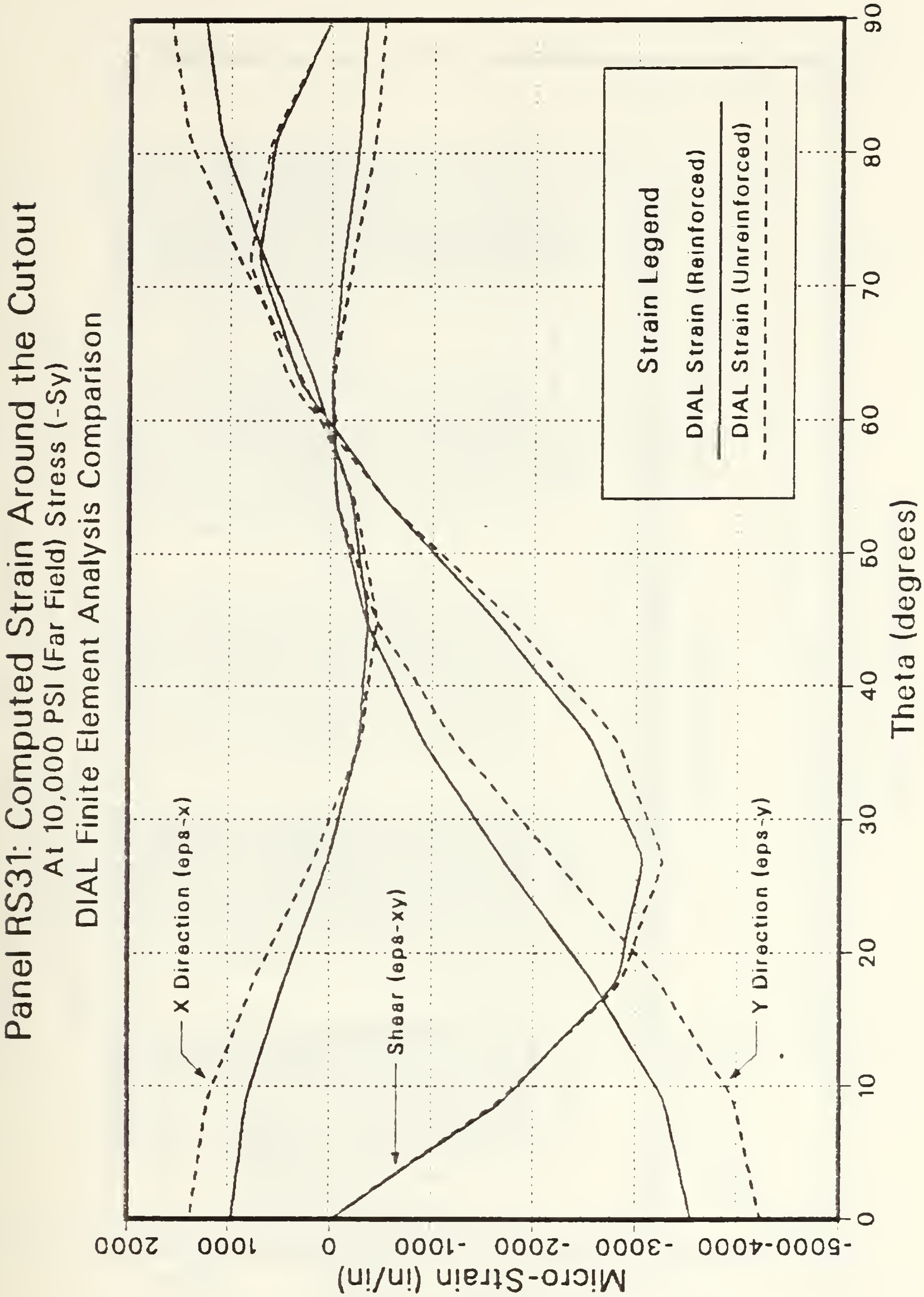

Figure H.2 Panel RS31: Strain Comparison Around the Cutout.

TABLE XXXI

PANEL RS31: LEFEA STRAIN DISTRIBUTION AROUND THE CUTOUT (-10,000 PSI).

NODE	X COORD	Y COORD	EPS-Y	EPS-X	EPS-XY
1	0.0000E+00	0.5000E+00	-0.3334E-03	0.1254E-02	0.1680E-04
2	0.3923E-01	0.4985E+00	-0.3002E-03	0.1173E-02	0.2789E-03
3	0.7822E-01	0.4938E+00	-0.2643E-03	0.1086E-02	0.5538E-03
4	0.1167E+00	0.4862E+00	-0.1886E-03	0.8772E-03	0.6385E-03
5	0.1545E+00	0.4755E+00	-0.1116E-03	0.6659E-03	0.7136E-03
6	0.1913E+00	0.4619E+00	-0.5570E-04	0.4215E-03	0.5191E-03
7	0.2270E+00	0.4455E+00	-0.7876E-07	0.1793E-03	0.3157E-03
8	0.2612E+00	0.4263E+00	-0.2523E-04	-0.1076E-04	-0.1095E-03
9	0.2939E+00	0.4045E+00	-0.5172E-04	-0.1973E-03	-0.5399E-03
10	0.3247E+00	0.3802E+00	-0.1969E-03	-0.2801E-03	-0.1069E-02
11	0.3536E+00	0.3536E+00	-0.3443E-03	-0.3600E-03	-0.1600E-02
12	0.3802E+00	0.3247E+00	-0.6218E-03	-0.3197E-03	-0.2076E-02
13	0.4045E+00	0.2939E+00	-0.9031E-03	-0.2770E-03	-0.2551E-02
14	0.4263E+00	0.2612E+00	-0.1293E-02	-0.1279E-03	-0.2807E-02
15	0.4455E+00	0.2270E+00	-0.1688E-02	0.2322E-04	-0.3058E-02
16	0.4619E+00	0.1913E+00	-0.2122E-02	0.2331E-03	-0.2942E-02
17	0.4755E+00	0.1545E+00	-0.2560E-02	0.4437E-03	-0.2814E-02
18	0.4862E+00	0.1167E+00	-0.2916E-02	0.6317E-03	-0.2267E-02
19	0.4938E+00	0.7822E-01	-0.3269E-02	0.8182E-03	-0.1707E-02
20	0.4985E+00	0.3923E-01	-0.3412E-02	0.8955E-03	-0.8566E-03
21	0.5000E+00	0.0000E+00	-0.3545E-02	0.9694E-03	-0.2429E-04

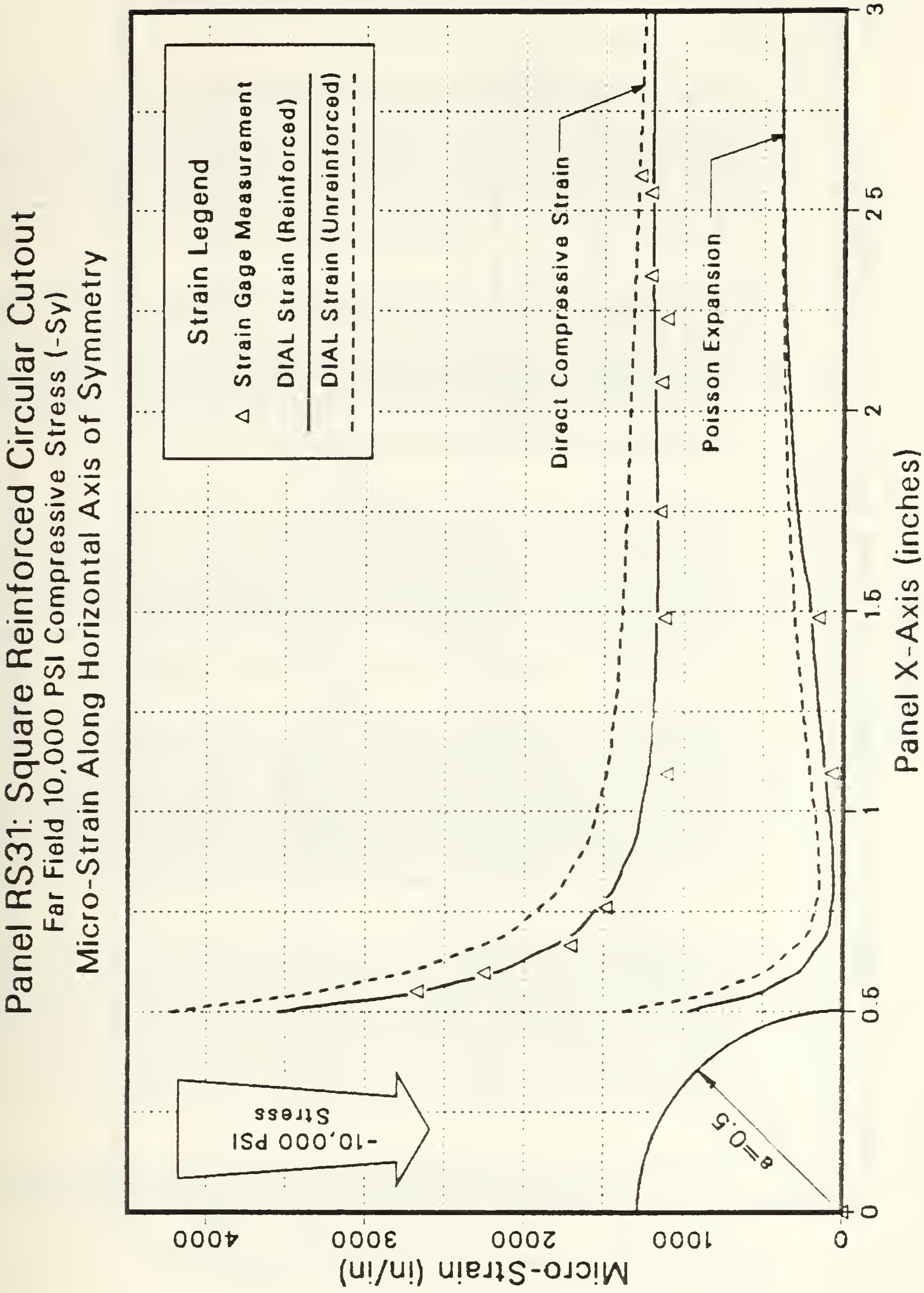

Figure H.3   Panel RS31: Strain Comparison Along the X Axis.

TABLE XXXII

PANEL RS31: LEFEA STRAIN DISTRIBUTION ALONG THE X AXIS (-10,000 PSI).

NODE	X COORD	Y COORD	EPS-Y	EPS-X	EPS-XY
21	0.5000E+00	0.0000E+00	-0.3545E-02	0.9694E-03	-0.2429E-04
32	0.5250E+00	0.0000E+00	-0.3099E-02	0.7313E-03	-0.1542E-04
53	0.5500E+00	0.0000E+00	-0.2663E-02	0.5013E-03	-0.4966E-05
64	0.5750E+00	0.0000E+00	-0.2428E-02	0.3933E-03	-0.3377E-05
85	0.6000E+00	0.0000E+00	-0.2172E-02	0.2730E-03	-0.1979E-05
96	0.6500E+00	0.0000E+00	-0.1914E-02	0.1780E-03	0.6641E-06
117	0.7000E+00	0.0000E+00	-0.1673E-02	0.9272E-04	0.1598E-05
128	0.7500E+00	0.0000E+00	-0.1566E-02	0.7686E-04	0.1969E-05
149	0.8000E+00	0.0000E+00	-0.1451E-02	0.5673E-04	0.2618E-05
160	0.8605E+00	0.0000E+00	-0.1383E-02	0.6209E-04	0.2551E-05
181	0.9210E+00	0.0000E+00	-0.1312E-02	0.6679E-04	0.2628E-05
192	0.1021E+01	0.0000E+00	-0.1263E-02	0.9236E-04	0.3406E-05
213	0.1120E+01	0.0000E+00	-0.1218E-02	0.1180E-03	0.3780E-05
224	0.1210E+01	0.0000E+00	-0.1204E-02	0.1423E-03	0.1611E-05
245	0.1300E+01	0.0000E+00	-0.1189E-02	0.1654E-03	-0.1529E-07
256	0.1350E+01	0.0000E+00	-0.1186E-02	0.1759E-03	0.4857E-06
277	0.1400E+01	0.0000E+00	-0.1182E-02	0.1870E-03	0.5659E-06
288	0.1450E+01	0.0000E+00	-0.1179E-02	0.1972E-03	0.2390E-05
309	0.1500E+01	0.0000E+00	-0.1176E-02	0.2076E-03	0.3845E-05
320	0.1550E+01	0.0000E+00	-0.1172E-02	0.2161E-03	0.6024E-05
341	0.1600E+01	0.0000E+00	-0.1168E-02	0.2416E-03	0.7863E-05
342	0.1771E+01	0.0000E+00	-0.1173E-02	0.2934E-03	0.5047E-05
343	0.1943E+01	0.0000E+00	-0.1180E-02	0.3276E-03	0.3707E-05
344	0.2114E+01	0.0000E+00	-0.1190E-02	0.3487E-03	0.2864E-05
345	0.2286E+01	0.0000E+00	-0.1198E-02	0.3697E-03	0.1669E-05
346	0.2457E+01	0.0000E+00	-0.1201E-02	0.3797E-03	0.1378E-05
347	0.2629E+01	0.0000E+00	-0.1204E-02	0.3897E-03	0.9517E-06
348	0.2800E+01	0.0000E+00	-0.1201E-02	0.3922E-03	0.7488E-06
349	0.2971E+01	0.0000E+00	-0.1199E-02	0.3948E-03	0.4958E-06
350	0.3143E+01	0.0000E+00	-0.1192E-02	0.3932E-03	0.3890E-06
351	0.3314E+01	0.0000E+00	-0.1186E-02	0.3917E-03	0.2582E-06
352	0.3486E+01	0.0000E+00	-0.1179E-02	0.3885E-03	0.2055E-06
353	0.3657E+01	0.0000E+00	-0.1172E-02	0.3854E-03	0.1397E-06
354	0.3829E+01	0.0000E+00	-0.1165E-02	0.3824E-03	0.1068E-06
355	0.4000E+01	0.0000E+00	-0.1159E-02	0.3796E-03	0.6790E-07
356	0.4125E+01	0.0000E+00	-0.1155E-02	0.3782E-03	0.3794E-07
357	0.4250E+01	0.0000E+00	-0.1151E-02	0.3768E-03	0.6505E-08

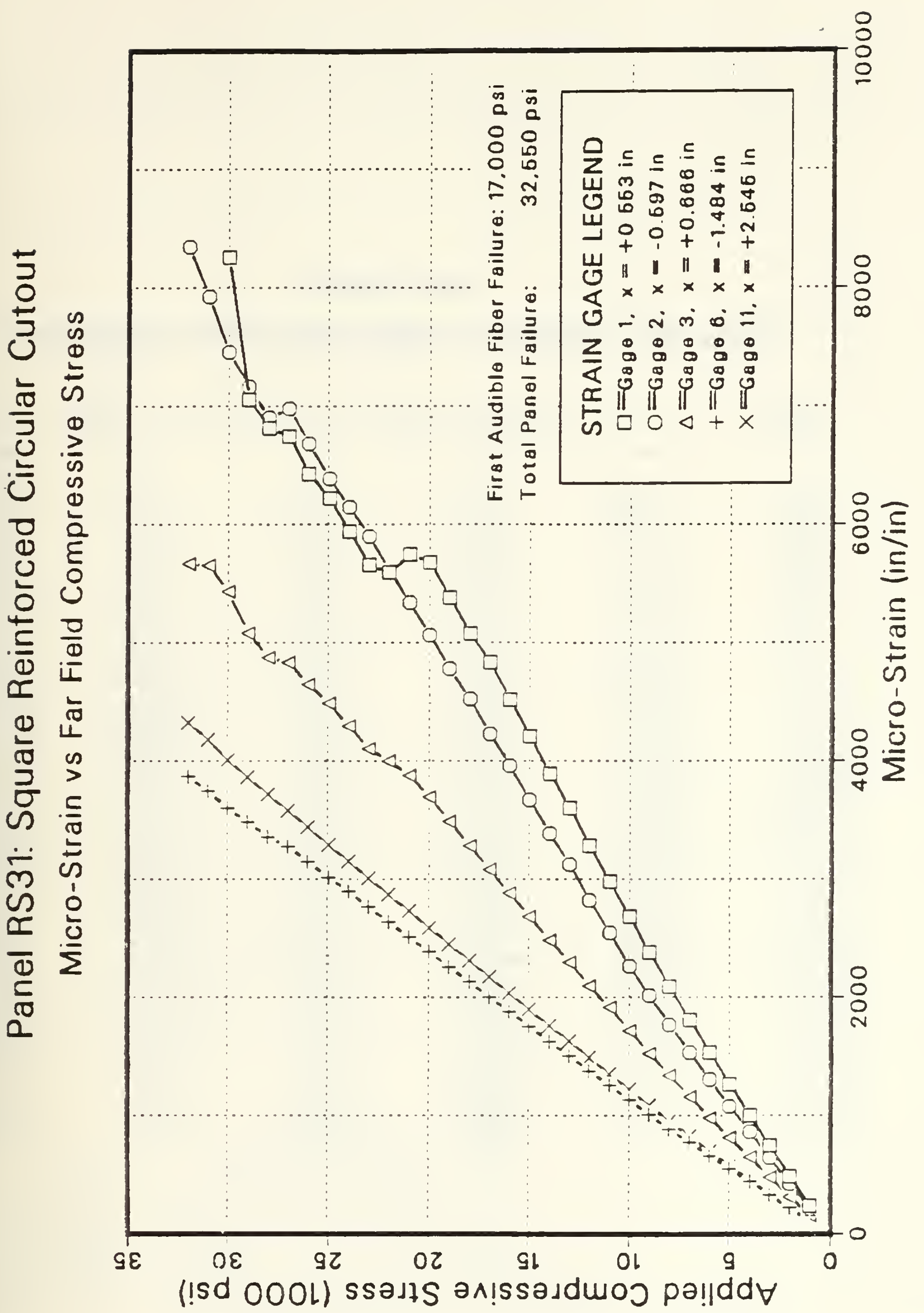

Figure H.4 Panel RS31: Microstrain vs. Compressive Stress.

TABLE XXXIII

PANEL RS31: SELECTED STRAIN GAGE VALUES DURING LOAD.

Load (psi)	Micro-Strain Indicated by Gage: #1	#2	#3	#6	#11
1000	-234	-207	-153	-107	-102
2000	-485	-420	-313	-219	-213
3000	-742	-642	-478	-330	-330
4000	-1003	-860	-645	-441	-451
5000	-1264	-1077	-811	-547	-572
6000	-1534	-1301	-982	-657	-695
7000	-1810	-1533	-1162	-770	-825
8000	-2090	-1767	-1341	-886	-953
9000	-2382	-2012	-1526	-1006	-1085
10000	-2681	-2263	-1719	-1131	-1213
11000	-2979	-2544	-1907	-1253	-1352
12000	-3281	-2823	-2098	-1375	-1487
13000	-3600	-3125	-2300	-1505	-1630
14000	-3893	-3389	-2485	-1624	-1757
15000	-4208	-3672	-2684	-1753	-1895
16000	-4520	-3960	-2881	-1878	-2034
17000	-4837	-4230	-3083	-2002	-2171
18000	-5074	-4522	-3285	-2131	-2310
19000	-5377	-4779	-3492	-2256	-2449
20000	-5677	-5065	-3696	-2383	-2589
21000	-5744	-5336	-3874	-2509	-2728
22000	-5590	-5606	-4000	-2635	-2868
23000	-5658	-5899	-4104	-2765	-3010
24000	-5940	-6144	-4298	-2894	-3153
25000	-6222	-6389	-4487	-3017	-3292
26000	-6430	-6680	-4651	-3148	-3438
27000	-6748	-6977	-4832	-3278	-3578
28000	-6817	-6903	-4876	-3356	-3716
29000	-7055	-7164	-5084	-3480	-3861
30000	-8252	-7454	-5432	-3602	-4004
31000	n/a	-7927	-5657	-3743	-4178
32000	n/a	-8343	-5672	-3871	-4327
32500	n/a	-8583	-4949	-3932	-4417

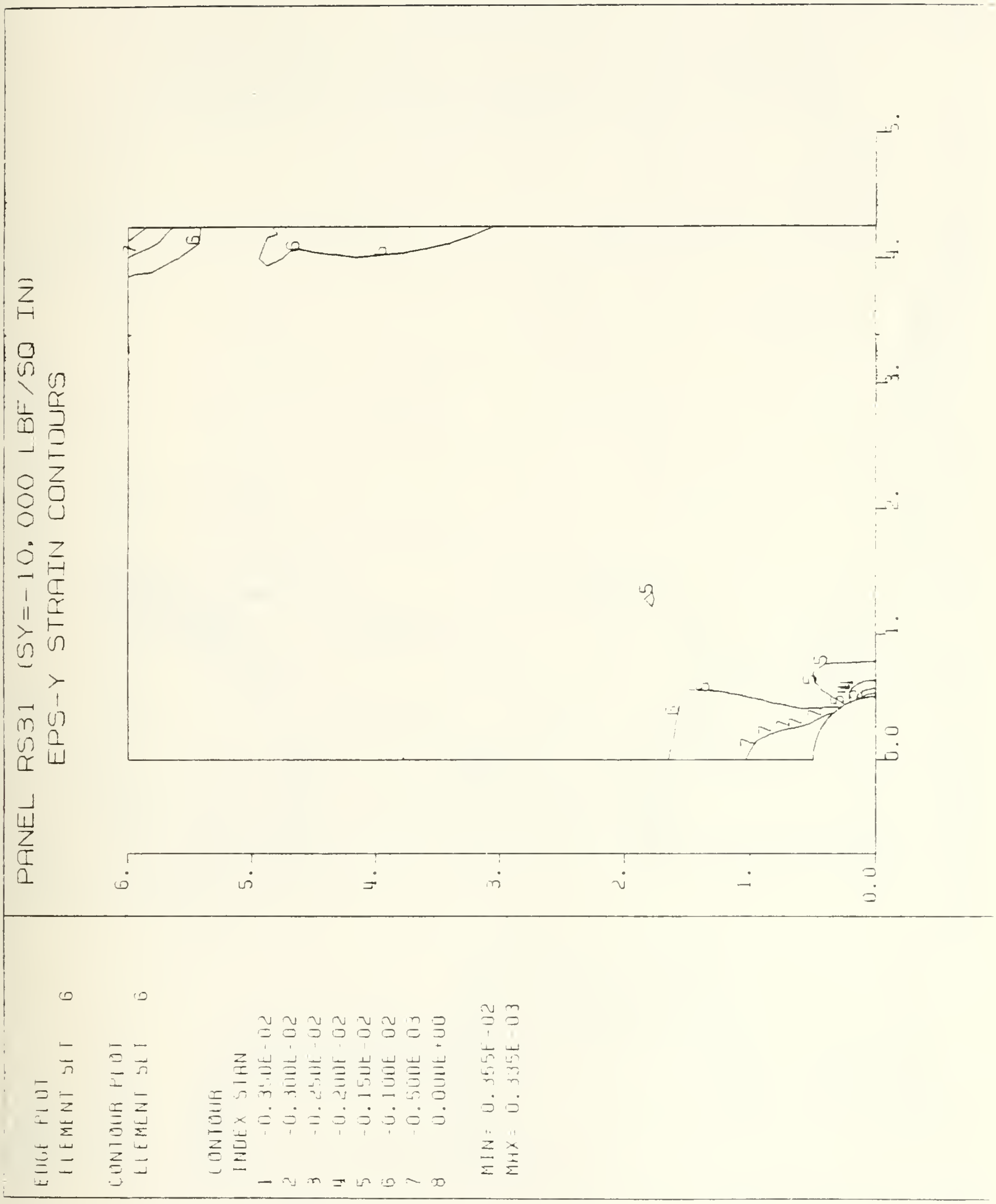

Figure H.5 Panel RS31: Eps-Y FEA Contours.

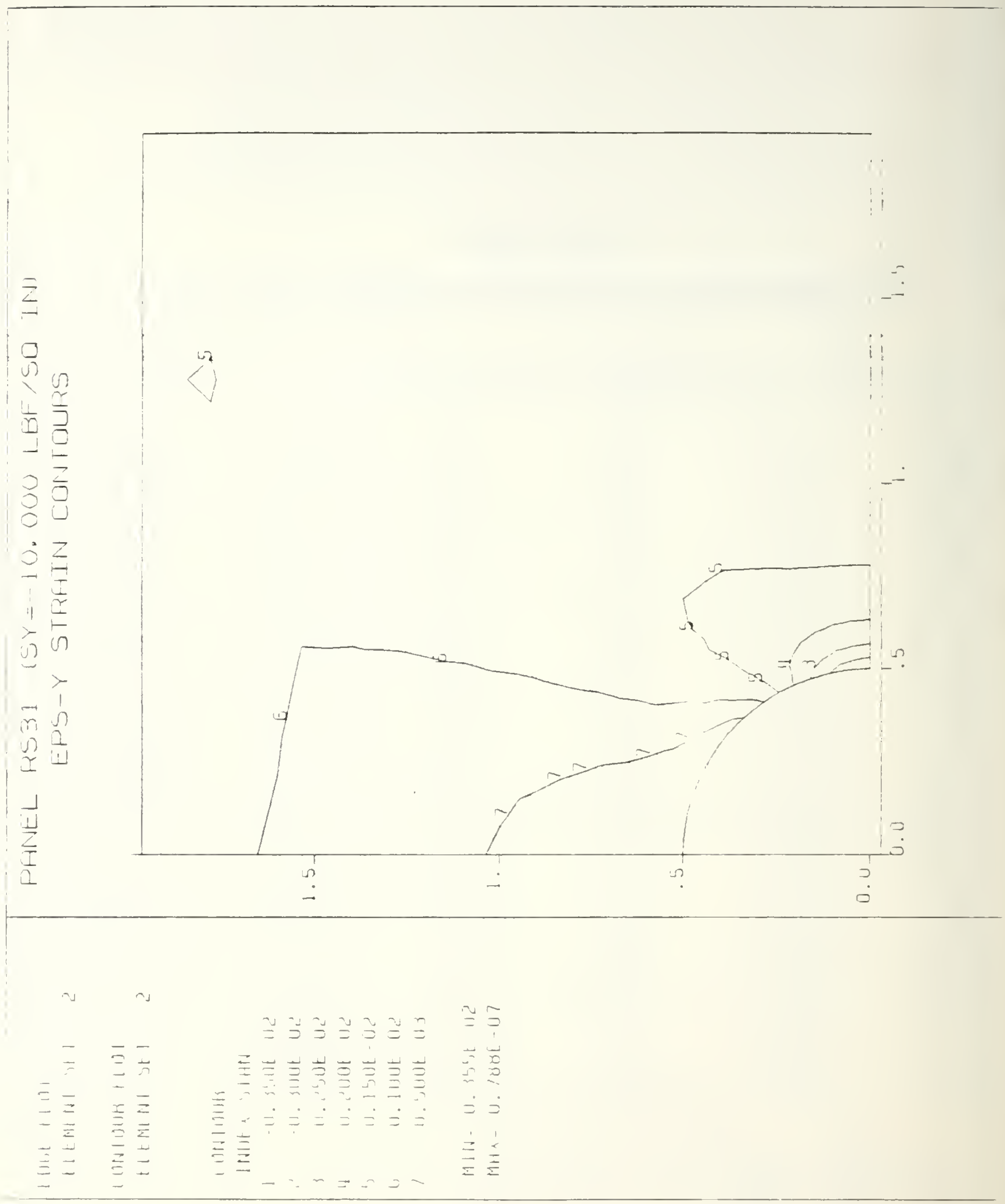

Figure H.6 Panel RS31: Eps-Y FEA Contours Near the Cutout.

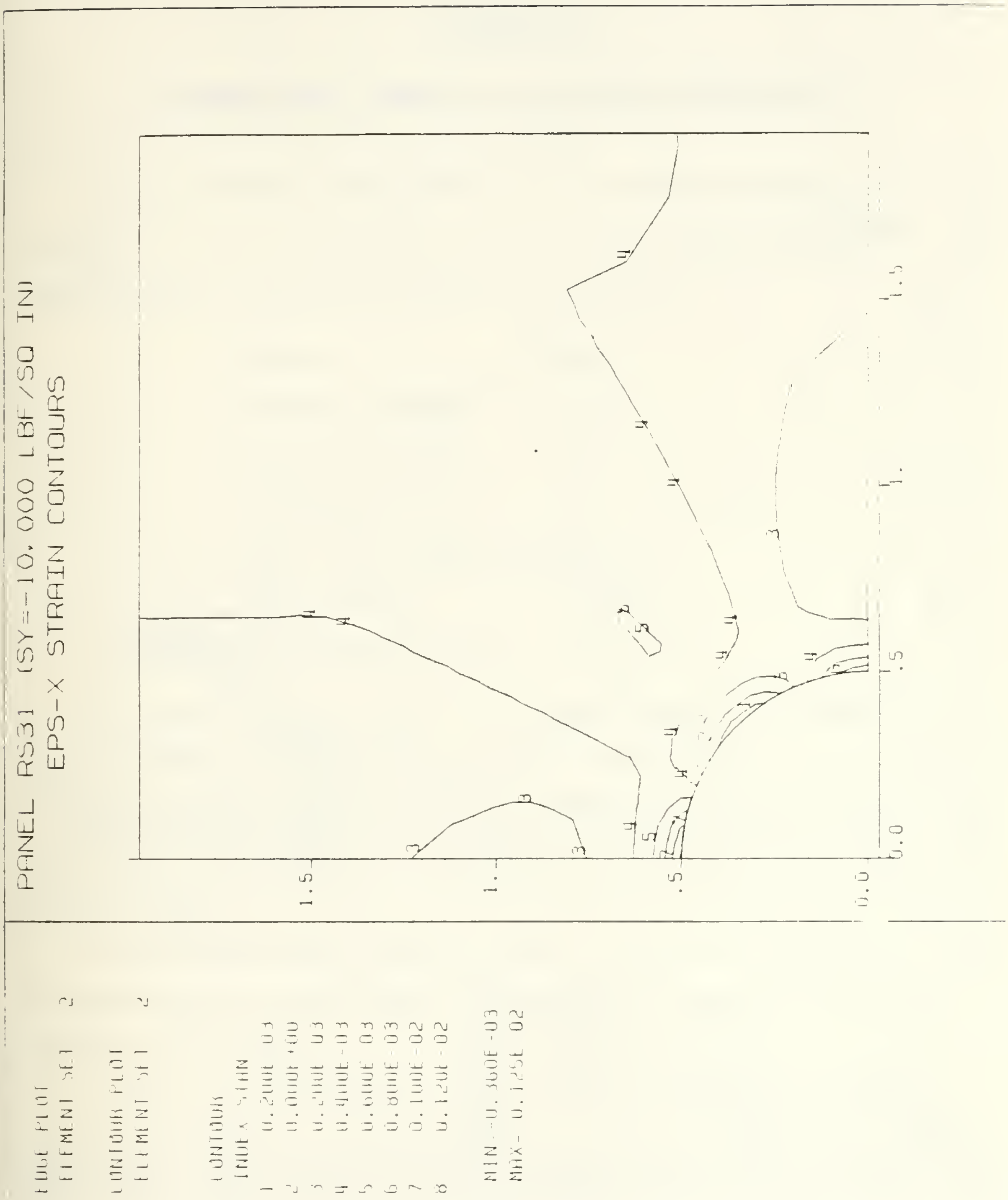

Figure H.7 Panel RS31: Eps-X FEA Contours Near the Cutout.

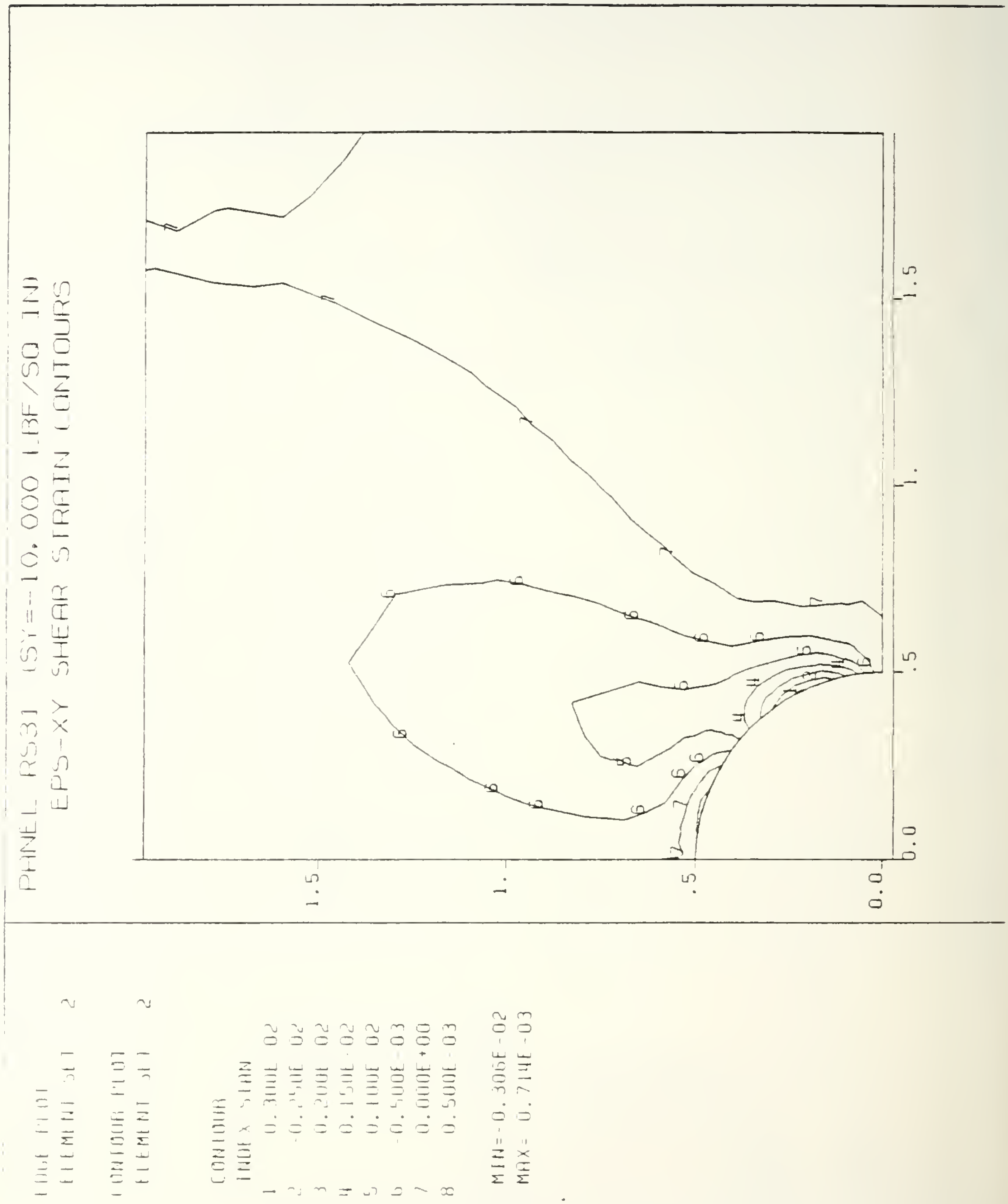

Figure H.8 Panel RS31: Eps-XY FEA Contours Near the Cutout.

APPENDIX I

PANEL RS51: ANALYTICAL AND EXPERIMENTAL DATA

Panel RS51 was reinforced with one square co-cured ply of G/Ep concentric with the cutout on the outside of each facesheet. The reinforcement had the following dimensions:

Shape:	Square
Inside Diameter:	1.00 in
Length & Width:	4.10 in
Thickness (each):	0.014 in (1 ply)
Area (each face):	16.025 in^2
Total Volume:	0.449 in^3
Net Cross Section:	0.087 in^2

The panel failed at the hole edge (Type-1) at an applied normal stress of about -16,000 psi. Based strictly on the failure of the unreinforced panel and the computed stress concentration factor of 2.46, however, the failure should have been close $\bar{\sigma}_n$ = -37,000 psi.

The finite element model (mesh) is shown in Figure I.1. The square area of reinforcement is denoted by the heavy outline around the cutout.

Figure I.2 compares the three (finite element) computed strains around the cutout between the unreinforced panel (POØØ) and RS51. These computed strain values are listed in Table XXXIV.

Figure I.3 compares the computed (solid and dashed lines) and experimental (triangles) strains in the Y and X (poisson expansion) directions in the panel and shows excellent correlation between analytical and experimental strain at -10,000 psi applied normal stress. There was some minor strain variation between the left and right sides of the hole. The edge of the reinforcement is very difficult to see in the figure as a very slight inflection point at about x = 2.0". Table XXXV gives the analytical strain values along the X axis.

Figure I.4 graphically shows the stress-strain state during the load sequence from $\bar{\sigma}_n$ = 0 to -21 ksi. Experimentally measured strain gage values are given in Table XXXVI. Up to about -16 ksi gage #1 next to the hole (x = +0.553") shows the expected almost linear stress-strain relation. However, just above $\bar{\sigma}_n$ = -16 ksi up to -19 ksi there begins a apparent loss in stiffness on the right side of the cutout which suddenly ends at -19 ksi where the strain next to the cutout drops to almost zero. Note that gage #3 on the right side of the cutout at x = 0.666" shows no corresponding increase in strain that would be caused by an increase in local stress near the cutout due to a shift in the load path. Gages #5 and #11 at x = 1.44" and -2.76" respectively reflect only the expected stress-strain relation. This can be explained by gages #1 and 3 showing the effect of a gage under compression when the facesheet under it suddenly buckles outward. The result was a near zero strain indication. It is difficult to see, but there is an appreciable increase in strain rate indicated in gages #5 and #11 at $\bar{\sigma}_n$ = -20 ksi. This confirms that there is a sudden increase in load in an area relatively far from the cutout, just as would be expected when the material close to the cutout begins to fail and the load paths are displaced away from it increasing the stain in the far-field.

Figures I.5 through I.8 show the strain contours at $\bar{\sigma}_n$ = -10,000 psi computed and plotted using DIAL. Figure I.5 is the full quarter panel with strain (Eps-Y) parallel to the applied load. Figures I.6 through I.8 (Eps-Y, Eps-X and Eps-XY) show the strains in detail close to the cutout.

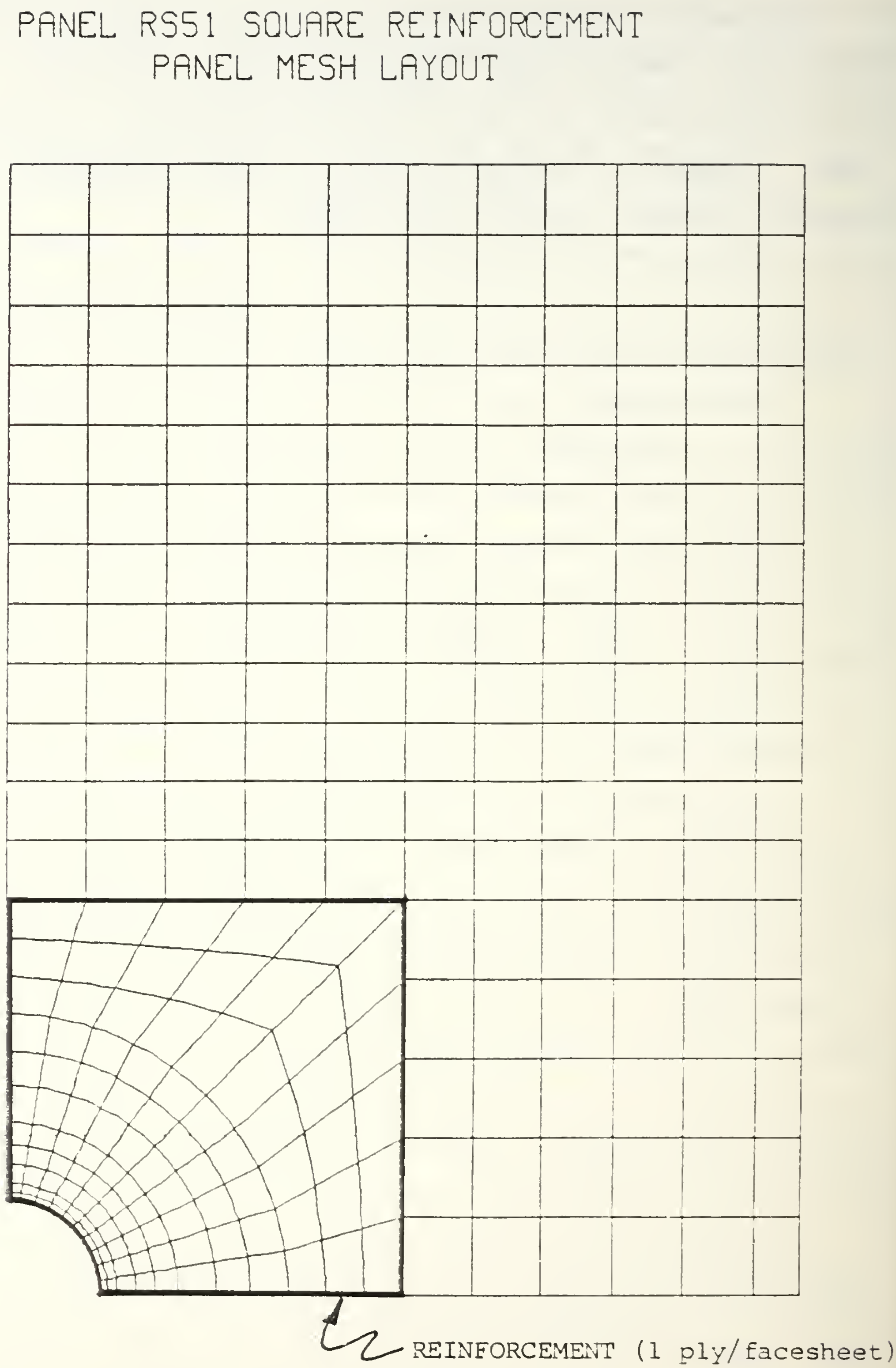

Figure I.1 Panel RS51: DIAL Finite Element Mesh.

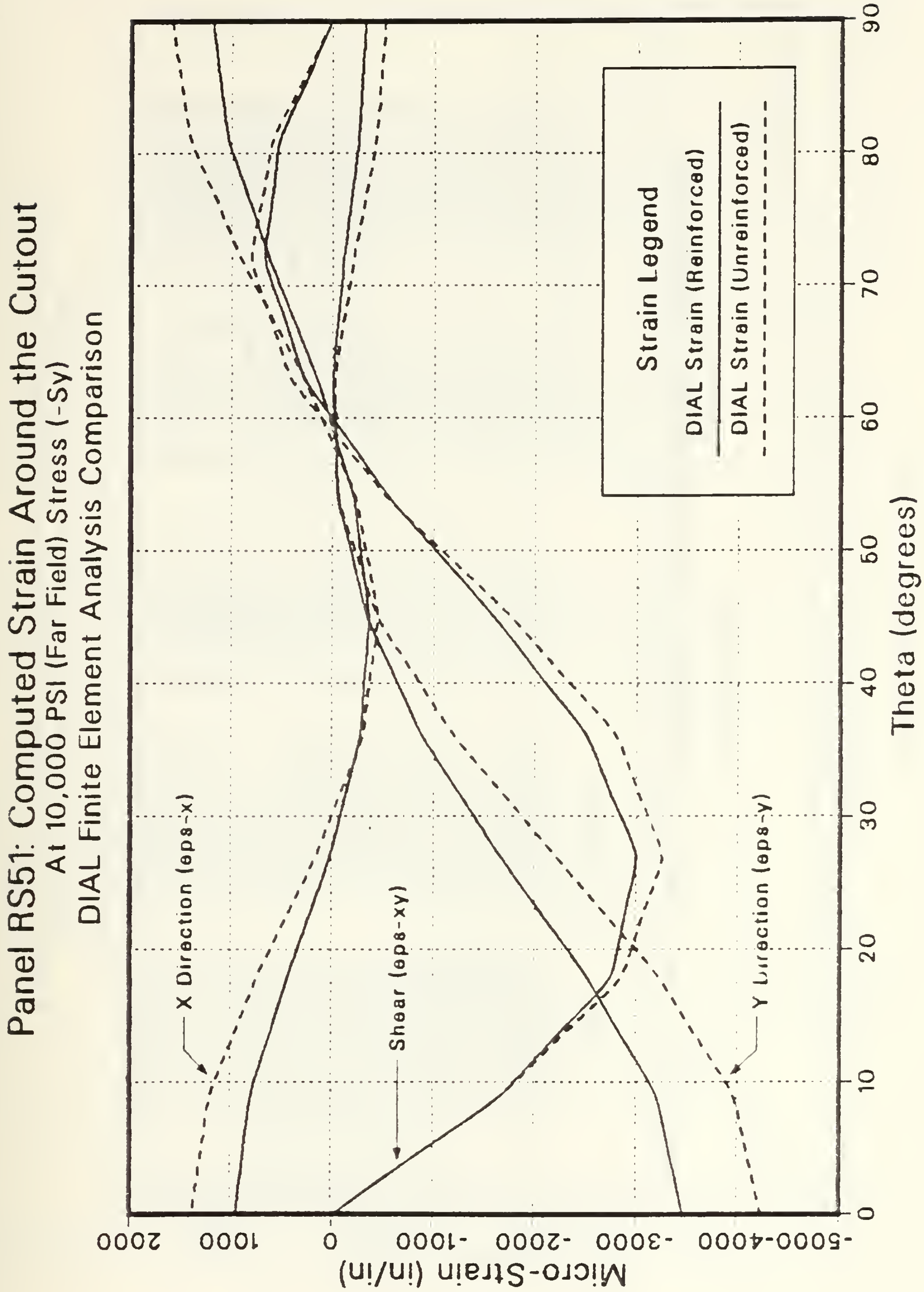

Figure I.2 Panel RS51: Strain Comparison Around the Cutout.

TABLE XXXIV

PANEL RS51: LEFEA STRAIN DISTRIBUTION AROUND THE CUTOUT (-10,000 PSI).

NODE	X COORD	Y COORD	EPS-Y	EPS-X	EPS-XY
1	0.0000E+00	0.5000E+00	-0.3171E-03	0.1193E-02	0.1624E-04
2	0.3923E-01	0.4985E+00	-0.2853E-03	0.1116E-02	0.2649E-03
3	0.7822E-01	0.4938E+00	-0.2508E-03	0.1032E-02	0.5258E-03
4	0.1167E+00	0.4862E+00	-0.1785E-03	0.8303E-03	0.6032E-03
5	0.1545E+00	0.4755E+00	-0.1049E-03	0.6268E-03	0.6714E-03
6	0.1913E+00	0.4619E+00	-0.5222E-04	0.3916E-03	0.4792E-03
7	0.2270E+00	0.4455E+00	0.2294E-06	0.1584E-03	0.2784E-03
8	0.2612E+00	0.4263E+00	-0.2605E-04	-0.2420E-04	-0.1367E-03
9	0.2939E+00	0.4045E+00	-0.5362E-04	-0.2033E-03	-0.5569E-03
10	0.3247E+00	0.3802E+00	-0.1967E-03	-0.2818E-03	-0.1072E-02
11	0.3536E+00	0.3536E+00	-0.3420E-03	-0.3574E-03	-0.1589E-02
12	0.3802E+00	0.3247E+00	-0.6138E-03	-0.3162E-03	-0.2051E-02
13	0.4045E+00	0.2939E+00	-0.8893E-03	-0.2727E-03	-0.2512E-02
14	0.4263E+00	0.2612E+00	-0.1270E-02	-0.1259E-03	-0.2758E-02
15	0.4455E+00	0.2270E+00	-0.1656E-02	0.2279E-04	-0.2999E-02
16	0.4619E+00	0.1913 [illegible]	-0.2079E-02	0.2282E-03	-0.2882E-02
17	0.4755E+00	0.1545E+00	-0.2505E-02	0.4343E-03	-0.2754E-02
18	0.4862E+00	0.1167E+00	-0.2852E-02	0.6178E-03	-0.2218E-02
19	0.4938E+00	0.7822E-01	-0.3196E-02	0.7999E-03	-0.1669E-02
20	0.4985E+00	0.3923E-01	-0.3335E-02	0.8753E-03	-0.8374E-03
21	0.5000E+00	0.0000E+00	-0.3465E-02	0.9473E-03	-0.2361E-04

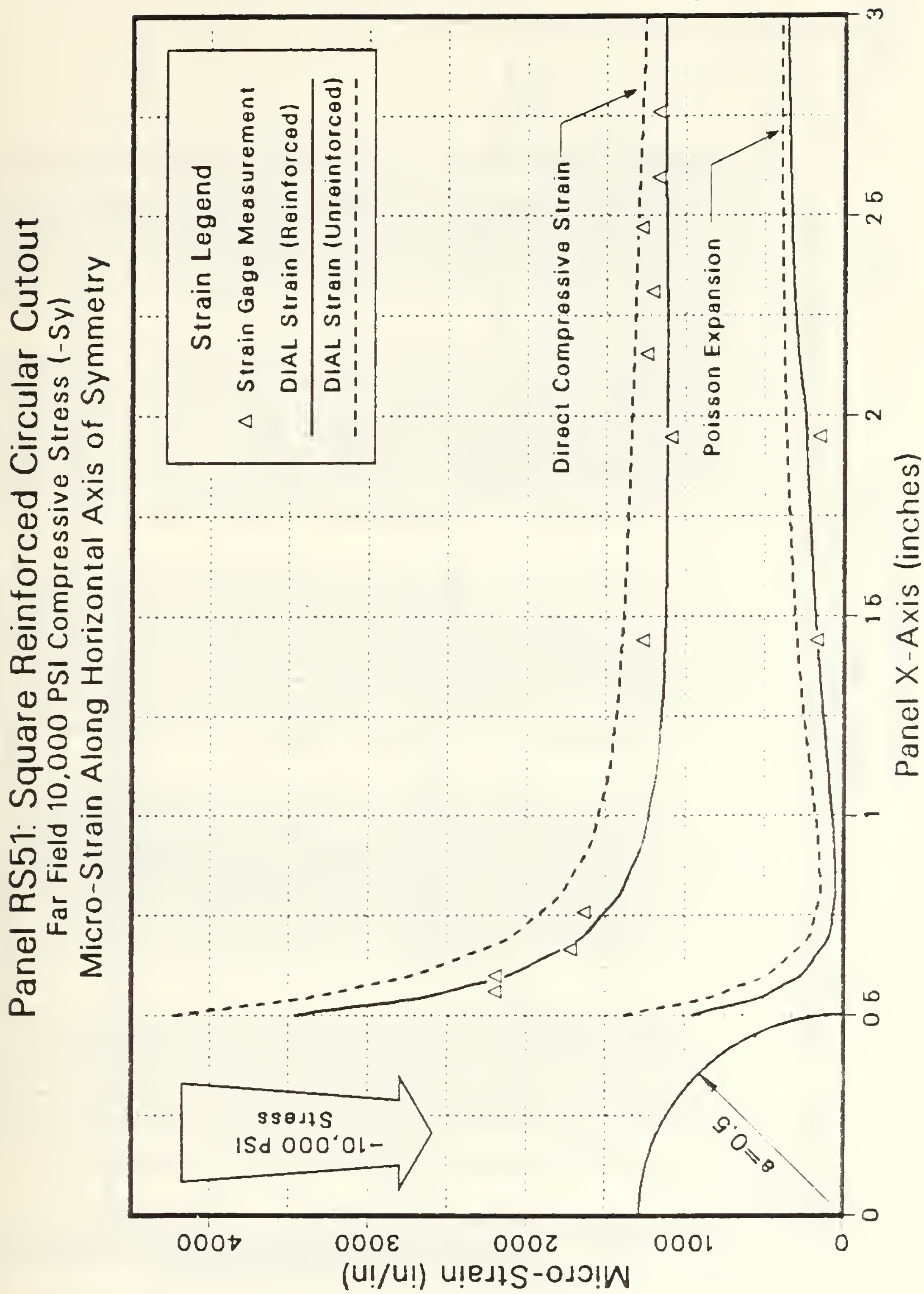

Figure I.3 Panel RS51: Strain Comparison Along the X Axis.

TABLE XXXV

PANEL RS51: LEFEA STRAIN DISTRIBUTION ALONG THE X AXIS (-10,000 PSI).

NODE	X COORD	Y COORD	EPS-Y	EPS-X	EPS-XY
21	0.5000E+00	0.0000E+00	-0.3465E-02	0.9473E-03	-0.2361E-04
32	0.5250E+00	0.0000E+00	-0.3029E-02	0.7148E-03	-0.1500E-04
53	0.5500E+00	0.0000E+00	-0.2605E-02	0.4901E-03	-0.4856E-05
64	0.5750E+00	0.0000E+00	-0.2375E-02	0.3842E-03	-0.3319E-05
85	0.6000E+00	0.0000E+00	-0.2125E-02	0.2662E-03	-0.1966E-05
96	0.6500E+00	0.0000E+00	-0.1872E-02	0.1722E-03	0.6020E-06
117	0.7000E+00	0.0000E+00	-0.1636E-02	0.8773E-04	0.1506E-05
128	0.7500E+00	0.0000E+00	-0.1530E-02	0.7091E-04	0.1819E-05
149	0.8000E+00	0.0000E+00	-0.1417E-02	0.4995E-04	0.2410E-05
160	0.8605E+00	0.0000E+00	-0.1349E-02	0.5354E-04	0.2494E-05
181	0.9210E+00	0.0000E+00	-0.1278E-02	0.5650E-04	0.2707E-05
192	0.1021E+01	0.0000E+00	-0.1227E-02	0.7846E-04	0.2852E-05
213	0.1120E+01	0.0000E+00	-0.1179E-02	0.1005E-03	0.2757E-05
224	0.1210E+01	0.0000E+00	-0.1162E-02	0.1217E-03	0.3015E-05
245	0.1300E+01	0.0000E+00	-0.1144E-02	0.1421E-03	0.3311E-05
256	0.1400E+01	0.0000E+00	-0.1135E-02	0.1614E-03	0.1769E-05
277	0.1500E+01	0.0000E+00	-0.1127E-02	0.1804E-03	0.7863E-06
288	0.1600E+01	0.0000E+00	-0.1123E-02	0.1950E-03	0.1405E-05
309	0.1700E+01	0.0000E+00	-0.1120E-02	0.2098E-03	0.1403E-05
320	0.1800E+01	0.0000E+00	-0.1119E-02	0.2221E-03	0.2396E-05
341	0.1900E+01	0.0000E+00	-0.1118E-02	0.2344E-03	0.3250E-05
352	0.2000E+01	0.0000E+00	-0.1117E-02	0.2436E-03	0.4289E-05
373	0.2100E+01	0.0000E+00	-0.1114E-02	0.2742E-03	0.5108E-05
374	0.2290E+01	0.0000E+00	-0.1118E-02	0.3143E-03	0.3502E-05
375	0.2480E+01	0.0000E+00	-0.1122E-02	0.33[illegible]E-03	0.2692E-05
376	0.2670E+01	0.0000E+00	-0.1127E-02	0.3435E-03	0.2120E-05
377	0.2860E+01	0.0000E+00	-0.1131E-02	0.3546E-03	0.1390E-05
378	0.3050E+01	0.0000E+00	-0.1132E-02	0.3599E-03	0.1185E-05
379	0.3240E+01	0.0000E+00	-0.1134E-02	0.3651E-03	0.9140E-06
380	0.3430E+01	0.0000E+00	-0.1132E-02	0.3667E-03	0.7752E-06
381	0.3620E+01	0.0000E+00	-0.1131E-02	0.3684E-03	0.5891E-06
382	0.3810E+01	0.0000E+00	-0.1129E-02	0.3684E-03	0.4589E-06
383	0.4000E+01	0.0000E+00	-0.1127E-02	0.3685E-03	0.2967E-06
384	0.4125E+01	0.0000E+00	-0.1125E-02	0.3680E-03	0.1566E-06
385	0.4250E+01	0.0000E+00	-0.1123E-02	0.3675E-03	0.5533E-07

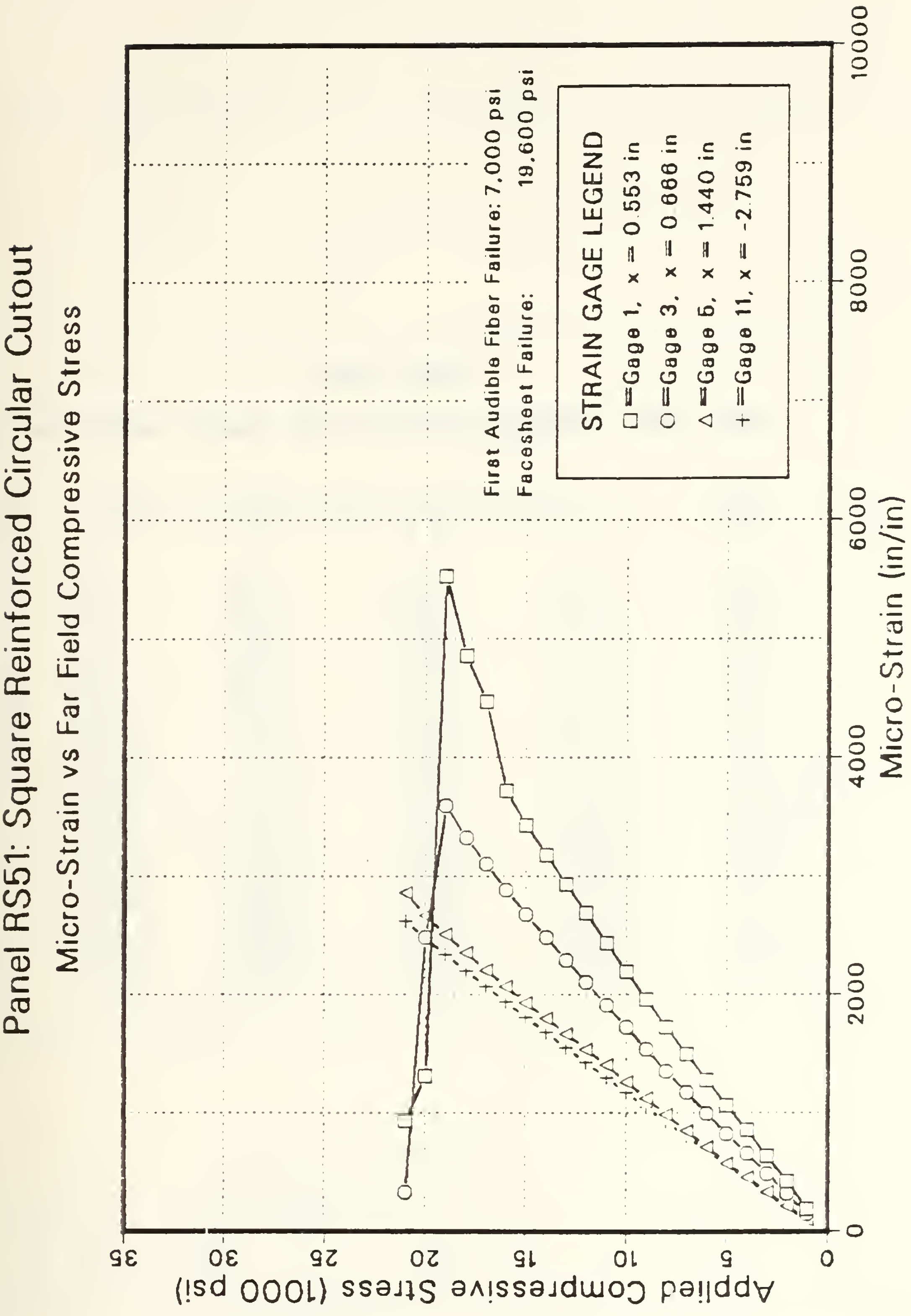

Figure I.4 Panel RS51: Microstrain vs. Compressive Stress.

TABLE XXXVI

PANEL RR51: SELECTED STRAIN GAGE VALUES DURING LOAD.

Load (psi)	Micro-Strain Indicated by Gage: #1	#3	#5	#[illegible]
1000	-189	-145	-94	-86
2000	-419	-318	-215	-203
3000	-636	-486	-333	-319
4000	-853	-657	-455	-438
5000	-1061	-820	-575	-557
6000	-1277	-995	-713	-679
7000	-1498	-1170	-847	-798
8000	-1723	-1351	-983	-921
9000	-1960	-1539	-11[illegible]	-1050
10000	-2194	-1725	-126[illegible]	-1175
11000	-2437	-1912	-14[illegible]	-1299
12000	-2687	-2102	-1541	-1427
13000	-2929	-2291	-1670	-1551
14000	-3182	-2482	-1801	-1680
15000	-3430	-2675	-1931	-1807
16000	-3715	-2880	-2068	-1937
17000	-4470	-3103	-2206	-2070
18000	-4856	-3322	-2349	-2203
19000	-5526	-3595	-2507	-2338
20000	-1309	-2480	-2668	-2471
21000	-933	-323	-2860	-2619

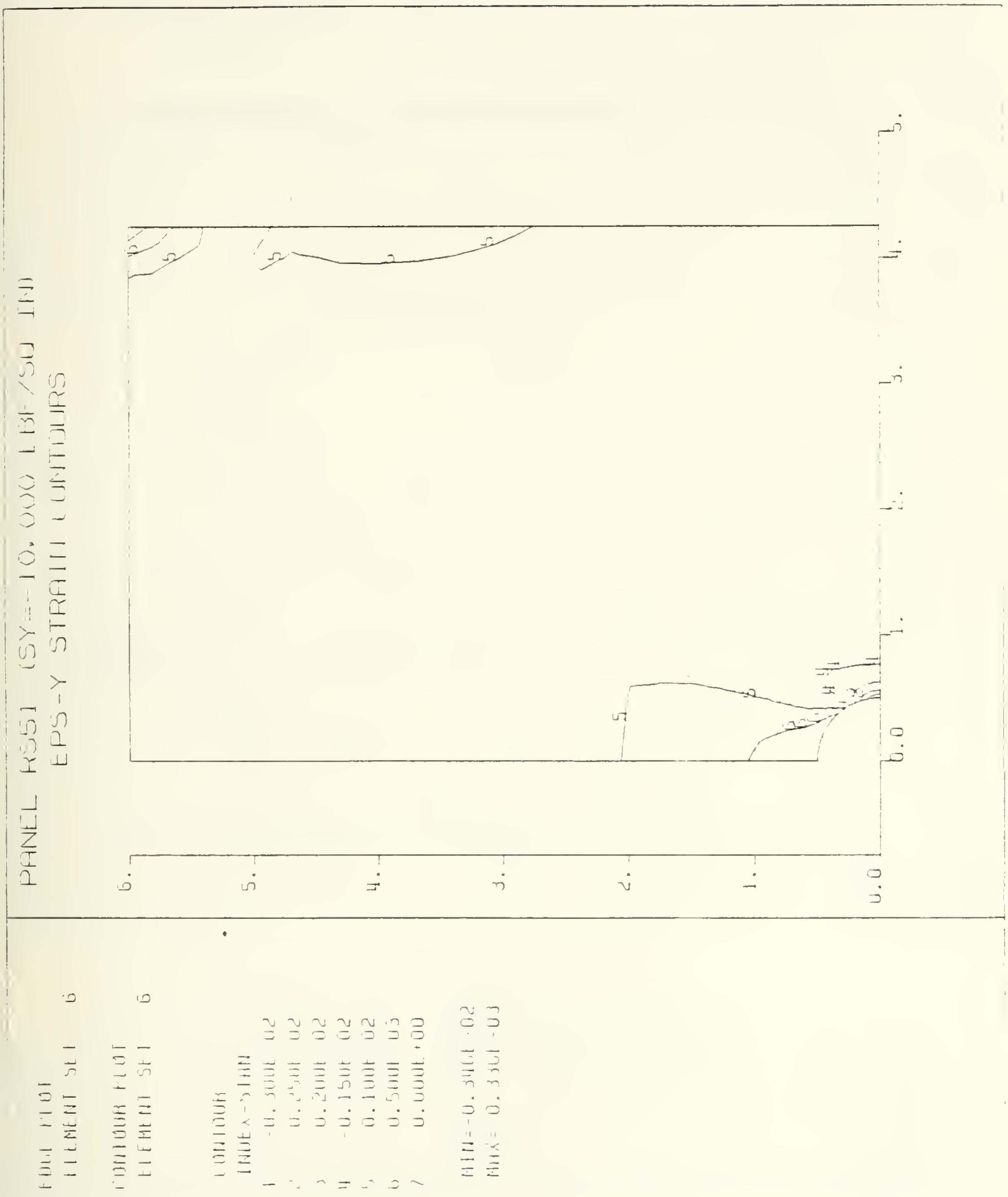

Figure I.5 Panel RS51: Eps-Y FEA Contours.

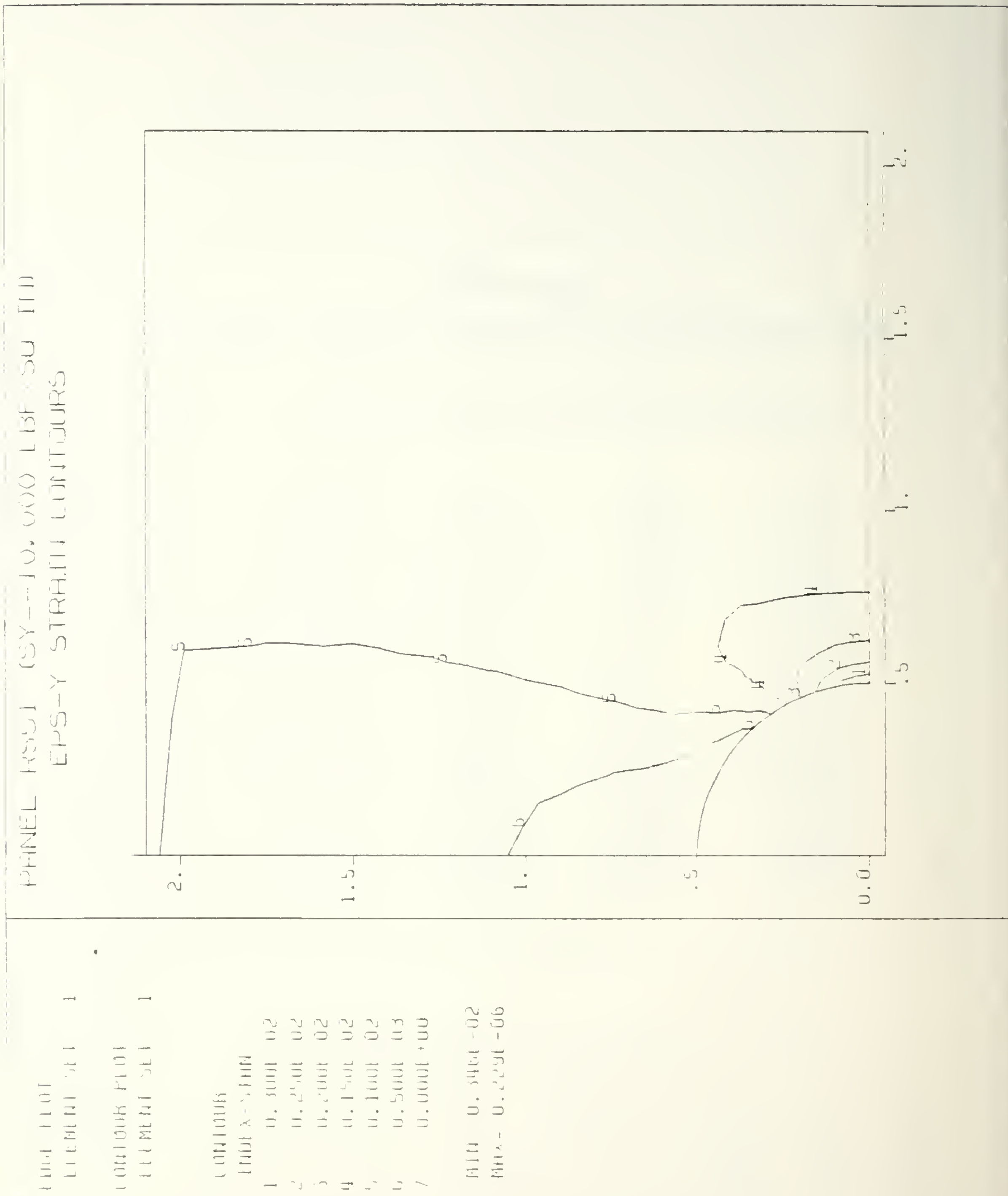

Figure I.6 Panel RS51: Eps-Y FEA Contours Near the Cutout.

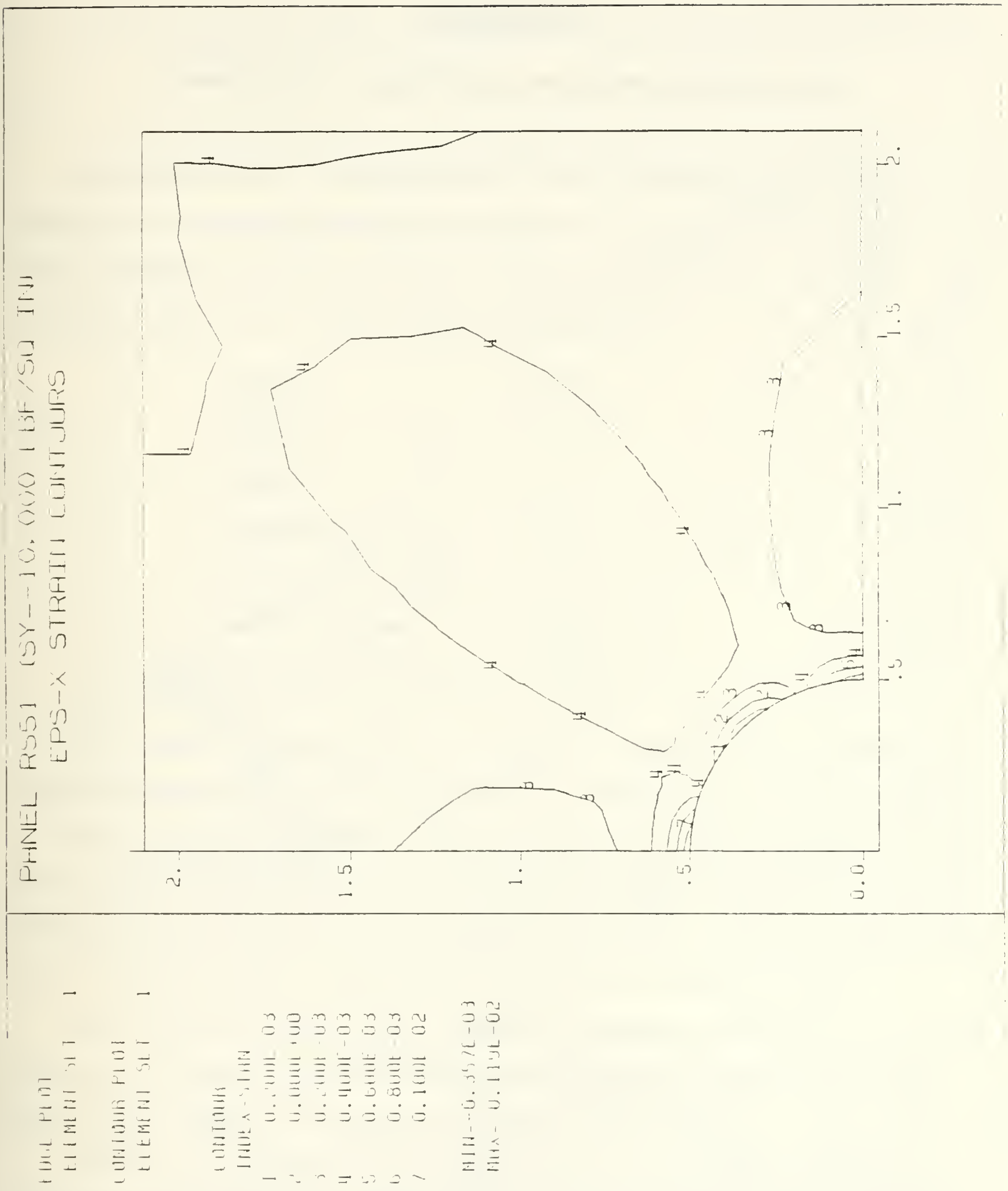

Figure I.7   Panel RS51: Eps-X FEA Contours Near the Cutout.

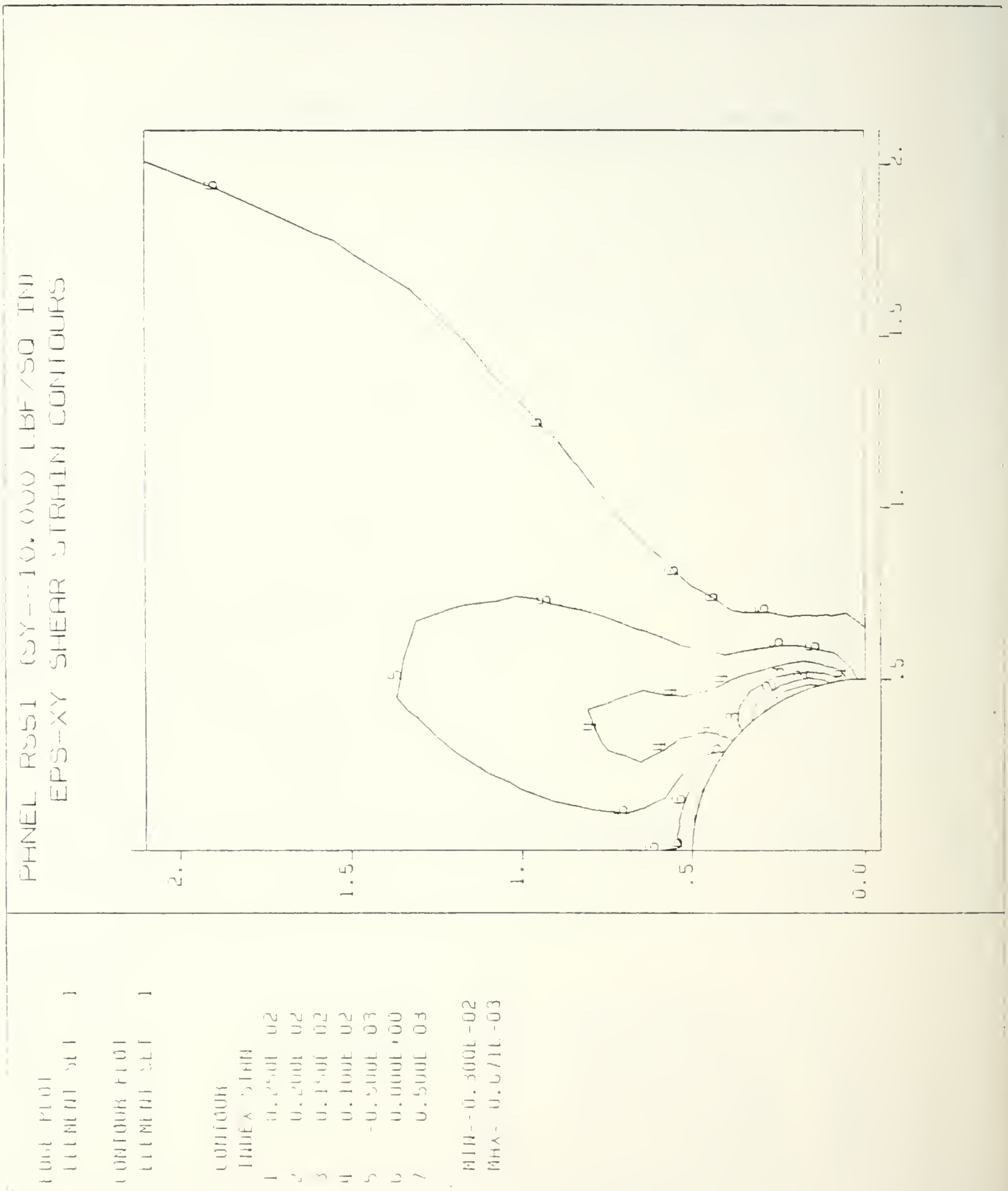

Figure I.8 Panel RS51: Eps-XY FEA Contours Near the Cutout.

APPENDIX J

PANEL RH11: ANALYTICAL AND EXPERIMENTAL DATA

Panel RH11 was reinforced with one co-cured ply of G/Ep in the shape of two strips on either side of the cutout on the outside of each facesheet offset 0.50 inch from the edge of the cutout. The reinforcement had the following dimensions:

Shape:	Strip
Length:	1.57 in
Width:	1.00 in
Thickness (each):	0.014 in (1 ply)
Area (each face):	3.14 in^2
Total Volume:	0.088 in^3
Net Cross Section:	0.056 in^2

The panel failed at the hole edge (Type-1) at an applied normal stress ($\bar{\sigma}_n$) of -29,960 psi. Based strictly on the failure of the unreinforced panel and the computed stress concentration factor of 3.02 (which was very slightly higher than the unreinforced panel), failure was predicted at $\bar{\sigma}_n$ = -30,200 psi. The panel failed within 0.6% of the predicted ultimate load.

The finite element model (mesh) is shown in Figure J.1. The area of the strip reinforcement is outlined by the heavy lines offset 0.50 inch to the right of the cutout edge.

Figure J.2 compares the three (finite element) computed strains around the cutout between the unreinforced panel (POØØ) and RH11. These computed strain values are listed in Table

XXXVII. There is no significant decrease in the strain due to the reinforcement. A very slight increase may be seen in Eps-Y near the 0 degree position (on the X axis). This increase in strain is due to the shifting of load paths to either side of the reinforcement. The slight load path shift <u>toward</u> the cutout acted to slightly <u>increase</u> the SCF.

Figure J.3 compares the computed and experimental strains in the X and Y (poisson) directions in the panel and shows almost perfect correlation between analytical and experimental strain at $\bar{\sigma}_n$ = -10,000 psi. There was virtually no measured strain variation between the left and right side of the hole. The edge of the reinforcement can not be seen in the figure; the effects of reinforcement is a decrease around the reinforcement and a subtle increase near the hole and in the far field (where x = 2.50") compared to the unreinforced panel (POØØ). Table XXXVIII gives the computed values of the strains along the X axis.

Figure J.4 shows the stress-strain state during the load sequence from 0 to -29 ksi. Experimentally measured strain values are given in Table XXXIX. Up to -23 ksi all gages indicated a normal stress-strain state. From -23 ksi there was a dramatic change; first gages #1 and #2 showed a load transfer from the area next to the right edge of the cutout to the left side. Then suddenly the roles were reversed and gage #2 (x = -0.583") indicated a load transfer to the right side of the cutout. Gage #1 (x = +0.568") shows a tremendous strain increase, off the scale on Figure J.4, as high as 12,800 microstrain (Table XXXIX). The effect of the load transfer is apparent on gage #6 (x = +0.681); it reflects the increased load away from the cutout edge on the right side of the hole. It appears that the fibers on the right side of the cutout began to buckle on the micro-mechanical level very near the edge.

Figures J.5 through J.8 show the strain contours at $\bar{\sigma}_n$ = -10,000 psi computed and plotted using DIAL. Figure J.5 is the full quarter panel with strain (Eps-Y) parallel to the applied load. Figures J.6 through J.8 (Eps-Y, Eps-X and Eps-XY) show the strains in detail close to the cutout.

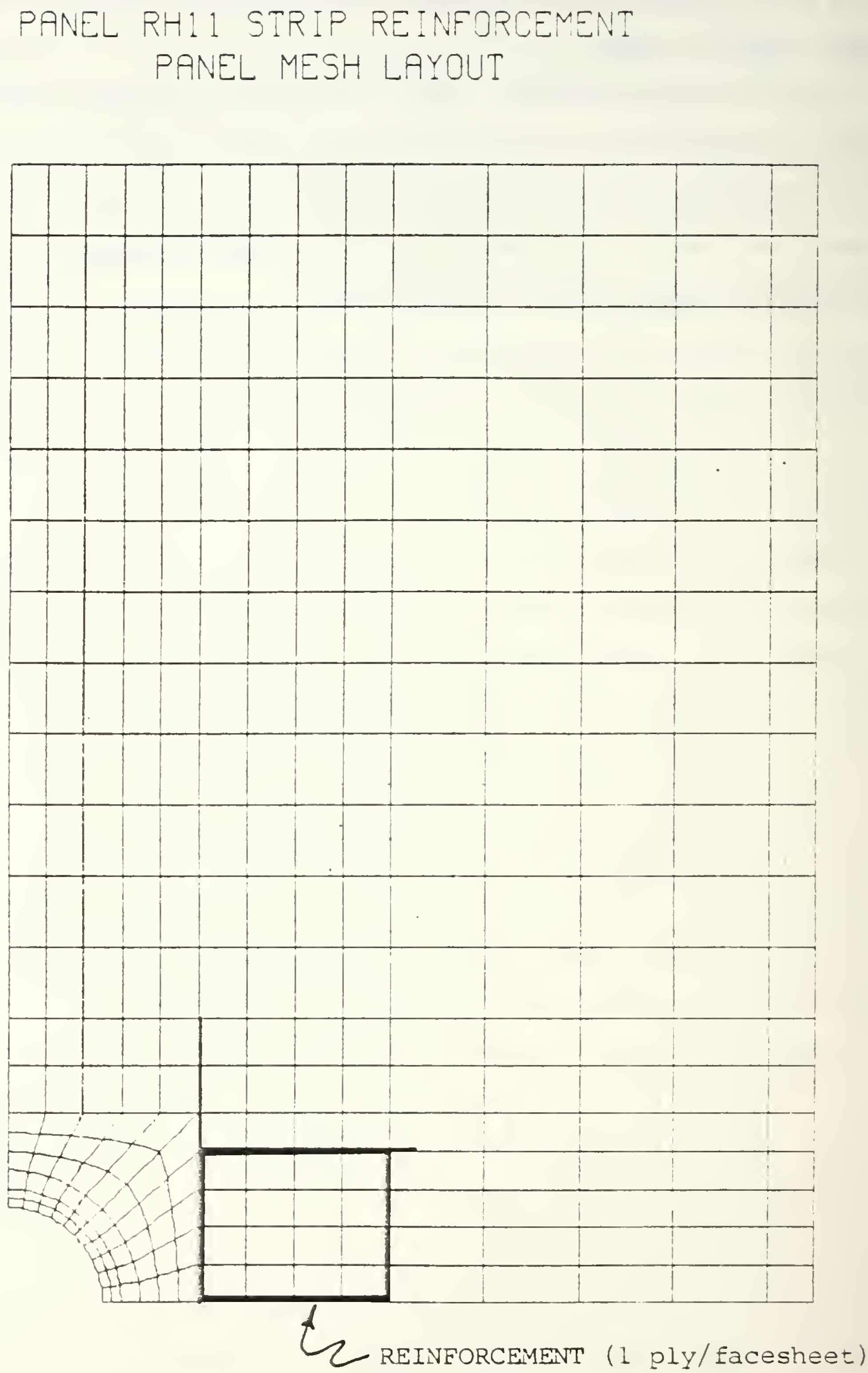

Figure J.1 Panel RH11: DIAL Finite Element Mesh.

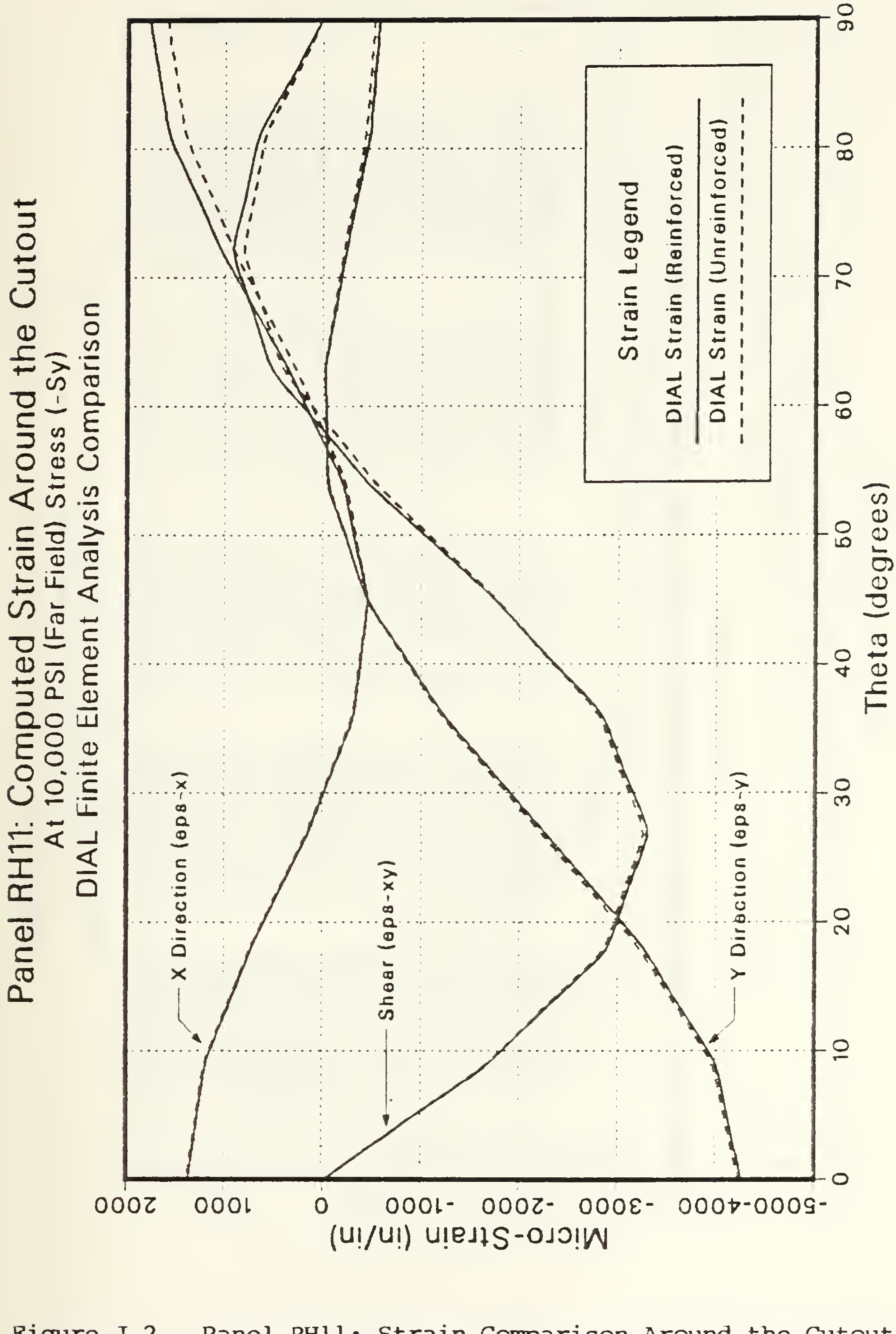

Figure J.2 Panel RH11: Strain Comparison Around the Cutout.

TABLE XXXVII

PANEL RH11: LEFEA STRAIN DISTRIBUTION AROUND THE CUTOUT (-10,000 PSI).

NODE	X COORD	Y COORD	EPS-Y	EPS-X	EPS-XY
1	0.0000E+00	0.5000E+00	-0.5635E-03	0.1777E-02	0.1795E-04
2	0.3923E-01	0.4985E+00	-0.5154E-03	0.1678E-02	0.3317E-03
3	0.7822E-01	0.4938E+00	-0.4628E-03	0.1573E-02	0.6603E-03
4	0.1167E+00	0.4862E+00	-0.3455E-03	0.1307E-02	0.7925E-03
5	0.1545E+00	0.4755E+00	-0.2257E-03	0.1037E-02	0.9155E-03
6	0.1913E+00	0.4619E+00	-0.1227E-03	0.7016E-03	0.7280E-03
7	0.2270E+00	0.4455E+00	-0.2059E-04	0.3654E-03	0.5289E-03
8	0.2612E+00	0.4263E+00	-0.3194E-04	0.8281E-04	0.3823E-04
9	0.2939E+00	0.4045E+00	-0.4750E-04	-0.1965E-03	-0.4617E-03
10	0.3247E+00	0.3802E+00	-0.2446E-03	-0.3241E-03	-0.1101E-02
11	0.3536E+00	0.3536E+00	-0.4478E-03	-0.4461E-03	-0.1743E-02
12	0.3802E+00	0.3247E+00	-0.8362E-03	-0.3786E-03	-0.2292E-02
13	0.4045E+00	0.2939E+00	-0.1230E-02	-0.3052E-03	-0.2837E-02
14	0.4263E+00	0.2612E+00	-0.1739E-02	-0.7907E-04	-0.3073E-02
15	0.4455E+00	0.2270E+00	-0.2250E-02	0.1506E-03	-0.3298E-02
16	0.4619E+00	0.191[illegible]E+00	0.2755E-02	0.4383E-03	-0.3100E-02
17	0.4755E+00	0.1545E+00	-0.3259E-02	0.7260E-03	-0.2890E-02
18	0.4862E+00	0.1167E+00	-0.3628E-02	0.9598E-03	-0.2290E-02
19	0.4938E+00	0.7822E-01	-0.3994E-02	0.1190E-02	-0.1682E-02
20	0.4985E+00	0.3923E-01	-0.4130E-02	0.1281E-02	-0.8422E-03
21	0.5000E+00	0.0000E+00	-0.4261E-02	0.1367E-02	-0.1978E-04

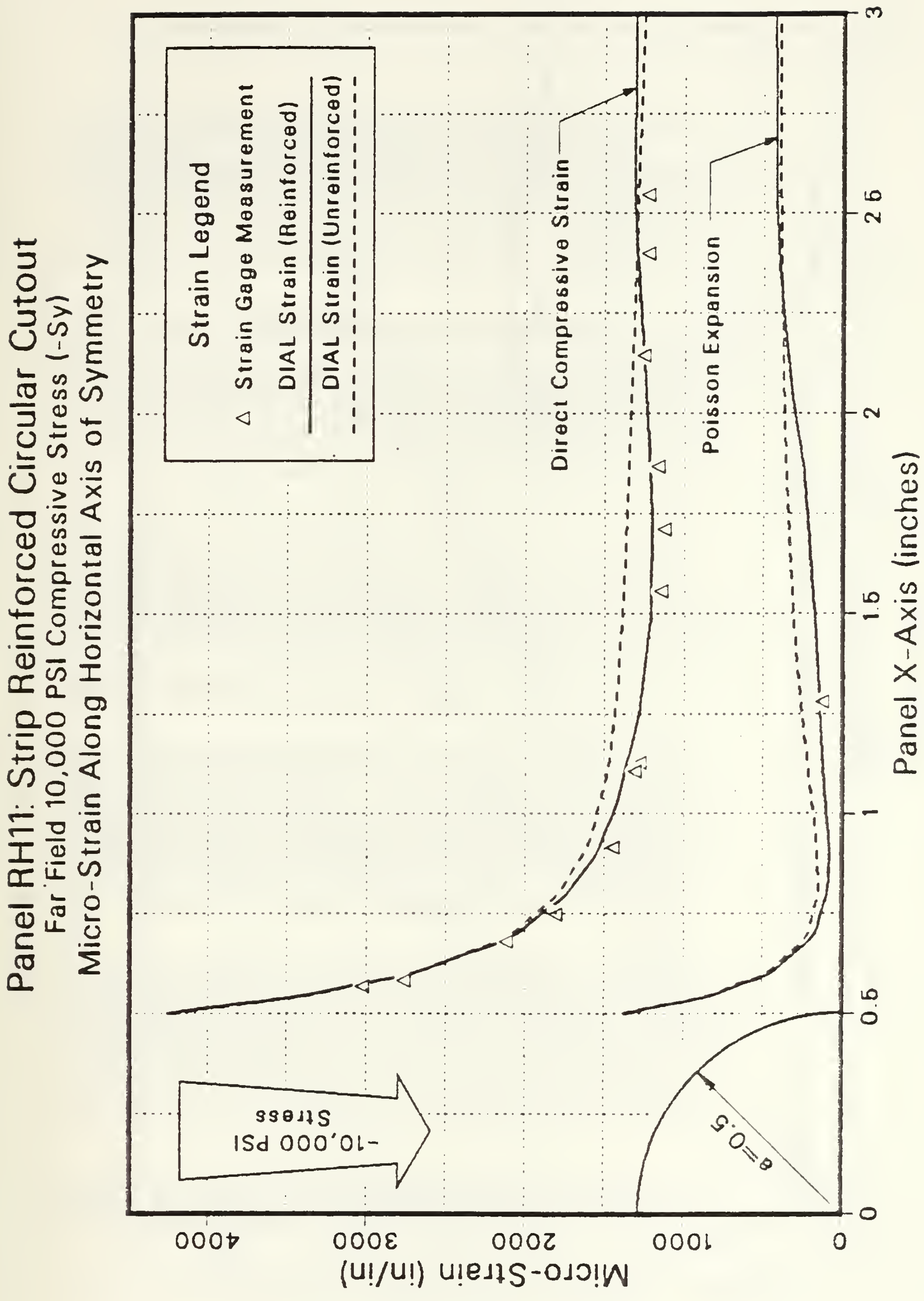

Figure J.3 Panel RH11: Strain Comparison Along the X Axis.

TABLE XXXVIII

PANEL RH11, LEFEA STRAIN DISTRIBUTION ALONG THE X AXIS (-10,000 PSI).

NODE	X COORD	Y COORD	EPS-Y	EPS-X	EPS-XY
21	0.5000E+00	0.0000E+00	-0.4261E-02	0.1367E-02	-0.1978E-04
32	0.5250E+00	0.0000E+00	-0.3794E-02	0.1075E-02	-0.1438E-04
53	0.5500E+00	0.0000E+00	-0.3333E-02	0.7884E-03	-0.8648E-05
64	0.5750E+00	0.0000E+00	-0.3040E-02	0.6293E-03	-0.7478E-05
85	0.6000E+00	0.0000E+00	-0.2728E-02	0.4575E-03	-0.4177E-05
96	0.6500E+00	0.0000E+00	-0.2381E-02	0.3060E-03	-0.1883E-05
117	0.7000E+00	0.0000E+00	-0.2056E-02	0.1691E-03	-0.1349E-05
128	0.7500E+00	0.0000E+00	-0.1900E-02	0.1333E-03	0.2972E-06
149	0.8000E+00	0.0000E+00	-0.1738E-02	0.9173E-04	-0.1418E-06
160	0.8500E+00	0.0000E+00	-0.1646E-02	0.8499E-04	0.2516E-06
181	0.9000E+00	0.0000E+00	-0.1553E-02	0.7778E-04	0.2424E-05
192	0.9500E+00	0.0000E+00	-0.1502E-02	0.8482E-04	0.9142E-05
213	0.1000E+01	0.0000E+00	-0.1447E-02	0.9746E-04	0.1233E-04
214	0.1125E+01	0.0000E+00	-0.1364E-02	0.1221E-03	0.6864E-05
215	0.1250E+01	0.0000E+00	-0.1285E-02	0.1392E-03	0.5219E-05
216	0.1375E+01	0.0000E+00	-0.1249E-02	0.1573E-03	0.3992E-05
217	0.1500E+01	0.0000E+00	-0.1213E-02	0.1761E-03	0.2407E-05
218	0.1625E+01	0.0000E+00	-0.1209E-02	0.1994E-03	0.2185E-05
219	0.1750E+01	0.0000E+00	-0.1206E-02	0.2233E-03	0.1590E-05
220	0.1875E+01	0.0000E+00	-0.1220E-02	0.2494E-03	0.1468E-05
221	0.2000E+01	0.0000E+00	-0.1236E-02	0.3010E-03	0.8826E-06
222	0.2250E+01	0.0000E+00	-0.1276E-02	0.3736E-03	0.5784E-06
223	0.2500E+01	0.0000E+00	-0.1314E-02	0.4190E-03	0.1137E-05
224	0.2750E+01	0.0000E+00	-0.1314E-02	0.4244E-03	0.4220E-06
225	0.3000E+01	0.0000E+00	-0.1312E-02	0.4291E-03	-0.1799E-06
226	0.3250E+01	0.0000E+00	-0.1293E-02	0.4210E-03	0.7590E-07
227	0.3500E+01	0.0000E+00	-0.1276E-02	0.4142E-03	-0.2994E-07
228	0.3750E+01	0.0000E+00	-0.1256E-02	0.4059E-03	0.3066E-07
229	0.4000E+01	0.0000E+00	-0.1237E-02	0.3982E-03	-0.5949E-07
230	0.4125E+01	0.0000E+00	-0.1229E-02	0.3952E-03	-0.2035E-07
231	0.4250E+01	0.0000E+00	-0.1221E-02	0.3922E-03	0.4322E-07

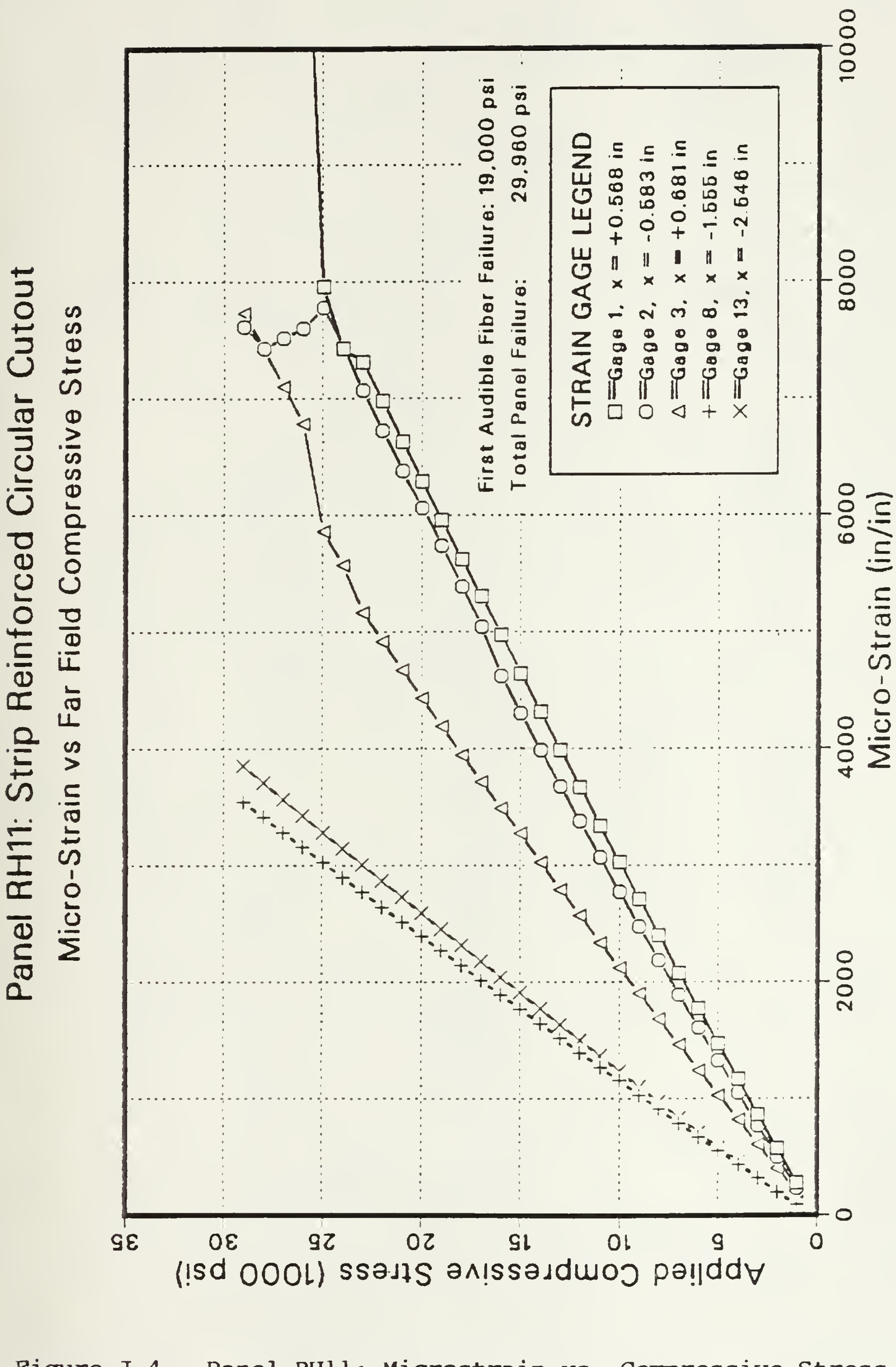

Figure J.4 Panel RH11: Microstrain vs. Compressive Stress.

TABLE XXXIX

PANEL RH11: SELECTED STRAIN GAGE VALUES DURING LOAD.

Load (psi)	Micro-Strain Indicated by Gage:				
	#1	#2	#3	#8	#13
1000	-275	-226	-194	-87	-78
2000	-569	-497	-402	-198	-194
3000	-861	-768	-608	-314	-320
4000	-1164	-1048	-820	-432	-452
5000	-1466	-1327	-1031	-551	-579
6000	-1772	-1606	-1244	-669	-708
7000	-2078	-1889	-1459	-786	-836
8000	-2399	-2185	-1681	-910	-971
9000	-2711	-2475	-1902	-1031	-1101
10000	-3025	-2769	-2121	-1150	-12[illegible]
11000	-3341	-3066	-2341	-1270	-1364
12000	-3670	-3376	-2572	-1396	-1499
13000	-3987	-3677	-2792	-1518	-1634
14000	-4315	-3988	-3025	-1642	-1770
15000	-4644	-4303	-3275	-1767	-1908
16000	-4975	-4622	-3489	-1892	-2044
17000	-5302	-5043	-3720	-2015	-2179
18000	-5620	-5389	-3948	-2142	-2318
19000	-5956	-5741	-4192	-2269	-2453
20000	-6293	-6060	-4432	-2394	-2590
21000	-6626	-6376	-4670	-2517	-2731
22000	-6977	-6725	-4920	-2643	-2869
23000	-7311	-7066	-5166	-2770	-3006
24000	-7427	-7443	-5573	-2899	-3148
25000	-7956	-7778	-5862	-3027	-3282
26000	-12134	-7601	-6783	-3158	-3425
27000	-12299	-7516	-7106	-3285	-3567
28000	-12543	-7430	-7423	-3411	-3708
29000	-12867	-7615	-7732	-3543	-3854

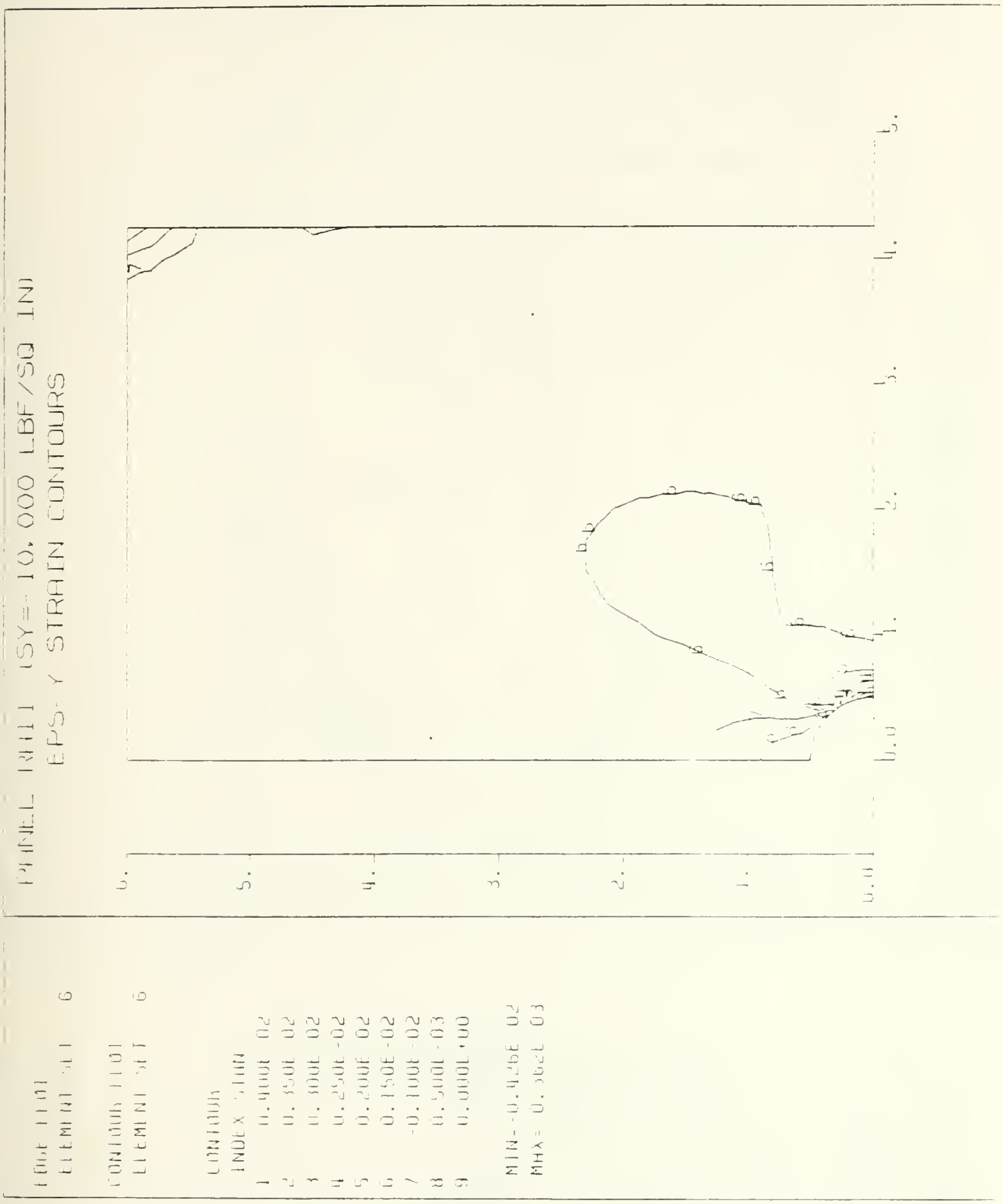

Figure J.5 Panel RH11: Eps-Y FEA Contours.

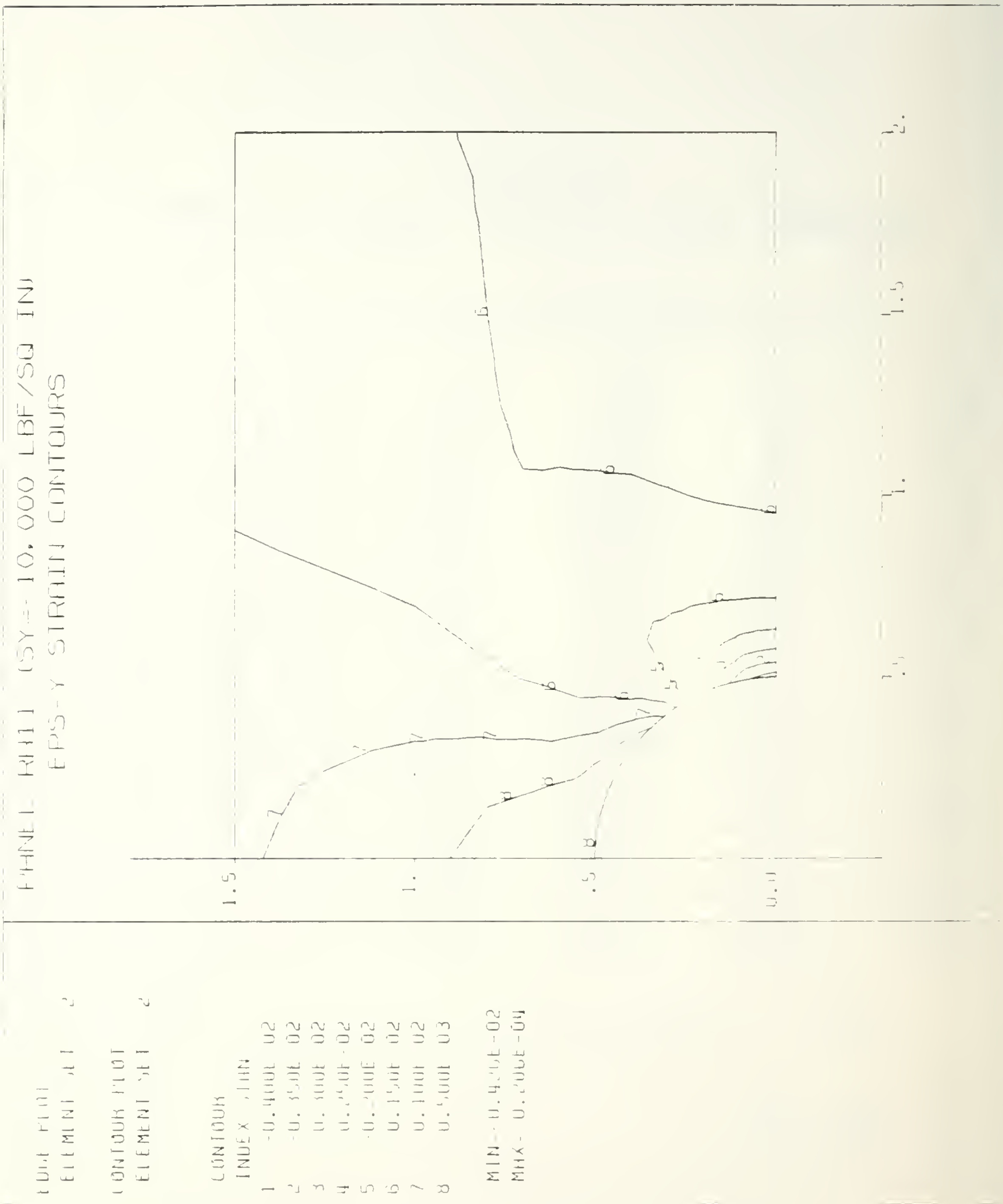

Figure J.6   Panel RH11: Eps-Y FEA Contours Near the Cutout.

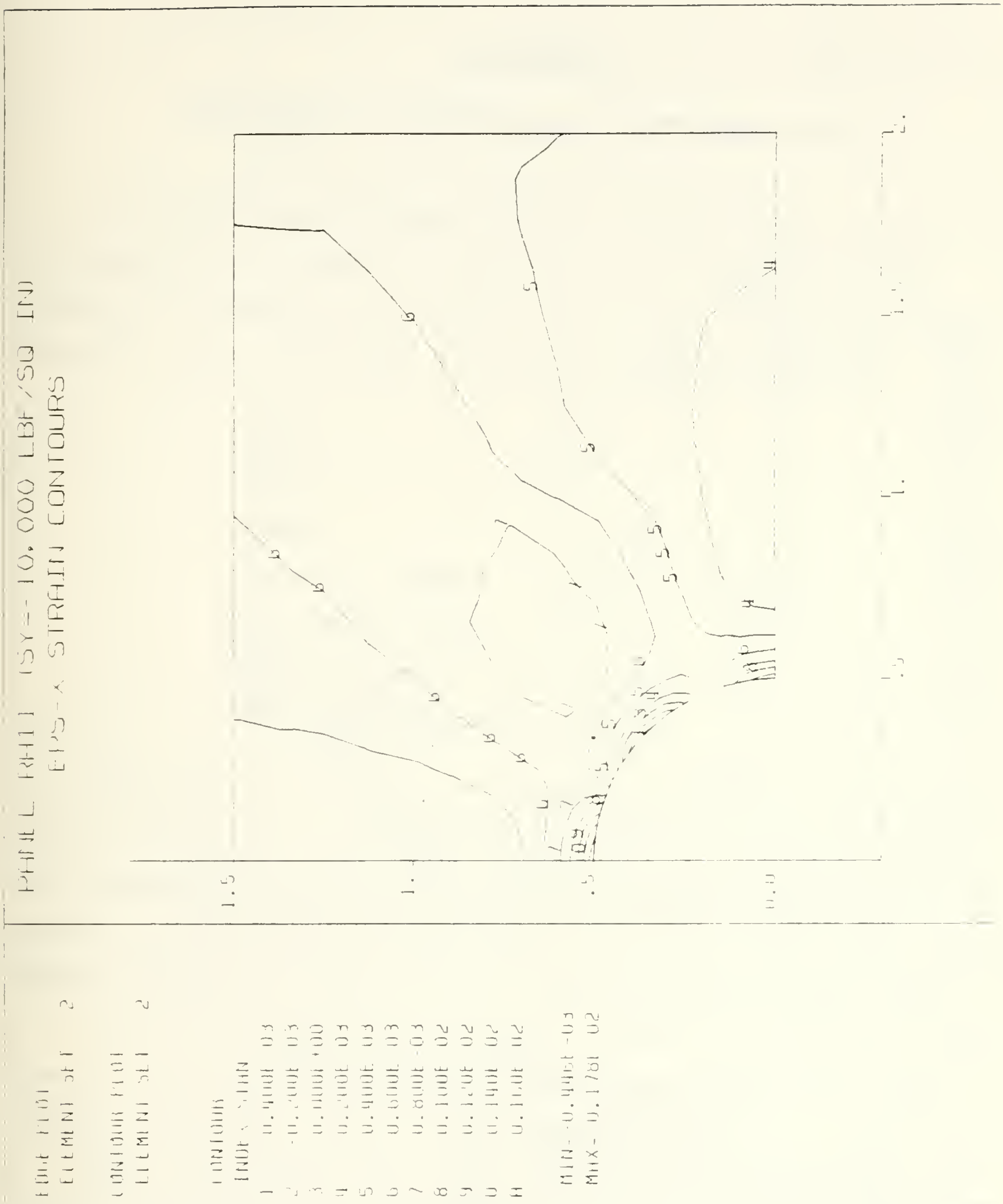

Figure J.7 Panel RH11: Eps-X FEA Contours Near the Cutout.

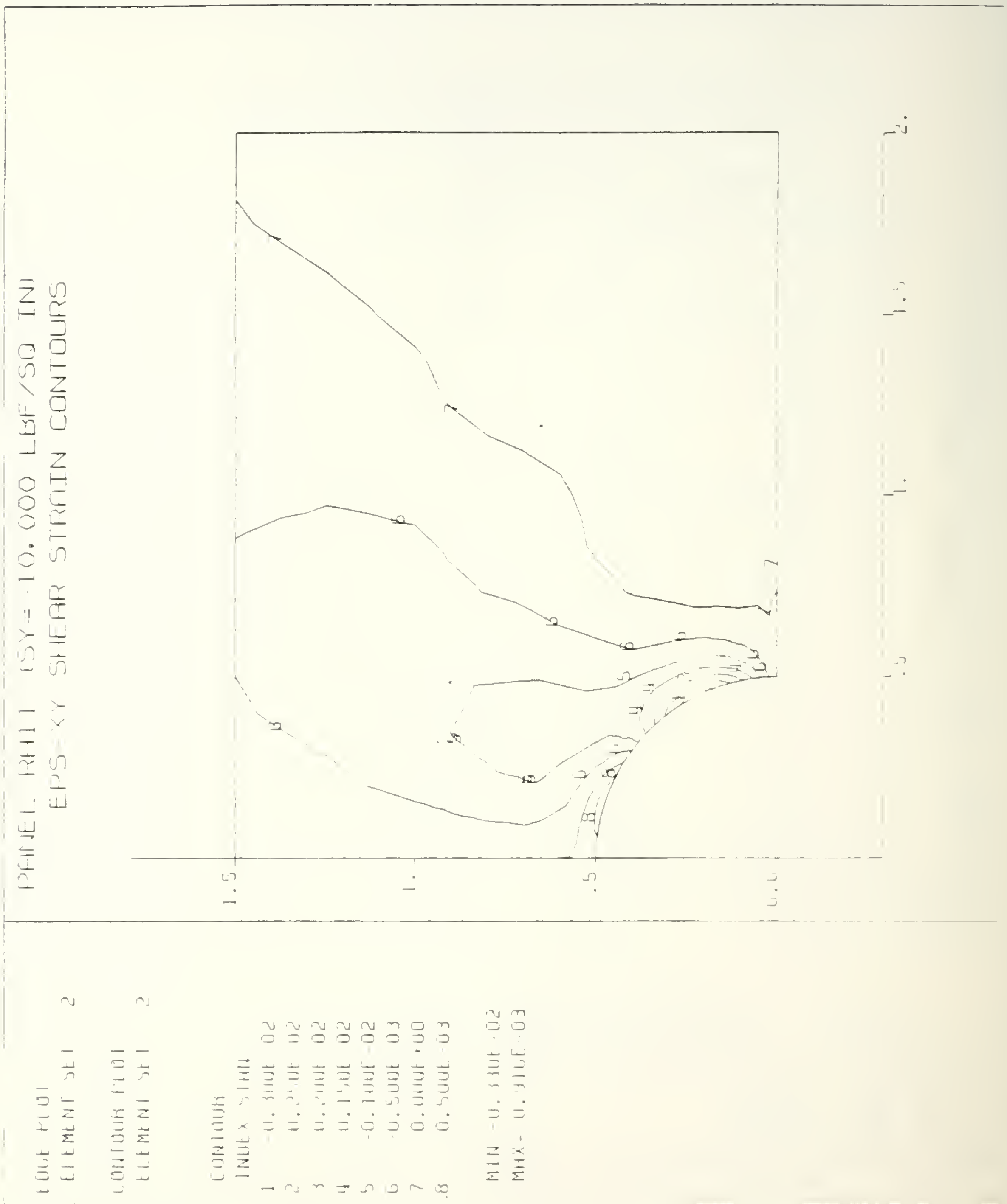

Figure J.8 Panel RH11: Eps-XY FEA Contours Near the Cutout.

APPENDIX K

PANEL RH22: ANALYTICAL AND EXPERIMENTAL DATA

Panel RH22 was reinforced with two co-cured plies of G/Ep in the shape of two strips on either side of the cutout on the outside of each facesheet offset 0.50 inch from the edge of the cutout. The reinforcement had the following dimensions:

Shape:	Strip
Length:	1.57 in
Width:	1.00 in
Thickness (each):	0.028 in (2 ply)
Area (each face):	3.14 in^2
Total Volume:	0.176 in^3
Net Cross Section:	0.112 in^2

The panel failed at the hole edge (Type-1) at an applied normal stress of -31,460 psi. Based strictly on the failure of the unreinforced panel and the computed stress concentration factor of 2.91, the predicted failure was $\bar{\sigma}_n$ = -31,500 psi. The actual failure was within 0.4% of the predicted ultimate load.

The finite element model (mesh) is shown in Figure K.1. The area of the strip reinforcement is outlined by the heavy lines offset 0.50" to the right of the cutout's edge.

Figure K.2 compares the three (finite element) computed strains around the cutout between the unreinforced panel (PO∅∅) and RH22. These computed strain values are listed in Table XXXX.

There is only a small decrease in the strain due to the reinforcement.

Figure K.3 compares the computed (solid and dashed lines) and experimentally measured (triangles) strains in the X and Y (poisson) directions in the panel and shows an excellent correlation between analytical and experimental strain at -10,000 psi applied stress. There was some very slight measured strain variation between the left and right side of the hole. The exact edge of the reinforcement can not be seen in the figure. The effects is a significant strain decrease (compared to the unreinforced panel, PO$\emptyset\emptyset$) under the reinforcement, a small decrease near the hole and a slight increase in the far field (where x = 2.50"). Table XLI gives the computed values of the strains along the X axis.

Figure K.4 shows the stress-strain state during the load sequence from $\bar{\sigma}_n$ = 0 to -30 ksi. Experimentally measured strain gage data are given in Table XLII. Up to about -9 ksi all gages indicated a normal stress-strain state. At -9 ksi gage #1 (x = +0.570") began showing decreasing reaction to the applied load. At -18 ksi, which coincided with the first audible ply failure (FAPF), the strain at gage #1 showed virtually no change up to -22 ksi. At -23 ksi, however, the strain suddenly doubles from 3100 to 6500$\mu\epsilon$ and resumes its normal stress-strain ratio. At -9 ksi it appears that the load path is being diverted away from the right side of the cutout to the left. Gage #2 (x = -0.614") demonstrates an increased strain rate from -9 to -25 ksi when it increases significantly. Gage #1 failed above -27 ksi at about 10,000$\mu\epsilon$ while Gage #2 continued to give reliable output up to almost 12,000$\mu\epsilon$. It can be assumed from the response of gages in the far-field that the stress-strain response of the panel as a whole remained constant with a slight decrease in stiffness with increased loads. The response of the facesheets close to the cutout show a very different response. It appears that there is a significant transfer of load from one side of the cutout to the other and to the opposing facesheet.

Figures K.5 through K.8 show the strain contours at $\bar{\sigma}_n$ = -10,000 psi computed and plotted using DIAL. Figure K.5 is the full quarter panel with strain (Eps-Y) parallel to the applied load. Figures K.6 through K.8 (Eps-Y, Eps-X and Eps-XY) show the strains in detail close to the cutout.

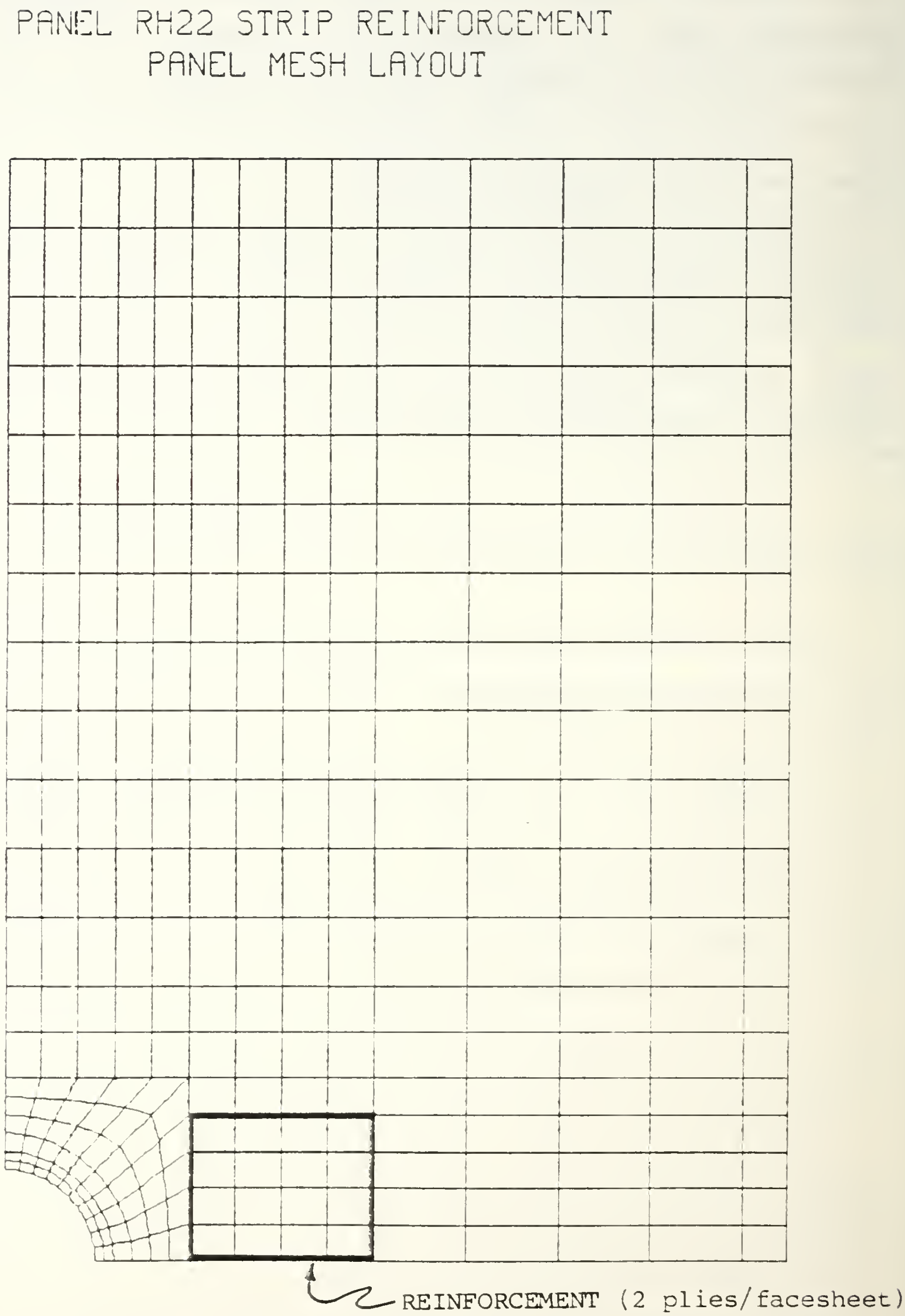

Figure K.1 Panel RH22: DIAL Finite Element Mesh.

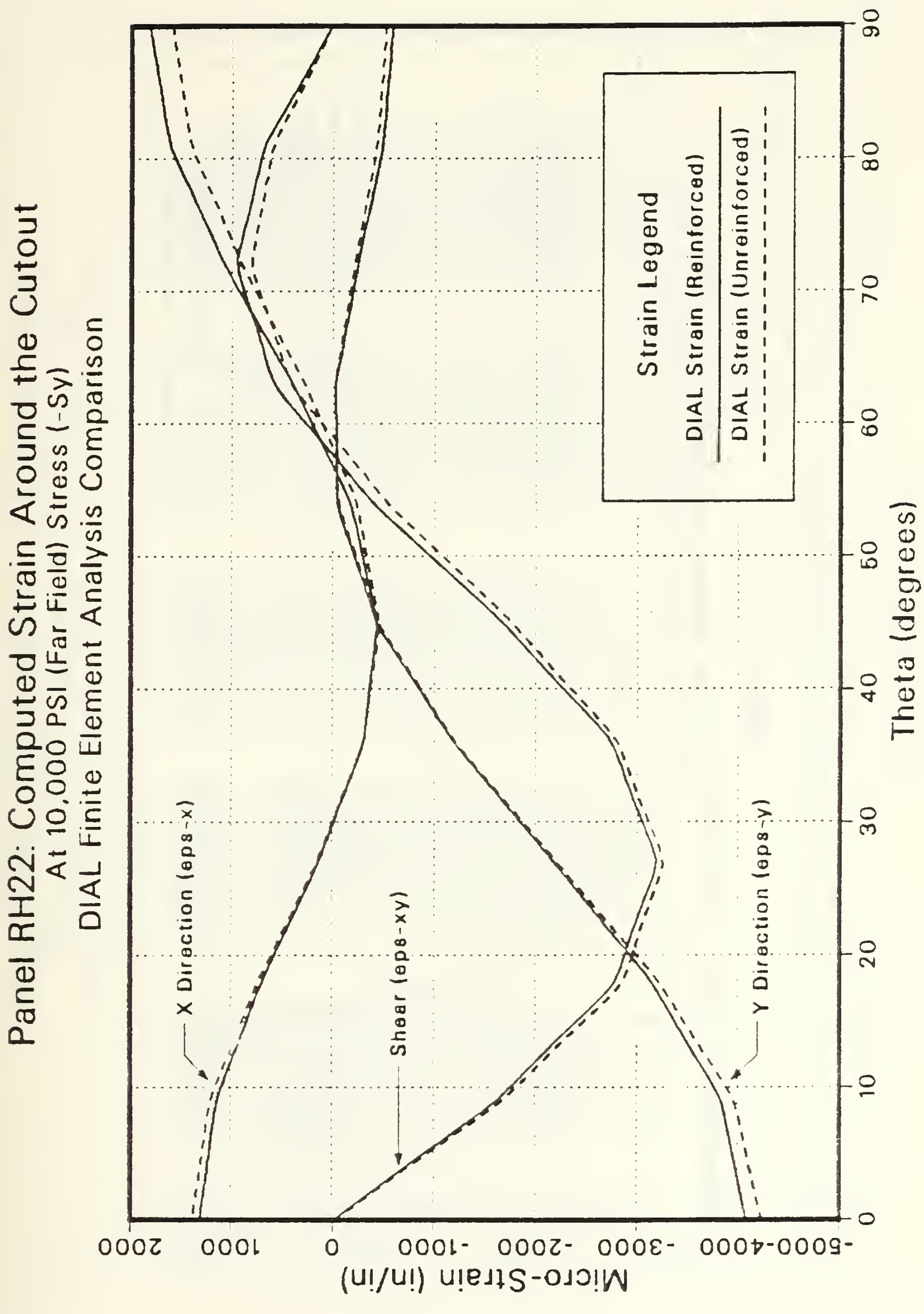

Figure K.2 Panel RH22: Strain Comparison Around the Cutout.

TABLE XL

PANEL RH22: LEFEA STRAIN DISTRIBUTION AROUND THE CUTOUT (-10,000 PSI).

NODE	X COORD	Y COORD	EPS-Y	EPS-X	EPS-XY
1	0.0000E+00	0.5000E+00	-0.5779E-03	0.1821E-02	0.1796E-04
2	0.3923E-01	0.4985E+00	-0.5293E-03	0.1722E-02	0.3410E-03
3	0.7822E-01	0.4938E+00	-0.4760E-03	0.1617E-02	0.6788E-03
4	0.1167E+00	0.4862E+00	-0.3569E-03	0.1350E-02	0.8202E-03
5	0.1545E+00	0.4755E+00	-0.2351E-03	0.1079E-02	0.9522E-03
6	0.1913E+00	0.4619E+00	-0.1288E-03	0.7406E-03	0.7729E-03
7	0.2270E+00	0.4455E+00	-0.2327E-04	0.4017E-03	0.5820E-03
8	0.2612E+00	0.4263E+00	-0.2986E-04	0.1154E-03	0.9786E-04
9	0.2939E+00	0.4045E+00	-0.4079E-04	-0.1677E-03	-0.3956E-03
10	0.3247E+00	0.3802E+00	-0.2314E-03	-0.2997E-03	-0.1029E-02
11	0.3536E+00	0.3536E+00	-0.4282E-03	-0.4259E-03	-0.1664E-02
12	0.3802E+00	0.3247E+00	-0.8064E-03	-0.3636E-03	-0.2207E-02
13	0.4045E+00	0.2939E+00	-0.1190E-02	-0.2953E-03	-0.2743E-02
14	0.4263E+00	0.2612E+00	-0.1682E-02	-0.7676E-04	-0.2971E-02
15	0.4455E+00	0.2270E+00	-0.2175E-02	0.1452E-03	-0.3188E-02
16	0.4619E+00	0.1913E+00	-0.2658E-02	0.4221E-03	-0.2991E-02
17	0.4755E+00	0.1545E+00	-0.3138E-02	0.6987E-03	-0.2783E-02
18	0.4862E+00	0.1167E+00	-0.3485E-02	0.9216E-03	-0.2202E-02
19	0.4938E+00	0.7822E-01	-0.3829E-02	0.1141E-02	-0.1613E-02
20	0.4985E+00	0.3923E-01	-0.3956E-02	0.1227E-02	-0.8075E-03
21	0.5000E+00	0.0000E+00	-0.4079E-02	0.1309E-02	-0.1836E-04

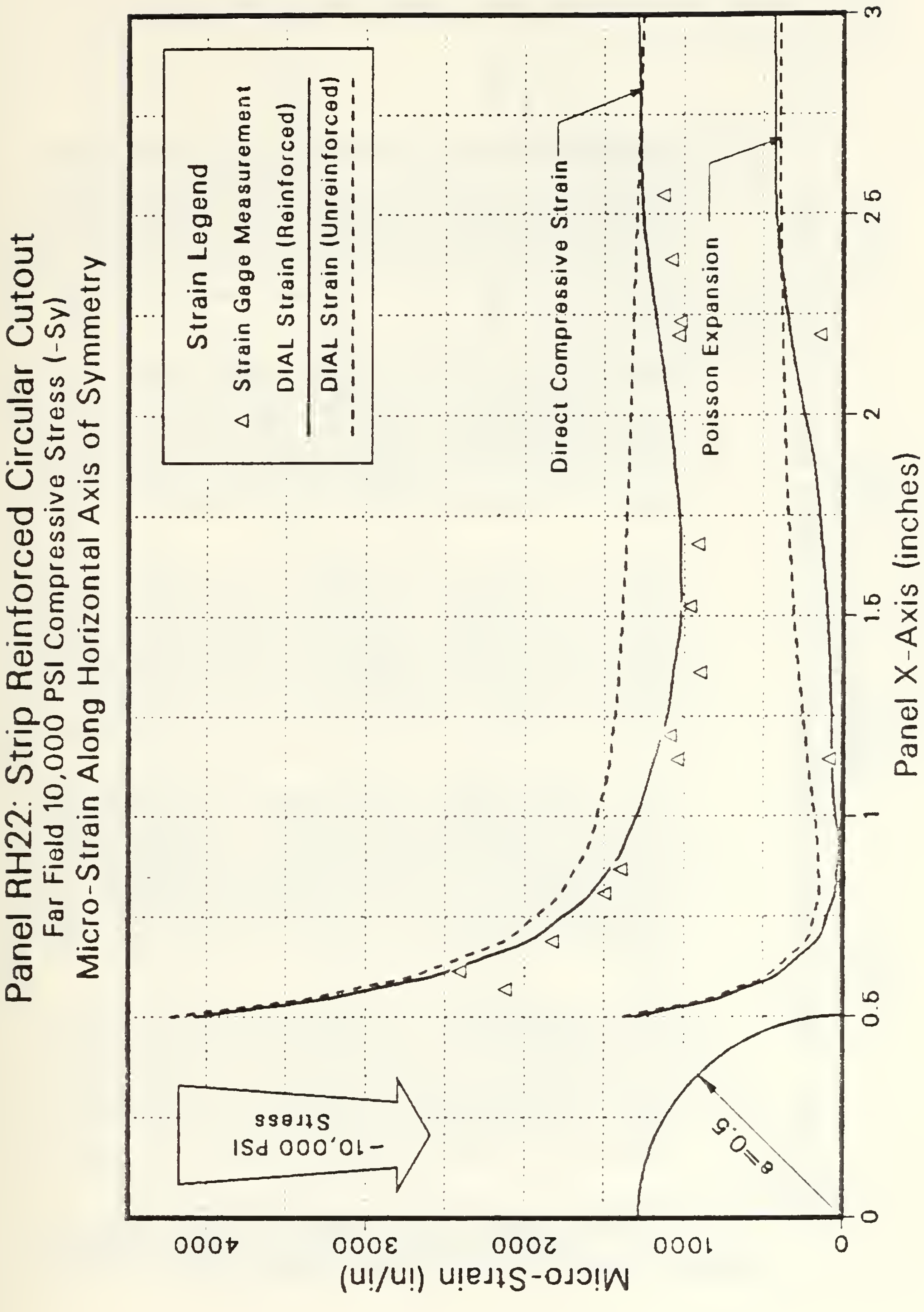

Figure K.3 Panel RH22: Strain Comparison Along the X Axis.

TABLE XLI

PANEL RH22, LEFEA STRAIN DISTRIBUTION ALONG THE X AXIS (-10,000 PSI).

NODE	X COORD	Y COORD	EPS-Y	EPS-X	EPS-XY
21	0.5000E+00	0.0000E+00	-0.4079E-02	0.1309E-02	-0.1836E-04
32	0.5250E+00	0.0000E+00	-0.3629E-02	0.1028E-02	-0.1364E-04
53	0.5500E+00	0.0000E+00	-0.3185E-02	0.7516E-03	-0.8665E-05
64	0.5750E+00	0.0000E+00	-0.2899E-02	0.5961E-03	-0.7624E-05
85	0.6000E+00	0.0000E+00	-0.2596E-02	0.4286E-03	-0.4455E-05
96	0.6500E+00	0.0000E+00	-0.2253E-02	0.2771E-03	-0.2390E-05
117	0.7000E+00	0.0000E+00	-0.1931E-02	0.1394E-03	-0.1972E-05
128	0.7500E+00	0.0000E+00	-0.1772E-02	0.9854E-04	-0.2148E-06
149	0.8000E+00	0.0000E+00	-0.1606E-02	0.5203E-04	-0.4398E-06
160	0.8500E+00	0.0000E+00	-0.1509E-02	0.3896E-04	-0.8359E-06
181	0.9000E+00	0.0000E+00	-0.1412E-02	0.2552E-04	0.1180E-05
192	0.9500E+00	0.0000E+00	-0.1358E-02	0.2704E-04	0.8782E-05
213	0.1000E+01	0.0000E+00	-0.1302E-02	0.4678E-04	0.1191E-04
214	0.1125E+01	0.0000E+00	-0.1205E-02	0.7024E-04	0.6395E-05
215	0.1250E+01	0.0000E+00	-0.1110E-02	0.7336E-04	0.4527E-05
216	0.1375E+01	0.0000E+00	-0.1066E-02	0.8463E-04	0.3508E-05
217	0.1500E+01	0.0000E+00	-0.1024E-02	0.9693E-04	0.2415E-05
218	0.1625E+01	0.0000E+00	-0.1027E-02	0.1208E-03	0.2365E-05
219	0.1750E+01	0.0000E+00	-0.1031E-02	0.1454E-03	0.1841E-05
220	0.1875E+01	0.0000E+00	-0.1061E-02	0.1769E-03	0.1491E-05
221	0.2000E+01	0.0000E+00	-0.1094E-02	0.2423E-03	0.7633E-06
222	0.2250E+01	0.0000E+00	-0.1180E-02	0.3494E-03	0.7797E-06
223	0.2500E+01	0.0000E+00	-0.1261E-02	0.4203E-03	0.1736E-05
224	0.2750E+01	0.0000E+00	-0.1278E-02	0.4293E-03	0.5196E-06
225	0.3000E+01	0.0000E+00	-0.1291E-02	0.4371E-03	-0.3192E-06
226	0.3250E+01	0.0000E+00	-0.1277E-02	0.4260E-03	0.7477E-07
227	0.3500E+01	0.0000E+00	-0.1265E-02	0.4171E-03	-0.8817E-07
228	0.3750E+01	0.0000E+00	-0.1250E-02	0.4075E-03	0.2020E-07
229	0.4000E+01	0.0000E+00	-0.1237E-02	0.3989E-03	-0.1204E-06
230	0.4125E+01	0.0000E+00	-0.1234E-02	0.3971E-03	-0.5578E-07
231	0.4250E+01	0.0000E+00	-0.1231E-02	0.3952E-03	0.7559E-07

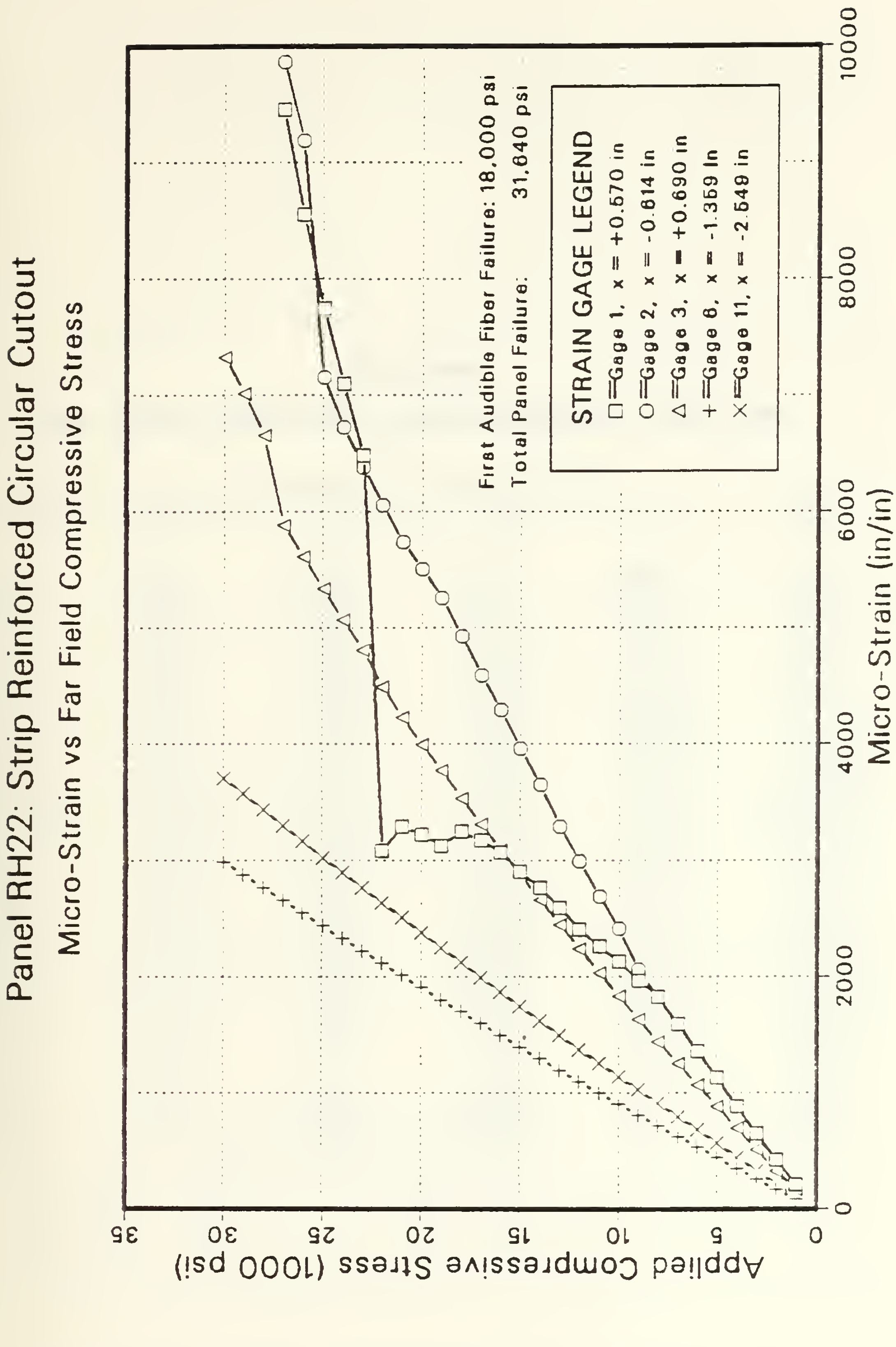

Figure K.4 Panel RH22: Microstrain vs. Compressive Stress.

TABLE XLII

PANEL RH22: SELECTED STRAIN GAGE VALUES DURING LOAD.

Load (psi)	Micro-Strain Indicated by Gage: #1	#2	#3	#6	#1
1000	-208	-208	-163	-80	-99
2000	-419	-417	-326	-163	-209
3000	-645	-642	-507	-254	-324
4000	-886	-875	-694	-348	-442
5000	-1128	-1115	-884	-441	-563
6000	-1361	-1346	-1067	-534	-680
7000	-1592	-1578	-1252	-624	-7[illegible]
8000	-1825	-1819	-1441	-717	-908
9000	-1968	-2060	-1636	-810	-1025
10000	-2129	-2411	-1833	-906	-1139
11000	-2260	-2693	-2036	-998	-1254
12000	-2408	-2992	-2244	-1093	-1375
13000	-2596	-3292	-2449	-1195	-1497
14000	-2765	-3646	-2662	-1295	-1622
15000	-2902	-3958	-2875	-1398	-1743
16000	-3067	-4290	-3093	-1499	-1872
17000	-3173	-4536	-3311	-1600	-1996
18000	-3247	-4926	-3533	-1702	-2121
19000	-3127	-5253	-3772	-1803	-2251
20000	-3224	-5503	-3991	-1908	-2377
21000	-3287	-5736	-4225	-2013	-2507
22000	-3084	-6057	-4492	-2115	-2636
23000	-6483	-6379	-4808	-2224	-2765
24000	-7098	-6724	-5067	-2329	-2898
25000	-7745	-7154	-5336	-2438	-3022
26000	-8553	-9183	-5612	-2549	-3168
27000	-9455	-9665	-5886	-2655	-3299
28000	n/a	-10442	-6053	-2768	-3434
29000	n/a	-11015	-7014	-2878	-3571
30000	n/a	-11548	-7327	-2983	-3706

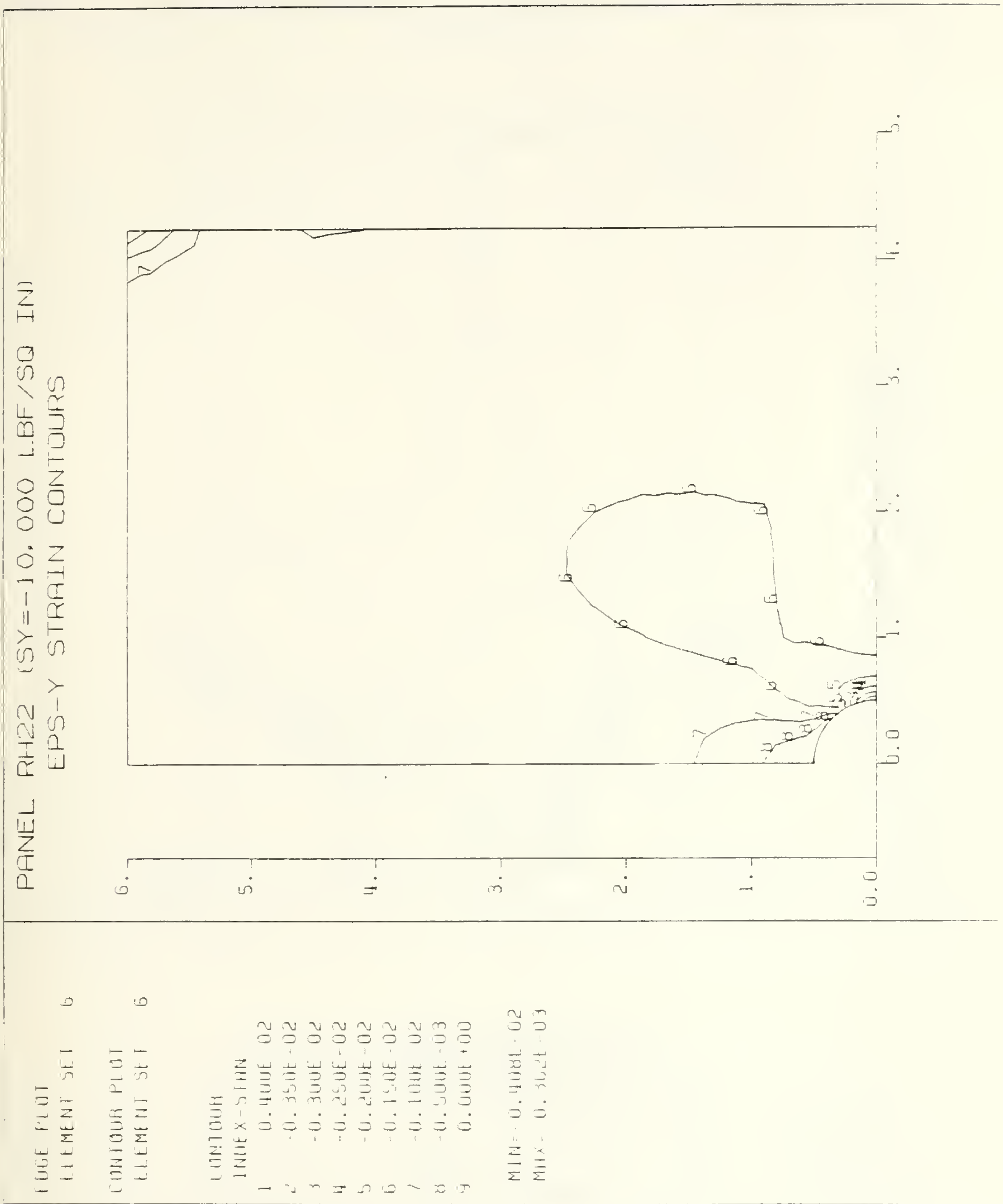

Figure K.5 Panel RH22: Eps-Y FEA Contours.

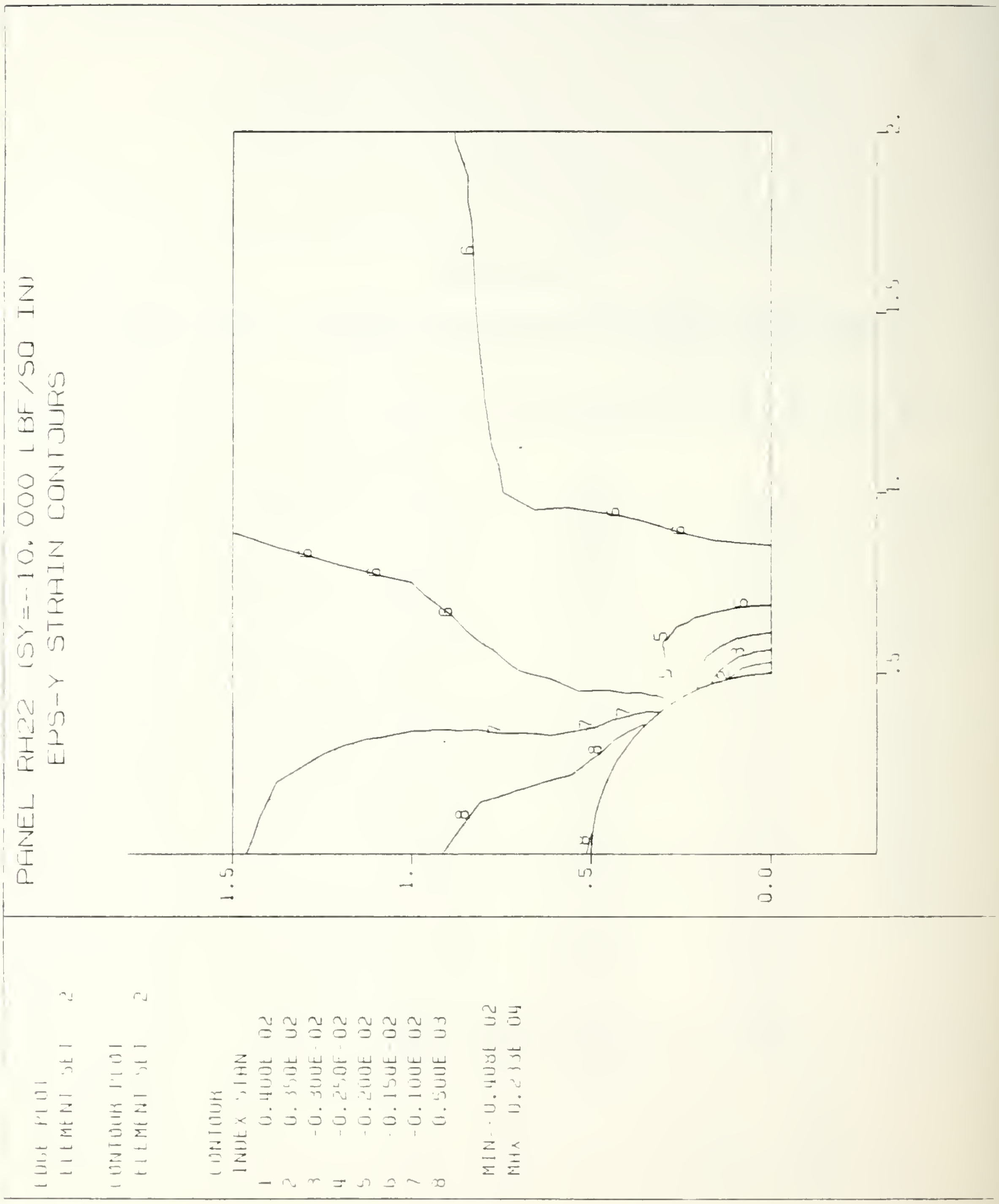

Figure K.6 Panel RH22: Eps-Y FEA Contours Near the Cutout.

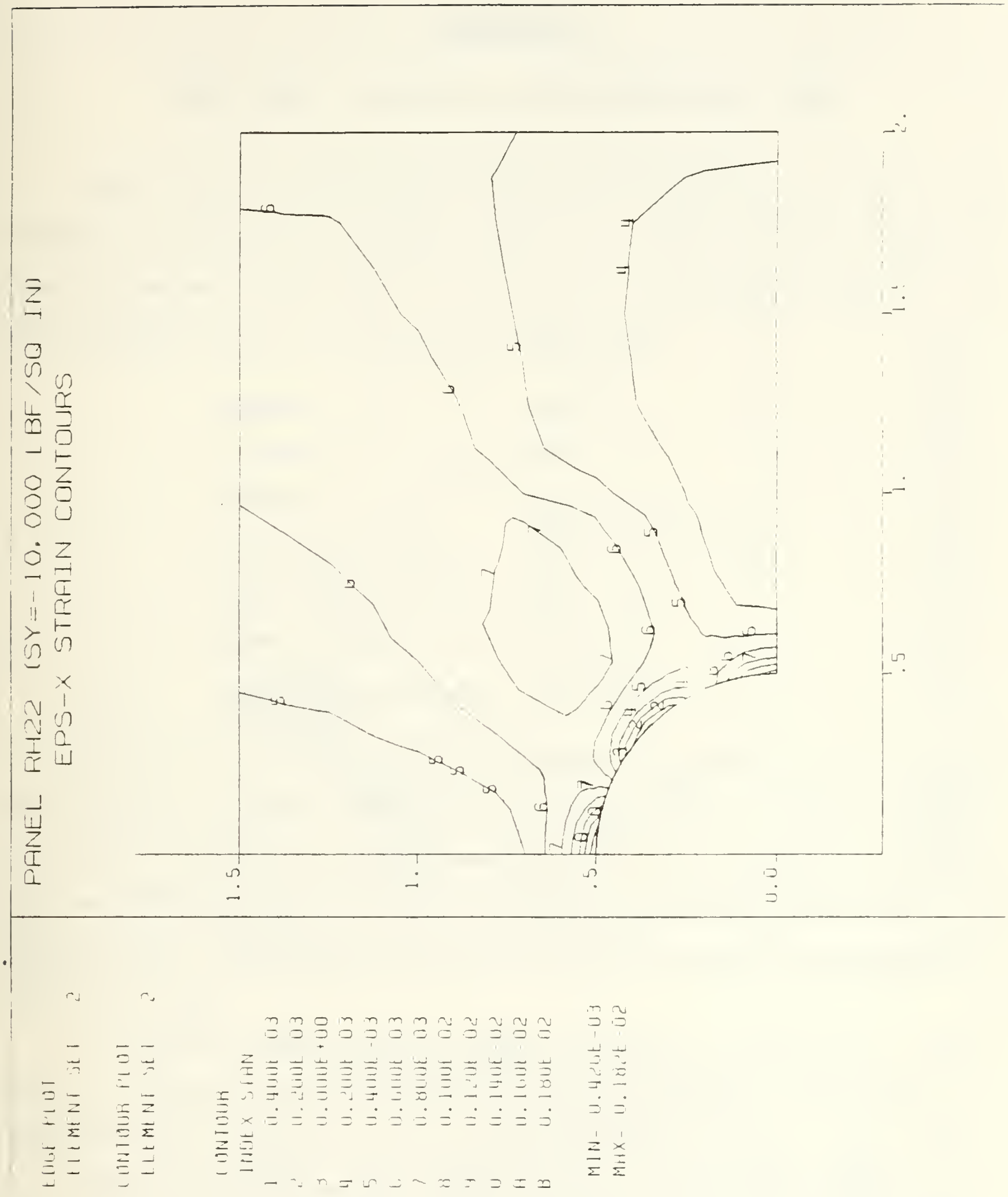

Figure K.7 Panel RH22: Eps-X FEA Contours Near the Cutout.

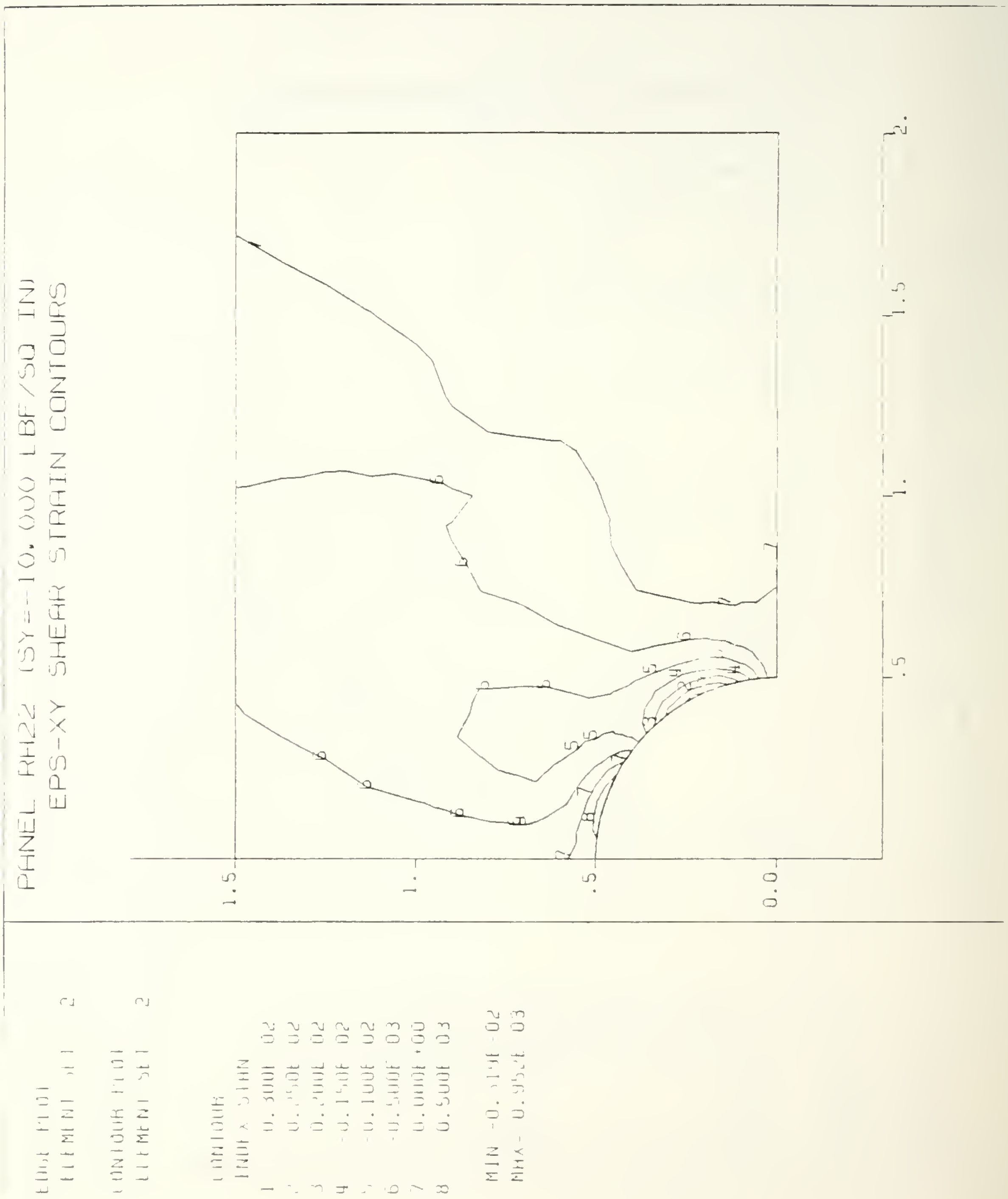

Figure K.8 Panel RH22: Eps-XY FEA Contours Near the Cutout.

APPENDIX L

PANEL RH31: ANALYTICAL AND EXPERIMENTAL DATA

Panel RH31 was reinforced with one co-cured ply of G/Ep in the shape of two strips on either side of the cutout on the outside of each facesheet offset 0.50 inch from the edge of the cutout. The reinforcement had the following dimensions:

Shape:	Strip
Length:	4.70 in
Width:	1.00 in
Thickness (each):	0.014 in (1 ply)
Area (each face):	9.40 in^2
Total Volume:	0.263 in^3
Net Cross Section:	0.056 in^2

The panel failed by facesheet separation and buckling (Type-2) at an applied normal stress of -21,500 psi ($\overline{\sigma}_n$). Based strictly on the failure of the unreinforced panel and the computed stress concentration factor of 2.82, the predicted failure was at $\overline{\sigma}_n$ = -32,400 psi. The panel failed at 33.6% less than the predicted ultimate load.

The finite element model (mesh) is shown in Figure L.1. The area of the strip reinforcement is outlined by the heavy lines 0.50 inch to the right of the cutout's edge.

Figure L.2 compares the three (finite element) computed strains around the cutout between the unreinforced panel (PO∅∅) and RH31. These computed strain values are listed in Table XLIII.

There was only a small decrease in the computed strain near the cutout due to the reinforcement.

Figure L.3 compares the computed (solid and dashed lines) and experimental (triangles) strains in the X and Y (poisson) directions in the panel and shows almost perfect correlation between analytical and experimentally measured strain at -10,000 psi applied normal stress. There was virtually no strain variation between the left and right side of the hole. The edge of the reinforcement can not be seen in the figure. The effect of reinforcement is a relatively small decrease in strain from the edge of the cutout out to about x = 3.0". Table XLIV gives the computed values of the strains along the X axis.

Figure L.4 shows graphically the stress-strain state during the load sequence from $\bar{\sigma}_n$ = 0 to -21 ksi. Strain gage values are given in Table XLV. Up to $\bar{\sigma}_n$ = -12 ksi all gages indicated a fairly normal stress-strain relation. At that point up to -18 ksi gage #2 demonstrated virtually no strain increase. At -18 ksi gage #1 (x = +0.572") suddenly indicated a strain decrease from 8900 to 6200 $\mu\epsilon$ and then an 1100 $\mu\epsilon$ increase at -19 ksi. From there it remained steady at about 7250 $\mu\epsilon$ to failure at $\bar{\sigma}_n$ = -21,500 ksi. Above -18 ksi gage #2 showed a steady decrease in strain which most probably indicated a separation of the facesheet from the core directly under the gage. As the load increased the facesheet buckled more and the indicated strain decreased. This panel shows how useful it would have been to instrument both facesheets of the panel to measure load transfer between them.

Figures L.5 through L.8 show the strain contours $\bar{\sigma}_n$ = -10,000 psi computed and plotted using DIAL. Figure L.5 is the full quarter panel with strain (Eps-Y) parallel to the applied load.

Figures L.6 through L.8 (Eps-Y, Eps-X and Eps-XY) show the strains in detail close to the cutout.

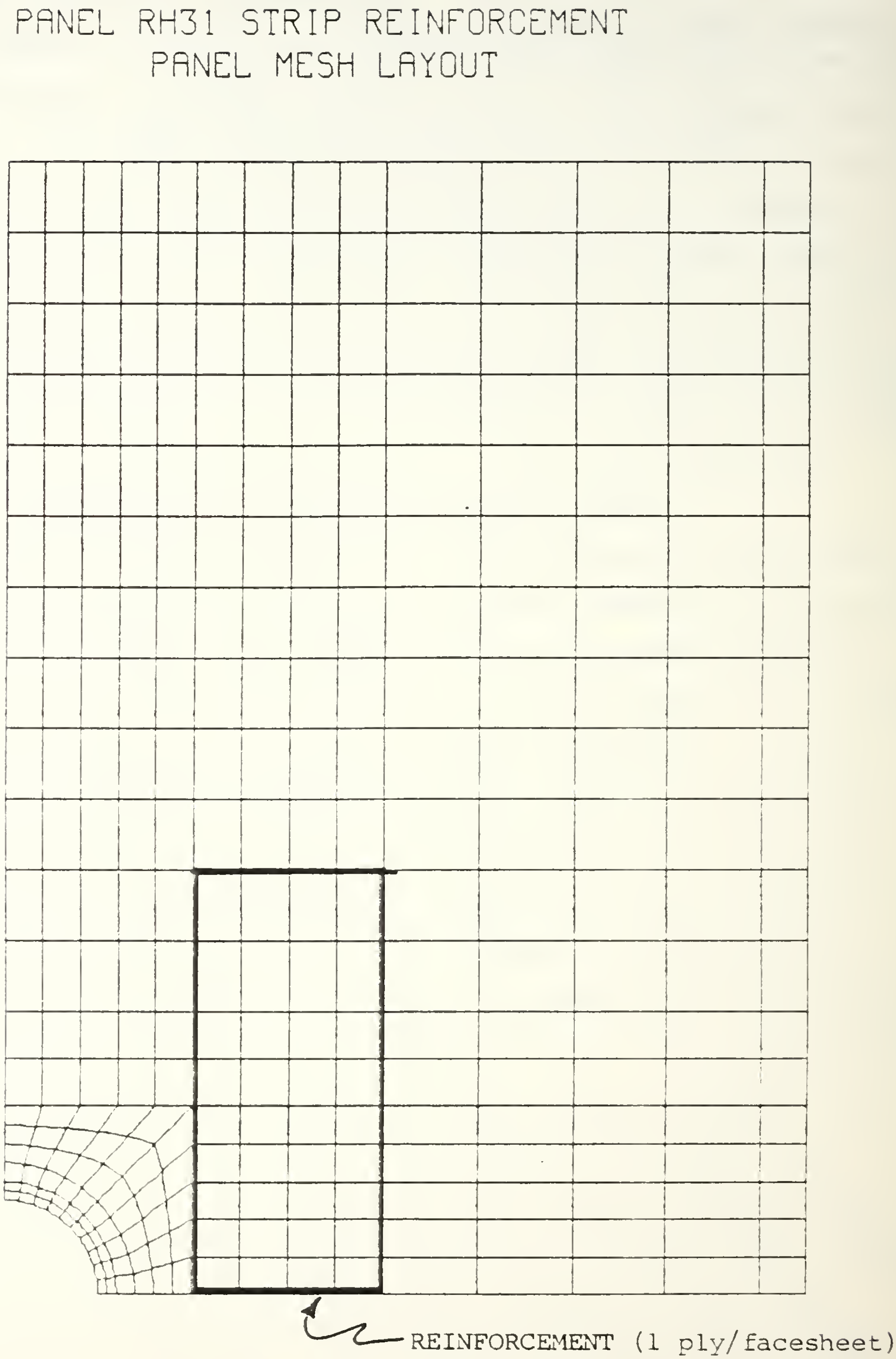

Figure L.1 Panel RH31: DIAL Finite Element Mesh.

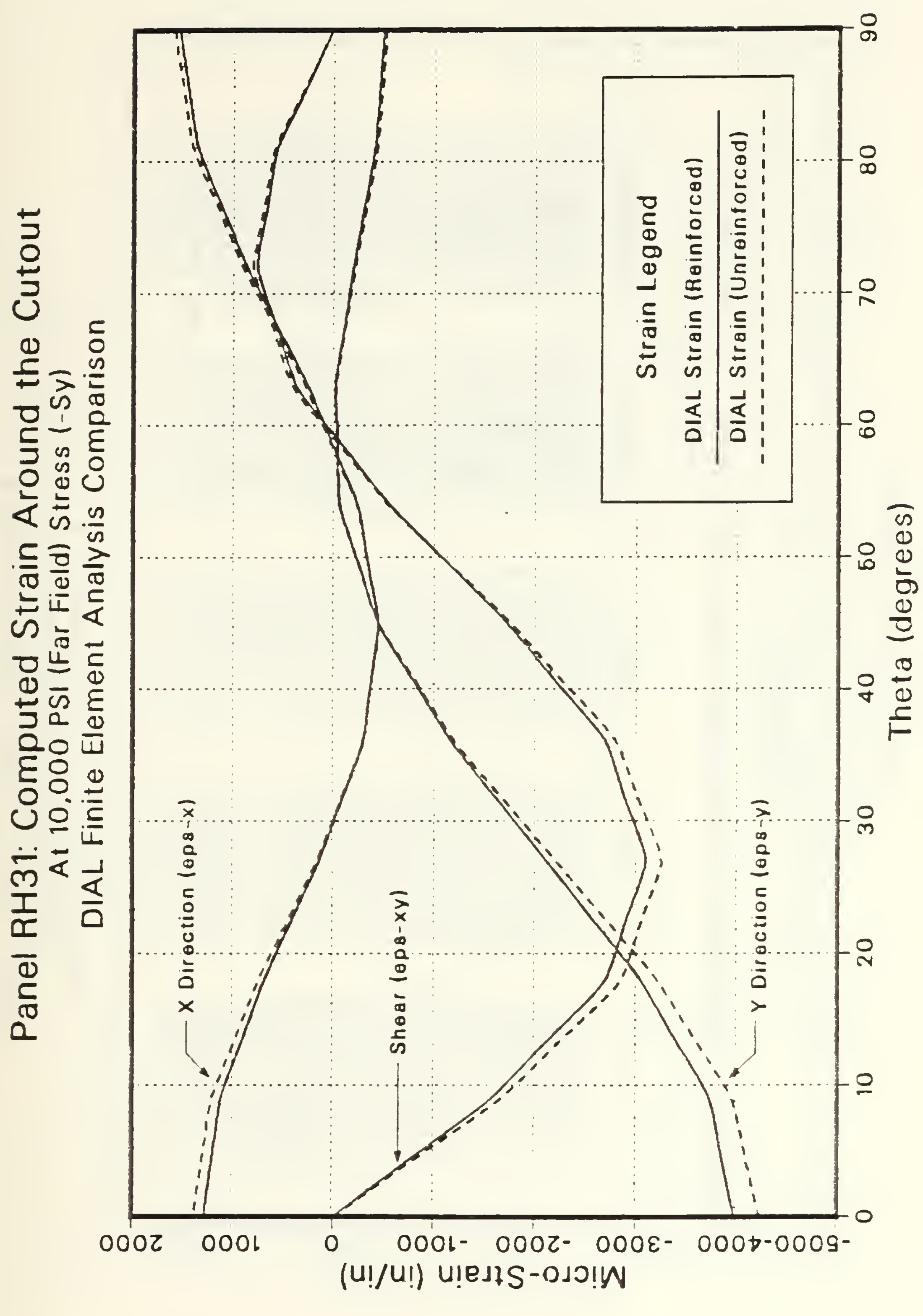

Figure L.2 Panel RH31: Strain Comparison Around the Cutout.

TABLE XLIII

PANEL RH31: LEFEA STRAIN DISTRIBUTION AROUND THE CUTOUT (-10,000 PSI).

NCDE	X COORD	Y COORD	EPS-Y	EPS-X	EPS-XY
1	0.0000E+00	0.5000E+00	-0.4894E-03	0.1545E-02	0.1667E-04
2	0.3923E-01	0.4985E+00	-0.4462E-03	0.1455E-02	0.2863E-03
3	0.7822E-01	0.4938E+00	-0.3988E-03	0.1358E-02	0.5695E-03
4	0.1167E+00	0.4862E+00	-0.2946E-03	0.1114E-02	0.6714E-03
5	0.1545E+00	0.4755E+00	-0.1882E-03	0.8671E-03	0.7646E-03
6	0.1913E+00	0.4619E+00	-0.1005E-03	0.5635E-03	0.5749E-03
7	0.2270E+00	0.4455E+00	-0.1385E-04	0.2598E-03	0.3747E-03
8	0.2612E+00	0.4263E+00	-0.3365E-04	0.1021E-04	-0.8451E-04
9	0.2939E+00	0.4045E+00	-0.5726E-04	-0.2361E-03	-0.5517E-03
10	0.3247E+00	0.3802E+00	-0.2468E-03	-0.3409E-03	-0.1134E-02
11	0.3536E+00	0.3536E+00	-0.4415E-03	-0.4406E-03	-0.1719E-02
12	0.3802E+00	0.3247E+00	-0.8032E-03	-0.3681E-03	-0.2212E-02
13	0.4045E+00	0.2939E+00	-0.1170E-02	-0.2905E-03	-0.2700E-02
14	0.4263E+00	0.2612E+00	-0.1640E-02	-0.7599E-04	-0.2903E-02
15	0.4455E+00	0.2270E+00	-0.2113E-02	0.1416E-03	-0.3097E-02
16	0.4619E+00	0.1913E+00	-0.2581E-02	0.4104E-03	-0.2906E-02
17	0.4755E+00	0.1545E+00	0.3048E-02	0.6793E-03	-0.2703E-02
18	0.4862E+00	0.1167E+00	-0.3392E-02	0.8975E-03	-0.2142E-02
19	0.4938E+00	0.7822E-01	-0.3733E-02	0.1113E-02	-0.1572E-02
20	0.4985E+00	0.3923E-01	-0.3861E-02	0.1198E-02	-0.7873E-03
21	0.5000E+00	0.0000E+00	-0.3983E-02	0.1278E-02	-0.1846E-04

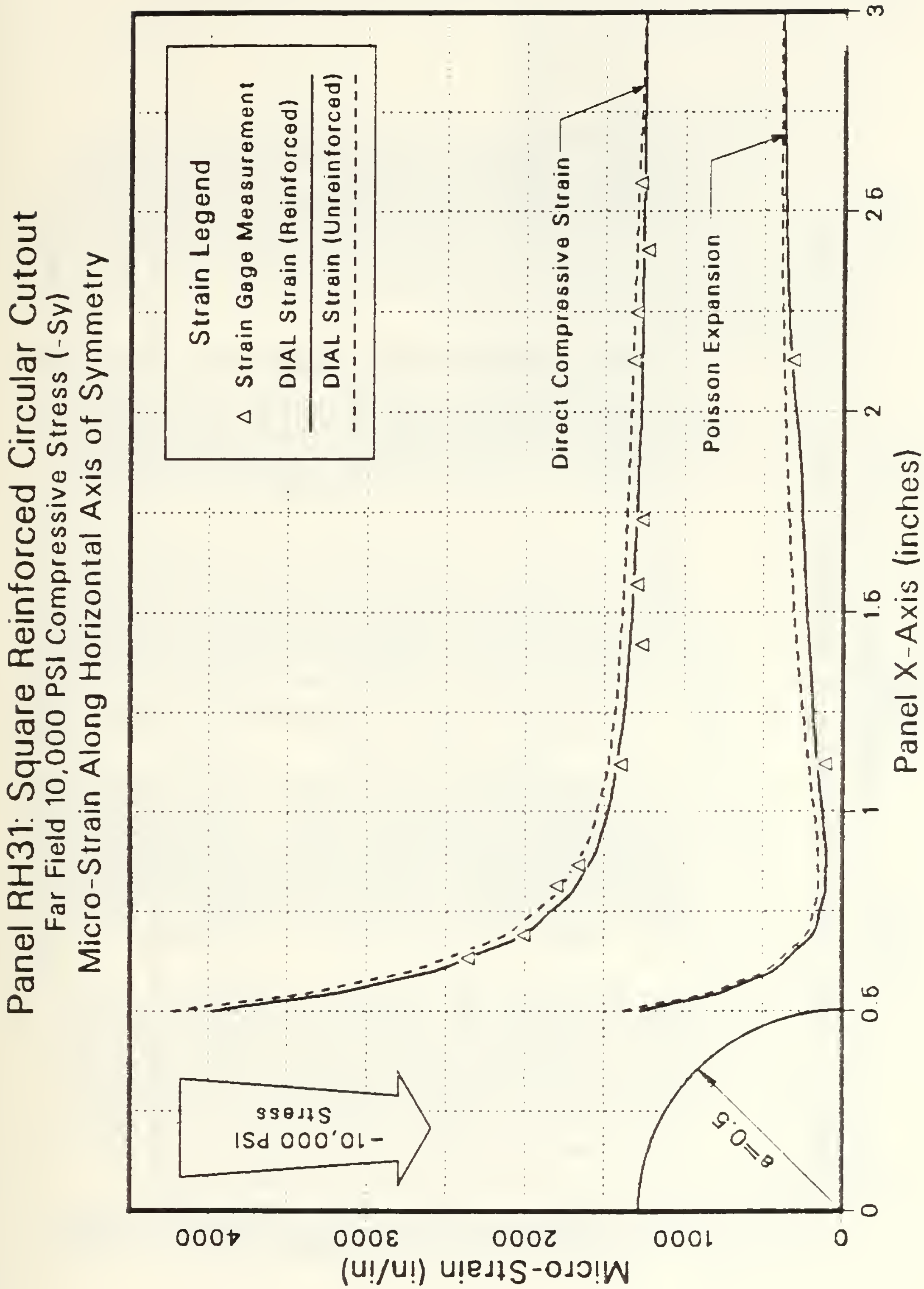

Figure L.3 Panel RH31: Strain Comparison Along the X Axis.

TABLE XLIV

PANEL RH31: LEFEA STRAIN DISTRIBUTION ALONG THE X AXIS (-10,000 PSI).

NODE	X COORD	Y COORD	EPS-Y	EPS-X	EPS-XY
21	0.5000E+00	0.0000E+00	-0.3983E-02	0.1278E-02	-0.1846E-04
32	0.5250E+00	0.0000E+00	-0.3555E-02	0.1008E-02	-0.1327E-04
53	0.5500E+00	0.0000E+00	-0.3133E-02	0.7421E-03	-0.7740E-05
64	0.5750E+00	0.0000E+00	-0.2866E-02	0.5950E-03	-0.6725E-05
85	0.6000E+00	0.0000E+00	-0.2581E-02	0.4360E-03	-0.3763E-05
96	0.6500E+00	0.0000E+00	-0.2269E-02	0.2966E-03	-0.1445E-05
117	0.7000E+00	0.0000E+00	-0.1977E-02	0.1708E-03	-0.7835E-06
128	0.7500E+00	0.0000E+00	-0.1843E-02	0.1405E-03	0.5327E-06
149	0.8000E+00	0.0000E+00	-0.1702E-02	0.1049E-03	-0.4216E-07
160	0.8500E+00	0.0000E+00	-0.1628E-02	0.1031E-03	0.7265E-06
181	0.9000E+00	0.0000E+00	-0.1554E-02	0.1008E-03	0.2693E-05
192	0.9500E+00	0.0000E+00	-0.1517E-02	0.1132E-03	0.8050E-05
213	0.1000E+01	0.0000E+00	-0.1479E-02	0.1278E-03	0.1071E-04
214	0.1125E+01	0.0000E+00	-0.1428E-02	0.1584E-03	0.6061E-05
215	0.1250E+01	0.0000E+00	-0.1379E-02	0.1855E-03	0.4928E-05
216	0.1375E+01	0.0000E+00	-0.1356E-02	0.2062E-03	0.3761E-05
217	0.1500E+01	0.0000E+00	-0.1331E-02	0.2270E-03	0.2204E-05
218	0.1625E+01	0.0000E+00	-0.1317E-02	0.2424E-03	0.1783E-05
219	0.1750E+01	0.0000E+00	-0.1303E-02	0.2580E-03	0.1128E-05
220	0.1875E+01	0.0000E+00	-0.1292E-02	0.2687E-03	0.1277E-05
221	0.2000E+01	0.0000E+00	-0.1279E-02	0.3024E-03	0.9095E-06
222	0.2250E+01	0.0000E+00	-0.1270E-02	0.3452E-03	0.2873E-06
223	0.2500E+01	0.0000E+00	-0.1262E-02	0.3650E-03	0.3868E-06
224	0.2750E+01	0.0000E+00	-0.1256E-02	0.3751E-03	0.3220E-06
225	0.3000E+01	0.0000E+00	-0.1250E-02	0.3850E-03	0.3242E-07
226	0.3250E+01	0.0000E+00	-0.1241E-02	0.3875E-03	0.9031E-07
227	0.3500E+01	0.0000E+00	-0.1231E-02	0.3901E-03	0.8932E-07
228	0.3750E+01	0.0000E+00	-0.1218E-02	0.3884E-03	0.6624E-07
229	0.4000E+01	0.0000E+00	-0.1205E-02	0.3867E-03	0.3280E-07
230	0.4125E+01	0.0000E+00	-0.1196E-02	0.3842E-03	0.3098E-07
231	0.4250E+01	0.0000E+00	-0.1188E-02	0.3819E-03	-0.2405E-07

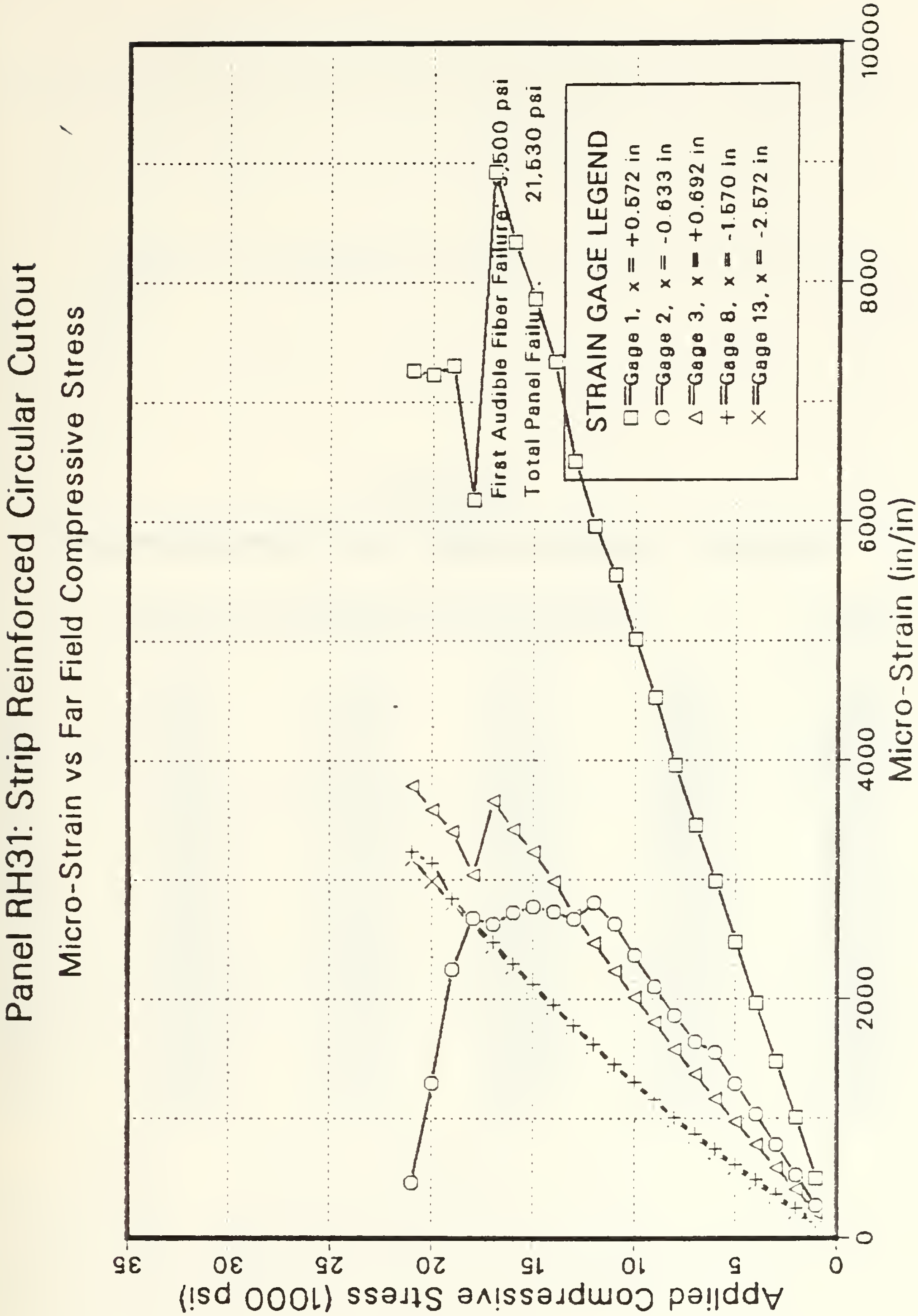

Figure L.4 Panel RH31: Microstrain vs. Compressive Stress.

TABLE XLV

PANEL RH31: SELECTED STRAIN GAGE VALUES DURING LOAD.

Load (psi)	Micro-Strain Indicated by Gage:				
	#1	#2	#3	#8	#13
1000	-496	-267	-207	-131	-116
2000	-1005	-527	-407	-245	-217
3000	-1475	-777	-589	-365	-339
4000	-1964	-1036	-777	-492	-463
5000	-2477	-1292	-970	-617	-589
6000	-2986	-1553	-1168	-743	-715
7000	-3452	-1644	-1371	-872	-848
8000	-3959	-1860	-1577	-1009	-987
9000	-4526	-2100	-1806	-1162	-1143
10000	-5015	-2364	-2012	-1302	-1285
11000	-5551	-2626	-2233	-1457	-1441
12000	-5962	-2809	-2468	-1618	-1601
13000	-6501	-2667	-2705	-1782	-1765
14000	-7336	-2732	-2989	-1952	-1931
15000	-7865	-2771	-3232	-2122	-2097
16000	-8337	-2722	-3419	-2297	-2268
17000	-8925	-2628	-3664	-2473	-2439
18000	-6176	-2678	-3038	-2655	-2615
19000	-7306	-2249	-3410	-2844	-2796
20000	-7227	-1299	-3583	-3141	-2986
21000	-7259	-461	-3788	-3234	-3171

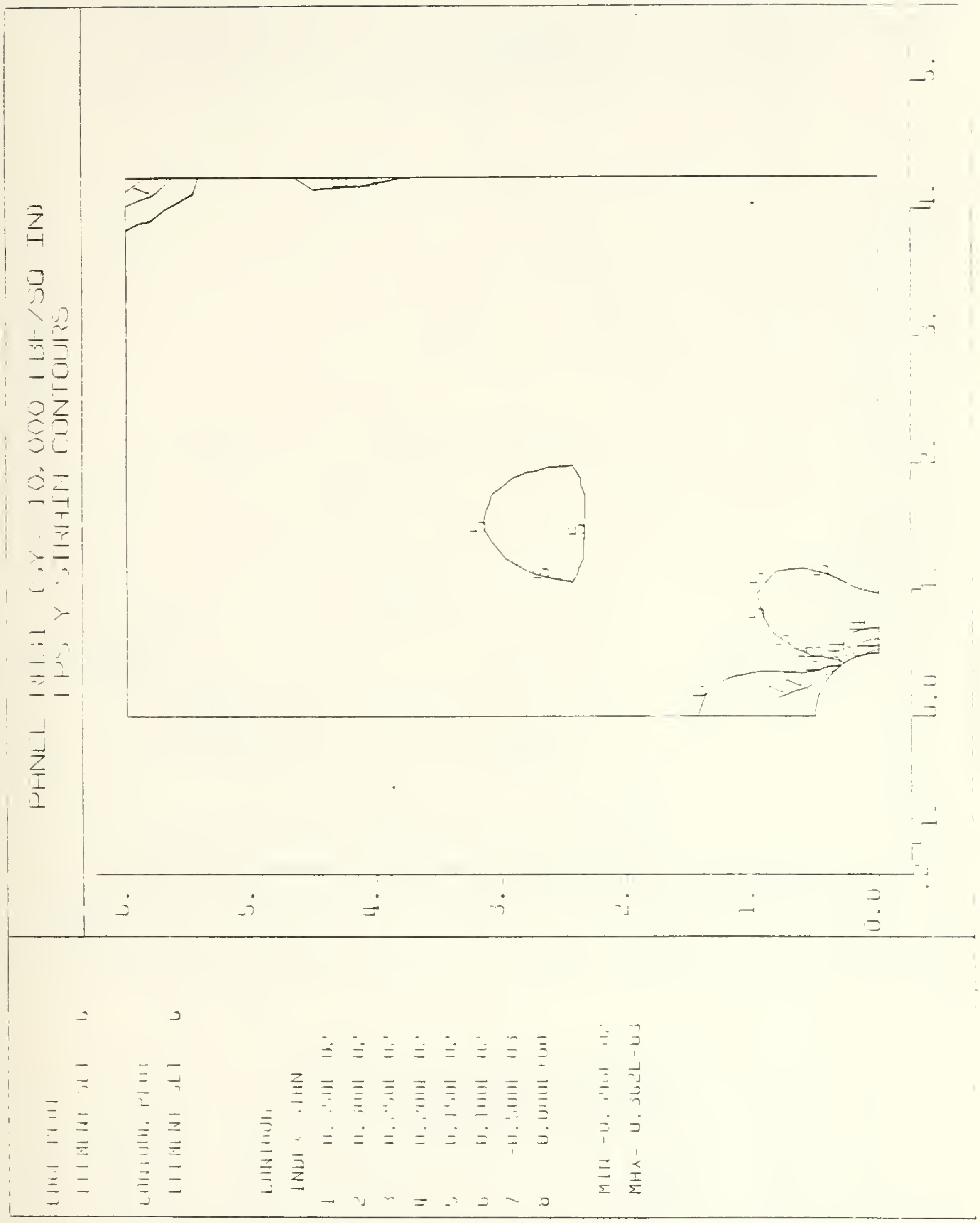

Figure L.5 Panel RH31: Eps-Y FEA Contours.

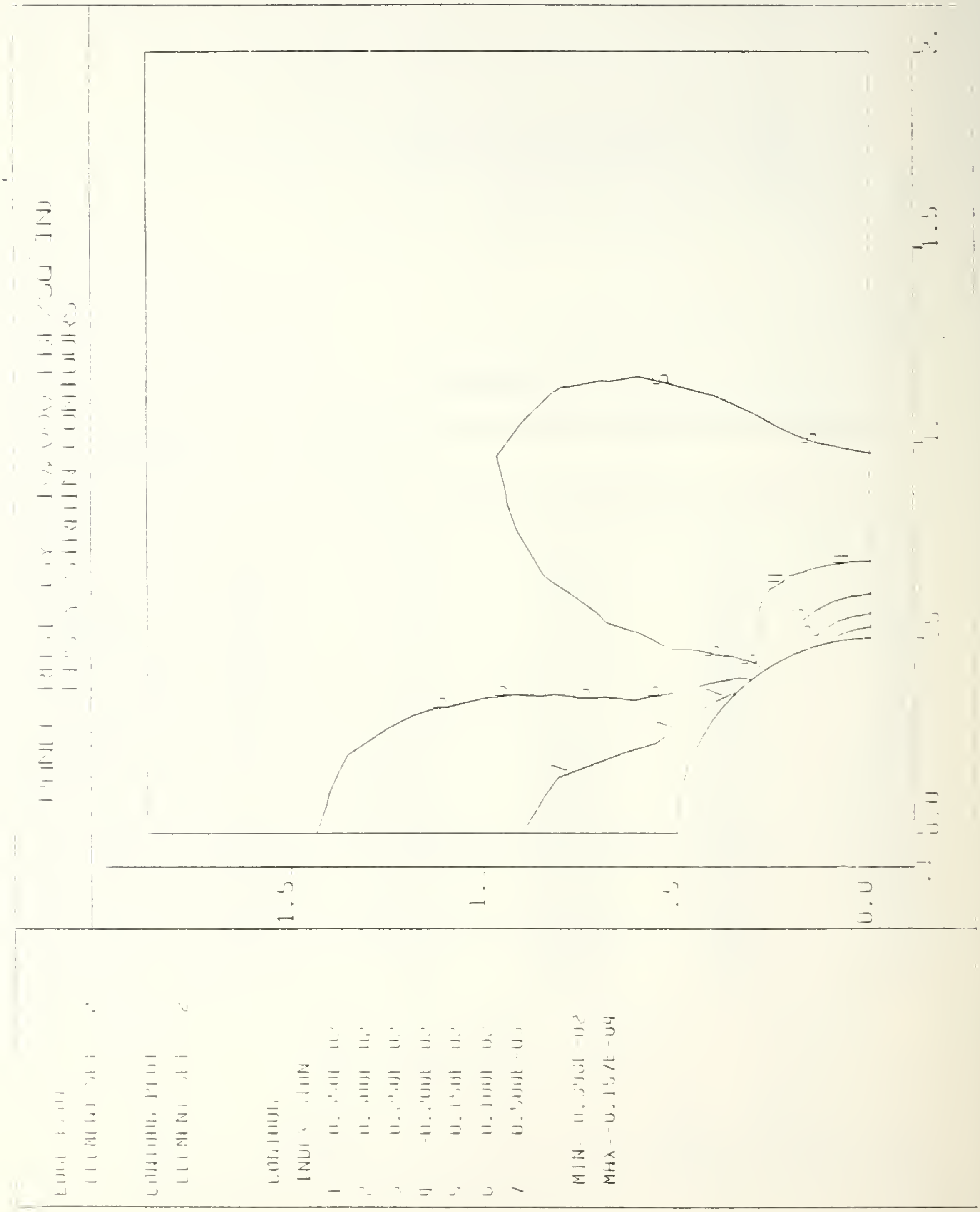

Figure L.6 Panel RH31: Eps-Y FEA Contours Near the Cutout.

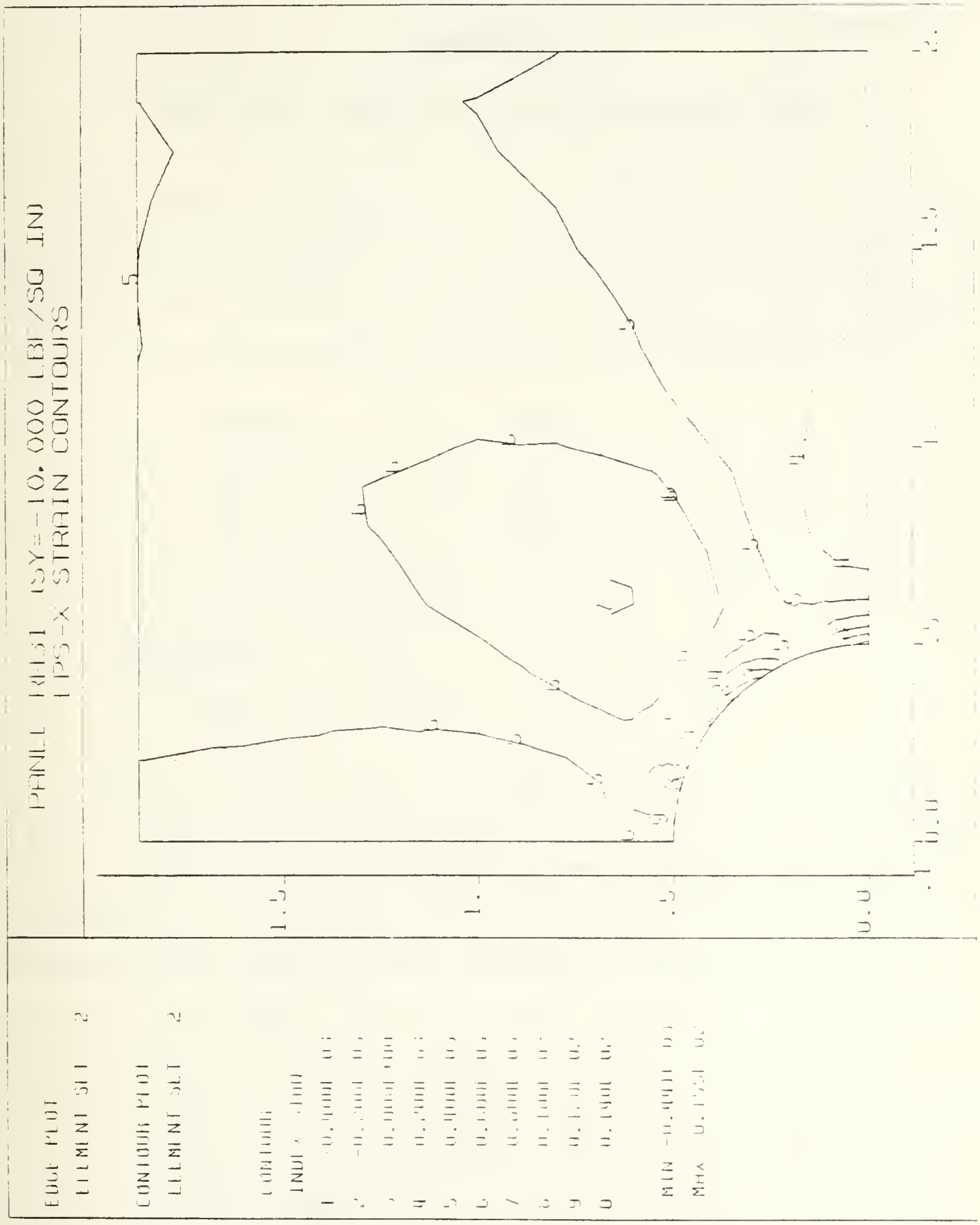

Figure L.7 Panel RH31: Eps-X FEA Contours Near the Cutout.

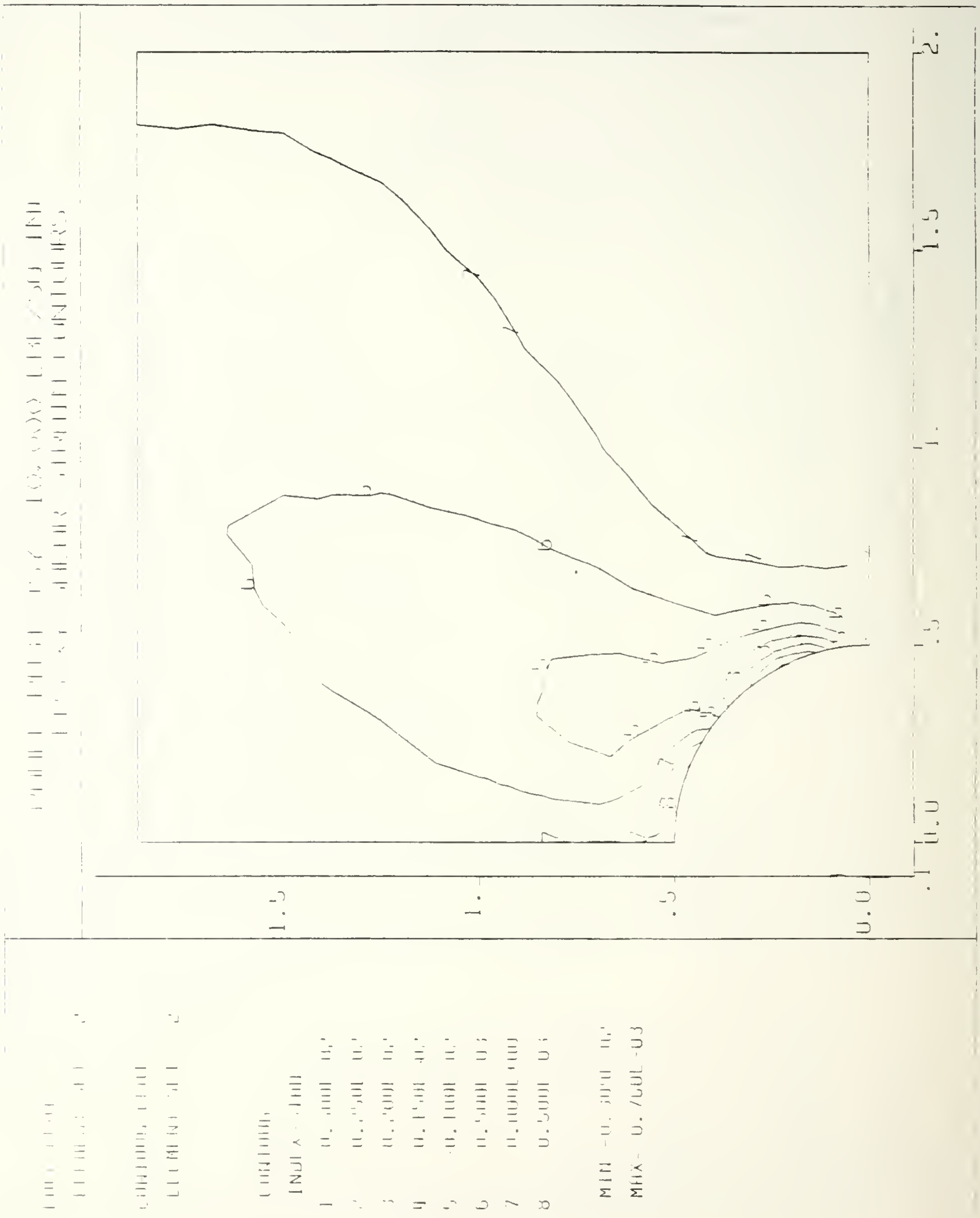

Figure L.8 Panel RH31: Eps-XY FEA Contours Near the Cutout.

APPENDIX M

PANEL RH42: ANALYTICAL AND EXPERIMENTAL DATA

Panel RH42 was reinforced with two co-cured plies of G/Ep in the shape of two strips on either side of the cutout on the outside of each facesheet offset 0.50 inch from the edge of the cutout. The reinforcement had the following dimensions:

Shape:	Strip
Length:	3.14 in
Width (each):	1.00 in
Thickness (each):	0.028 in (2 ply)
Area (each face):	6.280 in^2
Total Volume:	0.352 in^3
Net Cross Section:	0.112 in^2

The panel failed at the hole edge (Type-1) at an applied normal stress of -36,990 psi ($\bar{\sigma}_n$). Based strictly on the failure of the unreinforced panel and the computed stress concentration factor of 2.64 the predicted failure was $\bar{\sigma}_n$ = -34,650 psi. The panel failed at **106.8%** of the predicted ultimate stress. It sustained the <u>highest</u> load of any test specimen. The reinforcement increased the panel's weight little more than 3.6% and increased the failure strength by 21% over the unreinforced panel. It was one of the panels that led to the conclusion that several layers of reinforcement close to the cutout are more effective than spreading it out more thinly over a larger area.

The finite element model (mesh) is shown in Figure M.1. The area of the strip reinforcement is outlined by the heavy lines beginning 0.5" to the right of the cutout's edge.

Figure M.2 compares the three (finite element) computed strains around the cutout between the unreinforced panel (POØØ) and RH42. These computed strain values are listed in Table XLVI. There is a relatively small decrease in the strain due to the strip reinforcement compared with the equivalent amount of reinforcement concentrated next to the cutout.

Figure M.3 compares the computed (solid and dashed lines) and experimental (triangles) strains in the Y and X (poisson) directions in the panel and shows an excellent correlation between analytical and experimental strain at $\bar{\sigma}_n$ = -10,000 psi. There was some strain variation between the left and right sides of the hole. The exact edge of the reinforcement can not be seen in the figure. The effects of reinforcement is a significant strain decrease (compared to the unreinforced panel, POØØ) under the reinforcement, a small decrease near the hole and a slight increase in the far field (where x 2.50"). Table XLVII gives the computed values of the strains along the X axis.

Figure M.4 shows the stress-strain state during the load sequence from $\bar{\sigma}_n$ = 0 to -36 ksi. Experimentally measured strain data are given in Table XLVIII. Up to about $\bar{\sigma}_n$ = -24 ksi all gages indicated a normal stress-strain relation. At that load gage #2 (x = -0.571") demonstrated the "stair-step" phenomena. At -25 ksi gage #1 (x = +0.569") indicates what appears to be a softening or loss of stiffness--the strain rate drastically increased. Gage #2 seems to reflect the same behavior at -4 ksi higher stress. Gage #3 (x = +0.701") appears to pick up the load when gage #1 shows what appears to be local buckling. Note that gages #8 and #13 (x = -1.512" and -2.460") reflect none of what is occurring next to the cutout.

The reaction of this panel may help explain much of what occurs in the boundary region around the cutout on the other panels. At high levels of strain (8,000 to 10,000 $\mu\epsilon$) next to the cutout's edge, local delamination, buckling and fiber failure forces the transfer of the load path laterally away from the edge to the still intact and stiffer fibers and matrix farther from the cutout.

Figures M.5 through M.8 show the strain contours at $\bar{\sigma}_n$ = -10,000 psi computed and plotted using DIAL. Figure M.5 is the full quarter panel with strain (Eps-Y) parallel to the applied load. Figures M.6 through M.8 (Eps-Y, Eps-X and Eps-XY) show the strains in detail close to the cutout.

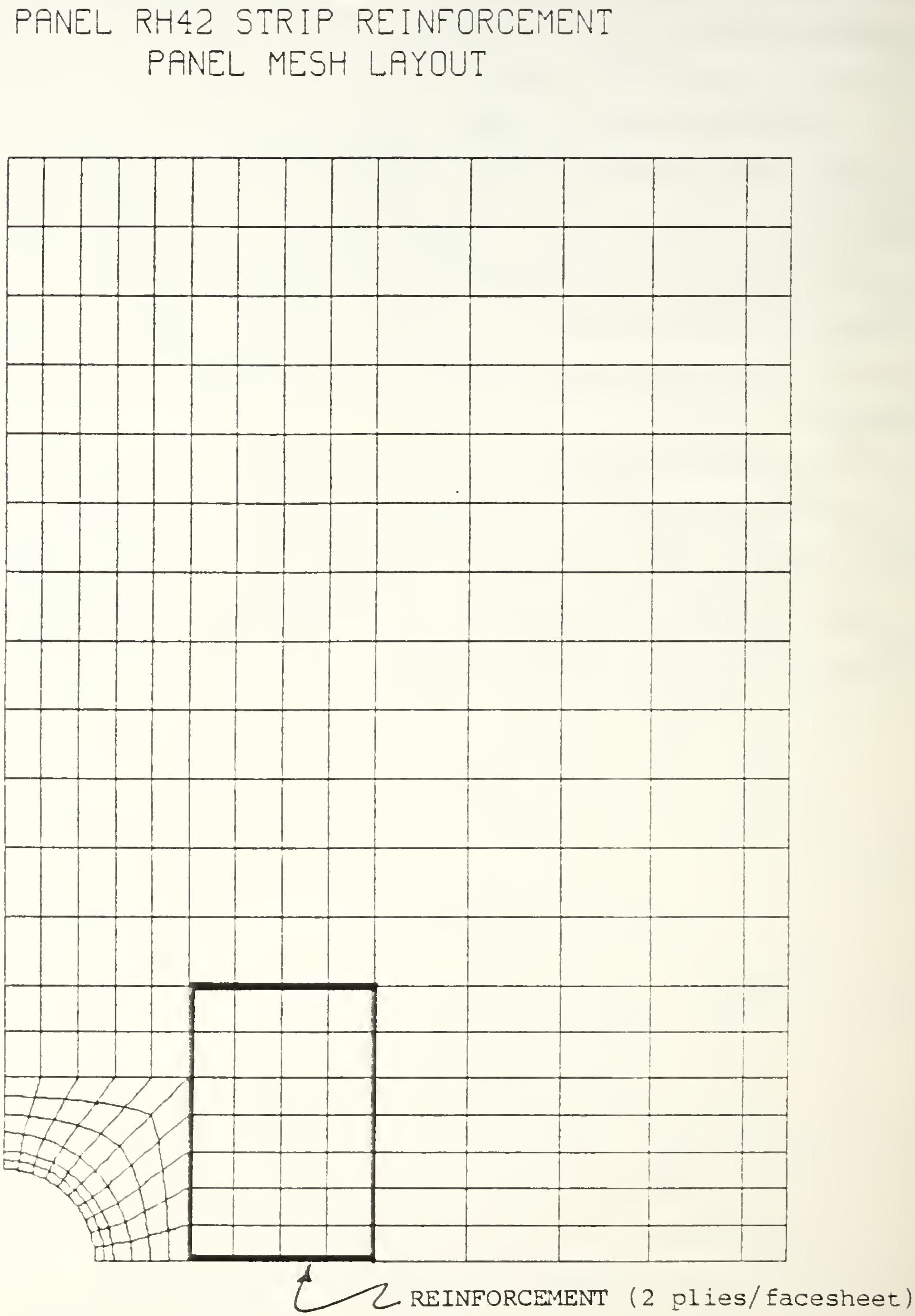

Figure M.1 Panel RH42: DIAL Finite Element Mesh.

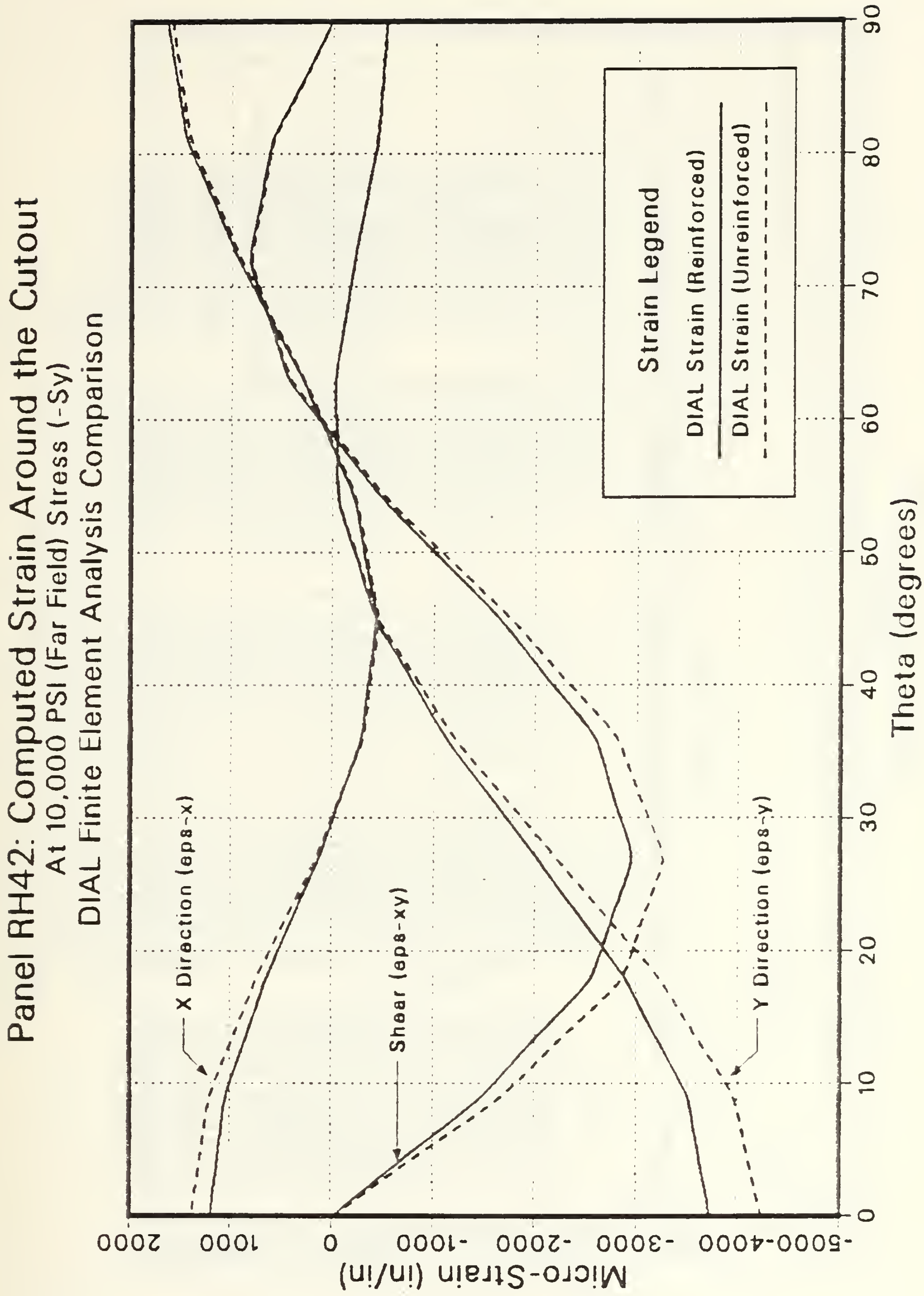

Figure M.2 Panel RH42: Strain Comparison Around the Cutout.

TABLE XLVI

PANEL RH42: LEFEA STRAIN DISTRIBUTION AROUND THE CUTOUT (-10,000 PSI).

NODE	X COORD	Y COORD	EPS-Y	EPS-X	EPS-XY
1	0.0000E+00	0.5000E+00	-0.5212E-03	0.1645E-02	0.1743E-04
2	0.3923E-01	0.4985E+00	-0.4756E-03	0.1549E-02	0.3051E-03
3	0.7822E-01	0.4938E+00	-0.4256E-03	0.1448E-02	0.6068E-03
4	0.1167E+00	0.4862E+00	-0.3155E-03	0.1193E-02	0.7197E-03
5	0.1545E+00	0.4755E+00	-0.2033E-03	0.9337E-03	0.8229E-03
6	0.1913E+00	0.4619E+00	-0.1097E-03	0.6175E-03	0.6347E-03
7	0.2270E+00	0.4455E+00	-0.1728E-04	0.3015E-03	0.4353E-03
8	0.2612E+00	0.4263E+00	-0.3238E-04	0.4369E-04	-0.2456E-04
9	0.2939E+00	0.4045E+00	-0.5162E-04	-0.2104E-03	-0.4922E-03
10	0.3247E+00	0.3802E+00	-0.2346E-03	-0.3188E-03	-0.1068E-02
11	0.3536E+00	0.3536E+00	-0.4228E-03	-0.4216E-03	-0.1644E-02
12	0.3802E+00	0.3247E+00	-0.7698E-03	-0.3528E-03	-0.2118E-02
13	0.4045E+00	0.2939E+00	-0.1121E-02	-0.2790E-03	-0.2587E-02
14	0.4263E+00	0.2612E+00	-0.1565E-02	-0.7371E-04	-0.2772E-02
15	0.4455E+00	0.2270E+00	-0.2010E-02	0.1341E-03	-0.2947E-02
16	0.4619E+00	0.1913E+00	-0.2444E-02	0.3876E-03	-0.2754E-02
17	0.4755E+00	0.1545E+00	-0.2876E-02	0.6407E-03	-0.2552E-02
18	0.4862E+00	0.1167E+00	-0.3190E-02	0.8436E-03	-0.2016E-02
19	0.4938E+00	0.7822E-01	-0.3500E-02	0.1044E-02	-0.1475E-02
20	0.4985E+00	0.3923E-01	-0.3616E-02	0.1122E-02	-0.7383E-03
21	0.5000E+00	0.0000E+00	-0.3727E-02	0.1196E-02	-0.1652E-04

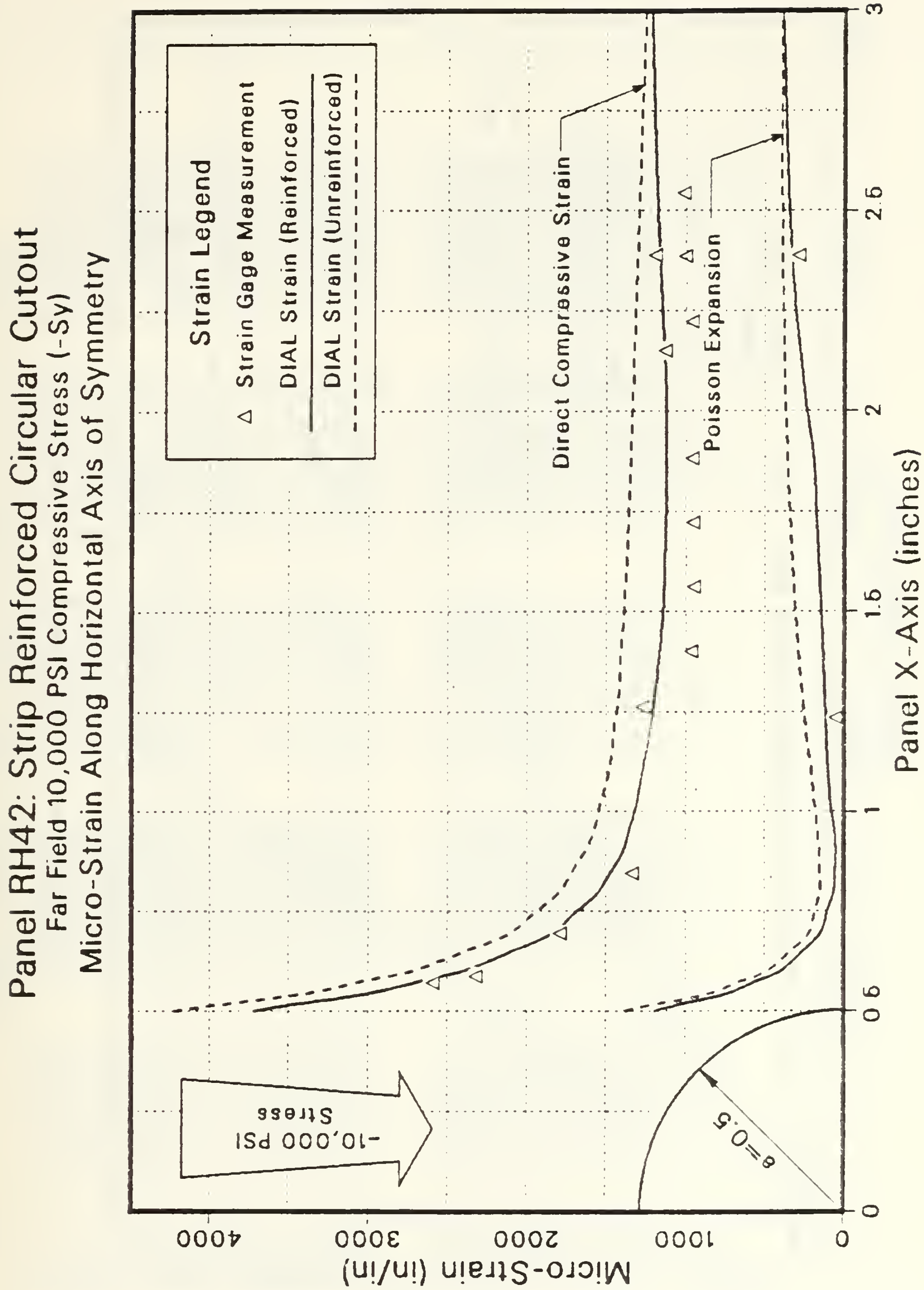

Figure M.3 Panel RH42: Strain Comparison Along the X Axis.

TABLE XLVII

PANEL RH42: LEFEA STRAIN DISTRIBUTION ALONG THE X AXIS (-10,000 PSI).

NODE	X COORD	Y COORD	EPS-Y	EPS-X	EPS-XY
21	0.5000E+00	0.0000E+00	-0.3727E-02	0.1196E-02	-0.1652E-04
32	0.5250E+00	0.0000E+00	-0.3326E-02	0.9418E-03	-0.1214E-04
53	0.5500E+00	0.0000E+00	-0.2930E-02	0.6921E-03	-0.7504E-05
64	0.5750E+00	0.0000E+00	-0.2675E-02	0.5510E-03	-0.6689E-05
85	0.6000E+00	0.0000E+00	-0.2406E-02	0.3990E-03	-0.3989E-05
96	0.6500E+00	0.0000E+00	-0.2104E-02	0.2616E-03	-0.1876E-05
117	0.7000E+00	0.0000E+00	-0.1822E-02	0.1370E-03	-0.1277E-05
128	0.7500E+00	0.0000E+00	-0.1688E-02	0.1025E-03	0.1125E-07
149	0.8000E+00	0.0000E+00	-0.1548E-02	0.6302E-04	-0.4469E-06
160	0.8500E+00	0.0000E+00	-0.1472E-02	0.5595E-04	-0.2354E-06
181	0.9000E+00	0.0000E+00	-0.1396E-02	0.4828E-04	0.1561E-05
192	0.9500E+00	0.0000E+00	-0.1360E-02	0.5645E-04	0.7340E-05
[illegible]	[illegible]	[illegible]	[illegible]	[illegible]	[illegible]
215	0.1250E+01	0.0000E+00	-0.1204E-02	0.1176E-03	0.4500E-05
216	0.1375E+01	0.0000E+00	-0.1174E-02	0.1311E-03	0.3297E-05
217	0.1500E+01	0.0000E+00	-0.1145E-02	0.1450E-03	0.2270E-05
218	0.1625E+01	0.0000E+00	-0.1137E-02	0.1605E-03	0.2190E-05
219	0.1750E+01	0.0000E+00	-0.1129E-02	0.1765E-03	0.1017E-05
220	0.1875E+01	0.0000E+00	-0.1129E-02	0.1912E-03	0.8616E-06
221	0.2000E+01	0.0000E+00	-0.1126E-02	0.2348E-03	0.7887E-06
222	0.2250E+01	0.0000E+00	-0.1151E-02	0.3053E-03	0.4017E-06
223	0.2500E+01	0.0000E+00	-0.1180E-02	0.3478E-03	0.4395E-06
224	0.2750E+01	0.0000E+00	-0.1201E-02	0.3700E-03	0.3135E-06
225	0.3000E+01	0.0000E+00	-0.1219E-02	0.3905E-03	0.2033E-06
226	0.3250E+01	0.0000E+00	-0.1221E-02	0.3935E-03	0.1556E-06
227	0.3500E+01	0.0000E+00	-0.1223E-02	0.3966E-03	0.6767E-07
228	0.3750E+01	0.0000E+00	-0.1221E-02	0.3940E-03	0.6649E-07
229	0.4000E+01	0.0000E+00	-0.1218E-02	0.3921E-03	0.2721E-07
230	0.4125E+01	0.0000E+00	-0.1218E-02	0.3918E-03	0.3485E-07
231	0.4250E+01	0.0000E+00	-0.1219E-02	0.3915E-03	-0.3617E-07

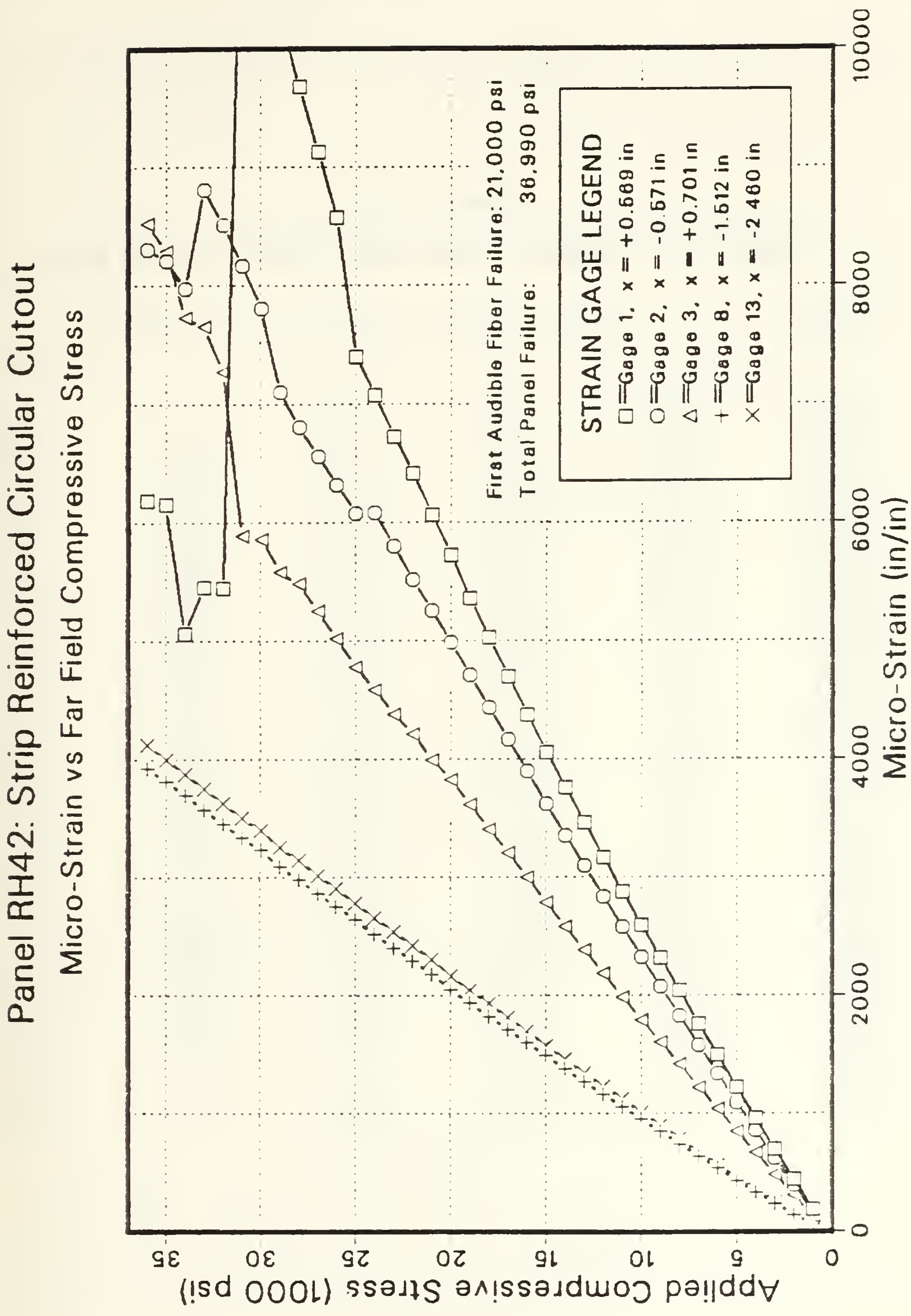

Figure M.4 Panel RH42: Microstrain vs. Compressive Stress.

TABLE XLVIII

PANEL RH42: SELECTED STRAIN GAGE VALUES DURING LOAD.

Load (psi)	Micro-Strain Indicated by Gage:				
	#1	#2	#3	#8	#13
1000	-185	-167	-127	-53	-57
2000	-443	-395	-307	-141	-146
3000	-699	-622	-485	-235	-246
4000	-957	-856	-666	-333	-350
5000	-1220	-1093	-849	-431	-451
6000	-1498	-1341	-1040	-536	-562
7000	-1759	-1576	-1222	-635	-667
8000	-2044	-1831	-1420	-741	-787
9000	-2315	-2073	-1604	-845	-894
10000	-2594	-2324	-1796	-950	-1004
11000	-2876	-2577	-1989	-1055	-1121
12000	-3167	-2834	-2185	-1161	-1229
13000	-3460	-3094	-2385	-1270	-1342
14000	-3756	-3355	-2584	-1378	-1459
15000	-4057	-3621	-2786	-1487	-1575
16000	-4374	-3897	-2999	-1603	-1700
17000	-4698	-4166	-3206	-1713	-1813
18000	-5025	-4435	-3409	-1823	-1930
19000	-5357	-4709	-3615	-1935	-2044
20000	-5726	-4984	-3825	-2049	-2163
21000	-6062	-5258	-3995	-2179	-2306
22000	-6417	-5517	-4211	-2289	-2423
23000	-6726	-5801	-4378	-2402	-2541
24000	-7078	-6083	-4584	-2514	-2656
25000	-7399	-6078	-4782	-2639	-2778
26000	-8570	-6318	-5018	-2749	-2902
27000	-9125	-6562	-5253	-2865	-3017
28000	-9675	-6806	-5481	-2981	-3142
29000	-10261	-7106	-5585	-3088	-3255
30000	-11239	-7808	-5865	-3232	-3400
31000	-11953	-8168	-5888	-3336	-3503
32000	-5449	-8508	-7275	-3454	-3627
33000	-5453	-8809	-7653	-3573	-3754
34000	-5062	-7973	-7729	-3695	-3876
35000	-6149	-8207	-8290	-3816	-4001
36000	-6188	-8306	-8521	-3925	-4121

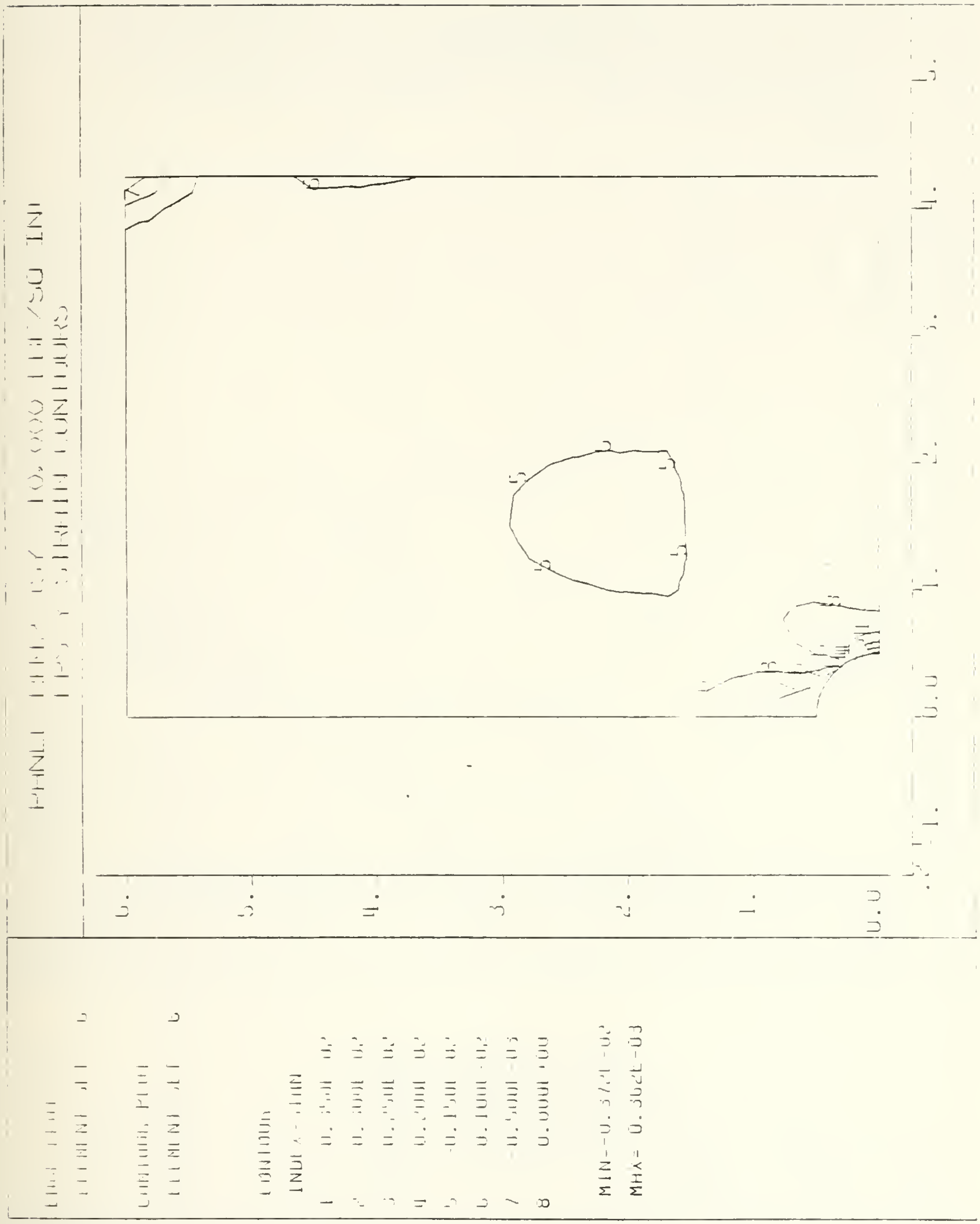

Figure M.5 Panel RH42: Eps-Y FEA Contours.

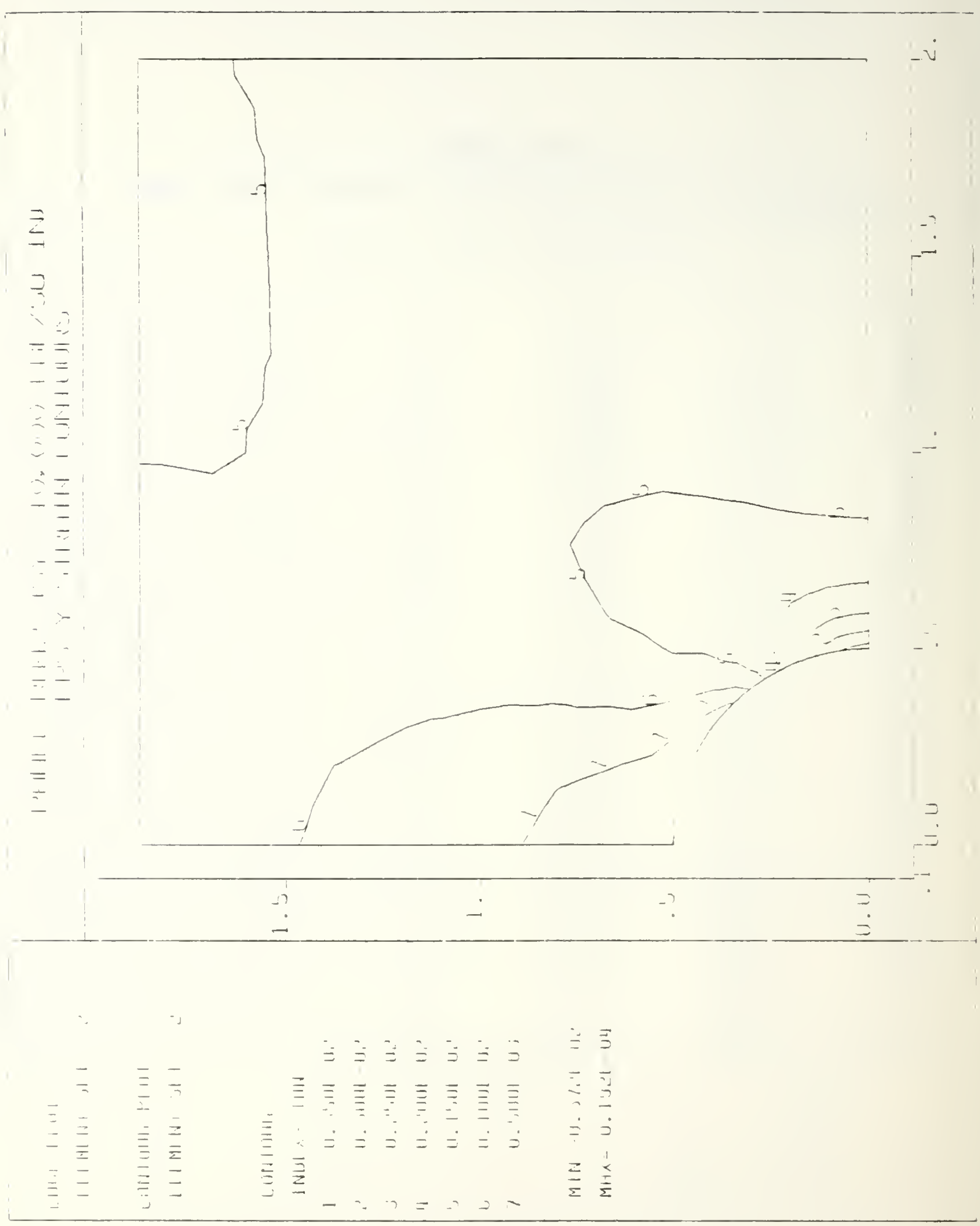

Figure M.6   Panel RH42: Eps-Y FEA Contours Near the Cutout.

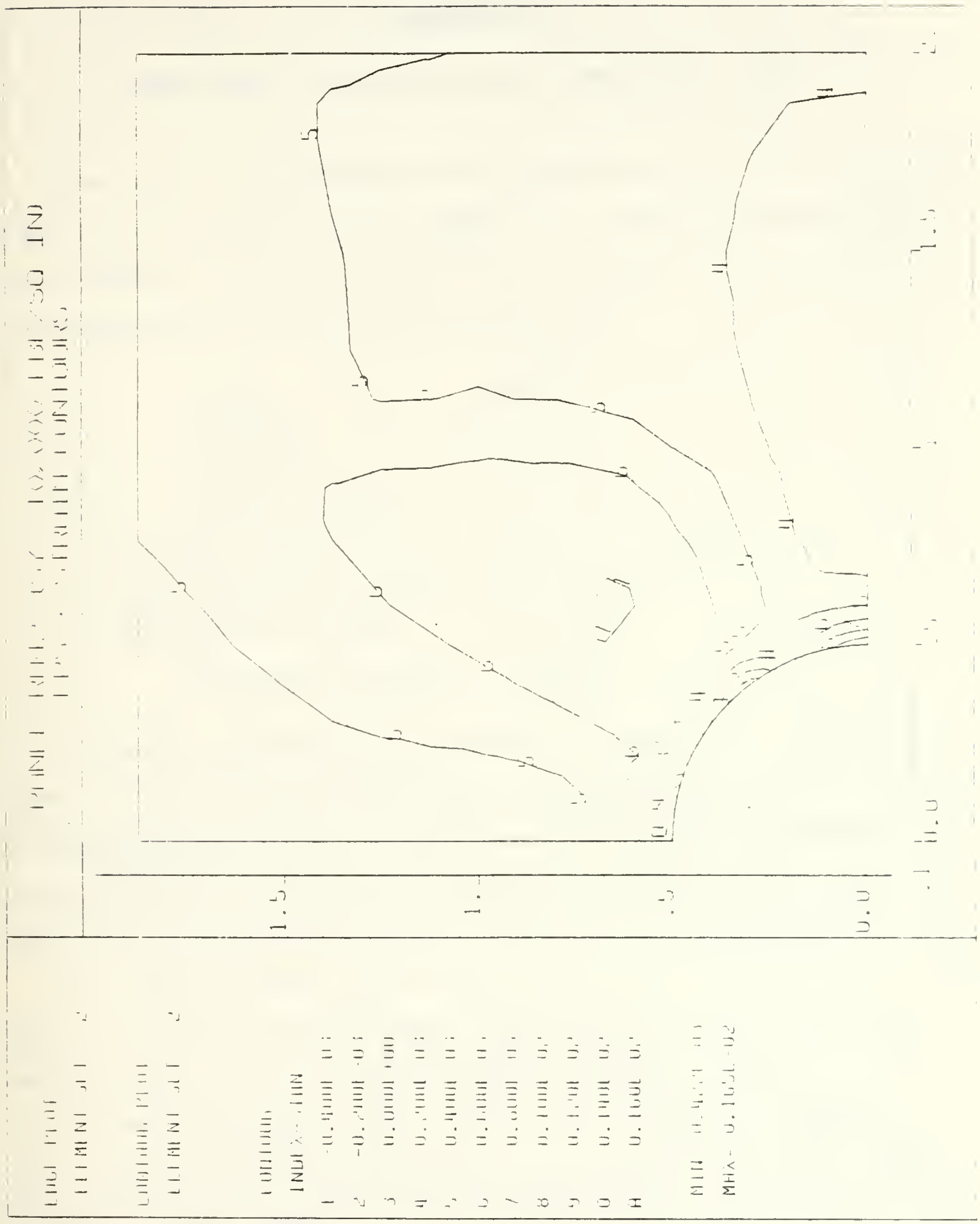

Figure M.7 Panel RH42: Eps-X FEA Contours Near the Cutout.

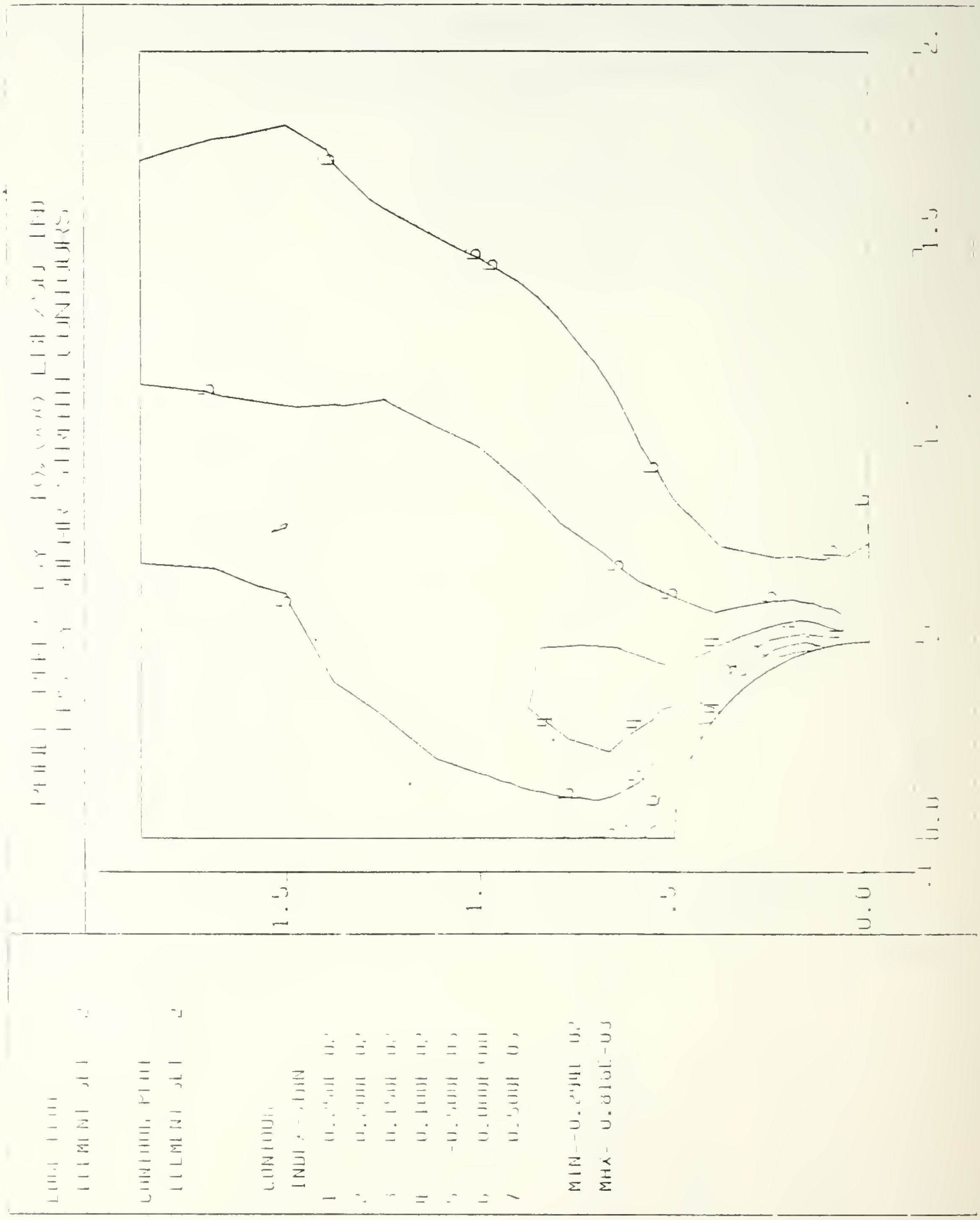

Figure M.8   Panel RH42: Eps-XY FEA Contours Near the Cutout.

APPENDIX N

PANEL RH51: ANALYTICAL AND EXPERIMENTAL DATA

Panel RH51 was reinforced with one co-cured ply of G/Ep in the shape of two strips on either side of the cutout on the outside of each facesheet offset 0.50 inch from the edge of the cutout. The reinforcement had the following dimensions:

Shape:	Strip
Length:	7.86 in
Width (each):	1.00 in
Thickness (each):	0.014 in (1 ply)
Area (each face):	15.720 in^2
Total Volume:	0.440 in^3
Net Cross Section:	0.056 in^2

The panel failed at the hole edge (Type-1) at an applied normal stress ($\bar{\sigma}_n$) of -31,630 psi. Based strictly on the failure of the unreinforced panel and the computed stress concentration factor of 2.83, the predicted failure was $\bar{\sigma}_n$ = -32,300 psi. The panel failed within 2.1% of the predicted ultimate load.

The finite element model (mesh) is shown in Figure N.1. The area of the strip reinforcement is outlined by the heavy lines beginning 0.50 inch to the right of the cutout's edge.

Figure N.2 compares the three (finite element) computed strains around the cutout between the unreinforced panel (PO∅∅) and RH51. These computed strain values are listed in Table XLIX.

There is only a small apparent decrease in the strain around the cutout due to the reinforcement.

Figure N.3 compares the computed (solid and dashed lines) and experimental (triangles) strains in the Y and X (poisson) directions in the panel and shows a poorer than usual correlation between analytical and experimental strain at $\bar{\sigma}_n$ = -10,000 psi. There was no apparent strain variation between the left and right side of the hole, but the finite element model predicted a higher level of strain at $\bar{\sigma}_n$ = -10 ksi. From the appearance of the panel during the load sequence, this can not be explained. The finite element model was rerun to verify the results and the data is consistent with the other models. The effect of reinforcement is a very slight strain decrease (compared to the unreinforced panel, PØØ0) under the reinforcement and a small decrease near the cutout. Table L gives the LEFEA computed values of the strains along the X axis.

Figure N.4 shows the stress-strain relation during the load sequence from $\bar{\sigma}_n$ = 0 to -31 ksi. Experimentally measured strain values are given in Table LI. Both gages #1 and #2 (x = +0.569" and -0.571") show much higher strain rate than equivalent gages on other RH panels. Gage #3 at first parallels the strain rate of #1 and #2, then seems to indicate a load transfer away at -3 ksi and then again picks up the load at -9 ksi. Gages #1 and #2 show somewhat the same phenomena described in Appendix M: significant buckling and fiber failure close to the cutout and a transfer of the load path away from the cutout's edge. There may have also been a transfer of load from one side of the cutout to the other and to the opposing facesheet.

Figures N.5 through N.8 show the strain contours at $\bar{\sigma}_n$ = -10,000 psi computed and plotted using DIAL. Figure N.5 is the full quarter panel with strain (Eps-Y) parallel to the applied load. Figures N.6 through N.8 (Eps-Y, Eps-X and Eps-XY) show the strains in detail close to the cutout.

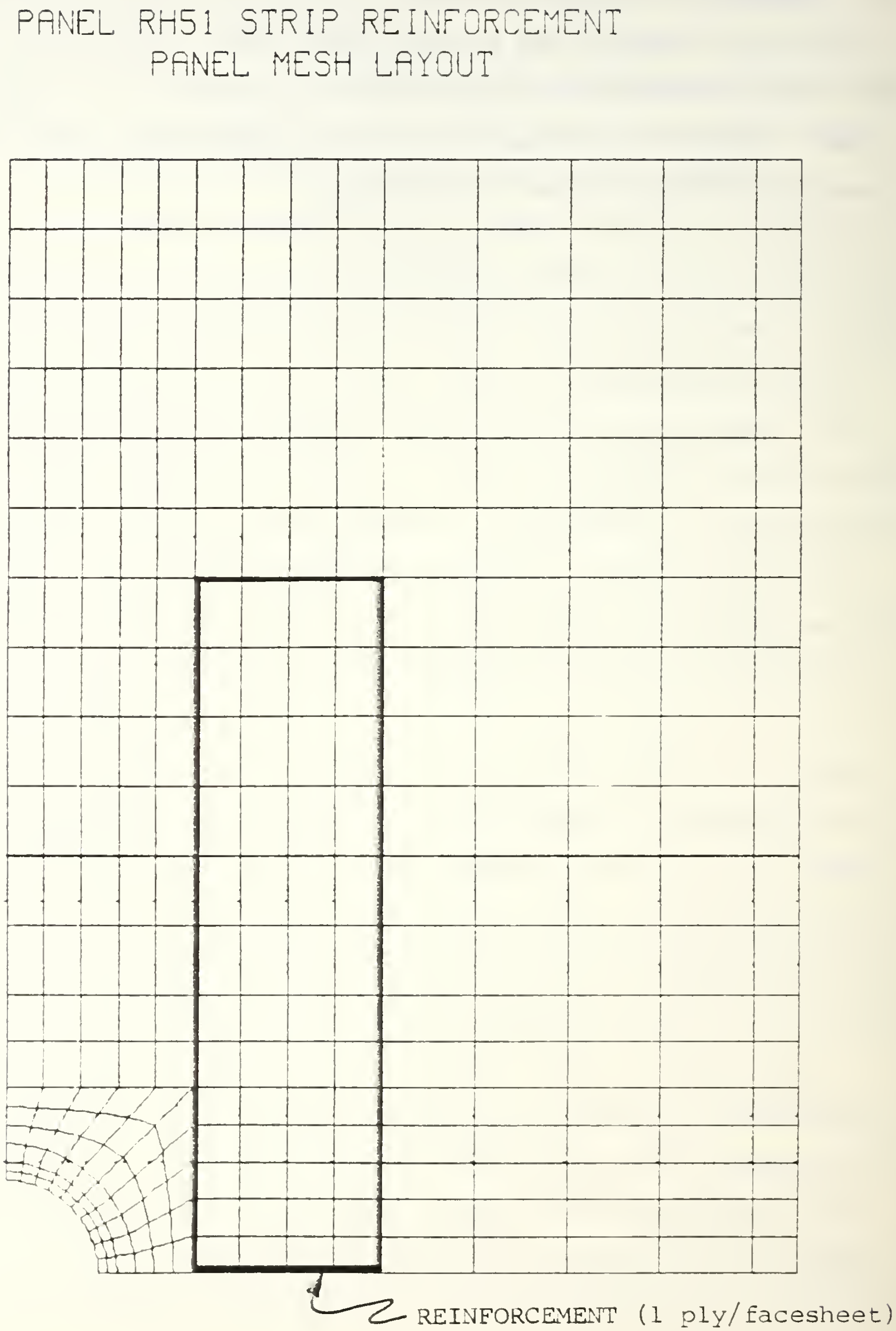

Figure N.1 Panel RH51: DIAL Finite Element Mesh.

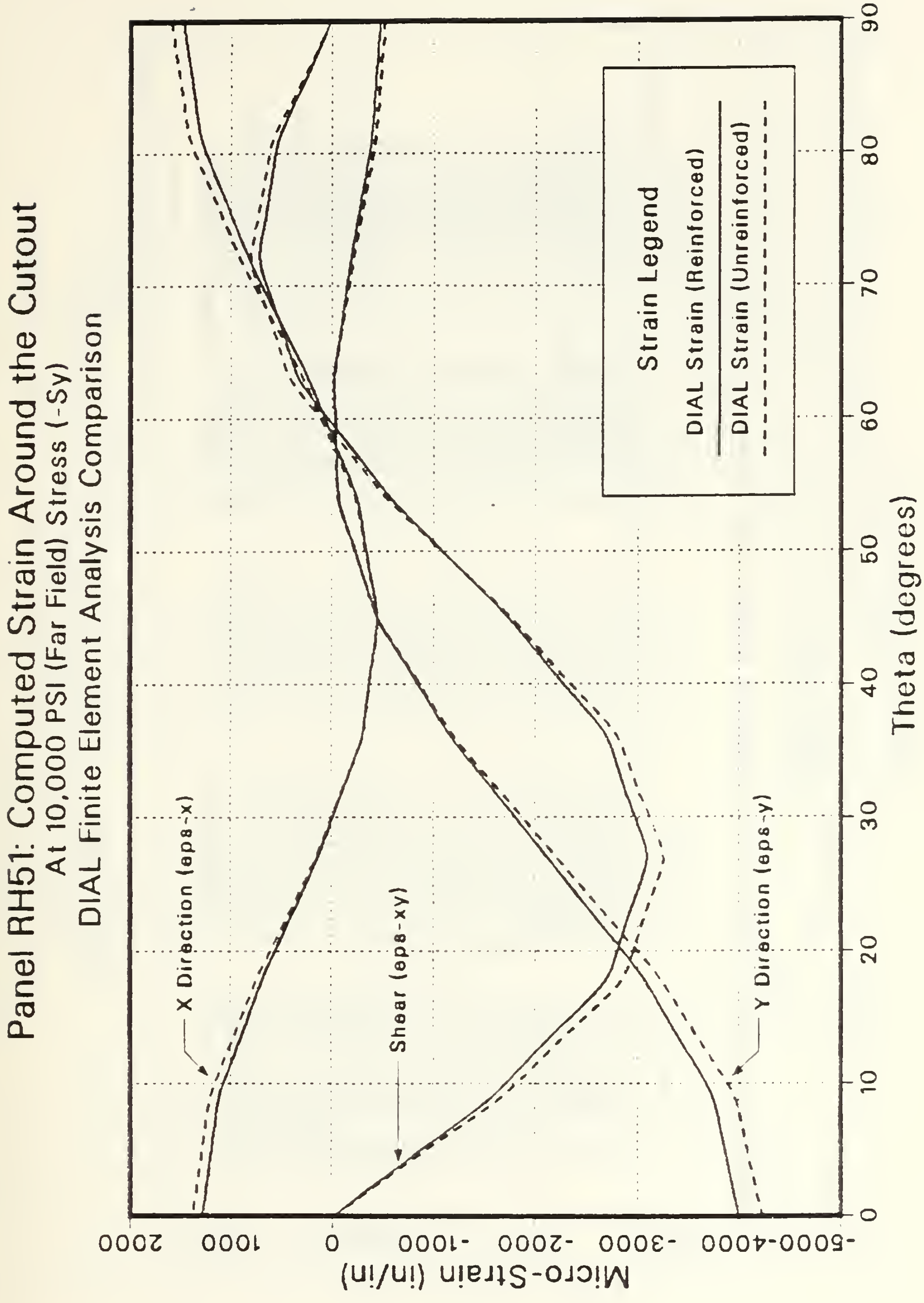

Figure N.2 Panel RH51: Strain Comparison Around the Cutout.

TABLE XLIX

PANEL RH51: LEFEA STRAIN DISTRIBUTION AROUND THE CUTOUT (-10,000 PSI).

NODE	X COORD	Y COORD	EPS-Y	EPS-X	EPS-XY
1	0.0000E+00	0.5000E+00	-0.4667E-03	0.1475E-02	0.1837E-04
2	0.3923E-01	0.4985E+00	-0.4255E-03	0.1387E-02	0.2728E-03
3	0.7822E-01	0.4938E+00	-0.3800E-03	0.1293E-02	0.5395E-03
4	0.1167E+00	0.4862E+00	-0.2802E-03	0.1059E-02	0.6336E-03
5	0.1545E+00	0.4755E+00	-0.1786E-03	0.8208E-03	0.7200E-03
6	0.1913E+00	0.4619E+00	-0.9578E-04	0.5283E-03	0.5318E-03
7	0.2270E+00	0.4455E+00	-0.1385E-04	0.2355E-03	0.3337E-03
8	0.2612E+00	0.4263E+00	-0.3596E-04	-0.5737E-05	-0.1176E-03
9	0.2939E+00	0.4045E+00	-0.6132E-04	-0.2441E-03	-0.5768E-03
10	0.3247E+00	0.3802E+00	-0.2498E-03	-0.3464E-03	-0.1151E-02
11	0.3536E+00	0.3536E+00	-0.4435E-03	-0.4430E-03	-0.1728E-02
12	0.3802E+00	0.3247E+00	-0.8052E-03	-0.3683E-03	-0.2215E-02
13	0.4045E+00	0.2939E+00	-0.1172E-02	-0.2894E-03	-0.2698E-02
14	0.4263E+00	0.2612E+00	-0.1642E-02	-0.7478E-04	-0.2900E-02
15	0.4455E+00	0.2270E+00	-0.2115E-02	0.1429E-03	-0.3094E-02
16	0.4619E+00	0.1913E+00	-0.2584E-02	0.4113E-03	-0.2903E-02
17	0.4755E+00	0.1545E+00	-0.3052E-02	0.6801E-03	-0.2703E-02
18	0.4862E+00	0.1167E+00	-0.3399E-02	0.8987E-03	-0.2141E-02
19	0.4938E+00	0.7822E-01	-0.3742E-02	0.1115E-02	-0.1572E-02
20	0.4985E+00	0.3923E-01	-0.3872E-02	0.1201E-02	-0.7895E-03
21	0.5000E+00	0.0000E+00	-0.3997E-02	0.1282E-02	-0.2178E-04

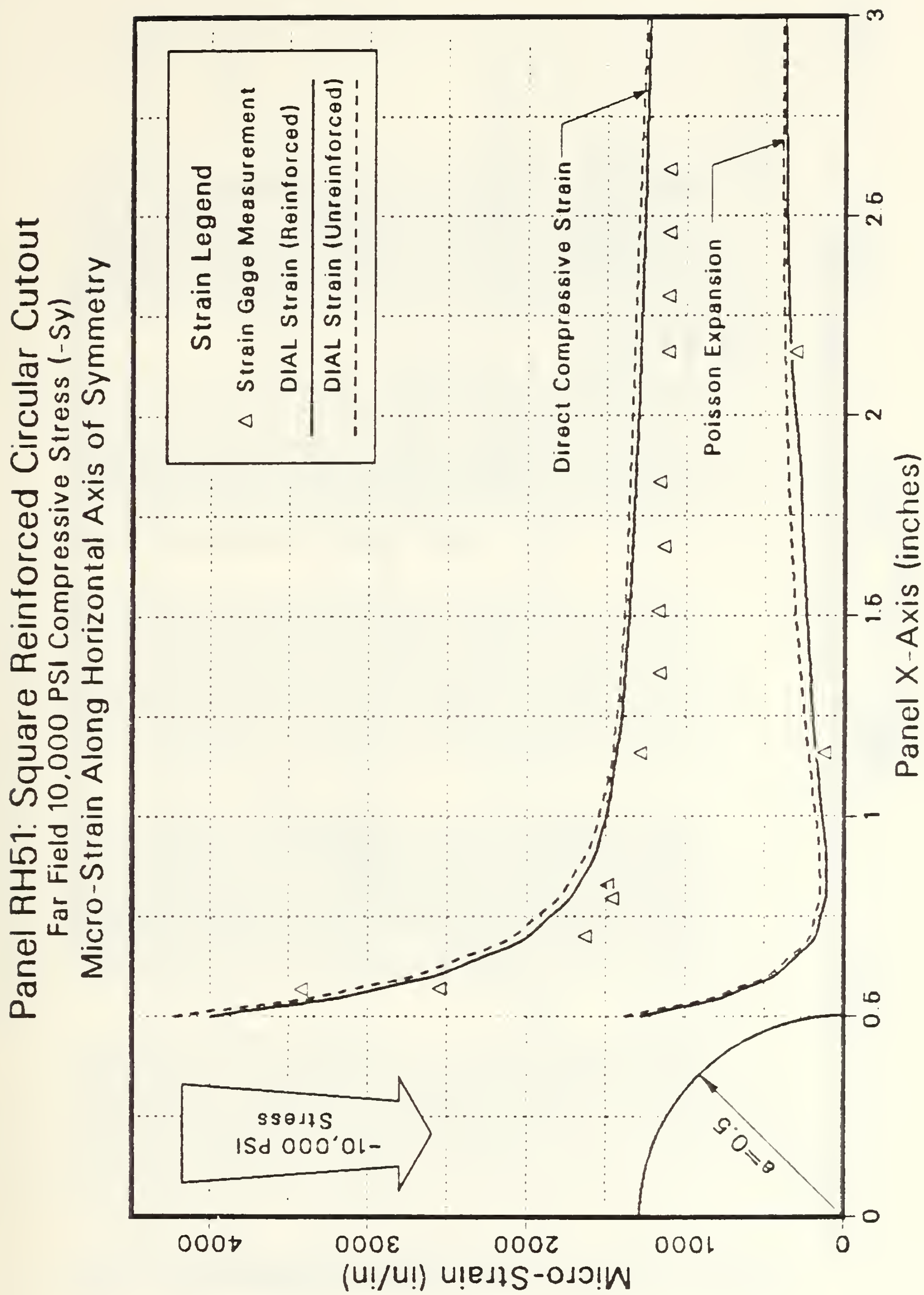

Figure N.3 Panel RH51: Strain Comparison Along the X Axis.

TABLE L

PANEL RH51: LEFEA STRAIN DISTRIBUTION ALONG THE X AXIS (-10,000 PSI).

NODE	X COORD	Y COORD	EPS-Y	EPS-X	EPS-XY
21	0.5000E+00	0.0000E+00	-0.3997E-02	0.1282E-02	-0.2178E-04
32	0.5250E+00	0.0000E+00	-0.3568E-02	0.1011E-02	-0.1326E-04
53	0.5500E+00	0.0000E+00	-0.3145E-02	0.7453E-03	-0.7814E-05
64	0.5750E+00	0.0000E+00	-0.2878E-02	0.5983E-03	-0.7024E-05
85	0.6000E+00	0.0000E+00	-0.2594E-02	0.4396E-03	-0.2882E-05
96	0.6500E+00	0.0000E+00	-0.2284E-02	0.3008E-03	-0.1633E-05
117	0.7000E+00	0.0000E+00	-0.1993E-02	0.1757E-03	-0.6529E-06
128	0.7500E+00	0.0000E+00	-0.1860E-02	0.1461E-03	0.5012E-06
149	0.8000E+00	0.0000E+00	-0.1721E-02	0.1112E-03	0.1457E-06
160	0.8500E+00	0.0000E+00	-0.1648E-02	0.1103E-03	0.7263E-06
181	0.9000E+00	0.0000E+00	-0.1575E-02	0.1087E-03	0.2789E-05
192	0.9500E+00	0.0000E+00	-0.1540E-02	0.1220E-03	0.8067E-05
213	0.1000E+01	0.0000E+00	-0.1503E-02	0.1366E-03	0.1062E-04
214	0.1125E+01	0.0000E+00	-0.1454E-02	0.1678E-03	0.5997E-05
215	0.1250E+01	0.0000E+00	-0.1407E-02	0.1964E-03	0.4871E-05
216	0.1375E+01	0.0000E+00	-0.1385E-02	0.2181E-03	0.3722E-05
217	0.1500E+01	0.0000E+00	-0.1362E-02	0.2398E-03	0.2185E-05
218	0.1625E+01	0.0000E+00	-0.1347E-02	0.2550E-03	0.1768E-05
219	0.1750E+01	0.0000E+00	-0.1331E-02	0.2703E-03	0.1118E-05
220	0.1875E+01	0.0000E+00	-0.1317E-02	0.2798E-03	0.1295E-05
221	0.2000E+01	0.0000E+00	-0.1302E-02	0.3135E-03	0.9340E-06
222	0.2250E+01	0.0000E+00	-0.1283E-02	0.3525E-03	0.2854E-06
223	0.2500E+01	0.0000E+00	-0.1265E-02	0.3672E-03	0.3989E-06
224	0.2750E+01	0.0000E+00	-0.1250E-02	0.3727E-03	0.3215E-06
225	0.3000E+01	0.0000E+00	-0.1233E-02	0.3782E-03	0.1473E-07
226	0.3250E+01	0.0000E+00	-0.1215E-02	0.3780E-03	0.7843E-07
227	0.3500E+01	0.0000E+00	-0.1197E-02	0.3780E-03	0.6651E-07
228	0.3750E+01	0.0000E+00	-0.1176E-02	0.3742E-03	0.5335E-07
229	0.4000E+01	0.0000E+00	-0.1154E-02	0.3703E-03	0.1729E-07
230	0.4125E+01	0.0000E+00	-0.1141E-02	0.3664E-03	0.2263E-07
231	0.4250E+01	0.0000E+00	-0.1128E-02	0.3627E-03	-0.1128E-07

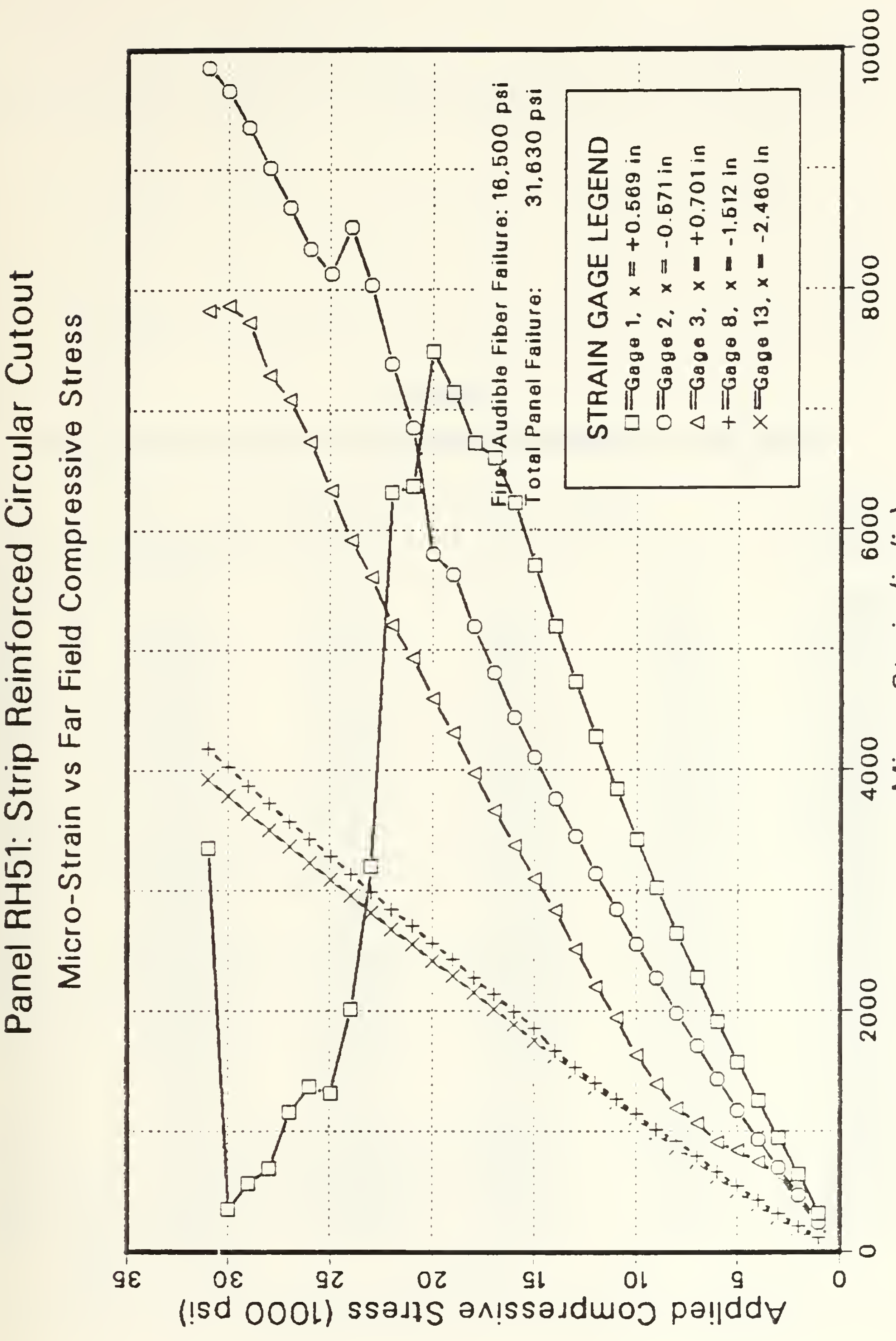

Figure N.4 Panel RH51: Microstrain vs. Compressive Stress.

TABLE LI

PANEL RH51: SELECTED STRAIN GAGE VALUES DURING LOAD.

Load (psi)	Micro-Strain Indicated by Gage:				
	#1	#2	#3	#8	#13
1000	-317	-241	-214	-116	-105
2000	-642	-469	-419	-215	-193
3000	-946	-696	-641	-313	-285
4000	-1256	-931	-745	-428	-393
5000	-1572	-1173	-839	-542	-503
6000	-1913	-1435	-907	-665	-622
7000	-2276	-1711	-1070	-793	-747
8000	-2639	-1980	-1191	-919	-865
9000	-3020	-2268	-1394	-1017	-989
10000	-3422	-2550	-1636	-1142	-111[illegible]
11000	-3841	-2841	-1944	-1272	-1238
12000	-4276	-3140	-2201	-1401	-1367
13000	-4733	-3446	-2511	-1534	-1493
14000	-5196	-3762	-2837	-1666	-1625
15000	-5706	-4101	-3098	-1858	-1755
16000	-6229	-4433	-3370	-1996	-1887
17000	-6601	-4808	-3663	-2136	-2017
18000	-6723	-5190	-3975	-2278	-2150
19000	-7148	-5630	-4308	-2427	-2292
20000	-7486	-5802	-4591	-2559	-2414
21000	-6367	-6847	-4933	-2704	-2550
22000	-6315	-7382	-5205	-2844	-2679
23000	-3197	-8035	-5605	-2988	-2817
24000	-2016	-8514	-5918	-3137	-2957
25000	-1314	-8133	-6331	-3285	-3093
26000	-1372	-8337	-6741	-3428	-3229
27000	-1160	-8686	-7092	-3575	-3365
28000	-690	-9015	-7289	-3721	-3501
29000	-566	-9354	-7730	-3872	-3641
30000	-349	-9656	-7866	-4025	-3765
31000	-3349	-9848	-7831	-4180	-3927

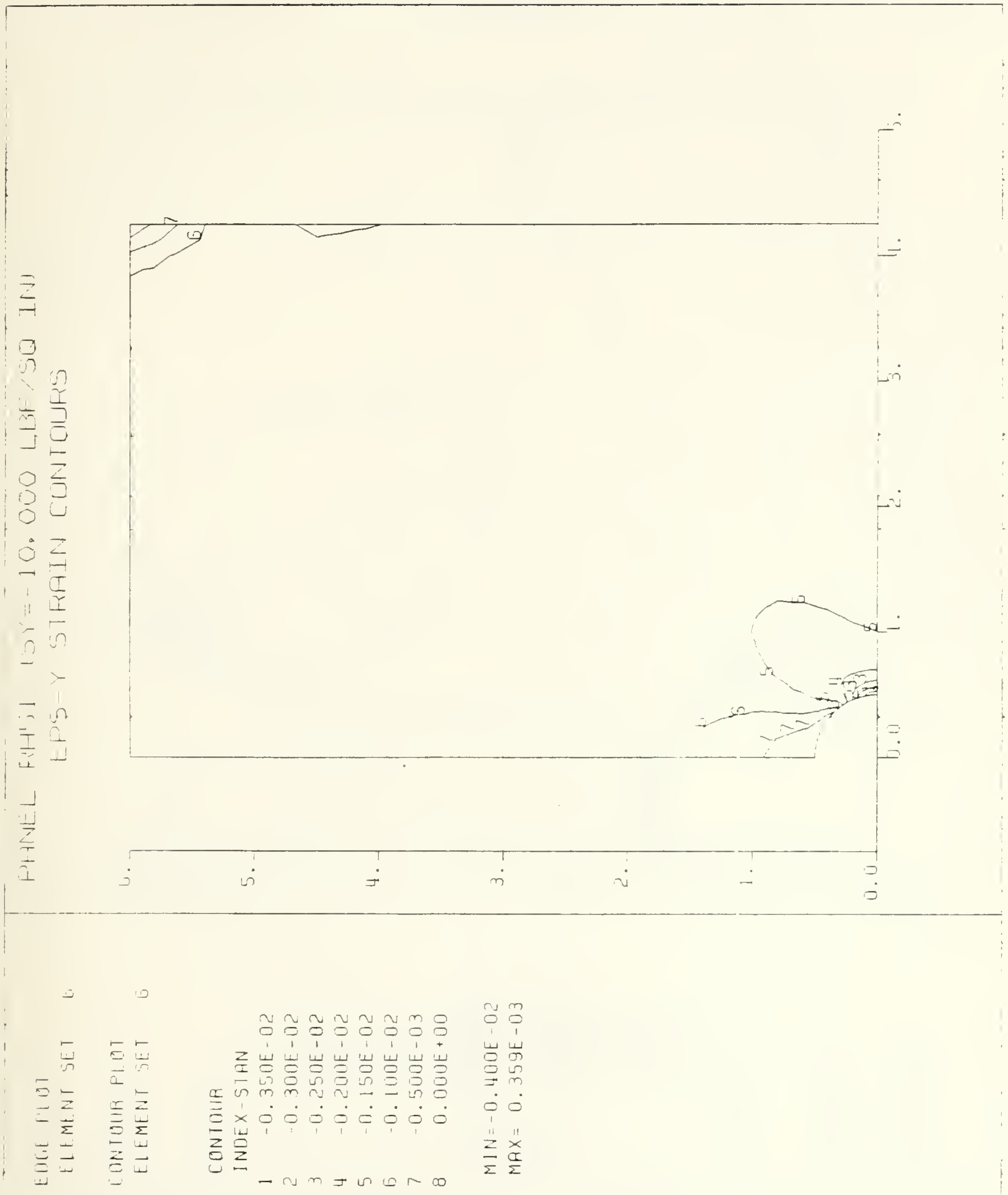

Figure N.5 Panel RH51: Eps-Y FEA Contours.

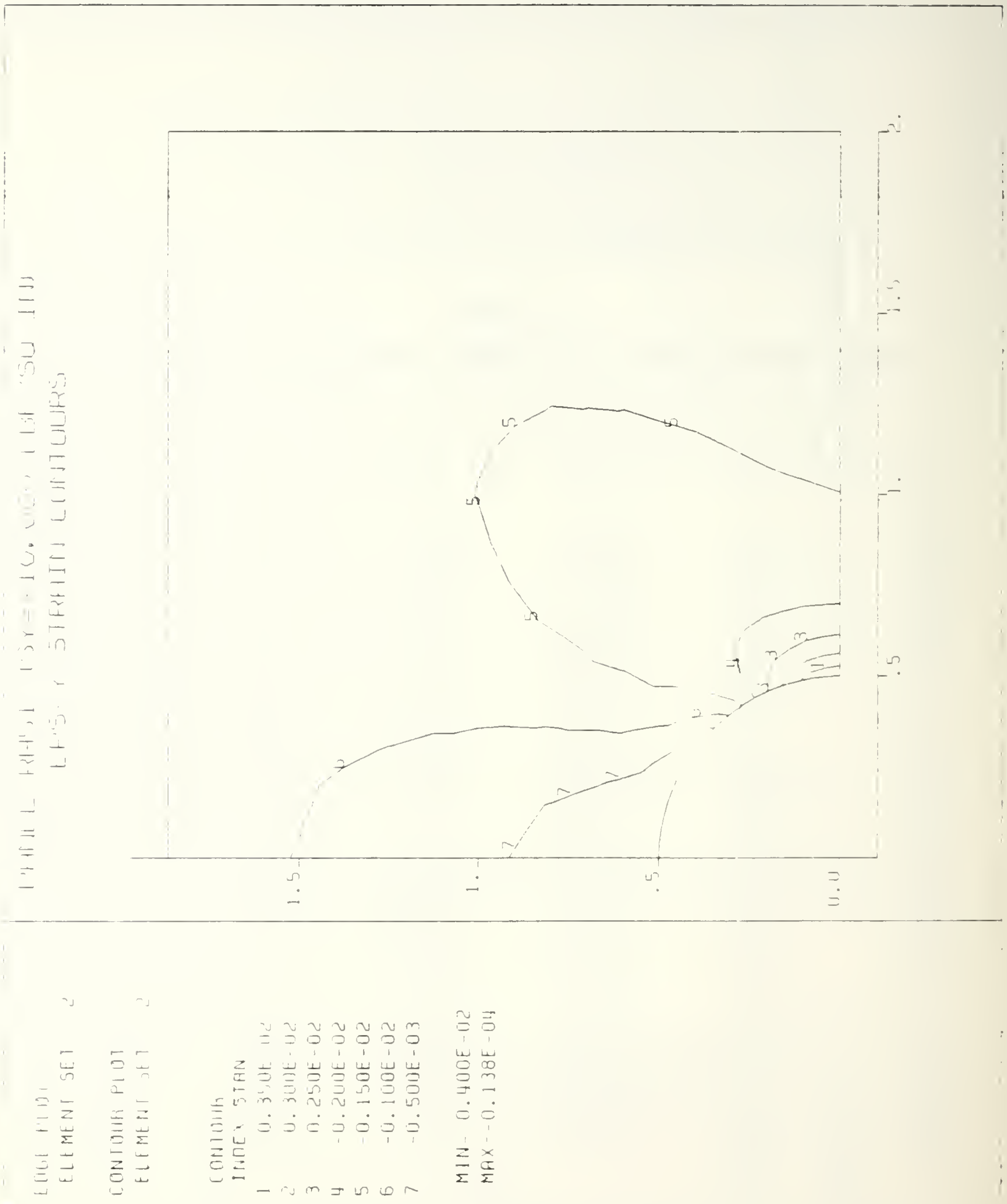

Figure N.6 Panel RH51: Eps-Y FEA Contours Near the Cutout.

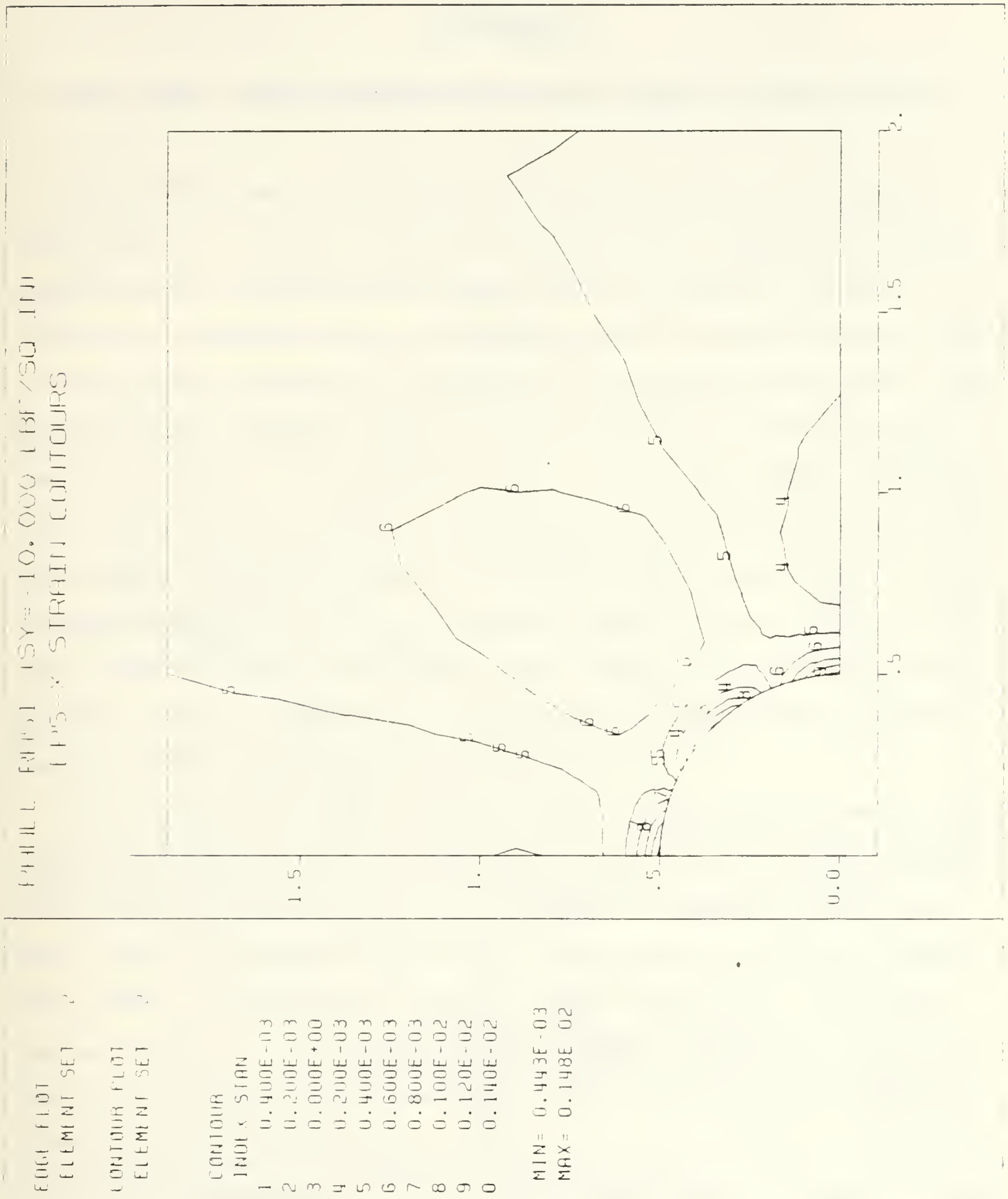

Figure N.7 Panel RH51: Eps-X FEA Contours Near the Cutout.

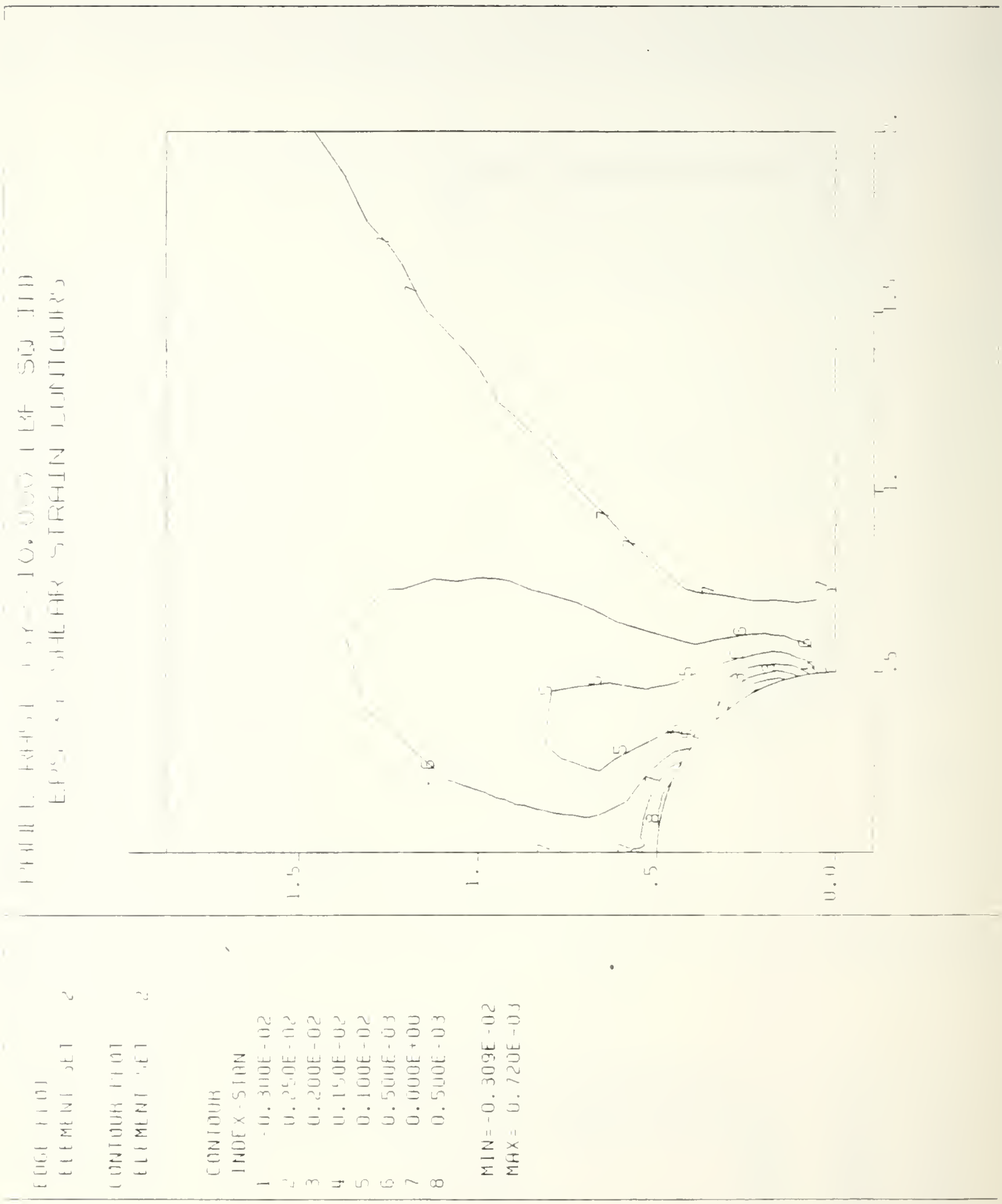

Figure N.8   Panel RH51: Eps-XY FEA Contours Near the Cutout.

APPENDIX O

PANEL RR22: THREE-DIMENSIONAL LINEAR FINITE ELEMENT ANALYSIS

Panel RR22 was reinforced with two co-cured round plies of G/Ep around the cutout on the outside of each facesheet. The reinforcement configuration should have been among the most efficient, concentrating the maximum amount of reinforcement close to the cutout. Figure 5.3 and Table VI show that the round, 200% reinforcement produced about a 22.5% reduction in maximum strain (eps-y) parallel to the applied load. The round, 400% reinforcement with twice the volume of additional weight provided only 3.1% additional strain reduction. It was therefore more than a little disconcerting when the most promising panel failed at $\bar{\sigma}_n$ = 21,050 psi, only 55% of the predicted load. Table IX gives the predicted failure (based on the actual failure of the unreinforced panels and the LEFEA computed SCF) at 38,250 psi.

When trying to explain the failure, it was postulated that the facesheet layup $[0_3,\pm45,90]$ may have caused out-of-plane stresses ($+\sigma_z$) sufficient to cause the facesheet to separate from the core. This, of course, would have invalidated the entire thesis that local reinforcement around a cutout could be a significant design benefit. The two-dimensional LEFEA (see section III C.1) used in the computational analysis was not able to give stress or strain in the Z direction.

A three-dimensional analysis was undertaken. Figure O.1 shows the three-dimensional mesh. In order to conserve computer time and provide an accurate solution, the quarter panel was modeled only from the midplane (z = 0.0). Modeling only half the core and and one facesheet did not affect the accuracy of the solution. In order to approximate the strain closer to the predicted failure, the model was subjected to an equivalent applied load of 30 ksi rather than the 10 ksi used on the 2-D models. The analysis was linear and did not take into account the very probable matrix cracking and non-linear behavior at high strain (10,000 $\mu\epsilon$). Table LII summarizes the results of the analysis.

TABLE LII

PANEL RR22: SUMMARY OF THREE-DIMENSIONAL LEFEA STRAIN

Direction:	Y	X	Z	XY	YZ	ZX
Maximum	1140	4690	92	2420	273	2100
Minimum	-10100	-2720	-11	-9300	-1060	-4220

Figure O.2 gives the strain parallel to the applied load. The maximum predicted stain was 10,100 $\mu\epsilon$ at $\overline{\sigma}_n$ = 30 ksi. This is exactly three times the maximum strain computed in the 2-D model described in Appendix C (see Figure C.5). The exact analytical correspondence of the 2- and 3-D FEA helps to validate it. Figure O.3 shows the ϵ_y strain near the cutout. Figure O.4 shows ϵ_x next to the cutout. This corresponds with Figure C.7.

The strain in the Z direction is shown in Figures O.5 and O.6. The maximum was 92 $\mu\epsilon$, the minimum -11 $\mu\epsilon$. The stress at the interface of the facesheet and honeycomb core is shown in Figures O.7 and O.8. It is obvious that the out-of-plane stress at the interface is virtually nil (less than +5 psi) and that premature failure was <u>not</u> due to the layup or the reinforcement configuration.

The shear strains ϵ_{xy}, ϵ_{yz} and ϵ_{zx} are shown in Figures O.9, O.10 and O.11 respectively. The three-dimensional analysis reversed the sign on the shear strain from the two-dimensional. Comparing the results of the 2- and 3-D analyses, the maximum and minimum ϵ_{xy}: 2420 and -9300 $\mu\epsilon$ in the 3-D (Figure O.9) are almost exactly 3 times the 2-D: 826 and -3110 $\mu\epsilon$ (Figure C.8).

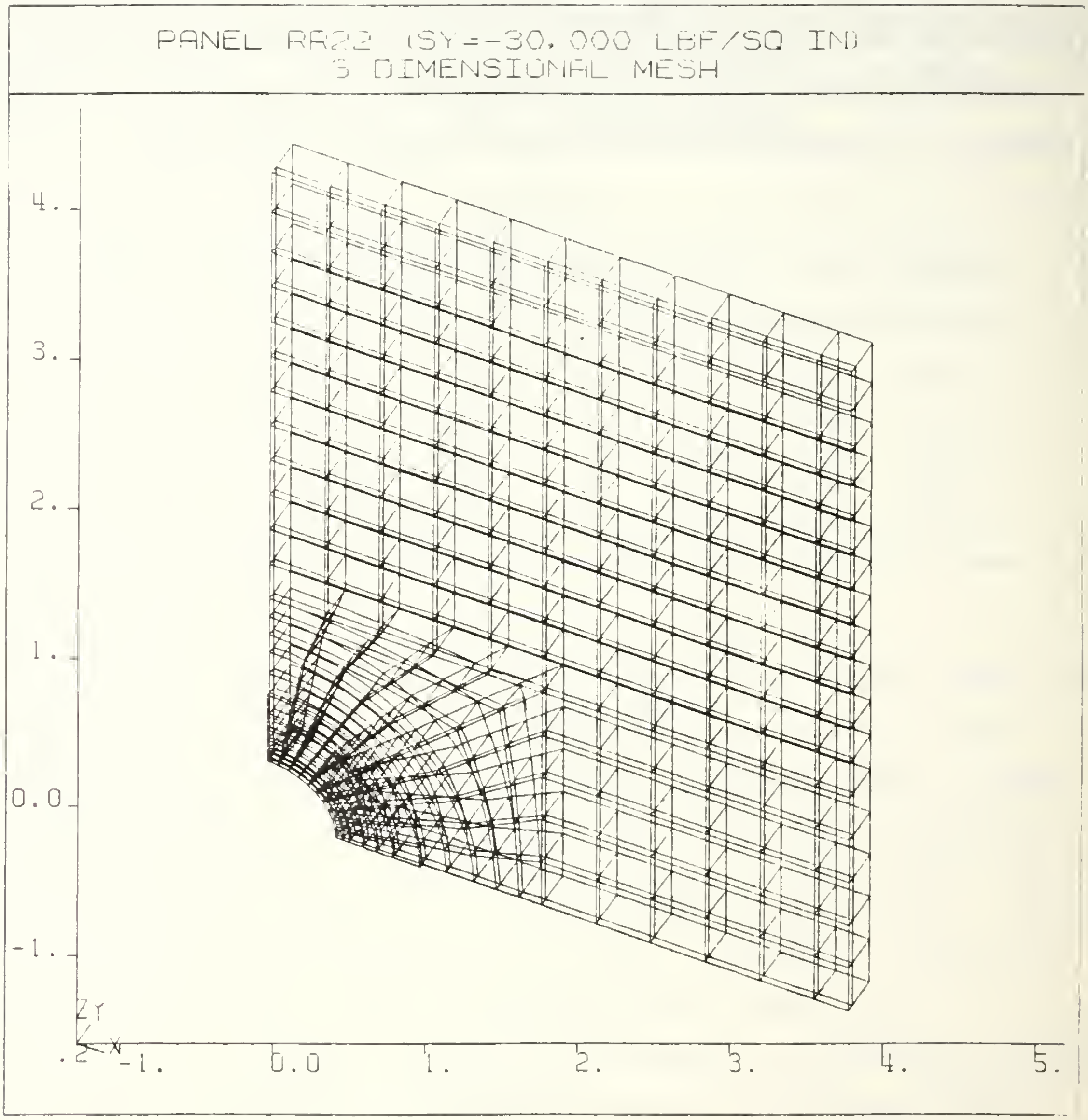

Figure O.1 Panel RR22: 3-D DIAL Finite Element Mesh.

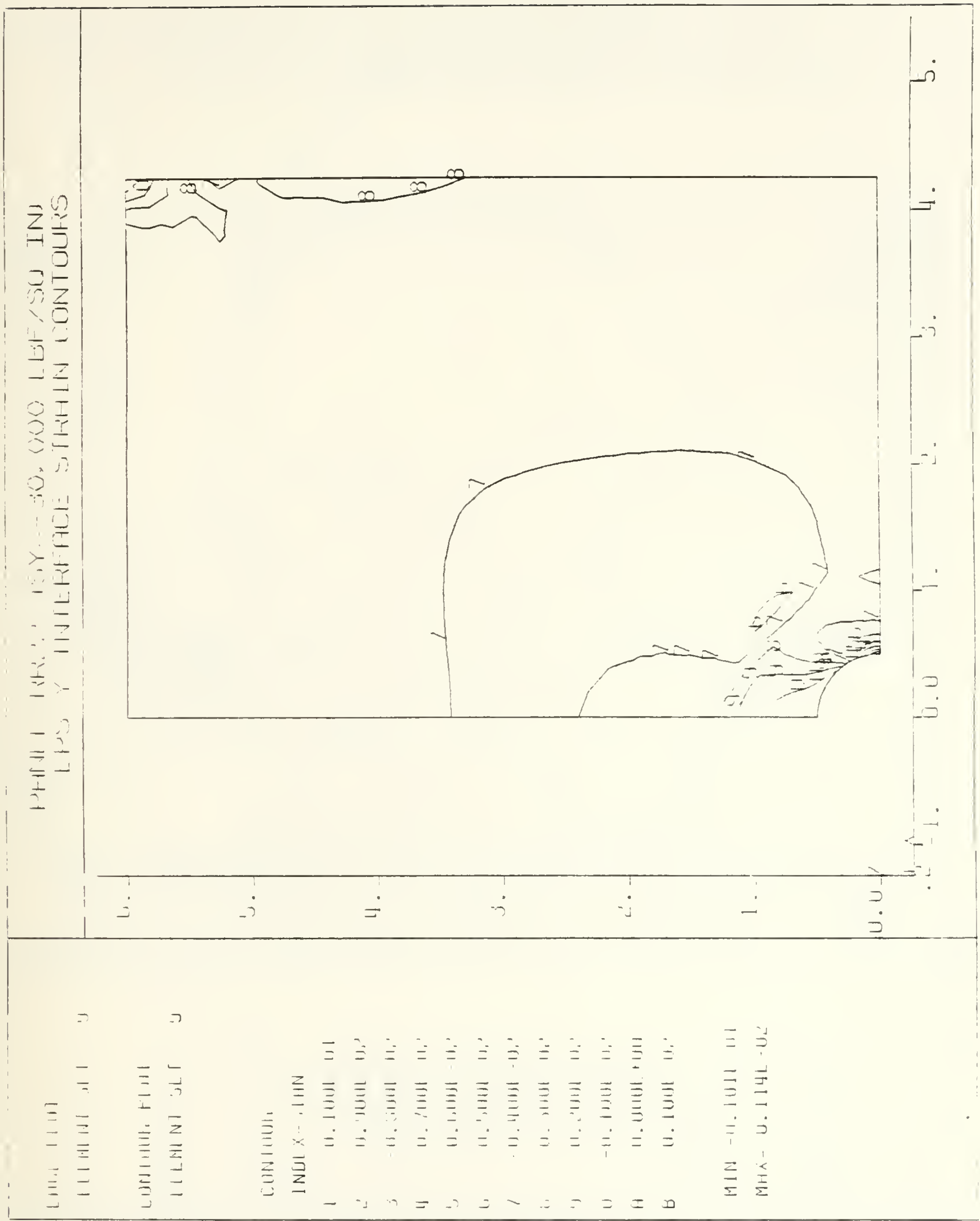

Figure O.2 Panel RR22: 3-D Eps-Y FEA Contours.

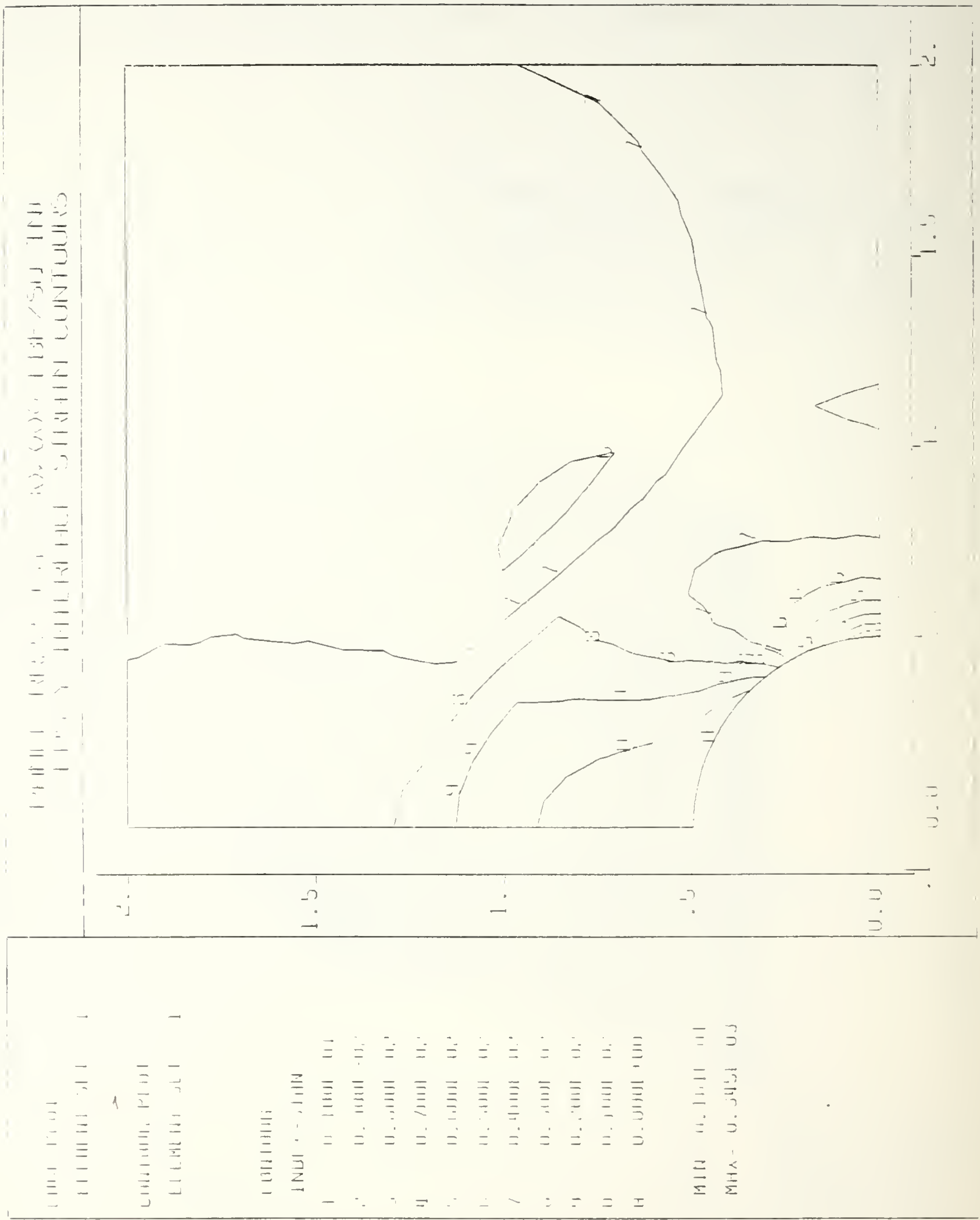

Figure O.3   Panel RR22: 3-D Eps-Y FEA Contours Near the Cutout.

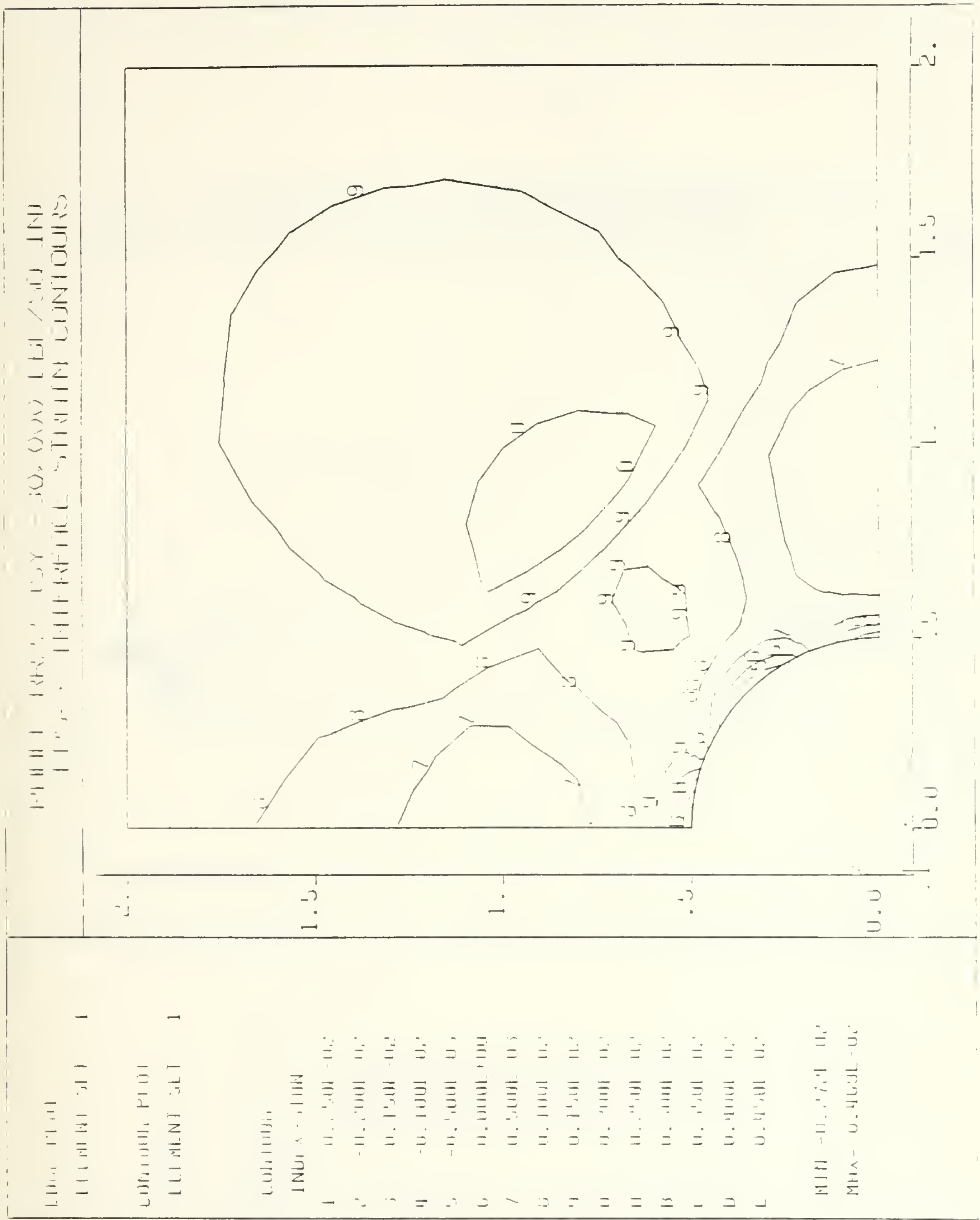

Figure O.4 Panel RR22: 3-D Eps-X FEA Contours Near the Cutout.

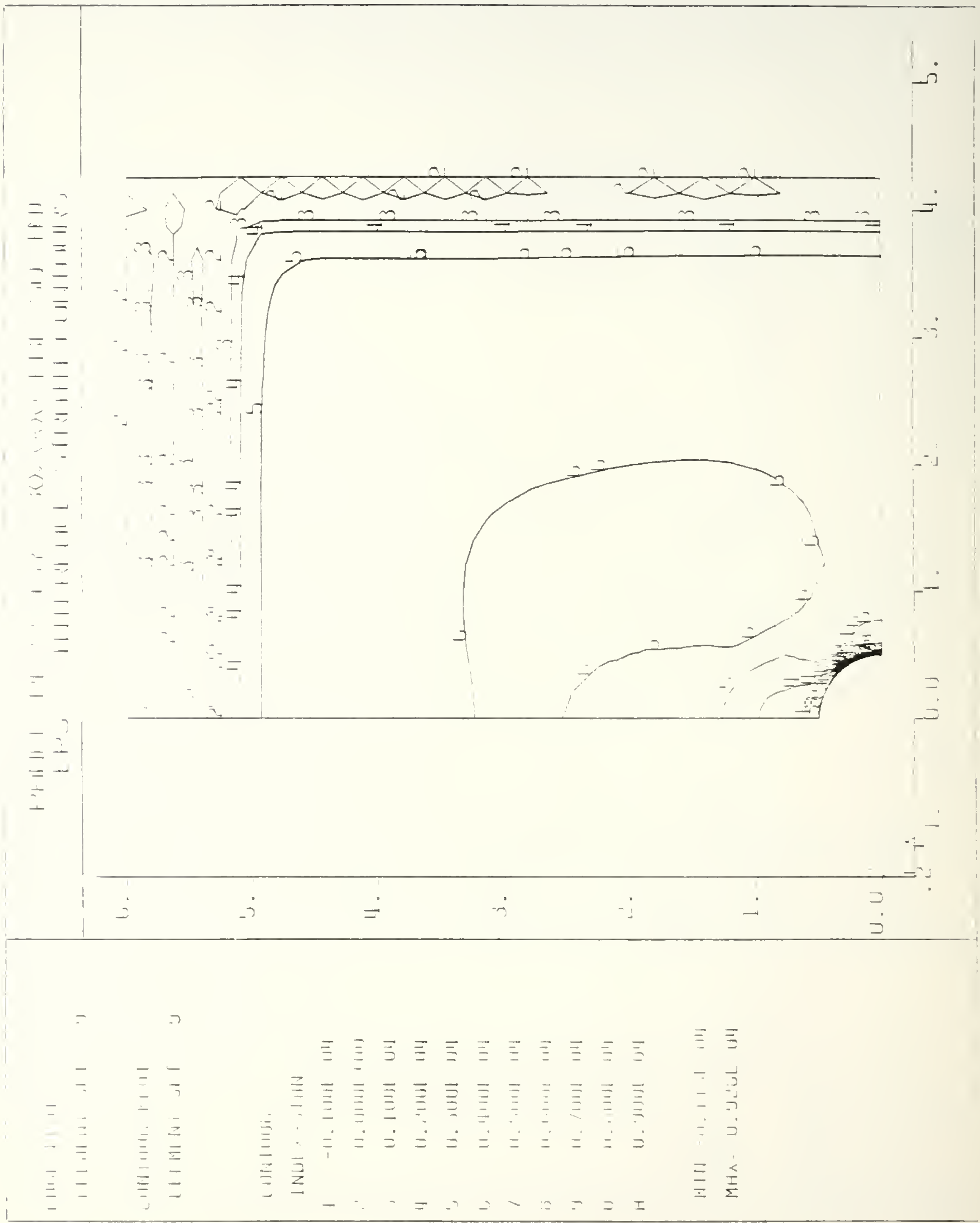

Figure O.5   Panel RR22: 3-D Eps-Z FEA Contours.

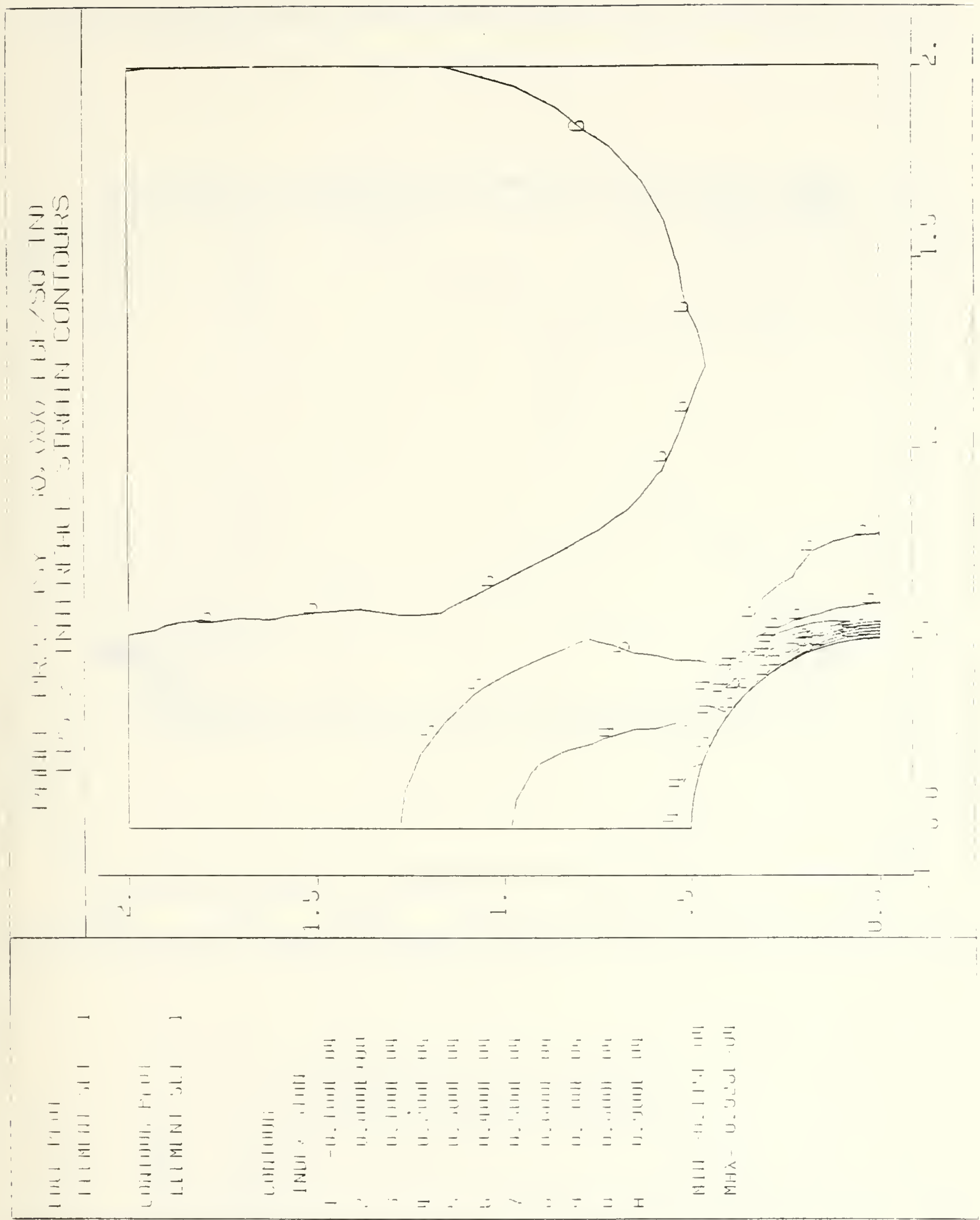

Figure O.6 Panel RR22: 3-D Eps-Z FEA Contours Near the Cutout.

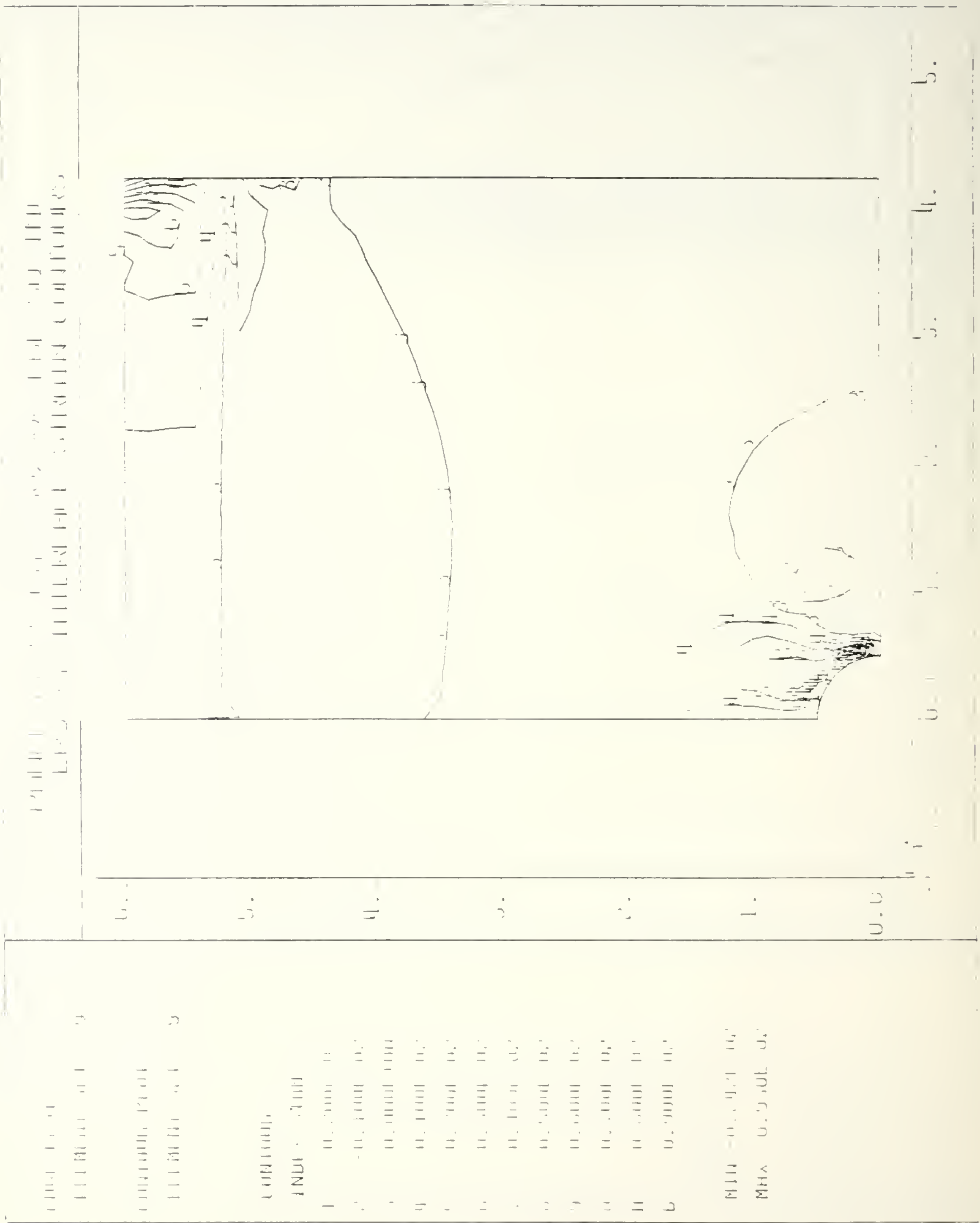

Figure O.7 Panel RR22: 3-D Eps-XY FEA Contours.

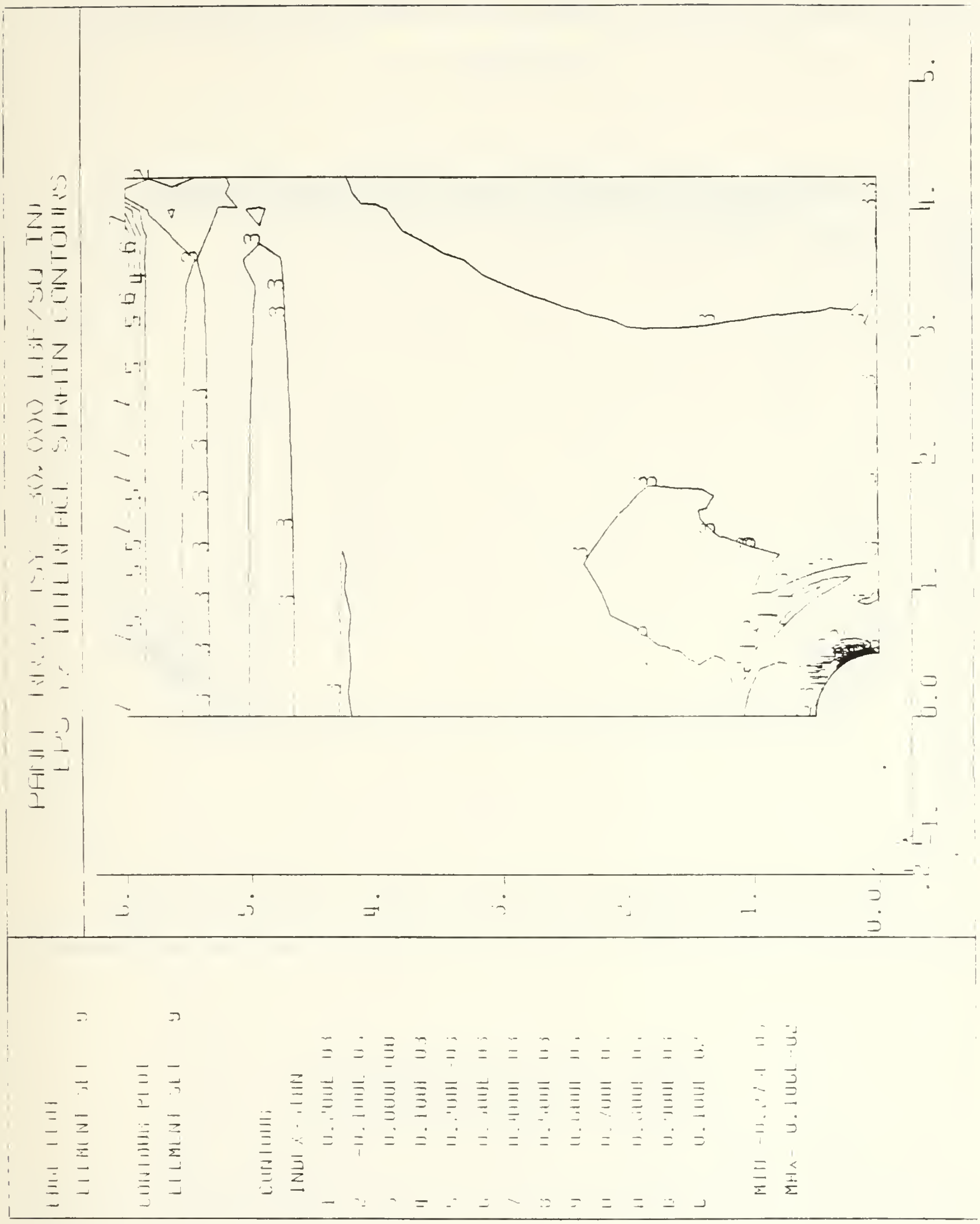

Figure O.8 Panel RR22: 3-D Eps-YZ FEA Contours.

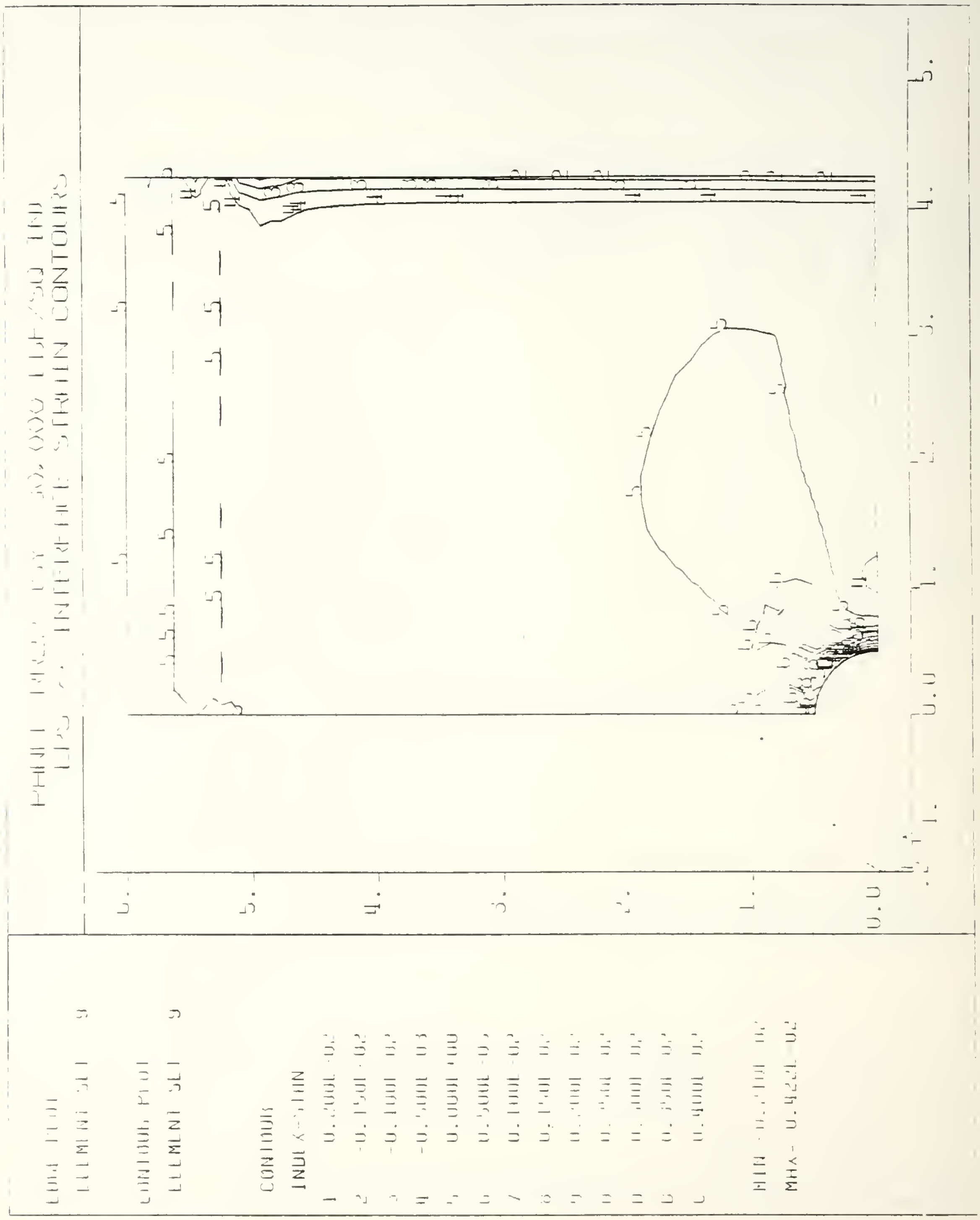

Figure O.9 Panel RR22: 3-D Eps-ZX FEA Contours.

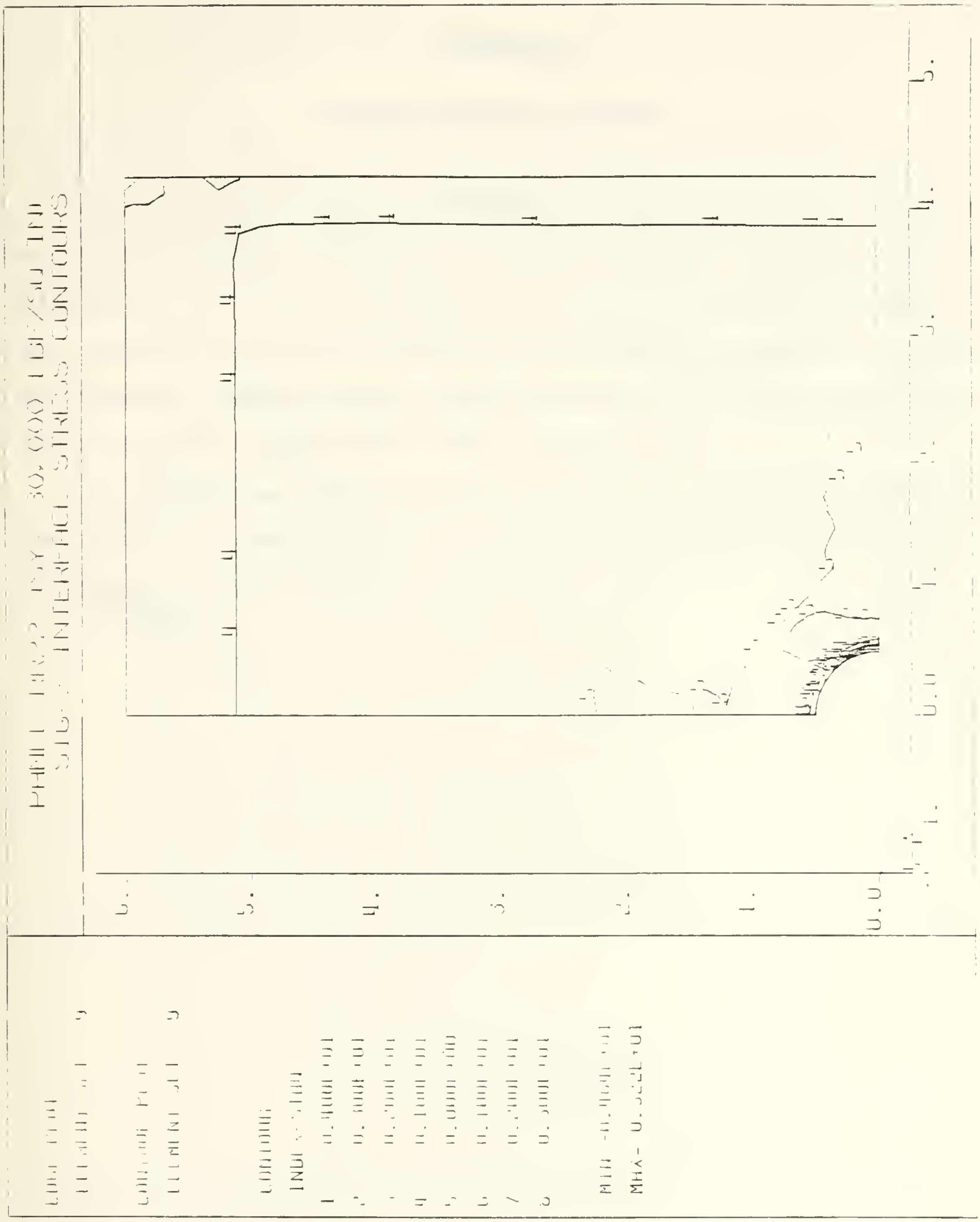

Figure O.10 Panel RR22: 3-D Sig-Z FEA Contours.

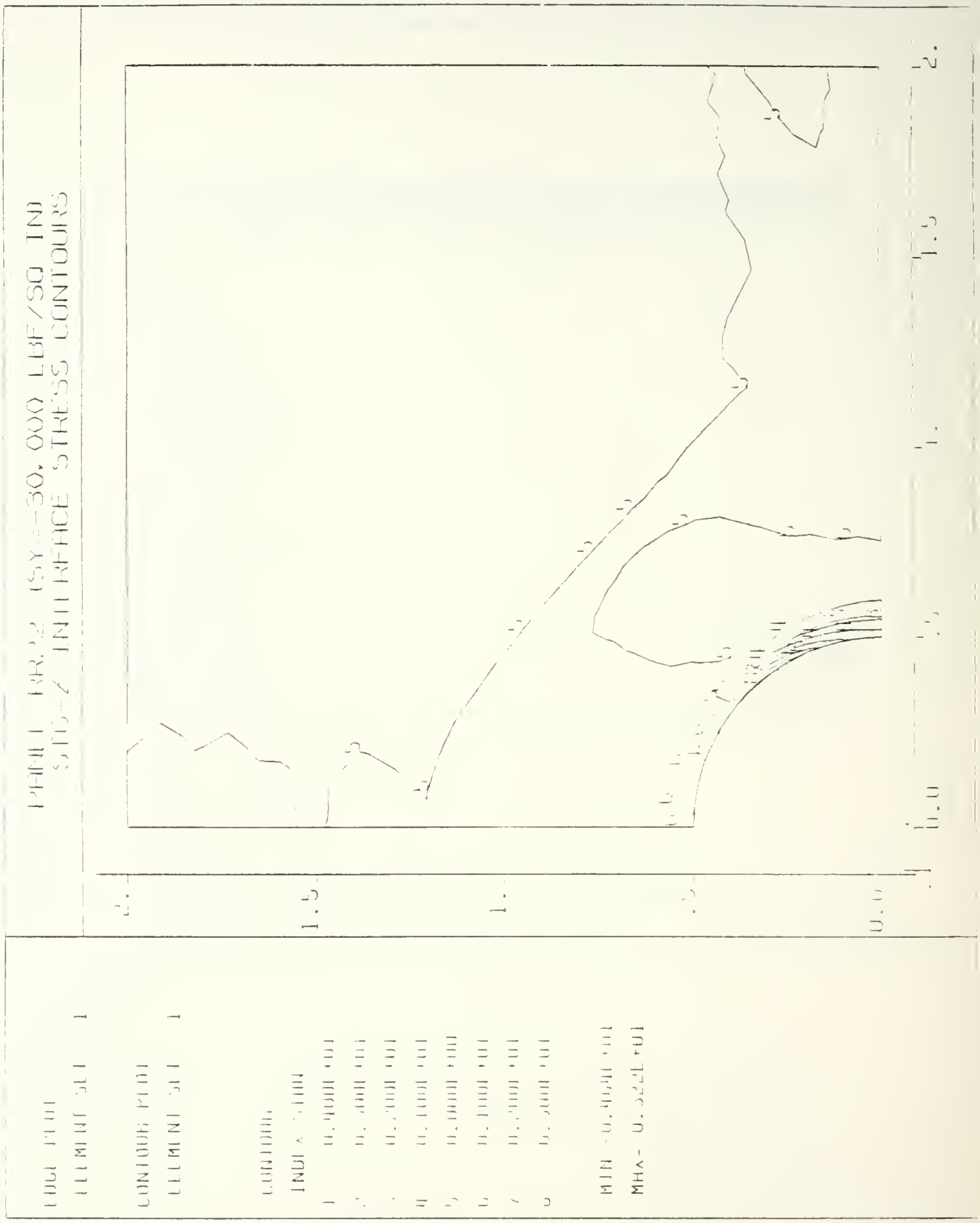

Figure O.11 Panel RR22: 3-D Sig-Z FEA Contours Near the Cutout.

APPENDIX P

FORTRAN PROGRAM "RBSFM"

This program written in FORTRAN was developed by S.P. Garbo and J.M. Ogonowski of McDonnell Aircraft Company, McDonnell-Douglas Aircraft Corporation, PO Box 516, St. Louis, MO 63166. It was published by the Air Force Flight Dynamics Laboratory, Wright Aeronautical Laboratories, Wright-Patterson Air Force Base, Ohio 45433 as report AFWAL-TR-81-3041, Volumes 1-3.

The program was modified by the author to run on the IBM 370. The code was renumbered, the input method and output format was altered for easier input.

```
C=======================================================================
C  BBSFM     VER 2.2     11/09/83     PAT SULLIVAN      AERO ENGINEERING  =
C  I/O MODIFICATION TO RUN FROM INPUT FILE.                               =
C=======================================================================
C  FILES:  01-READ DATA, 02-WRITE RESULTS, 03-SUMMARY OF INPUT            =
C=======================================================================
      COMMON /ONE/ E1(3),E2(3),G12(3),V12(3)
      COMMON /TWO/ IOUT(15),NUMPLY,NUMMAT,ANG(8),PLYTHK(8),MATID(8)
      COMMON /THREE/ IANG,ILOW,IHIGH,STPINK,NUMSTP
      COMMON /FOUR/ PX,PY,PXY,P,PW,ALPHA,BETA,DIA,CORREC
      COMMON /FIVE/ FXT(3),FXC(3),FYT(3),FYC(3),FXY(3),IFAIL
      COMMON /SIX/ AI(3,3)
      COMMON /SEVEN/ S(3,3)
      COMMON /EIGHT/ STRESS(3,20,91),STRAIN(3,20,91)
      COMMON /NINE/ STR1(8,20,91),STR2(8,20,91),STR12(8,20,91)
      INTEGER ANS,ANS2,YES,IANG,ILOW,IHIGH,RANGE
      DIMENSION TITLE(16)
      DATA RANGE/0/
C-----------------------------------------------------------------------
C  READ INPUT FILE IN FREE FORMAT FOR ALL REQUIRED DATA.                  -
C-----------------------------------------------------------------------
      DO 10 L=1,15
      IOUT(L)=0
10    CONTINUE
C
      READ (1,80)  TITLE
      READ (1,*)  (IOUT(L),L=1,10)
      READ (1,*)  NUMPLY,NUMMAT
      READ (1,*)  (E1(J),E2(J),G12(J),V12(J),J=1,NUMMAT)
      READ (1,*)  (FXT(J),FXC(J),FYT(J),FYC(J),FXY(J),J=1,NUMMAT)
      READ (1,*)  (ANG(J),PLYTHK(J),MATID(J),J=1,NUMPLY)
      READ (1,*)  PX,PY,PXY,BETA,P,ALPHA
      READ (1,*)  W,DIA,IFAIL
      READ (1,*)  ILOW,IHIGH,IANG,STPINK,NUMSTP
C
      IF (NUMSTP.GT.20) NUMSTP=20
      IF (IANG.EQ.0) GO TO 20
      RANGE=IFIX(FLOAT(IHIGH-ILOW)/FLOAT(IANG))
20    CONTINUE
      IF (RANGE.GT.91) WRITE (2,180)
      IF (RANGE.GT.91) STOP
      BL=P*DIA
      PW=0.0
      IF (P.NE.0.0.AND.W.NE.0.0) PW=BL/(2.0*W)
      WD=W/DIA
C-----------------------------------------------------------------------
C WRITE A SUMMARY OF THE INPUT DATA TO THE OUTPUT FILE                    -
C-----------------------------------------------------------------------
      WRITE (2,90) TITLE
      WRITE (2,100)  (IOUT(L),L=1,10)
      WRITE (2,110)  NUMPLY,NUMMAT
      DO 30 J=1,NUMMAT
      WRITE (2,120)  (J,E1(J),E2(J),G12(J),V12(J),FXT(J),FXC(J),FYT(J),FY
     1C(J),FXY(J))
30    CONTINUE
      WRITE (2,130)
      DO 40 J=1,NUMPLY
      WRITE (2,140)  (J,ANG(J),PLYTHK(J),MATID(J))
40    CONTINUE
      WRITE (2,150)  PX,PY,PXY,BETA,P,ALPHA
      WRITE (2,160)  W,DIA
      WRITE (2,170)  ILOW,IHIGH,IANG,RANGE,STPINK,NUMSTP
      IF (WD.LT.4.0.AND.W.NE.0.0) WRITE (3,190)
      WRITE (2,200)
      IF (IFAIL.EQ.1) WRITE (2,210)
      IF (IFAIL.EQ.2) WRITE (2,220)
      IF (IFAIL.EQ.3) WRITE (2,230)
      IF (IFAIL.EQ.4) WRITE (2,240)
      IF (IFAIL.EQ.5) WRITE (2,250)
      IF (IFAIL.LE.0.OR.IFAIL.GE.6) WRITE (2,260)
C-----------------------------------------------------------------------
C  BRANCH TO SUBROUTINES AS DIRECTED BY THE OPTION LIST                   -
C-----------------------------------------------------------------------
      IF (PUTOUT(IOUT,2).EQ.0.0) GO TO 60
      ALPH=ALPHA
      CALL ABD (ALPH)
```

```
      CORREC=1.0
      DUMMY=PUTOUT(ICUT,98)
50    CONTINUE
C
      IF (PUTOUT(IOUT,3).EQ.0.0) GO TO 60
      CALL LAMSTR
C
      IF (PUTOUT(IOUT,7).EQ.0.0) GO TO 60
      CALL PLYSTR (IFAIL)
C
      IF (PUTOUT(IOUT,9).EQ.0.0) GO TO 60
      CALL FAIL
C
      IF (PUTOUT(IOUT,10).EQ.2.0) DUMMY=PUTOUT(IOUT,99)
      IF (CORREC.LT..999.OR.CORREC.GT.1.001) GO TO 50
C
60    CONTINUE
      DUMMY=PUTCUT(ICUT,98)
      IF (PUTOUT(IOUT,1).NE.2.0) GO TO 70
70    CCNTINUE
C-----------------------------------------------------------------------
      STCP
80    FORMAT (16(A4))
90    FORMAT (15X,39HEOLTED JOINT STRESS FIELD MODEL (RBJSF),//,5X,31HCO
     1MPOSITE MATERIALS LABORATCRY,,2X,25HDEPARTMENT OF AERONAUTICS,/,11
     2X,26HNAVAL POSTGRADUATE SCHOOL,,2X,19HMCNTEREY,  CA 93943,////,5X,6
     3HTITLE:,16(A4),///)
100   FORMAT (5X,21H1) CPTIONS IN EFFECT:,2X,10(I3),//)
110   FORMAT (5X,40H2) NUMEER OF DIFFERENT PLY ORIENTATIONS:,I3,///,5X,3
     17H3) NUMBER OF DIFFERENT PLY MATERIALS:,I6,//)
120   FORMAT (5X,45H4) MATERIAL CONSTANTS & ALLOWABLES, MATERIAL:,I2,//,
     110X,6HE1 =  ,1PE11.3,6X,6HE2 =  ,E11.3,/,10X,6HG12 = ,E11.3,6X,6HV
     212 = ,E11.3,//,10X,6HFXT = ,E11.3,6X,6HFXC = ,E11.3,/,10X,6HFYT =
     3,E11.3,6X,6HFYC = ,E11.3,/,10X,6HFXY = ,E11.3,/)
130   FORMAT (/,5X,12H5) PLY DATA:,//,10X,6HNUMBER,5X,5HANGLE,5X,9HTHICK
     1NESS,5X,8HMATERIAL,/)
140   FORMAT (12X,I2,4X,F8.1,5X,F8.4,9X,I2)
150   FORMAT (//,5X,18H6) APPLIED STRESS:,//,10X,7HPX =    ,1PE11.4,2X,5HP
     1Y = ,E11.4,2X,6HPXY = ,E13.4,/,10X,7HBETA = ,E11.4,2X,5HP =  ,E11.
     24,2X,8HALPHA = ,E11.4,//)
160   FORMAT (5X,14H7) PANEL DATA:,//,10X,6HWIDTH:,F16.3,/,10X,14HHOLE D
     1IAMETER:,F8.3,//)
170   FORMAT (5X,21H8) SEARCH PARAMETERS:,//,10X,11HLOW ANGLE: ,I17,4H D
     1EG,/,10X,11HHIGH ANGLE:,I17,4H DEG,/,10X,16HANGLE INCREMENT:,I12,4
     2H DEG,/,10X,22HNUMBER OF ANGLE STEPS:,I7,5X,13H(MAXIMUM: 91),/,10X
     3,19HDISTANCE INCREMENT:,F13.3,2X,/,10X,25HNUMBER OF DISTANCE STEPS
     4:,I4,5X,13H(MAXIMUM: 20),/)
180   FORMAT (15X,30H*******  INPUT  ERROR  *******,/,5X,59HANGULAR INCR
     1EMENT BETWEEN HIGH AND LOW ANGLES IS TOO SMALL.,/,5X,51HDECREASE T
     2HE RANGE OR INCREASE THE INCREMENT ANGLE.,/,5X,21HEXECUTION IS STO
     3PPED.,/)
190   FORMAT (5X,38HCAUTION: WIDTH-TC-DIAMETER RATIOS LESS,/,5X,31HTHAN
     14.0 GIVE ERRONEOUS RESULTS/)
200   FORMAT (/,5X,34H9) FAILURE ANALYSIS CRITERIA USED:,//)
210   FORMAT (9X,14HMAXIMUM STRAIN,//)
220   FORMAT (9X,14HMAXIMUM STRESS,//)
230   FORMAT (9X,9HTSAI-HILL,//)
240   FORMAT (9X,17HMODIFIED TSAI-WU,//)
250   FORMAT (9X,7HHOFFMAN,//)
260   FORMAT (9X,14HNONE REQUESTED,//)
      END
      FUNCTION PUTOUT (IOUT,IN)
C=======================================================================
C  S/R PUTOUT      VER 1.1     4/25/83        PDS      AERO ENGINEERING  =
C=======================================================================
      DIMENSION IOUT(15)
C-----------------------------------------------------------------------
      DATA=0.0
      PUTOUT=0.0
      DO 10 J=1,15
      IF (IOUT(J).GE.IN) PUTOUT=1.0
10    CONTINUE
      DO 20 J=1,15
      IF (IOUT(J).EQ.IN) PUTOUT=2.0
20    CONTINUE
      IF (DATA.EQ.1.0.AND.IN.LT.10) PUTOUT=0.5
```

```
C----------------------------------------------------------------------
      RETURN
      END
      SUBROUTINE ABD (ALPHA)
C======================================================================
C   S/R ABD          VER 1.1      4/25/83        PDS      AERO ENGINEERING  =
C   SUBROUTINE CALCULATES A,B,D MATRICIES AND INVERSION MATRICI             =
C======================================================================
      COMMON /ONE/ E1(3),E2(3),G12(3),V12(3)
      COMMON /TWO/ IOUT(15),NUMPLY,NUMMAT,ANG(8),PLYTHK(8),MATID(8)
      COMMON /SIX/  AI(3,3)
      COMMON /SEVEN/ S(3,3)
      DIMENSION V21(3),DIV(3),Q11(3),Q22(3),Q12(3),Q66(3),U1(3),U2(3),U3
     1(3),U4(3),U5(3),QBAR(8,3,3),ZZ(20),Z(20),Q(3,3),AA(3,3),A(3,3)
      DATA PI/3.1415926535/
C----------------------------------------------------------------------
C   CALCULATE THE REDUCED STIFFNESS MATRIX FOR EACH MATERIAL           -
C----------------------------------------------------------------------
      DO 10 M=1,NUMMAT
      V21(M)=E2(M)*V12(M)/E1(M)
      DIV(M)=1.0-V12(M)*V21(M)
      Q11(M)=E1(M)/DIV(M)
      Q22(M)=E2(M)/DIV(M)
      Q12(M)=V12(M)*E2(M)/DIV(M)
      Q66(M)=G12(M)
10    CONTINUE
C----------------------------------------------------------------------
C   CALCULATE THE INVARIENTS (U) FROM THE Q MATRIX FOR EACH MATERIAL   -
C----------------------------------------------------------------------
      DO 20 M=1,NUMMAT
      U1(M)=(3.0*Q11(M)+3.0*Q22(M)+2.0*Q12(M)+4.0*Q66(M))/8.0
      U2(M)=(Q11(M)-Q22(M))/2.0
      U3(M)=(Q11(M)+Q22(M)-2.0*Q12(M)-4.0*Q66(M))/8.0
      U4(M)=(Q11(M)+Q22(M)+6.0*Q12(M)-4.0*Q66(M))/8.0
      U5(M)=(Q11(M)+Q22(M)-2.0*Q12(M)+4.0*Q66(M))/8.0
20    CONTINUE
C
      DO 30 I=1,3
      DO 30 J=1,3
      A(I,J)=0.0
      AA(I,J)=0.0
30    CONTINUE
C----------------------------------------------------------------------
C   TRANSFORMED REDUCED STIFFNESS MATFIX FOR EACH PLY                  -
C----------------------------------------------------------------------
      THICK=0.
      DO 40 L=1,NUMPLY
      DEG=ANG(L)*PI/180.0
      M=MATID(L)
C
      QBAR(L,1,1)=U1(M)+U2(M)*COS(2.0*DEG)+U3(M)*COS(4.0*DEG)
      QBAR(L,1,2)=U4(M)-U3(M)*COS(4.0*DEG)
      QBAR(L,2,2)=U1(M)-U2(M)*COS(2.0*DEG)+U3(M)*COS(4.0*DEG)
      QBAR(L,1,3)=0.5*U2(M)*SIN(2.0*DEG)+U3(M)*SIN(4.0*DEG)
      QBAR(L,2,3)=0.5*U2(M)*SIN(2.0*DEG)-U3(M)*SIN(4.0*DEG)
      QBAR(L,3,3)=U5(M)-U3(M)*COS(4.0*DEG)
      QBAR(L,2,1)=QBAR(I,1,2)
      QBAR(L,3,1)=QBAR(I,1,3)
      QBAR(L,3,2)=QBAR(L,2,3)
C
      THICK=PLYTHK(L)+THICK
      ZZ(L+1)=THICK
40    CONTINUE
      Z(1)=-1.0*THICK/2.0
C----------------------------------------------------------------------
C   CALCULATE THE A MATRIX                                             -
C----------------------------------------------------------------------
      DO 70 I=1,3
      DO 60 J=1,3
      DO 50 L=1,NUMPLY
      Z(L+1)=Z(1)+ZZ(L+1)
      ZA=Z(L+1)-Z(L)
      A(I,J)=A(I,J)+QBAR(L,I,J)*ZA
50    CONTINUE
C----------------------------------------------------------------------
C   MATRIX Q AND QQ ARE MATRICIES USED IN CALCULATIONS FOR THE MANIPU-  -
```

```
C  LATION OF OTHER MATRICIES                                            -
C-----------------------------------------------------------------------
      Q(I,J)=A(I,J)/THICK
60    CONTINUE
70    CONTINUE
C-----------------------------------------------------------------------
C     COMPUTE A/THICK INVERSE MATRIX                                    -
C-----------------------------------------------------------------------
      ISTEP=1
      CALL INVERS (Q,AI)
C-----------------------------------------------------------------------
C  LAMINATE MID-PLANE PROPERTIES CAN BE CALCULATED HERE AS FOL          -
C-----------------------------------------------------------------------
      EX1=1.0/AI(1,1)
      EY1=1.0/AI(2,2)
      VXY1=-EX1*AI(1,2)
      GXY1=1.0/AI(3,3)
      SCF=1.0+SQRT(2.0*(SQRT(EX1/EY1)-VXY1)+EX1/GXY1)
      WRITE (2,160) EX1,GXY1,EY1,VXY1,SCF
C-----------------------------------------------------------------------
C  CALCULATE MATERIAL PROPERTIES FOR OFF-AXIS BOLT LOAD, TRANSFORMED    -
C  REDUCED STIFFNESSES PER PLY                                          -
C-----------------------------------------------------------------------
      THICK=0.0
      ALPHA=ALPHA*PI/180.0
      DO 80 L=1,NUMPLY
      DEG=ANG(L)*PI/180.0
      DEG=DEG-ALPHA
      M=MATID(L)
C
      QBAR(L,1,1)=U1(M)+U2(M)*COS(2.0*DEG)+U3(M)*COS(4.0*DEG)
      QBAR(L,1,2)=U4(M)-U3(M)*COS(4.0*DEG)
      QBAR(L,2,2)=U1(M)-U2(M)*COS(2.0*DEG)+U3(M)*COS(4.0*DEG)
      QBAR(L,1,3)=0.5*U2(M)*SIN(2.0*DEG)+U3(M)*SIN(4.0*DEG)
      QBAR(L,2,3)=0.5*U2(M)*SIN(2.0*DEG)-U3(M)*SIN(4.0*DEG)
      QBAR(L,3,3)=U5(M)-U3(M)*COS(4.0*DEG)
      QBAR(L,2,1)=QBAR(L,1,2)
      QBAR(L,3,1)=QBAR(L,1,3)
      QBAR(L,3,2)=QBAR(L,2,3)
C
      THICK=PLYTHK(L)+THICK
      ZZ(L+1)=THICK
80    CONTINUE
      Z(1)=-1.0*THICK/2.0
C-----------------------------------------------------------------------
C CALCULATE AA MATRIX                                                   -
C-----------------------------------------------------------------------
      DO 110 I=1,3
      DO 100 J=1,3
      DO 90 L=1,NUMPLY
      Z(L+1)=Z(1)+ZZ(L+1)
      ZA=Z(L+1)-Z(L)
      AA(I,J)=AA(I,J)+QBAR(L,I,J)*ZA
90    CONTINUE
      Q(I,J)=AA(I,J)/THICK
100   CONTINUE
110   CONTINUE
C-----------------------------------------------------------------------
C  COMPUTE AA/THICK INVERSE MATRIX                                      -
C-----------------------------------------------------------------------
      ISTEP=4
      CALL INVERS (Q,S)
C-----------------------------------------------------------------------
C  PRINT MATRIX AND LAMINATE DATA                                       -
C-----------------------------------------------------------------------
      IF (PUTOUT(IOUT,2).NE.2.) GO TO 120
      WRITE (2,130) ((AA(I,1),AA(I,2),AA(I,3)),I=1,3)
      WRITE (2,140) ((Q(I,1),Q(I,2),Q(I,3)),I=1,3)
      WRITE (2,150) ((S(I,1),S(I,2),S(I,3)),I=1,3)
120   CONTINUE
C-----------------------------------------------------------------------
C  OFF-AXIS LAMINATE PROPERTIES                                         -
C-----------------------------------------------------------------------
      EX2=1.0/S(1,1)
      EY2=1.0/S(2,2)
      VXY2=-EX2*S(1,2)
```

```
      GXY2=1.0/S(3,3)
C-----------------------------------------------------------------------
      RETURN
130   FORMAT (10X,9HA MATRIX:,//,3(10X,3(1PE14.3),/),/)
140   FORMAT (10X,11HA/T MATRIX:,//,3(10X,3(1PE14.3),/),/)
150   FORMAT (10X,15HA/T INV MATRIX:,//,3(10X,3(1PE14.3),/),/)
160   FORMAT (/,5X,24H10) LAMINATE PROPERTIES:,//,10X,5HEX = ,1PE11.3,5X
     1,6HGXY = ,E11.3,/,10X,5HEY = ,E11.3,5X,6HVXY = ,0PF8.4,//,10X,30HS
     2TRESS CONCENTRATION FACTOR = ,F5.3,//)
      END
      SUBROUTINE INVERS (X,XI)
C=======================================================================
C  S/R INVERS         VER 1.1      4/25/83       PDS       AERO ENGINEERING  =
C  CALCULATES THE INVERSE OF A 3X3 MATRIX                                    =
C=======================================================================
      DIMENSION X(3,3),XI(3,3)
      COMMON ISTEP
C-----------------------------------------------------------------------
      DET=(X(1,1)*X(2,2)*X(3,3))+(X(1,2)*X(2,3)*X(3,1))+(X(1,3)*X(2,1)*X
     1(3,2))-(X(1,3)*X(2,2)*X(3,1))-(X(1,1)*X(2,3)*X(3,2))-(X(1,2)*X(2,1
     2)*X(3,3))
      IF (DET.EQ.0.0) GO TO 10
C
      XI(1,1)=(X(2,2)*X(3,3)-X(2,3)*X(3,2))/DET
      XI(1,2)=(X(2,3)*X(3,1)-X(2,1)*X(3,3))/DET
      XI(1,3)=(X(2,1)*X(3,2)-X(2,2)*X(3,1))/DET
      XI(2,2)=(X(1,1)*X(3,3)-X(1,3)*X(3,1))/DET
      XI(2,3)=(X(1,2)*X(3,1)-X(1,1)*X(3,2))/DET
      XI(3,3)=(X(1,1)*X(2,2)-X(1,2)*X(2,1))/DET
      XI(2,1)=(X(3,2)*X(1,3)-X(1,2)*X(3,3))/DET
      XI(3,1)=(X(1,2)*X(2,3)-X(2,2)*X(1,3))/DET
      XI(3,2)=(X(2,1)*X(1,3)-X(1,1)*X(2,3))/DET
C
      GO TO 20
10    WRITE (2,30) ISTEP
20    CONTINUE
C-----------------------------------------------------------------------
      RETURN
30    FORMAT (49H SUBROUTINE INVERSE CALCULATES A SINGULAR MATRIX ,7HAT
     1STEP,I3)
      END
      SUBROUTINE LAMSTR
C=======================================================================
C  S/R LAMSTR         VER 1.1      4/25/83       PDS       AERO ENGINEERING  =
C  CALCULATES THE LAMINATE STRESSES AND STRAINS DUE TO AN INPLANE LOAD =
C  AND A BOLT LOAD                                                           =
C=======================================================================
      COMMON /TWO/ ICOT(15),NUMELY,NUMMAT,ANG(8),PLYTHK(8),MATID(8)
      COMMON /THREE/ IANG,ILOW,IHIGH,STPINK,NUMSTP
      COMMON /FOUR/ PX,PY,PXY,P,PW,ALPHA,BETA,DIA,CORREC
      COMMON /SIX/ AI(3,3)
      COMMON /SEVEN/ S(3,3)
      COMMON /EIGHT/ STRESS(3,20,91),STRAIN(3,20,91)
      INTEGER IANG,ILOW,IHIGH
      DIMENSION STR(3,20,91),U(20,91),V(20,91),UX(20,91),VY(20,91)
      DATA NUMPT/1/,PI/3.1415926535/
C-----------------------------------------------------------------------
      PX=CORREC*PX
      PY=CORREC*PY
      PXY=CORREC*PXY
      P=CORREC*P
      PW=CORREC*PW
C
      IF (IANG.EQ.0) GO TO 10
      NUMPT=((IHIGH-ILOW)/IANG)+1
10    CONTINUE
      DO 20 J=1,NUMSTP
      DO 20 K=1,NUMPT
      U(J,K)=0.0
      V(J,K)=0.0
      DO 20 I=1,3
      STRESS(I,J,K)=0.0
      STRAIN(I,J,K)=0.0
20    CONTINUE
C-----------------------------------------------------------------------
C  CALCULATE UNLOAD HOLE STRESSES                                            -
```

```
C----------------------------------------------------------------------
      IF (PX.EQ.0.0) GO TO 30
      BETA0=BETA
      CALL UNLOAD (PX,DIA,AI,BETA0,STRESS,U,V)
30    CONTINUE
      IF (PY.EQ.0.0) GO TO 50
      BETA90=BETA+90.0
      CALL UNLOAD (PY,DIA,AI,BETA90,STR,UX,VY)
      DO 40 J=1,NUMSTP
      DO 40 K=1,NUMPT
      U(J,K)=U(J,K)+UX(J,K)
      V(J,K)=V(J,K)+VY(J,K)
      DO 40 I=1,3
      STRESS(I,J,K)=STRESS(I,J,K)+STR(I,J,K)
40    CONTINUE
C----------------------------------------------------------------------
50    CONTINUE
      IF (PXY.EQ.0.0) GO TO 80
      BETA45=BETA+45.0
      CALL UNLOAD (PXY,DIA,AI,BETA45,STR,UX,VY)
      DO 60 J=1,NUMSTP
      DO 60 K=1,NUMPT
      U(J,K)=U(J,K)+UX(J,K)
      V(J,K)=V(J,K)+VY(J,K)
      DO 60 I=1,3
      STRESS(I,J,K)=STRESS(I,J,K)+STR(I,J,K)
60    CONTINUE
C
      BETA45=BETA-45.0
      PXYN=-PXY
      CALL UNLOAD (PXYN,DIA,AI,BETA45,STR,UX,VY)
      DO 70 J=1,NUMSTP
      DO 70 K=1,NUMPT
      U(J,K)=U(J,K)+UX(J,K)
      V(J,K)=V(J,K)+VY(J,K)
      DO 70 I=1,3
      STRESS(I,J,K)=STRESS(I,J,K)+STR(I,J,K)
70    CONTINUE
80    CONTINUE
C----------------------------------------------------------------------
C  CALCULATE LOADED HOLE STRESSES                                     -
C----------------------------------------------------------------------
      IF (P.EQ.0.0) GO TO 110
      ALPHA0=ALPHA
      PB=P
      CALL LOAD (PB,DIA,S,ALPHA0,STR,UX,VY)
      DO 90 J=1,NUMSTP
      DO 90 K=1,NUMPT
      U(J,K)=U(J,K)+UX(J,K)
      V(J,K)=V(J,K)+VY(J,K)
      DO 90 I=1,3
      STRESS(I,J,K)=STRESS(I,J,K)+STR(I,J,K)
90    CONTINUE
C----------------------------------------------------------------------
      ALPHA0=ALPHA
      CALL UNLOAD (PW,DIA,AI,ALPHA0,STR,UX,VY)
      DO 100 J=1,NUMSTP
      DO 100 K=1,NUMPT
      U(J,K)=U(J,K)+UX(J,K)
      V(J,K)=V(J,K)+VY(J,K)
      DO 100 I=1,3
      STRESS(I,J,K)=STRESS(I,J,K)+STR(I,J,K)
100   CONTINUE
110   CONTINUE
      IF (PUTOUT(IOUT,3).EQ.2.) WRITE (2,210)
C----------------------------------------------------------------------
C  CALCULATE PRINCIPAL STRESSES                                       -
C----------------------------------------------------------------------
      IF (PUTOUT(IOUT,3).NE.2.) GO TO 130
      DO 120 JJ=1,NUMSTP
      DO 120 NN=1,NUMPT
      PRINA=(STRESS(1,JJ,NN)-STRESS(2,JJ,NN))*(STRESS(1,JJ,NN)-STRESS(2,
     1JJ,NN))/4.0
      PRINA=SQRT(PRINA+STRESS(3,JJ,NN)*STRESS(3,JJ,NN))
      PRIN1=(STRESS(1,JJ,NN)+STRESS(2,JJ,NN))/2.0+PRINA
      PRIN2=(STRESS(1,JJ,NN)+STRESS(2,JJ,NN))/2.0-PRINA
```

```
      TSTS=STRESS(1,JJ,NN)-STRESS(2,JJ,NN)
      DIRCT=0.0
      IF (TSTS.NE.0.0) DIRCT=0.5*ATAN(2.0*STRESS(3,JJ,NN)/TSTS)
      DIRCT=180.0*DIRCT/3.1415926535
C
      IF (PUTOUT(IOUT,3).NE.2.0) GO TO 130
      ANGLE=(NN-1)*IANG+ILOW
      DIST=(JJ-1)*STPINK
C     IF (DIST.LE.0.0005) DIST=0.001
      WRITE (2,220) DIST,ANGLE,STRESS(1,JJ,NN),STRESS(2,JJ,NN),STRESS(3,
     1JJ,NN),PRIN1,PRIN2,DIRCT
120   CONTINUE
130   CONTINUE
      IF (PUTOUT(IOUT,4).EQ.2.) WRITE (2,230)
C-----------------------------------------------------------------------
C  CALCULATE LAMINATE STRAINS                                          -
C-----------------------------------------------------------------------
      DO 140 JJ=1,NUMSTP
      DO 140 NN=1,NUMPT
      DO 140 KK=1,3
      DO 140 MM=1,3
      STRAIN(KK,JJ,NN)=AI(KK,MM)*STRESS(MM,JJ,NN)+STRAIN(KK,JJ,NN)
140   CONTINUE
C-----------------------------------------------------------------------
C  CALCULATE PRINCIPAL STRAINS                                         -
C-----------------------------------------------------------------------
      IF (PUTOUT(IOUT,4).NE.2.0) GO TO 160
      DO 150 JJ=1,NUMSTP
      DO 150 NN=1,NUMPT
      PRINA=(STRAIN(1,JJ,NN)-STRAIN(2,JJ,NN))*(STRAIN(1,JJ,NN)-STRAIN(2,
     1JJ,NN))/4.
      PRINA=SQRT(PRINA+STRAIN(3,JJ,NN)*0.25*STRAIN(3,JJ,NN))
      PRIN1=(STRAIN(1,JJ,NN)+STRAIN(2,JJ,NN))/2.0+PRINA
      PRIN2=(STRAIN(1,JJ,NN)+STRAIN(2,JJ,NN))/2.0-PRINA
      TSTS=STRAIN(1,JJ,NN)-STRAIN(2,JJ,NN)
      DIRCT=0.0
      IF (TSTS.NE.0.) DIRCT=0.5*ATAN(2.0*STRAIN(3,JJ,NN)/TSTS)
      DIRCT=180.0*DIRCT/3.1415926535
      DIST=(JJ-1)*STPINK
C     IF (DIST.LE.0.0005) DIST=0.001
      ANGLE=(NN-1)*IANG+ILOW
C     IF (CORREC.NE.1.00
      WRITE (2,240) DIST,ANGLE,STRAIN(1,JJ,NN),STRAIN(2,JJ,NN),STRAIN(3,
     1JJ,NN),PRIN1,PRIN2,DIRCT
150   CONTINUE
160   CONTINUE
C-----------------------------------------------------------------------
C  CALCULATE CIRCUMFERENTIAL AND RADIAL STRESSES & STRAINS             -
C-----------------------------------------------------------------------
      IF (PUTOUT(IOUT,5).EQ.2.) WRITE (2,250)
      IF (PUTOUT(IOUT,5).NE.2.) GO TO 180
      DO 170 J=1,NUMSTP
      DO 170 N=1,NUMPT
      ENERGY=.5*(STRESS(1,J,N)*STRAIN(1,J,N)+STRESS(2,J,N)*STRAIN(2,J,N)
     1+STRESS(3,J,N)*STRAIN(3,J,N))
      ANGLE=(N-1)*IANG+ILOW
      D=ANGLE*PI/180.0
      DIST=(J-1)*STPINK
C     IF (DIST.LE.0.0005) DIST=0.001
      RADSTS=STRESS(1,J,N)*COS(D)*COS(D)+STRESS(2,J,N)*SIN(D)*SIN(D)+2.*
     1STRESS(3,J,N)*SIN(D)*COS(D)
      CIRSTS=STRESS(1,J,N)*SIN(D)*SIN(D)+STRESS(2,J,N)*COS(D)*COS(D)-2.*
     1STRESS(3,J,N)*SIN(D)*COS(D)
      SHRSTS=-1.*STRESS(1,J,N)*SIN(D)*COS(D)+STRESS(2,J,N)*SIN(D)*COS(D)
     1+STRESS(3,J,N)*(COS(D)*COS(D)-SIN(D)*SIN(D))
      RADSTN=STRAIN(1,J,N)*COS(D)*COS(D)+STRAIN(2,J,N)*SIN(D)*SIN(D)+STR
     1AIN(3,J,N)*SIN(D)*COS(D)
      CIRSTN=STRAIN(1,J,N)*SIN(D)*SIN(D)+STRAIN(2,J,N)*COS(D)*COS(D)-STR
     1AIN(3,J,N)*SIN(D)*COS(D)
      SHRSTN=-1.*STRAIN(1,J,N)*SIN(D)*COS(D)+STRAIN(2,J,N)*SIN(D)*COS(D)
     1+STRAIN(3,J,N)*(COS(D)*COS(D)-SIN(D)*SIN(D))
      WRITE (2,260) DIST,ANGLE,CIRSTS,RADSTS,SHRSTS,CIRSTN,RADSTN,SHRSTN
170   CONTINUE
180   CONTINUE
C-----------------------------------------------------------------------
C  WRITE THE OUTPUT DISPLACEMENTS                                      -
```

```
C-----------------------------------------------------------------------
      D3=3.0*DIA
      DISP=DIA/2.0+NUMSTP*STPINK
      IF (PUTOUT(IOUT,6).EQ.2.0.AND.P.NE.0.0.AND.DISP.GT.D3) WRITE (2,27
     10)
      IF (PUTOUT(IOUT,6).EQ.2.0) WRITE (2,280)
      IF (PUTOUT(IOUT,6).NE.2.0) GO TO 200
      DO 190 J=1,NUMSTP
      DO 190 K=1,NUMPT
      ANGLE=(K-1)*IANG+ILOW
      DIST=(J-1)*STPINK
C     IF (DIST.LE.0.0005) DIST=0.001
      WRITE (2,290) DIST,ANGLE,U(J,K),V(J,K)
190   CONTINUE
200   CONTINUE
C-----------------------------------------------------------------------
      RETURN
210   FORMAT (//,29(1H-),21H  LAMINATE STRESSES  ,29(1H-),//,8HDISTANCE,
     12X,5HANGLE,3X,5HSIG-X,6X,5HSIG-Y,5X,6HSIG-XY,5X,7HMAXIMUM,4X,7HMIN
     2IMUM,2X,9HDIRECTICN,/,49X,20HPRINCIPAL  PRINCIPAL,/)
220   FORMAT (F7.3,F8.2,F9.1,4F11.1,F8.1)
230   FORMAT (//,29(1H-),20H  LAMINATE STRAINS  ,30(1H-),//,8HDISTANCE,2
     1X,5HANGLE,4X,5HEPS-X,6X,5HEPS-Y,5X,6HEPS-XY,4X,7HMAXIMUM,4X,7HMINI
     2MUM,2X,9HDIRECTICN,/,49X,20HPRINCIPAL  PRINCIPAL,/)
240   FORMAT (F7.3,F8.2,F10.6,4F11.6,F7.1)
250   FORMAT (//,15(1H-),49H  CIRCUMFERENTIAL AND RADIAL STRESSES & STRA
     1INS  ,15(1H-),//,8HDISTANCE,2X,5HANGLE,3X,5HTHETA,6X,6HRADIAL,5X,5
     2HSHEAR,5X,5HTHETA,5X,6HRADIAL,5X,5HSHEAR,/,18X,6HSTRESS,5X,6HSTRES
     3S,5X,6HSTRESS,4X,6HSTRAIN,4X,6HSTRAIN,4X,6HSTRAIN,//)
260   FORMAT (F7.3,F7.1,3F11.1,3F10.6)
270   FORMAT (56H CAUTION:  DISPLACEMENTS AT POINTS GREATER THAN 3D AWAY
     1 ,30H FROM THE HOLE MAY BE IN ERROR)
280   FORMAT (///,13(1H-),16H  DISPLACEMENT  ,13(1H-),//,8HDISTANCE,4X,5
     1HANGLE,9X,1HU,11X,1HV,/)
290   FORMAT (F7.3,F10.2,F13.6,F12.6)
      END
      SUBROUTINE UNLOAD (P,DIA,AI,BETA,STRESS,U,V)
C=======================================================================
C  S/R UNLOAD       VER 1.1      4/25/83        PDS       AERO ENGINEERING  =
C  CALCULATE STRESS DISTRIBUTION ARCUND AN UNLOADED HOLE                    =
C=======================================================================
      COMMON /THREE/ IANG,ILOW,IHIGH,STPINK,NUMSTP
      INTEGER IANG,ILOW,IHIGH
      DIMENSION STRESS(3,20,91),U(20,91),V(20,91),AI(3,3)
      DIMENSION WORK(5),COEF(5),RTR(4),RTI(4)
      COMPLEX R1,R2,COMPLX,XI1,XI2,CCM1,COM2,DEN1,DEN2,PHI1,PHI2
      COMPLEX Z,Z1,Z2,P1,P2,Q1,Q2
      DATA NUMPT/1/,PI/3.1415926535/
C-----------------------------------------------------------------------
C  CALCULATE COMPLEX PARAMETERS, INITIALIZE COMPLEX NUMBER: SQRT(-1.0) -
C-----------------------------------------------------------------------
      COMPLX=(0.0,1.0)
      NUMCO=4
      COEF(1)=AI(2,2)*1000000.0
      COEF(2)=-2.0*AI(2,3)*1000000.0
      COEF(3)=(2.0*AI(1,2)+AI(3,3))*1000000.0
      COEF(4)=-2.0*AI(1,3)*1000000.0
      COEF(5)=AI(1,1)*1000000.0
      CALL ROOTS (COEF,WORK,NUMCO,RTR,RTI,IE)
      R1=RTR(1)+COMPLX*RTI(1)
      IF (RTI(2).GT.0.0) R1=RTR(2)+CCMPLX*RTI(2)
      R2=RTR(3)+COMPLX*RTI(3)
      IF (RTI(4).GT.0.0) R2=RTR(4)+CCMPLX*RTI(4)
      P1=AI(1,1)*R1*R1+AI(1,2)-AI(1,3)*R1
      P2=AI(1,1)*R2*R2+AI(1,2)-AI(1,3)*R2
      Q1=AI(1,2)*R1+AI(2,2)/R1-AI(2,3)
      Q2=AI(1,2)*R2+AI(2,2)/R2-AI(2,3)
      BETA=BETA*PI/180.0
      IF (IANG.EQ.0) GO TO 10
      NUMPT=((IHIGH-ILOW)/IANG)+1
10    CONTINUE
C
      DO 30 JJ=1,NUMSTP
      DO 20 NN=1,NUMPT
      U(JJ,NN)=0.0
      V(JJ,NN)=0.0
```

```
      NNN=NN-1
      JJJ=JJ-1
      THETA=(NNN*IANG+ILOW)*PI/180.0
      RADIUS=JJJ*STPINK+DIA/2.0
C-----------------------------------------------------------------------
C  CALCULATE X & Y COORDINATES OF POINTS AROUND UNLOADED HOLE          -
C-----------------------------------------------------------------------
      X=RADIUS*COS(THETA)
      Y=RADIUS*SIN(THETA)
C-----------------------------------------------------------------------
C  CALCULATE LOCATION PARAMETERS FOR UNLOADED HOLE EQUATIONS           -
C-----------------------------------------------------------------------
      Z1=X+R1*Y
      Z2=X+R2*Y
      Z=X+COMPLX*Y
C-----------------------------------------------------------------------
C  COMPLEX MAPPING FUNCTION                                            -
C-----------------------------------------------------------------------
      XI1=CSQRT(Z1*Z1-DIA*DIA/4.0-R1*R1*DIA*DIA/4.0)
      XI2=CSQRT(Z2*Z2-DIA*DIA/4.0-R2*R2*DIA*DIA/4.0)
C-----------------------------------------------------------------------
C  CHOOSE THE ROOT WITH THE CORRECT SIGN                               -
C-----------------------------------------------------------------------
      XI1=Z1/XI1
      XI2=Z2/XI2
      IF (REAL(XI1).LT.-0.00001) XI1=-1.0*XI1
      IF (REAL(XI2).LT.-0.00001) XI2=-1.0*XI2
      XI1=1.0-XI1
      XI2=1.0-XI2
C-----------------------------------------------------------------------
C  CALCULATE PHI PRIME                                                 -
C-----------------------------------------------------------------------
      COM1=R2*SIN(2.0*BETA)+2.0*COS(BETA)*COS(BETA)+COMPLX*(2.0*R2*SIN(B
     1ETA)*SIN(BETA)+SIN(2.0*BETA))
      COM2=R1*SIN(2.0*BETA)+2.0*COS(BETA)*COS(BETA)+COMPLX*(2.0*R1*SIN(B
     1ETA)*SIN(BETA)+SIN(2.0*BETA))
C-----------------------------------------------------------------------
      DEN1=2.0*DIA*(R1-R2)*(1.0+COMPLX*R1)
      DEN2=2.0*DIA*(R1-R2)*(1.0+COMPLX*R2)
      PHI1=-COMPLX*P*DIA*COM1*XI1/(2.0*DEN1)
      PHI2=COMPLX*P*DIA*COM2*XI2/(2.0*DEN2)
C-----------------------------------------------------------------------
C      CALCULATE STRESSES AROUND HOLE                                  -
C-----------------------------------------------------------------------
      STRESS(1,JJ,NN)=P*COS(BETA)*COS(BETA)+2.0*REAL(R1*R1*PHI1+R2*R2*PH
     1I2)
      STRESS(2,JJ,NN)=P*SIN(BETA)*SIN(BETA)+2.0*REAL(PHI1+PHI2)
      STRESS(3,JJ,NN)=P*SIN(BETA)*COS(BETA)-2.0*REAL(R1*PHI1+R2*PHI2)
C-----------------------------------------------------------------------
C  CALCULATE DISPLACEMENTS                                             -
C-----------------------------------------------------------------------
      XI1=1.0-XI1
      XI2=1.0-XI2
      XI1=Z1/XI1
      XI2=Z2/XI2
      DEN1=16.0*(R1-R2)*(Z1+XI1)
      DEN2=16.0*(R1-R2)*(Z2+XI2)
      PHI1=-P*DIA*DIA*(COMPLX+R1)*COM1/DEN1
      PHI2=P*DIA*DIA*(COMPLX+R2)*COM2/DEN2
      U(JJ,NN)=2.0*REAL(P1*PHI1+P2*PHI2)
      V(JJ,NN)=2.0*REAL(Q1*PHI1+Q2*PHI2)
20    CONTINUE
30    CONTINUE
C-----------------------------------------------------------------------
      RETURN
      END
      SUBROUTINE LOAD (P,DIA,S,ALPHA,STRESS,U,V)
C=======================================================================
C  S/R LOAD          VER 1.1      4/25/83       PDS       AERO ENGINEERING  =
C  CALCULATES STRESS DISTRIBUTION AROUND A LOADED HOLE ASSUMING A      =
C  COSINE BOLT LOAD DISTRIBUTION                                       =
C=======================================================================
      COMMON /TWO/ ICUT(15),NUMPLY,NUMMAT,ANG(8),PLYTHK(8),MATID(8)
      COMMON /THREE/ IANG,ILOW,IHIGH,STPINK,NUMSTP
      INTEGER IANG,ILOW,IHIGH
      COMPLEX R1,R2,COMPLX,Z,Z1,Z2,CPOS(50),CNEG(50),CZERO,CM,AK1,AK2,XI
```

```
     11,XI2,PHI1,PHI2,COM1,COM2,XXI1,XXI2
      COMPLEX CHECK1,CHECK2,P1,P2,Q1,Q2
      COMPLEX A1(50),A2(50)
      DIMENSION AMATRX(4,4),BMATRX(4),STRESS(3,20,91)
      DIMENSION U(20,91),V(20,91),S(3,3)
      DIMENSION WORK(5),COEF(5),RTR(4),RTI(4)
      DATA NUMPI/1/,PI/3.1415926535/
C-----------------------------------------------------------------------
C  INITIALIZE COMPLEX NUMBER:   SQRT(-1.0)                            -
C-----------------------------------------------------------------------
      COMPLX=(0.0,1.0)
C-----------------------------------------------------------------------
C  CALCULATE COMPLEX PARAMETERS                                        -
C-----------------------------------------------------------------------
      NUMCO=4
      COEF(1)=S(2,2)*1000000.0
      COEF(2)=-2.0*S(2,3)*1000000.0
      COEF(3)=(2.0*S(1,2)+S(3,3))*1000000.0
      COEF(4)=-2.0*S(1,3)*1000000.0
      COEF(5)=S(1,1)*1000000.0
      CALL ROOTS (COEF,WORK,NUMCO,RTR,RTI,IE)
      R1=RTR(1)+COMPLX*RTI(1)
      IF (RTI(2).GT.0.0) R1=RTR(2)+COMPLX*RTI(2)
      R2=RTR(3)+COMPLX*RTI(3)
      IF (RTI(4).GT.0.0) R2=RTR(4)+COMPLX*RTI(4)
      P1=S(1,1)*R1*R1+S(1,2)-S(1,3)*R1
      P2=S(1,1)*R2*R2+S(1,2)-S(1,3)*R2
      Q1=S(1,2)*R1+S(2,2)/R1-S(2,3)
      Q2=S(1,2)*R2+S(2,2)/R2-S(2,3)
      THICK=0.0
      DO 10 N=1,NUMPLY
      THICK=THICK+PLYTHK(N)
10    CONTINUE
      P=4.0*P/PI
C-----------------------------------------------------------------------
C  A COSINE SHAPED LOAD DISTRIBUTION OVER HALF OF HOLE AT AN ANGLE     -
C  ALPHA TO X AXIS.  CALCULATE THE COMPLEX CONSTANTS                   -
C-----------------------------------------------------------------------
      PI2=PI/2.0
      M=-1
20    CONTINUE
      M=M+1
      IF (M.EQ.1) GO TO 40
30    CONTINUE
      C1=SIN((M-1)*PI2)/(2*(M-1))
      C2=SIN((M+1)*PI2)/(2*(M+1))
      C3=SIN((M-1)*(-PI2))/(2*(M-1))
      C4=SIN((M+1)*(-PI2))/(2*(M+1))
      C5=COS((M-1)*PI2)/(2*(M-1))
      C6=COS((M+1)*PI2)/(2*(M+1))
      C7=COS((M-1)*(-PI2))/(2*(M-1))
      C8=COS((M+1)*(-PI2))/(2*(M+1))
      CM=P*((C1+C2-C3-C4)-COMPLX*(-C5-C6+C7+C8))/(2.0*PI)
      IF (M.EQ.0) CZERO=CM
      IF (M.GT.1) CPOS(M)=CM
      IF (M.LT.-1) MN=-1*M
      IF (M.LT.-1) CNEG(MN)=CM
      IF (M.LE.0) GO TO 50
      M=-1*M
      GO TO 30
40    CONTINUE
      C1=PI2
      C2=SIN(2.0*(PI2))/4.0
      C3=SIN(2.0*(-PI2))/4.0
      C4=SIN(PI2)*SIN(PI2)/2.0
      C5=SIN(-PI2)*SIN(-PI2)/2.0
      CM=P*((C1+C2-C3)-M*COMPLX*(C4-C5))/(2.0*PI)
      IF (M.EQ.1) CPOS(1)=CM
      IF (M.EQ.-1) CNEG(1)=CM
      IF (M.EQ.-1) GO TO 50
      M=-1*M
      GO TO 40
50    CONTINUE
      M=IABS(M)
      IF (M.LT.49) GO TO 20
C-----------------------------------------------------------------------
```

```
C   SERIES TRUNCATED AFTER 25 TERMS.                                          -
C   TRANSFORM COMPLEX PARAMETERS INTO REAL AND IMAGINARY PARTS.               -
C-----------------------------------------------------------------------------
      S1=REAL(R1)
      S2=REAL(R2)
      T1=AIMAG(R1)
      T2=AIMAG(R2)
C-----------------------------------------------------------------------------
C   EQUATE COEFFICIENTS AND SOLVE FOR CONSTANTS                               -
C-----------------------------------------------------------------------------
      DO 80 M=1,45
      MN=M-1
      IF (MN.NE.0) GO TO 60
      BMATRX(1)=REAL(-CZERO*DIA/2.0)
      BMATRX(2)=AIMAG(-CZERO*DIA/2.0)
      GO TO 70
60    CONTINUE
      BMATRX(1)=REAL(-CPOS(MN)*DIA/(2.0*(MN+1)))
      BMATRX(2)=AIMAG(-CPOS(MN)*DIA/(2.0*(MN+1)))
70    CONTINUE
      MN=M+1
      MNEG=-1*MN
      BMATRX(3)=REAL(-CNEG(MN)*DIA/(2.0*(MNEG+1)))
      BMATRX(4)=AIMAG(-CNEG(MN)*DIA/(2.0*(MNEG+1)))
      AMATRX(1,1)=T1+1.0
      AMATRX(1,2)=S1
      AMATRX(1,3)=T2+1.0
      AMATRX(1,4)=S2
      AMATRX(2,1)=S1
      AMATRX(2,2)=-T1-1.0
      AMATRX(2,3)=S2
      AMATRX(2,4)=-T2-1.0
      AMATRX(3,1)=1.0-T1
      AMATRX(3,2)=-S1
      AMATRX(3,3)=1.0-T2
      AMATRX(3,4)=-S2
      AMATRX(4,1)=S1
      AMATRX(4,2)=1.0-T1
      AMATRX(4,3)=S2
      AMATRX(4,4)=1.0-T2
      CALL SIMULT (AMATRX,BMATRX,4,J)
      IF (J.EQ.1) WRITE (2,170)
      A1(M)=BMATRX(1)+COMPLX*BMATRX(2)
      A2(M)=BMATRX(3)+COMPLX*BMATRX(4)
80    CONTINUE
C
      PX=2.0*PI*AIMAG(COMPLX*DIA*CNEG(1)/2.0)
      PY=2.0*PI*REAL(COMPLX*DIA*CNEG(1)/2.0)
C
      AMATRX(1,1)=T1
      AMATRX(1,2)=S1
      AMATRX(1,3)=T2
      AMATRX(1,4)=S2
      AMATRX(2,1)=0.0
      AMATRX(2,2)=1.0
      AMATRX(2,3)=0.0
      AMATRX(2,4)=1.0
      AMATRX(3,1)=2.0*S1*T1
      AMATRX(3,2)=S1*S1-T1*T1
      AMATRX(3,3)=2.0*S2*T2
      AMATRX(3,4)=S2*S2-T2*T2
      AMATRX(4,1)=-T1/(S1*S1+T1*T1)
      AMATRX(4,2)=S1/(S1*S1+T1*T1)
      AMATRX(4,3)=-T2/(S2*S2+T2*T2)
      AMATRX(4,4)=S2/(S2*S2+T2*T2)
      BMATRX(1)=PX/(4.0*PI)
      BMATRX(2)=-PY/(4.0*PI)
      BMATRX(3)=(S(1,2)*PY+S(1,3)*PX)/(4.0*PI*S(1,1))
      BMATRX(4)=-(S(1,2)*PX+S(2,3)*PY)/(4.0*PI*S(2,2))
      CALL SIMULT (AMATRX,BMATRX,4,J)
      IF (J.EQ.1) WRITE (2,180)
      AK1=BMATRX(1)+COMPLX*BMATRX(2)
      AK2=BMATRX(3)+COMPLX*BMATRX(4)
      NUMPT=1
      IF (IANG.EQ.0) GO TO 90
      NUMPT=((IHIGH-ILOW)/IANG)+1
```

```
90    CONTINUE
      ALPHA=-ALPHA*PI/180.0
      ALPH=-ALPHA
      DO 160 JJ=1,NUMSTP
      DO 150 NN=1,NUMPT
      U(JJ,NN)=0.0
      V(JJ,NN)=0.0
      NNN=NN-1
      JJJ=JJ-1
      THETA=(NNN*IANG+ILOW)*PI/180.0
      RADIUS=JJJ*STPINK+DIA/2.0
C----------------------------------------------------------------------
C  CALCULATE X AND Y COORDINATES OF POINTS AROUND LOADED HOLE         -
C----------------------------------------------------------------------
      X=RADIUS*COS(THETA+ALPHA)
      Y=RADIUS*SIN(THETA+ALPHA)
C----------------------------------------------------------------------
C  CALCULATE PARAMETERS FOR LOADED HOLE EQUATIONS                     -
C----------------------------------------------------------------------
      Z1=X+R1*Y
      Z2=X+R2*Y
      Z=X+COMPLX*Y
C----------------------------------------------------------------------
C     MAPPING FUNCTION                                                -
C----------------------------------------------------------------------
      XXI1=CSQRT(Z1*Z1-DIA*DIA/4.0-R1*R1*DIA*DIA/4.0)
      XXI2=CSQRT(Z2*Z2-DIA*DIA/4.0-R2*R2*DIA*DIA/4.0)
C----------------------------------------------------------------------
C  CHOOSE THE CORRECT SIGN OF CSQRT                                   -
C----------------------------------------------------------------------
100   CONTINUE
      XI1=Z1+XXI1
      XI2=Z2+XXI2
      XI1=2.0*XI1/(DIA*(1.0-COMPLX*R1))
      XI2=2.0*XI2/(DIA*(1.0-COMPLX*R2))
      COX1=REAL(XI1)*REAL(XI1)+AIMAG(XI1)*AIMAG(XI1)
      COX2=REAL(XI2)*REAL(XI2)+AIMAG(XI2)*AIMAG(XI2)
      IF (COX1.GE.0.99999) GO TO 110
      XXI1=-XXI1
      GO TO 100
110   CONTINUE
      IF (COX2.GE.0.99999) GO TO 120
      XXI2=-XXI2
      GO TO 100
120   CONTINUE
      XXI1=XI1
      XXI2=XI2
C----------------------------------------------------------------------
C  CALCULATE PHI PRIME                                                -
C----------------------------------------------------------------------
      COM1=(0.0,0.0)
      COM2=(0.0,0.0)
      DO 130 M=1,45
      COM1=COM1+M*A1(M)*XI1**(-1*M)
      COM2=COM2+M*A2(M)*XI2**(-1*M)
130   CONTINUE
C----------------------------------------------------------------------
C     CHECK SIGN OF CSQRT                                             -
C----------------------------------------------------------------------
      XI1=CSQRT(Z1*Z1-DIA*DIA/4.0-DIA*DIA*R1*R1/4.0)
      XI2=CSQRT(Z2*Z2-DIA*DIA/4.0-DIA*DIA*R2*R2/4.0)
      CHECK1=Z1/XI1
      CHECK2=Z2/XI2
      IF (REAL(CHECK1).LT.-0.00001) XI1=-1.0*XI1
      IF (REAL(CHECK2).LT.-0.00001) XI2=-1.0*XI2
      PHI1=(AK1-COM1)/XI1
      PHI2=(AK2-COM2)/XI2
C----------------------------------------------------------------------
C  CALCULATE STRESS COMPONENTS IN LAMINATE AT COORDINATES X,Y         -
C----------------------------------------------------------------------
      STRX=2.0*REAL(R1*R1*PHI1+R2*R2*PHI2)
      STRY=2.0*REAL(PHI1+PHI2)
      STRXY=-2.0*REAL(R1*PHI1+R2*PHI2)
      STRESS(1,JJ,NN)=STRX*COS(ALPH)*COS(ALPH)+STRY*SIN(ALPH)*SIN(ALPH)-
     12.0*STRXY*SIN(ALPH)*COS(ALPH)
      STRESS(2,JJ,NN)=STRX*SIN(ALPH)*SIN(ALPH)+STRY*COS(ALPH)*COS(ALPH)+
```

```
     12.0*STRXY*SIN(ALPH)*COS(ALPH)
      STRESS(3,JJ,NN)=STRX*SIN(ALPH)*COS(ALPH)-STRY*SIN(ALPH)*COS(ALPH)+
     1STRXY*(COS(ALPH)*COS(ALPH)-SIN(ALPH)*SIN(ALPH))
C-----------------------------------------------------------------------
C  CALCULATE DISPLACEMENTS                                             -
C-----------------------------------------------------------------------
      XI1=XXI1
      XI2=XXI2
      COM1=(0.0,0.0)
      COM2=(0.0,0.0)
      DO 140 M=1,45
      COM1=COM1+A1(M)*XI1**(-1*M)
      COM2=COM2+A2(M)*XI2**(-1*M)
140   CONTINUE
      XXI1=CLOG(XI1)
      XXI2=CLOG(XI2)
      PHI1=AK1*XXI1+COM1
      PHI2=AK2*XXI2+COM2
      U(JJ,NN)=2.0*REAL(P1*PHI1+P2*PHI2)
      V(JJ,NN)=2.0*REAL(Q1*PHI1+Q2*PHI2)
150   CONTINUE
160   CONTINUE
C-----------------------------------------------------------------------
      RETURN
170   FORMAT (41H SIMULT CALCULATES A SINGULAR SET OF EQS.)
180   FORMAT (41H SIMULT CALCULATES A SINGULAR SET OF EQS.)
      END
      SUBROUTINE PLYSTR (IFAIL)
C=======================================================================
C     TRANSFORMS LAMINATE STRAINS TO PLY STRESSES/STRAINS BY ASSU      =
C     CONSTANT STRAIN THROUGH THE THICKNESS                            =
C=======================================================================
      COMMON /ONE/ E1(3),E2(3),G12(3),V12(3)
      COMMON /TWO/ IOUT(15),NUMPLY,NUMMAT,ANG(8),PLYTHK(8),MATID(8)
      COMMON /THREE/ IANG,ILOW,IHIGH,STPINK,NUMSTP
      COMMON /EIGHT/ STRESS(3,20,91),STRAIN(3,20,91)
      COMMON /NINE/ STR1(8,20,91),STR2(8,20,91),STR12(8,20,91)
      INTEGER IANG,ILOW,IHIGH
      DATA NUMPT/1/,PI/3.1415926535/
C-----------------------------------------------------------------------
C  CALCULATE THE STRAINS                                               -
C-----------------------------------------------------------------------
      MOVE=0
      IF (IANG.EQ.0) GO TO 10
      NUMPT=((IHIGH-ILOW)/IANG)+1
10    CONTINUE
      IF (PUTOUT(IOUT,7).EQ.2.) WRITE (2,60)
20    CONTINUE
      DO 30 JJ=1,NUMSTP
      DO 30 NN=1,NUMPT
      DO 30 L=1,NUMPLY
      D=ANG(L)*PI/180.0
      STRANX=STRAIN(1,JJ,NN)
      STRANY=STRAIN(2,JJ,NN)
      GAMA=STRAIN(3,JJ,NN)
C-----------------------------------------------------------------------
      STRAN1=STRANX*COS(D)*COS(D)
      STRAN2=STRANY*SIN(D)*SIN(D)
      GAMA12=GAMA*SIN(D)*COS(D)
      STR1(L,JJ,NN)=STRAN1+STRAN2+GAMA12
      STRAN1=STRANX*SIN(D)*SIN(D)
      STRAN2=STRANY*COS(D)*COS(D)
      GAMA12=-1.0*GAMA*SIN(D)*COS(D)
      STR2(L,JJ,NN)=STRAN1+STRAN2+GAMA12
      STRAN1=-2.0*STRANX*SIN(D)*COS(D)
      STRAN2=2.0*STRANY*SIN(D)*COS(D)
      GAMA12=GAMA*COS(D)*COS(D)-GAMA*SIN(D)*SIN(D)
      STR12(L,JJ,NN)=STRAN1+STRAN2+GAMA12
      ANGLE=(NN-1)*IANG+ILOW
      DIST=(JJ-1)*STPINK
C     IF (DIST.LE.0.0005) DIST=0.001
      IF (PUTOUT(IOUT,7).EQ.2.) WRITE (2,70) DIST,ANGLE,ANG(L),STR1(L,JJ
     1,NN),STR2(L,JJ,NN),STR12(L,JJ,NN)
30    CONTINUE
      IF (MOVE.EQ.1) GO TO 50
C-----------------------------------------------------------------------
```

```
C  CALCULATE THE STRESS IN EACH PLY                                       -
C-------------------------------------------------------------------------
      IF (PUTOUT(IOUT,8).EQ.2.0) WRITE (2,80)
      DO 40  JJ=1,NUMSTP
      DO 40  NN=1,NUMPT
      DO 40  L=1,NUMPLY
      M=MATID(L)
      V21=V12(M)*E2(M)/E1(M)
      DEN=1.0-V12(M)*V21
      ABC=STR2(L,JJ,NN)/DEN
      BCA=STR1(L,JJ,NN)
      STR1(L,JJ,NN)=E1(M)*STR1(L,JJ,NN)/DEN+V12(M)*E2(M)*ABC
      STR2(L,JJ,NN)=V12(M)*E2(M)*BCA/DEN+E2(M)*ABC
      STR12(L,JJ,NN)=STR12(L,JJ,NN)*G12(M)
      ANGLE=(NN-1)*IANG+ILOW
      DIST=(JJ-1)*STPINK
C     IF (DIST.LE.0.0005)  DIST=0.001
      IF (PUTOUT(IOUT,8).EQ.2.0)  WRITE (2,90) DIST,ANGLE,ANG(L),STR1(L,J
     1J,NN),STR2(L,JJ,NN),STR12(L,JJ,NN)
40    CONTINUE
      MOVE=1
      IF (IFAIL.EQ.1) GO TO 20
50    CONTINUE
C-------------------------------------------------------------------------
      RETURN
60    FORMAT (///,20(1H-),19H PLY-BY-PLY STRAIN ,20(1H-),//,8HDISTANCE,2
     1X,5HANGLE,4X,3HPLY,7X,5HEPS-1,7X,5HEPS-2,6X,6HEPS-12,/)
70    FORMAT (F7.3,F8.2,F8.1,3F12.6)
80    FORMAT (///,20(1H-),19H PLY-BY-PLY STRESS ,20(1H-),//,2X,4HDIST,4X
     1,5HANGLE,4X,3HPLY,7X,5HSIG-1,7X,5HSIG-2,6X,6HSIG-12,/)
90    FORMAT (F7.3,F8.2,F8.1,3F12.1)
      END
      SUBROUTINE FAIL
C=========================================================================
C  POINT STRESS/STRAIN ANALYSIS FOR FAILURE USING UNIDIRECTION           =
C  MATERIAL ALLOWABLES                                                   =
C=========================================================================
      COMMON /TWO/ IOUT(15),NUMPLY,NUMMAT,ANG(8),PLYTHK(8),MATID(8)
      COMMON /THREE/ IANG,ILOW,IHIGH,STPINK,NUMSTP
      COMMON /FOUR/ PX,PY,PXY,P,PW,ALPHA,BETA,DIA,CORREC
      COMMON /FIVE/ FXT(3),FXC(3),FYT(3),FYC(3),FXY(3),IFAIL
      COMMON /NINE/ STR1(8,20,91),STR2(8,20,91),STR12(8,20,91)
      INTEGER IANG,ILOW,IHIGH
      DIMENSION PLYFAL(3,8),FAILS(3,8),RTO(3,8),PLYRTO(3,8)
C-------------------------------------------------------------------------
      IF (PUTOUT(IOUT,9).NE.2.) GO TO 20
      IF (IFAIL.GT.2) GO TO 10
      WRITE (2,210)
      GO TO 20
10    CONTINUE
      WRITE (2,220)
20    CONTINUE
      CHECK=0.0
      KKK=1
      F2=0.0
      F3=0.0
      NUMPT=1
      IF (IANG.EQ.0) GO TO 30
      NUMPT=((IHIGH-ILOW)/IANG)+1
30    CONTINUE
      DO 140  JJ=1,NUMSTP
      DO 140  KK=1,NUMPT
      SIG=1.0
      DO 130  II=1,NUMPLY
      X=STR1(II,JJ,KK)
      Y=STR2(II,JJ,KK)
      XY=STR12(II,JJ,KK)
      MATII=MATID(II)
      GO TO (40,40,50,60,70), IFAIL
C-------------------------------------------------------------------------
C  MAXIMUM STRESS/STRAIN CRITERIA                                         -
C-------------------------------------------------------------------------
40    CONTINUE
      FX=FXT(MATII)
      IF (X.LT.0.0)  FX=FXC(MATII)
      FY=FYT(MATII)
```

```
      IF (Y.LT.0.0)  FY=FYC(MATII)
      F1=X/FX
      F2=Y/FY
      F3=XY/FXY(MATII)
      GO TO 80
C-----------------------------------------------------------------------
C     TSAI-HILL CRITERIA                                               -
C-----------------------------------------------------------------------
50    CONTINUE
      FX=FXT(MATII)
      IF (X.LT.0.0)  FX=FXC(MATII)
      FY=FYT(MATII)
      IF (Y.LT.0.0)  FY=FYC(MATII)
      F1=X*X/(FX*FX)+Y*Y/(FY*FY)-X*Y/(FX*FX)+XY*XY/(FXY(MATII)*FXY(MATII
     1))
      RTOX=(X/FX)/SQRT(F1)
      RTOY=(Y/FY)/SQRT(F1)
      RTOXY=(XY/FXY(MATII))/SQRT(F1)
      GO TO 80
C-----------------------------------------------------------------------
C  MODIFIED TSAI-WU CRITERIA                                           -
C-----------------------------------------------------------------------
60    CONTINUE
      F1=1.0/FXT(MATII)-1.0/FXC(MATII)
      F2=1.0/FYT(MATII)-1.0/FYC(MATII)
      F11=1.0/(FXT(MATII)*FXC(MATII))
      F22=1.0/(FYT(MATII)*FYC(MATII))
      F66=1.0/(FXY(MATII)*FXY(MATII))
      F1=F1*X+F2*Y+F11*X*X+F22*Y*Y+F66*XY*XY
      FX=FXT(MATII)
      IF (X.LT.0.0)  FX=FXC(MATII)
      FY=FYT(MATII)
      IF (Y.LT.0.0)  FY=FYC(MATII)
      F1=ABS(F1)
      RTOX=(X/FX)/SQRT(F1)
      RTOY=(Y/FY)/SQRT(F1)
      RTOXY=(XY/FXY(MATII))/SQRT(F1)
      GO TO 80
C-----------------------------------------------------------------------
C     HOFFMAN FAILURE CRITERIA                                         -
C-----------------------------------------------------------------------
70    CONTINUE
      F1=1.0/FXT(MATII)-1.0/FXC(MATII)
      F2=1.0/FYT(MATII)-1.0/FYC(MATII)
      F11=1.0/(FXT(MATII)*FXC(MATII))
      F22=1.0/(FYT(MATII)*FYC(MATII))
      F66=1.0/(FXY(MATII)*FXY(MATII))
      F12=-1.0/(FXT(MATII)*FXC(MATII))
      F1=F1*X+F2*Y+F11*X*X+F22*Y*Y+F12*X*Y+F66*XY*XY
      FX=FXT(MATII)
      IF (X.LT.0.0)  FX=FXC(MATII)
      FY=FYT(MATII)
      IF (Y.LT.0.0)  FY=FYC(MATII)
      F1=ABS(F1)
      RTOX=(X/FX)/SQRT(F1)
      RTOY=(Y/FY)/SQRT(F1)
      RTOXY=(XY/FXY(MATII))/SQRT(F1)
      GO TO 80
80    CONTINUE
      ANGLE=(KK-1)*IANG+ILOW
      DIST=(JJ-1)*STPINK
C     IF (DIST.LE.0.0005) DIST=0.001
      IF (IFAIL.GT.2) GO TO 90
      IF (PUTOUT(IOUT,9).EQ.2.) WRITE (2,230) DIST,ANGLE,ANG(II),F1,F2,F
     13
      GO TO 100
90    CONTINUE
      IF (PUTOUT(IOUT,9).EQ.2.) WRITE (2,240) DIST,ANGLE,ANG(II),F1,RTOX
     1,RTOY,RTOXY
100   CONTINUE
C-----------------------------------------------------------------------
C  AUTOMATIC SEARCH FOR FAILURE                                        -
C-----------------------------------------------------------------------
      IF (SIG.EQ.2.) FAILS(1,II)=F1
      IF (SIG.EQ.2.) FAILS(2,II)=F2
      IF (SIG.EQ.2.) FAILS(3,II)=F3
```

```
      IF (SIG.EQ.2.) RTC(1,II)=RTOX
      IF (SIG.EQ.2.) RTC(2,II)=RTOY
      IF (SIG.EQ.2.) RTC(3,II)=RTOXY
      IF (JJ.NE.2) GO TO 120
      PLYFAL(1,II)=F1
      PLYFAL(2,II)=F2
      PLYFAL(3,II)=F3
      PLYRTO(1,II)=RTOX
      PLYRTO(2,II)=RTOY
      PLYRTO(3,II)=RTOXY
      CHK=CHECK
      IF (ABS(CHECK).LT.ABS(F1)) CHECK=F1
      IF (ABS(CHECK).LT.ABS(F2)) CHECK=F2
      IF (ABS(CHECK).LT.ABS(F3)) CHECK=F3
      IF (CHECK.EQ.CHK) GO TO 120
      KKK=KK
      III=II
      SIG=2.0
      DO 110 M=1,III
      DO 110 N=1,3
      FAILS(N,M)=PLYFAL(N,M)
      RTC(N,M)=PLYRTC(N,M)
110   CONTINUE
120   CONTINUE
130   CONTINUE
140   CONTINUE
C
      IF (CHECK.EQ.0.0) GO TO 190
      IF (IFAIL.EQ.1) CORREC=1.0/ABS(CHECK)
      IF (IFAIL.EQ.2) CORREC=1.0/ABS(CHECK)
      IF (IFAIL.EQ.3) CORREC=1.0/SQRT(CHECK)
      IF (IFAIL.EQ.4) CORREC=1.0/SQRT(CHECK)
      IF (IFAIL.EQ.5) CORREC=1.0/SQRT(CHECK)
      WRITE (2,200) CORREC
      IF (PUTOUT(IOUT,10).NE.2.) GO TO 180
      IF (CORREC.LT..999.OR.CORREC.GT.1.001) GO TO 180
      ANGLE=(KKK-1)*IANG+ILOW
      IF (IFAIL.GT.2) GO TO 160
      WRITE (2,250) PX,PY,PXY,P
C-----------------------------------------------------------------------
      DO 150 I=1,NUMPLY
      WRITE (2,260) STPINK,ANGLE,ANG(I),FAILS(1,I),FAILS(2,I),FAILS(3,I)
150   CONTINUE
      GO TO 190
C-----------------------------------------------------------------------
160   CONTINUE
      WRITE (2,270) PX,PY,PXY,P
      DO 170 I=1,NUMPLY
      WRITE (2,280) STPINK,ANGLE,ANG(I),FAILS(1,I),RTO(1,I),RTO(2,I),RTO
     1(3,I)
170   CONTINUE
180   CONTINUE
190   CONTINUE
      IF (PUTOUT(IOUT,10).NE.2.) CORREC=1.0
C-----------------------------------------------------------------------
      RETURN
200   FORMAT (/,5X,34HFAILURE LOAD MAGNIFICATION FACTOR:,F9.4)
210   FORMAT (//,10(1H-),26H FAILURE CRITERIA PER PLY ,10(1H-),//,15H
     1DIST      ANG,8H      PLY,12X,15HFAILURE NUMBERS,/,35X,23H1
     22          SHEAR)
220   FORMAT (//,18(1H-),26H FAILURE CRITERIA PER PLY ,18(1H-),//,8HDIST
     1ANCE,2X,5HANGLE,4X,3HPLY,4X,7HFAILURE,7X,14HFAILURE RATIOS,/,27X,6
     2HNUMBER,6X,1H1,7X,1H2,6X,5HSHEAR,//)
230   FORMAT (F7.3,F8.2,F8.1,3F12.1)
240   FORMAT (F7.3,F8.2,F8.1,4F9.3)
250   FORMAT (//,10X,29HAUTOMATIC SEARCH FOR FAILURE:,//,25X,16HFAILURE
     1STRESSES,/,18X,2HPX,10X,2HPY,10X,3HPXY,10X,1HP/,11X,4F12.1,//,8X,4
     24HDISTANCE   ANGLE     PLY     FAILURE NUMBERS,/,36X,19H1         2
     3     SHEAR)
260   FORMAT (F11.3,F9.2,F10.2,3F8.3)
270   FORMAT (//10X,29HAUTOMATIC SEARCH FOR FAILURE://,25X,16HFAILURE ST
     1RESSES,/,18X,2HPX,10X,2HPY,10X,3HPXY,10X,1HP,/,11X,4F12.1,//,6X,33
     2HDISTANCE   ANGLE   PLY     FAILURE,9X,14HFAILURE RATIOS,/,35X,6HNU
     3MBER,7X,1H1,9X,1H2,7X,5HSHEAR)
280   FORMAT (F11.3,F9.2,F10.2,4F10.3)
      END
```

```
      SUBROUTINE SIMULT (A,B,N,KS)
C=====================================================================
C     TEST FOR ALGORITHMIC SINGULARITY ADDED 01/10/79                 =
C     MACHINE EPSILON FOR CYBER SINGLE PRECISION                      =
C=====================================================================
      DIMENSION A(1),B(1)
      DATA EPS/7.11E-15/
C---------------------------------------------------------------------
      TOL=3.18*EPS*(N-1)
      BETA=0.0
      KS=0
      JJ=-N
      DO 80 J=1,N
      JY=J+1
      JJ=JJ+N+1
      BIGA=0.0
      IT=JJ-J
      DO 20 I=J,N
      IJ=IT+I
      IF (ABS(BIGA)-ABS(A(IJ))) 10,20,20
10    BIGA=A(IJ)
      IMAX=I
20    CONTINUE
      IF (ABS(BIGA).GT.BETA) BETA=ABS(BIGA)
      IF (ABS(BIGA)-TOL*BETA) 30,30,40
30    KS=1
      RETURN
40    I1=J+N*(J-2)
      IT=IMAX-J
      DO 50 K=J,N
      I1=I1+N
      I2=I1+IT
      SAVE=A(I1)
      A(I1)=A(I2)
      A(I2)=SAVE
50    A(I1)=A(I1)/BIGA
      SAVE=B(IMAX)
      B(IMAX)=B(J)
      B(J)=SAVE/BIGA
      IF (J-N) 60,90,60
60    IQS=N*(J-1)
      DO 80 IX=JY,N
      IXJ=IQS+IX
      IT=J-IX
      DO 70 JX=JY,N
      IXJX=N*(JX-1)+IX
      JJX=IXJX+IT
70    A(IXJX)=A(IXJX)-(A(IXJ)*A(JJX))
80    B(IX)=B(IX)-(B(J)*A(IXJ))
90    NY=N-1
      IT=N*N
      DO 100 J=1,NY
      IA=IT-J
      IB=N-J
      IC=N
      DO 100 K=1,J
      B(IB)=B(IB)-A(IA)*B(IC)
      IA=IA-N
100   IC=IC-1
      RETURN
      END
```

```
      SUBROUTINE ROOTS (XCOF,COF,M,ROOTR,ROOTI,IER)
C=========================================================================
C                                                                        =
C=========================================================================
      DIMENSION XCOF(M),COF(M),ROOTR(M),ROOTI(M)
      REAL*8 XO,YO,X,Y,XPR,YPR,UX,UY,V,YT,XT,U
     1 ,XT2,YT2,SUMSQ,DX,DY,TEMP,ALPHA,FI,RMPREC,TOL
C     RELATIVE MACHINE PRECISION (TEST FOR *ALMOST ZERO*)
      DATA RMPREC/1.0D-14/,TOL/1.0D-4/
      IFIT=0
      N=M
      IER=0
      IF (XCOF(N+1)) 10,30,10
10    IF (N) 20,20,50
20    IER=1
      GO TO 290
30    IER=4
      GO TO 290
40    IER=2
      GO TO 290
50    IF (N-36) 60,60,40
60    NX=N
      NXX=N+1
      N2=1
      KJ1=N+1
      DO 70 L=1,KJ1
      MT=KJ1-L+1
70    COF(MT)=XCOF(L)
80    XO=0.00500101D0
      YO=0.01000101D0
      IN=0
90    X=XO
      XO=-10.0D0*YO
      YO=-10.0D0*X
      X=XO
      Y=YO
      IN=IN+1
      GO TO 110
100   IFIT=1
      XPR=X
      YPR=Y
110   ICT=0
120   UX=0.0D0
      UY=0.0D0
      V=0.0D0
      YT=0.0D0
      XT=1.0D0
      U=COF(N+1)
      IF (DABS(U).LE.RMPREC) GO TO 230
      DO 130 I=1,N
      L=N-I+1
      TEMP=COF(L)
      XT2=X*XT-Y*YT
      YT2=X*YT+Y*XT
      U=U+TEMP*XT2
      V=V+TEMP*YT2
      FI=I
      UX=UX+FI*XT*TEMP
      UY=UY-FI*YT*TEMP
      XT=XT2
130   YT=YT2
      SUMSQ=UX*UX+UY*UY
      IF (SUMSQ.LE.RMPREC) GO TO 190
      DX=(V*UY-U*UX)/SUMSQ
      X=X+DX
      DY=-(U*UY+V*UX)/SUMSQ
      Y=Y+DY
      IF (DABS(DY)+DABS(DX).LE.TOL) GO TO 170
      ICT=ICT+1
      IF (ICT-500) 120,140,140
140   IF (IFIT) 170,150,170
150   IF (IN-5) 90,160,160
160   IER=3
      GO TO 290
170   DO 180 L=1,NXX
      MT=KJ1-L+1
```

```
      RTEMP=XCOF(MT)
      XCOF(MT)=COF(L)
180   COF(L)=RTEMP
      ITEMP=N
      N=NX
      NX=ITEMP
      IF (IFIT) 210,100,210
190   IF (IFIT) 200,90,200
200   X=XPR
      Y=YPR
      GO TO 170
210   IFIT=0
      IF (DABS(Y)-1.0D-4*DABS(X)) 240,220,220
220   ALPHA=X+X
      SUMSQ=X*X+Y*Y
      N=N-2
      GO TO 250
230   X=0.0D0
      NX=NX-1
      NXX=NXX-1
240   Y=0.D0
      SUMSQ=0.D0
      ALPHA=X
      N=N-1
250   COF(2)=COF(2)+ALPHA*COF(1)
      DO 260 L=2,N
260   COF(L+1)=COF(L+1)+ALPHA*COF(L)-SUMSQ*COF(L-1)
270   ROOTI(N2)=Y
      ROOTR(N2)=X
      N2=N2+1
      IF (SUMSQ.LE.RMPREC) GO TO 280
      Y=-Y
      SUMSQ=0.D0
      GO TO 270
280   IF (N.GT.0) GO TO 80
290   RETURN
      END
```

LIST OF REFERENCES

1. Timoshenko, S.P. and Goodier, A.A., Theory of Elasticity, 2nd ed., McGraw-Hill Book Co., New York, 1951.

2. Air Force Materials Laboratory Technical Report 72-15, Analytical Investigation of Stress Concentrations Due to Holes in Fiber Reinforced Plastic Laminated Plates, Two-Dimensional Models, by E.F. Rybicki and A.T. Hopper, (AD A775 732), Battelle Columbus Laboratories, Columbus, Ohio, March 1972.

3. Kirsch, G., "Die Theorie der Elastizitat und Die Bedurfnisse Der Festiqkeitslehre," Zeitschrift Verein Deutscher Ingenieure, v. 32, pp. 797-807, July 1898.

4. Howland, R.C.J., "On the Stresses in the Neighbourhood of a Circular Hole in a Strip Under Tension," Philosophical Transactions of the Royal Society (London), Series A, v. 229, pp. 49-86, January, 1930.

5. Levy, S., Wolley, R.M. and Kroll, W.D., "Instability of Simply Supported Square Plate with Reinforced Circular Hole in Edge Compression," Journal of Research of the National Bureau of Standards, Report Paper 1849, v. 39, p. 571, December 1947.

6. Lekhnitskii, S.G., Anisotropic Plates, Gordon and Breach, New York, 1968.

7. NASA Technical Translation TT F-607, Stress Distribution Around Holes, by G.N. Savin, Translation of "Raspredeleniye Napryazheniy Okolo Otverstiy," "Naukova Dumka" Press, Kiev 1968.

8. Air Force Wright Aeronautical Laboratories Technical Report 81-3041, Effect of Variances and Manufacturing Tolerances on the Design Strength and Life of Mechanically Fastened Composite Joints, by S.P. Garbo and J.M. Ogonowski, v. 1-3, April 1981.

9. Greszczuk, L. B. "Stress Concentrations and Failure Criteria for Orthotropic and Anisotropic Plates with Circular Openings," Composite Materials: Testing and Design (Second Conference), ASTM STP 479, American Society for Testing Materials, pp. 363-381, 1972.

10. Air Force Materials Laboratory Technical Report 76-92, Three Dimensional Finite Element Stress Analysis of Laminated Plates Containing a Circular Hole, by E.F. Rybicki and D.W. Schmueser, Battelle Columbus Laboratories, June 1976.

11. Kocher, L.H. and Cross, S.L., "Reinforced Cutouts in Graphite Composite Structures," Composite Materials: Testing and Design (Second Conference), ASTM STP 497, American Society for Testing and Materials, pp. 382-395, 1972.

12. McKenzie, D.O., The Analysis of Reinforced Holes in Carbon Fibre Plates, Ph.D. Thesis, University of Bristol, U.K., February 1976.

13. Daniel, I.M., Rowlands, R.E. and Whiteside, J.B., "Effects of Material and Stacking Sequence on Behavior of Composite Plates with Holes," Experimental Mechanics, v. 13, pp. 1-9, January 1974.

14. Rowlands, R.E. Daniel, I.M. and Whiteside, J.B., "Geometric and Loading Effects on Strength of Composite Plates with Cutouts," Composite Materials: Testing and Design (Third Conference), ASTM STP 546, American Society for Testing and Materials, p. 361, 1974.

15. Daniel, I.M., Rowlands, R.E. and Whiteside, J.B., "Deformation and Failure of Boron-Epoxy Plate with Circular Hole," Analysis of the Test Methods for High Modulus Fibers and Composites, ASTM STP 521, American Society for Testing and Materials, August 1973.

16. Air Force Wright Aeronautical Laboratories Technical Report 73-48, The Behavior of Advanced Filamentary Composite Plates with Cutouts, by J.B. Whiteside, I.M. Daniel and R.E. Rowlands, (AD A764 362), June 1973.

17. Rowlands, R.E., Daniel, I.M. and Whiteside, J.B., "Stress and Failure Analysis of a Glass-Epoxy Composite Plate with a Circular Hole," Proceedings of the Society for Experimental Stress Analysis, v. XXX, No. 1, pp. 31-37, 1973.

18. Knauss, J.F., Starnes, J.H. and Henneke, E.G., The Compressive Failure of Graphite/Epoxy Plates with Circular Holes, Virginia Polytechnic Institute and State University, Blacksburg, VA, February 1978.

19. Herman, R., Postbuckling Behavior of Graphite/Epoxy Cloth Shear Panels with 45 Degree Flanged Lighting Holes, M.S. Thesis, Naval Postgraduate School, Monterey, California, March 1982.

20. O'Neill, G.S., Asymmetric Reinforcement of a Quasi-Isotropic Graphite-Epoxy Plate Containing a Circular Hole, M.S. and A.Eng. Thesis, Naval Postgraduate School, Monterey, California, June 1982.

21. Pickett, D.H. and Sullivan, P.D., Analysis of Symmetric Reinforcement of Quasi-isotropic Graphite/Epoxy Plates with a Circular Cutout Under Uniaxial Tensile Loading, M.S. Thesis, Naval Postgraduate School, Monterey, California, December 1983.

22. Bank, M.H., Sullivan, P.D., O'Neill, G.S. and Pickett, D.H., An Analysis of Graphite/Epoxy Panels with Reinforced Circular Cutouts Under Tensile Loading, Proceedings of the Twelfth Southeastern Conference On Theoretical and Applied Mechanics (SECTAM XII), Callaway Gardens, GA, 10 May 1984.

23. Ashton, J.E., Haplin, J.C. and Petit, P.H., Primer on Composite Materials, Technomic Publishing Co., Westport, CN, 1969.

24. Tsai, S.W. and Hahn, T.H., Introduction to Composite Materials, Technomic Publishing Co., Westport, CN, 1980.

25. National Aeronautics and Space Administration Technical Paper 1469, Stress-Concentration Factors for Finite Orthotropic Laminates with a Circular Hole and Uniaxial Loading, by C.S. Hong and J.H. Crews Jr., May 1979.

26. Whitney, J.M. and Nuismer, R.J., "Stress Fracture Criteria for Laminated Composites Containing Stress Concentrations," Journal of Composite Materials, v. 8, pp. 253-256, July 1974.

27. Nuismer, R.J. and Whitney, J.M., "Uniaxial Failure of Composite Laminates Containing Stress Concentrations," Fracture Mechanics of Composites, ASTM STP 593, American Society for Testing and Materials, pp. 117-142, 1975.

28. Watson, J.C., "AV-8B Composite Fuselage Design," Journal of Aircraft, v. 19, no. 3, p. 235, March 1982.

29. Bailie, J.A., Woven Fabric Aerospace Structures, private communication, November 1982.

30. Dally, J.W. and Riley, W.F., Experimental Stress Analysis, McGraw-Hill Co., New York, 1965.

31. Konish, H.J. and Whitney, J.M., "Approximate Stresses in an Orthotropic Plate Containing a Circular Hole," Journal of Composite Materials, v. 9, pp. 157-166, January 1979.

32. Peterson, R.E., Stress Concentration Factors, Wiley-Interscience, New York, 1974.

33. Nuismer, R.J. and Labor, J.D., "Applications of the Average Stress Failure Criterion: Part II - Compression," Journal of Composite Materials, v. 13, pp. 49-60, January 1979.

34. Tang, S., "Interlaminar Stresses around Circular Cutouts in Composite Plates Under Tension," AIAA Journal, v. 15, pp. 1631-1637, November 1977.

35. Air Force Materials Laboratory Technical Report 73-100, Analytical Investigation of Stress Concentrations Due to Holes in Fiber Reinforced Plastic Laminated Plates, Three-Dimensional Models, by E.F. Rybicki and A.T. Hopper, Battelle Columbus Laboratories, Columbus, Ohio, June 1973.

36. Hsu, P.W. and Herakovich, C.T., "A Perturbation Solution for Inter-Laminar Stress in Composite Laminates," Composite Materials: Testing and Design (Fourth Conference), ASTM 617, American Society for Testing and Materials, 1976.

37. Advisory Group for Aerospace Research and Development, Lecture Series No. 124., Practical Considerations of Design, Fabrication and Tests for Composite Materials, "Micromechanical Models for the Stiffness and Strength of Composite Materials" and "Introduction to Thin Laminate Theory," by R.B. Pipes, AGARD-LS-124, (AD A123 450), 1982.

38. Love, A.E.H., A Treatise on the Mathematical Theory of Elasticity, 4th ed., Dover, New York, 1944.

39. Feynman, R.P., Leighton, R.B. and Sands, M., The Feynman Lectures on Physics, Addison-Wesley Publishing Co., Reading, MA, 1964.

40. Jones, R.M., "Stress-Strain Relations for Materials with Different Modulii in Tension and Compression," AIAA Journal, v. 15, pp. 16-25, January 1977.

41. Garbo, S.P. and Ogonowski, J.M., "Strength Predictions of Composite Laminates with Unloaded Fastener Holes," AIAA Journal, v. 18, pp. 585-589, May 1980.

42. Cook, R.D., Concepts and Applications of Finite Element Analysis, 2nd ed., John Wiley & Sons, New York, 1981.

43. Zienkiewicz, O.C., The Finite Element Method in Engineering Science, McGraw-Hill, London, 1971.

44. Ferguson, G.H., Cyr, N., DIAL User's Manual, Lockheed Missiles and Space Co., Sunnyvale, CA, 1982.

45. "Accurate Strain Gage Measurements at Stress Concentrations," Epsilonics, Measurements Group, Inc., P.O. Box 27777, Raleigh, NC 27611, v. 1, pp. 10-11, July 1982.

46. Measurements Group, Inc., Technical Note 502, Optimizing Strain Gage Excitation Levels, Raleigh, NC 27777, 1979.

47. Measurements Group, Inc., Catalog 200, Gage Listing Section, Raleigh, NC 27777, June 1981.

48. Measurements Group, Inc., Technical Tip 603, The Proper Use of Bondable Terminals in Strain Gage Applications, Raleigh, NC 27777, 1983.

49. Measurements Group, Inc., Instruction Bulletin B-127-7, Strain Gage Installations with M-Bond 200 Adhesive, Raleigh, NC 27777, 1979.

50. Measurements Group, Inc., Instruction Bulletin B-129-3, Surface Preparation for Strain Gage Bonding, Raleigh, NC 27777, 1976.

51. Measurements Group, Inc., Instruction Bulletin B-141-2, Application of M-Coat G and GL Protective Coatings, Raleigh, NC 27777, 1978.

BIBLIOGRAPHY

Agarwal, B.D. and Broutman, L.J., *Analysis and Performance of Fiber Composites*, John Wiley and Sons, New York, NY, 1980.

Crossman, F.W. and Wang, A.S.D., "Stress Field Induced by Transient Sorption In Finite-Width Composite Laminates," *Journal of Composite Materials*, v. 12, pp. 2-18, January 1978.

DeJong, T., "Stresses Around Pin-Loaded Holes in Elastically Orthotropic or Isotropic Plates," *Journal of Composite Materials*, v. 11, pp. 313-331, July 1977.

England, A.H., *Complex Variable Methods in Elasticity*, Wiley-Interscience, 1971.

Hahn, H.T. and Pagano, J.J., "Curing Stresses in Composite Laminates," *Journal of Composite Materials*, v. 9, pp. 91-106, January 1975.

Hahn, H.T. and Tsai, S.W., "On Behavior of Composite Laminates After Initial Ply Failure," *Journal of Composite Materials*, v. 8, pp. 288-305, July 1974.

Jennings, A., *Matrix Computation for Engineers and Scientists*, Wiley-Interscience, 1977.

Kuske, A. and Robertson, G., *Photoelastic Stress Analysis*, Wiley, 1974.

Lekhnitskii, S.G., *Theory of Elasticity of An Anisotropic Elastic Body*, (Translated by P. Fern), Holden-Day, 1963.

Loos, A.C. and Springer, G.S., "Effects of Thermal Spiking on Graphite-Epoxy Composites," *Journal of Composite Materials*, v. 13, pp. 17-34, January 1979.

Nuismer, R.J., Labor, J.D., "Applications of the Average Stress Failure Criterion: Part I-Tension," *Journal of Composite Materials*, v. 12, p. 238, July 1978.

Pagano, N.J., "On the Calculation of Interlaminar Normal Stress in Composite Laminate," *Journal of Composite Materials*, v. 8, pp. 65-81, January 1974.

Pagano, N.J. and Rybicki, E.F., "On the Significance of Effective Modulus Solutions for Fibrous Composites," *Journal of Composite Materials*, v. 8, pp. 214-228, July 1974.

Predecki P. and Barrett, C.S., "Stress Measurement in Graphite/Epoxy Composites By X-Ray Diffraction from Fillers" *Journal of Composite Materials*, v. 13, pp. 61-71, January 1979.

Prezemienicki, J.S., Theory of Matrix Structural Analysis, McGraw-Hill Book Co., New York, NY, 1968.

Rowlands, R.E., Daniel, I.M. and Whiteside, J.B., "Stress and Failure Analysis of a Glass-Epoxy Plate with a Circular Hole," Experimental Mechanics, p. 31, January 1973.

Royal Aeronautical Society, Stress Concentration Data, London, UK September 1965.

Tang, S., "A Boundary Layer Theory - Part I: Laminated Composites in Plane Stress," Journal of Applied Mechanics, v. 9, pp. 33-41, January 1975.

Tang, S., "Interlaminar Stresses around Circular Cutouts in Composite Plates under Tension," AIAA Journal, v. 15, pp. 1631-1637, November 1977.

Ugural, A.C. and Fenster, S.K., Advanced Strength and Applied Elasticity, Elsevierl, 1981.

Wang, A.S.D. and Crossman, F.W., "Some New Results on Edge Effect in Symmetric Composite Laminates," Journal of Composite Materials, v. 11, pp. 92-106, January 1977.

Wang, S.S. and Choi, I., "Boundary-Layer Effects in Composite Laminates: Part 1 - Free-Edge Stress Singularities," Journal of Applied Mechanics, v. 19, pp. 541-548, September 1982.

Wang, S.S. and Choi, I., "Boundary-Layer Effects in Composite Laminates: Part 2 - Free-Edge Stress Solutions and Basic Characteristics," Journal of Applied Mechanics, v. 19, pp. 549-560, September 1982.

INITIAL DISTRIBUTION LIST

		No. Copies
1.	Defense Technical Information Center Cameron Station Alexandria, Virginia 22304-6145	2
2.	Library, Code 0142 Naval Postgraduate School Monterey, California 93943-5100	2
3.	Department Chairman, Code 67 Department of Aeronautics Naval Postgraduate School 93943-5100	1
4.	Professor Milton H. Bank, Code 034Bt Aviation Safety Programs Naval Postgraduate School Monterey, California 93943-5100	8
5.	Dr. J.A. Bailie Organization 81-12, Building 154 Lockheed Missiles and Space Company PO Box 504 Sunnyvale, California 90486	5
6.	Composite Materials Laboratory Code 67Bt Department of Aeronautics Naval Postgraduate School Monterey, California 93943-5100	5
7.	CDR P.D. Sullivan, USN 9226 Whitney St. Silver Spring, Maryland 20901	5
8.	LCDR G. H. O'Neill, USN COMNAVAIRPAC (Code 722) San Diego, California 93125	1
9.	S.P. Garbo McDonnell-Douglas Aircraft Corporation PO Box 516 St. Louis, MO 63166	1

215809

Thesis
S85983 Sullivan
c.1 An analysis of symmetric reinforcement of graphite/epoxy honeycomb sandwich panels with a circular cutout under uniaxial compressive loading.